Fundamentele studie van uitwisselingsprocessen in rivierecosystemen

A Fundamental Study on Exchange Processes in River Ecosystems

Liesbet De Doncker

Promotoren: prof. dr. ir. R. Verhoeven, prof. dr. ir. P. Troch
Proefschrift ingediend tot het behalen van de graad van
Doctor in de Ingenieurswetenschappen: Bouwkunde

Vakgroep Civiele Techniek
Voorzitter: prof. dr. ir. J. De Rouck
Faculteit Ingenieurswetenschappen
Academiejaar 2009 - 2010

UNIVERSITEIT
GENT

ISBN 978-90-8578-324-4
NUR 956
Wettelijk depot: D/2009/10.500/82

Universiteit Gent
Faculteit Ingenieurswetenschappen
Vakgroep Civiele Techniek

Supervisors:

Prof. dr. ir. Ronny Verhoeven
Prof. dr. ir. Peter Troch

Members of the exam committee:

Prof. dr. ir. Ronny Verhoeven (supervisor, Faculty of Engineering, UGent)
Prof. dr. ir. Peter Troch (supervisor, Faculty of Engineering, UGent)

Prof. dr. ir. Rik Van de Walle (chairman, Faculty of Engineering, UGent)
ir. Kerst Buis (Faculty of Sciences, UA)
Prof. dr. ir. Renaat De Sutter (Faculty of Engineering, UGent)
Prof. dr. ir. Patrick Meire (Faculty of Sciences, UA)
Prof. dr. ir. Tomasz Okruszko
(Faculty of Agricultural Engineering, University of Warschau)
Prof. dr. ir. Rudy Van Impe (Faculty of Engineering, UGent)

Proefschrift tot het behalen van de graad van
Doctor in de Ingenieurswetenschappen: Bouwkunde
Academiejaar 2009-2010

Acknowledgement

Na 6 jaar op het Labo Hydraulica is het tijd om eens terug te kijken en een aantal mensen te bedanken. Een bijzonder woord van dank gaat uiteraard naar Prof. Ronny Verhoeven, mijn promotor vanaf het prille begin. Hij gaf me het vertrouwen om dit onderzoek aan te vatten en heeft me de hele weg gesteund om er iets van te maken. Toen ook het numerieke deel van dit doctoraat uitbreidde, raakte ook Prof. Peter Troch betrokken bij het onderzoek. Ook hem ben ik heel erg dankbaar voor de steun in de voorbije jaren.

Toen ik hier in 2003 arriveerde, was ik blij me verder te kunnen verdiepen in de rivierhydraulica. Dat er toen nog een heleboel andere dingen zouden bijkomen had ik enigszins wel verwacht, maar ik had nooit durven dromen dat het hier zo'n boeiende en verrijkende periode zou worden.
Toen werd er in het Labo nog zowel bloed als water bestudeerd en het was hier gezellig druk, maar ook soms hectisch. Bedankt Ilse, Kris, Koen, Fadi, Stijn, Guy, Lieve, Sebastian, Ivo, Jurgen, Dirk, Prof. Segers, Prof. Verdonck en vooral Sunny om me hier de weg te wijzen.

De Hydraulica-afdeling werd bemand door Robert en Edawi: bedankt allebei voor de gesprekjes en een plaatsje in jullie bureau. Toen na enkele jaren de biomedische afdeling verhuisde, ging dat gepaard met twee nieuwe collega's, Binod en Kevin, blij dat jullie er waren! Nog later kwamen Sieglien en Dieter de groep versterken. Ik wens hen allemaal veel succes en doorzettingsvermogen bij hun onderzoek en Dieter, geniet van je extra dimensie bij het bestuderen van de rivieren.

Gedurende al die tijd waren Manuella, Marcel, Martin en Stefaan de constante aanwezigen. Bedankt, Manuella om me weg te wijzen in de doolhof van de universiteit, voor alle administratieve hulp en voor je welgemeende interesse in Daan. Bedankt, Marcel voor de geruststellende gesprekken en de labohulp, telkens het nodig was. Bedankt, Martin en Stefaan voor alle metingen op de Aa, zonder jullie was dit boek er wellicht niet gekomen. Martin, geniet van je extra vrije tijd de komende jaren en

Davy, de Aa heb je gemist, maar er zijn nog genoeg boeiende onderzoeken... Verder ben ik ook nog dank verschuldigd aan Yvan om dit werk te redden van meer dan *éé*n computercrash.

Verder ook nog een woordje van dank aan alle thesisstudenten die de voorbije jaren hun weg naar het Labo hebben gevonden en mijn onderzoek interessant genoeg vonden om er zich verder in te verdiepen: Sarah, Barbara, Maarten, Joris, Maximiliaan, Stoffel, Frederik, Pieter, Maarten, Bruno, Steven, Jan, Bert en Michael. Het ga jullie goed en hopelijk denken jullie met veel plezier terug aan deze periode.

Mijn werk als assistent liet mij toe om heel wat lessen te verzorgen in de opleiding burgerlijk bouwkundig ingenieur, een zeer aangename afwisseling. Aan al de studenten, ik hoop dat jullie leuke herinneringen hebben aan 'de hydraulica' en dat jullie je weg vinden in het leven.

Dit onderzoek is gekoppeld aan een FWO-project (Uitwisselingsprocessen in rivierecosystemen - G.0306.04) en bijgevolg gaat er ook een woord van dank uit naar de andere partners. Bedankt aan de mensen van Ecobe (Universiteit Antwerpen): Prof. Meire, Kris, Sofie, Jonas en in het bijzonder Kerst en Nele. Kerst, voor 'Femme', alle hulp hieromtrent en je inspanningen om het project mee op poten te zetten, Nele, voor de gezellige meetcampagnes en de constructieve samenwerking. Verder ook nog een woord van dank aan de VUB (Afdeling Hydrologie en Hydraulica), Christian en Prof. Batelaan: bedankt om de grondwaterwereld van de Aa te verkennen en te verduidelijken. Resultaten met betrekking tot de Biebrza rivier waren er niet gekomen zonder de jaarlijkse meetcampagnes in samenwerking met de groep van Prof. Okruszko aan de Universiteit van Warschau (Warsaw Agricultural University).

Bedankt aan familie en vrienden die in me bleven geloven, zelfs als ze niet meer wisten waar ik nu eigenlijk mee bezig was.

Daan, bedankt om ons leven te verrijken. Jouw lach en jouw enthousiasme maken alles de moeite waard. We houden heel veel van je en zullen er altijd voor je zijn.

Bedankt, broer of zus van Daan, om samen met je mama dit boek te schrijven. We kijken reikhalzend uit naar je komst. Welkom!

En Jan, voor alles.

Gent, december 2009
Liesbet De Doncker

Table of Contents

List of Figures

List of Tables

List of Acronyms and Symbols

A

a	[-]	coefficient depending on the position of the weir in the calibration formula of the weir
A	[m^2]	wetted cross section area
A_0	[m^2]	average cross-sectional area at zero flow
A_1	[-]	hydraulic-geometry coefficient
A_2	[-]	exponent for area
A_b	[m^2]	surface of inundation area at weir level
A_v	[m^2]	part of the cross section taken by plants
$\Delta A_{i,j}$	[m^2]	part of the wetted cross section A
ADCP		Acoustic Doppler Current Profiler

B

b	[-]	coefficient depending on the position of the weir in the calibration formula of the weir
b	[m]	width of the weir between the river channel and the storage basin
B	[m]	section width at water surface
B	[-]	blockage
B_{SA}	[-]	surface area blockage factor
B_V	[-]	volumetric blockage factor
B_X	[-]	cross sectional blockage factor
β	[1/°C]	temperature correction
BOD	[mg/l]	biochemical oxygen demand

C

C	[mol/kg water]	concentration in water
C_0	[g/l]	natural background concentration of the river
C_1	[g/l]	concentration of the injected solution
C_2	[g/l]	concentration balance at point of measurement, further downstream the river
C_d	[-]	discharge coefficient
C_d	[-]	drag coefficient
C_j	[-]	coefficient in the continuity equation
$C_j^{'}$	[-]	coefficient in the momentum equation
$C_{x,t}$	[mg/l]	nutrient concentration at location x at time t
Cl		chlorine
CO_2		carbon dioxide

D

df	[-]	dilution factor
d_m	[-]	absolute deviation
D_j	[-]	coefficient in the continuity equation
$D_j^{'}$	[-]	coefficient in the momentum equation
D_L	[m^2/s]	hydrodynamic dispersion coefficient
δ_v	[m]	thickness of the viscous sublayer

E

EC	[μS/cm]	electrical conductivity
E_j	[-]	auxiliary variable in the double sweep algorithm

F

f	[-]	friction factor of Darcy-Weisbach
F_j	[-]	auxiliary variable in the double sweep algorithm
F	[-]	a factor that relates the discrete sum over the finite number of verticals to the integral of the continuous function over the cross section
FHR		Flanders Hydraulic Research
FWO		Fund for Scientific Research

G

g	[m/s^2]	gravity acceleration
G_j	[-]	coefficient in the continuity equation
$G_j^{'}$	[-]	coefficient in the momentum equation
γ	[N/m^3]	specific density

H

h	[m]	water depth
h	[m]	water level over the weir
h_{afw}	[m TAW]	downstream water level
h_b	[m]	water height in the storage basin above the weir
h_{kr}	[m TAW]	crest level
h_o	[m]	height of the weir for each of the positions of the downstream weir
h_{opw}	[m TAW]	upstream water level
h_p	[m]	water height in the river channel above the weir
h_w	[m]	water depth over the upstream weir
h_v	[m]	velocity head
H	[m]	water depth
H_j	[-]	coefficient in the continuity equation

$H_j^{'}$	[-]	coefficient in the momentum equation
H_{weir3}	[m]	water level at weir 3
H_{weir4}	[m]	water level at weir 4
Δh	[m]	difference in water surface elevation
Δh_v	[m]	upstream velocity head minus downstream velocity head
HIC		Hydrological Information Centre

I

I	[W/m^2]	intensity of light
I	[m/s^2]	turbulence intensity
I_j	[-]	coefficient in the continuity equation
$I_j^{'}$	[-]	coefficient in the momentum equation

J

K

k	[-]	von Karman constant
k	[mm]	roughness height in the flow
k_s	[mm]	equivalent bottom roughness
k_{growth}	[1/day]	intrinsic growth rate
k_{decay}	[1/day]	intrinsic mortality rate
K	[s/m^3]	conveyance
K_I	[W/m^2]	light limitation
$K_{biomass}$	[g/m^2]	biomass limitation

L

l	[m]	width of the weir between two inundation areas
l	[m]	length of the channel reach
L	[m]	distance between the first and last cross-section sampled
L	[m]	length of the vegetated area
L_j	[-]	auxiliary variable in the double sweep algorithm
ΔL_{x1-x2}	[mg/l]	change in nutrient load

M

m	[-]	number of verticals
m	[-]	correction factor for meandering
m	[-]	coefficient depending on the position of the weir in the calibration formula of the weir
M_j	[-]	auxiliary variable in the double sweep algorithm
μ	[Pa.s]	dynamic viscosity

N

n	[-]	coefficient depending on the position of the weir in the calibration formula of the weir
n	$[s/m^{1/3}]$	Manning's coefficient
n	[-]	number of measurements
n	[-]	number of measurement depths over the vertical
n_0	$[s/m^{1/3}]$	Manning roughness - basic value for a straight uniform channel
n_1	$[s/m^{1/3}]$	Manning roughness - irregularities of the bottom

n_2	$[s/m^{1/3}]$	Manning roughness - variations in the geometry of the channel
n_3	$[s/m^{1/3}]$	Manning roughness - obstacles
n_4	$[s/m^{1/3}]$	Manning roughness - vegetation
n_{eff}	$[s/m^{1/3}]$	Manning's coefficient of the plants
n_{meas}	$[s/m^{1/3}]$	measured Manning's coefficient
n_{pl}	$[s/m^{1/3}]$	Manning's coefficient over the vegetated flume
n_{pred}	$[s/m^{1/3}]$	predicted Manning's coefficient
N	[1/s]	number of revolutions
N_j	[-]	auxiliary variable in the double sweep algorithm
ν	$[m^2/s]$	kinematic viscosity
ν	[m/s]	pore water flow velocity
N		nitrogen
Na		natrium
$NaHCO_3$		sodium bicarbonate
NH_4		ammonium
NO_3		nitrate

O

O		oxygen

P

P	[m]	wetted perimeter

Q

q	$[m^3/s/m]$	lateral in- or outflow discharge per unit length
q	$[m^3/s]$	constant injection discharge
Q	$[m^3/s]$	discharge
Q_{down}	$[m^3/s]$	downstream discharge

$Q_{downstream}$	[m^3/s]	downstream discharge
Q_{in2}	[m^3/s]	free flow in storage basin
Q_{in3}	[m^3/s]	submerged flow in storage basin
Q_{uit4}	[m^3/s]	free flow out of storage basin
Q_{uit5}	[m^3/s]	submerged flow out of storage basin
Q_{flood}	[m^3/s]	flooding discharge
Q_{up}	[m^3/s]	upstream discharge
$Q_{upstream}$	[m^3/s]	upstream discharge
Q_{meas}	[m^3/s]	measured discharge
Q_{sim}	[m^3/s]	simulated discharge
$Q_{x,t}$	[m^3/s]	discharge at location x at time t
ΔQ_j	[m^3/s]	difference in discharge in node je between two timesteps

R

r	[expressed as mol/kg water in the pores]	concentration in the solid phase
R	[m]	hydraulic radius
ρ	[kg/m^3]	density

S

S_0	[m/m]	channel bottom slope
S_b	[m/m]	water surface slope
S_f	[m/m]	friction slope
$S_{f,b}$	[m/m]	friction slope in the empty flume
$S_{f,eff}$	[m/m]	friction slope in the flume with floating plants

T

t	[s]	time
t	[s]	measurement duration
T	[°C]	temperature

T_0	[°C]	reference temperature
T_a	[s]	time of arrival of the tracer at the measurement point compared to the time of injection
T_c	[s]	equilibrium time
T_i	[s]	injection time
T_p	[s]	transit time
T_p	[s]	time of passage from the tracer at the measuring point
τ	[s]	travel time
τ	[N/m^2]	shear stress
τ_0	[N/m^2]	bottom shear stress
$\tau_{x,z}$	[N/m^2]	total shear stress
θ	[]	angle of the flap of the weir in the calibration formula
θ	[-]	parameter in the numerical scheme
Δt	[s]	time step
Traveltime	[s]	time the water in the river needs to travel from upstream to downstream
TAW	[m]	Tweede Algemene Waterpassing
TDS	[mg/l]	Total Dissolved Solids

U

U	[m/s]	velocity
$U_{i,j}$	[m/s]	local water velocity
u	[m/s]	measured velocity
$\overline{u}$	[m/s]	average velocity
u′	[m/s]	turbulence
u_m	[%]	uncertainty on the limited number of verticals
u_{bi}	[%]	relative (percentage) standard uncertainties in the width at vertical i
u_{di}	[%]	relative (percentage) standard uncertainties in the depth at vertical i
u_{vi}	[%]	relative (percentage) standard uncertainties in the mean velocity at vertical i
u_s	[%]	systematic uncertainty due to to calibration errors

u_{pi}	[%]	uncertainty due to the limited numbers of depths at which velocity measurements are made
u_{ci}	[%]	uncertainty on the characteristics of the measurement instrument
u_{ei}	[%]	uncertainty due to fluctuation of the velocity during the measurement
u^*_{bi}	[%]	percentage systematic uncertainty in the instrument measuring width
u^*_{di}	[%]	percentage systematic uncertainty in the instrument measuring depth
u^*_{ci}	[%]	percentage systematic uncertainty in the registration of the current meter
UA		University of Antwerp
UGent		Ghent University

V

v	[m/s]	velocity
v^x	[m/s]	friction velocity
v_{gem}	[m/s]	average velocity
v_{max}	[m/s]	maximum velocity
$v_x^{'}$	[m/s]	fluctuating velocity
$\overline{v_x}$	[m/s]	averaged velocity in the x-direction
$v_{sensor,i}$	[m/s]	measured velocity
$\overline{v_{sensor}}$	[m/s]	average velocity
V	[m/s]	velocity
V	[m/s]	mean velocity
V	[m^3]	volume of the injected solution
V_0	[m/s]	velocity of the inflow in the storage area perpendicular to the weir
V_b	[m^3]	volume of the storage basin at time step t
V_p	[m/s]	velocity within the plants
V_{Sys}	[m^3]	total volume in the river system

W

w	[m/s]	measured velocity
$w^{'}$	[m/s]	turbulence
w_i	[-]	coefficient of weight
$\overline{w}$	[m/s]	average velocity
W	[m]	wetted perimeter
W_1	[-]	hydraulic-geometry coefficient
W_2	[-]	exponent for width

X

x	[-]	location
x	[m]	distance
x	[-]	coordinate along the river channel
Δx	[m]	cell width

Y

$y^{'}$	[m]	flexible roughness
y_0	[m]	distance from bottom where v=0
y_n	[m]	depth of flow

Z

z	[m]	water level
z	[m]	water level in the river channel
z_0	[m]	height where the velocity equals 0
z_b	[m]	bed elevation
z_b	[m]	bottom elevation of the river channel
z_b	[m]	water level in the storage basin
z_d	[m]	treshold value, height of the weir
z_j	[m]	water level in the river channel

Z_{cr}	[m TAW]	level of the crest of the weir
z_{gem}	[m]	height with v(z_{gem})=v_{gem}
Z_{sv}	[m TAW]	water level
Z_{meas}	[m]	measured water level
Z_{sim}	[m]	simulated water level
Z_{up}	[m TAW]	upstream water level
$Z_{upstream}$	[m TAW]	upstream water level
$Z_{bottomup}$	[m TAW]	upstream bottom level
Z_{down}	[m TAW]	downstream water level
$Z_{downstream}$	[m TAW]	downstream water level
$Z_{bottomdown}$	[m TAW]	downstream bottom level
ΔZ_j	[m]	difference in water levels in node j between two timesteps

Nederlandse samenvatting –Summary in Dutch–

HOOFDSTUK 1: INLEIDING

Het hoofddoel van deze doctoraatsthesis is de studie van de interactie tussen oppervlaktewater en ecosysteem. In het eerste hoofdstuk worden, samen met de bestudeerde studiegebieden en de introductie van uitwisselingsprocessen in rivierecosystemen, de doelstellingen voor het onderzoek vastgelegd. Er is vooral aandacht besteed aan de aanwezigheid van vegetatie in de rivier en dat effect op debiet, waterpeil en waterkwaliteitvariabelen. Er zijn zowel metingen uitgevoerd in het labo als op het terrein, waar 2 studiegebieden zijn beschouwd: de Aa (België) en de Biebrza (Polen). De uitwisselingsprocessen worden gemodelleerd met behulp van een geïntegreerd pakket met belangrijke hydraulische module, de drijvende kracht van de interactieprocessen.
De eerste doelstelling heeft betrekking op de samenstelling van een uitgebreide dataset waarbij zowel data in het labo als op het veld worden verzameld. Deze dataset laat toe fysische processen te bestuderen, en dan vooral de interactie tussen waterkwantiteitparameters (debiet en waterpeil) en de aanwezigheid van vegetatie in de rivier. Deze studie is terug te vinden in hoofdstukken 4 en 5. Ten tweede wordt een numerieke code, Strive (STream RIVer Ecosystem), opgebouwd die toelaat geïntegreerde processen in rivierecosystemen te modelleren. Dit wordt toegelicht in hoofdstukken 2 en 3. De derde doelstelling slaat op het gebruik van de uitgebreide dataset, meer specifiek de veldwaarden, om het model te calibreren en valideren (zie hoofdstuk 6). Tenslotte worden doorheen het werk verschillende aspecten van geïntegreerde modellering en geïntegreerde processen toegelicht. Dit staat beschreven in hoofdstuk 7. In hoofdstuk 8 worden de conclusies geformuleerd en worden suggesties voor verder onderzoek naar voor geschoven.

HOOFDSTUK 2: HYDRAULISCHE MODELLERING

De ontwikkeling van het Strive model is het resultaat van een zoektocht in de wereld van de numerieke codes. Het doel is een code te selecteren

die in staat is uitwisseling en interactie tussen oppervlaktewater, grondwater en ecosysteem correct te modelleren. Verder moet het model vrij beschikbaar en de code toegankelijk zijn zodat aanvullingen en aanpassingen mogelijk zijn. Aangezien de ecosysteemhydraulica een innovatief studiegebied is, werd ervoor geopteerd de studie aan te vatten in 1 dimensie om op die manier inzicht te krijgen in de heersende processen. Een laatste vereiste is dat de hydraulica, met name de stromingsvergelijkingen, correct en niet vereenvoudigd worden geïmplementeerd.

HOOFDSTUK 3: EENDIMENSIONALE VERGELIJKINGEN VOOR NIET - PERMANENTE STROMING

Aangezien geen geschikt bestaand model werd gevondendat aan bovenstaande eisen voldoet, is ervoor gekozen een nieuwe code te ontwikkelen: 'Strive'. Dit model is uitgebouwd binnen de 'Femme' omgeving. 'Femme' is een modelleeromgeving geschikt voor ontwikkeling en toepassing van ecologische, tijdsafhankelijke processen. Het Strivemodel bestaat uit verschillende modules waarbij de hydraulische module de belangrijkste is. Het betreft een 1D hydrodynamisch model dat toelaat niet-permanente stroming te modelleren. Het 1D model is gebaseerd op de Saint-Venant vergelijkingen, welke bestaan uit de continuiteitsvergelijking en de bewegingsvergelijking. De oplossing van deze set niet-lineaire differentiaalvergelijkingen gebeurt met behulp van het Preissmann schema en het Double Sweep algoritme. Bijzondere aandacht is besteed aan de verschillende types randvoorwaarden en de Manning coëfficiënt die de weerstand beschrijft in de Saint-Venant vergelijkingen. Vervolgens werden ook modules, die het transport van opgeloste stoffen en deeltjes en de reactieprocessen van de aanwezige vegetatie beschrijven, toegevoegd. In dit onderzoek wordt vooral aandacht besteed aan de transportmodule en de interactie met de aanwezige biomassa in de rivier.

HOOFDSTUK 4: GEGEVENS VERZAMELD IN LABO- EN VELDMETINGEN

Om het model te calibreren en te valideren is een uitgebreide set van gegevens verzameld. Bijzondere aandacht is besteed aan de verschillende types meettoestellen om hydraulische data te bepalen. Er zijn metingen uitgevoerd in de meetgoot in het laboratorium en in het veld om hydraulische parameters te bepalen. De verschillende meetinstrumenten zijn verder bekeken en tevens zijn ook biomassa metingen uitgevoerd. Continue metingen van snelheid en debiet zijn te verkiezen, maar vrij duur. Discrete metingen maken gebruik van molentjes of electromagnetische instrumenten. Deze laatste kunnen ook eenvoudig meten in rivieren waar vegetatie aanwezig is. Tot slot zijn ook peilmetingen uitgevoerd. Het debiet wordt dan berekend via integratie van de snelheden over de dwarsdoorsnede. Een gecalibreerde overlaat, waarbij waterpeilen worden gemeten en debie-

ten berekend, is een handige en snelle manier om debieten op een continue wijze te kunnen meten. Resultaten voor debiet en waterpeil worden getoetst aan registraties van het Hydrologisch InformatieCentrum (HIC). In het veld zijn gedurende 4 jaar metingen uitgevoerd in het studietraject van de Aa. Aanvullend zijn ook intensieve meetcampagnes gehouden. Met betrekking tot biomassametingen worden invasieve methodes gebruikt om de hoeveelheid vegetatie per oppervlakte-eenheid te bepalen. In het veld is verder ook een gevoeligheidsanalyse uitgevoerd en de registratie van een piekdebiet is geanalyseerd. In de meetgoot zijn snelheidsprofielen opgemeten in duidelijk vastgelegde omstandigheden. De vegetatie blijkt een grote invloed te hebben op de snelheidsprofielen. Aanwezigheid van vegetatie zorgt voor afwijking van het logaritmisch snelheidsprofiel dat optreedt in 'onbegroeide' stromingsgoten. Tussen de planten worden lagere snelheden geregistreerd dan errond.

HOOFDSTUK 5: VERWERKING VAN DE DATA

Na het verzamelen van gegevens worden deze resultaten uitgebreid geanalyseerd. De weerstand tegen stroming, uitgedrukt door de Manning coëfficiënt, tengevolge van de aanwezigheid van planten wordt verder bestudeerd, net als de relatie tussen Manning coëfficiënt, debiet en biomassa. In de meetgoot is aangetoond dat het bepalen van de Manning coëfficiënt heel nauwkeurig moet gebeuren tengevolge van de kleine waterhelling. In het geval van drijvende planten blijkt dat het waterpeil een grote invloed heeft op de Manning coëfficiënt, wat erop wijst dat de weerstand tegen stroming vooral wordt veroorzaakt door obstructie. In het veld zijn een aantal snelheidsprofielen verder bestudeerd net als het aspect 'blockage' tengevolge van de aanwezige vegetatie. Over het algemeen varieert de Manning coëfficiënt zowel over de breedte als over de lengte van een rivier wat bepalend is voor de optredende waterpeilen in het rivierpand. De analyse van de volledige dataset laat toe een aantal fysische processen beter te begrijpen, waarbij de dataset zelf een succesvolle modellering toelaat.

HOOFDSTUK 6: BASISVALIDATIE VAN HET STRIVE MODEL

In hoofdstuk 6 worden enkele eenvoudige toepassingen nagerekend met het Strive model om verzekerd te zijn van goede resultaten zowel voor permanente als niet-permanente stroming. Eveneens wordt een gevoeligheidsanalyse gedaan. Tot slot wordt het model uitgebreid gecalibreerd met behulp van de gegevens verzameld in het studiegebied van de Aa. Deze calibratie is gebaseerd op de afhankelijkheid van de Manning coëfficiënt van debiet en biomassa. Naast een continue vergelijking werden ook 2 korte-termijn relaties getest waarbij wordt gewezen op de moeilijkheid om natuurlijke processen in *éé*n wiskundig verband te vatten. Het gebruik van de correcte Manning coëfficiënt in het model laat toe debieten, waterpeilen

en niet-reactieve tracers zoals de elektrische conductiviteit correct te berekenen. Hierbij zal de afwijking op het debiet telkens hoger zijn dan op de andere variabelen, waterpeil en conductiviteit.

HOOFDSTUK 7: GEÏNTEGREERDE MODELLERING MET STRIVE

In dit hoofdstuk wordt alle kennis uit het voorgaande verzameld om tot een geïntegreerde modellering te komen. Twee aspecten worden daarbij in detail bestudeerd: de aanwezigheid van overstromingsgebieden bij rivieren en de waterkwaliteit van de rivier.
Bij het bestuderen van de rivierhydraulica hebben overstromingsgebieden eveneens hun nut. Een extra module laat toe om het 1D model als quasi 2D te beschouwen. Het vullen en ledigen van deze overstromingszones werd experimenteel getest en vervolgens numeriek geïmplementeerd met behulp van verschillende methodes. De methode waarbij tussen rivier en overstromingsbekken een overlaat wordt beschouwd levert de beste resultaten, maar heeft wel tot gevolg dat het in- en uitstromend debiet niet op zich wordt bekeken.
Tot slot wordt naast de stroming ook het transport in de rivier bestudeerd. Naast niet-reactieve tracers worden ook reactieve componenten gemodelleerd. Het blijkt dat Strive zeer geschikt is om de waterkwaliteit van beken en rivieren te bestuderen, maar dat aandacht moet worden besteed aan implementatie van reactieprocessen in rivieren in het model.

HOOFDSTUK 8: CONCLUSIES

Dit werk toont het belang van de studie van uitwisselingsprocessen in ecosystemen aan. Een uitgebreide set van gegevens laat toe conclusies te trekken met betrekking tot de impact van plantengroei in de rivier op de stroming, de impact van obstakels op de stroming in de rivier en in de meetgoot, de voor- en nadelen van verschillende meetinstrumenten en het belang van de Manning coëfficiënt om de stroming te beschrijven. Een goed uitgebouwd model (Strive) maakt het mogelijk de interactieprocessen effectief te modelleren. Het model is uitgebreid gecalibreerd en gevalideerd en biedt mogelijkheden voor verder onderzoek, ook in andere rivieren.

English summary

CHAPTER 1: INTRODUCTION

The main aim of this thesis is the study of the interaction between surface water flow and the ecosystem. In the first chapter, the aim of the research is established, as well as the study areas and an introduction to exchange processes in river ecosystems. Attention is particularly paid to the presence of in-stream vegetation and its effect on discharge, water level and also on water quality variables. Measurements are performed in the laboratory flume and in the field where two study areas are considered: the river Aa (Belgium) and the Biebrza river (Poland). The mentioned interactions are incorporated in an integrated model with an important hydraulic component, the driving force of the ecological processes. First, data collection in the lab as well as in the field is performed. This data set allows for the study of physical processes and in particular the interaction between water quantity parameters (discharge and water level) and the presence of in-stream vegetation. This study is described in chapter 4 and chapter 5. Second, the numerical code 'Strive' (STream RIVer Ecosystem), which allows for modelling of integrated river ecosystems, is built. This can be found in chapter 2 and 3. The third aim is based on the use of the extended dataset, in particular the field measurements, for calibration and validation of the model (chapter 6). Finally, several aspects of integrated modelling and integrated processes are described in chapter 7. Chapter 8 summarizes the conclusions and suggestions for further research.

CHAPTER 2: HYDRAULIC MODELLING

The development of the Strive model is the result of a search between existing numerical codes. The aim is to select a code which allows for accurate modelling of the exchange and interaction of surface water flow, groundwater flow and the ecosystem. The model has to be freely available without black box properties: an open source code allows for additions and adaptations. As ecosystem hydraulics is an innovative research area, the study is started in 1 dimension to gain an insight into the present processes. A last requirement is the correct implementation of the full Saint-Venant equations, describing the hydraulics.

CHAPTER 3: EQUATIONS OF 1D UNSTEADY OPEN CHANEL FLOW

As no existing model was appropriate, a new code, 'Strive', is developed and built in the 'Femme' environment. 'Femme' is a modelling environment suitable for development and application of ecological, time-dependent processes. The Strive model consists of different modules from which the hydraulic module makes up the core of the model. This part is a 1D hydrodynamic model which allows for modelling of non-permanent flow, based on the Saint-Venant equations, which consist of the continuity equation and the momentum equation. The solution to this set of non-linear differential equations is obtained by using the Preissmann scheme and the Double Sweep algorithm. Special attention is paid to the different types of boundary conditions and Manning's coefficient which describes the resistance in the Saint-Venant equations. Consequently, also modules which describe the transport of solutes and solids and reaction processes of the in-stream vegetation are added. In this research, particular attention is paid to the transport module and the interaction with the biomass in the river.

CHAPTER 4: LABORATORY AND FIELD DATA COLLECTION

An extensive dataset is collected for model calibration and validation. Special attention is paid to the different types of measurement instruments to collect hydraulic data. Hydraulic measurements are performed in the flume and in the field, the different measurement instruments are discussed and the results are completed with biomass measurements. Continuous measurements of velocity and discharge are preferable but expensive. Discrete measurements use propellers or electromagnetic instruments. The latter allows for measurements in vegetated areas. Gauge data completes the set of measurements. The discharge is calculated based on the integration of the velocity over the cross section. A calibrated weir allows for fast and accurate calculation of discharges in a continuous way by measuring water levels. Measuring results for discharge and water level are compared to the registrations of the Hydrologic Information Centre (HIC). In the field, measurements are performed in the studied reach of the river Aa during 4 years. Additional, intensive measurement campaigns are organised. Concerning the biomass measurements, invasive techniques are used to measure the amount of vegetation for each m^2 of the river bottom. Different experiments are performed including a sensitivity analysis and the registration of a flood wave. In the flume, measurements are performed in an empty flume, in a flume with gravel bottom and in a flume with floating plants. Also, the influence of different obstacles is tested. Measurements in the Hydraulics lab allow to determine the influence of vegetation on velocity profiles. In the flume, velocity profiles are measured in different

set-ups and under well controlled conditions. The large influence of vegetation on the velocity profile is indicated. Presence of vegetation disturbs the logarithmic velocity profile which occurs in non-vegetated channels. Between the vegetation, lower velocities are registered than around the vegetation.

CHAPTER 5: DATA PROCESSING

All the gathered information is studied and conclusions are drawn about the flow resistance of in-stream vegetation, expressed by Manning's coefficient, and the relation between this Manning coefficient, discharge and biomass is explored. In the flume, it was shown that determination of Manning's coefficient demands large accuracy due to the small fall of the water level. The influence of varying Manning coefficient over the width and the length of the channel is studied. The study of the floating plants showed the large influence of the water level on Manning's coefficient which indicates that the stream flow resistance is especially caused by obstruction. In the field, velocity profiles and blockage aspects due to vegetation are studied in more detail. This data set allows for a better understanding of physical processes and is used for numerical modelling.

CHAPTER 6: BASIC VALIDATION OF THE STRIVE NUMERICAL MODEL

In chapter 6, practical examples of steady and non-permanent flow are simulated with the Strive model to ensure good results. A sensitivity analysis is also performed. Furthermore, the model is extensively calibrated using the measurement values gathered in the study area of the river Aa. This calibration is based on the dependence of Manning's coefficient on discharge and biomass. A long-term relationship is used as well as 2 short-term relationships and the difficulty to express natural processes in one mathematical relationship is stressed. Use of the correct Manning coefficient in the Strive model allows for accurate calculation of discharge, water level and non-reactive tracers as the electrical conductivity. The deviation on simulated discharge values is larger than the deviation on water level and conductivity.

CHAPTER 7: INTEGRATED MODELLING USING STRIVE

This chapter summarizes all information from the previous chapters to end up with the subject of integrated modelling. Two aspects are studied in detail: integration of inundation areas to rivers and water quality in rivers. While studying river hydraulics, flooding areas are an important topic. An extra module to the Strive model considers the 1D model as a quasi 2D model. Filling and emptying of storage basins and inundation areas is tested experimentally and numerically implemented according to different me-

thods. The method considering a weir between river and inundation area results in the most accurate values, but, as a consequence, in- and outflow are not studied separately. Finally, after study of flow, also transport of tracers and reactive components in the river is researched. Non-reactive tracers as well as reactive tracers are modelled. The Strive model is very appropriate for studying water quality of rivers, but attention has to be paid to implementation of reaction processes in rivers.

CHAPTER 8: CONCLUSIONS

This work describes the importance of the study of exchange processes in river ecosystems. An extensive dataset delivers plenty of information and a well developed model (Strive) allows for modelling of the exchange processes. The model is extensively calibrated and validated and offers possibilities for further research, also in other rivers.

1 Introduction

1 Exchange processes in river ecosystems

An ecosystem is a natural unit consisting of all plants, animals and micro organisms (biotic factors, related to living organisms) in an area functioning together with all of the non-living physical (abiotic, as temperature, light, water, etc.) factors of the environment [1].

Knowledge of the hydraulics of open channel flow includes flow resistance [2, 3], flow types [4–7], velocity and turbulence [8–11] and the role of flood plains in open channel flow [12].
It is widely acknowledged that hydrology plays a critical role in present-day fluvial systems and associated ecosystems [13]. Models are being developed, for example, to assist in providing rapid estimates of the ecological instream flow requirements of rivers [14]. Ecohydrology has close links with hydraulics [15–17].

It is evident that river form, process and behaviour can be understood in a scale sensitive, spatial and temporal, hierarchical manner. This requires that the spatial and temporal complexities of fluvial systems need understanding. Thus, while small scale process studies are vital, these need to be nested within the context of broad scale, long-term studies [18–25]. Much of the accumulated process knowledge should be used to bring longer-term and broader-scale perspectives of landscape change

back to prominence [13, 26]. Fluvial geomorphology is also in a stronger position now than it ever has been. Research has broadened and strengthened, and the contribution of fluvial geomorphology to resolving complex interdisciplinary problems is now widely recognized [27–29]. This represents both an opportunity and a challenge, as too many policy decisions are made without adequate consideration of the spatial and temporal complexity of systems; this is an area in which fluvial geomorphologists can offer crucial insight [13, 30].

Through drainage of sediments, organic matter and nutrients to the coastal seas, rivers largely influence the marine ecosystem. The qualitative and quantitative characteristics of this input and the temporal dynamics depend on processes in the upstream parts of the rivers [31]. In that upstream part, terrestrial material is removed through drainage and groundwater flow, while geomorphological, hydraulic and biological processes lead to storage and transport of the material. Over the years, transport of water, sediments and solutes is described in models on macro scale level. In the contact area between water and land, particular exchange processes occur with a particular fauna and flora and an intensive transformation and storage of material [32]. Transport to the downstream areas is determined by the transport velocity (determined by the type of component, ie. particular matter reaches higher velocities compared to dissolved solutes), transformation processes (which can remove, store or transform components) and the lateral connectivities (ie. exchange between river and inundation area or groundwater and surface water).

Interactions between surface water, groundwater and ecological processes are already studied in different fields [13, 33–47]. Surface water and groundwater interaction are discussed in [48, 49] and the ecological importance of it in [50–52]. The influence of biomass on surface water flow works on the hydraulic aspects as blockage of the river [53–60] and on the nutrient processes [61, 62]. Sediment processes in rivers and their interaction with the presence of macrophytes in rivers and inundation areas is studied in [40, 63–65]. Modelling of the interaction processes is studied in [66, 67] and described here in Chapter 2, 3, 6 and 7.

An integrated study focusses on aspects as sediment, river and floodplain interaction, influence of vegetation and management aspects. All of them are studied worldwide as is explained in the following.
The transfer of sediment from hillslopes to rivers, flood plains, lakes and transitional and coastal waters is, in part, a function of sediment deli-

very. Delivery is spatially and temporally highly variable [68] and requires hillslope-channel/flood plain coupling [69, 70]. Sourcing sediment is also critical for understanding transfer and for targeted management [71, 72].
The limitations of sediment and bed load equations are widely known and predictions of all transport formulae show large uncertainties. Difficulties introduced by sediment packing, variability of the near-bed turbulent velocity field, modification of the velocity field by the upstream presence of grains and variable supply mean that a universal transport equation has not been developed. Field measurements of sediment transport confirm the limits of applying transport equations for prediction [73]. Despite these challenges, researchers continue to develop new models for prediction [74–84]. It is suggested that a better understanding of transport-storage relations may improve predictive model capacity in the future [85]. Studies that emphasize the collection of field data are rare, but important [86–91].

Flood plains are an integral part of the fluvial system. Much of the work on flood plains is directed towards understanding present [92–96] and past sedimentation rates [97–100] and their relationship to the transportation of nutrients, organics [101], contaminants [102–104], vegetation [105, 106] and to hydrology [107, 108]. Flood plain research is critical for understanding material fluxes, contaminant storage, longitudinal and lateral connectivity and riverine ecology [109].

Vegetation plays an important role as an agent in fluvial geomorphology. At finer scales, this is effected through its influence on local hydraulics that determines sediment transport. At this scale, vegetation reduces bed shear through absorbing momentum by drag on the stems [110–112]. This enhances deposition and reduces sediment transport capacity [113, 114]. Complexity is introduced through large spatial and temporal variations between different vegetation types, growth stages, densities and locations [115–118]. Flexible vegetation also behaves differently with stage changes and, as a consequence, roughness becomes variable and dynamic [39, 119]. Consideration of the hydraulics of flow through and over vegetation therefore remains an important field of study, both experimentally [120–124] and in the field [125, 126]. The important question remains the prediction of velocity profiles in open channels.
At larger scales vegetation is also of importance [127, 128]. At the flood plain scale for example, the importance of vegetation in reducing the risk of flooding in the Waal River, the Netherlands, is recognized [129]. At the channel-type scale, Gradzinski et al. [130] has shown how in-channel

vegetation enhances channel aggradation and contributes to separation by blocking channels. Similarly, Gumbricht et al. [131] has demonstrated that local topographic features and channel flanking vegetation exert an important influence on the distribution of water in the Okavango Delta, Botswana. At the reach scale, it is also generally accepted that riparian vegetation increases bank stability and reduces stream bank erosion through enhancing resistance to erosion [132–135].
Over thousands of years, channel capacity, hydraulics, bed load transport rates and bank erosion are influenced substantially by vegetation and wood, both within the channel and on the flood plain [136].

The management of rivers as 'integrated ecosystems' [137] comprises at least four interacting subsystems: the active channel, flood plain (or, where absent, macro-channel), alluvial aquifer and riparian vegetation [138]. Together these comprise the integrated fluvial system, emphasizing the importance of lateral and longitudinal connectivity and interdependence. Four broad themes are considered under river management and remediation. These are: river landscape and classification, ecological water requirements, the European Water Framework Directive and river restoration and remediation [13].

All of the mentioned aspects concerning exchange processes in river ecosystems and their modelling are studied in literature, however, considering integrational aspects is rare and is subject of this research project.

2 Study areas and their characteristics

One study area is located in Belgium: the river Aa, another study area is located in Poland: the Biebrza river.

2.1 The river Aa

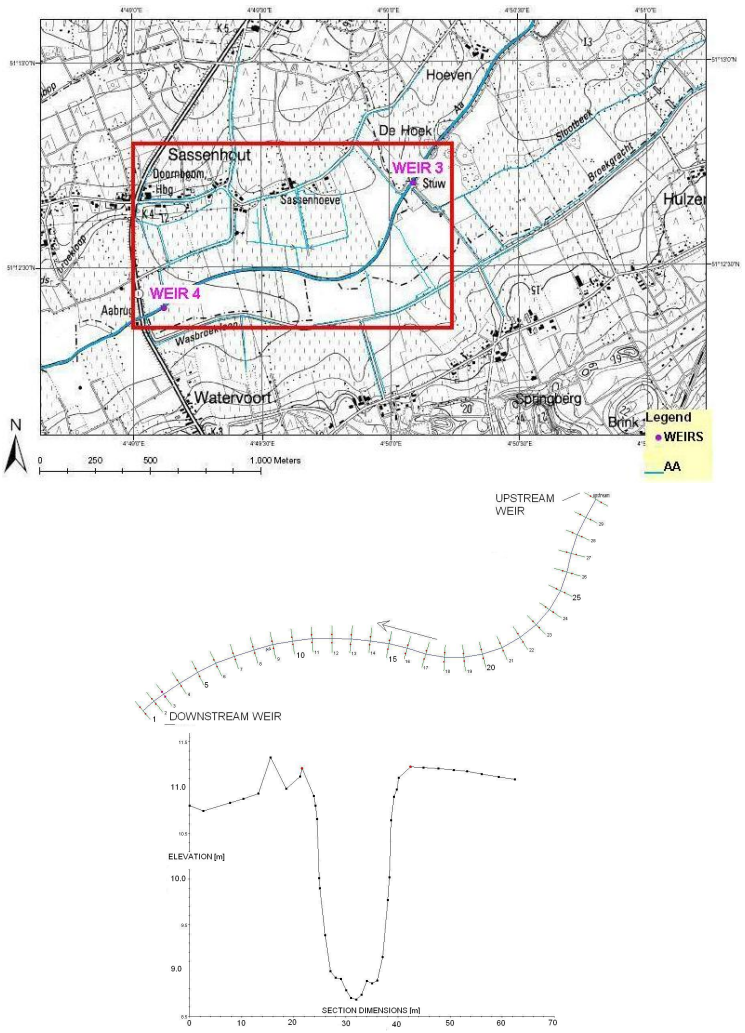

Figure 1.1: Study area of the river Aa, Poederlee, province of Antwerp, Belgium: localisation, plan view and cross section

In Belgium, focus of the study is the downstream part of the river Aa.
The catchment basin of the river Aa is situated in the region of Antwerp in Belgium and is hydrographically part of the Nete basin. The most important rivers of this basin are the Kleine Nete and the Grote Nete, both influenced by the tidal bore. More than 40 % of the water in the Nete basin is carried by the river Aa, which is consequently the most important tributary of the Kleine Nete. The river Aa flows into the Kleine Nete near the city of Grobbendonk. The well of the river Aa is found in the northern part of the Kempic Plateau near the communities of Merksplas and Turnhout. It has a total length of 36.8 km and a drainage area of about 23 700 ha. The study area is focused on the downstream part of the Aa, near the village of Poederlee, on a 1.4 km reach controlled by two weirs at the up-and downstream end.
The river Aa is a typical lowland river with low velocities, a small fall and so, a strongly meandering character. Over the years, the river has been straightened and the section was enlarged. The water inflow originates from drainage of rain water and seepage of ground water. The water is rather acid, without chalk and a low amount of minerals, not suitable for organisms. Living conditions for them are caused by food supply in the way of organic drainage of fertilizers from the fields of agriculture along the banks of the river.
The subsoil is predominantly formed by coarse sand. One million year old tertiary sand (as the Formations of Diest, Kasterlee and Berchem) is covered by 10 000 years old quartaire sand. Under these permeable sandy soils, a less permeable clay layer, the Boomse Klei, is present.
In the neighbourhood of the river, land is predominantly used for agriculture (48 %). Also living areas (17 %) and woods (25 %) are present, next to some recreational (3 %) and industrial (7 %) areas [139].

2.2 The river Biebrza

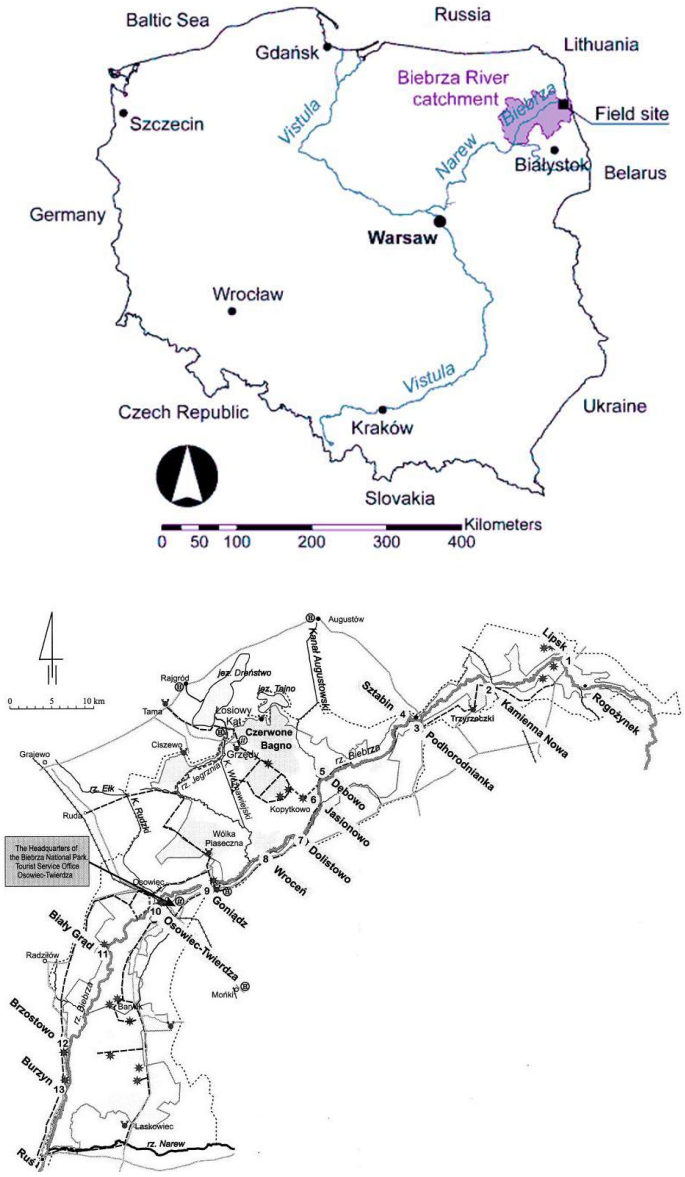

Figure 1.2: Study area of the Biebrza river, Poland

The Biebrza River and surrounding wetlands are situated in the north-eastern part of Poland, in an ice-marginal valley, an area of 195 000 ha. This region forms the last extensive, fairly undisturbed river-marginal peatland in Europe, containing endangered plant and animal species in a large variety of fully developed ecosystems. It is internationally recognised as a reference area for restoration of deteriorated peatlands.
Biebrza Valley, according to the geomorphologic description, is an extensive depression formed during the last glaciation. It is filled with several thick deposits of fluvioglacial sands. There are 3 major basins, respectively identified as the Upper Basin reaching from the springs of Biebrza to the mouth of the Netta River; the Middle Basin covering the area from Netta to the mouth of Rudzki Channel and the Lower Basin situated in the southern part of the valley up to the alluvial cone of the recipient Narew River. The Upper Basin has a length of some 40 km (62 km along the river) and a width of 2-3 km, with two basin-lake widenings: in its middle part and in the transition zone to the Middle Basin. The Middle Basin is the biggest, 40 km long and up to 20 km wide. It forms a vast, very flat depression paludified by the surface waters of Biebrza and its tributaries flowing from the Lake District, as well as by the ground waters of two aquifers. The river in Lower Basin has a length of 30 km and a width ranging from 12 to 15 km. The flood plain composes of flat peatlands and a mud zone of 2 km along the river border.
The Biebrza river, as a whole, is a typical lowland river. It has mild slopes (in average about 10 cm per km) and a strong meandering character. It features varying cross-sections and an irregular longitudinal profile. The variability of the hydrological characteristics along the river is also typical. This is due to the fact that the valley intensively drains the surrounding plateau and the outwash plain into the river. The surface water system is quite complicated consisting of a complex drainage system, network of inundation fields and storage areas. The flow is highly influenced by the dense vegetation [140].
The upstream reach of the Biebrza River is generally unpolluted, but two discharges of untreated domestic waste water are present in this reach. Diffuse sources are negligible. Further downstream, main tributaries, like the Augustowski Canal and the Rudzki Canal, discharge relatively polluted water into the Biebrza River [141].

3 The overall project

3.1 Setting

This research is part of the multidisciplinary research project 'A fundamental study on exchange processes in river ecosystems' (University of Antwerp, Vrije Universiteit Brussel, Ghent University, 2004 - 2007), funded by the FWO (Fund for Scientific Research) - Flanders (G.0306.04). Ghent University collects and analyses hydrometric data and develops a mathematical model for surface water flow. The Vrije Universiteit Brussel collects and analyses data from groundwaterflow and sets up a groundwater model. The growing process of macrophytes, their interaction and their relation with the amount of nutrients is studied by the University of Antwerp.

Quantity and quality of the input of sediments, organic matter and nutrients in coastal seas are determined by upstream processes in the river basin and output of the upstream system is input for the downstream sytems, and determines its structure and function. This output or input may be understood as hydraulic, chemical and biological characteristics of the interaction. To investigate how the diverse physical and biological processes and their interactions determine the exchange of water, dissolved compounds and suspended matter in margins and floodplains of water courses, it is necessary to develop models for land-water interfaces and their integration on the ecosystem level (Fig. 1.3) [142, 143].
The overall objective of the project is to study the physical and biological exchange processes in margins and inundation areas of water courses and how their interactions determine the exchange of water, dissolved compounds and particulate matter.

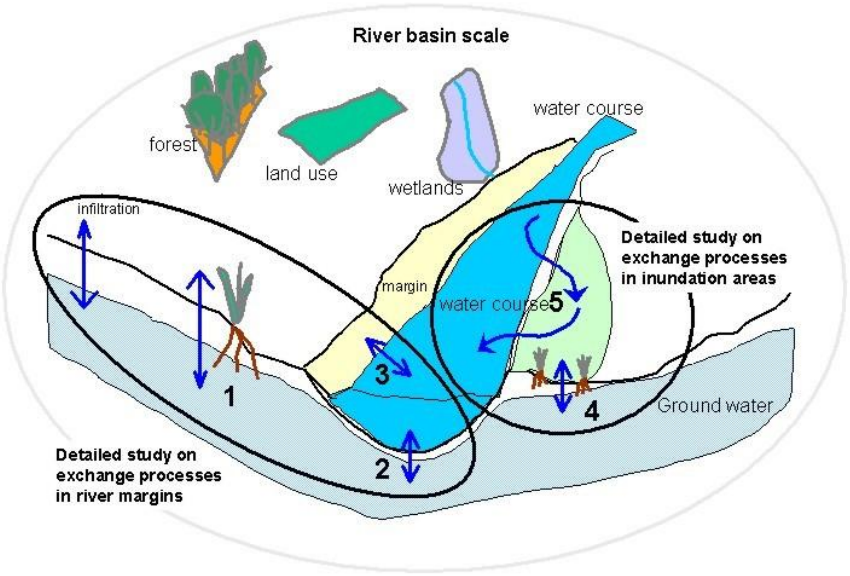

Figure 1.3: Considering the river basin at a macro level, detailed models of wetland - margin - stream areas and the inundation area allow a better definition of the intern boundary conditions and processes. Zones of interaction for water, dissolved solutes and suspended matter are important.

3.2 Niche

The project is based on data collection, data processing and model development. Hydrological and hydraulic data are important for the mass balances of rivers, while morphology and vegetation dynamics are characteristics of the system. The model development is focussed on the coupling of hydraulic and ecological processes.

Expertise in the field of geomorphology, hydrodynamics and ecology is widespread, but what is missing is the integrational aspect of these disciplines ie. a synthesis of physical and ecological descriptions in one model structure to analyse land-water interactions. Therefore, this project is fundamental for integrated stream basin research. This work, in particular, focusses on the influence of the in-stream vegetation on the hydraulic processes.

Furthermore, the European Union demands for an integrated vision in the 'Water Framework Directive' which includes a part of sustainable water management and water quality [144, 145]. In Flanders, recent management strategies stress the importance of efficient drainage of surface water, together with the conservation of biodiversity, the storage and the removal of nutrients to come to an adequate approach of ecosystems. This is described in the Flemish Environmental Policy Plan (MINA, [146]).

3.3 Results

As a conclusion, the results of the project partly described in this work are as follows:

- data generation on river ecosystem scale and derived from experiments
- collection of field data
- methodology set up for discharge determination in rivers and flumes and experiments with macrophytes
- integrated model development

The 1D integrated model generation allows study of the influence of macrophytes on the surface water flow, the water flux between surface water and the water bottom and exchange between river and inundation areas. Implementation of the behaviour of particular matter is included in the aspects for further research. It includes reactivity, sedimentation and erosion of the material and determines the retention of nutrients in the river system. Further 2D modelling will include the heterogeneities of flow velocity and vegetation patches which influence the nutrient behaviour [147].

4 Aim and organisation of this research

Physical processes in river ecosystems are studied in detail. Therefore, the development of an integrated numerical model is a useful tool.

In short, the research described in this work is focussed on four research objectives:

1. Data is collected from lab and field measurements. Lab tests allow studies in controlled conditions, while environmental measurements return effective field information. This dataset allows the description of physical processes, especially the interaction of the water quantity parameters (discharge and water level) and the presence of biomass (i.e. amount of vegetation, g/m^2) in the river using Manning's coefficient.

2. Development of the Strive (STream RIVer Ecosystem) model, a numerical model which allows integrated modelling. Aim is to study hydraulic as well as ecological variables and their interaction. The core hydraulic module is based on the Saint-Venant equations. The model meets the lack of integrated numerical models for river ecosystem studies.

3. The collected data set in the field (the river Aa in Poederlee, Belgium) is used for calibration and validation of the Strive model. Consequently, the hydraulic model results into accurate results.

4. Through this study, different aspects of integrated modelling are discussed. Examples are the interaction between biomass and flow, but next to flow aspects also flooding and transport are considered.

After this introduction, Chapter 2 gives an overview of numerical codes, (more or less) appropriate for integrated modelling. Chapter 3 summarizes the flow equations for 1D unsteady open channel flow used for hydraulic modelling. In Chapter 4, data collection in the laboratory as well as in the field is presented. Chapter 5 processes the collected data. Chapter 6 shows the accuracy of the Strive model while Chapter 7 presents some examples of more advanced and integrated modelling using the Strive model. Chapter 8 contains some conclusions and aspects for further research.

5 Publications

5.1 Publications in international journals

1. De Doncker, L., Troch, P., Verhoeven, R., 2008. Accuracy of discharge measurements in a vegetated river. Flow Measurement and Instrumentation (19) 29-40. ISSN 0955-5986, IF 0.819.

2. De Doncker, L., Troch, P., Verhoeven, R., Bal, K., Meire, P., Brandyk, A., Chormanski, J., Quintelier, J., 2009. Determination of the Manning roughness coefficient influenced by vegetation in the river Aa and Biebrza river. Environmental Fluid Mechanics (9)5 549-567. ISSN 1567-7419, IF 1.000.

3. De Doncker, L., Troch, P., Verhoeven, R., Bal, K., Desmet, N., Meire, P., 2009. Relation between resistance characteristics due to aquatic weed growth and the hydraulic capacity of the river Aa. River Research and Applications (25)10. ISSN 1535-1459, IF 1.959.

4. (submitted 11/05/09 Journal of Hydraulic Research, accepted with considering comments) De Doncker, L., Deneckere, M., Troch, P., Verhoeven, R., Study of flow resistance of floating plants in flume experiments. ISSN 0022-1686, IF 0.833.

5. (submitted 24/07/09 Journal of Hydroinformatics, accepted with considering comments) De Doncker, L., Troch, P., Verhoeven, R., Buis, K., Desmet, N., Meire, P., Numerical simulation of the interaction between ecological processes and surface water flow making use of the coupled Strive model. ISSN 1464-7141, IF 0.681.

6. (submitted 26/08/09 River Research and Applications) De Doncker, L., Troch, P., Verhoeven, R., Buis, K., Desmet, N., Meire, P., Importance of Manning's coefficient for the calibration of the coupled Strive model. ISSN 1364-8152, IF 1.959.

7. (submitted 08/10/09 Ecological Engineering) Bal, K., Struyf, E., Vereecken, H., Viaene, P., De Doncker, L., de Deckere, E., Mostaert, F., Meire, P., How do macrophyte distribution patterns affect hydraulic resistances?. ISSN 0925-8574, IF 1.836.

5.2 Publications in national journals

1. Buis, K., Anibas, C., Bal, K., Banasiak, R., De Doncker, L., De Smet, N., Gerard, M., Van Belleghem, S., Batelaan, O., Troch, P., Verhoeven,

R., Meire, P., 2007. Fundamentele studie van uitwisselingsprocessen in rivierecosystemen - Geintegreerde modelontwikkeling. Water, Vol. 32. p 51-54.

2. De Doncker, L., Troch, P., Verhoeven, R., Desmet, N., Buis, K., Meire, P., 2007. Stromingsweerstand in rivieren door de aanwezigheid van macrofyten. Water, Vol. 32. p 55-59.

5.3 Publications in international conferences

1. Anibas, C., Buis, K., De Doncker, L., 2005. Estimation of groundwater fluxes on a local scale via streambed temperature measurements. EGU General Assembly, Geophysical Research Abstracts, Vol. 7, 05596, Vienna, Austria.

2. De Doncker, L., Troch, P., Verhoeven, R., Bal, K., Meire, P., Chormanski, J., Miroslaw-Swiatek, D., Okruszko, T., 2005. Impact of vegetation development on the hydraulic characteristics and flow patterns in lowland rivers. W3M, Wetlands: Monitoring, Modelling, Management, 22-25 September 2005, Wierzba, Poland. ISBN13 978-0-415-40820-2, p 165-172.

3. Buis, K., Anibas, C., Banasiak, R., De Doncker, L., De Smet, N., Gerard, M., Van Belleghem, S., Batelaan, O., Troch, P., Verhoeven, R., Meire, P., 2005. A multidisciplinary study on exchange processes in river ecosystems. W3M, Wetlands: Monitoring, Modelling, Management., 22-25 September 2005, Wierzba, Poland.

4. De Doncker, L., Troch, P., Verhoeven, R., Bal, K., Meire, P., 2005. Influence of aquatic plants on the flow resistance and the hydraulic capacity of vegetated rivers. River Flow 2006, 06-08 September 2006, Lisboa, Portugal. ISBN 0-415-40815-6, p 593-602.

5. Buis, K., Anibas, C., Bal, K., Banasiak, R., De Doncker, L., Desmet, N., Gerard, M., Van Belleghem, S., Batelaan, O., Verhoeven, R., Meire, P., 2006, A multidisciplinary study on exchange processes in river ecosystems - The interaction between hydraulics and ecology on the retention of matter. EGU General Assembly, 02-07 April 2006, Geophysical Research Abstracts, Vol. 8, 05928, Vienna, Austria.

6. Anibas, C., Buis, K., Bal, K., Banasiak, R., De Doncker, L., Desmet, N., Gerard, M., Van Belleghem, S., Batelaan, O., Verhoeven, R., Troch, P., Meire, P., 2007, Hyporheic groundwater fluxes at the lower river Aa, Belgium. EGU General Assembly, 02-07 April 2006, Geophysical Research Abstracts, Vol. 8, 05151, Vienna, Austria.

7. De Doncker, L., Troch, P., Verhoeven, R., Bal, K., Meire, P., 2006. Interaction of river Hhydraulics and vegetation dynamics. EGU General Assembly, 02-07 April 2006, Geophysical Research Abstracts, Vol. 8, 07409, Vienna, Austria.

8. Desmet, N., Anibas, C., Bal, K., Bouma T.J., Buis K., De Doncker L., Seuntjens P., Van Belleghem S., Van Duren L.A., Batelaan O., Verhoeven R., Meire, P., 2006, The effects of aquatic macrophytes on river water quality. EGU General Assembly, 02-07 April 2006, Vienna, Austria.

9. De Doncker, L., Troch, P., Verhoeven, R., Buis, K., Meire, P., 2007. Flood routing in the river Aa using Femme. EGU General Assembly, 15-20 April 2007, Vienna, Austria.

10. Anibas, C., Buis, K., Bal, K., Banasiak, R., De Doncker, L., Desmet, N., Gerard, M., Van Belleghem, S., Batelaan, O., Verhoeven, R., Troch, P., Meire, P., 2007, Quantification of the groundwater-surface water interaction by analysing temperature gradients in the streambed of the Aa river, Belgium. EGU General Assembly, 15-20 April 2007, Geophysical Research Abstracts, Vol. 9, 03114, Vienna, Austria.

11. De Doncker, L., Troch, P., Verhoeven, R., Buis, K., Meire, P., 2007. Flood routing using Femme. Computational Civil Engineering 2007, 25 May 2007, Iasi, Romania. ISBN 978-973-8955-14-1, p 1-10.

12. Anibas, C., Bal, K., Banasiak, R., Batelaan, O., Buis, K., De Doncker, L., De Smet, N., Gerard, M., Meire, P., Troch, P., van Belleghem, S., Verhoeven, R., 2007. Determination of groundwater fluxes via sensing and simulation of hydraulic head and streambed temperatures in lowland rivers. IUGG-IAHS General Assembly 2-13 July 2007, Perugia, Abstract for Session HS1002 A New Focus on Integrated Analysis of Groundwater/Surface-Water Systems: Process Understanding, Conceptualisation and Modelling.

13. De Doncker, L., Troch, P., Verhoeven, R., Desmet, N., Meire, P., 2008. Influence of the vegetation on the propagation of flood waves, Applied Fluid Mechanics, Wessex, Institute of Technology, 2008, 331-340.

14. De Doncker, L., Troch, P., Verhoeven, R., Buis, K., Desmet, N., Meire, P., 2008. Computational aspects of river hydraulics. Computational Civil Engineering 2008, 30 May 2008, Iasi, Romania. ISBN 978-973-8955-41-7, p 168-177.

15. De Doncker, L., Troch, P., Verhoeven, R., Buis, K., Meire, P., 2009. Modelling of river hydraulics and ecological processes using Femme. 2nd International Multidisciplinary Conference on Hydrology and Ecology, 20-25 April 2009, Vienna, Austria.

16. Batelaan, O., Okruszko, T., Anibas, C., Verbeiren, B., Dams, J., Chormanski, J., Grygoruk, M., Miroslaw, D., Opdekamp, W., El Kahloun, M., Bal, K., Meire, P., De Doncker, L., Troch, P., Verhoeven, R., Penning, E., Biebrza ecohydrological research experiences: embracing the science of place. 2nd International Multidisciplinary Conference on Hydrology and Ecology, 20-25 April 2009, Vienna, Austria.

17. Batelaan, O., Okruszko, T., Anibas, C., Verbeiren, B., Dams, J., Chormanski, J., Grygoruk, M., Miroslaw, D., Opdekamp, W., El Kahloun, M., Bal, K., Meire, P., De Doncker, L., Troch, P., Verhoeven, R., Penning, E., Biebrza wetland research: required science for sustainable management. 15th Annual International Sustainable Development Research Conference, 3-8 July 2009, Utrecht, The Netherlands.

18. Meire, D., De Doncker, L., Troch, P., Verhoeven, R., 2009. Simulation of the filling and emptying processes between a river and its storage areas. International workshop on environmental hydraulics, 29-30 Octobre 2009, Valencia, Spain.

5.4 Publications in national conferences

1. De Doncker, L., Troch, P., Verhoeven, R., 2005. Influence of aquatic weed growth on the flow resistance of the river Aa. 6th FirW PhD Symposium, 30th November 2005, Ghent University, Belgium.

2. De Doncker, L., Troch, P., Verhoeven, R., Bal, K., Meire, P., 2006. Velocity profiles in vegetated rivers. NCTAM 2006, 29-30 May 2006, Mons, Belgium.

3. Bal, K., Vereecken, H., De Doncker, L., Meire, P., Viaene, P., Verhoeven, R., Troch, P., Mostaert, F., 2006, Waterplanten en waterkwantiteit. Studiedag voor gemeentebesturen met betrekking tot kruidruiming in rivieren, Belgium.

4. De Doncker, L., Troch, P., Verhoeven, R., Desmet, N., Buis, K., Meire, P., 2007. Stromingsweerstand in rivieren door de aanwezigheid van macrofyten, 3 Mei 2007, Congres Watersysteemkennis - Modellen voor integraal waterbeheer in Vlaanderen, Brussel, Belgium.

5. Buis, K., Anibas, C., Bal, K., Banasiak, R., De Doncker, L., Desmet, N., Gerard, M., Van Belleghem, S., Batelaan, O., Verhoeven,, R., Meire, P., 2007, Fundamentele studie van uitwisselingsprocessen in rivierecosystemen, 26 April 2007, Congres Watersysteemkennis - De interactie tussen bodem, grondwater en ecosysteem, Leuven, Belgium.

6. De Doncker, L., Troch, P., Verhoeven, R., 2008. Coupled ecosystem-hydrodynamic modelling. 9th FirW PhD Symposium, 3rd December 2008, Ghent University, Belgium.

References

[1] R.W Christopherson. *Geosystems: an introduction to physical geography*. 1996.

[2] J.C. Bathurst. *At-a-site variation and minimum flow resistance for mountain rivers*. Journal of Hydrology, (269):11–26, 2002.

[3] G. Katul, P. Wiberg, J. Albertson, and G. Hornberger. *A mixing layer theory for flow resistance in shallow streams*. Water resources Research, 38(11):32–1–32–8, 2002.

[4] J.M. Crowley. *Rough water, smooth water: a comprehensive classification of water-flow characteristics*. Focus, 46(4):29–32, 2002.

[5] V. Ferro and F.G. Carollo. *Discussion on 'estimating depth-averaged velocities in rough channels'*. Earth Surface Processes and Landforms, 27:1021–1025, 2002.

[6] P.M. Biron, A. Richer, A.D. Kirkbride, A.G. Roy, and S. Han. *Spatial patterns of water surface topography at a river confluence*. Earth Surface Processes and Landforms, 27:913–928, 2002.

[7] A.A. Jordanova, C.S. James, and A.L. Birkhead. *The role of hydraulics in holistic instream flow requirement assessment*. In D. Bousmar and Y. Zech, editors, River flow 2002: Proceedings of the international conference on fluvial hydraulics, volume 1, pages 515–519, Louvain-La-Neuve, Belgium, September 2002. Balkema Publishers.

[8] P. De Vries. *Bedload layer thickness and disturbance depth in gravel bed streams*. Journal of Hydraulic Engineering, 128(10):983–991, 2002.

[9] A.J. Lee and R.I. Ferguson. *Velocity and flow resistance in step-pool streams*. Geomorphology, (46):59–71, 2002.

[10] K. Babaeyan-Koopaei, D.A. Ervine, P.A. Carling, and Z. Cao. *Velocity and turbulence measurements for two overbank flow events in the River Severn*. Journal of Hydraulic Engineering, 128(10):891–900, 2002.

[11] X. Chen and Y.M. Chiew. *Response of velocity and turbulence to sudden change of bed roughness in open channel flow*. Journal of Hydraulic Engineering, 129(1):35–43, 2002.

[12] P.A. Carling, Z. Cao, and D.A. Ervine. *Flood plain contribution to open channel flow structure*. In F.J. Dyer, M.C. Thoms, and J.M. Olley, editors, The structure, function and management of fluvial sedimentary

systems, number 276 in Wallingford, IAHS Publication, pages 227–237, 2002.

[13] E.S.J. Dollar. *Fluvial geomorphology*. Progress in Physical Geography, 28(3):405–450, 2004.

[14] D.A. Hughes and P. Hannart. *A desktop model used to provide an initial estimate of the ecological instream flow requirements of rivers in South Africa*. Journal of Hydrology, (270):167–181, 2003.

[15] D.J. Booker. *Hydraulic modelling of fish habitat in urban rivers during high flows*. Hydrological Processes, 17:577–599, 2003.

[16] M. Odeh. *Discharge rating equation and hydraulic characteristics of Standard Denil fishways*. Journal of Hydraulic Engineering, 129(5):341–348, 2003.

[17] E.R. Rowland, R.H. Hitchkiss, and M.E. Barber. *Predicting fish passage design flows at ungauged streams in eastern Washington*. Journal of Hydrology, (273):177–187, 2003.

[18] L.H. Cammeraat. *A review of two strongly contrasting geomorphological systems within the context of scale*. Earth Surface Processes and Landforms, 27:1201–1222, 2002.

[19] S. Fukuoka. *River management for hydraulic harmony between flood control and environmental considerations*. In D. Bousmar and Y. Zech, editors, River flow 2002: Proceedings of the international conference on fluvial hydraulics, volume 1, pages 45–54, Louvain-La-Neuve, Belgium, September 2002. Balkema Publishers.

[20] A.S. Goudie. *Aesthetics and relevance in geomorphological outreach*. Geomorphology, (47):245–249, 2002.

[21] C.R. Thorne. *Geomorphic analysis of large alluvial rivers*. Geomorphology, (44):203–219, 2002.

[22] J. Vandenberghe. *The relation between climate and river processes, landforms and deposits during the Quaternary*. Quaternary International, 91:17–23, 2002.

[23] H.R. Beckedahl, P.D. Sumner, and G. Garland. *South African geomorphology: critical choices for the future*. South African Geographical Journal, 84(1):145–152, 2002.

[24] T.R. Kjeldsen, J.C. Smithers, and R.E. Schulze. *Regional flood frequency analysis in the KwaZulu-Natal province, South Africa, using the index flood method*. Journal of Hydrology, (255):194–211, 2002.

[25] J.D. Phillips. *Sources of nonlinearity and complexity in geomorphic systems*. Progress in Physical Geography, 27(1):1–23, 2003.

[26] B.J. Smith, P.A. Warke, and W.B. Whalley. *Landscape development, collective amnesia and the need for integration in geomorphological research*. Area, 33(4):409–418, 2002.

[27] A. Conacher. *A role for geomorphology in integrated catchment management*. Australian Geographical Studies, 40(2):179–195, 2002.

[28] L.E. Benda, N.L. poff, C. tague, M.A. Palmer, J. Pizzuto, S. Cooper, E. Stanley, and G. Moglen. *How to avoid train wrecks when using science in environmental problem solving*. Bioscience, 52(12):1127–1136, 2002.

[29] A. Frei, R.L. Armstrong, M.P. Clark, and M.C. Serreze. *Catskill Mountain water resources: vulnerability, hydroclimatology, and climate-change sensitivity*. Annals of the Association of American Geographers, 92(2):203–224, 2002.

[30] P.L.K. Knuepfer and J.F. Petersen. *Introduction: geomorphology in the public eye: policy issues, education, and the public*. Geomorphology, (47):95–105, 2002.

[31] G. Billen, C. Lancelot, and M. Meybeck. *N, P and Si retention along the aquatic continuum from land to ocean*. Ocean Margin Processes in Global Change, pages 19–44, 1991.

[32] J.B. Lachavanne and R. Juge. *Biodiversity in land-inland water ecotones*. Man and the Biosphere Series. Unesco and The Parthenon Publishing Group, 1997.

[33] M.C. Acreman and M.J. Dunbar. *Defining environmental river flow requirements - a review*. Hydrology and Earth System Science, 8:861–876, 2004.

[34] B.J.F. Biggs, V.I. Nikora, and T.H. Snelder. *Linking scales of flow variability to lotic ecosystem structure and function*. River Research and Application, 21:283–298, 2005.

[35] J.A. Cotton, G. Wharton, J.A.B. Bass, C.M. Heppell, and R.S. Wotton. *The effects of seasonal changes to in-stream vegetation cover on patterns of flow and accumulation of sediment*. Geomorphology, 77:320–334, 2006.

[36] F.H. Dawson. *Seasonal effects of aquatic plant growth on the flow of water in a small stream*. In European Weed Research Society 5th International Symposium on Aquatic Weeds, September 1978.

[37] W.W. Gregg and F.L. Rose. *The effects of aquatic macrophytes on the stream micro-environment*. Aquatic Botany, 14:309–324, 1982.

[38] R.J. Wilcock, P.D. Champion, J.W. Nagels, and G.F. Croker. *The influence of aquatic macrophytes on the hydraulic and physico-chemical properties of a New Zealand lowland stream*. Hydrobiologia, 416:203–214, 1999.

[39] U. Stephan and D. Gutknecht. *Hydraulic resistance of submergend flexible vegetation*. Journal of Hydrology, 269(1-2):27–43, 2002.

[40] K. Sand-Jensen. *Influence of submerged macrophytes on sediment composition and near-bed flow in lowland streams*. Freshwater Biology, 39:663–679, 1998.

[41] T. Riis, A.M. Suren, B. Clausen, and K. Sand-Jensen. *Vegetation and flow regime in lowland streams*. Freshwater Biology, 2008.

[42] T. Riis and B.J.F. Biggs. *Hydrologic and hydraulic control of macrophye establishment and performance in streams*. Limnology and Oceanography, 48:1488–1497, 2003.

[43] P.S. Naden, P. Rameshwaran, and P. Vienot. *Modelling the influence of instream macrophytes on velocity and turbulence*. In IAHR, editor, Proceedings of the fifth international symposium on ecohydraulics, volume 2, pages 1118–1122, 2004.

[44] J.D. Madsen, P.A. Chambers, W.F. James, E.W. Koch, and D.F. Westlake. *The interaction between water movement, sediment dynamics and submersed macrophytes*. Hydrobiologia, 444:71–84, 2001.

[45] C. Neal, W.A. House, B.A. Whitton, and G.J.L. Leeks. *Conclusions to special issue: water quality and biology of United Kingdom rivers entering the North Sea: the Land Ocean Interaction Study (LOIS) and associated work*. The Science of the Total Environment, 210/211:585–594, 1998.

[46] M.I. Stutter and D.G. Lumsdon. *Inteactions of land use and dynamic river conditions on sorption equilibria between benthic sediments and river soluble reactive phosphorus concentrations*. Water Research, 42:4249–4260, 2008.

[47] K.M. Ivkovic. *A top-down approach to characterise aquifer-river interaction processes*. Journal of Hydrology, 35:145–155, 2009.

[48] M. Sophocleus. *Interactions between groundwater and surface water: the state of the science*. Hydrogeology Journal, 10:52–67, 2002.

[49] T.C. Winter. *Relation of streams, lakes, and wetlands to groundwater flow systems*. Hydrogeology Journal, 7(1):28–45, 1999.

[50] A.J. Boulton, S. Findlay, P. Marmonier, E.H. Stanley, and H.M. Valett. *The functional significance of the hyporheic zone in streams and rivers*. In Annual Review of Ecological Systems, volume 29, pages 59–81, 1998.

[51] M. Brunke and T. Gonser. *The ecological significance of exchange processes between rivers and groundwater*. Freshwater Biology, 37(1):1–33, 1997.

[52] J.L. Meyer, D.L. Strayer, J.B. Wallace, S.L. Eggert, G.S. Helfman, and N.E. Leonard. *The contribution of headwater streams to biodiversity in river networks*. Journal of the American Water Resources Association, 43(1):86–103, 1997.

[53] R.S. Jadhav and S.G. Buchberger. *Effects of vegetation on flow through free water surface wetlands*. Ecological Engineering, 5(4):481–496, 1995.

[54] J.C. Green. *Modelling flow resistance in vegetated streams: review and development of new theory*. Hydrological Processes, 19(6):1245–1259, 2005.

[55] J.C. Green. *Effect of macrophyte spatial variability on channel resistance*. Advances in Water Resources, (65):232–243, 2005.

[56] J.C. Green. *Comparison of blockage factors in modelling the resistance of channels containing submerged macrophytes*. River Research and Applications, (21):671–686, 2005.

[57] J.C. Green. *Velocity and turbulence distribution around lotic macrophytes*. Aquatic Ecology, 39(1-2):1–10, 2005.

[58] P. Franklin, M. Dunbar, and P. Whitehead. *Flow controls on lowland river macrophytes: a review*. Science of the total environment, 400:369–378, 2008.

[59] D.S. White and S.P. Hendricks. *Chapter 15: Lotic Macrophytes and surface-subsurface exchange processes*, volume In: Streams and ground waters of *Academic Press, San Diego, California*. J.J. Jones and P.J. Mulholland, 2000.

[60] N. Desmet, S. Van Belleghem, P. Seuntjens, T. Bouma, K. Buis, and P. Meire. *Quantification of the impact of macrophytes on oxygen dynamics and nitrogen retention in a vegetated lowland river*. Physics and Chemistry of the Earth, 2008.

[61] C.C. Tanner. *Plants for constructed wetland treatment systems - A comparison of the growth and nutrient uptake of eight emergent species*. Ecological Engineering, 7(1), 1996.

[62] R.H. Kadlec, C.C. Tanner, V.M. Hally, and M.M. Gibbs. *Nitrogen spiraling in subsurface-flow constructed wetlands: implications for treatment response*. Ecological Engineering, 25(4):365–381, 2005.

[63] J. Vandenberghe and V. Vanacker. *Towards a system approach in the study of river catchments*. Geomorphology, 98(3-4):173–175, 2008.

[64] N.I. Alekseevskiy, K.M. Berkovich, and R.S. Chalov. *Erosion, sediment transport and accumulation in rivers*. International Journal of Sediment Research, 23(2):93–105, 2008.

[65] J.P.M. Lenssen, F.B.J. Menting, W.H. van der Putten, and C.W.P.M. Blom. *Effects of sediment type and water level on biomass production of wetland plant species*. Aquatic Botany, 64(2):151–165, 1999.

[66] G. Steinebach, S. Rademacher, P. Rentrop, and M. Schulz. *Mechanisms of coupling in river flow simulation systems*. Journal of Computational and Applied Mathematics, 168:459–470, 2004.

[67] Y. Lian, I. Chi Chan, J. Singh, M. Demissie, V. Knapp, and H. Xie. *Coupling of hydrologic and hydraulic models for the Illinois River Basin*. Journal of Hydrology, 344:210–222, 2007.

[68] J.J. Macaire, S. Bellemlih, C. Di-Giovanni, P. De Luca, L. Visset, and J. Bernard. *Sediment yield and storage variations in the Negron River catchment (South Western Parisian Basin, France) during the Holocene period*. Earth Surface Processes and Landforms, 27:991–1009, 2002.

[69] K. Michaelides and J. Wainwright. *Modelling the effects of hillslope-channel coupling on catchment hydrological response*. Earth Surface Processes and Landforms, 27:1441–1457, 2002.

[70] M.C. Slattery, P.A. Gares, and J.D. Philips. *Slope-channel linkage and sediment delivery on North Carolina coastal plain cropland*. Earth Surface Processes and Landforms, 27:1377–1387, 2002.

[71] R.J. Wasson, G. Caitcheon, A.S. Murray, M. McCulloch, and J. Quade. *Sourcing sediment using multiple tracers in the catchment of Lake Argyle, northwestern Australia*. Environmental Management, 29(5):643–646, 2002.

[72] P.A. Cawood, A.A. Nemchin, M. Freeman, and K. Sircombe. *Linking source and sedimentary basin: detrital zircon record of sediment flux along a modern river system and implications for provenance studies*. Earth and Planetary Science Letters, 1-2:259–268, 2003.

[73] J.T. Pearce, F.J. Pazzaglia, E.B. Evenson, D.E. Lawson, R.B. Alley, D. Germanoski, and J.D. Denner. *Bedload component of glacially discharged sediment: insights from the Matanuska Glacier, Alaska*. Geology, 31(1):7–10, 2003.

[74] N.S. Cheng. *Exponential formula for bedload transport*. Journal of Hydraulic Engineering, 128(10):942–746, 2002.

[75] J.P. Le Roux. *Shape entropy and settling velocity of natural grains*. Journal of Sedimentary Research, 72(3):363–366, 2002.

[76] W.R. Richardson. *Simplified model for assessing meander bend migration rates*. Journal of Hydraulic Engineering, 128(12):1094–1097, 2002.

[77] R.P. Hunziker and M.N.R. Jaeggi. *Grain sorting processes*. Journal of Hydraulic Engineering, 128(12):1060–1068, 2002.

[78] H.L. Monteith and G. Pender. *The response of graded sediment beds to flow abstraction*. In D. Bousmar and Y. Zech, editors, River flow 2002: Proceedings of the international conference on fluvial hydraulics, volume 1, pages 699–702, Louvain-La-Neuve, Belgium, September 2002. Balkema Publishers.

[79] H.M. Nagy, K. Watanabe, and M. Hirano. *Prediction of sediment load concentration in rivers using artificial neural network model*. Journal of Hydraulic Engineering, 128(6):588–595, 2002.

[80] E. Pea, J. Fe, J. Puertas, and F. Sanchez-Tembleque. *A 2D numerical model using finite volume method for sediment transport in rivers*. In D. Bousmar and Y. Zech, editors, River flow 2002: Proceedings of the international conference on fluvial hydraulics, volume 1, pages 693–698, Louvain-La-Neuve, Belgium, September 2002. Balkema Publishers.

[81] J.S. Ribberink, A. Blom, P. van der Scheer, and M.P. van Stralen. *Multi-fraction techniques for sediment transport and morphological modelling in sand-gravel rivers*. In D. Bousmar and Y. Zech, editors, River flow 2002: Proceedings of the international conference on fluvial hydraulics, volume 1, pages 731–739, Louvain-La-Neuve, Belgium, September 2002. Balkema Publishers.

[82] S. Wongsa, T. Nakui, M. Iwai, and Y. Shimizu. *Runoff and sediment transport modelling for mountain river*. In D. Bousmar and Y. Zech, editors, River flow 2002: Proceedings of the international conference on fluvial hydraulics, volume 1, pages 683–691, Louvain-La-Neuve, Belgium, September 2002. Balkema Publishers.

[83] P.R. Wilcock and J.C. Crowe. *Surface-based transport model for mixed-size sediment*. Journal of Hydraulic Engineering, 129(2):120–128, 2002.

[84] S.Q. Yang and S.Y. Lim. *Total load transport formula for flow in alluvial channels*. Journal of Hydraulic Engineering, 129(1):68–72, 2002.

[85] T.E. Lisle and M. Church. *Sediment transport-storage relations for degrading, gravel bed channels*. Water resources Research, 38(11):1–1–1–14, 2002.

[86] B.C. Eaton and M.F. Lapointe. *Effects of large floods on sediment transport and reach morphology in the cobble-bed Sainte Marguerite River*. Geomorphology, (40):291–309, 2002.

[87] H.M. Habersack and J.B. Laronne. *Evaluation and improvement of bed load discharge formulas based on Helley-Smith sampling in an alpine gravel bed river*. Journal of Hydraulic Engineering, 128(5):484–499, 2002.

[88] S.K. Hayes, D.R. Montgomery, and C.G. Newhall. *Fluvial sediment transport and deposition following the eruption of Mount Pinatubo*. Geomorphology, (45):211–224, 2002.

[89] P.Y. Julien, G.J. Klaassen, W.B.M. ten Brinke, and A.W.E. Wilbers. *Case study: bed resistance of Rhines River during 1998 flood*. Journal of Hydraulic Engineering, 128(12):1042–1050, 2002.

[90] J. Rodriguez, D.M. Admiraal, F. Lopez, and M.H. Garcia. *Unsteady bed shear stresses induced by navigation: laboratory observations*. Journal of Hydraulic Engineering, 128(5):515–526, 2002.

[91] S.E. Ryan, L.S. Porth, and C.A. Troendle. *Defining phases of bedload transport using piecewise regression*. Earth Surface Processes and Landforms, 27:971–990, 2002.

[92] M. Brunke. *Floodplains of a regulated southern Alpine river (Brenno, Switzerland): ecological assessment and conservation options*. Aquatic Conservation: Marine and Freshwater Ecosystems, 12(6):583–599, 2002.

[93] H. Middelkoop. *Reconstructing floodplain sedimentation rates from heavy metal profiles by inverse modelling*. Hydrological Processes, 16:47–64, 2002.

[94] N.E.M. Asselman and M. van Wijngaarden. *Development and application of a 1D floodplain sedimentation model for the River Rhine in The Netherlands*. Journal of Hydrology, (268):127–142, 2002.

[95] A.P. Nicholas and C.A. Mitchell. *Numerical simulation of overbank processes in topographically complex floodplain sediments*. Hydrological Processes, 17:727–746, 2002.

[96] S. Lusk, K. Halaoka, and V. Luskova. *Rehabilitating the floodplain of the lower River Dye for fish*. River Research and Applications, 19(3):281–288, 2003.

[97] D.E. Walling and P.N. Owens. *The role of flood plain sedimentation in catchment sediment and contaminant budgets*. In F.J. Dyer, M.C. Thoms, and J.M. Olley, editors, The structure, function and management of fluvial sedimentary systems, number 276 in Wallingford, IAHS Publication, pages 407–416, 2002.

[98] I.D.L. Foster, J.A. Lees, A.R. Jones, A.S. Chapman, and S.E. Turner. *The possible role of agricultural land drains in sediment delivery to a small reservoir, Worcestershire, UK: a multiparameter fingerprint study*. In F.J. Dyer, M.C. Thoms, and J.M. Olley, editors, The structure, function and management of fluvial sedimentary systems, number 276 in Wallingford, IAHS Publication, pages 433–442, 2002.

[99] J.L. Paine, J.S. Rowan, and A. Werritty. *Reconstructing historic floods using sediments from embanked floodplains: a case study of the river Tay in Scotland*. In F.J. Dyer, M.C. Thoms, and J.M. Olley, editors, The structure, function and management of fluvial sedimentary systems, number 276 in Wallingford, IAHS Publication, pages 211–218, 2002.

[100] K.J. Page, G.C. Nanson, and P.S. Fraziezr. *Floodplain formation and sediment stratigraphy resulting from oblique accretion on the Murrumbidgee River, Australia*. Journal of Sedimentary Research, 73(1):5–14, 2002.

[101] G.S. Morozova and N.D. Smith. *Organic matter deposition in the Saskatchewan River floodplain (Cumberland Marshes, Canada): effects of progradational avulsions*. Sedimentary Geology, 157:15–29, 2003.

[102] J.S. Rowan and S.W. Franks. *Heavy metal mining and flood plain response in the upper Clyde basin, Scotland*. In F.J. Dyer, M.C. Thoms, and J.M. Olley, editors, The structure, function and management of fluvial sedimentary systems, number 276 in Wallingford, IAHS Publication, pages 143–153, 2002.

[103] L. Maurice-Bourgoin, R. Aalto, and J.L. Guyot. *Sediment-associated mercury distribution within a major Amazon tributary: century-scale contamination history and importnace of floodplain accumulation*. In F.J. Dyer, M.C. Thoms, and J.M. Olley, editors, The structure, function and management of fluvial sedimentary systems, number 276 in Wallingford, IAHS Publication, pages 161–168, 2002.

[104] H. Middelkoop, I. Thonon, and M. van der Perk. *Effective discharge for heavy metal deposition in the lower River Rhine flood plains*. In F.J. Dyer, M.C. Thoms, and J.M. Olley, editors, The structure, function and management of fluvial sedimentary systems, number 276 in Wallingford, IAHS Publication, pages 151–159, 2002.

[105] N.C. Sims and M.C. Thoms. *What happens when flood plains wet themselves: vegetation response to inundation on the lower Balonne flood plain*. In F.J. Dyer, M.C. Thoms, and J.M. Olley, editors, The structure, function and management of fluvial sedimentary systems, number 276 in Wallingford, IAHS Publication, pages 195–202, 2002.

[106] A.A. Webb, W.D. Erskine, and D. Dragovitch. *Flood-driven formation and destruction of a forested flood plain and in-channel benches on a bedrock-confined stream: Wheeny Creek, southeast Australia*. In F.J. Dyer, M.C. Thoms, and J.M. Olley, editors, The structure, function and management of fluvial sedimentary systems, number 276 in Wallingford, IAHS Publication, pages 203–210, 2002.

[107] F.J. Dyer. *Assessing the hydrological changes to flood palin wetland inundation caused by river regulation*. In F.J. Dyer, M.C. Thoms, and J.M. Olley, editors, The structure, function and management of fluvial sedimentary systems, number 276 in Wallingford, IAHS Publication, pages 245–253, 2002.

[108] R. Aalto, T. Dunne, C.A. Nittrouer, L. Maurice-Bourgoin, and D.R. Montgomery. *Fluvial transport of sediment across a pristine tropical fore-*

land basin: channel-flood plain interaction and episodic flood palin deposition. In F.J. Dyer, M.C. Thoms, and J.M. Olley, editors, The structure, function and management of fluvial sedimentary systems, number 276 in Wallingford, IAHS Publication, pages 339–344, 2002.

[109] G.C. Nanson and J.C. Croke. *Emerging issues in flood plain research*. In F.J. Dyer, M.C. Thoms, and J.M. Olley, editors, The structure, function and management of fluvial sedimentary systems, number 276 in Wallingford, IAHS Publication, pages 271–278, 2002.

[110] C.A.M.E. Wilson and M.S. Horritt. *Measuring the flow resistance of submerged grass*. Hydrological Processes, 16:2589–2598, 2002.

[111] P.G. Samuels, M.E. Bramley, and E.P. Evans. *Reducing uncertainty in conveyance estimation*. In D. Bousmar and Y. Zech, editors, River flow 2002: Proceedings of the international conference on fluvial hydraulics, volume 1, pages 293–302, Louvain-La-Neuve, Belgium, September 2002. Balkema Publishers.

[112] A.A. Jordanova and C.S. James. *Experimental study of bed load transport through emergent vegetation*. Journal of Hydraulic Engineering, 129(6):474–478, 2002.

[113] T. Helmio. *Unsteady 1D flow model of compound channel with vegetated floodplains*. Journal of Hydrology, 269:89–99, 2002.

[114] M. Righetti and A. Armanini. *Flow resistance in open channel flows with sparsely distributed bushes*. Journal of Hydrology, 269(1-2):55–64, 2002.

[115] J. Jarvela. *Determination of flow resistance of vegetated channel banks and floodplains*. In D. Bousmar and Y. Zech, editors, River flow 2002: Proceedings of the international conference on fluvial hydraulics, volume 1, pages 311–318, Louvain-La-Neuve, Belgium, September 2002. Balkema Publishers.

[116] J. Jarvela. *Flow resistance of flexible and stiff vegetation: a flume study with natural plants*. Journal of Hydrology, 269(1-2):44–54, 2002.

[117] R.H.J. Sellin and D.P. van Beesten. *Berm vegetation and its effect on flow resistance in a two-stage river channel: an analysis of field data*. In D. Bousmar and Y. Zech, editors, River flow 2002: Proceedings of the international conference on fluvial hydraulics, volume 1, pages 319–327, Louvain-La-Neuve, Belgium, September 2002. Balkema Publishers.

[118] H. Yoshida and A. Dittrich. *A 1D unsteady state flow simulation of a section in the upper Rhine*. Journal of Hydrology, (269):79–88, 2002.

[119] Z. Shi and j.M.R. Hughes. *Laboratory flume studies of microflow environments of aquatic plants*. Hydrological Processes, 16:3279–3289, 2002.

[120] P.M. Rowinski and J. Kubrak. *Velocity profiles on vegetated flood plains*. In D. Bousmar and Y. Zech, editors, River flow 2002: Proceedings of the international conference on fluvial hydraulics, volume 1, pages 303–309, Louvain-La-Neuve, Belgium, September 2002. Balkema Publishers.

[121] P.M. Rowinski and J. Kubrak. *A mixing length model for predicting vertical velocity distribution in flows through emergent vegetation*. Hydrological Sciences Journal, 47(6):893–899, 2002b.

[122] S.J. Bennett, T. Pirim, and B.D. Barkdoll. *Using simulated emergent vegetation to alter stream flow direction within a straight experimental channel*. Geomorphology, 44:115–126, 2002.

[123] F.G. Carollo, V. Ferro, and D. Termini. *Flow velocity measurements in vegetated channels*. Journal of Hydraulic Engineering, 128(7):664–673, 2002.

[124] C.S. James, A.A. Jordanova, and C.R. Nicolson. *Flume experiments and modelling of flow-sediment-vegetation interactions*. In F.J. Dyer, M.C. Thoms, and J.M. Olley, editors, The structure, function and management of fluvial sedimentary systems, number 276 in Wallingford, IAHS Publication, pages 3–9, 2002.

[125] M.J. Baptist and E. Mosselman. *Biogeomorphological modelling of secondary channels in the Waal river*. In D. Bousmar and Y. Zech, editors, River flow 2002: Proceedings of the international conference on fluvial hydraulics, volume 1, pages 773–782, Louvain-La-Neuve, Belgium, September 2002. Balkema Publishers.

[126] J.M. Goodson, A.M. Gurnell, P.G. Angold, and I.P. Morrissey. *Evidence for hydrochory and the deposition of viable seeds within winter flow-deposted sediments: the River Dove, Derbyshire, UK*. River Research and Applications, 19(4):317–334, 2003.

[127] J. Steiger and A.M. Gurnell. *Spatial hydrogeomorphological influences on sediment and nutrient deposition in riparian zones: observations from the Garonne River, France*. Geomorphology, (49):1–23, 2002.

[128] M. Huisink, J.J.W. De Moor, C. Kasse, and T. Virtanen. *Factors influencing periglacial fluvial morphology in the northern European Russian tundra and Taiga*. Earth Surface Processes and Landforms, 27:1223–1235, 2002.

[129] J.S. Ribberink, A. Blom, P. van der Scheer, and M.P. van Stralen. *Large-scale floodplain lowering along the River Waal: a stochastic prediction of morphological impacts*. In D. Bousmar and Y. Zech, editors, River flow 2002: Proceedings of the international conference on fluvial hydraulics, volume 1, pages 903–912, Louvain-La-Neuve, Belgium, September 2002. Balkema Publishers.

[130] R. Gradzinski, J. Baryla, M. Doktor, D. Gmur, M. Gradzinski, A. Kedior, M. Paszkowski, R. Soja, T. Zielinski, and S. Zurek. *Vegetation-controlled modern anastomosing system of the upper Narew River (NE Poland) and its sediments*. Sedimentary Geology, 157:253–276, 2003.

[131] T. Gumbricht, T.S. McCarthy, and C.L. Merry. *The topography of the Okavango Delta, Botswana, and its tectonic and sedimentological implications*. South African Journal of Geology, 104:243–264, 2001.

[132] E.R. Micheli and J.W. Kirchner. *Effects of wet meadow riparian vegetation on streambank erosion. Remote sensing measurements of streambank migration and erodibility*. Earth Surface Processes and Landforms, 27:627–639, 2002.

[133] A.B. Murray and C. Paola. *Modelling the effect of vegetation on channel pattern in bedload rivers*. Earth Surface Processes and Landforms, 27:131–143, 2002.

[134] W.C. Hession, J.E. Pizzuto, T.E. Johnson, and R.J. Horwitz. *Influence of bank vegetation on channel morphology in rural and urban watersheds*. Geology, 31(2):147–150, 2003.

[135] L.A. McKergow, D.M. Weaver, I.P. Prosser, R.B. Grayson, and A.E.G. Reed. *Before and after riparian management: sediment and nutrient exports from a small agricultural catchment, Western Australia*. Journal of Hydrology, (270):253–272, 2002.

[136] A.P. Brooks and G.J. Brierley. *Mediated equilibrium: the influence of riparian vegetation and wood on the long-term evolution and behaviour of a near-pristine river*. Earth Surface Processes and Landforms, 27:343–367, 2002.

[137] J.C. Rodda. *Water under pressure*. Hydrological Sciences Journal, 46(6):841–853, 2001.

[138] G.C. Poole. *Fluvial landscape ecology: addressing uniqueness within the river discontinuum*. Freshwater Biology, 47(641-660), 2002.

[139] Aminal. *De Kleine Nete, computer modelling as a method, high water control as a target (in Dutch) - computermodellering als methode, hoogwaterbeheer als doel*, 2004. Grontmij Belgroma nv, in order of Aminal.

[140] R. Verhoeven, R. Banasiak, D. Swiatek, J. Chormanski, and T. Okruszko. *Surface water modeling of the Biebrza River network*. In River Flow '04, number ISBN 90-5809-688-2, pages 1057–1064, Italy, Naples, June 2002.

[141] M. van der Perk and M. Bierkens. *The identifiability of parameters in a water quality model of the Biebrza River, Poland*. Journal of Hydrology, (200):307–322, 1997.

[142] C. Amoros, J. Gibert, and M.T. Greenwood. *Interactions between units of the fluvial hydrosystem*. Fluvial Hydrosystems, pages 184–210.

[143] A. Brookes and F.D. Shields. *River channel restoration: guiding principles for sustainable development*. John Wiley and sons, 1996.

[144] T. Moss. *The governance of land use in river basins: prospects for overcoming problems of institutional interplay with the EU Water Framework Directive*. Land Use Policy, 21:85–94, 2004.

[145] T. Petersen, B. Klauer, and R. Manstetten. *The environment as a challenge for governmental responsibility - The case of the European Water Framework Directive*. Ecological Economics, 68:2058–2065, 2009.

[146] N.N. *Milieubeleidsplan - Flemish Environmental Policy Plan*. Technical report, Flemish Government - Ministerie van de Vlaamse Gemeenschap (in dutch), 2003. Mina 2 (1997 - 2001), Mina 3 (2003 - 2007), Mina 3+ (2007 - 2010), Mina 4 (2011 - 2015).

[147] K. Buis, C. Anibas, K. Bal, R. Banasiak, L. De Doncker, N. Desmet, M. Gerard, S. Van Belleghem, O. Batelaan, P. Troch, R. Verhoeven, and P. Meire. *Fundamentele studie van uitwisselingsprocessen in rivierecosystemen - gentegreerde modelontwikkeling*. Water, 2007.

2 Hydraulic modelling

After the description of the interaction processes in river ecosystems, this chapter indicates the most important criteria for integrated modelling, with particular attention to the aspect of hydraulic modelling. The importance of the interaction of groundwater, surface water and ecosystem is presented, as well as an overview of existing models. The choice of the model used in this study is explained.

1 Interaction of groundwater, surface water and ecosystem

In nature, groundwater, surface water and ecosystem are interacting permanently. So is, on the one hand, evaporation of vegetation part of the balance for surface water and are, on the other hand, groundwater level and water quality boundary conditions for the presence and functionning of vegetation. In inundation areas, the vegetation influences the stream flow, the residence time of the water and the sedimentation of suspended solids. Vice versa is the flooding influencing the type of vegetation developping in these areas. Therefore, an integration of the different disciplines is necessary to develop the scientific know how of ecosystems. For this purpose, numerical modelling is a useful tool.

Numerical models and studies often consider only a part of the river basin or transport of a limited number of components. However, exchange processes on the basin level ask for good understanding of land-water areas with special attention to temporal dynamics and spatial heterogenity ('hot moments' and 'hot spots' according to [1]). The interaction between processes and structures determining the flow of water with dissoved solids and solutes has to be understood. The interaction of physical, chemical and biological processes influence the exchange of water, dissolved solids and particular matter.
The integrated study of ecological processes and surface water flow is situated in a multidisciplinary research field were attention is paid to the interaction of groundwater, surface water and the ecological system in order to describe the transport of matter through river basins [2]. The ecosystem consists of different subsystems: the surface water (the river), the parts with saturated sediments and groundwater flow, and the riparian zone, which are all hydrologically connected. Water and its suspended and dissolved load move through the subsystems. Chemical transformations result in a change of the quantity of materials in transport [3]. Furthermore, at terrestrial-aquatic interfaces, so-called 'hot spot' and 'hot moment' activity is seen. Hot spots are patches with high reaction rate, while hot moments are periods of time with high reaction rate [1]. In ecosystem studies, not only the river discharge, but also the biochemical processes of the nutrients in the water body are important. The path of these nutrients is connected with the hydrologic variability. Doyle [4] looked for what discharges were connected with what nutrient retention. Rivers seem to be important corridors for nutrient transport, yet they can also be critical reactors or regions where nutrients are removed or transformed [5].

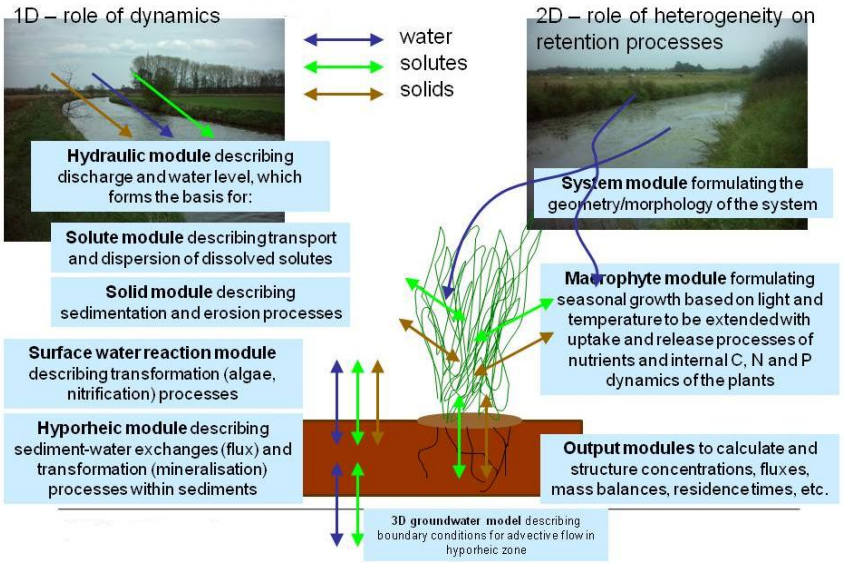

Figure 2.1: Illustration of the modular stream ecosystem model. Modules are depicted as blocks. [2]

Fig. 2.1 [2] shows the different processes which take place in ecosystems. The different processes are incorporated in different modules to result in an integrated model. Water as well as solids, solutes and vegetation have their particular function. The model has to deal with this wide range of processes and effects. Following aspects have to be incorporated.

- Formulation of geometry of the river (width, bottom slope, etc.).

- Hydraulics of the water system based on the Saint-Venant equations with Manning's coefficient as imported calibration parameter. As water flows in the river, this is the core module of the model.

- Transport of dissolved solutes. From upstream to downstream, solutes (Cl^-,NO_3^-, NH_4^+, etc.) are transported by the river. In the study of the solutes, following parameters are considered: the electrical conductivity (presence of Na, K, Cl and NH4), Cl, O and minerals (NO_3, NH_4).

- Transport of suspended solids, sedimentation and erosion processes. The transport of sediments by the flow has consequences for the morphology of the river. Concerning the solids; BOD, organic N (N

Kjehldahl), detritus (dead organic matter can cause eutrophication) and suspended solids were implemented.

- Macrophyte growth over the year based on temperature and light. Vegetation influences the stream flow and vice versa.

- Reactions in the surface water (algae growth, nitrification).

- Water bottom model with diffusive and advective transport in a vertical way and reactivity of components. It is a connection between groundwater and surface water. Mineralisation processes in the bottom and fluxes of nitrate, ammonium, tracers or other components over the edge of the water bottom

- Output variables are determined, based on the research question. Discharges or water levels, the amount of nutrients in the river, the macrophyte growth and reaction, etc. are possible subjects of interest.

The properties of the upstream river basin determine the quantity (discharge and water level) and quality (eg. amount and type of nutrients due to hydrological, chemical and biological processes which will transform and remove material [3, 6]) of the water flowing to the sea.
Brock [7] stated that physical, chemical and biological properties of the environment determine if plants can occur and vice versa, these plants influence the environment. Important aspect is the amount of biomass and the production of biomass [g/m^2]. Macrophytes contribute to the rivers fauna and to the accumulation of organic matter in the bottom. The influence on the environment of in-stream vegetation is large: anorganic carbon (CO_2 and $NaHCO_3$) uptake, uptake and storage of minerals (N, P, K, Na), excretion of nutriments and organic compounds, decomposition of the plants and the material produced by the macrophytes, increase of nutrients due to decomposition, influence on O_2 concentration, oxidation of the rhizosphere, influence on the water movement, competition for light, influence on the environment temperature, evaporation, etc.

The development of integrated numerical ecosystem models is essential in ecosystem studies [8]. Interaction processes as well as integrated model development is described in [9]: exchange processes in rivers require integrated model development. 'Integrated' is described in [9] as the connection between disciplines as groundwater, surface water and ecology and the interactive study of cascade and feedback relations. Interaction between different parts of and processes in the water system are coupled to

describe cascade and feedback relations for transport and retention of material. An example will illustrate this.
Presence of macrophytes in lowland rivers causes higher resistance to flow. Vegetation grows in a heterogeneous way and due to these macrophyte patches, stream flow is not uniform. In the patches, velocity is lower then in the free area. Therefore, large sedimentation of particles occurs between these macrophytes. A change in mineralisation processes will take place due to the higher amount of organic matter in the vegetated areas.
Other microbial decomposition processes gain importance due to the smaller amount of oxygen that reaches the water bottom.
Denitrification causes the remove of nitrate of the water ('cascade'). On the other hand, the amount of nutrients in the bottom will increase due to decomposition of organic matter. Consequently, macrophyte growth increases ('feedback'). It is a stimulating process: more wealthy growth causes higher retention of particular matter, etc. Another cascade effect is found in the macrophytes which are a habitat for organisms, certainly macro-invertebrates.

The presence of vegetation on the riverbed has an influence on the hydrodynamic characteristics of the flow; moreover, a seasonal variation of the vegetation causes variation of the depth of flow and variation of the resistance. Vegetation affects the fluvial processes as exchange of sediment, nutrients and contaminants [10, 11]. In this research, the vegetation type consists of macrophytes with their spatial and temporal variation. The variation of vegetation is expressed as a change in flow resistance characteristics which has consequently a major effect on the flow, i.e. on the hydraulic capacity of the river and the flow velocity profiles.

2 Integrated Modelling

An integrated model study of hydraulic, groundwater, biogeochemical and ecological processes is required for the prediction of dynamic ecosystem behaviour, such as retention of matter in a river ecosystem and the associated resilience. However, most of the available models do not allow the integration of surface water flow, groundwater flow and ecosystem processes.

In general, for modelling surface water flow, the groundwater level is taken as a boundary condition. Vice versa, when modelling groundwater flow, the surface water level is taken as a boundary condition. In cases of strong interaction, however, it is useful to couple models. Smits [12] devel-

oped a method to couple Duflow, for surface water flow and based on the 1D Saint-Venant equations, and MicroFem (finite elements), for groundwater flow, according to an iterative procedure. This model does not take into account environmental aspects. Whigham [13] developed a simple water movement model allowing the prediction of the environmental impact of flow scenarios in lowland rivers and their floodplains. The model is a good initial framework, but has its constraints due to its simplification. Querner [14] combined the regional groundwater flow model Simgro with the surface water flow model Simwat and developed Mogrow, using the simplified Saint-Venant equations (parabolic model) to describe the river flow. Another widely used code is Hec-Ras (Hydrologic Engineering Centers River Analysis System), suitable for 1D, steady and unsteady, surface water flow. Rodriguez [15] describes the coupling of Hec-Ras with Modflow. To study integrated hydrodynamic - ecological modelling, it is not advisable to model complex ecological processes with simplified conceptual hydrodynamic models. In a multidisciplinary approach, different research areas have to be integrated to study properly the interaction between surface water and vegetation. In [16], some criteria for code selection are studied in detail. Some of them are used for the present code selection. they vary from availability (commercial packet, research code, etc.), possibilities for data processing (high requirements on data quality and/or quantity), complexity of the model (conceptual, detailed, etc.) to possibilities for presentation of results.

3 Overview of hydraulic models

3.1 Code selection

3.1.1 Introduction

There is a distinction between the terms 'code' and 'model'. A 'model' refers to the tool that provides a simplified representation of the specific field situation, while 'code' refers to a generic program or set of commands that is used to solve the governing equations representing the physical processes. A model is site and objective-specific, whereas a code is generic and can be applied to many sites and problems [16].

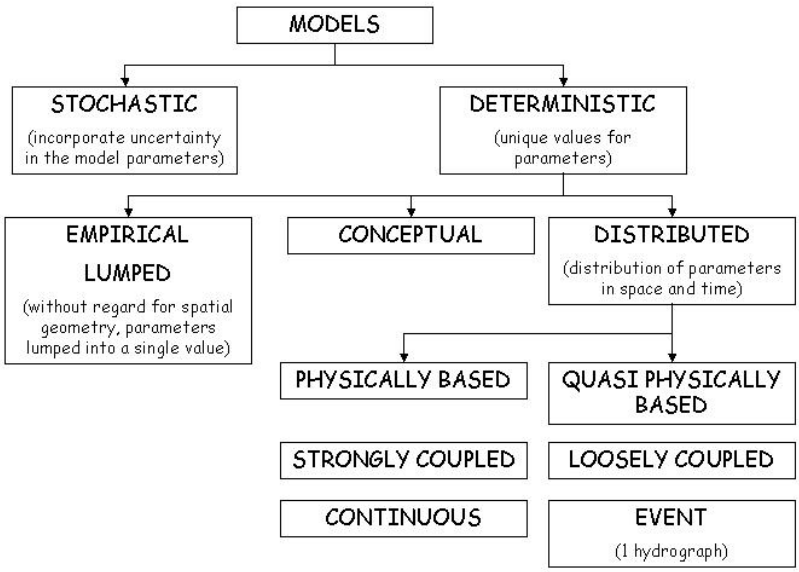

Figure 2.2: Classification of hydraulic models according to the way they treat the randomness and space and time variability of hydrologic phenomena, according [17]

Increasing concerns in predicting the impacts of land use management on the hydrological cycle have led researchers to construct three types of hydrological models which are gathered in Fig. 2.2. Trying to develop a model with random variables that depend on space dimensions and time is a big task and for most practical purposes it is necessary to simplify the model by neglecting some sources of variation. Hydraulic models may be classified (Fig. 2.2) by the ways in which this simplification is accomplished [17]. A deterministic model does not consider randomness; a given input always produces the same output. A stochastic model has outputs that are at least partially random. Further, the treatment of spatial variation is considered. Hydrologic phenomena vary in all three space dimensions, but all of this taken into account makes the model too complicated for practical use. In a deterministic lumped model, the system is spatially averaged or regarded as a single point in space without dimensions. A deterministic distributed model considers the hydrologic processes taking place at various points in space and defines the model variables as a function of the

space dimensions. Stochastic models are classified as space-independent or space-correlated according to whether or not random variables at different points in space influence each other.
Firstly, considering the discharge, an important variable in hydraulic modelling, the simplest case is the deterministic lumped steady flow model. Inflow and outflow are equal and constant in time. Secondly, for a deterministic lumped unstaedy flow model, the inflow and outflow are not allowed to vary in time. Thirdly, there is a deterministic distributed unsteady flow model, variation in space and time are allowed. This method allows a more accurate model of channel flow than a lumped model.

The most detailed models are spatial distributed and physically based: there, physical hydrological processes are described in a 3D view. The study is limited to certain points where the calculations are performed. Numerical equations are discreted to perform the calculations in different 'blocs'. Advantages are the wide range of possibilities to describe the natural situation, on the other hand, a lot of (ground)parameters are needed and calculation times are high.
There are two types of physically-based distributed models. The first type of models views the watershed as an ensemble of inter-connected reservoirs and describes water routing with various types of discharge expressions and conceptual models (eg. Topmodel [18–20]). The second type of model discretizes the watershed into a number of control volumes and models water routing using combinations of partial differential equations for mass and momentum conservation and phenomenological models (eg. Kineros [21–23] and Thales [24, 25]).

On another front, the adverse effects of agricultural, industrial and urban runoff on surface and ground waters have motivated the development and application of different approaches to predict the transport of various water contaminants in the environment (i.e. eroded soil particles, adsorbed and dissolved nutrients and pesticides as well as organic matter). In soil erosion modelling, these concerns have led researchers to construct nonpoint source pollution models for evaluating the impacts of alternative land management practices on water quality [26].

Another aspect of modelling are the uncertainties. Natural situations of water and nutrient transport are that complicated that it is not possible to model the situation on the field. Therefore, simplifications are added in the modelling structure, which simultaneously result in inaccurate calculations. Aim is to look for an equilibrium between field situation and model according to the goal of the project while minimising uncertainties.

While hydraulic models simulate the behaviour of the water in the river, the hydrologic model describes and calculates the water supply of the river (eg. due to rainfall). In this study, attention is paid to the hydraulic capacities of rivers. Consequently, the hydraulic capacities of the model are more important than the hydrologic possibilities in the model selection.

3.1.2 Selection criteria

The selection of a useful code for integrated modelling is based on a number of general considerations based on the demands with regard to the expected results [16] and gathered in Table 2.1.

General considerations	Significance for selected code
Commercially-available	Code should be available free/for purchase by anyone who wants to run the model
Project objectives	Requires high resolution, predictive accuracy, and ability to work at various scales
Data quality and quantity	Both are high, not a limitation on code selection
Conceptual model	Allows modelling of all aspects: surface water flow, groundwaterflow and ecological processes
Project constraints	Project schedule requires a flexible and efficient code
Graphical Interface	Ability to be interfaced with GIS and graphical tools

Table 2.1: Selection criteria for a useful code for integrated modelling, based on [16]

The selection criteria for model choice are presented in Table 2.1 and completed with the following considerations. In this study, integrated modelling is performed by a one dimensional approach. The description of the river section is one-dimensional and thus simplified equations are used. 1D modelling assumes that the modelled flow characteristics only change along the length of the river. This means that all variables are averaged over the river cross section. Such a description is in many cases adequate when the main interest is to model hydraulic aspects and transformation processes over relatively long distances. On the other hand, it makes the application of the river section compartment to local mixing phenomena impossible.
Furthermore, 1D modelling has some advantages compared to other, more complex, models for 2D and 3D calculations. The modelling approach is

more clear and the 1D model is a basic tool for further development of the model to more dimensions.
Flooding areas and construction works can be incorporated in the model. Modelling of flood plains is done in two different ways. The first technique includes the extension of the river to the flood plains. Cross sections are split up in different parallel parts with their own conveyance. This is important for the correct calculation of the transport capacity. So, a higher roughness is asigned to the flood plains. The water level in the river and in the flood plain is considered as the same. A second possibility connects the river and the storage areas by using weirs. This technique is more accurate because the difference in water level between river and flood plains is modelled. The storage in the flood plains is determined, but the flow profile is not incorporated. This is in contrast with the first technique. An alternative to the 1D modelling is the quasi 2D modelling where the floodplains are described as a network of extra streams and canals. The cross section from these rivers corresponds with the geometry of the actual storage area. Rivers and floodplains are connected by weirs. A distinction is made between storage reservoirs (without stream flow) and floodplains (with stream flow). This quasi 2D technique of modelling and the solution of the Saint Venant equations (full, non-simplified) are close to an optimal way of working. Floodplain modelling using a 1D code is explained more in detail in Chapter 7.

The choice of an accurate code for integrated modelling is determined by the requirements and the expectations of the hydraulic engineer and so starts from the point of view of the surface water. A hydraulic code models discharge (velocity) and water level. Therefore, description of the river geometry, possibilities to describe friction losses (Manning, etc.), lateral inflow, possibilities for steady flow, unsteady flow and flooding, addition of boundary conditions in different forms (discharge, water level, QH relation, etc.) and the possibility to generate results in different sections of the river, has to be included. Further, to come to an integrated model, water quality analysis, sediment transport and interaction with groundwater flow need to be added. This implies that the specific characteristics of ecology and groundwater have to be studied. Groundwater flow is two dimensional flow in a vertical plane, has a timescale in the order of magnitude of 1 hour and a scale of distance in the order of magnitude of 50 m. The ecology part consists of vegetation in the river which uses water and transpirates next to the biomass growth. The flow is two dimensional in a horizontal plane with attention to a spatial distribution of the patches. The time scale is in the order of days (24 hour) and the studied boxes are

smaller.

Boundary conditions are set down based on the available data, but most of the time, discharges are used as an upstream boundary condition and water levels are used as a downstream boundary condition.

3.1.3 Available models

A selection of numerical codes is collected in Table 2.2. Each of them has the possibility to model stream flow. Some of them allow to add groundwater or ecosystem aspects, but most of them operate as a black box and do not allow to add or delete modules. A first code selection is perfomed from the hydraulic point of view, what includes an accurate description of the hydraulics based on the Saint-Venant equations [27]; so simplified equations are not allowed. Further, a one dimensional approach is preferred for several reasons. Firstly, velocity measurements in the lab and in the field are only performed in 1 dimension due to available equipment. Secondly, the study of interactions between groundwater, surface water and the ecological system is rather complex. Therefore, a gradual set-up of a model is preferred and starting in 1 dimension is recommended. Later, extensions to 2 dimensions are advisable [28]. Thirdly, from a hydraulic point of view, longitudinal streamflow is far more important compared to cross-sectional flow.
The possibility to model aspects of water quality can be broad or small and therefore, the mentioned aspect of water quality in Table 2.2 is not limited. The indication of 'water quality' in Table 2.2 only means that some possibilities for water quality modelling are incorporated in the program code.

Model	Description	Name	Reference
Accessus	SVE, no groundwater or water quality	Accessus	[29, 30]
Aquasim	kinematic or diffusive flow, sediment transport, ecological processes	Aquasim	[31, 32]
Branch	SVE, overbank storage, conservative tracer	Branch	[33–35]
CASC2D	2D watershed modelling	CASC2D	[36, 37]
Daflow	diffusion analogy form of the flow equations and unsuitable for reversing flow or backwater situations, accurate in steep channels where there is a unique relation between stage and discharge	Daflow	[38–40]
DHSVM	watershed modelling	Distributed Hydrology Soil Vegetation Model	[41–43]
DYNHYD5	SVE, rectangular geometry, moderate bottom slope, hydrodynamic module of water quality model WASP5	Dynamic Estuary Model Hydrodynamics Program	[44, 45]
FEQ	SVE, complete hydraulic model	Full Equations Model	[46–48]
Fluent	3D, fully equipped	Fluent	[49, 50]
FourPt	SVE, unsteady, one dimensional, open channel flow model	Four-PoinT-implicit finite difference method	[51]
*HEC-RAS (formerly UNET)	SVE, sediment transport, water quality	Hydrologic Engineering Center-River Analysis System	[52, 53]
HSPF	land use, kinematic wave, water quality	Hydrological Simulation Program–Fortran	[54]
Hymos	only used for data management	Hymos	[55]
	continued on next page		

Hysep	discharge analysis	Hydrograph Seperation Program	[56, 57]
INHM	integrate surface and subsurface flow and transport processes	Integrated Hydrology Model	[58–60]
ISGW (HSPF and Modflow)	kinematic wave, surface water and groundwater	Integrated Surface-Groundwater Model	[61, 62]
Kineros	kinematic flow, runoff modelling	Kinematic Runoff and Erosion Model	[21–23]
MIKE 11	SVE, water quality	Mike 11	[63]
Modbranch (Modflow and Branch)	surface- and groundwater interactions, conservative tracer		[64, 65]
Modflow - SURfact 2000	3D, finite difference, saturated groundwater flow		[66, 67]
Modflow / Daflow	surface- and groundwater interactions	Modflow/Daflow	[68]
MODHMS	based on Modflow, watershed modelling		[69, 70]
Mogrow (SimWat and SimGro)	surface water and groundwater	Modelling GROundwater flow and the flow in surface Water systems	[14, 71]
Mohid	1,2,3D, surface water, ground water and water quality modelling, modular, free	Water Modelling System	[72, 73]
PRMS, now MMS	land use, kinematic flow, sediment	Precipitation Runoff Modelling System	[74, 75]
RWQM	integrated water quality model	River Water Quality Model	[76]

continued on next page

Simgro	regional groundwater flow	SIMulation of GROundwater flow and surface water levels	[77, 78]
Simwat	SVE, surface water flow	SIMulation of flow in surface WATer networks	[78, 79]
Swat	river basin scale model to quantify the impact of land management practices in large, complex watersheds	Soil and Water Assessment Tool	[80, 81]
SwatMod (Swat and Modflow)	surface water and ground water	Swat and Modflow	[82, 83]
SWMM	SVE, water quality, sediment transport, urban areas	Storm Water Management Model	[84]
SWRRB	for agricultural use, no flood routing, no water quality	Simulator for Water Resources in Rural Basins-Water Quality	[85, 86]
Telemac	2D- 3D SVE	Telemac	[53, 87, 88]
Thales	watershed modelling	Thales	[24, 25]
TopModel	watershed modelling	TopModel	[18–20]
Topog-Dynamic	kinematic flow, groundwater interaction, chemical transport	Topog-Dynamic	[89, 90]
QUAL2E	only steady state, surface water flow and water quality	Qual 2E	[91]

Table 2.2: Overview of available models, describing the interaction groundwater, surface water and ecosystem

The one model listed in Table 2.2 is more suitable than the other. Some considerations are gathered below. The first criterion for model selection is the possibility of the code to model surface water flow very accurately. Secondly, possibilities to add aspects of water quality or groundwater flow have to be available. The availability of codes (free, commercial packet, etc.) is also taken into account. The remaining codes are studied in more detail and a choice is made.

Models as Fluent, Modhms, Modflow-Surfact, Mike, Aquasim, Telemac, etc. are not free and are not considered as primary options. For example, Mike She represents each of the three main hydrologic processes and their dynamic interaction (surface flow, unsaturated zone flow, and groundwater flow). It is based on the complexity of the governing physical equations, which can, however, be simplified as justified for each hydrologic process, so that the overall computational efficiency of the integrated hydrologic model can be optimized. It utilizes spatial and temporal data easily, and is capable of providing a variety of output types. An advantage of the model is the flexibility in defining boundary conditions and grid resolutions. On the other hand, the model is not free and is useful to model the hydrological cycle rather than hydraulic streamflow.

Accessus [29, 30] is describing surface water flow in detail. Accessus is developed by the Hydraulics Laboratory of Ghent University since 1990. The program describes surface water flow in rivers using the implemented Saint-Venant equations. Equations are solved using the Preissmann discretisation scheme and the Proganka or double sweep solution algorithm. Initial conditions for unsteady state calculations are obtained by performing a steady state calculation. The Manning equation is implemented to calculate the friction. Groundwater flow and quality modules are not included.
Aquasim [31] is a program for data analysis and simulation of aquatic systems. The Saint-Venant equations are included in a simplified version: the kinematic or diffusive approximation. The river section compartment of Aquasim can be used to describe river hydraulics, advective-dispersive transport of substances dissolved or suspended in the water column, exchange of substances between the water column and the sediment, and transformation processes of substances in the water column or the sediment in a river section without abrupt hydraulic controls.
Models as Daflow, Hec-Ras, Branch, and Topmodel are only used for surface water flow and so less appropriate for integrated modelling. All of them are describing 1 dimensional flow, which is the scope of the project.

HSPF and Mike 11 are used for flow and constituent transport [92]. Models as Topog-Dynamic, HSPF, PRMS, SWRBB do not describe surface flow by the full Saint-Venant equations. As all transport and reaction processes studied by the ecological engineer are based on and coupled with the flow, the use of the Saint-Venant equations for 1 dimensional flow is an important criterion in the model choice.

The most important criterion concerns the surface water flow, but also aspects of water quality are important for the integrated model. The QUAL-2E model [91] is a good example of a moderately complex water quality model where advection-dispersion and temperature effects on several water characteristics and contaminants are considered under 1 dimensional steady flow conditions. BLTM (Branched Lagrangian Transport Model) models water quality and needs coupling with Daflow [93, 94]. OTEQ is a 1 dimensional model used to characterize the fate and transport of trace metals in streams and rivers [95] and OTIS (One-dimensional Transport with Inflow and Storage) is a 1-dimensional model used to characterize the fate and transport of water quality constituents in streams and rivers based on the advection-dispersion equation [96]. In these water quality models, the hydraulic modules are rather conceptual and do not describe in detail the flow.

In literature codes, which already couple two of the three considered aspects of integrated modelling, are described. The hydrological ISGW code [97] couples HSPF [54] and Modflow [98, 99]. The main limitation for this code is its implementation of time-stepping, which does not offer the flexibility necessary to simulate the type of rapid precipitation events and runoff. Furthermore, it does not consider unsaturated zone flow rigorously. This is important in arid and semi-arid zone hydrology . This is also the case for the SWATMOD code [100], which also couples an existing code, SWAT, with Modflow [16]. Swatch [101] was developed as a Ph.D. dissertation in a comparatively physically-based approach, but does not have been applied outside this academic environment [16]. Mogrow [14], couples two codes, SimWat and SimGro, to integrate surface and groundwater flow. Other distributed parameter hydrologic codes like TopModel [20], Thales [24], or Kineros [23], adequately handle only some of the hydrologic processes. For example, groundwater is typically handled too simply, where the partial differential equation describing flow is greatly simplified to the point where it is a lumped or conceptual model component [16]. The US Army Corps of Engineers supports development of GMS, SMS, and WMS codes that respectively deal with groundwater, surface water,

and watershed management. These codes do not currently permit the direct coupling of the surface- and groundwater flow modules [16]. Codes mentioned in this paragraph are not retained as they ar more suited for hydrologic and watershed modelling and do not meet the aims of the integration of hydraulic and environmental processes.

Computer models that simulate groundwater and surface water flow are widely used to evaluate and manage ground- and surface water resources. The Modflow model [98, 99] simulates 3 dimensional groundwater flow and includes the effects of many steady state or transient processes, such as areal recharge, rivers, drains, evapotranspiration, and pumpage. Modflow simulates groundwater flow through a three dimensional grid of cells. The models are coupled by adding an exchange between each subreach and a specified groundwater cell. The water exchange for each subreach is computed on the basis of the stream-aquifer head difference, the streambed thickness, stream width, and streambed hydraulic conductivity.
Although other methods of simulating surface-water interaction have been previously incorporated within Modflow [99, 102, 103], Daflow provides a highly stable solution scheme that is simple to run and requires a minimum of field data and calibration.

MMS (Modular Modeling System) is a modelling framework that enables a user to selectively couple the most appropriate process algorithms from applicable models to create an 'optimal' model for the desired application. Where existing algorithms are not appropriate, new algorithms can be developed and easily added to the system. This modular approach to model development and application provides a flexible method for identifying the most appropriate modeling approaches given a specific set of user needs and constraints. The framework includes a pre-process component to input, analyze, and prepare spatial and time-series data for use in model applications, a post-process component to display and analyze model results, and to pass results to management models or other types of software, and a GIS interface for the analysis and manipulation of spatial data. Models that have been incorporated into MMS [104] include PRMS, Topmodel, and RZWQM (Root Zone Water Quality Model). The options for routing flow include a simple Muskingum routing module and Daflow [16].

Due to the limitations of existing codes, the idea of a modelling framework is used in the following to incorporate all surface water, groundwater

and environmental processes in one code including different modules.

3.2 Tested models

Although we were looking for a code applicable to integrated modelling, first, some hydraulic codes are studied. This aspect is rather important and useful as the hydraulic module will be the core of the final code. Therefore, tests were performed with two other models i.e. Hec-Ras and Daflow. The use of these codes supplies useful information for the final model decision.

3.2.1 Hec-Ras

HEC-RAS (Hydrologic Engineering Centers River Analysis System) is designed to perform one-dimensional hydraulic calculations for a full network of natural and constructed channels [105], for steady and unsteady flow as for sediment transport and water quality analysis. The model is used worldwide [15, 52, 53, 106] and has plenty of features. Several calculations in this work are perfomed using the Hec-Ras code. The model is not retained due to the impossibility to write, add or change code.

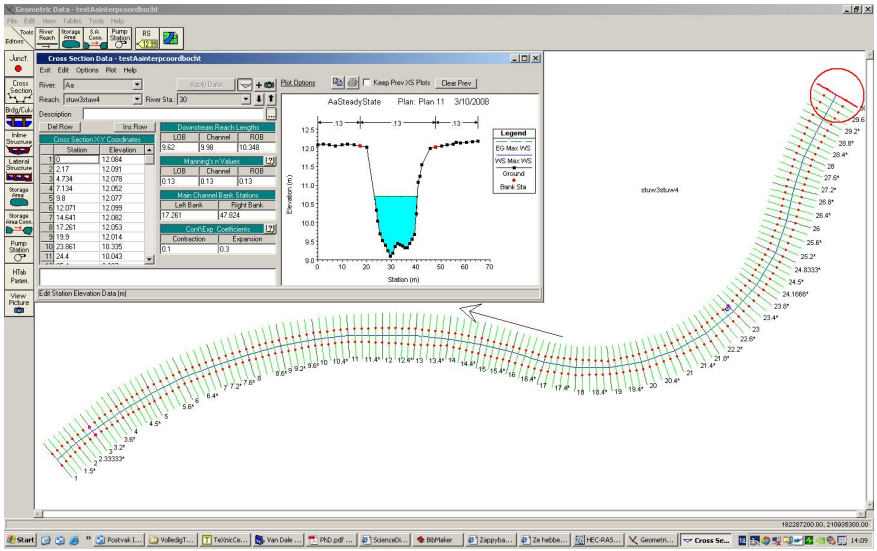

Figure 2.3: Screen shot of the Hec-Ras interface

3.2.2 Daflow

The Daflow model calculates flows through a system of interconnected 1 dimensional channels and subdivides the system into a series of branches, with each branch divided into a number of subreaches. Daflow approximates the flow distribution in a stream as reaches of steady uniform flow separated by transitions of unsteady flow. The Daflow model [38] simulates 1 dimensional flow through a system of interconnected channels by solving the diffusive wave form of the flow equations. The acceleration terms are not included in the equations (Chapter 3), which is acceptable for rivers with small slopes. The model accuracy degrades as the wave diffusion increases relative to advection. It is designed to simulate flow in upland stream systems where flow reversals do not occur and backwater conditions are not severe. If these two conditions are satisfied, Daflow can be applied with reasonable accuracy using minimal field data.

3.3 Final choice: Strive developed in Femme

We present a STream-RIVer-Ecosystem package (STRIVE), that enables the construction of integrated river ecosystems to capture cascade effects and feedbacks, along with their effect on retention. This is performed within the Femme software environment [107].
After exploring a wide range of codes, the environment 'Femme' is selected to develop an integrated numerical model. Some general characteristics are described here. The used equations are given in Chapter 3. The coupling of different subsystems form a methodological challenge.
Subsystems of different complexity can be linked to study the dynamic behaviour of water, dissolved and/or particulate matter. There are core modules for the description of river geometry, hydraulics, transport and reaction of dissolved and particular matter, growth of macrophyte vegetation, etc. developed.

3.3.1 Femme environment

'Femme' or 'a flexible environment for mathematically modelling the environment' is developed by NIOO (Netherlands Institute of Ecology) [107]. 'Femme' is a modelling environment for the development and application of ecological time dependent processes by use of numerical integration in the time of differential equations. The program is written in Fortran.
'Femme' has a library of numerical calculations and model manipulations (such as integration functions, forcing functions, linking to observed data, calibration possibilities, etc.). These technical possibilities allow the user to focus on the scientific part of the model and detailed research of the model

without the confrontation with real program linked problems.
'Femme' is focused on ecosystem modelling, is open source and exists of a modular hierarchical structure (implementation of different models next to each other). What was missing up till now was the implementation of a hydrodynamic surface water model to couple ecology and surface water in each timestep. For the study of the interaction of ecological processes and flow in the river, a realistic modelling of the surface water flow is necessary.

The Strive package has been developed using the 'Femme' environment. A 1D hydrodynamic model for unsteady free surface flow based on the Saint-Venant equations has been implemented, yielding accurate modelling of surface flow characteristics, which subsequently has been coupled to ecological processes to achieve the required interaction between the subsystems of the ecosystem.
A large number of simulations, comparing model results with analytical and numerical results from other models, has been carried out [108].

3.3.2 Modular structure

In a first stage, a water transport model is developed in Femme. This model uses the Saint-Venant equations to describe the surface water flow in rivers. In a multidisciplinair approach of ecosystem studies, also sediment transport, macrophyte growth and suspended solids have to be incorporated. Therefore, using a modular approach in the Femme environment allows to study the interaction of macrophytes, water transport, sediments and suspended solids. Furthermore, different stream models (constant discharge, simplified equations, full Saint-Venant equations, etc.) and varying biomass can easily be incorporated.
The program code is split into several parts as the water transport part (TransWater), the biomass part (Macrophytes) and the part with the general river characteristics (System) (Fig. 2.4). An extra module where the massbalances are checked is added (MassBalances). For each of these modules the specifications of constants, boundary conditions, parameters and variables is performed in separated files, which are brought together in the declaration files. The main menu is bringing the separated parts of the program code together in the parts 'Initialise', 'Initialise2', 'Dynamics' and 'Finalise'.
The implementation of the solution algorithm for the flow equations is explored more in detail in Chapter 3 and Chapter 6.

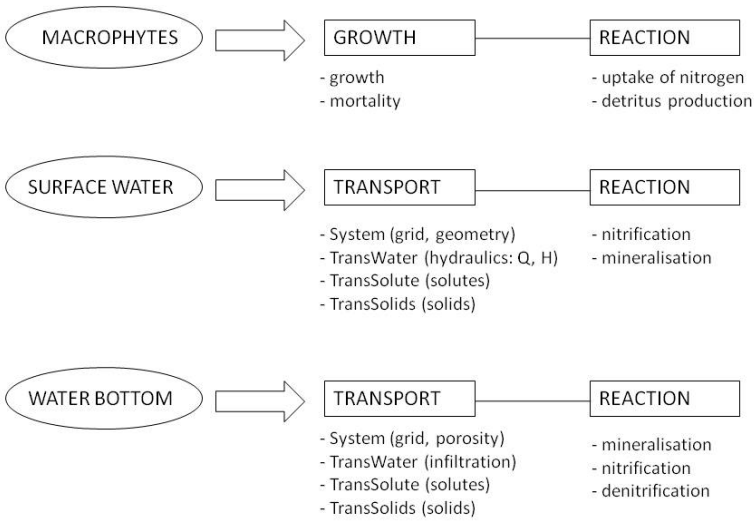

Figure 2.4: Simple flowchart of the Strive package [2]

4 Conclusions

The importance of the interaction of groundwater, surface water and ecosystem is presented and some conditions for the most appropriate model are discussed. The model code should contain a wide range of processes and effects: formulation of geometrical characteristics of the river, description of the hydraulics, the transport of solutes and solids, the macrophyte growth and reaction and possibilities for output representation.

This chapter indicates the most important criteria for integrated modelling. The code has to be widely available. The hydraulic aspect makes up the core of the integrated model and therefore, the full description of 1-dimensional flow by the Saint-Venant equations is necessary. Further, possibilities for adding aspects of water quality and groundwater flow need to be present. Open source characteristics are useful.

An overview of existing models is given and their characteristics are

studied in detail. At the end, the decision about the model used in this study is explained. Although some model codes are good for describing several aspects of integrated modelling, none of them meet requirements for ecosystem modelling. Therefore, a totally new code is developed in an existing environment ('Femme'). The core of the model is the hydraulic flow description, but modules for macrophyte growth, transport of solutes and solids, etc. are added.

References

[1] M.E. McClain, E.W. Boyer, C.L. Dent, S.E. Gergel, N.B. Grimm, P.M. Groffman, S.C. Hart, J.W. Harvey, C.A. Johnston, E. Mayorga, W.H. McDowell, and G. Pinay. *Biogeochemical hot spots and hot moments at the interface of terrestrial and aquatic ecosystems*. Ecosystems, 6:301–312, 2003.

[2] K. Buis, C. Anibas, R. Banasiak, L. De Doncker, N. Desmet, M. Gerard, S. Van Belleghem, Batelaan O., P. Troch, R. Verhoeven, and P. Meire. *A multidisciplinary study on exchange processes in river ecosystems*. In W3M, Wetlands: Monitoring, Modelling, Management, Wierzba, Poland, 2005.

[3] G.F. Fisher, N.B. Grimme, E. Marti, R.M. Holmes, and J.B. Jones. *Material spiraling in stream corridors: a telescoping ecosystem model*. Ecosystems, 1:19–34, 1998.

[4] M.W. Doyle. *Incorporating hydrologic variability into nutrient spiraling*. Journal of Geophysical Research, 110, 2005.

[5] B.J. Peterson, W.M. Wollheim, P.J. Mulholland, J.R. Webster, J.L. Meyer, J.L. Tank, E. Marti, W.B. Bowden, H.M. Valett, A.E. Hershey, W.H. mcDowell, W.K. Dodds, S.K. Hamilton, S. Gregory, and D.D Morall. *Control of nitrogen export from watersheds by headwater streams*. Science, 292:86–90, 2001.

[6] G. Billen, C. Lancelot, and M. Meybeck. *N, P and Si retention along the aquatic continuum from land to ocean*. Ocean Margin Processes in Global Change, pages 19–44, 1991.

[7] T.C.M. Brock. *Waterplanten en waterkwaliteit*. Number 45. Stichting Uitgeverij Koninklijke Nederlandse Natuurhistorische Vereniging, 1988. ISBN 90-5011-014-2.

[8] C. Amoros, J. Gibert, and M.T. Greenwood. *Interactions between units of the fluvial hydrosystem*. Fluvial Hydrosystems, pages 184–210.

[9] K. Buis, C. Anibas, K. Bal, R. Banasiak, L. De Doncker, N. Desmet, M. Gerard, S. Van Belleghem, O. Batelaan, P. Troch, R. Verhoeven, and P. Meire. *Fundamentele studie van uitwisselingsprocessen in rivierecosystemen - gentegreerde modelontwikkeling*. Water, 2007.

[10] F.G. Carollo, V. Ferro, and D. Termini. *Experimental investigation of flow characteristics in vegetated channels.* In River Flow 2006, Portugal, 2006.

[11] S. Schneider, F. Nestmann, and B. Lehmann. *Interaction of vegetation, current and sedimantation*. In River Flow 2006, Portugal, 2006.

[12] F. Smits and K. Hemker. *Koppeling Duflow-Microfem*, 2002.

[13] P.A. Whigham and W.J. Young. *Modelling river and floodplain interactions for ecological response*. Mathematical and Computer Modelling, 33:635–647, 2001.

[14] E.P. Querner. *Description and application of the combined surface and groundwater flow model MOGROW*. Journal of Hydrology, 192:158–188, 1997.

[15] L.B. Rodriguez, P.A. Cello, C.A. Viommet, and D. Goodrich. *Fully conservative coupling of Hec-Ras with Modflow to simulate stream-aquifer interactions in a drainage basin*. Journal of Hydrology, 2008.

[16] *Model code and scenario selection report, site - wide water balance, rocky flats environmental technology site*, 2001. Kaiser-Hill Company.

[17] V. T. Chow, D. R. Maidment, and L. W. Mays. *Applied Hydrology*. McGrawHill, New-York, 1988.

[18] R. Vertessy, E. O'Loughlin, E. Beverly, and T. Butt. *Austrailian experiences with the CSIRO Topog model in land and water resources management.* In Proceedings of UNESCO International Symposium on Water Resources Planning in a Changing World, pages 135–1444, Karlsruhe, Germany, June 1994.

[19] D. Short, W.R. Dawes, and I. White. *The practicability of using Richard's equation for general purpose soil-water dynamics models*. Environment International, 21(5):723–730, 1995.

[20] K.J. Beven and M.J. Kirkby. *A physically based variable contributing area model of basin hydrology*. Hydrology Science Bulletin, 1979.

[21] J.O. Duru and A.T. Hjehnfelt. *Investigating prediction capability of HEC-1 and KINEROS kinematic wave runoff models*. Journal of Hydrology, 157:87–103, 1994.

[22] R.E. Smith and D.C. Goodrich. *Investigating prediction capability of HEC-1 and KINEROS kinematic wave runoff models*. Journal of Hydrology, 179:391–393, 1996.

[23] D.A. Woolhiser, R.E. Smith, and D.C. Goodrich. *KINEROS. Kinematic Runoff and Erosion Model: documentation and user manual*. Technical Report 77, USDA-ARS, 1990.

[24] R.B. Grayson, I.D. Moore, and T.A. McMahon. *Physicallu based hydrologic modelling. A terrain-based model for investigative purposes.* Water Resources Research, 28(10):2639–2658, 1992.

[25] R.B. Grayson, G. Blschl, and I.D. Moore. *Computer models of watershed hydrology*, chapter Distributed parameter hydrologic modelling using vector elevation data: Thales and Tape-C, pages 669–696. Water Resources Publications, Highlands Ranch, 1995.

[26] J.P. Villeneuve, P. Hubert, A. Mailhot, and A.N. Rousseau. *La modlisation hydrologique et la gestion de l'eau/Hydrological modelling and water management*. Revue des sciences de l'eau, pages 19–39, 1998. nspecial.

[27] V. T. Chow. *Open Channel Hydraulics*. McGrawHill, New-York, 1959.

[28] D. Meire, P. Troch, K. Buis, and P. Meire. *Using optical imaging techniques and 2D modelling for studying spatial heterogeneity in vegetated streams and rivers*. Technical report, 2009. Submitted project for FWO funding (Flanders).

[29] P. Cosyn. *Mathematische simulatie van tijgolven op rivieren*. Master's thesis, Ghent University, Faculty of Engineering, 1989.

[30] P. Troch. *Mathematische simulatie van niet-permanente stroming op een waterwegennet*. Master's thesis, Ghent university, 1991.

[31] P. Reichert. *Computer program for the identification and simulation of aquatic systems*. Technical report, Swiss federal Institute for Environmental Science and Technology, 1998. ISBN: 3-906484-16-5.

[32] U. Uehlinger, C. Konig, and P. Reichert. *Variability of photosynthesis-irradiance curves and ecosystem respiration in a small river*. Freshwater Biology, 44:493–507, 2000.

[33] R.W. Schaffranek, R.A. Baltzer, and D.E. Goldberg. *A model for simulation of flow in singular and interconnected channels*. Technical report, U.S. Geological Survey Techniques of Water-Resources Investigations, 1981. Book 7, chap 3, 110p.

[34] R.W. Schaffranek. *Flow model for open-channel reach or network*. Technical report, U.S. Geological Survey Professional Paper 1384, 1987. 12p.

[35] P.A. Conrads and P.A. Smith. *Simulation of water level, streamflow, and mass transport for the Cooper and Wando Rivers near Charleston, South*

Carolina. Technical report, USGS Water - Resources Investigations Report 96-4237, 1996. 51 p.

[36] P.Y. Julien and B. Saghafian. *CASC2D users manual - a two dimensional watershed rainfall-runoff model*. Civil engineering report, Colorado State University, Fort Collins, 1991. CER90-91PYJ-BS-12.

[37] M. Marsik and P. Waylen. *An application of the distributed hydrologic model CASC2D to a tropical montane watershed*. Journal of Hydrology, 330(3-4):481–495, 2006.

[38] H.E. Jobson. *Users manual for an open-channel streamflow model based on the diffusion analogy*. Technical report, U.S. Geological Survey Water-Resources Investigations Report 89-4133. 73p.

[39] H.E. Jobson and A.W. Harbaugh. *Modifications to the diffusion analogy surface-water flow model (DAFLOW) for coupling to the modular finite-difference ground-water flow model (MODFLOW)*. Technical report, U.S. Geological Survey Water-Resources Investigations Report 99-217, 1999. 107p.

[40] J.B. Wiley. *Flow and solute-transport models for the New River in the New River Gorge National River, West Virginia*. Technical report, U.S. Geological Survey Open-File Report 92-65, 1992.

[41] M.S. Wigmosta and S.J. Burges. *An adaptive modeling and monitoring approach to describe the hydrologic behaviour of small catchments*. Journal of Hydrology, 202:48–77, 1997.

[42] M.S. Wigmosta, B. Nijssen, P. Storck, and D.P. Lettenmaier. *Mathematical models of small watershed hydrology and applications*, chapter The distributed hydrology soil vegetation model, pages 7–42. Water Resource Publications, Littleton, 2002.

[43] C.O. Doten and D.P. Lettenmaier. *Prediction of sediment erosion and transport with the distributed hydrology-soil-vegetation model*. Water Resources Series 178, University of Washington, Seattle, 2004.

[44] R.B. Ambrose, T.A. Wool, and J.L. Martin. *The Dynamic Estuary Model Hydrodynamics Program, DYNHYD5, Model documentation and user manual*. Technical report, US Environmental Protection Agency, Environmental Research Lab, Athens, Georgia, 1993.

[45] J.J. Warwick and Heim K.J. *Hydrodynamic modelling of the Carson River and Lahontain Reservoir, Nevada*. Water Resources Bulletin, 31(1):67–77, 1995.

[46] D.D. Franz and C.S. Melching. *Full equations (FEQ) model for the solution of the full dynamic equations of motions for one-dimensional unsteady flow in open channels through control structures*. Technical report, USGS Water-Resources Investigations Report 96-4240, 1996.

[47] M.J. Turner, A.P. Pulokas, and A.L. Ishii. *Implementation and verification of a one-dimensional, unsteady flow-model for Spring Brook near Warrenville, Illinois*. Technical report, U.S. Geological Survey Water-Supply Paper 2455, 1996. 35p.

[48] A.L. Ishii and J.E. Wilder. *Effect of boundary condition selection on unsteady-flow model calibration*. In Proceedings of the XXV Congress of International Association for Hydraulic Research, pages 193–200, 1993. Tokyo.

[49] A.P. Nicholas and G.H.S. Smith. *Numerical simulation of three-dimensional hydraulics in a braided channel*. Hydrological processes, 13(6):913–929, 1999.

[50] P. Kumar, A. Garmory, M. Ketzel, R. Berkowicz, and R. Britter. *Comparative study of measured and modelled number concentrations of nanoparticles in an urban street canyon*. Atmospheric Environment, 43(4):949–958, 2009.

[51] L.L. Delong, D.B. Thompson, and J.K. Lee. *The computer program FOURPT-A model for simulating one-dimensional, unsteady, open channel flow*. Technical report, U.S. Geological Survey Water-Resources Investigations Report 97-4016, 1997.

[52] F. Pappenberger, K. Beven, H. Morrit, and S. Blazkova. *Uncertainty in the calibration of effective roughness parameters in Hec-Ras using inundation and downstream level observations*. Journal of Hydrology, 302(1-4):46–69, 2005.

[53] M.S. Horritt and P.D. Bates. *Evaluation of 1D and 2D numerical models for predicting river flood inundation*. Journal of Hydrology, 268(1-4):87–99, 2002.

[54] B.R. Bicknell, J.C. Imhoff, J.L. Kittle, A.S. Donigian, and R.C. Johanson. *Hydrological Simulation Program-Fortran, User's manual for version 11*. Technical report, Environmental Protection Agency, National Exposure Research Laboratory, Athens, Ga., 1997. EPA/600/R-97/080, 755p.

[55] H.J.M. Ogink and J.I. Crebas. *Hymos - A database-management and processing system for hydrometeorologic data*. In A. Verwey, A.W. Minns, V. Babovic, and C. Maksimovic, editors, Hydroinformatics '94, volume 1-2, pages 97–102, 1994.

[56] R.A. Sloto and M.Y. Crouse. *HYSEP: a computer program for streamflow hydrograph separation and analysis*. US Geological Survey Water-Resources Investigations Report 96-4040, 1996. 46p.

[57] M. Stewart, J. Cimino, and M. Ross. *Calibration of base flow separation methods with streamflow conductivity*. Groundwater, 45(1):17–27, 2007.

[58] K. Loague and J.E. VanderKwaak. *Physics-based hydrologic response simulation: Platinum bridhge, 1958 Edsel, or useful tool*. Hydrologic Processes, 18:2949–2956, 2004.

[59] S. Panday, P.S. Huyakorn, and J.E. VanderKwaak. *Rigorous coupling of surface water and vadose zone flow with Modflow*. In E. Poeter, C. Zheng, and M. Hill, editors, Proceedings Modflow 98, number 2, pages 707–714. Colorado School of Mines, Boulder, 1998.

[60] R.G. McLaren, P.E. Forsyth, E.A. Sudicky, J.E. VanderKwaak, F.W. Schwartz, and J.H. Kessler. *Flow and transport at Yucca Mountain: numerical experiments on fast preferential flow mechanisms*. Journal of Contaminant Hydrology, 43:211–238, 2000.

[61] M. Ross, J. Geurink, A. Said, A. Aly, and P. Tara. *Evapotransporation conceptualization in the HSPF-Modflow integrated models*. Journal of the American Water Resources Association, 41(5):1013–1025, 2005.

[62] J. Cho, V.A. Barone, and S. Mostaghimi. *Simulation of land use impacts on groundwater levels and streamflow in a Virginia watershed*. Agricultural Water Management, 96(1):1–11, 2009.

[63] K. Havno, M.N. Madsen, and J. Dorge. *Mike 11: a generalized river modelling package*. Water Resources Publications, Highlands Ranch, Colorado, 1995.

[64] E.D. Swain. *Incorporating hydraulic structures in an open-channel model*. In Proceedings of the National Hydraulic Engineering Conference, pages 1118–1123, New York, 1992. American Society of Civil Engineers.

[65] E.D. Swain and E.J. Wexler. *A coupled surface-water and groundwater flow model (MODBRNCH) for simulation of stream-aquifer interaction*. Technical report, U.S. Geological Survey Techniques of Water-Resources Investigations, 1996. Book 6, chap A6, 125p.

[66] S. Panday and P.S. Huyakorn. *Modflow Surfact: a stat-o-the-art use of vadose zone flow and transport equations and numerical techniques for environmental evaluations*. Vadose Zone Journal, 7(2):610–631, 2008.

[67] J. Doherty. *Improved calculations for dewatered cells in Modflow*. Ground Water, 39(6):863–869, 2001.

[68] Y.C. Lin and M.A. Medina. *Incorporating transient storage in conjunctive stream-aquifer modelling*. Advances in Water Resources, 26(9):1001–1019, 2003.

[69] A.D. Werner and M.R. Gallagher. *Characterisation of sea-water intrusion in the Pioneer Valley, Australia using hydrochemistry and three-dimensional numerical modelling*. Hydrogeology Journal, 14(8):1452–1469, 2006.

[70] A.D. Werner, M.R. Gallagher, and S.W. Weeks. *Regional-scale, fully coupled modelling of stream-aquifer interaction in a tropical catchment*. Journal of Hydrology, 328(3-4):497–510, 2006.

[71] E.P. Querner. *The combined surface and groundwater flow model Mogrow applied to the Hupselse-beek drainage basis*. In Friend: flow regimes from international experimental and network data, number 221 in IAHS Publications, pages 381–389, Germany, 1994.

[72] A.R. Trancoso, S. Saraiva, L. Fernandes, P. Pina, P. Leitao, and R. Neves. *Modelling macroalgae using a 3D hydrodynamic-ecological model in a shallow, temperate estuary*. Ecological Modelling, 187(2-3):232–246, 2005.

[73] N. Vaz, J.M. Dias, and P.C. Leitao. *Three-dimensional modelling of a tidal channel: The Espinheiro Channel (Portugal)*. In Continental Shelf Research (13th Biennial Conference on the Physics of Estuaries and Coastal Seas), volume 29, pages 29–41, Astoria, 2009.

[74] G.H. Leavesly, R.W. Lichty, B.M. Troutman, and L.G. Saindon. *Precipitation-Runoff Modelling System: user manual*. Technical report, U.S. Geological Survey Water-Resources Investigations Report 83-4238, 1983. 207p.

[75] W.A. Flugel. *Delineating hydrological response units by geographical information system analyses for regional hydrological modelling using PRMS/MMS in drainage basin of the river Brol, Germany*. Hydrological Processes, 9(3/4):423, 1195.

[76] L. Somlyody, M. Henze, L. Koncsos, W. Rauch, P. Reichert, P. Shanahan, and P. Vanrolleghem. *River water quality modelling: III Future of the art*. Water Science and Technology, 38(11):253–260, 1998.

[77] E.P. Querner. *Description of a regional groundwater flow model SIMGRO and some applications*. Agricultural Water Management, 14:209–218, 1988.

[78] E.P. Querner, J.A. Morabito, M. Manzanera, J.A. Pazos, N.C. Ciancaglini, and M. Menenti. *The use of hydrological models in the irrigated areas of Mendoza, Argentina*. Agricultural Water Management, 35:11–28, 1997.

[79] M. Manzanera, E.P. Querner, and N.C. Ciancaglini. *Utilisation of SIMWAT model in an irrigated area of Mensoza, Argentina*. In International Workshop on the Application of Mathematical Modelling for the Improvement of Irrigation Canal Operation, pages 55–65, Montpellier, France, 1992.

[80] Q. Yang, F. Meng, Z. Zhao, T. Chow, G. Benoy, H.W. Rees, and C. Bourque. *Assessing the impacts of flow diversion terraces on stream water and sediment yields at a watershed level using SWAT model*. Agriculture, Ecosystems and Environment, 2009. in press.

[81] J. Schuol and K.C. Abbaspour. *Using monthly weather statistics to generate daily data in a SWAT model application to West Africa*. Ecological Modelling, 201:301–311, 2007.

[82] N.W. Kim, I.M. Chung, Y.S. Won, and J.G. Arnold. *Development and application of the integrated SWAT-MODFLOW model*. Journal of Hydrology, 356:1–16, 2008.

[83] M.A. Sophocleus, J.K. Koelliker, R.S. Govindaraju, T. Birdie, S.R. Ramireddygari, and S.P. Perkins. *Integrated numerical modeling for basin-wide water management: the case of the Rattlesnake Creek basin in south-central Kansas*. Journal of Hydrology, 214:179–186, 1999.

[84] A. Lewis. *Storm Water Management Model user's manual - Version 5.0*. Technical report, Water Supply and Water Resources Divison National Risk Management, U.S. Environmental Protection Agency, Research Laboratory Cincinnati, OH 45268, 2008. EPA/600/R-05/040.

[85] J.G. Arnold and J.R. Williams. *Validation of SWRRB - Simulator for water-resources in rural basins*. Journal of Water Resources Planning and Management, 113(2):243–256, 1987.

[86] N.D. MacAlpine, S.M. Ahmed, R.A. Young, j.G. Arnold, A.J. Sosiak, and D.O. Trew. *Validation of non-point source pollution models for a northern Great Plains lake*. In Water Quality Modelling - Proceedings of the international symposium, volume 95 of *ASAE Publication*, pages 154–163, 1995.

[87] C. Le Normant. *Three-dimensional modelling of cohesive sediment transport in the Loire estuary*. Hydrological Processes, 14(13):2231–2243, 2000.

[88] D.A. Tyrell and K.J. George. *Finite element modelling of the hydrodynamics and water quality of the Patos Lagoon System, Brazil*. Journal of Coastal Research, 3(39):1594–1599, 2006.

[89] S.H. Davis, R.A. Vertessy, and R.P. Silberstein. *The sensitivity of a catchment model to soil hydraulic properties obtained by using different measurement techniques*. Hydrological Processes, 13(5):677–688, 1999.

[90] R.P. Silberstein, R.A. Vertessy, J. Morris, and P.M. Feikema. *Modelling the effects of soil moisture and solute conditions on long-term tree growth and water use: a case study from the Shepparton irrigation area, Australia*. Agricultural Water Management, 39(2-3):283–315, 1999.

[91] T.O. Barnwell and L.C. Brown. *The enhanced stream water quality models QUAL2E and QUAL2E-UNCAS: Documentation and user manual*. Technical report, US environmental Protection Agency, 1987. EPA/600/3-87/007 and EPA/823/B/95/003.

[92] Smic. *Model Matrix*. USGS. Surface water and water quality models information clearinghouse.

[93] H.E. Jobson. *Enhancements to the Branched Lagrangian Transport Modelling System*. Technical report, USGS WRIR 97-4050, 1997.

[94] H.E. Jobson and D.H. Schoellhamer. *Users manual for a Branched Lagrangian Transport Model*. Technical report, USGS-WRIR 87-4163, 1987.

[95] R.L. Runkel. *One dimensional transport with equilibrium chemistry 5OTEQ): a reactive transport model for streams and rivers*. Technical report, U.S. Geological Survey Water-resources Investigation Report, 1999.

[96] R.L. Runkel. *One dimensional transport with inflow and storage (OTIS): a solute transport model for streams and rivers*. Technical report, U.S. Geological Survey Water-Resources Investigation Report 98-4018, 1998. 73 p.

[97] P.R. Davis. *ISGW: The integrated surface water and groundwater model couplinf MODFLOW and HSPF*. In Proceedings from Modflow 98, volume II, pages 715–722, Golden Colorado, 1998.

[98] A.W. Harbaugh and M.G. McDonald. *Programmer's documentation for MODFLOW-96, an update to the U.S. geological Survey modular finite-difference ground-water flow model*. Technical report, U.S. geological Survey, 1996.

[99] M.G. McDonald and A.W. Harbaugh. *A modular three-dimensional finite-difference ground-water flow model*. Technical report, U.S. Geological Survey, 1988. Techniques of Water-Resources Investigations, Book 6.

[100] S.R. Ramireddygari. *A comprehensive integrated computer model for basin-wide water resources managemnet*. PhD thesis, Kansas State University, Kansas, 1998. 221p.

[101] S.A. Alhassoun. *A physically-based distributed hydrologic simulation watershed model (rainfall, runoff, stream-aquifer system)*. PhD thesis, Colorado State University, Fort Collin, Colorado, 1987. 333p.

[102] D.E. Prudic. *Documentation of a computer program to simulate stream-aquifer relations using a modular, finite-difference, ground-water flow model*. Technical report, U.S. Geological Survey, 1989. Open-File Report 88-729.

[103] E. Swain and E. Wexler. *A coupled surface-water and ground-water flow model for simulation of stream-aquifer interaction*. Technical report, U.S. Geological Survey, 1993. Open-File Report 92-138.

[104] G.H. Leavesley, P.J. Restrep, S.L. Markstrom, M. Dixon, and L.G. Stannard. *The Modular Modelling System (MMS)*. Technical report, U.S. Geological Survey open file report 96-151, 1996.

[105] Hydrologic Engineering Center, US Army Corps of Engineers. *HEC-RAS River Analysis System, Version 2.1.4*, 2004. `http:\\www.hec.usace.army.mil`.

[106] G. Schumann, P. Matgen, L. Hoffmann, R. Hostache, F. Pappenberger, and L. Pfister. *Deriving distributed roughness values from satellite radar data for flood inundation modelling*. Journal of Hydrology, 344:96–111, 2007.

[107] K. Soetaert, V. de Clippele, and P. Herman. *Femme: a flexible environment for mathematically modelling the environment*. NIOO: Netherlands Institute of Ecology, 2006.

[108] L. De Doncker, P. Troch, R. Verhoeven, K. Buis, and P. Meire. *Coupled ecosystem-hydrodynamic modelling using Femme*. 2008. In review.

3

Equations of 1D unsteady open channel flow

In this chapter, the equations of 1D unsteady open channel flow are studied in more detail. These equations will make up the core of a hydraulic model. Special attention is paid to the determination of Manning's roughness coefficient as an important parameter.

1 Introduction: flood routing

River hydraulics is characterised by changing discharges and water levels due to rain fall. Studies about this topic have to take into account this non-permanent character of the flow. Over decades, both the accurate prediction of flood magnitude and the capability to manage and minimize the flood risks have become increasingly important goals. Among others, selection of an appropriate wave model for channel network flood routing has been of great interest to researchers and engineers in hydrology and hydraulics. In applications, the river channel is divided into a number of computational reaches and the shallow water wave equations (so called Saint-Venant equations) are applied to each reach. By using an implicit finite difference scheme (so called Preissmann scheme), the equations for all reaches are solved simultaneously [1].

Surface water flow is mathematically seen as the propagation of a wave in a river. Registration of the hydrograph (i.e. the discharge as a function of time) in two different sections of the river shows a time shift of the peak and flattening of the peak due to storage and dissipation of the energy by bottom friction. Time shift and flattening of the peak of the wave are observed by studying waves at two different places in rivers (Figure 3.1). The hydrograph of the wave is shown in section I as well as in the more downstream section II. Flood routing or the calculation of the propagation of waves in a river bed can give information about maximal discharge (design of bridges, channel sections), maximum water level (flooding), determination of the flooded area, etc. [2]).

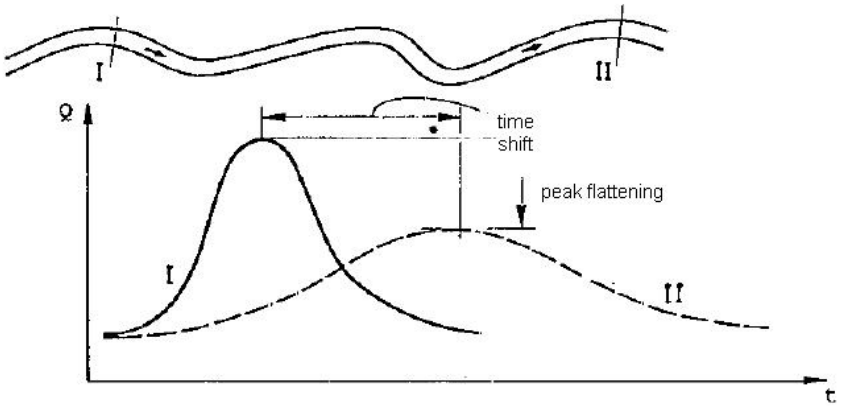

Figure 3.1: Hydrograph in two sections (I and II) of the river, with indication of time shift and peak flattening

2 Saint-Venant equations

This phenomenon, i.e. unsteady flow of surface water, is ususally described using the Saint-Venant equations which include the continuity equation (3.1) and the momentum equation (3.2). These equations are the one dimensional expression (time-averaged and cross-section averaged [3]) of the Navier-Stokes equations. These last equations describe fluid flow in three dimensions [4, 5] and are the base of hydrodynamic modelling. More simplified forms are given by the Bresse-equation (for steady flow) and the Manning equation (for steady and uniform flow). The integral form of the Saint-Venant equations can be found in [5–7]. Here, the differential form is used which assumes that the dependent flow variables (discharge, water

level, waterdepth, etc.) are continuous and differentiable functions.

$$\frac{\partial Q}{\partial x} + B\frac{\partial h}{\partial t} = \quad q \tag{3.1}$$

$$\frac{\partial Q}{\partial t} + \frac{\partial}{\partial x}(\frac{Q^2}{A}) + gA(\frac{\partial h}{\partial x} - S_o + S_f) = \quad qA \tag{3.2}$$

with Q = discharge [m^3/s], B = section width at water surface [m], h = water depth [m], g = gravity acceleration [m/s^2], A = wetted cross section area [m^2], S_0 = tan α = channel bottom slope [m/m] (small, so tan α = sin α, cos α = 1), S_f = friction slope (energy gradient needed to overcome frictional resistance of channel bed and banks in steady flow) [m/m], q = lateral in- or outflow, discharge per unit length, positive for inflow [$m^3/s/m$] ([5]).

The Saint-Venant equations form a system of non-linear partial differential equations (hyperbolic type). An analytical solution of this system is not possible, but the use of numerical models allows a numerical solution. Three types of dynamic models can be used [5–8]. For each of these solution methods, boundary conditions and initial conditions are necessary.

- *Method of characteristics.* The system is changed to a system of 2 differential equations which are valid on the 2 characteristic curves and solved in a rectangular x,t-grid (Fig. 3.2). The method of characteristics discovers curves (called characteristic curves or just characteristics) along which the partial differential equation becomes an ordinary differential equation. Once the ordinary differential equation is found, it can be solved along the characteristic curves and transformed into a solution for the original partial differential equation.

- *Finite difference method.* Finite-difference methods approximate the solutions to differential equations by replacing partial derivative expressions with approximately equivalent finite difference quotients. Derivatives in the partial differential equation are approximated by linear combinations of function values at the grid points. Different methods are used. The implicit scheme of Preissmann is used further in this research. Solutions follow out of the x,t-grid (Fig. 3.2). The solution starts from a well known initial condition at t = 0, taking into account the boundary conditions. Values of discharge and water level are calculated each time step in the x,t grid. The most attractive feature of finite differences is that it can be very easy to implement.

- *Finite element method.* The x,t-surface (Fig. 3.2) is divided into small elements in which the equations are solved. The solution approach is based on rendering the partial differential equation into an approximating system of ordinary differential equations, which are then numerically integrated using standard techniques such as Euler's method, Runge-Kutta, etc. The most attractive feature of this method is its ability to handle complicated geometries (and boundaries) with relative ease.

In the x,t grid (Fig. 3.2), discharge and water level are dependent variables, while distance x and time t are independent variables. Knowing the solutions in two points and calculating the differences Δ t and Δ x, the discharge and water level are calculated in another point, using linear equations. Further, time steps are very small and so the computer time is rather large, intern boundary conditions are difficult to take into account and the x,t-grid (Fig. 3.2) is not regular due to the dependence of Δ t and Δ x of discharge and water level. The raster is smaller if discharge and water level are changing faster and problems occur when the geometry of the channel is only known in a few sections.

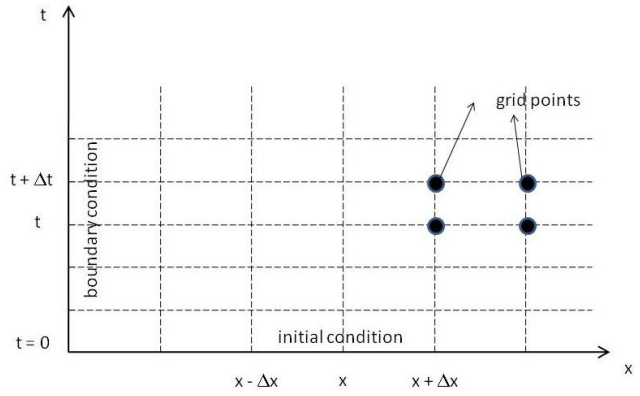

Figure 3.2: x,t grid for solving the differential equations

Implementing the Saint-Venant equations in this study is performed by the implicit scheme of Preissmann. A solution to the resulting system of equations is found by using the double sweep algorithm [5–8].

3 Basic assumptions

The Saint-Venant equations are based upon the following series of assumptions [5]:

- The flow is one-dimensional i.e. the velocity is uniform over the cross section and the water level across the section is horizontal;
- The streamline curvature is small and vertical accelerations are negligible hence the pressure is hydrostatic;
- The effects of boundary friction and turbulence can be accounted for through resistance laws analogous to those used for steady state flow;
- The average channel bed slope is small so that the cosine of the angle it makes with the horizontal may be replaced by unity.

4 Differential form of the Saint-Venant equations

The Saint-Venant equations consist of the continuity equation and the momentum equation [5, 7]. The differential form is used, which is derived by manipulating the integral form or an approximation. The last one is obtained by taking limits as the time and distance intervals approach zero.

Continuity equation The continuity equation is the description of the storage of the water in the different cells: 'the net rate of flow into the volume is equal to the rate of change of storage inside the volume'. There are three terms: (a) convective flow, (b) storage and (c) lateral in- and outflow. The continuity equation is written according 3 different notations.

in Q(x,t) and A(x,t)

$$\frac{\partial Q}{\partial x} + \frac{\partial A}{\partial t} = q \tag{3.3a}$$

in Q(x,t) en z(x,t)

$$\frac{\partial Q}{\partial x} + B\frac{\partial z}{\partial t} = q \tag{3.3b}$$

in Q(x,t) en h(x,t)

$$\frac{\partial Q}{\partial x} + B\frac{\partial h}{\partial t} = q \tag{3.3c}$$

(a) (b) (c)

where z [m] is the water level relative to chart datum.

Momentum equation The momentum equation describes the transport of the water between the neighbouring cells: 'the net rate of momentum entering the volume plus the sum of all external forces (pressure, gravity, friction) acting on the volume is equal to the rate of accumulation of momentum'. The equation has following terms: (a) local acceleration term (change in momentum, due to change in velocity over time), (b) convective acceleration term (change in momentum, due to change in velocity along the channel), (c) gravity force term: proportional to the bed slope S_0, (d) friction force term: proportional to the friction slope S_f, (e) pressure force term: proportional to change in water depth along the channel and (f) lateral inflow. Also the momentum equation is written according 3 different notations.

in Q(x,t) and A(x,t):

$$\frac{\partial Q}{\partial t} + \frac{\partial}{\partial x}(\frac{Q^2}{A}) - gA(S_0 - S_f - \frac{\partial h}{\partial x}) = q\frac{Q}{A} \tag{3.4a}$$

in Q(x,t) and z(x,t):

$$\frac{\partial Q}{\partial t} + \frac{\partial}{\partial x}(\frac{Q^2}{A}) + gA(S_f + \frac{\partial z}{\partial x}) = q\frac{Q}{A} \tag{3.4b}$$

in Q(x,t) and h(x,t):

$$\frac{\partial Q}{\partial t} + \frac{\partial}{\partial x}(\frac{Q^2}{A}) - gA(S_0 - S_f - \frac{\partial h}{\partial x}) = q\frac{Q}{A} \tag{3.4c}$$

(a) (b) (c) (d) (e) (f)

with water level and water depth related as follows:

$$\frac{\partial z}{\partial x} = \frac{\partial h}{\partial x} - S_0 \tag{3.5}$$

Using Manning's formula (cf. infra) as resistance law:

$$V = \frac{1}{n}R^{2/3}S_f^{1/2} \tag{3.6}$$

where V = velocity [m/s], R = hydraulic radius [m] and n = Manning's coefficient [$m^{-1/3}s$]

and introducing the conveyance K [5]:

$$S_f = \frac{Q|Q|}{K^2} \tag{3.7}$$

Eq.(3.6) and (3.7) yield:

$$K^2 = \frac{A^{10/3}}{P^{4/3}n^2} \tag{3.8}$$

$$K = \frac{AR^{(2/3)}}{n} \tag{3.9}$$

with all parameters defined as follows (Fig. 3.4):

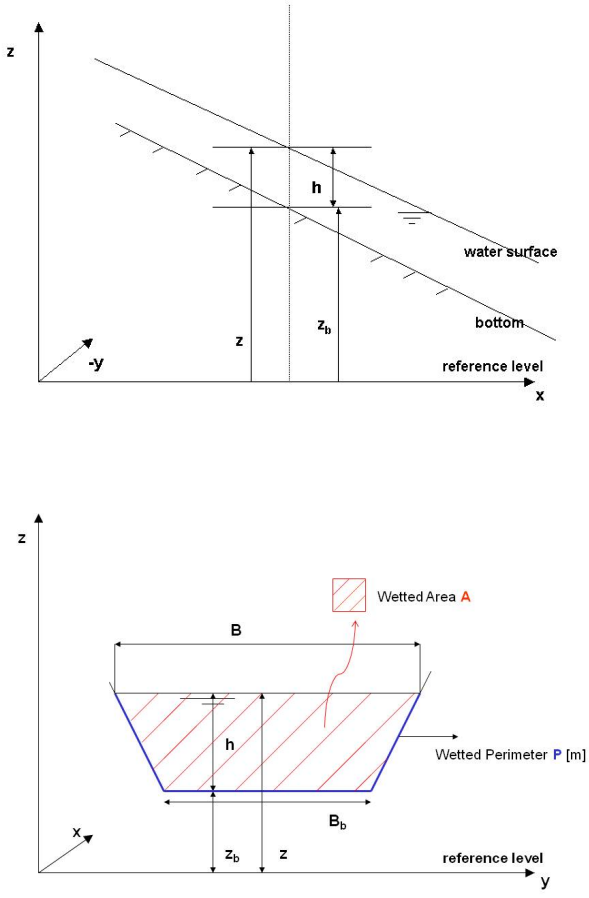

Figure 3.3: Longitudinal section along the channel and cross section of the channel with indication of all parameters

with x,t independent variables for position x and time t, z(x,t) = water level relative to chart datum (or free surface elevation) [m], h(x,t) = water depth (vertical distance between bottom and free surface) [m], z_b(x,t) = bottom level relative to chart datum (or bottom elevation) [m], B(z) = channel width at free surface [m], V(x,t) = Q/A = uniform (cross-sectional) velocity [m/s], K = conveyance factor of the channel [s/m^3]

S_0 and S_f are related to each other. The bottom slope equals:

$$S_0 = -\frac{\partial z_b}{\partial x} \tag{3.10}$$

The friction slope is defined by [9]:

$$S_f = \frac{f}{8g}\frac{V^2}{R} \tag{3.11}$$

with f [-] = friction factor of Darcy-Weisbach.

The water depth:

$$h = z - z_b \tag{3.12}$$

yields:

$$\frac{\partial h}{\partial t} = \frac{\partial z}{\partial t} \tag{3.13}$$

$$\frac{\partial h}{\partial x} = \frac{\partial z}{\partial x} - \frac{\partial z_b}{\partial x} = \frac{\partial z}{\partial x} - S_0 \tag{3.14}$$

The Saint-Venant equations can be simplified in some typical cases: a parabolic model and a kinematic model. These simplifications were often used in the past and can be easily solved. For rivers with a small slope, the acceleration terms ($\frac{\partial Q}{\partial t}$ and $\frac{\partial Q}{\partial x}$) (without (a) and (b) in the momentum equation) are negligible and the equation is known as a parabolic model, which is the convection-diffusion equation. The model describes the attenuation of the wave due to storage and friction. The maximum discharge will decrease and the minimum discharge will increase in the downstream direction, due to the influence of the diffusion parameter. So, the wave will become flatter and wider, because the total amount of water has to be the same.

When also the distance between two sections is short, the peak flattening is negligible ($\frac{\partial Q}{\partial x}$) and the most simplified model is the kinematic model (without (a), (b) and (e) in the momentum equation) which includes only the friction and the translation of the wave. Peak flattening is not incorporated. It assumes that $S_0 = S_f$ and the friction and gravity forces balance each other.

5 Solution of the Saint-Venant equations using the Preissmann scheme and the double sweep algorithm

5.1 Definition sketch

A longitudinal and cross section are presented to indicate notation and references (Fig. 3.4). At the longitudinal section, the bottom level and the water surface level are indicated as well as the bottom slope. The cross section shows the bottom width B_b of the river channel and the width at the water surface B. Further, the water depth and the bank angles are indicated. Bottom level and water level of the river channel are depicted at both sketches.

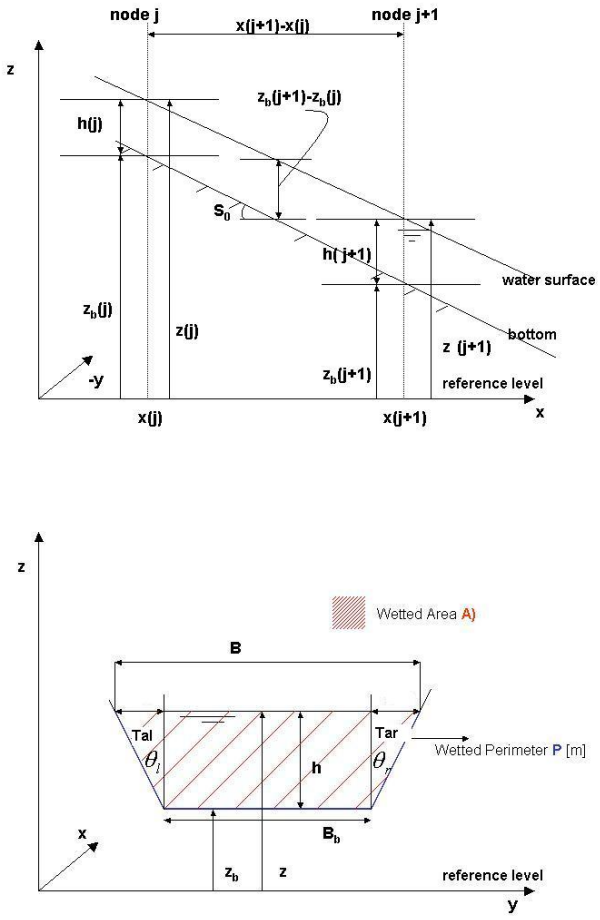

Figure 3.4: Longitudinal section along the channel and cross section of the channel with indication of all parameters

5.2 Numerical solution

The Saint-Venant equations are a set of non-linear differential equations. Discretisation is performed by the implicit scheme of Preissmann where the equations are linearised using a Taylor expansion. Implicit methods deal with the limitations imposed on the time step Δt when using explicit schemes. A numerical solution of the resulting system of linear equations is found by using the double sweep algorithm. Fig. 3.5 depicts the scheme.

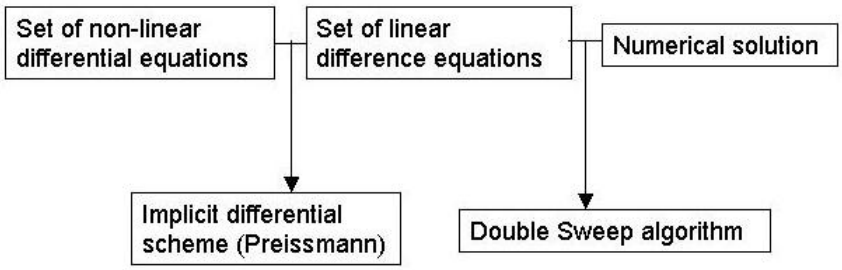

Figure 3.5: Numerical solution of the Saint-Venant equations

5.3 Discretisation of flow equations using Preissmann scheme

The implicit difference scheme of Preissmann proposes expressions between different points in the (x,t) grid to replace the non-linear differential equations. It uses a combination of forward difference quotients on two following columns for t (time) (with weighting coefficient 0.5 and 0.5 for these partial derivatives) and two following rows for x (distance) (weighting coefficient θ and 1- θ for these partial derivatives). The partial derivatives are replaced by finite difference quotients and the coefficients are replaced by weighted averages of the values in the 4 points (Fig. 3.6). The second form of the formulas is based on $f^{n+1} = f^n + \Delta f$ and $f^n = f$.

$$
\begin{aligned}
& f(x,t) \\
& \quad = \theta\frac{1}{2}(f_{j+1}^{n+1} + f_j^{n+1}) + (1-\theta)\frac{1}{2}(f_{j+1}^{n} + f_j^{n}) \\
& \quad = \frac{\theta}{2}(\Delta f_{j+1} + \Delta f_j) + \frac{1}{2}(f_{j+1} + f_j)
\end{aligned}
\tag{3.15}
$$

$$
\begin{aligned}
& \frac{\partial f}{\partial t} \\
& \quad = \frac{1}{2}\frac{1}{\Delta t}(f_{j+1}^{n+1} - f_{j+1}^{n}) + \frac{1}{2}\frac{1}{\Delta t}(f_{j}^{n+1} - f_{j}^{n}) \\
& \quad = \frac{\Delta f_{j+1} + \Delta f_j}{2\Delta t}
\end{aligned}
\tag{3.16}
$$

$$\frac{\partial f}{\partial x} = \theta\frac{1}{\Delta x}(f_{j+1}^{n+1} - f_j^{n+1}) + (1-\theta)\frac{1}{\Delta x}(f_{j+1}^{n} - f_j^{n}) = \frac{f_{j+1} - f_j}{\Delta x} + \theta\frac{\Delta f_{j+1} - \Delta f_j}{\Delta x} \tag{3.17}$$

with weighting coefficient θ:

$$0 < \theta < 1 \tag{3.18}$$

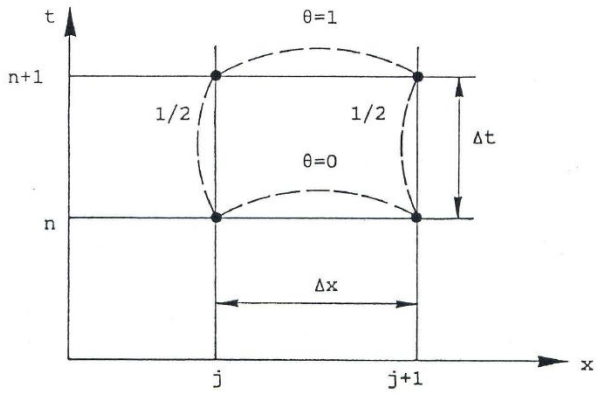

Figure 3.6: Preissmann scheme

Replacing Eq.(3.15) to (3.17) in the Saint-Venant equations in Q and z (Eq.(3.3b) and Eq.(3.4b)) results in two equations in Δz_j, Δz_{j+1}, ΔQ_j and ΔQ_{j+1}. The continuity equation and the momentum equation are then written symbolically as 3.19 and 3.20. The coefficients H_j, I_j, C_j, D_j, G_j and $H_j^{'}$, $I_j^{'}$, $C_j^{'}$, $D_j^{'}$, $G_j^{'}$ are gathered in Appendix A [4, 10, 11].

Continuity equation:

$$H_j\Delta z_{j+1} + I_j\Delta Q_{j+1} = \quad C_j\Delta z_j + D_j\Delta Q_j + G_j \tag{3.19}$$

Momentum equation:

$$H_j^{'}\Delta z_{j+1} + I_j^{'}\Delta Q_{j+1} = \quad C_j^{'}\Delta z_j + D_j^{'}\Delta Q_j + G_j^{'} \tag{3.20}$$

This is a system of 2 equations with four unknown variables (Δ z_j, Δ z_{j+1}, Δ Q_j and Δ Q_{j+1}). Considering N (j = 1,...,N) nodes, this results in 2(N-1) equations for 2N unknown variables. Eq.(3.19) and (3.20) may be written for any pair of computational points (j,j+1). They are not sufficient to find the values of Δz_j, Δz_{j+1}, ΔQ_j and ΔQ_{j+1} because for these four unknowns only two equations are available. But if there are N computational points in the model(j = 1,...,N) one can write 2(N-1) equations for 2N unknowns. As two boundary conditions must be available, there is actually a system of 2(N-1)+2 = 2N algebraic equations for 2N unknowns (Δ Q_j,Δ z_j). Then, this system may be solved for any time step Δt. Therefore, up- and downstream boundary conditions have to be linearised and written as a function of Δ z_1 and Δ Q_1, respectively Δ z_N and Δ Q_N. The result is a system of 2 equations and 2 unknown variables. All equations express relations between the previous (j) and the following node (j+1). Consequently, the double sweep algorithm, which takes into account the upstream and downstream boundary conditions, is used to come to a numerical solution.

5.4 Double Sweep solution algorithm

5.4.1 Basic idea

The Double Sweep algorithm uses the auxiliary variables E_j, F_j, L_j,M_j and N_j for each of the nodes. These variables are mutually connected: E_{j+1}=E(E_j), F_{j+1}=F(E_j,F_j), L_j=L(E_j,F_j), M_j=M(E_j,F_j) and N_j=N(E_j,F_j). These recurrence relationships suggest the method of computing z^{n+1} and Q^{n+1} for all points j = 1,...,N of a given reach.

Fig. 3.7 shows schematically the principle of the double sweep algorithm.

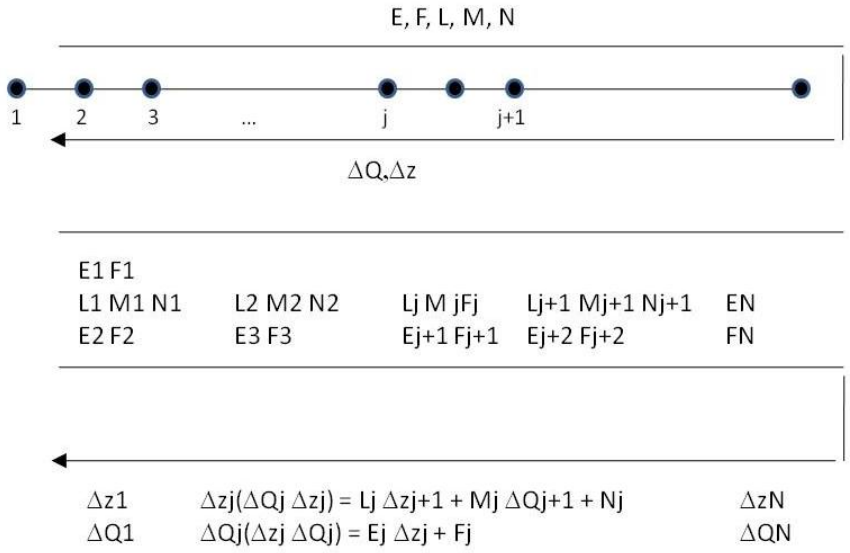

Figure 3.7: Double Sweep Algorithm

The practical meaning of the algoritm is that the number of elementary operations (and consequently the computer time required) necessary to solve the system is proportional to the number of points N.

5.4.2 Solution algorithm for flow equations

Fig. 3.8 depicts the flowchart, which explains the Double Sweep solution method in more detail. Based on the upstream boundary condition, the auxiliary variables E_1, F_1, L_1, M_1 and N_1 are calculated in the upstream node (node 1). In the forward sweep, the auxiliary variables are calculated in nodes 2, 3, ..., N. Based on the result in the downstream node and the downstream boundary condition, discharge and water level are calculated in the downstream node. Consequently, the variables discharge and water level are calculated in the backward sweep in the nodes N-1, N-2,... 1. Eq.(3.26) and Eq.(3.27) are the result of this procedure.

Forward sweep:

In the forward sweep, following helping variables are calculated:

$$L_j = \frac{H_j}{C_j+D_jE_j} \tag{3.21}$$

$$M_j = \frac{I_j}{C_j+D_jE_j} \tag{3.22}$$

$$N_j = -\frac{G_j+D_jF_j}{C_j+D_jE_j} \tag{3.23}$$

$$E_{j+1} = \frac{H_j(C_j^{'}+D_j^{'}E_j)-H_j^{'}(C_j+D_jE_j)}{I_j^{'}(C_j+D_jE_j)-I_j(C_j^{'}+D_j^{'}E_j)} \tag{3.24}$$

$$F_{j+1} = \frac{(G_j^{'}+D_j^{'}F_j)(C_j+D_jE_j)-(G_j+D_jF_j)(C_j^{'}+D_j^{'}E_j)}{I_j^{'}(C_j+D_jE_j)-I_j(C_j^{'}+D_j^{'}E_j)} \tag{3.25}$$

Backward sweep:

The variables z and Q are calculated in the backward sweep:

$$\Delta z_j = L_j\Delta z_{j+1} + M_j\Delta Q_{j+1} + N_j \tag{3.26}$$

$$\Delta Q_j = E_j\Delta z_j + F_j \tag{3.27}$$

Indicated at the Preissmann scheme, the final result of z and Q are calculated according Eq.(3.28) and Eq.(3.29).

$$z_j^{n+1} = z_j^n + \Delta z_j \tag{3.28}$$

$$Q_j^{n+1} = Q_j^n + \Delta Q_j \tag{3.29}$$

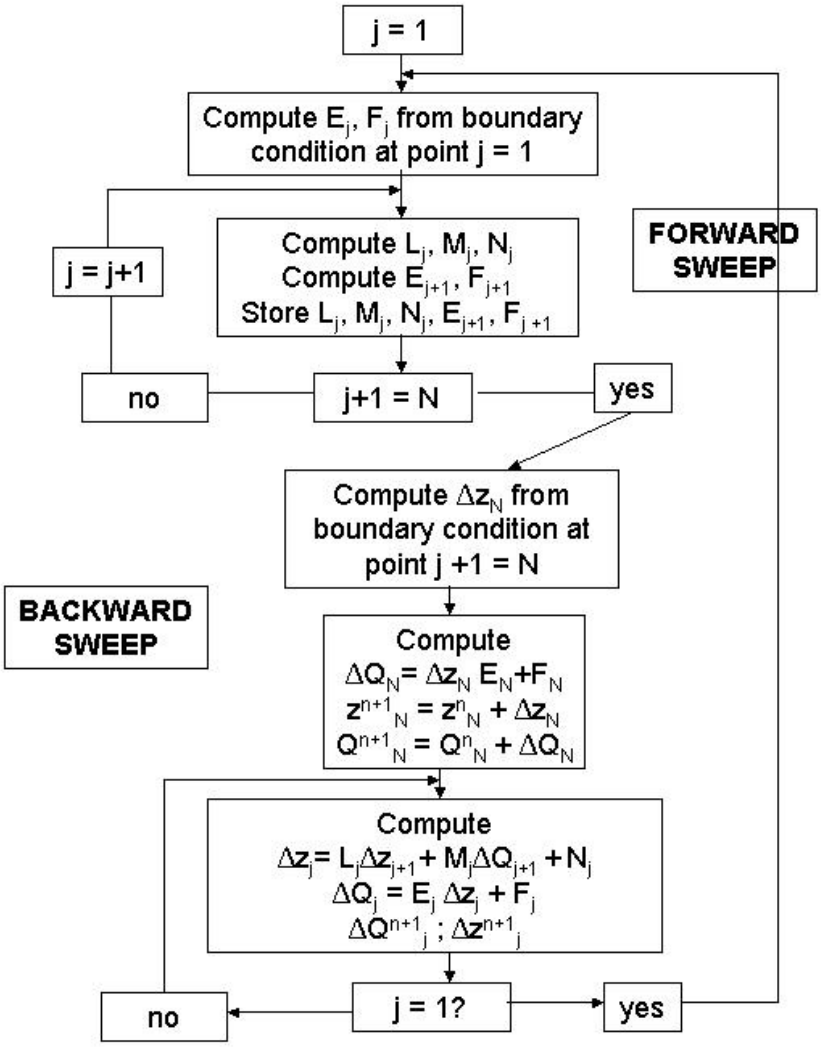

Figure 3.8: Flow chart for the Double Sweep method of solution - Proganka algorithm

5.4.3 Boundary conditions

The boundary conditions, used in the solution algorithm, can occur in different forms. They must be locally linearized. Exterior boundary condi-

tions should furnish either the values of coefficients E_1, F_1 or the value of the water stage increment Δz.

Upstream boundary condition (exterior): Compute E(1), F(1) from boundary condition at point j = 1

- Q1 = Q1(t) is given
  - $E_{(1)}$ = 0.0
  - $F_{(1)}$ = QUpstream - $QUpstream_{oldtimelevel}$
- Z1 = Z1(t) is given
  - $E_{(1)}$ = 1000000.
  - $F_{(1)}$ = -1000000.*(QUpstream - $QUpstream_{oldtimelevel}$)

with 'oldtimelevel', the value in the previous timestep

Downstream boundary condition (exterior): Compute Δ Z(N) from boundary condition at point j+1 = N

- QN = QN(t) is given
  - Δ Q(NumberOfNodes) = QDownstream - $QDownstream_{oldtimelevel}$
  - Δ Z(NumberOfNodes) = ZDownstream - $ZDownstream_{oldtimelevel}$
- ZN = ZN(t) is given
  - Δ Z(NumberOfNodes)
    = 1/E(NumberOfNodes)*(Δ Q(NumberOfNodes)
    - F(NumberOfNodes))
- QN = f(ZN(t))
  Starting from a calculated water level, a corresponding discharge is determined. Indeed, there exists a unique relation between water level above the crest of the weir and the discharge over the weir.
  - Δ Z(NumberOfNodes) = (fzN - Q(NumberOfNodes)
    - F(NumberOfNodes))/(E(NumberOfNodes)- dfdz)

Internal boundary conditions: cf. infra. Tributaries to the river and storage basins linked to the river are examples of interior boundary conditions.

6 Manning's roughness coefficient

6.1 Definition

Using the Saint-Venant equations, it is assumed that the effects of boundary friction are included using resistance laws analoguous to those used for steady flow. The friction of channels is easily linked to the Bresse equation and the expression for the energy slope S_f by the roughness coefficient of Darcy-Weisbach f (Eq.(3.11)).

Plenty of methods are available to describe the roughness value. The roughness coefficient of Darcy-Weisbach is linked to other roughness expressions as the Chézy-formula, the formula of Bazin and the equation of Manning and Strickler [2, 9]. All of them are used in literature. Examples of the use of the Chézy-formula are found in [12, 13], while the roughness according Bazin is provided in [14, 15] . Manning's coefficient as a roughness value is the base of studies in [16–19]. Next to that, also tables and figures with indication of roughness coefficients for rivers of different type and dimensions are available. Manning's coefficient as a roughness coefficient is widely used and has been implemented in the following of this research. Manning's coefficient n is defined as:

$$S_f = \frac{n^2 P^{4/3} Q^2}{A^{10/3}} \tag{3.30}$$

6.2 Determination of Manning's coefficient

In general, hydraulic models for open channel flow are based on the Saint-Venant equations [6]. These equations (continuity equation and momentum equation) are the one dimensional expression (time-averaged and cross-section averaged [3]) of the Navier Stokes equations. These last equations describe fluid flow in three dimensions. By calculation of the discharge and the water levels, the Saint-Venant equations allow for the calibration of the roughness of the channel (expressed by the roughness coefficient or friction factor) by comparing with field data. Here, this roughness is represented by Manning's coefficient n and is calculated from the energy slope.

For steady flow, the momentum equation (Eq.(3.4b)) is simplified and is known as the Bresse equation (Eq.(3.31)).

$$\frac{dh}{ds} = \frac{S_0 - S_f}{\sqrt{(1 - S_0^2) - \frac{Q^2 B}{g A^3}}} \tag{3.31}$$

with Q = discharge [m^3/s], A = wetted cross section [m^2], B = channel width [m], g = gravity [m/s^2], S_f = energy slope [-], S_0 = bottom slope [-], h [m] = water depth, s [m] = distance along the channel.

The Manning coefficient n [$m^{-1/3}s$] is easily linked to the Bresse equation (Eq.(3.31)) and the expression for the energy slope S_f (Eq.(3.32)) by the roughness coefficient of Darcy-Weisbach f [-] (Eq.(3.33)):

$$S_f = \frac{fPQ^2}{8gA^3} \tag{3.32}$$

$$f[-] = 8g\frac{n^2}{R^{1/3}} \tag{3.33}$$

with P = wetted perimeter [m], R = hydraulic radius [m] and n = Manning coefficient [$m^{-1/3}s$].

In steady state conditions and assuming uniform flow, the energy slope is equal to the bottom slope ($S_0 = S_f$) and discharge, water levels and Manning coefficient are linked directly by Manning's equation (Eq.(3.34)) [6]. The roughness coefficient is determined from the measurements of discharge and water levels by (Eq.(3.34)).

Substituting (Eq.(3.33)) in (Eq.(3.32)) yields:

$$n[m^{-1/3}s] = = \frac{S_f^{1/2}A^{5/3}}{QP^{2/3}} \tag{3.34}$$

i.e. the Manning equation.

6.3 Methods for determination of the roughness coefficient

Calculation of Manning's coefficient is difficult. The Manning formula is most used for expressing resistance [2]. Next to the definition, other methods are available to obtain the value of Manning's roughness coefficient. It might be determined by empirical formula, e.g. Cowan [20] who splitted channel resistance into several parts, including the bed material, presence of vegetation in the river, meandering, etc.

$$n = (n_o + n_1 + n_2 + n_3 + n_4)m \tag{3.35}$$

where
n_0 = basic value, for a straight, uniform channel (0.020 - 0.028 $m^{-1/3}s$),
n_1 = irregularities of the bottom (0 - 0.020 $m^{-1/3}s$),
n_2 = variations in the geometry of the channel (0 - 0.015 $m^{-1/3}s$),
n_3 = obstacles (0 - 0.060 $m^{-1/3}s$),
n_4 = vegetation (0.005 - 0.1 $m^{-1/3}s$),
m = correction factor for meandering (1 - 1.3)

Important is to take into account not to double conditions that are already included in another parameter. The equation requires an estimate of separate n factors for different channel conditions. What is missing in this formula is the dependence from Manning's coefficient on the discharge. In the following, this relation is further investigated.

Furthermore, the large variability of the coefficients involved leaves too many degrees of freedom to allow an accurate determination of the roughness coefficient. Another method is to use a set of pictures from literature which represent a comparable situation or to make use of graphs and tables [21]. One can find photographs and descriptive data of typical rivers for which Manning's coefficient is determined in [22], for United States rivers, and [23], for New Zealand rivers. Their main advantage derives from a wider range of bank vegetation types and density and multiple roughness values for each river calculated at different discharges. Using the books demands for a lot of experience in the field and looking for comparable rivers. As this research started from scratch, measurements over the year were carried out to determine the roughness coefficient of the river. Next to these mentioned methods, also formulas to determine the roughness coefficient based on the bed material are published. [24] related the Manning coefficient to hydraulic radius and particle size on the basis of samples from 11 stream channels having bed material ranging from small gravel to medium-sized boulders. Analogous research, based on the characteristic bed material, is carried out by [25].

Channel roughness is influenced by the grain size of the bed material, the surface irregularities of the channel, the channel bed forms (such as ripples and dunes), erosion and deposition characteristics, meandering tendencies, channel obstructions (downed trees, exposed root wads, debris, etc.), geometry changes between channel sections, vegetation along the bankline and in the channel, etc. [21].
One single value of the roughness coefficient has to include all these parameters (cf. Bresse equation, where the roughness is presented as f). Furthermore, as vegetation is strongly dependent on the season, the roughness coefficient can be fairly different for summer and winter conditions.

To determine Manning's roughness coefficient using Eq.(3.34), it is necessary to measure the water surface slope. Calculation of Manning's coefficient is based on the determination of the energy slope S_f. This value is composed of the water surface slope ($\frac{\Delta h}{l}$) and the difference in velocity energy ($\frac{\Delta h_v}{L}$) [18]:

$$S_f = \frac{\Delta h}{l} + \frac{\Delta h_v}{L} \tag{3.36}$$

$$h_v = \alpha \frac{V^2}{2g} \tag{3.37}$$

where Δh [m] is the difference in water surface elevation ; l is the length of channel reach; L is the distance between the first and last cross-section sampled and is potentially shorter than the length of the channel reach; Δh_v [m] is the upstream velocity head minus downstream velocity head; h_v [m] is the velocity head; g [m/s^2] is the gravity acceleration and α is a coefficient and equals 1 according [22]. Most of the time, it is a good idea to determine the water surface slope over a channel reach as long as possible (without special effects etc.) to minimize measurement errors as the slope is equal for the entire reach. Measurements are sometimes performed in a shorter part of the reach.

The kinematic wave approximation [9] assumes that the velocity energy term does not change due to limited velocity and water level changes. Then, the water surface slope equals the energy slope.

In case of an empty river or flume, height differences are so small, that very precise readings are required. Even in the situation with vegetation placed in the flume or found in the river, in which the slope of the water surface is considerably larger than in case of the empty situation, a high accuracy is necessary. Different instruments to measure the water level were investigated. The gauging errors of divers (0.005 m) and mechanical gauges (0.0015 m) were found to be too big, so finally precise measurements for calculating the slope of the water surface were obtained by using a gauge tube with a damper based on the principle of communicating vessels (Fig. 4.22). In order to obtain maximal accuracy, the distance between up- and downstream gauging locations was taken as long as possible. It is clear that the measurement error increases with shorter distance and lower velocities, according the Manning equation.

Accurate measurement of the water level is rather hard and therefore, theoretical procedures are adapted. [26] proposed a method based on the

Reynolds stresses. Measurements are performed in one cross section.

$$S_b = \frac{1}{g}\frac{\partial \overline{u'w'}}{\partial z} \tag{3.38}$$

with S_b [m/m] = water surface slope, u' = u-$\overline{u}$ and w' = w-$\overline{w}$ = turbulence terms with u, w = measured velocity and $\overline{u}$, $\overline{w}$ = average velocity in x and z direction. This formula is only useful over the water depth where the stresses show a linear distribution ($z_1 < z < z_2$, with z_1 and z_2 boundary values of the linear distribution). This linear area is according results in [26]. The slope of the linear line is used in (Eq.3.38).

[3] describes the roughness using the energy losses:

$$S_f = \frac{1}{\gamma A V}\int \tau_{ij}\frac{\partial u_i}{\partial x_j}dA \tag{3.39}$$

with S_f [m/m] = energy slope; γ [N/m^3] = specific density; V [m/s]= velocity, A [m^2] = cross section; τ [N/m^2]= shear stress equally to $\rho\ \overline{u'w'}$ [27]; u_i/x_i determines the velocity profile. The formula may be used for a linear distribution of the shear stresses.

Also, other formulations to determine Manning's coefficient are proposed as the formula of Colebrook White, Thijsse or Reinius (Chapter 5).

As different approaches show great variability of n, they do not guarantee accurate values for the roughness coefficient and a determination of the roughness starting from measurements is recommended.

The importance of the use of a correct value of Manning's coefficient for the river is clearly illustrated by this example, representing the variation of a flood wave along a 25 km long trapezoidal shaped river reach, increasing the roughness coefficient by a factor 2, causes a large reduction of the discharge. While Manning's coefficient of 0.02 m$^{-1/3}$s reduces the peak discharge of the inflow hydrogram after 12 km with 17 %, Manning's coefficient of 0.04 m$^{-1/3}$s reduces the value with 23 %. So, accurate knowledge of Manning's coefficient is necessary to guarantee reliable predictions.

7 Conclusions

Numerical modelling of 1D open channel flow is based on the Saint-Venant equations, which consist of the continuity equation and the momentum equation. This set of non-linear differential equations is converted into a set of linear difference equations using the implicit differential scheme of Preissmann. Consequently, the Double Sweep algorithm is used to come to a numerical solution. Different types of boundary conditions are mentioned in the solution procedure.
An important parameter in the Saint-Venant equations is Manning's roughness coefficient calculated from the energy slope. Different methods and procedures are described in literature to come to the value of Manning's coefficient. As all the different approaches in determining the roughness coefficient show great variability of n, they do not guarantee accurate values. All existing methods are based on particular research in selected rivers or flumes. These values are only indicative and not simply transferable to other measurement set ups or rivers. Therefore, it is recommended to determine the roughness starting from measurements. For steady state conditions and assuming uniform flow, the roughness coefficient in the Saint-Venant equations is described using the Manning equation.

References

[1] C.W. Tsai. *Applicability of kinematic, noninertia, and quasi-steady dynamic wave models to unsteady flow routing*, volume 129. Journal of Hydraulic Engineering, 2003.

[2] V. T. Chow. *Open Channel Hydraulics*. McGrawHill, New-York, 1959.

[3] B. Yen. *Open channel flow equations revisited*. Journal of the Engineering Mechanics Division, 99(5):979–1009, 1973.

[4] K. Mahmood and V. Yevjevich. *Unsteady flow in open channels*, volume 1. 1975.

[5] J.A. Cunge, F.M. Holly, and A. Verwey. *Practical aspects of computational river hydraulics*. Pitman Advanced Publishing Program, 1980.

[6] V. T. Chow, D. R. Maidment, and L. W. Mays. *Applied Hydrology*. McGrawHill, New-York, 1988.

[7] K. Mahmood and V. Yevjevich, editors. *Unsteady flow in open channels*, volume 1. Water Resources Publications, 1975.

[8] R. Verhoeven, R. Banasiak, D. Swiatek, J. Chormanski, and T. Okruszko. *Surface water modeling of the Biebrza River network*. In River Flow '04, number ISBN 90-5809-688-2, pages 1057–1064, Italy, Naples, June 2002.

[9] J. Berlamont. *Theorie van de verhanglijnen*. L. Wouters, 6 edition, 2004.

[10] P. Troch. *Mathematische simulatie van niet-permanente stroming op een waterwegennet*. Master's thesis, Ghent university, 1991.

[11] P. Cosyn. *Mathematische simulatie van tijgolven op rivieren*. Master's thesis, Ghent University, Faculty of Engineering, 1989.

[12] S.S. Medvedev, V.N. Utesinov, and O.M. Churmayev. *Formulation and solution of the problem of determining erosion and deposition in open channels for loose soils*. Journal of Applied Mathematics and Mechanics, 69:585–592, 2005.

[13] E.Y. Kra and G.P. Merkley. *Mathematical modeling of open channel velocity profiles for float method calibration*. Agricultural Water management, 70:229–244, 2004.

[14] G. Corriga, S. Sanna, and G. Usai. *Frequency response and dynamic behaviour of canal networks with self-levelling gates*. Applied Mathematical Modelling, 4(2):125–129, 1980.

[15] H. Chanson. *Environmental Hydraulics of open channel flows*. Elsevier, 2004. ISBN 07506 6165 8.

[16] A. Ghaffar. *Determination of Manning's flow resistance coefficient for rivers in Malaysia.* In Rivers '04, 2004. First International Conference on managing rivers in the 21st Century: Issues and Challenges.

[17] C.A.M.E. Wilson. *Flow resistance models for flexible submerged vegetation*. Journal of Hydrology, 342:213–222, 2007.

[18] J.C. Green. *Effect of macrophyte spatial variability on channel resistance*. Advances in Water Resources, (65):232–243, 2005.

[19] F. Pappenberger, K. Beven, H. Morrit, and S. Blazkova. *Uncertainty in the calibration of effective roughness parameters in Hec-Ras using inundation and downstream level observations*. Journal of Hydrology, 302(1-4):46–69, 2005.

[20] W.L. Cowan. *Estimating hydraulic roughness coefficients*. Agricultural Engineering, 37(7):473–475, 1956.

[21] G. Dyhouse, J. Hatchett, and J. Benn. *Floodplain Modeling using Hec-Ras*. Haestad Methods Inc., 2003. ISBN 0-9714141-0-6.

[22] H.H. Barnes. *Roughness Characteristics of Natural Channels*. Technical report, USGS Water Supply Paper, 1967.

[23] D.M. Hicks and P.D. Mason. *Roughness characteristics of New Zealand Rivers*. Water Resources Publications, 1998. ISBN 0-477-02608-7.

[24] J.T. Limerinos. *Determination of the Manning Coefficient from Measured Bed Roughness in Natural Channels.* Technical report, USGS Water Supply Paper 1898-B, 1970.

[25] A. Strickler. *Beiträge zur Frage der Geschwindigkeits formel und der Rauhigkeitszahlen für Ströme, Kanale und geschlossene Leitungen (Some contributions to the problems of a velocity formula and roughness coefficients for rivers, canals, and closed conduits).* Technical report, Mitteilungen des Eidgenössischen Amtes für Wasserwirtschaft No. 16, Bern, Switzerland. (as cited in Chow, 1959), 1923.

[26] M. Ghisalberti and H. Nepf. *The limited growth of vegetated shear layers*. Water Resources Research, 40(W07502), 2004.

[27] I. Nezu. *Open-channel flow turbulence and its research prospect in the 21st century*. Journal of Hydraulic Engineering, 131(4):229–246, 2005.

4

Laboratory and field data collection

In chapter 4, hydraulic measurements performed in a laboratory flume as well as in the field are described. The measurement instruments and their calibration and accuracy, are discussed. In the flume, some measurement techniques are tested in controlled conditions and the velocity profiles in the flume are studied. In the field, the measurement results are presented together with specific attention to continuous measurements and registration of flood waves. The method used to collect vegetation from the river is also explained.

1 Hydraulic measurements

Hydraulic measurements are necessary to calibrate numerical models and to collect information about the situation under field and laboratory conditions. The accuracy of the measurements depends on several factors. The better the quality of the discharge measurements, the more reliable determination of the roughness coefficient is possible, leading to an improved accuracy of hydraulic modelling.
Laboratory research is carried out to evaluate the accuracy of different techniques and methods under well controlled conditions. Field measurements are performed to evaluate the impact of natural conditions on the accuracy of the measurements.

Several measurement techniques and instruments (as hydrometric propellers and electromagnetic devices) are discussed. Further, the possibility of continuous measurements is investigated, next to the influence of macrophytes on discharge measurement in vegetated rivers and the influence of vegetation on velocity profiles. Therefore, biomass measurements are studied more in detail.

1.1 Introduction

A numerical model, describing the exchange processes between surface water, groundwater and vegetation, needs calibration data to provide accurate results and to allow conclusions about interaction processes in the study area of a vegetated river. As water flow is the driving force of most of these processes, accurate information on discharges and velocities is of major importance. In the research field of environmental engineering, hydraulic measurements are carried out on a regular base.

For that purpose, measurements of surface water flow have to be carried out. Chow [1], ISO [2] and Hershy [3] describe classical flow velocity measurements with a propeller current meter. More advanced techniques use electromagnetic devices. Stone [4] tested ADCP, as a potential alternative to traditional point-velocity measurements in natural streams, against ADV and Price current meter to data accuracy, velocities and required sampling time. Ward and Tepper [5], demonstrated the possibilities of the use of the Doppler technology for velocity measurements. Chow [1] also mentions the use of gauges to measure the water level.

Although, over the years, advantages and disadvantages of the traditional techniques have been encountered, they all have demonstrated their value, both in the lab and in the field. To avoid the disadvantages, Bass [6] presents the constant temperature anemometry (CTA) systems. The device comprises three main parts. The temperature probe allows continuous monitoring of the water temperature. Five velocity probes consist of a hot-wire film encased within a resin attached to a tin steel rod. The hot-wire film records voltages, a conversion to velocities is provided. This system can be used in vegetation without disturbing the environmental conditions. A high sampling frequency is possible, so that variations in velocity can be registered.

Fenton [7] presents some applications of mathematical and computational methods to the practice of flow measurement, resulting in more accurate and possibly simpler hydrographic procedures, whereas Thomas [8] discusses the benefits and practical advantages in introducing a standards programme in the field of open channel flow measurement.

Voet [9] indicates the limitations of measurement instruments. Continuous registration demands for the possibility to measure a wide variation of water depth or water velocity. While carrying out continuous measurements, the results have to be checked to eliminate deviations due to different disturbing influences such as obstacles in the river.

Discharges are easily computed by integration of the measured velocities over the cross section [3]. In general, it is normal practice to establish a relationship (rating curve) between the stage at a particular gauging station and the discharge. Most of the time, discharges are calculated out of registered water levels using a QH-curve. A QH-curve is determined by measurements of discharge and water level, the relation between these parameters is based on a polynomial function determined by the use of the least square method. From observation of the stage, the discharge can be calculated. However, for unsteady flow, rating curves are not always single valued [10]. Velocity measurements, which are carried out with the most care and precision, can add accuracy to this curve. Problems are detected for small rivers where the manual discharge measurements have to be carried out fast due to the short reaction time of the system. Further more, for heavy rainfall, a constant discharge during the measurements is not realistic. Increase and decrease of water levels occur very fast [11]. Determination of the discharge of a river by direct measurement is laborious and time consuming and cannot be used directly for daily information. It may not always be possible to carry out direct measurements of discharge or its computation through the measurement of velocity in a large number of locations at the cross section, because this is expensive and the site may be remote and inaccessible. Therefore, Rahimpour [12] presents a single-point method of velocity measurement in order to estimate the discharge. Further, discharge calculation may be based on tracer measurements and on a calibrated-weir formula. The last method counters the difficulties with the measurements which are not performed in a continuous way. Unlike discharge measurements, stage measurements are relatively easy to automate, therefore, it is measured continuously.

Field measurements are difficult to perform due to the continuously changing conditions. As a consequence, repetition of a test is not possible. Accuracy of the measurements is therefore a responsibility of the operator.

In order to upgrade the overall quality of the measurements, 'International Standards' describing correct measuring techniques have been elaborated. ISO748 consists of the description of *'Velocity-Area methods'* for the measurement of open channel flow, while ISO2537 has to be used for propeller measurements in open channels, ISO6416 for the use of acoustic measurement instruments and ISO15768 for the electromagnetic devices.

1.2 Importance of measurements

Hydraulic measurements are carried out in a laboratory flume (Hydraulics Lab, Ghent University) to check the accuracy of the measurement instruments and to study the influence of vegetation on stream flow. Hydraulic and biomass data collection (cf. infra) in the river Aa and Bierbza river (cf. chapter 1) is performed for studying measurement results under different conditions (e.g. vegetational influence). Accurate measured data are essential for calibration and validation of a hydraulic model.

2 Measuring material and methods

2.1 Introduction

Three different methods to measure the discharge are applied and compared. The methods are meant for discharge measuring in the field, but can also be used for measurements in a flume. Firstly, methods making use of velocity measurements are used. The techniques used are hydrometric propellers, electromagnetic devices and a Doppler instrument. Secondly, the calibration formula of the downstream weir, obtained from a laboratory model study is used. Thirdly, attention is paid to tracer measurements. The first and second technique are used in the river Aa. For the third method, the University of Antwerp performed measurements in the river Aa, but on a smaller scale and to test dilution methods, experiments in a smaller river are also performed by Ghent University. The study of the results of both tracer measurement techniques are no part of this research.
Different measurement techniques are suitable for different goals. On the one hand, calibrated weirs are necessary for long term registration and deliver information for longer periods. A continuous registration of the water level and the position of the flap of the weir allows for a continuous calculation of the discharge. The set up of mass balances in river reaches, on the other hand, is important on a shorter term and needs discrete measurements.
The techniques presented here are classified into two groups: the 'global' measurements and the 'local' measurements. As an example, (chemical) tracer measurements are part of the first group. Here, an average velocity over a certain distance is measured. The other techniques mentioned are based on the local measurement of the velocity in each point of a grid over the cross section and on integration of these velocities over the section.
Discontinuous measurements with the other techniques only deliver good results if the discharge is constant during the measurement period.

Next to velocity and discharge data, also water levels are measured

using a levelled gauge. The limnimetric data set acquired by HIC (Hydrologisch Informatie Centrum, Hydrologic Information Centre, Borgerhout) mentioned further is discussed and compared to the Ghent Hydraulics Laboratory measurements.

2.2 Methods making use of velocity measurements

2.2.1 In general

Knowing the dimensions of the river section and the measured velocities, the flow is calculated using the principal of integration of the velocities over the cross section (4.1) [1]:

$$Q = \sum_{i=1}^{m} \sum_{j=1}^{n} V_{ij} \Delta A_{ij} \tag{4.1}$$

with Q = discharge in river section [m^3/s], V_{ij} = local water velocity [m/s], Δ A_{ij} = part of the wetted cross section A to which V_{ij} is attributed [m^2].

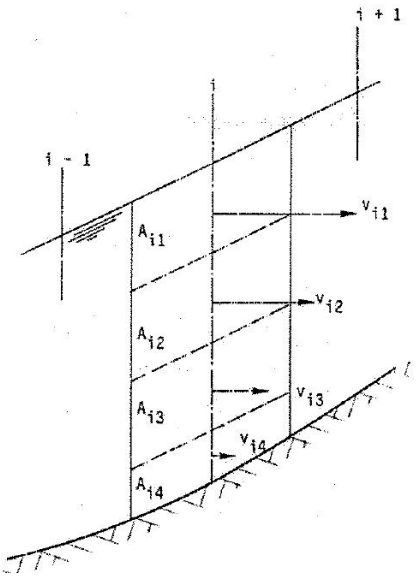

Figure 4.1: Integration of the velocity field over the cross section for the determination of the discharge

The section is divided into several (m) vertical parts. For each of these vertical parts, the velocity of the water is measured on different (n) depths, so that the velocity profile is known over the entire water depth. The result of the measurements is an overview of velocities over the section. Integration of the values over the wetted area yields the discharge, from which the spatially averaged velocity over the cross section is calculated by dividing the discharge by the wetted cross section area.
In general, a limited number (1 or 2) of measurements on each vertical are carried out according standards, supposing a Prandtl Von Karman velocity profile. However, this profile is not seen in vegetated rivers [13], so more intensive gauging in a larger number of measurement points per vertical is needed.
Good performance of the measurements with electromagnetic and acoustic devices is prescribed by the 'International Standards Organisation' [2]. For measurement of liquid flows in open channels, ISO 2537 reports the use of hydrometric propellers. ISO 9213 describes the electromagnetic method and ISO 6416 the ultrasonic or acoustic method. Doppler devices are discussed in ISO/TS 24154.

2.2.2 Hydrometric propellers

First, flow measurements have been carried out using hydrometric propellers (Type: OTT, C31 Universal Current Meter, Fig. 4.2). This instrument is designed for flow metering in combination with a cable suspended from a bridge or boat. The rotation rate of the calibrated propeller is proportional to the water velocity. The velocity is determined by registration of the time period over a pre-selected number of propeller revolutions with a counter unit. Knowing the dimensions of the river channel and the measured velocities, the flow is calculated using Eq.(4.1). The simple visual and acoustic verification of the correct functioning of this equipment is an advantage. Indeed, each rotation of the propeller is visible and indicated by a signal. On the other hand, the instrument interferes with vegetation in rivers, which disturbs the measurements.

Figure 4.2: Hydrometric propeller for measuring velocities: OTT [14]

2.2.3 Electromagnetic devices

Further, an electromagnetic instrument (Type: OTT, Nautilus C2000/SENSA Z300 and Valeport, Type 801, Fig. 4.3) is used. The advantage of this device is that it can be used in vegetated rivers. There are no moving parts which can interfere with the macrophytes, the device is wear-resistant and maintenance-free. The reach of measurements is preferably between 0.0 m/s and 2.5 m/s. The instrument can be used in shallow water. The measurements are independent of any parameters, such as temperature, suspended sediment concentration and salinity. As there is no visual or any other control of the reliable functioning of the instrument during the measurements, regular verification by calibration is advised.

The electromagnetic flow meter is based on Faraday's Law that a conductor (water) moving in a magnetic field, produced by a coil in the sensor, produces a voltage. This voltage is perpendicular to the movement of the conductor and perpendicular to the direction of the magnetic field. The voltage is proportional to the velocity of the water. The sampling volume is measured above the surface of the sensor (OTT), or is a sphere around the body of the sensor (Valeport) of approximately 120 mm diameter. For the flat sensor (Valeport), the sampling volume is a small cylinder whose height extends 10 mm above the surface of the sensor.

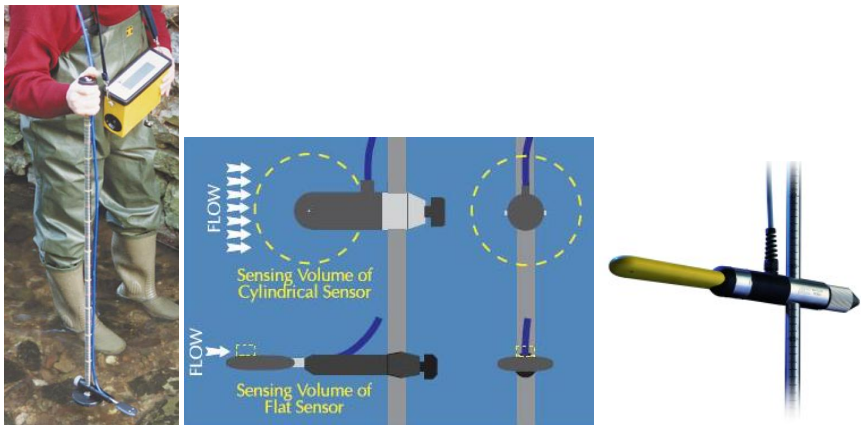

Figure 4.3: Electromagnetic device for measuring velocities: Valeport [15] (left) and OTT [14] (right) and the working principle (middle)

2.2.4 ADV

The Nortek ADV [16] (Fig. 4.4) is an accurate solution fo 3 axis velocity measurements in the laboratory flume. The ADV uses Doppler technique to measure flow in a remote sampling volume. The measured flow is practically undisturbed by the presence of the probe. Data are available at an output rate of 25 Hz and the velocity range is 2.5 m/s. The acoustic sensor consits of one transmit transducer and three receive transducers. The receive transducers are mounted on short arms around the transmit transducer. The acoustic beams are oriented so that the receive beams intercept the transmit beam at a point located at 5 cm below the sensor. The interception of these four beams, together with the width of the transmit pulse, define the sampling volume. This volume is 3, 6 or 9 mm long and approximately 6 mm in diameter. The minimum water depth for measuring is 0.06 m while the maximum water depth is 30 m. The sampling volume stays 0.005 m from the boundary.
The ADV is used for measurements in the laboratory flume. Experiments in the flume without vegetation and in the flume with floating plants are performed (cf. chapter 4, chapter 5). Measurements are performed in a sampling volume of 6 mm height with a sample frequancy of 25 Hz and a nominal velocity of 0.10 to 0.30 m/s.

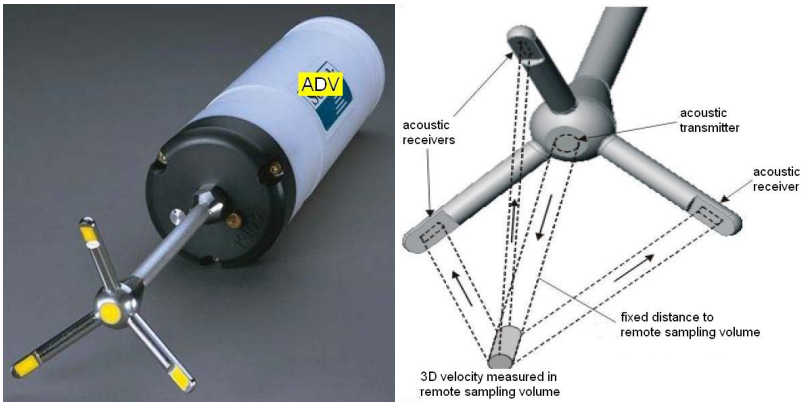

Figure 4.4: Acoustic Doppler Velocitimeter [16]

2.2.5 ADCP

Thirdly, the Streampro ADCP (Acoustic Doppler Current Profiler) is used to measure the velocities. This instrument is applied for shallow water (max. 2 m) discharge measurement. Doppler technology is used to measure the vertical velocity profile and the depth in a chosen number of sections across the river. The device is pulled over the cross section with a constant velocity perpendicular to the flow. The velocity of the water is measured on 'every' point of the cross section, i.e. the slower the movement of the device, the more verticals can be sampled. Next, the value of the velocity is measured over the entire water depth, at different distances from the bottom. As a result, a vertical surface of velocities in the cross section is composed. This faster measurement method allows more measurements and more data collection. Velocity and depth information are combined to estimate the discharge. Internally, sensors to register the movement of the ADCP are incorporated. This information is used to correct the measured flow velocities with the instrument movement. Due to the risk of false reflections, measurements start and end at 1 m from the river banks. Presence of vegetation or other obstructions will show these influences on the results in the area where the obstruction is found. When vegetation affects the transducers, no results are obtained. Only illustrative, an example of discharge results (14th April 05) obtained by the ADCP is shown in Fig. 4.5. It is a cross-section near weir 4 of the studied reach of the river Aa where the vegetation was removed before the measurement. Discharge values vary between 0 and 0.8 m^3/s. The results give good indication of the total discharge in the cross-section and the bottom profile, but control of local values is necessary.

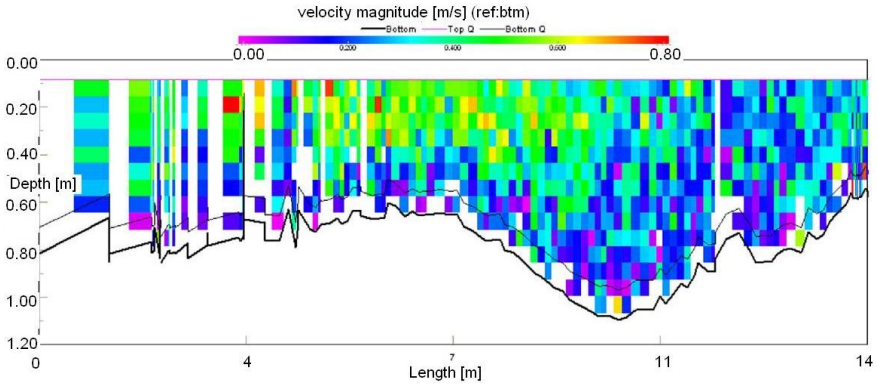

Figure 4.5: Illustrative ADCP results in a cross-section at the river Aa upstream weir 4

2.3 Methods making use of a calibrated weir

The calibration formula, for different positions of the downstream weir in the measurement reach of the river Aa, mentioned above, was determined in 1995 by the Hydraulics Laboratory (UGent) [17], using a scale model (scale: 1/5) of the weir in the lab. The results of this calibration are presented in Appendix 4.

After obtaining the calibration formula for the downstream weir, the discharge is calculated as a function of the upstream water level h_{opw}, the flap crest level h_{kr} and the weir angle according Eq.(D.1) and (D.2).

For this study, the discharge calculated using the calibration formula is used as a value of comparison for the discharge measured downstream making use of the methods discussed in the previous paragraph.

Figure 4.6: Weir downstream (view downstream (left) and upstream (right) direction)

2.4 Tracer methods

The discharge is determined based on conductivity measurements. An advection-dispersion-reaction model of the river can be developed to determine the discharge in the river [18, 19]. Therefore, in- and output signals of the tracers in the river are used. If the water volume of the river system between the gauging sections is known and the time the signal needs to move from upstream to downstream is registered, the discharge can be estimated:

$$Q = \frac{V_{Sys}}{Traveltime} \tag{4.2}$$

with V_{Sys} [m^3] = total volume in the river system and Traveltime [s] = time the water in the river needs to travel from upstream to downstream.

In the most ideal case, the output signal is exactly the same as the input signal, with a time delay between both of them. However, in realistic river systems, the input and output signal will differ. A possible reason for that is the uncertainty on the sensor (accuracy of 1 % of the reading, use of Hydrolab DS3 and YSI 600XLM probes). Further, dispersion in the river will occur: the wave peak of the input signal will be lower and more dispersed. In the numerical model, it is advised to limit the box length to avoid as much as possible the numerical dispersion aspect. A third possibility is the occurence of dilution in the reach. This dilution is due to lateral inflow on the one hand and groundwater in-and outflow on the other hand. The conductivity of these incoming discharges is important to estimate the signal change from upstream to downstream.
The total volume in the river system is determined by measuring water levels in the river and using the knowledge of the bathymetry of the river.

2.4.1 Measuring electrical conductivity and related parameters

Concentration of tracers is measured by the electrical conductivity, which is related to the streamflow. The more ionisation of the tracer, the more conductivity [μS/cm] and the higher the velocity. For the range of the measurements, conductivity and concentration are linear related.
Conductivity measurements are carried out by the University of Antwerp [UA, Ecosystem Management Research Group], partner in the project. Analysis is performed in [20], headpoints are mentionned below. Upstream and downstream the river reach basic water quality characteristics were permanently monitored and water samples were taken at regular time intervals over a 48 h period. The monitored parameters are water tempera-

ture (°C), electric conductivity (μS/cm), pH and dissolved oxygen (mg/l, % saturation). For these parameters measurements were automatically recorded at 5 min intervals by multiparameter monitoring instruments (Hydrolab DS3 and YSI 600XLM probes) (Fig. 4.7). The multiparameter probes utilize a cell with four pure nickel electrodes for the measurement of solution conductance. This cell is usually referred as the conductivity probe. Two electrodes in the cell are current driven, and two are used to measure the voltage drop. The measured voltage drop is converted to a conductance value in milli-Siemens. To convert the measurement to a conductivity value in milli-Siemens per cm (mS.cm^{-1}), the conductance is multiplied by the cell constant that has units of reciprocal cm (cm^{-1}). The cell constant for the conductivity probe is approximately 5.0 cm^{-1}. The exact cell constant is set with each deployment of the system by following the calibration procedure. Prior to each measurement campaign the conductivity probe of each multiparameter sonde is calibrated against a standard solution of 1.409 mS.cm^{-1} (at 25 C). The conductivity probes are known to be very linear over the 0-100 mS.cm^{-1} range. Therefore, a single reference point is sufficient for calibration. The applied tolerance range for the conductivity calibration constant (i.e. the cell constant) is 4.55 - 5.45 cm^{-1}. Only if the calibration constant is within the aforementioned range, the calibration is accepted [20].

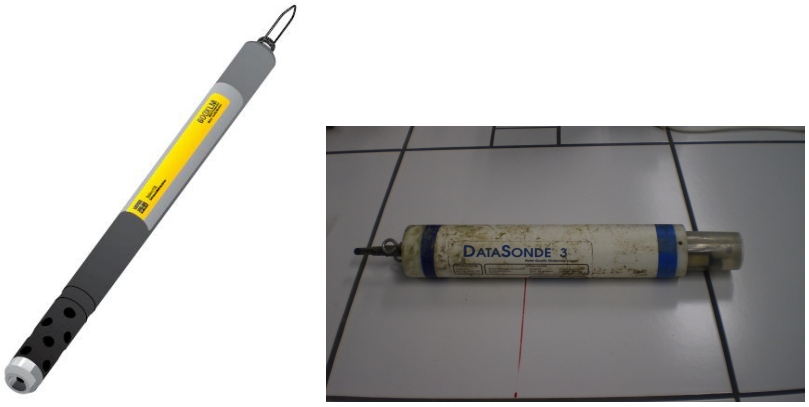

Figure 4.7: YSI 600 XLM and Hydrolab DS3 probes for measuring electrical conductivity

Intensive water sampling occurred at 2 or 3 h intervals, conditional upon the water travelling time. Samples were taken less frequently at low discharges (in summer). The water samples were stored in cool boxes and transported to the laboratory as soon as possible. In the laboratory follow-

ing concentrations were determined in the water samples: NH_4-N, NO_2-N, NO_3-N, Kjeldahl-N, total-N, PO_4-P, total-P, and Cl.

The water transport characteristics of the system were derived from discharge measurements and from an inverse analysis of the passage of salt tracer peaks through the river reach. Breakthrough curves were obtained by automatically recording electric conductivity and by measuring chloride concentrations in the water. The software package Hydrus-1D [21] was used for the inverse modelling analysis and parameters of the advection-dispersion equation were optimized to the observations using non-linear least squares methods. The travel time τ and the dilution factor df were derived from this analysis. The travel time could be assessed from the breakthrough of the tracer peaks and the dilution factor could be assessed from the tracer mass balance. Both parameters were used to calculate for some period (from t_0 until t_n) the change in nutrient load ΔL_{x1-x2} between the upstream (x1) and the downstream (x2) border of the 1.4 km river reach. This difference in nutrient load is defined as:

$$\Delta L_{x1-x2} = \sum [(C_{x_1,t} Q_{x_1,t}) - (C_{x_2,t+\tau} Q_{x_2,t+\tau})] \tag{4.3}$$

But, as only one discharge value was known, tracer data were required to compute the dilution factor which is defined as the ratio between the downstream and the upstream discharge. Using the dilution factor, the difference in nutrient load can be calculated according to the following equation.

$$\Delta L_{x1-x2} = \sum [(C_{x_1,t} Q_{x_1,t}) - (df_i C_{x_2,t+\tau} Q_{x_1,t})] \tag{4.4}$$

In the above equations, $C_{x,t}$ is the nutrient concentration at location x at time t, and $Q_{x,t}$ is the discharge at location x at time t.

Conductivity measurements and their analysis are explained detailed in [20] and is beyond the scope of this work.

2.4.2 Overview of chemical methods for discharge measurements

Two chemical methods for discharge measurements are studied: the gulp method and the constant rate injection method [22] (Fig.2.4.2). These 'dilution' methods are based on the injection of a solution with a well known concentration of tracer and the measurement of the concentration further downstream in the river. The measurements can be carried out in rather turbulent rivers, necessary for the mixing of the tracer in the flow. Conditions for optimal mixture are gathered in [22]. Retention zones in the river

are influencing the discharge measurements in a negative way. Therefore, vegetated rivers are not ideal for that kind of measurements, absorption of tracer will influence the measurement. Further, it is not advisable to measure during varying discharge.
Measurement errors are experimental or systematic. Systematic errors are due to errors of the measurement device and to the specific circumstances of the measurements. Errors of the tracer, e.g. reactions in the river, wrong measuring periods, bad mixture, discharge change, etc. are all systematic errors. Experimental errors are varying errors linked to the experiments. By repeating of the measurements, the standard deviation can indicate this error.

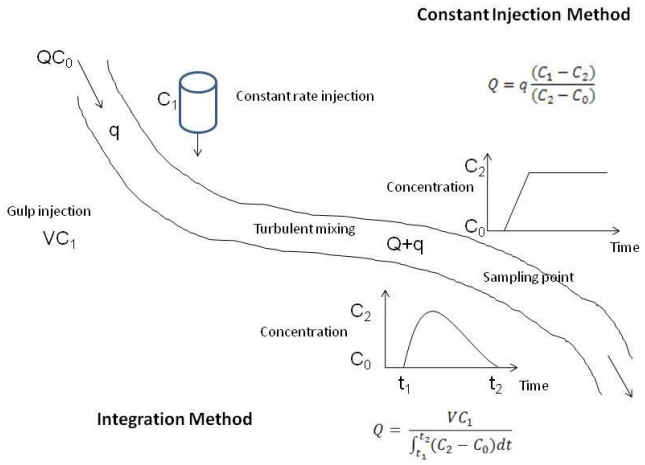

Figure 4.8: Two basic methods for dilution gauging: constant rate injection method and gulp method [23]

Constant rate injection method The discharge of the river is based on the assumption that all tracer passes the measuring point and is determined by [24]:

$$Q = \frac{q(C_1 - C_2)}{C_2 - C_0} \tag{4.5}$$

with Q = discharge of the river [m^3/s], q = constant injection discharge [m^3/s], C_0 = natural background concentration of the river [$g/l = kg/m^3$], C_1 = concentration of the injected solution [kg/m^3], C_2 = concentration balance at point of measurement, further downstream the river [kg/m^3].

In an upstream section 1, a discharge q of a solution with concentration C_1 is injected continu during a certain period. The natural concentration of the river is C_0. Downstream, in section 2, the concentration C_2 is measured and the discharge of the river is calculated using Eq.(4.5). The concentration at the measuring point has to be stable for a sufficient long time. The method is simple, rather fast en accurate [25]. Good mixing of the tracer over the cross sections is necessary which requires a certain turbulence in the river.

The injection time T_i is determined by the transit time T_p and has to result into an equilibrium time T_c, which is long enough [26], 10 to 15 min according [27]: $T_i = T_p + T_c$. The equilibrium concentration is measured.

[28] describes the necessary injection volume and [29] proposes some positions of the measuring points. Different appliances can be used to inject the solution in the river. Important is the long injection time to reach an equilibrium. According [26], the Mariotte bottle, a floating siphon, a tank with constant discharge or a pump are appliances which proved their worth.

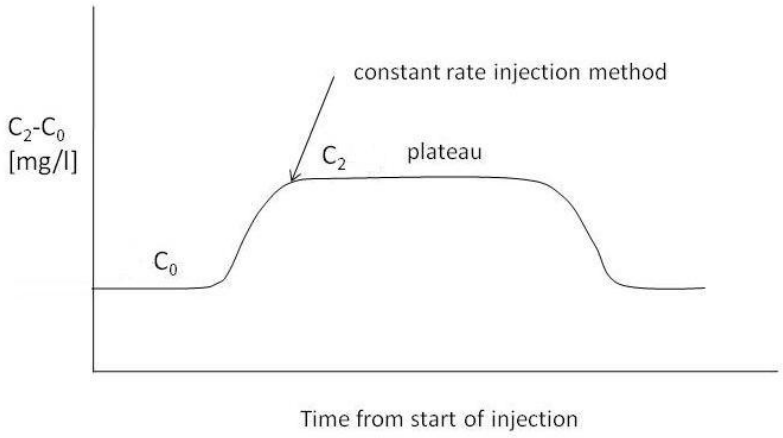

Figure 4.9: Constant rate injection method: concentration as a function of time [27]

Gulp method The discharge of the river is based on the assumption that all tracer passes the measuring point and is determined by [25]:

$$Q = \frac{V(C_1 - C_0)}{\int_{T_a}^{T_a+T_p}(C_2 - C_0)dt} - \frac{V}{T_p} \tag{4.6}$$

with Q = discharge of the river [m^3/s], V = volume of the injected solution [m^3], C_0 = natural background concentration of the river [kg/m^3], C_1 = concentration of the injected solution [kg/m^3], C_2 = concentration balance at point of measurement, further downstream the river [kg/m^3], T_a = time of arrival of the tracer at the measurement point compared to the time of injection [s], T_p = time of passage from the tracer at the measuring point [s].

In an upstream section 1, a volume V with concentration of the tracer is injected. Further downstream, the concentration C_2 is measured as a function of time. Good mixing is required. The method is fast, cheap (less tracer than for constant rate injection method) and simple (no measurement of q as with constant rate injection method).

Here, the concentration as a function of time is measured (Fig. 4.10) and not the equilibrium concentration. The surface A in the graph of the concentration C_2-C_0 as a function of time is the integration value of Eq.(4.6). Longitudinal dispersion determines the shape of the graph. The equilibrium concentration can be measured by discrete measurements, continue measuring and by measuring the average concentration [26].

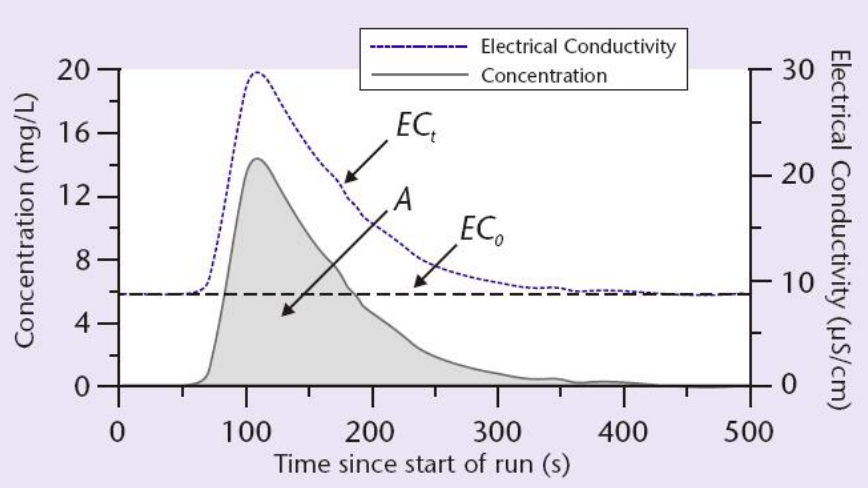

Figure 4.10: Gulp method: concentration as a function of time [30]

Measurements on the Zwedebeek Discharge measurements, using both methods, are carried out on the Zwedebeek [22, 31]. Salt is used as a tracer and conductivities are measured using two conductivity meters: WTW LF 340 and Hanna. An extensive sensitivity analysis is performed

and important parameters, error calculation, determination of the measuring length, etc. are studied.
For the constant rate injection method, the value of q and C_1 are chosen. For an increasing value of q, the influence on the discharge Q of the time is larger and the influence of concentrations C_0, C_1 and C_2 is smaller on the result. For an increasing value of C_1, the influence of the concentrations is smaller, while the influence of time is not changing. The difference between C_0 and C_2 has to be large enough. Indeed, for a high discharge and therefore a high dilution of C_1, the difference could be too small. Therefore, it is advisable to increase q or C_1.
Volume V and concentration C_1 are the parameters of the gulp method. The higher the volume and the higher the concentration C_1, the smaller the influence of the concentrations on the result.

In conclusion: two chemical methods to determine the discharge are tested. However, these methods are not usable in the river Aa and Biebrza river due to the enormous amounts of added water that is necessary for larger discharges occurring in these rivers.

2.5 Gauge data

Registration of the water level is executed in each measurement section, in the field as well as in the lab measurements. Therefore, a levelled gauge is necessary. On the river Aa, each weir is equipped with a gauge, so water level measurement is performed. Variation of water level during the measurement is registered by reading the gauge during the measurement of the discharge. The presence of 3 limnimeters of Flanders Hydraulics Lab (HIC) in the reach between weir 3 and weir 4 allows to study the evolution of the slope of the water surface as a function of time.

2.6 Overview of measuring instruments and measuring locations

Tabel 4.1 gives an overview of the measurement instruments and their specifications used during this research and Fig. 4.11 indicates the measuring locations at the river Aa.

Measurement instrument	Measured parameter	Properties	
levelled gauge	Z	range	not applicable
		resolution	0.5 cm
		accuracy	0.5 cm
		technique	reading
		measurement	simultaneous with the velocity measurements
limnimeter	Z	range	not applicable
		resolution	1 mm
		accuracy	1 mm
		technique	floating system
		measurement	the average of the water level is registered each 15 min
calibrated weir	Q	resolution	0.5 cm on reading off the water level
		accuracy	5 % for free flow and 10 % for submerged flow
		technique	measuring the water level over the weir
		measurement	simultaneous with the velocity measurements
propeller OTT Universal Current Meter	V	range	depends on type, from 0.025 m/s to 10 m/s
		accuracy	1 % of the measured value
		technique	point measurements of the velocity in the cross section
		measurement	the discharge is calculated by integration of the velocities over the cross section, an accuracy for the discharge of 2 to 5 % is obtained

continued on next page

electromagnetic instrument: - OTT Nautilius C2000 Sensa Z300 - Valeport single axis meter, model 801	V	range	depends on type from 0 m/s to 2.5 m/s
		accuracy	0.5 % of the measured value
		technique	based on Faraday's law
		measurement	the discharge is calculated by integration of the velocities over the cross section, an accuracy for the discharge of 2 to 5 % is obtained
ADCP Acoustic Doppler Current Profiler	V,Q,Z		no extended measurements performed
ADV	V_x,V_y,V_z	range	0.03 - 2.50 m/s
		resolution	0.01 cm/s
		accuracy	1 % of measured velocity
		technique	continuous velocity measurement in sampling volume
		measurement	flume measurements
mowing device [32]	biomass	accuracy	1 g/m^2
		technique	sampled from a circular plot using a mowing device
		measurement	10 sampling points at each location

continued on next page

Hydrolab DS3	EC	range	0-100 mS/cm
		resolution	0.001 mS/cm
		accuracy	0.5 % of the reading $\pm$ 0.001 mS/cm
		technique	automatically monitoring
		measurement	registration each 5 min, also registration of dissolved oxygen
YSI 600 XLM	EC	range	0-100 mS/cm
		resolution	0.001 to 0.1 mS/cm
		accuracy	0.5 % of the reading $\pm$ 0.001 mS/cm
		technique	automatically monitoring
		measurement	registration each 5 min
YSI 600 XLM	dissolved oxygen	range	0-50 mg/l
		resolution	0.01 mg/l
		accuracy	0-20 mg/l ($\pm$ 0.2 mg/l) and 20-50 mg/l ($\pm$ 0.6 mg/l)
		technique	automatically monitoring
		measurement	registration each 5 min
Hanna	EC	range	0-2 g/l
		resolution	1 μS/cm
		accuracy	1 % of the measurement
WTW LF 340	EC	range	0-5 g/l
		resolution	0.001 μS/cm - 1mS/cm
		accuracy	1 % of the measurement

Table 4.1: Overview of measurement instruments and their particular indications

Initially, more measurements of velocity and biomass were performed over the reach, without deviant results. Therefore, the upstream and downstream section are chosen as the measurements locations. As biomass occurs in patches, an extra measurement is performed in the middle of the studied strech.

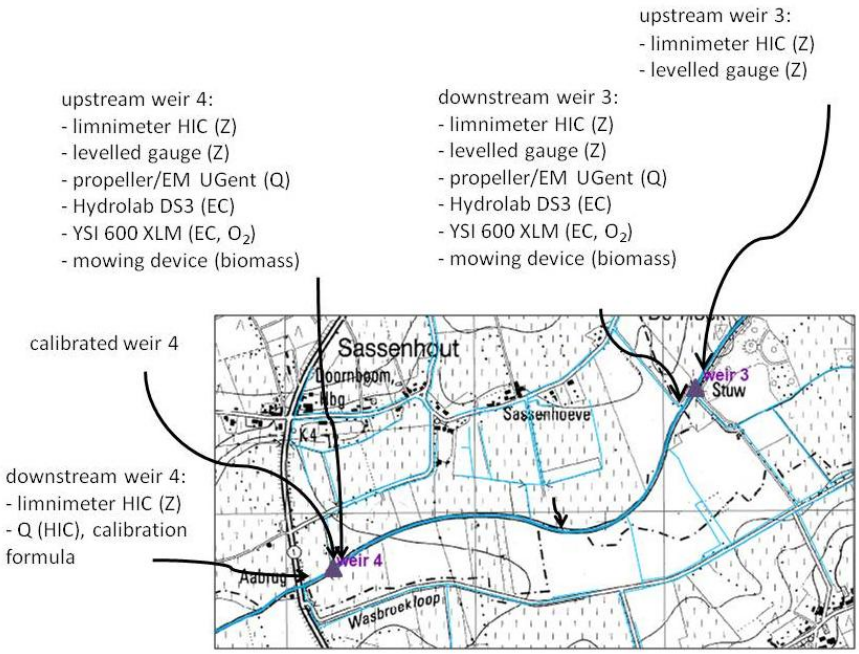

Figure 4.11: Overview of measurements and measurement locations in the studied reach of the river Aa

3 Calibration of the measurement instruments

All measurement instruments need calibration.

The conductivity meters WTW LF 340 and Hanna, used for the determination of discharges based on chemical methods, are calibrated in the Hydraulics Lab using demineralized water [22, 31]. Discharge calculation is carried out using Eq.(4.5) and Eq.(4.6), based on concentrations of the tracer. The relation between the measured conductivity and the concentration is given by Eq.(4.7) for the Hanna [range 0.0 g/l to 2.0 g/l, max. conductivity 4000 μS/cm] and Eq.(4.8) for the WTW LF 340 [range 0.0 g/l to 5.0 g/l, max. conductivity 500000 μS/cm]:

$$concentration[g/l] = 0.00054.conductivity[\mu S/cm] - 0.08192 \quad (4.7)$$

$$concentration[g/l] = 0.00055.conductivity[\mu S/cm] - 0.05739 \quad (4.8)$$

Hydrolab DS3 and YSI 600 XLM probes are used by the University of Antwerp to measure conductivities in the river Aa.

The electromagnetic devices and the hydrometric propellers are calibrated in the lab. Next to the hydrometric propellers (OTT C31 Universal Current Meter) and the electromagnetic instruments (OTT, Nautilus C2000 / SENSA Z300), a third instrument was tested (Valeport, Single Axis Electromagnetic Flow Meter, Model 801).

Calibrations are executed in a rectangular channel (length of 40 m, width of 1 m and depth of 1 m) in quiescent water. The propeller is installed on a lorry in the middle of the channel and is pulled through this channel with a constant velocity. Distance, time and revolutions of the propeller or the reading of the electromagnetic instrument are acquired by a computer. The same measurements are carried out for different velocities allowing calibration formulas to be developed (Eq.(4.9) with an accuracy which is better than 1 % of the actual velocity. For the used propeller (C31-87200, A-67619):

$$\begin{cases} V = 0.129n + 0.019 & 0 < n < 4.374 \\ V = 0.128n + 0.022 & 4.374 < n < 10 \end{cases} \quad (4.9)$$

with V = velocity [m/s]; n = N/t; N = number of revolutions [1/s]; t = measurement duration [s].

Also, further measurements are carried out with two different propellers (22558 and 23088), also calibrated in the Hydraulics Laboratory. The measurement range (V_{min} and V_{max}) of each propeller is determined. These values indicate the importance of using the instrument with specific measurement range under specific conditions. For propeller 22558, V_{min} = 0.025 m/s and V_{max} = 0.583 m/s, while propeller 23088 is more suitable for higher velocities (V_{min} = 0.008 m/s and V_{max} = 1.051 m/s). All propellers are calibrated each year.

Both electromagnetic devices are also calibrated in the lab, in the same way as the propellers, where following formulas (V [m/s]) are obtained.

For the Valeport, 801, cylindrical:

$$\begin{cases} V = 0.9514V(EM) + 0.0129 & 0 < V(EM) < 0.22 \\ V = \quad V(EM) & 0.22 < V(EM) \end{cases} \tag{4.10}$$

For the Valeport, 801, flat:

$$\begin{cases} V = 1.024V(EM)^{0.867} & 0 < V(EM) < 0.15 \\ V = \quad 0.918V(EM) + 0.034 & 0.15 < V(EM) \end{cases} \tag{4.11}$$

For the OTT, Nautilius:

$$\begin{cases} V = 0.8582V(EM) + 0.0075 & 0.049 < V(EM) < 0.276 \\ V = 1.0227V(EM) - 0.0401 & 0.276 < V(EM) < 0.883 \\ V = \quad 1.014V(EM) - 0.0305 & 0.883 < V(EM) < 2.205 \end{cases} \tag{4.12}$$

4 Accuracy of measurement methods

Hydraulic measurements are associated with a specific uncertainty because the obtained values are only an approximation of the exact value, as explained in e.g. [33]. So, the measurement error has to be included in any data analysis. To learn about the accuracy and the reliability of the results, all various sources of errors in the measurement have to be examined. Random errors and systematic errors are distinguished. Some of the random errors (also called experimental errors) can be reduced by increasing the number of observations. These errors are the most important to be considered in river gauging. Systematic errors are present in the water level registration, the current meter accuracy or in the position of the flap crest. By calibration of the instruments and serious control of all measurements, the errors can be reduced to a minimum.

The discharge is calculated from discrete velocity measurements (using the velocity area method); with F, a factor that relates the discrete sum over the finite number of verticals to the integral of the continuous function over the cross-section:

$$Q = F \sum_{i=1}^{n} \sum_{j=1}^{m} U_{ij} \Delta A_{ij} \tag{4.13}$$

In small rivers, velocity profiles are rather irregular and the accuracy of the measurements is function of the number of verticals and the number of points at each vertical [25]. For rivers with width comparable to

the river Aa, each vertical can be associated with a part of the discharge which is maximum 11 % of the total discharge. At least 11 verticals are gauged. For depths between 94 and 150 cm, five measurement points are taken (at 1/6, 2/6, etc. to 5/6). This method allows an accuracy better than 5 %, but the method is time intensive. Consequently, in the upstream and downstream section of the river Aa, velocities are measured each meter over the width of the section and at regular distances over the vertical (5 to 7 points). Gauging sufficient points over the depth allows to generate a realistic velocity profile.

To generate a reliable measurement, a sufficient number of verticals needs to be gauged. In normal circumstances a total of 13 verticals (m = 13) is considered to deliver a value 1 of the coefficient F. If too little verticals are measured, the discharge is underestimated and a value greater than 1 for F is applied. For a single determination of the discharge, the uncertainty at the 95 % confidence limit is up to 7 %. The choice of a sufficient number of verticals can reduce this value [33].

The uncertainty on the discharge is given as:

$$u(Q)^2 = u_m^2 + u_s^2 + \frac{\sum((b_i d_i v_i)^2 (u_{bi}^2 + u_{di}^2 + u_{vi}^2))}{(\sum(b_i d_i v_i))^2} \quad (4.14)$$

$$u_{vi}^2 = u_{pi}^2 + u_{ci}^2 + u_{ei}^2 \quad (4.15)$$

$$u_s^2 = u *_{bi}^2 + u *_{di}^2 + u *_{ci}^2 \quad (4.16)$$

with: u_m = uncertainty on the limited number of verticals; u_{bi}, u_{di}, u_{vi} = relative (percentage) standard uncertainties in the width, depth and mean velocity at vertical i, u_s = systematic uncertainty due to calibration errors; u_{pi} = uncertainty due to the limited number of depths at which velocity measurements are made; u_{ci} = uncertainty on the characteristics of the measurement instrument, u_{ei} = uncertainty due to fluctuation of the velocity during the measurement, u^*_{bi} = percentage systematic uncertainty in the instrument measuring width, u^*_{di} = percentage systematic uncertainty in the instrument measuring depth, u^*_{ci} = percentage systematic uncertainty in the registration of the current meter [2, 3].
For the values of the uncertainties, reference is made to ISO 748 and others [2].
For u_s, an estimated practical value of 1 % is taken.

If the segment discharges ($b_i d_i v_i$) are nearly equal and the random uncertainties X_i are nearly equal and of value X then:

$$u(Q)^2 = u_m^2 + u_s^2 + \frac{1}{m}(u_b^2 + u_d^2 + u_e^2 + u_p^2 + u_c^2) \quad (4.17)$$

which is the simplified error equation with m the number of verticals. Calculations in [3] show that there is only little difference between the original and the simplified error equation.

Measurements carried out with a propeller are the most accurate if the instrument is used as a standard wading unit, as this makes it possible to have an accurate measurement of the water depth. Determination of the water depth from a bridge is more difficult with deviations of 1 to 2 cm. This leads to an error of 3.5 to 7 % on a water depth of 30 cm. Measurements performed in the river (standing in the river or from a boat) allow to choose a section which is smaller, with better flow conditions and to take into account the condition of the bottom. By this more accurate results can be obtained [34], [11].

Accuracy of electromagnetic devices is up to 0.5 % while for propellers the accuracy is 1 % of the actual value. Deviations are larger for lower ranges of velocities. Also flow characteristics and the precision of the measurement depth influence the accuracy of the result. This leads to an overall accuracy of 2 to 5 % for the determination of the discharge.

Calculations of the discharge, using the formulas of a calibrated weir lead to an accuracy of 5 % (free overflow) to 10 % (submerged flow) [34].
In the analysis of the laboratory measurements, absolute and relative deviations are calculated to check the accuracy of the measurements.

Calculating the accuracy according to Herschy [3] results in following values: for thin plate weirs, an accuracy of 1 % is obtained. Using the measurement techniques and values of the river Aa, following calculation is made for one of the field measurements. The uncertainty values mentioned are percentage standard deviations at the 95 % confidence limits. These values are used because the true value of the discharge is unknown. An estimate of the true value has therefore to be made by calculating the uncertainty in the measurement, the uncertainty being defined as the range in which the true value is expected to lie expressed at the 95 % confidence level. For discharge calculation, it is not possible to calculate the standard deviation, because no repeated measurements can be performed under the same conditions. Therefore, an estimate of the true value has to be made by examining all the various sources of errors in the measurement.
On December 6th 2006, a discharge of 3.08 m^3/s was measured with an electromagnetic device. Measurements were carried out on 20 verticals and the average velocity in the cross section was 0.198 m/s. Further; u_m =

5 %, u_e = 15 %, u_b = 0.1 %, u_d = 1 %, u_p = 5 % (for 5 measurement points), u_c = 1.5 %, u^*_b = 0.5 %, u_d = 0.5 %, u^*_c = 1.0 %. For the value of the systematic uncertainty, 1 % is used as practical value, this value is almost independent of the instrument type (propeller or electromagnetic device). The random accuracy is much more stringent. The high value of u_e is due to a rather low velocity in the river and a short measurement time. For velocities over 0.3 m/s, an exposure time of 30 s is sufficient, for lower velocities, the measurement time is preferable up to 3 min. This is necessary to eliminate the fluctuation of the velocity. The measurements on the river Aa are carried out in dry periods and with a fixed position of the weir, which can result in lower velocity fluctuations and can allow a lower value of u_e. With the above mentioned values, the random uncertainty on the discharge is 6.1 %, to obtain a value within the 95 % confidence interval.

A levelled gauge measures water levels with an accuracy of 0.05 cm (1 to 2 %).

The ADV has an accuracy of 1 % of the measured velocity. The measurement range of the Nortek ADV is 0.03 to 2.5 m/s an dthe resolution is 0.01 cm/s. For the Streampro ADCP, following values are found. The accuracy is 1 % $\pm$ 0.2 cm/s of the reading. The measurement range is 0.15 m to 2 m water depth and velocities up to 2 m/s. The resolution is 0.1 cm/s.

The Hydrolab DS3 and the YSI 600 XLM probes have an accuracy of 0.5 % $\pm$ 0.001 mS/cm of the reading. The measurement range of the Hydrolab DS3 conductivity sensor is 0-100 mS/cm and the resolution is 0.001 mS/cm. The same values for the measurement range and the accuracy are found for the YSI 600XLM conductivity sensor. For the latter instrument, the resolution is range dependent (0.001-0.1 mS/cm).
The accuracy of the Hanna conductivity meter is up to 1 μS/cm, the accuracy of the WTW LF 340 meter depends of the measurement interval and varies from 0.001 μS/cm up to 1 mS/cm.

5 Flume measurements

5.1 Laboratory flume

In a flume of the Hydraulics Laboratory, measurements are carried out to calibrate instruments, to compare the results of the different measurement instruments and to check measurement influences under well known and controlled conditions. Also, measurements are carried out to check the influence of in-stream vegetation on the stream patterns. Aim is to obtain information for analogous patterns in rivers.

Experiments are carried out in a flume of 12 m long and 0.70 m wide. The bottom slope is measured using a leveling instrument and results in an average slope of 1/400 m/m. An upstream weir allows to measure discharges up to 120 l/s and water levels to 60 cm in the glass-walled flume. Discharge Q [m^3/s] is calculated by using Eq.(4.18) with h_w [m], the water depth over the upstream weir.

$$Q = 0.044 * (h_w - 348.7)^{1.5031} \tag{4.18}$$

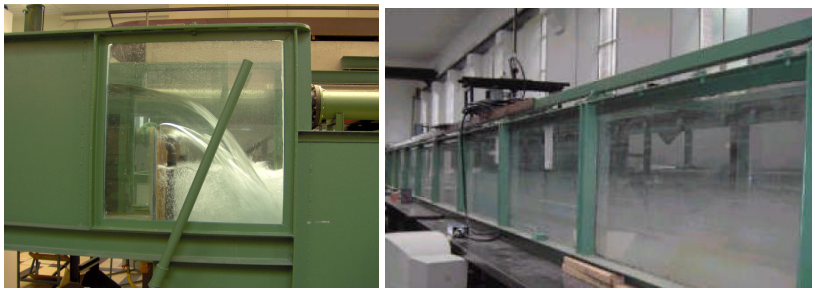

Figure 4.12: Calibrated upstream weir in the flume in the Hydraulics Laboratory

This formula (R^2=0.9993) results out of calibration of the upstream weir [35]. Attenuation of the turbulence and obtaining a uniform flow is organized by use of a damper and a metal frame. The downstream weir is placed in different fixed positions, varying from 5 cm to more than 50 cm above the flume bottom, to adjust the water level. An overview of the flume set-up is given in Fig. 4.13.

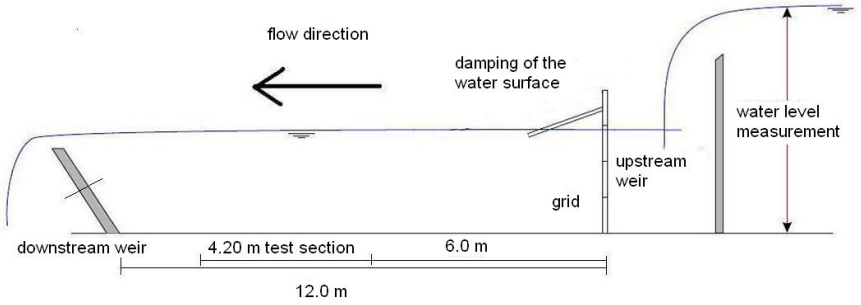

Figure 4.13: Flume set-up in the Hydraulics Laboratory for different types of measurements

5.2 Comparison of velocity measurement instruments

Comparative tests with three devices (OTT propeller, OTT electromagnetic device, Valeport electromagnetic instrument) were performed in the flume. Three different discharges were chosen and the corresponding velocities in the middle of the channel were measured with the hydrometric propeller and the electromagnetic instruments. The results are presented in Table 4.2 and show only small deviations. The value UG_{canal} is obtained by using the discharge formula of the calibrated weir at the upstream end of the test flume (Eq.(4.18)). The velocity is obtained by dividing this value by the wetted cross section. This velocity is lower because this is an average uniform value over the rectangular section.

Q [l/s]	12.22	69.93	100.52
UG_{canal}	0.058	0.250	0.326
$EM_{Valeport}$	0.075	0.294	0.393
EM_{OTT}	0.069	0.273	0.368
Propeller	0.069	0.299	0.396/0.398/0.382

Table 4.2: Velocities [m/s] measured in the lab by the different measuring instruments and corrected with the calibration formulas. Three values are indicated for the propeller measurement due to the three different propellers (OTT: 2-23092 1-22566, A-67619) used in the test.

To avoid turbulence influence in the stream flow, for various measurements the velocity is calculated in each measurement point based on n measurements. For each measurement, the accuracy using an electromagnetic device is 0.5 %. Next to that, the absolute deviation is also based on the standard deviation of n measurements compared to the average value.

So, the absolute deviation d_m is the largest value of Eq.(4.19) and Eq.(4.20), with $v_{sensor,i}$, the measured velocity [m/s], $\overline{v_{sensor}}$, the average velocity [m/s] and n, the number of measurements in each point .

$$d_m = \frac{1}{\sqrt{n}} \frac{\sum_{i=1}^{n} (\overline{v_{sensor}} - v_{sensor,i})^2}{\sqrt{n-1}} \tag{4.19}$$

$$d_m = 0.005 \overline{v_{sensor}} \tag{4.20}$$

5.3 Influence of the measurement duration

In order to evaluate the influence of unsteadiness of steady flow, for a chosen discharge, more measurements are carried out with the hydrometric propellers and the electromagnetic device. Therefore, two different propellers (22558 and 23088) and the electromagnetic instrument (Valeport) are used for a varying measurement time or varying number of rotations. Velocity measurements are performed at 3 verticals in the cross section (10, 35 and 50 cm) at different heights (4, 8, 12, 16, 20 en 24 cm) while the water depth in the flume was 27 cm. The discharge is calculated using the method of the integration of the velocities over the cross section.

For each of the situations (different propellers and a different number of rotations), the measurements were repeated 10 times. Each of the measured discharges is compared to the calibration value (discharge measured with a calibrated weir) and the minimum and maximum discharge of the 10 measured values (cf. infra) is mentioned in Table 4.3. Also the accuracy of the results is checked by calculation of the absolute and relative deviation, next to the standard deviation. The absolute deviation is determined for each of the 10 measurements, calculating the absolute deviation on the velocity and on the geometric dimensions. For each of the 10 measurements, the absolute deviation is more or less the same, and the average value is mentioned in Table 4.3. The small variation in the absolute deviation is confirmed by the small variation on the discharge under these laboratory conditions. Hydrometric propellers used in good flow conditions and in an accurate way can measure with an accuracy to 1 % of the actual value, which is confirmed by the values in Table 4.3.

The average velocity for the measurements is 0.317 m/s. Considering the measurement range of the propellers, it is expected (and confirmed in Table 4.3) that propeller 22558 is more suitable for these measurements than propeller 23088, which has been manufactured for use with higher velocities. Higher deviations are observed for the results of the second propeller, which is attributed to differences in calibration formulas and/or

application range. It should be mentioned that, the measured average velocity is situated in the middle of the range for propeller 22558, while propeller 23088 is more suitable for higher values of the velocity.

propeller	22558			23088	
	10 rot.	20 rot.	10 s	10 rot.	20 rot.
Qcal [l/s]	59.42	59.42	59.42	59.42	59.42
Qmin [l/s]	59.33	59.15	59.31	59.32	59.36
Qmax [l/s]	60.08	60.07	59.85	59.91	59.98
abs. dev. [l/s]	1.34	1.34	1.34	1.81	1.81
rel. dev. [%]	2.25	2.24	2.25	3.04	3.04
stand. dev. [l/s]	0.224	0.303	0.199	0.199	0.229

Table 4.3: Measurements in the lab with a hydrometric propeller and different number of rotations and measurement time

The measurement of the time with a fixed number of rotations or the measurement of the number of rotations during a certain time period to calculate the velocity does not show significant differences, which indicates that measurement time and number of rotations is of minor importance under lab conditions.

The same measurements are performed with an electromagnetic device (Valeport, cylindrical sensor) (Table 4.4) at 3 verticals (10, 35 and 55 cm) at different heights (5, 15, 25 cm). These heights are chosen taking into account the spherical measurement volume (diameter of 12 cm) of the electromagnetic device. In each point, 10 measurements are carried out and the constant value of the discharge (comparing Q_{min} and Q_{max} of the 10 measurements) indicates stable conditions and accurate measurements. Velocities up to 0.3 m/s lead to a relative deviation of 1.5 % which corresponds with the technical information (deviation up to 3 % for velocities of 0.1 m/s). For higher velocities, the deviation is smaller.

Valeport		
	10 s	20 s
Qcal [l/s]	59.06	59.06
Qmin [l/s]	59.80	59.71
Qmax [l/s]	61.27	60.75
abs. dev. [l/s]	1.41	1.41
rel. dev. [%]	2.33	2.33
stand. dev. [l/s]	0.363	0.352

Table 4.4: Measurements in the lab with an electromagnetic device and different measurement time

As a conclusion, all used instruments, hydrometric propellers and electromagnetic devices, lead to accurate results in well controlled lab conditions. Variations in measurement time are of less importance. It also becomes clear that application of a device (propeller) which is appropriate for the velocities under concern leads to better quality of the results.

5.4 Influence of vegetation on velocity profiles

5.4.1 Velocity profile with smooth bottom

Prandtl and Von Karman described theoretically the velocity distribution in permanent flow [36]. Therefore, the velocity in the x-direction is written as the sum of a time averaged velocity $\overline{v_x}$ and a fluctuating velocity $v_x^{'}$. Use of the expression for momentum conservation shows that the fluctuating velocities cause an extra flux of momentum, and are added to the value of the shear stress τ_{zx}. The total shear stress is written as:

$$\tau_{zx}[Pa] = \mu \frac{d\overline{v_x}}{dz} - \rho \overline{v_x^{'} v_y^{'}} \tag{4.21}$$

with μ = dynamic viscosity [Pa.s] and ρ = density [kg/m^3]

The first part of Eq.(4.21) is the shear stress due to molecular momentum transport of the water and is determined by the dynamic viscosity μ [Pa.s] and the differences in velocity over the water height. The second part is the Reynolds shear stress and is due to the turbulence of the flow. In the neighbourhood of the wall, the viscosity is determining and the shear stress equals τ_0, the bottom shear stress. So, in the viscous sublayer, the velocity follows a linear profile:

$$\tau_{zx}[Pa] = \mu \frac{d\overline{v_x}}{dz} = \tau_0 \tag{4.22}$$

$$\overline{v_x}(z) = \frac{\tau_0}{\mu} z \tag{4.23}$$

with $\overline{v_x}$(z) [m/s] = average velocity in x-direction, τ_0 [N/m^2] = bottom shear stress, μ [Pa.s] = dynamic viscosity and z [m] = height over the water depth

In the turbulent layer, where the Reynolds stresses are dominant, it is supposed that the fluctuating velocities are the result of the movement of the fluid in the vertical direction, over the mixing length L. Hence, the velocity profile results in [37]:

$$\overline{v_x}(z) = \frac{v_*}{k} ln \frac{z}{z_0} \tag{4.24}$$

with $v_* = \sqrt{\tau_0/\rho}$, z_0 the height where the velocity equals 0 [m] and k = von Karman constant (value of 0.4).

5.4.2 Velocity profile with rough bottom

The flow can be hydraulically either smooth or rough [38]. Hydraulically smooth flow occurs when the surface irregularities are so small that all roughness elements are entirely submerged in the laminar sublayer [37]. Therefore, the bed roughness will not affect the velocity distribution. The velocity profile is linear in the viscous sublayer and logarithmic on top of it. According to [39], the flow is smooth if:

$$0 < \frac{v_* k_s}{\nu} < \frac{1}{200} \tag{4.25}$$

where v* is the friction velocity [m/s], k_s is the roughness height [mm] and $\nu = \mu/\rho$ = kinematic viscosity [m^2/s].

The flow is rough when bed roughness is so large that it produces eddies close to the bottom [40]. There is no viscous sublayer and the velocity distribution is affected only by bed roughness and is logarithmic due to Reynolds tensions which are larger than the shear stresses. The flow is turbulent over the entire height. According to [39], the flow is hydraulically rough if:

$$\frac{7}{100} < \frac{v_* k_s}{\nu} \tag{4.26}$$

The flow is in the transition region if:

$$\frac{1}{200} < \frac{v_* k_s}{\nu} < \frac{7}{100} \tag{4.27}$$

In this case, the velocity distribution is affected by bed roughness and viscosity [37]. Nikuradse [35] defined the water height at which the velocity equals zero in the logarithmic velocity profile, this height is defined by the type of flow (smooth, rough or transition) that is occuring. In [40], expressions are found for respectively smooth, rough and transitional flow:

$$z_0 = 0.11\frac{\nu}{v_*} \tag{4.28}$$

$$z_0 = 0.033 k_s \tag{4.29}$$

$$z_0 = 0.11\frac{\nu}{v_*} + 0.033 k_s \tag{4.30}$$

5.4.3 Velocity profile in a vegetated reach

Study of the interaction of stream flow and in-stream vegetation demands for some theoretical background about the influence of vegetation on the velocity profile. The macrophytes in the river are obstructing the flow, which consequently surrounds the vegetation [41]. Between the vegetation, velocity is low, above and next to the plants, higher velocities are registered. In front of and behind the plants, the velocity is decreasing (Fig. 4.14). In presence of floating plants, maximum velocities will not be measured at the water surface.

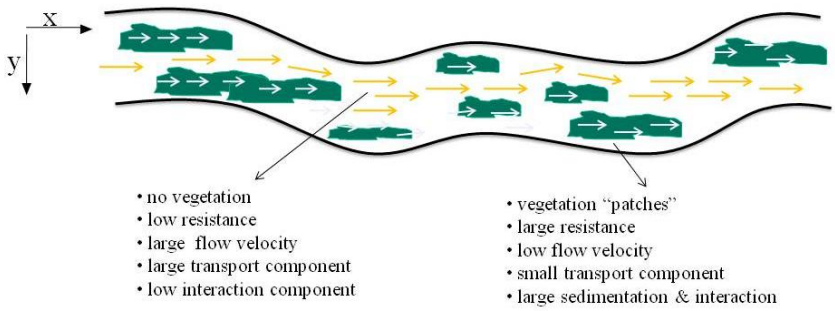

Figure 4.14: Influence of vegetation on stream flow [42]

Reynolds shear stresses are influenced by vegetation. The logarithmic velocity profile for undisturbed rivers is based on constant Reynolds shear stress, which is obviously not the case in vegetated rivers. [43] shows that maximum Reynolds shear stresses are found above the top of the bended plants. These stresses decrease in higher and lower regions. [44] described the influence of the leaves of the plants. Than, the velocity is decreasing even more and Reynolds shear stresses are lower, as well as turbulence. At the top of the vegetation a horizontal friction layer is seen and behind the plant patch, more turbulence is registered [41]. Flow through vegetation is studied by [45], where a model is developed for forces, turbulence and diffusion of flow through vegetation. Flume experiments for submerged and emergent plants are carried out by [46]. Reynolds shear stresses over the water height are calculated by [47] and [48]. Vice versa, the stream flow will also influence the vegetation.

The presence of vegetation can be included in the Manning equation by increasing the bottom roughness. [49] proposed following equation:

$$n = \frac{R^{(1/6)}}{18} \frac{1}{log(\frac{12R}{k_s})} \tag{4.31}$$

with n, Manning's coefficient [$m^{-1/3}s$]; R, hydraulic radius [m] and k_s, the equivalent roughness [m].

This parameter allows to include the extra roughness due to vegetation but fails in the description of the physical phenomena. After all, vegetation is not an extended part of the bottom structure and stream flow between vegetation differs from the logarithmic velocity profile.

Other and more adapted methods propose a velocity profile based on different zones over the water height (Fig. 4.15a) and a profile according a hyperbolic tangent (Fig. 4.15b). [49] divided the water height in 4 zones (Fig. 4.15a):

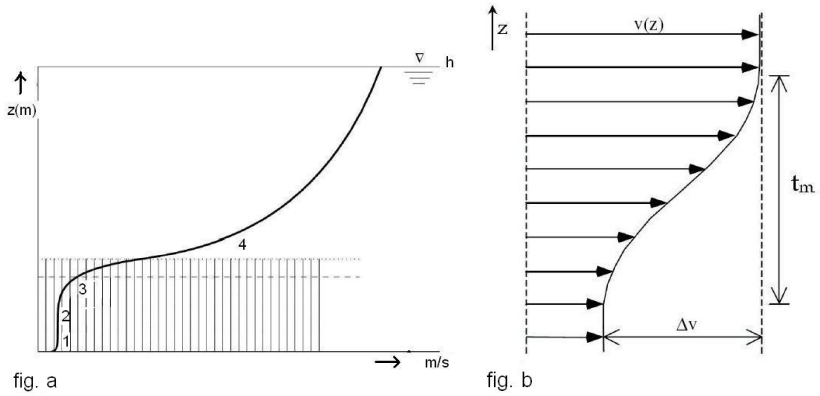

Figure 4.15: Velocity profile influenced by vegetation

- Zone 1: zone close to the bottom, the bottom is rough and so is the flow, the velocity profile follows the logarithmic one.
- Zone 2: is located in the vegetation, a uniform velocity is mentioned
- Zone 3: is found around the top of the vegetation, it is a transition zone and the velocity profile is described by an exponential function
- Zone 4: is the zone above the vegetation where the logarithmic velocity profile is seen.

In [50] is shown that the stream flow through a vegetation patch is comparable to a mixture layer. The velocity profile has two areas with constant velocity and in between is a transition zone described by a hyperbolic tangent, with inflection point at the top of the plants (Fig. 4.15b).

5.4.4 Stream patterns in and around vegetation

It is often shown that flow in rivers and waterways slows down within and in the proximity of vegetation. Presence of vegetation increases the water level upstream these plants and screens the flow behind the vegetated area [45, 51, 52]. Consequently, higher resistance against flows occurs. To allow the same discharge in the river when compared to the situation without vegetation, the difference in water levels before and after the vegetation has to increase resulting in backwater influence in the upstream part of the river. Due to the occurence of macrophytes, the drainage capacity of the river decreases, leading to higher flood risks during peak flow.

All experiments with vegetation were performed with *Hydrocotyle ranunculoides* ('floating pennywort'), an invasive, widespread; 'alien' freshwater plant (Fig. 4.16). Its rapid growth and high biomass (dry mass of 1,5 kg/m^2) leads to a high influence on the flow. [53] proposes a checklist with vegetation properties which increase the inundation risk. These properties are applicable for floating pennywort: in a short delay, the plant covers the whole river with a large density of impermeable vegetation. Plant growth is seen over the entire year and also dead plants form a layer on the water surface. *Hydrocotyle ranunculoides* has fine roots, fleshy stalks and grows horizontally. It has shiny, kidney-shaped leaves (up to 7 cm diameter) with crinkled edge, the leaves are frequently broader than long and can be floating or emergent. The stalks are attached between the lobes of the leave. The dry biomass of the collected plants is 1.5 kg/m, which will be substantially larger in summer periods. Plant growth is seen over the entire year and also dead plants form a layer on the water surface.

Figure 4.16: Floating pennywort

The research performed in the following is based on velocity measurements in x, y and z direction, using an ADV. Results are not studied into detail due to the abscence of an analoguous instrument for field measurements. In January 2009, the Vectrino (Nortek) has arrived at the Hydraulics Lab. This instrument allows velocity measurements in 3 directions in the lab as well as in the field. The working principle of the instrument is based on Doppler theory. The study of velocity measurements in 3 directions is no part of this work and therefore, lab results are only mentioned for completeness.

5.4.4.1 Measurements

Measurement set-up: test flume Experiments are carried out in the flume described in section 5.1. A calibrated upstream weir allows to measure discharges up to 120 l/s. The maximum water level is 0.60 m.

An overview of the flume set-up is given in Fig. 4.13, Fig. 4.17 and Fig. 4.19. The set-up for measurements in the empty flume is shown in Fig. 4.17 and differs from the set-up with floating plants (Fig. 4.19). With 'empty flume', it is meant the flume filled with water, but without obstructions as vegetation, etc. In Fig. 4.13, the test section for the floating plants is also indicated.

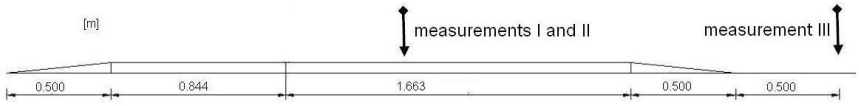

Figure 4.17: Location of velocity measurement positions in the flume without obstacles

For the flume without obstacles, the test section is installed 6.0 m behind the upstream boundary. For the tests with floating vegetation, the test section is 4.20 m long and is also installed 6.0 m behind the upstream boundary condition (Fig. 4.13):

- To allow placement of vegetation, the bottom of the flume was raised with 5 cm. The transition has a slope of 1/5.

- A flat zone of 1.25 m at the up- and downstream boundary of the test section, to decrease the effect of the run-up slope.

- The test zone (gravel, vegetation, etc.) is 1.20 m long and allows installation of vegetation at the bottom. In case of floating vegetation, the baskets with the plants were hanging in top of the test zone to a depth of 0.07 m below the water surface (Fig. 4.18). The gravel bed is retained to approach the situation in natural rivers.

Figure 4.18: Set-up of floating plants: baskets with plants hanging in top of the test zone

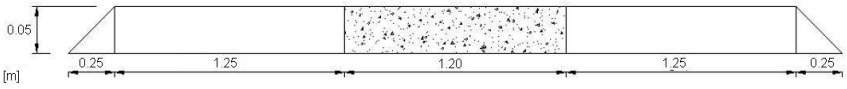

Figure 4.19: Measurement set-up for floating plants, vertical scale is 5 times larger than the horizontal scale

Measurements are carried out in the 'empty' flume and in the flume with floating plants or plants at the bottom.

Measuring instrument: ADV Velocity measurements were performed using a 3D Nortek Velocitimeter (ADV). This apparatus consists of a source sending acoustic waves towards the bottom of the flume. Three receivers are inclined in such a way the receiving waves intersect 5 cm below, in the sample volume. The waves are reflected by particles in that volume and the reflection is captured. Using the Doppler shift principle, the velocity can be determined. The data contains regular electronic noise and has to be filtered.

Errors in the velocity profile and consequently in discharge and Manning's coefficient (cf. infra) are due to errors in measuring the water height (see 3.1.2.) and in measuring the velocity. The velocity decreases very fast closer to the bottom. Also the orientation (vertical position and in line of the flow) of the ADV influences the measurements. A heavy frame kept the ADV in position, so errors due to movement of the measurement instru-

ment or deviation from its position are negligible. Comparison of the ADV-results with the velocity in the flow direction measured using the electro-magnetic sensor (Valeport), shows a systematic difference of 1 mm/s.

Measurements: test series In order to determine the undisturbed conditions, three series of measurements (velocity profiles and water level) were carried out in the flume without obstacles. Measurement series I and II are performed on the raised bottom, while series III is carried out in front of the test section (Fig. 4.17). At each location, the velocity profile is determined central of the width of the flume, the flume is too small to measure different verticals without influence of the side walls. For series I and II, the discharge is 88.8 l/s and the water level 38.5 cm. For series III, the discharge is 66.2 l/s and the corresponding water level is 35.5 cm. The discharge is calculated from the calibration formula of the upstream weir. Maximum velocities in the flume are 35 cm/s (I), 38.5 cm/s (II) and 30.1 cm/s (III). The vertical position of the downstream weir is at 19.14 cm. The energy slope is determined by measuring the water level in 2 points 9 m apart (Fig. 4.22).

To come to a more natural situation, gravel is added to the test area. At 4 points (A, B, C, D at Fig. 4.20), the velocity profiles were measured. Next to that, also the turbulence intensity and the Reynolds shear stresses are determined.

Figure 4.20: A gravel bed is added in the flume set-up

Two frames with plants are placed in a hanging position. The frames with plants have dimensions of 0.35 m length to 0.65 m width, so that plants cover the total flume width. Height of the filled baskets is about 0.10 to 0.12 m. Between the two frames, a gap of 20 cm is left to allow measurements with the ADV (Fig. 4.21).

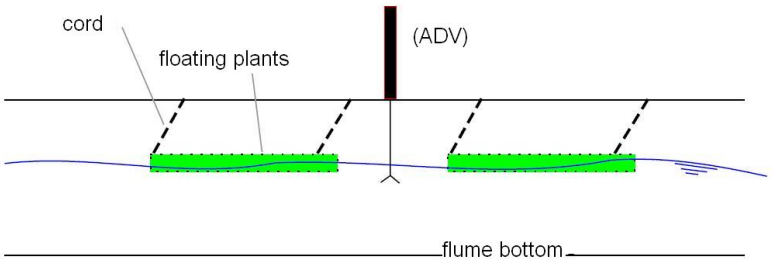

Figure 4.21: Set-up of floating plants in the flume

Several measurements were performed to check the influence of the floating vegetation. Firstly, to determine Manning's coefficient accurately, next to the discharge also the water levels are determined precisely at 4 points (Fig. 4.22): two points in front of the vegetation, one inbetween (which was not useful due to moving of the plants) and one behind the vegetated area. Secondly, velocity measurements were carried out under different conditions: the water level in the flume was first kept constant and then varied. During the measurements with constant water level, different discharges were measured, but the water level was kept constant by changing the position of the downstream weir. Series with water levels of 0.225 m, 0.25 m and 0.33 m were studied. Also velocity measurements with variabel water level were performed. Here, the downstream weir is kept on its fixed position and consequently water levels are changing with varying discharge. Two series of measurements are registered: for a downstream weir position of 13.21 cm (series 2) and 19.14 cm (series 1).

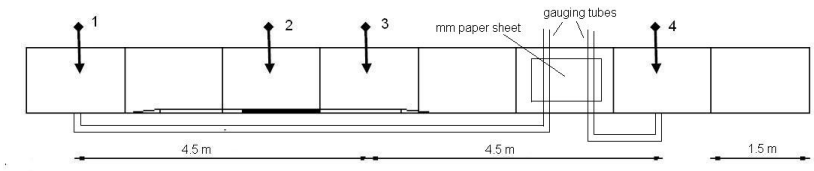

Figure 4.22: Locations of water level measurements in the flume

5.4.4.2 Results The influence of vegetation on the velocity profile is checked in different situations. First of all, the 'empty' flume was tested to have a reference situation. Second, some gravel was added in the test area. Third, floating plants were used, equally and not equally distributed over the width of the flume.

Velocity profiles in the flume without obstacles Theoretical velocity profiles, mentioned in literature [37], are only valid in a part of the flow. Therefore, different layers are distinguished in Fig. 4.23 [40]: the viscous sublayer (I) with low velocity and laminar flow, where the shear stress equals the bottom shear stress. Further, there is the transition layer (II). The turbulent logarithmic layer (III) has only turbulence effects to take into account. The shear stress is constant in this layer and therefore described with the mixing-length theory [54]. The outer layer (IV) occupies the largest part of the flow and big eddies smooth the velocity.

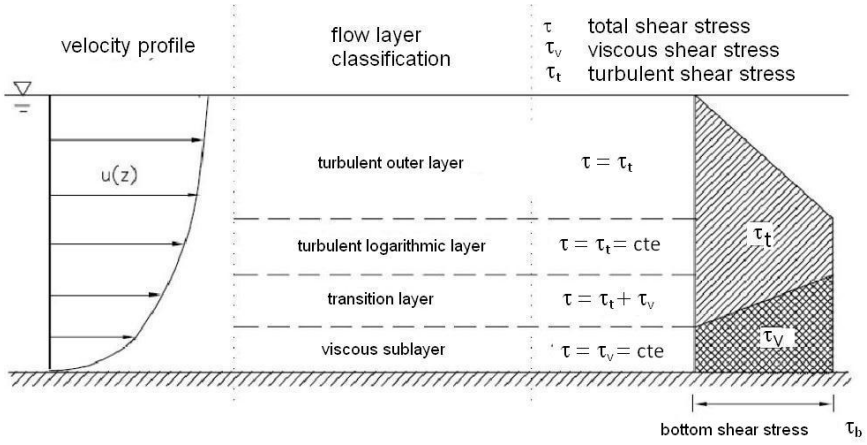

Figure 4.23: Classification of stream flow [40]

The laminar sublayer (I) is only found in a very small part of the flow ($z/h < 1/1000$), the velocity is given by Eq.(4.22) [55]. This thin layer cannot be measured by the ADV.
In the turbulent layer (III), the velocity profile is described by Eq.(4.24) [37].

Three series of measurements were carried out in the flume without obstacles (Fig. 4.17). The measured velocities are plotted in Fig. 4.24. Lowest velocities are measured for series III, due to the lower discharge.

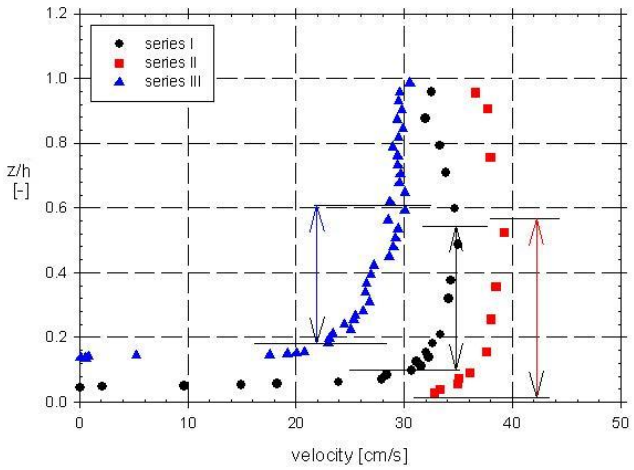

Figure 4.24: Velocity profile in the flume without obstacles for different series of measurements

As explained before, three layers are found. The measurement range does not include the laminar layer (I). The logarithmic part (III) is indicated (arrows) in Fig. 4.24. In [39], the applicability of this profile up to 0.2(z/h) is mentioned, while here reasonable values up to 0.5(z/h) to 0.6 (z/h) are found. For higher (z/h) values, closer to the free surface, the velocity decreases in the third layer (IV).

For each of the measurements, a logarithmic velocity profile, according to Eq.(4.24), is fitted to determine the shear velocity v_* and the water depth for zero velocity z_0 in the equation. Other parameters as S_0 (bottom slope), δ_v (thickness of the viscous sublayer) and k_s (equivalent bottom roughness)(Eq.(4.28)) are also calculated and mentioned in Table 4.5. The bottom slope S_0 is based on the determination of the friction velocity u^* [40], $v_*=\tau/\rho$ and $\tau=\rho g R S_0$. δ_v is determined by a theoretical viscous sublayer thickness ($11.6\mu/v_*$ based at the elevation $z = \delta_v$ where the linear velocity distribution intersects with the logarithmic velocity distribution).

properties	series I	series II	series III
v_* [cm/s]	1.0	0.9	1.5
S_0 (*10^{-6})	64.4	6.3	65
δ_v [cm]	1.0	1.1	0.69
z_0 [m]	2.9 *10^{-5}	1.3 *10^{-8}	2.7 *10^{-4}
k_s (*10^{-6} m)	28.6	11.3	821
$v_* k_s/\nu$	0.33	0.11	137
classification	smooth	smooth	rough

Table 4.5: Properties of the measurements carried out in the flume without obstacles

Measurement I and II are carried out at the same location. Consequently, results are similar. The third measurement results in different values. The first two series are measured above the wooden plate while the third one is performed above the part with rougher surface. The value of k_s is larger and a different classification of bottom roughness is obtained. The equivalent bottom roughness k_s is used in engineering classification of the flow.

Next to that, [56, 57] proposes to use a power law instead of the logarithmic profile Eq.(4.32).

$$\overline{v}(z) \quad = \quad v_{max}(\frac{z}{h})^{1/m} \tag{4.32}$$

where m is proposed to be 7. Correlations of 0.933 (I), 0.958 (II) and 0.877 (III) are obtained. The m-value is 7 for the third series, while it is 14.3 for series I and 16.1 for series II. The value for v_{max} is indeed the maximum velocity for series I and II, a lower value is found for series III. Problem with this power method is that properties of the bottom are not easy to obtain while this is rather simple with the logarithmic profile.

All these equations are valid for fully developed 2D flow in channels with large width compared to the water height, then the influence of the side walls is negligible [58, 59]. This is in canals where the width of the channel is 5 to 7 times the water depth in the channel. However, in the lab flume (where a large width would imply a water level of less than 10 cm) the velocity in the upper part of the flow will decrease due to secondary currents [60, 61] caused by the presence of the sidewalls of the flume. So, the maximal velocity will occur under the water surface. This phenomenon occurs close to the walls, while in the center of the flume, the presented logarithmic profile is seen. Corrections of the profile for this dip phenomenon

are proposed in [62–64] (Fig. 4.25).

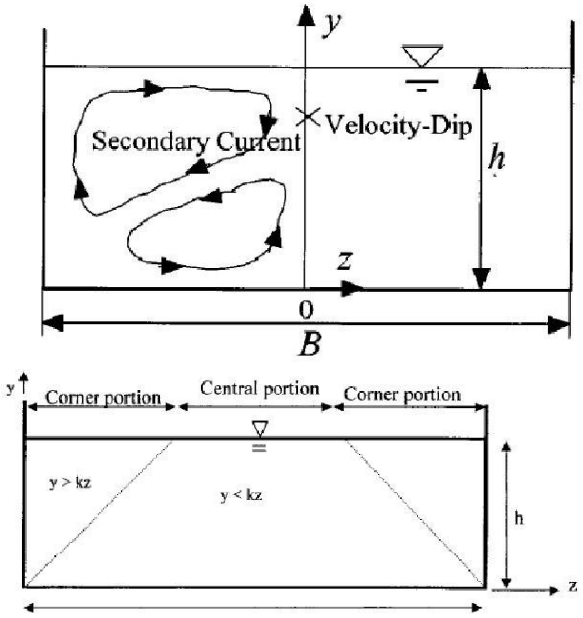

Figure 4.25: Presence of secondary currents in small flumes or canals [63]

Comparing measurement series I, II and III, differences are observed in the outer layer: while the first and second series show a dip-phenomenon near the water surface, the values of the third series are more or less constant. According to [55], the maximum velocity is seen at 0.6h to 0.7h for B = 2.5 h. [63] said that, due to secondary currents (turbulence close to sidewalls), the measured profile differs from the theoretical logarithmic one according ln(1-z/h) with z = distance from the measured point to the water surface. This correction gives good results for the decrease of the velocity closer to the water surface. This is a flume study to get any idea of the effects of floating plants on the water flow, the velocity and the roughness. Lots of effects give indication of the behaviour of floating plants in rivers, but this basic study in the flume is not sufficient. The experiments need performance on a larger scale, in larger flume set-ups and real rivers.

Velocity profiles in the flume with gravel bed Measurements in x, y, and z direction are carried out in the flume with gravel bed (Fig. 4.19 and Fig. 4.20), but only x-values are retained for useful evaluation. Fig. 4.26 shows the result, with A, B, C and D measurement points as indicated on Fig. 4.20.

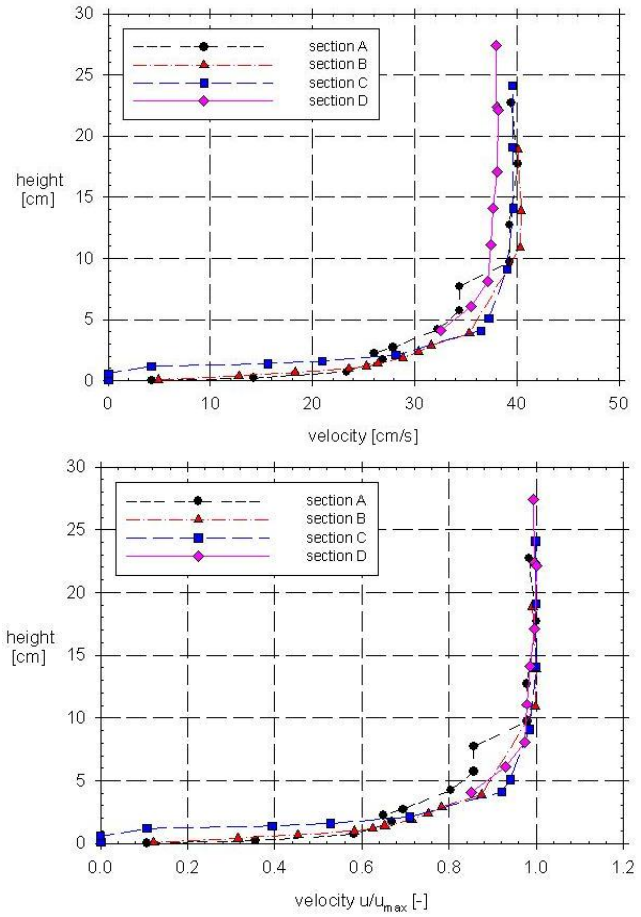

Figure 4.26: Velocity profile in the flume with gravel bed at different locations

Velocity profiles for A, B and C are equal, the maximum velocity for these measurements is respectively 40.1; 40.4 and 39.6 cm/s. Deviations of the profile in D are unexpected because the bottom surface is equal to the bottom in A. The gravel is well incorporated in the bottom surface and so it is unlikely that it will influence the water with consequently higher water levels and lower average velocities before the gravel bed. Probably,

the influence of the small slope was still noticeable.
Comparison of the measurements with gravel bed to the measurements with the flat bottom result in differences in the velocity above the bottom. A flat bottom will only decrease the velocity over a little height while rougher bottoms slow down more water and the velocity only increases slow. This aspect was not clear during the measurements, the increase of the velocity over the water depth is almost equal for each of the points.

To come to a more detailed analysis of the influence of the gravel on the velocity profiles, a logarithmic profile is fitted to the data points ($R^2 > 0.97$) and z_0 and k_s are calculated. The profile at position C is not retained because logarithmic analysis is not possible. The measurement point above the gravel (B) has a k_s of 8 cm, larger than the value for the wooden plate (D), nl. 0.1 mm. The value of 1 cm (little larger than in D) in A is due to the decreasing influence of the gravel part (boundary layer, cf. infra). Analogous conclusions are found for z_0: at position B, the value is 10 times larger than at A, where it is still little higher than at the upstream part of the flume. Fig. 4.15b shows the hyperbolic tangent, the velocity profile of the mixing layer according [50].
Based on the velocity profiles, analysis of the area where the stream velocity is lower than 90 % of the maximum velocity is possible. This value is an indication for the height of the boundary layer according [65]. For points C, D, the height of the mixing layer is 4 cm, at C, the turbulence caused by the gravel bed is fully developed. At point B, the mixing layer is 5.4 cm, while 10 cm is obtained in A. Thus, the layer caused by the gravel bed needs a certain distance to develop and is only fully manifested behind the gravel bed .

Also the Reynolds shear stresses are useful to study the different layers. Reynolds shear stresses and turbulence intensity are plotted in Figure 4.27. The Reynolds shear stress [N/m^2] equals $\rho\ \overline{u'w'}$ according [54] (Eq.4.21). The density is a constant value and is not taken into account in plotting the results in the following. The turbulence intensity I is based on the turbulences in different directions x, y and z: $I = \sqrt{u'^2 + v'^2 + w'^2}$. The turbulences u', v' and w' are an indication of the deviation of the stream flow compared to the average velocity: $u' = u(t) - \overline{u}$ with u(t), the measured velocity, and $\overline{u}$ the average velocity. For a certain time interval the turbulence equals the standard deviation of the velocity: $u' = \sqrt{\overline{u'^2(t)}}$

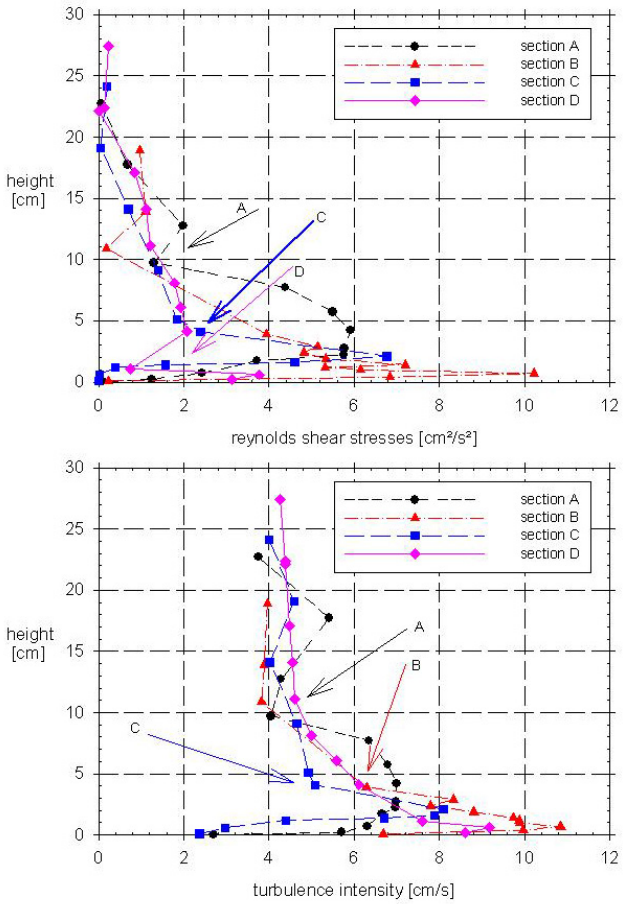

Figure 4.27: Reynolds shear stresses and turbulence intensity in the flume with gravel bed at different locations

The Reynolds shear stresses before the gravel bed are comparable to the values in the 'empty' flume, the value is more or less constant and reaches a maximum just above the bottom. Further, for the measurements above the gravel bed, the height of the peak increases with increasing distance over the gravel bed. The boundary layer is defined as the area where the peak of the Reynolds shear stress switches to a linear path (Fig. 4.28). These values are equal to the ones determined by using the velocity profiles, based on the value of 90 % of the maximum stream velocity. Both definitions define the boundary layer. At Fig. 4.28, the stress distribution due to the rougher bottom, according [66] is plotted, and a boundary layer is formed. The measured Reynolds stresses are smaller than the theoretical distribution.

The profiles are comparable to those measured in this research.

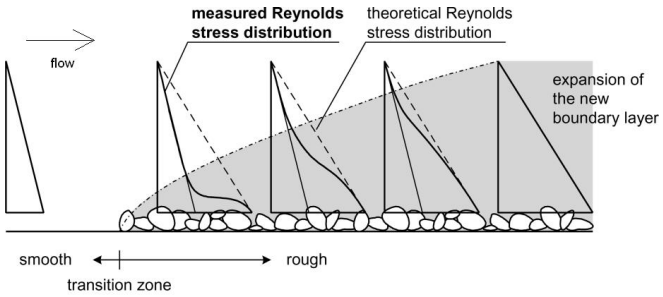

Figure 4.28: Development of the Reynolds stress distribution behind a roughness transition

Velocity profiles in the flume with floating plants Measurements are carried out according the described test series and set-up and results are presented in Fig.4.29.

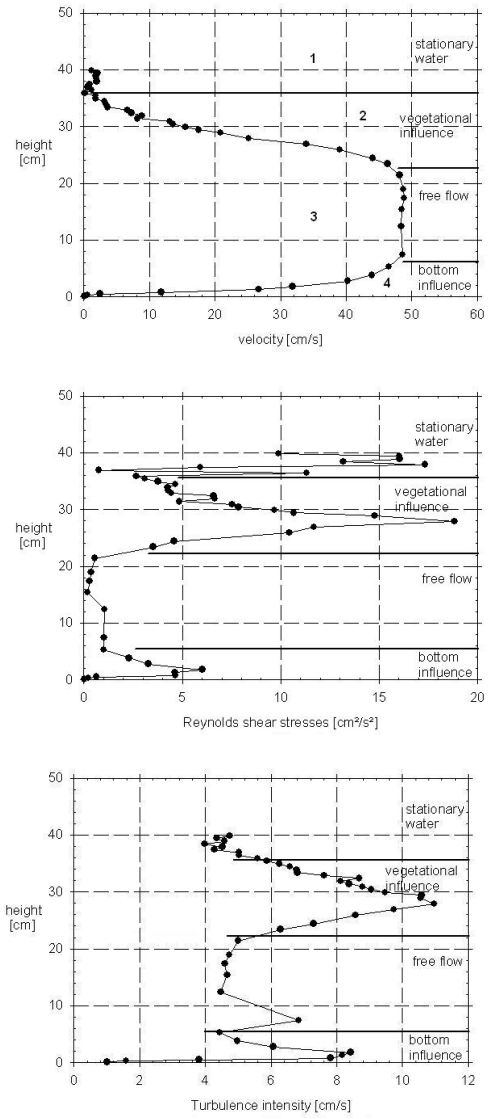

Figure 4.29: Velocity, Reynolds shear stresses and turbulence intensity: results of measurements with floating plants

Fig. 4.29 shows that approximately 4 layers are seen in the flow. In the area of the plants (layer 1), the flow is obstructed and so velocities are very small. Also the area above the plants is influenced by this zone and there, velocities are low. The turbulences are not that clear: the turbulence intensity is small while the Reynolds shear stresses are large. Underneath the plants (layer 2), no obstructions occur and the flow increases, slower or faster depending on the resistance of the plants. In the transitional zone between the area influenced by the plants and the area with free flow, an S-shaped profile is measured. At the bottom of the frame with the plants, a peak of turbulence intensity and Reynolds shear stresses is measured, due to the difference in resistance between the two zones and therefore the difference in stream flow. A large shear stress occurs between the areas with different velocities [50]. This phenomenon is seen in all studies concerning the influence of vegetation, rigid or flexible, on the stream flow [67].
The influence of the bottom is seen (layer 4) and the velocity follows a logarithmic profile. Reynolds shear stresses and the turbulence intensity show a peak. In between (layer 3), there is a free area, not influenced by the vegetation and by the bottom, with constant velocity and low Reynolds shear stresses. In the layer between the floating plants and the free stream flow, one can study the vegetational influence.

In a first phase, the analogy between the velocity close to the bottom and the velocity close to the plants is studied. In both cases, zero velocities are measured (Fig. 4.30). The velocity profile close to the plants also approaches a logarithmic one (with high correlation), however, this is not the best fit.

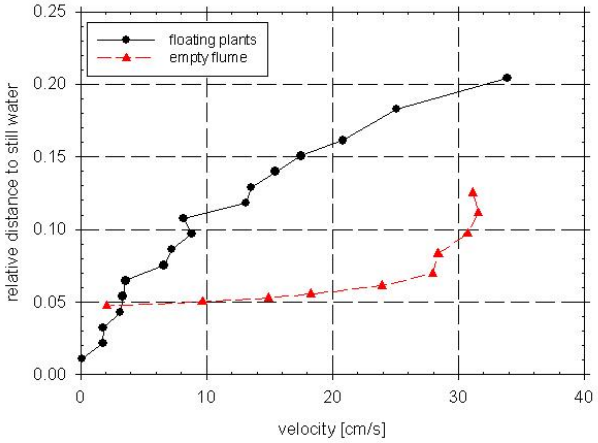

Figure 4.30: Comparison between the velocity close to the bottom and close to the floating plants

The curvature of both profiles is different and the velocity profile in the area between free flow and floating plants shows a S-pattern. It seems that [50, 65] flow obstructed by vegetation patches corresponds not to a boundary layer but to a mixing layer (Fig. 4.31). A mixing layer is a free shear layer (i.e. one where the shear does not arise from boundary conditions) characterized by two regions of constant velocity separated by a confined region of shear containing an inflection point (Fig. 4.15b).

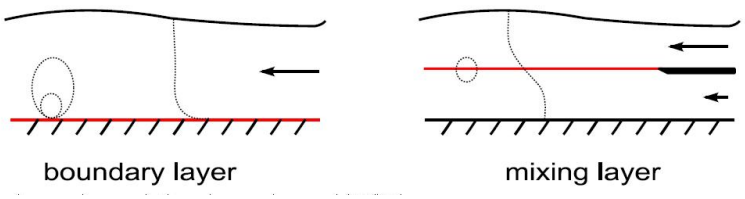

Figure 4.31: Comparison between boundary layer and mixing layer

In case of a mixing layer, the velocity profile is comparable to an S-shape approximated by a tangens hyperbolicus [35, 50] or an arc tangens [68]. Both are comparable, so only the first type is retained.

To fit a theoretical profile, 2 options are considered. The first determines the values of A, B, C and D in u(z) = A + B tanh(Cz+D), (R^2 = 0.995) while the second [50] is based on the velocity profile (v(z) - v_{gem})/Δv = 1/2

tanh(z - z_{gem})/2θ) with tangent lines at constant velocities v_1 and v_2 with $\Delta v = v_2 - v_1$, the difference in velocities, v_{gem} = the average velocity and z_{gem} is the height with $v(z_{gem}) = v_{gem}$. The second equation (R^2 = 0.954) is a theoretical better choice. It is based on 2 flows with constant velocity v_1 and v_2 and inbetween the mixing layer. The last method also allows easier calculation, because no 4-parameter-equation has to be solved and the velocities at each point are not necessary. Comparison is made in Fig. 4.32.

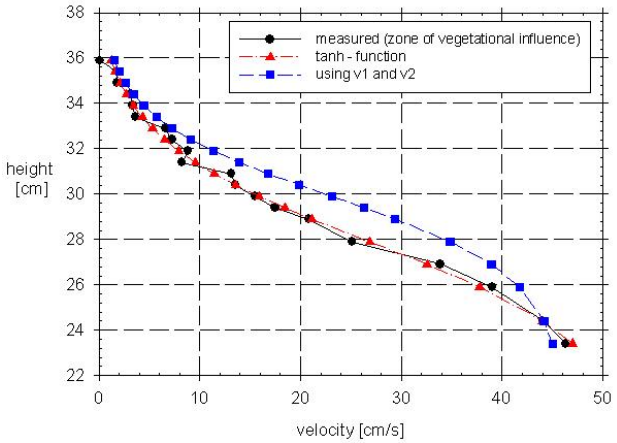

Figure 4.32: Comparison between the measured and theoretical velocity profile in the layer influenced by plants, under the layer where the plants are present

The Monami-phenomenon [50], which is expressed as a kind of waving of plants at the bottom, is also seen for the floating plants. The frames are moving with a period of 2 to 3 seconds and an amplitude of 2 to 3 cm.

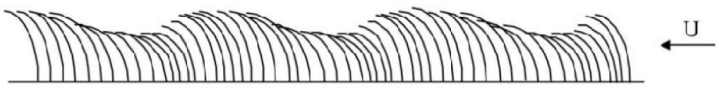

Figure 4.33: Monami effect

This movement has an influence on the measured velocity. Between the two grids, the velocity is zero, but due to the movement of the floating plants, a certain value is measured. To reduce the movements, the frames were fixed to the bottom.

The influence of the position of the plants on the velocity is also interesting in river systems. In natural rivers, mowing patterns are applied to

come to a compromise between ecosystem development and flood protection. According to the previous, velocities are influenced by the pattern of mowing. Therefore, an analysis of the velocity in x, y and z direction is carried out in this lab research. Measurements are performed at 33 points, at 20, 35 and 60 cm from the left side in the areas where no plants were applied and at 35, 45, 60 cm in the vegetated area. For plants equally distributed over the width of the flume, the u' turbulence (x-direction) and v' turbulence (y-direction) is almost equal. Presence of vegetation increases the turbulence with factor 2.5 while the Reynolds stresses are 121 times larger. Also for partially applied plants in the flume, the Reynolds shear stresses are larger (10 times) compared to the 'empty' flume. After the vegetated area, the turbulence is about three times higher, with v' two times larger than u' after the vegetated area. However, measuring the effect of mowing patterns is not possible in this flume because 2D effects will occur: the water is pushed up before the vegetated zones. The lab-flume and its instruments have not the accuracy to measure these small differences. Furthermore, different (also extended) patterns have to be compared which demands for plenty of space and plenty of plants. The study of mowing patterns is described in [69]. [70] describes the effect of mowing on the roughness coefficient.

6 Field measurements

6.1 Data set

Measurements are performed in, especially, the river Aa and, also, Biebrza river and are presented in this section. Further discussion and analysis is presented in Chapter 5.

Field measurements allow study and description of physical processes and provide a data set for calibration and validation of numerical models. Measurements of discharge (Q), water level (Z) and, more limited, electrical conductivity (EC) have been performed for more than 4 years in the river Aa, during regular measurements at monthly intervals and during several intensive campaigns with a duration of 1 week. Discharge measurements in Bierbrza river were carried out annually.

6.1.1 The river Aa

Hydraulic data as water levels and discharges are necessary, but also topographical data of the river bed and banks has to be collected aiming at numerical modelling. Therefore, the study area of the river Aa is monitored. The reach covers 1.4 km and every 50 m, a section is surveyed. So a set of 30 sections is available containing detailed information on the different cross sections and the bottom slope of the river. The cross sections are irregular due to the meandering aspect of the river. The average bottom slope (from upstream to downstream) is 0.0002 m/m. The monitoring results of the cross sections date from 1997.
Several intensive measurement campaigns (April and August 05, February, May and September 06) have been organised to collect hydraulic data (water levels and discharges).
The discharge of the river Aa was also measured monthly upstream and downstream the selected reach since September 04 till April 07. Water levels at the weirs on both sides of the reach are registered continuously by the Hydrological Information Centre (HIC) of Flanders Hydraulics Research by using a limnimeter. Water levels were measured, making use of levelled staff gauges (accuracy 0.5 cm), to calculate the energy slope and to check the influence of the aquatic plant growth on the water stage. Absence of an univocal relation between discharge and water level at a gauge (HIC) is attributed to seasonal changes in the amount of vegetation, quantitatively represented by the biomass, and to the presence of the movable weirs.
Table 4.6 provides an overview of all field measurements that heve been carried out in the river Aa between September 04 and April 07 by the institutions involved in the research.

who	what	where	when
UA	biomass [g/m^2]	upstream (5112'41"N, 450'5"E) - middle (5112'28"N, 449'44"E) - downstream (5112'25"N, 449'9"E)	monthly, from September 04 to April 07 measurement campaigns (2005: April, August - 2006: February, May)
	10 sampling points were randomly selected from a 14 m by 7 m grid and per point the above-ground vegetation was sampled from a circular plot of 0.221 m^2 using a mowing device		
VUB	groundwater	upstream, downstream and 10 points in between	monthly
HIC	water level [m]	upstream weir 4 (0633) - downstream weir 3 (0631)	continuously (2004 - 2007)
	limnimeter measures each 2 min, the average of these values per hour is retained		
UGent	velocity [m/s], water depth [m]	upstream - downstream	monthly and during measurement campaigns
	propellers (Type: OTT, C31 Universal Current Meter) and EM (Type OTT, Nautilus C2000/SENSA Z300 and Valeport, Type 801) gauges)		
UGent	water level [m]	upstream - downstream	monthly and during measurement campaigns
	reading of the levelled gauges		

Table 4.6: Overview of all field measurements that have been carried out in the river Aa between September 04 and April 07 by the institutions involved in the research. The measurement location and measuring instruments are indicated.

6.1.2 Sensitivity analysis of discharge measurements at the river Aa

In the reach of the river Aa, discharges were measured during the period 2004 - 2007 once a month and in 2005 (April, August) and 2006 (February, May, July, September) extended campaigns were organised.

To check the sensitivity of the results to measurement errors, the different discharge measurements are compared. The results are also related to the values obtained by HIC and to the values calculated from the calibration formula of the downstream weir. For the comparison, river characteristics (as the wetted section and the river width) are used as measured.

HIC has registered the water levels upstream and downstream the studied reach from 2004 to 2007. Also the discharge is determined in this area. It should be mentioned that the values of HIC are estimated starting from the measurements in two neighbouring stations and taking into account the surface of the corresponding catchment areas. Due to this approximative determination of these discharges, differences with the values obtained from the measurements of Ghent University are observed. The calibration parameters of the weir allow a more accurate calculation when the position of the weir and the water height over the weir is registered continuously, which was not possible during the reported period. Also, it is important that for a reliable measurement the weir should be kept free from plants.

Table 4.7 presents the results of the discharges measured (Q upstream and Q downstream), their average value, the estimations of HIC and the discharge obtained by using the calibration formula of the weir. Individual deviations are due to differences in determination methods. Largest differences can be remarked in Spring 06, certainly for the values of HIC when compared to the others.

Date	Qupstream	Qdownstream	Qaverage	QHIC downstream	Qcalibration-weir downstream
29/09/2004	0.98	1.02	1.00	1.37	-
28/10/2004	1.47	1.27	1.37	2.13	-
23/11/2004	2.81	3.00	2.91	3.25	2.77
15/12/2004	1.33	1.28	1.31	1.73	1.25
25/01/2005	2.98	3.21	3.10	3.01	2.67
23/02/2005	2.86	3.20	3.03	2.96	3.31
17/03/2005	1.64	1.84	1.74	1.92	1.84
12/04/2005	1.81	1.62	1.72	1.70	1.73
		1.7		1.77	1.73
		1.91		1.71	1.73
13/04/2005	1.69	1.46	1.58	1.69	1.73
14/04/2005	2.74	2.79	2.77	2.88	2.99
		2.89		2.88	2.99
10/05/2005	2.45	2.42	2.44	2.58	-
23/05/2005	1.42	1.18	1.30	1.06	1.25
23/06/2005	0.69	0.60	0.65	0.52	0.52
14/07/2005	1.06	0.94	1.00	1.13	1.36
22/08/2005	0.72	0.73	0.73	1.00	0.60
	0.72	0.77	0.75	0.98	0.60
23/08/2005	0.68	0.77	0.73	1.00	0.68
23/08/2005	0.80	0.79	0.8	1.01	0.68
24/08/2005	0.69	0.80	0.75	1.10	0.60
24/08/2005	0.78	0.84	0.81	1.09	0.68
25/08/2005	0.84	0.82	0.83	1.11	0.60
25/08/2005	0.91	0.87	0.89	1.11	0.59
26/08/2005	1.47	1.46	1.47	2.34	1.13
		1.44			1.13
28/09/2005	1.05	0.99	1.02	1.37	0.94
26/10/2005	1.20	1.26	1.23	1.32	1.60
30/11/2005	2.18	1.99	2.09	2.02	2.11
21/12/2005	1.80	1.86	1.83	1.81	2.53
11/01/2006	1.28	1.44	1.36	1.18	1.60
07/02/2006	1.24	1.35	1.30	0.89	2.39
07/02/2006	1.32	1.15	1.24	0.89	2.39
	1.47			0.88	-
08/02/2006	2.17	2.13	2.15	1.29	2.83
	2.84	2.99	2.82	1.89	2.83
	2.59			1.53	-
09/02/2006	2.61	2.67	2.64	1.92	2.39
		2.64		1.63	
		2.37		1.63	
15/03/2006	2.56	2.63	2.60	1.60	2.67
19/04/2006	1.97	1.95	1.96	1.25	1.98
15/05/2006	0.85	0.99	0.92	0.70	0.94
16/05/2006	0.82	1.01	0.92	0.73	0.94
17/05/2006	1.16	1.00	1.08	0.83	1.04
17/05/2006	1.03	1.14	1.09	0.85	1.04
18/05/2006	1.07	1.16	1.12	0.90	1.25
	1.08			0.93	-
05/07/2006	0.64	0.66	0.65	0.64	0.52
06/07/2006	0.69	0.72	0.71	0.90	0.52
26/09/2006	0.90	0.95	0.93	0.79	0.76
28/09/2006	1.11	0.89	1	0.79	1.05
18/10/2006	0.89	0.92	0.91	0.81	1.15
09/11/2006	0.96	0.97	0.97	0.83	1.36
06/12/2006	3.08	2.91	3.00	2.74	3.96
25/01/2007	2.82	2.89	2.86	2.95	3.45
22/02/2007	2.71	2.66	2.69	2.62	3.43
30/04/2007	0.79	0.89	0.84	0.77	0.94

Table 4.7: Comparison of the results of the discharge measurements [m^3/s] upstream and downstream the studied reach for the period from September 07 to April 04

In Fig. 4.34, discharges determined according different methods are plotted together. Values for each period are comparable. Deviations are seen for October 05 and Spring 06 where HIC calculates respectively higher and lower values. For Winter 06-07, the values determined with the calibration formula of the downstream weir are higher then expected.

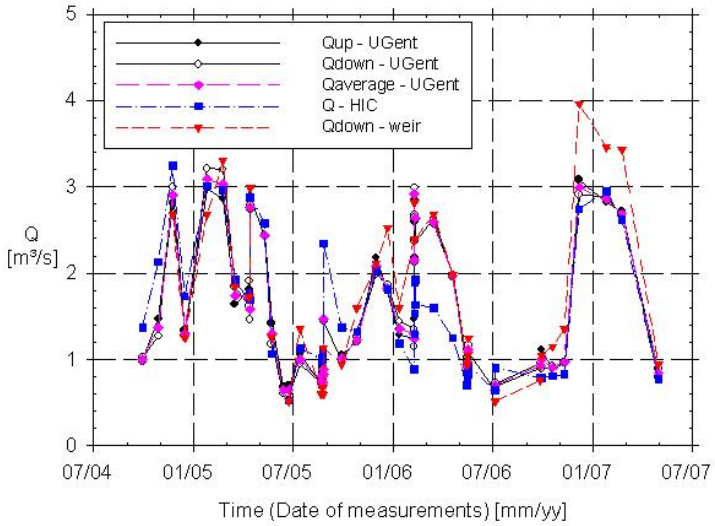

Figure 4.34: Comparison of the discharges determined according different methods upstream and downstream the studied reach for the period from September 07 to April 04

Next to the comparison of the discharge at monthly intervals, during the measurement campaigns, discharges were measured repetitively in the same sections with different instruments and at the same day (Table 4.8). As can be seen from the measurements of Ghent University (Qmeas), only small deviations occur while measuring in the same section. Also when different measurement instruments are used, the results are comparable. Exception is made for the use of propellers in periods with a wealthy plant growth (cf. infra, Chapter 5, 2.4.2). Remarkable is also that the results for the discharge determined by HIC are higher in 2005 and lower in 2006, with a similar offset value.

Date	Time	Instrument	Qmeas	QHIC	Qcalibration-weir
12/04/2005 downstream	10:30 - 11:21	A106202	1.70	1.77	-
	13:35 - 15:30	A67619	1.62	1.70	1.73
	15:45 - 17:00	Valeport	1.91	1.71	-
14/04/2005 downstream	11:20 - 12:45	Valeport	2.79	2.88	-
	13:15 - 14:20	Valeport	2.89	2.88	-
22/08/2005 downstream	11:45 - 13:10	Valeport	0.73	1.00	-
	15:40 - 17:00	Valeport	0.77	0.98	-
23/08/2005 upstream	10:15 - 12:10	A106202	0.68	1.00	-
	13:35 - 15:10	Valeport	0.80	1.01	-
23/08/2005 downstream	09:45 - 11:50	Valeport	0.77	1.01	0.68
	13:32 - 15:20	A106202	0.79	1.01	-
24/08/2005 upstream	09:25 - 11:20	A106202	0.69	1.10	-
	12:15 - 13:40	Valeport	0.78	1.09	-
07/02/2006 upstream	11:10 - 12:05	A106202	1.24	0.89	-
	12:20 - 13:25	Valeport	1.32	0.89	-
	09:50 - 11:30	Valeport	1.47	0.88	-
08/02/2006 upstream	09:10 - 10:15	Valeport	2.17	1.29	-
	11:20 - 12:48	A106202	2.84	1.89	-
	09:50 - 11:30	Valeport	2.59	1.53	-
08/02/2006 downstream	09:30 - 11:00	A106202	2.13	1.40	2.82
	12:00 - 13:15	Valeport	2.99	2.03	-
09/02/2006 downstream	10:40 - 11:45	A106202	2.64	1.63	1.73
	10:45 - 11:45	Valeport	2.37	1.63	-
16/05/2006 upstream	10:15 - 11:35	Valeport	0.93	0.73	-
	12:36 - 13:30	OTT	0.82	0.72	-
16/05/2006 downstream	11:41 - 13:30	Valeport	1.02	0.72	0.94
	10:16 - 11:50	OTT	1.01	0.73	-
17/05/2006 upstream	09:30 - 10:30	Valeport	1.16	0.83	-
	10:40 - 11:35	Valeport	1.03	0.85	-
17/05/2006 downstream	09:30 - 10:55	OTT	1.00	0.83	1.04
	11:20 - 12:25	OTT	1.14	0.89	-
18/05/2006 upstream	09:21 - 10:25	OTT	1.07	0.90	-
	10:30 - 11:15	OTT	1.08	0.93	-
26/09/2006 downstream	09:05 - 10:29	Valeport	0.88	0.79	-
	9:10 - 10:04	OTT	0.95	0.79	0.76
28/09/2006 downstream	09:00 - 10:12	Valeport	0.89	0.76	1.05
	11:15 - 12:06	Valeport	0.95	0.765	-

Table 4.8: Comparison of the results of the discharge measurements [m^3/s], at the same place and on the same day

In April 05, some measurements were carried out using the ADCP (Streampro). Measurements are performed in the downstream end of the river Aa, near weir 4. The measured values are mentioned in Table 4.9 and further compared in the following section.

Date	Time u	Q m^3/s
12/04/2005	14:40-15:45	1.259
14/04/2005	12:00-12:40	2.631
14/04/2005	13:50-14:30	2.551

Table 4.9: Discharges measured downstream of the river Aa, registered by the ADCP in April 05

6.1.3 The Biebrza river

In the Biebrza river, measurements have been carried out each year in Spring. The campaigns started in 1999 and are still going on. Specific measurement points on the river are selected as is indicated on Figure 4.35. A substantial contribution of the tributaries to the total discharge in the river and the importance of the groundwater inflow between the tributaries becomes clear. Table 4.10 shows all discharge measurements over the years in the river Biebrza.

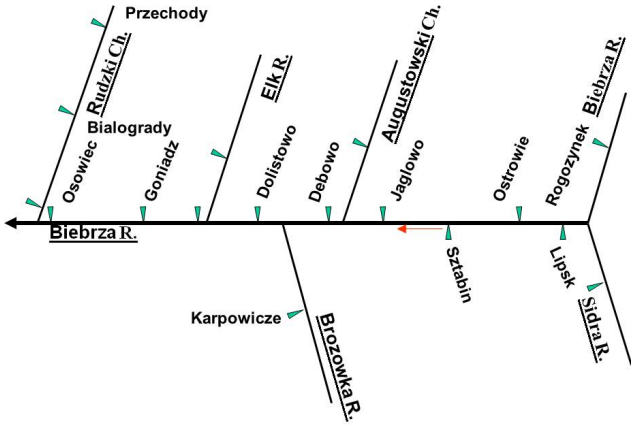

Figure 4.35: Study area of the Biebrza river, Poland: schematic view, with indication of the location of the measuring points

	Location	1999	2000	2001	2002	2003	2004	2005	2006	2007	2008
1	Rudzki Ch. - Przechody	4.40	7.00	10.52	5.17	9.15	-	12.60	3.08	3.51	4.65
2	Rudzki Ch. - Bialogrady	-	6.88	10.48	6.04	8.58	-	13.12	3.87	-	-
3	Rudzki Ch. - Osowiec	3.60	6.88	10.78	-	7.18	-	13.85	-	3.33	4.26
4	Bierbza R. - Osowiec	5.12	9.17	15.85	5.39	18.10	17.08	26.26	4.55	7.18	4.87
5	Bierbza R. - Goniadz	5.83	8.06	10.00	5.47	16.57	15.45	19.20	4.13	6.24	5.01
6	Elk R.	-	-	5.00	0.17	2.67	-	-	-	-	-
7	Bierbza R. - Dolistowo	5.40	5.98	9.56	4.23	13.63	10.50	15.67	2.84	5.28	3.30
8	Brozowka R. - Karpowicze	0.81	0.91	1.41	0.61	1.90	1.14	1.26	0.60	0.80	0.95
9	Bierbza R. - Debowo	4.65	3.94	7.80	3.88	10.77	10.20	12.46	1.70	4.34	3.31
10	Augustowski Ch.	-	3.43	5.52	2.94	6.14	-	-	-	-	-
11	Bierbza R. - Jaglowo	1.15	1.33	1.81	1.00	3.48	2.59	6.30	1.45	1.08	1.14
12	Bierbza R. - Sztabin	1.40	1.15	0.89	0.38	3.04	2.30	3.09	0.70	0.97	0.86
13	Bierbza R. - Ostrowie	0.78	0.86	1.09	0.54	2.36	2.35	2.57	0.60	0.95	0.80
14	Bierbza R. - Lipsk	1.05	0.89	1.01	0.49	1.79	3.04	1.35	0.74	0.82	1.28
15	Bierbza R. - Rogozynek	-	0.24	0.98	0.14	0.52	0.46	0.38	0.21	0.22	0.34
16	Sidra R.	-	0.24	-	0.14	0.85	4.51	-	-	-	-

Table 4.10: Discharge measurement from 1999 to 2008 (Q [m^3/s]) in the study area of the Biebrza river

The tabulated values are presented in Fig. 4.36 and Fig. 4.37, for discharges and water levels.

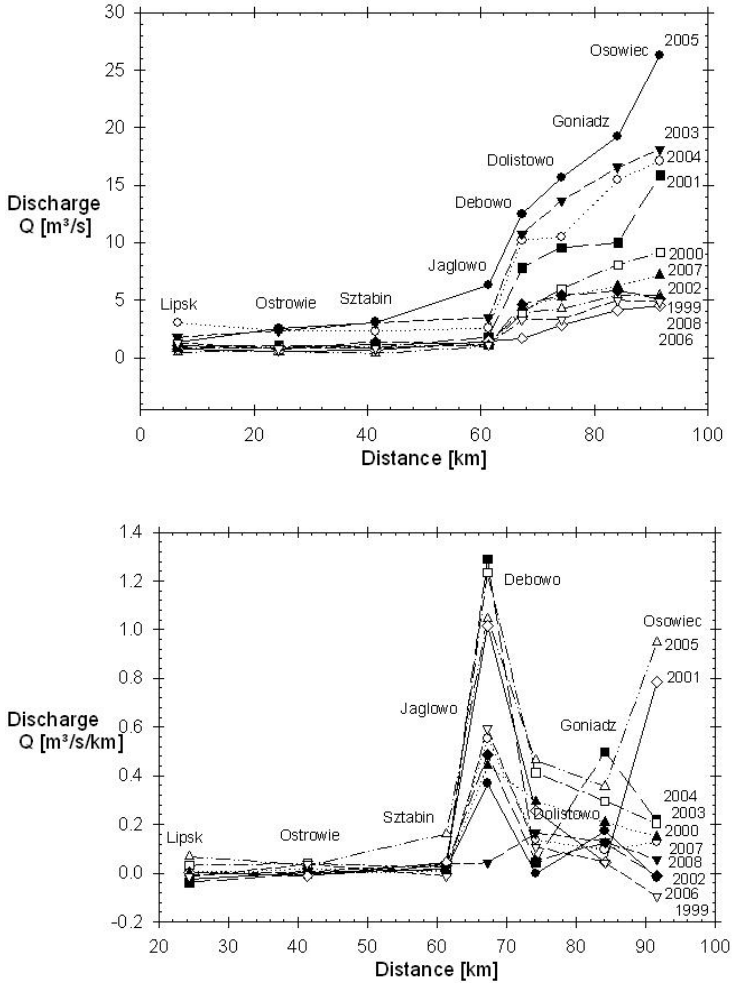

Figure 4.36: Overview of the discharges in the study area of the Biebrza river of Table 4.10 and Fig. 4.35. Fig. 4.36a (top) shows the accumulating discharge over the reach. Fig. 4.36b (bottom) shows the discharge added each km.

Fig. 4.36a depicts the measured discharges from upstream to downstream for each measurement campaign in the period 1999 to 2008. Lowest discharges were measured in 2006. Highest values were seen in 2005, when, in Osowiec, discharges up to 26 m^3/s are measured, 6 times higher

than the values occuring one year later. Between Jaglowo and Debowo, the discharge increases the most due to the inflow from Augustowski Channel. Fig. 4.36b shows the discharge added each km, the increasing discharge between Jaglowo and Debowo is clear. The water levels (Fig. 4.37a) vary between 118.5 m upstream and 108 m downstream, while depth's vary between 0.5 m upstream and 1.5 m downstream. Highest water levels correspond with higher discharges.

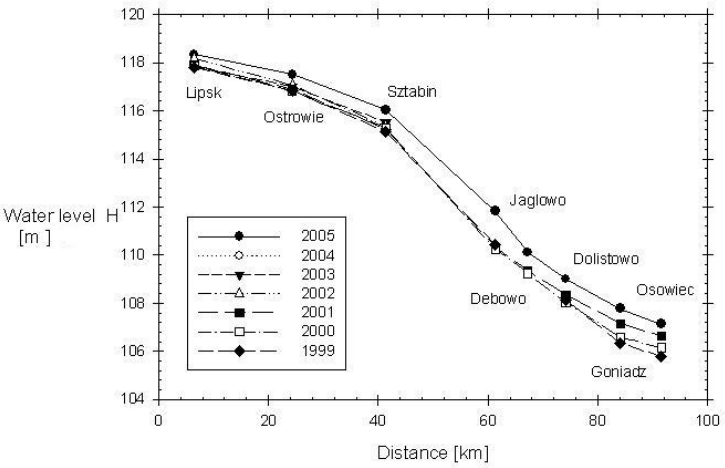

Figure 4.37: Overview of the water levels in the study area of the Biebrza river in the reach of Fig. 4.35 over the years

Next to the discharge measurements at the mentioned locations, biomass and discharge measurements are also performed in the reach between Rogozyn and Rogozynek, to measure the influence of the vegetation. This reach is found upstream Lipsk, at the Biebrza River (Fig. 4.35). Results are shown in chapter 5 and indicate that there is no need to cut the vegetation for measuring discharges when using electromagnetic devices.

6.2 Measurements using the calibrated weir

The Flemish Government (Afdeling Water, VMM) is responsible for the control of the 4 weirs on the river Aa. Weir 3 and weir 4 are respectively the upstream and downstream edge of the studied reach. The control is based on the ultrasonic measurement of the water level upstream the weir. The position of the weirs changes following five zones around the target or reference level. For weir 3 this level equals 11.55 m, while 10.20 m is

the reference level for weir 4. The high water situation is obtained for water levels 20 cm above this reference level. The zones for weir control are indicated as follows:

- dead zone: the measured water level is found between reference level - 3 cm and reference level + 3 cm. Then, the position of the weir does not change.
- zone of discontinuous rise: the water level is found between the dead zone and 5 cm lower than the reference level. The flap rises discontinuously (3s rise, 27 s rest).
- zone of continuous rise: water level is lower than 5 cm lower than the reference level. The flap rises continuously.
- zone of discontinuous decrease: the water level is found between the dead zone and 5 cm higher than the reference level. The flap comes down discontinuously (3s decrease, 27 s rest).
- zone of continuous decrease: water level is higher than 5 cm higher than the reference level. The flap comes down continuously.

Water levels were measured downstream of weir 3 and up- and downstream of weir 4. Using the water levels H [m] downstream weir 4 and a calibration table [71]), the discharge Q [m^3/s] is calculated at the location downstream weir 4 according $Q = a_0 + a_1H + a_2H^2 + a_3H^3$. This formula was working well until the amount of macrophytes started to increase rapidly over the years. Downstream weir 4, in winter period, the stream flow is not obstructed by vegetation and the calibration relation is still valid. Between weir 3 and weir 4, calibration relations are more difficult to set up and to use due to the varying amount of vegetation in the river.
As a consequence, to obtain discharges between weir 3 and weir 4, a measurement of the velocity is necessary, the water level seems not to be sufficient for determining discharges.
Another possibility, a relation $Q = f(H_{weir})$ as a function of curves H_{weir3} - H_{weir4} is only possible in non-vegetated areas. Here is H_{weir3}, the water level at weir 3 and H_{weir4}, the water level at weir 4.
The position of the flap of the weir is not registered and therefore, discharges cannot be determined based on the calibration formula of the weir (see Chapter 4, 2.3).
Here, to have a good indication of the discharge in Poederlee, HIC based its results on the discharge of Grobbendonk, which is more or less the sum of

the discharge at Poederlee (Aa, 20 to 30 %) and the discharge of Herentals (Kleine Nete).

The discharge over the weir, calculated with the weir equation is compared with the measured discharges at weir 4 using the propellers, the electromagnetic devices and the tracers. The calibration of the weir is only carried out for specific positions. However, looking at Fig. D.2, linear interpolation of the values in between is acceptable and will not introduce significant errors.
During the 4 years of this study, the discharges are measured monthly upstream and downstream of the reach. At the same time, also the thickness of the waterlayer overflowing weir 4 is measured. Then, the calibration formula is used and the discharge is determined in a second way. The values are compared in Fig. 4.38.

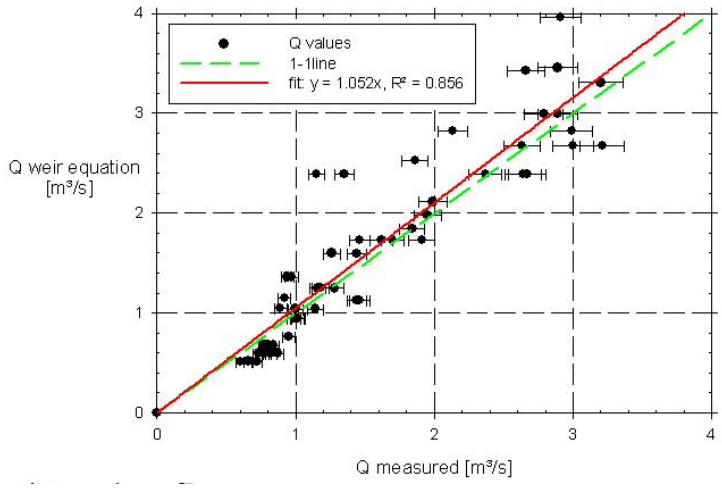

Figure 4.38: Comparison between measured discharges and calculated discharges based on the weir equation. Deviations of 5 % on the measured discharge values are indicated by the horizontal error bars. The linear regression line is shown in red and the 1:1 line is shown in green.

Fig. 4.38 shows the correspondance between the discharge measurements at the downstream weir (comparison with upstream discharges is not useful) and the discharge calculated out of weir calibration. It is seen that the agreement is very good for a wide range of discharges. This result allows to come to an easier way in calculating discharges in the river Aa. A good maintenance of the weir and registration of the water height over

the weir crest and the position of the weir crest allows a fast and easy way for determining the discharge, using the calibration formula.

Determining the discharge by using the calibration formula introduces errors at two points. First, errors can be found in the calibration formula itself. However, an accuracy up to 1 % is found [72]. Second, measurement errors are limited when determining the crest level and the water height over the crest by reading the leveling gauge. The position of the weir is not registered, so the levels are measured with an accuracy up to 0.5 cm. Both mentioned errors are small and negligible. To check the influence of measurement errors, a comparison is made of the results for higher and lower water heights over the weir crest. First, the water level is overestimated (1 cm), second, the water level is seen as lower (- 1 cm). The discharge is calculated using the calibration formula. The results are plotted in Fig. 4.39 A systematic error on the gauge reading will introduce deviations from the original result from 2 to 10 %. Errors up to 5 cm would lead to deviations from 26 to 40 %.

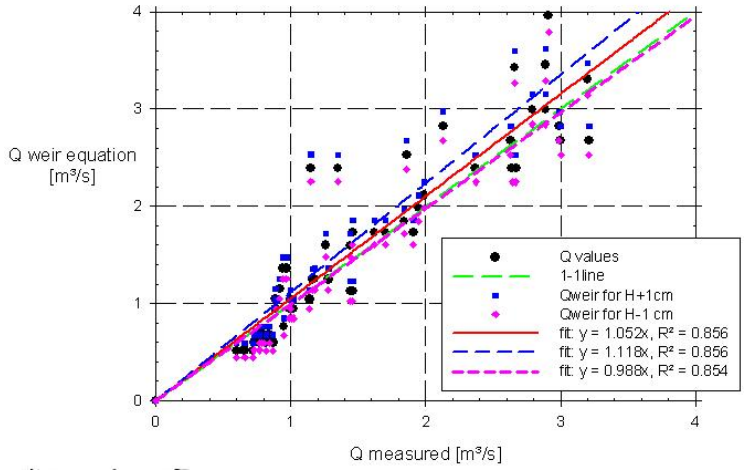

Figure 4.39: Incorporation of a reading error of 1 cm on the gauge to determine the water height over the weir, an overestimation (+1 cm) and an underestimation (-1 cm) are studied

6.3 Continuous discharge measurement

During the measurement campaign in April 05, a hydrometric propeller has been installed for three days on a fixed location in the downstream end of the river reach. So, continuous velocity measurements ('velocity measurements') were carried out. In the same period, discontinuous discharge measurements are performed in the same section for calibration. With this velocity and compared to the velocities at the same place during the discontinuous discharge measurements, a value for the continuous discharge can be determined. Fig. 4.40 shows the result of the continuous propeller measurements (velocities) and the continuous discharges ('continuous discharges') based on the discontinuous discharge values. The discontinuous discharge measurements ('triangels') are carried out in the neighbourhood of the downstream weir (weir 4) on April 12th (1.62 m^3/s), April 13th (1.46 m^3/s), April 14th (2.79 m^3/s) and April 14th (2.89 m^3/s). Also some ADCP results ('dots') and the values presented by HIC ('discharges HIC') are added. As can be seen, the increase in discharge on April 14th is clearly registered, due to heavy rainfall during the night.

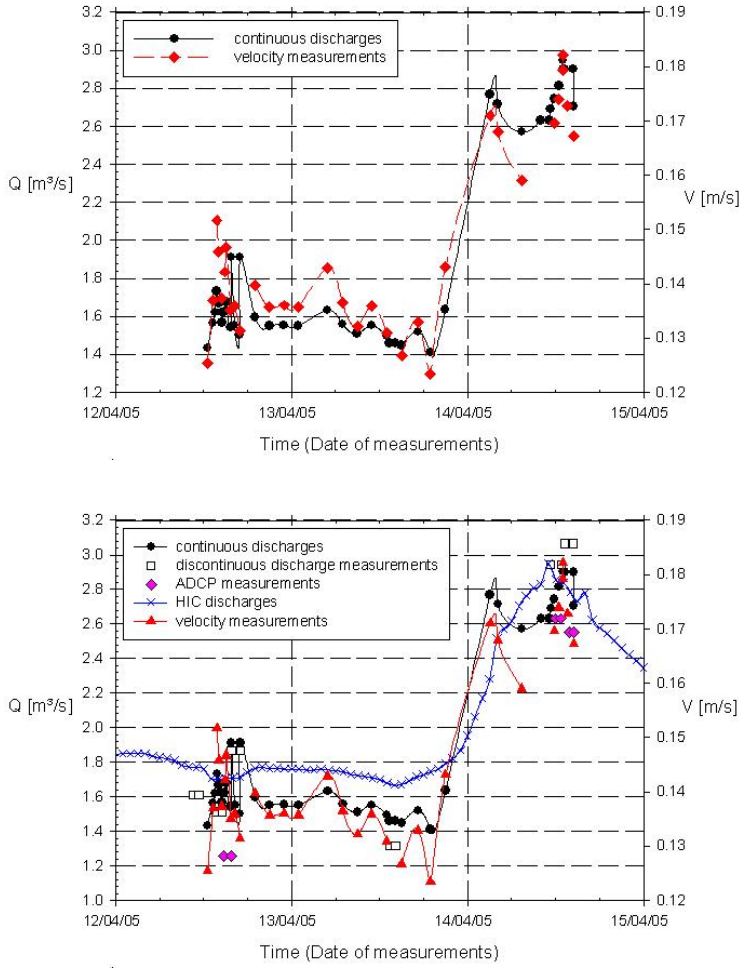

Figure 4.40: Continuous downstream discharge measurement during the measurement campaign (April 12th to April 14th). Measured values with the fixed propeller and corrected values based on the particular measurements.

It is checked whether it is possible to deliver accurate continuous discharge measurements with the fixed propeller. The propeller measures velocities in 1 point from which the discharge over the cross-section has to be determined. Therefore, the measured values for the velocity are corrected using the discrete discharge determinations in the downstream section.

The position of the propeller was based on the discontinuous discharge

measurements in that section. Out of all the results, the vertical and the water depth were selected where the average velocity was found. With that velocity and knowledge of the wetted cross section, the discharge can be calculated. Difficulty is to find the right combination between the velocity in that fixed point and the wetted cross section, which depend on the geometry and the bottom. Discontinuous discharge measurements deliver a number of calibration points (A = 9.5 m^2 for Q = 1.70 m^3/s and A = 10.9 m^2 for Q = 1.91 m^3/s), but a correct determination of the location where to install the fixed propeller meter is difficult due to presence of vegetation, sedimentation and erosion, geometry of the section, etc. After all, the wetted cross section increases if the discharge increases. An option is to set up a table or graph with the combination velocity - wetted cross section derived from the discontinuous discharge calculation. Therefore, a lot of measurements have to be carried out for different discharge situations. Further more, this relation will be different for summer and winter situations in vegetated rivers.
For the determination of the location for the continuous measurement use is made of the theoretical, logaritmic Prandtl Von Karman profile, where the average velocity is found at 0.37 times the water depth. This is about the position of the fixed propeller at the beginning of the measurements (April 12th). On April 14th, a peak flow is measured together with a water level rise of 11 cm. In this situation the velocities are registered at a depth which is lower than the depth corresponding with average velocities. So, the water level rise of about 10 % includes a correction on the calculation of the discharge, by correcting the registered velocity.

From Figure 4.40, it can be seen that using a fixed velocity measurement instrument leads to a good indication for the discharge if discontinuous discharge measurements are used to correct the velocity measurements. The curve obtained from HIC gives higher discharge values which is normal as the calculation by HIC is only approximative. This can be due to the estimations as done by HIC introduce deviations.

6.4 Measurement of a flood wave

Next to intensive discharge measurements upstream and downstream the selected reach of the river Aa, also a dynamic measurement was carried out. Therefore, the upstream weir was put in a fixed position to retain the water. After a certain period, the flap of the weir was lowered and a large amount of water flew into the river. This experiment was carried out on the 18th of May 2006, between 12:00u and 14:00u. Discharges were measured upstream (1.07 m^3/s between 9:20u and 10:25u) and downstream (1.16 m^3/s between 9:25 u and 11:20 u) before the experiment was performed. During the period of the measurement, Flanders Hydraulics Lab determined a series of water levels and discharges (12u: 0.953 m^3/s, 13u: 1.132 m^3/s, 14u: 1.154 m^3/s) (Table 4.11).

Date	Time	Q	$H_{upstream}$	$H_{downstream}$
	u	m^3/s	m	m
18/05/2006	12	0.953	10.660	10.240
18/05/2006	13	1.132	10.616	10.268
18/05/2006	14	1.154	10.624	10.206

Table 4.11: Discharges and upstream and downstream water levels in the river Aa measured by HIC

Divers are placed at different positions along the reach to measure the variation of the water height during the passing of the wave. Four pressure meters are installed at distances 207.7 m (12) (upstream), 726.9 m (7), 1038.5 m (4) and 1350 m (1) (downstream). During the test, the water levels were measured using the gauges upstream and downstream, so six levels over the reach are registered. Further, the velocities were measured upstream and downstream in one point of the section. Upstream, velocities were measured with an electromagnetic velocity instrument (OTT). Due to the huge amount of water, a lot of plants were moving together with the water flow and the propeller had to be removed. Downstream, a hydrometric propeller was installed in the section (middle of the section), while the velocities were also measured with an electromagnetic device (Valeport) (middle of the right flap of the weir).

Fig. 4.41 presents the height of the wave in different locations during the experiment. The water depth is not included. The registration by the divers caused no problem, the reading off the gauge (upstream and downstream level) was sometimes difficult due to the fast rise of the water. The large amount of water in a short time caused problems with the manual reading, especially for the upstream gauge, and therefore, some deviation

can be remarked. The downstream diver was placed near the downstream gauge, so differences are only small. Registrations by HIC are not useful, they are only available at the upstream weir and sampling is only performed each 15 minutes. This value is the average water level of the last 15 minutes. Only two registration points are available during the passing of the wave and only one of them is found in the range of the peak.

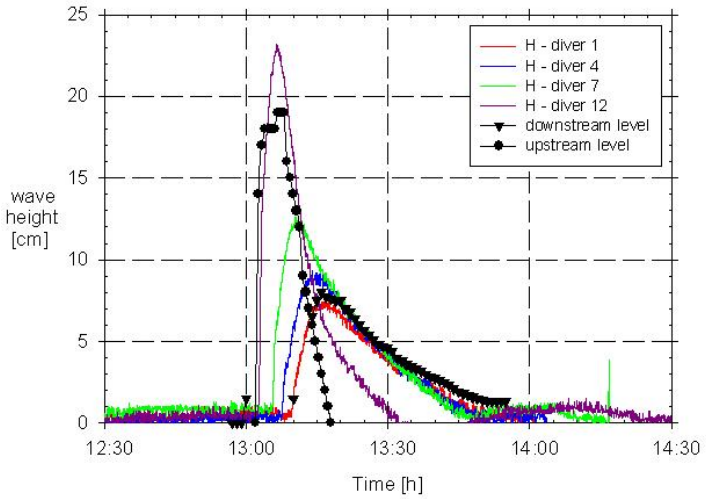

Figure 4.41: Water level measurements during the passing of the wave over the entire reach of the river Aa

Also the velocities were registered during the test and results are depicted in Fig. 4.42.

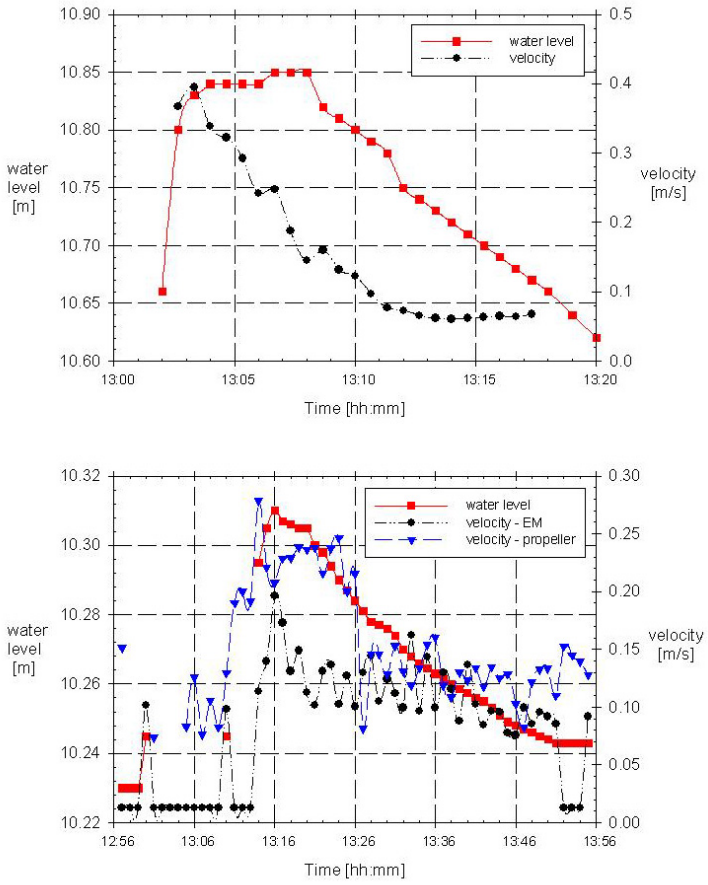

Figure 4.42: Water level and velocity measurements at the upstream weir (top) and downstream weir (bottom) in the river Aa

At the upstream weir, the velocity is measured by an electromagnetic velocity meter (OTT) in 1 point at 1/3 of the width, starting from the left bank and at 2/3 of the initial water level. Velocity and water level follow the same path. Based on the wetted cross section which is measured during the discharge measurements earlier that day (A = 15.8 m^2), the discharge is estimated and results vary from 6 m^3/s during the peak of the wave to 1 m^3/s after the wave passes (at 13:15u). This last value agrees with the values measured a couple of hours before and with the values estimated by HIC.
At the downstream weir, the velocity is measured by a propeller and by

using an electromagnetic velocity meter (Valeport). The propeller is positioned at 4.5 m of the left bank, which is close to the pillar inbetween the two flaps of the weir. The electromagnetic meter is positioned at 3/4 of the width of the river, starting from the left bank. The velocity measurements follow the water level. For the lowest values of the velocity, measurements obtained by propeller and by the electromagnetic meter result in similar values. For the peak of the wave, the propeller registrates higher velocities. This is due to the different position of the two instruments. For higher velocities, the influence of the pillar is probably more important.

6.5 Biomass measurements

The Ecosystem Management Reasearch Group of the University of Antwerp measured the biomass in the studied reach of the river Aa. The biomass, is the amount of vegetation in the channel and is expressed in g/m^2, which means the amount of vegetation for each m^2 of the river bottom. However, for calculation of blockage effects (cf. infra) caused by biomass, the amount of vegetation per volume is probably more significant. Therefore, the water depth is also taken into account. Aquatic macrophytes are growing all over this river, reaching biomass densities up to 0.5 kg dry weight per m^2. The aquatic vegetation in the river Aa includes mainly submerged and floating plants, although some emergent species can be found as well. The most common species are *Callitriche platycarpa* Ktz., *Ceratophyllum demersum* L., *Elodea nuttalli* (Planch) St John, *Sparganium emersum* Rehm., *Stucenia pectinatus* L., *Potamogeton natans* L., *Rorippa amphibia* (L.) Besser and *Sagittaria sagittifolia* L. (Fig. 4.43).

Figure 4.43: Sparganium emersum Rehm., Potamogeton natans L., Callitriche platycarpa Ktz.

The evolution of macrophyte biomass density in the study area was

monitored by quantitative sampling on a monthly base. Samples collected at three locations along the river reach: upstream, in the middle and downstream. At each location 10 sampling points were randomly selected from a 14 m by 7 m grid and per point the aboveground vegetation was sampled from a circular plot of 0.221 m^2 using a mowing device [32]. This instrument has no moving parts, its primary components are a cutting blade fixed to the base of a vertical shaft to shear off plant stems at the substrate surface, and a collection rake to allow retrieval of the freed vegetation. The sampler is well suited for the measurements in this study, because a large variety of macrophytes over a range of conditions can be sampled. Also, the instrument is lightweight and easily handled. The fresh vegetation samples were stored in plastic bags and transported to the lab for cleaning (removing debris and mud) and sorting. Finally, all fresh samples were weighed, dried at 70 °C and weighed again. Based on fresh and dry weight values the fresh and dry macrophyte biomass density [g/m^2] could be assessed.

The most common problem when sampling biomass is the heterogeneity of the vegetation. A large spreading on the data through the river is found and even large differences on the samples of the same cross section are remarked. The heterogeneity is largest in spring and autum with empty verticals and verticals with a rather large amount of vegetation in the same section. A larger sampling area of the instrument will reduce the uncertainty and the spreading on the results [73].

7 Conclusions

The quality and accuracy of a numerical model strongly depends on the data available to build and to calibrate the model. Therefore, regular measurement campaigns are an important tool.

Hydraulic measurements are performed in the laboratory flume and in the field. Measuring materials and methods are explained in detail. According to the scope of the research, one measurement instrument is more useful than another. Measurements in the lab differ from those in the field, due to the controlled conditions. Also the accuracy will be varying. Continuous registrations can give information over a longer time period in contrast to discontinuous ones. Next to surface water measurements, also geometrical characteristics and the presence of vegetation has to be taken into account. HIC registers, in a rather continuous way, water levels and calculates discharges, however, the velocity measurements performed by Ghent University are useful in the integrated view which considers groundwater

influence and vegetation interaction.

These traditional techniques are not all easy to use to measure flow velocities through vegetation. Hydrometric propellers can be fouled in vegetation. For acoustic devices, the vegetation interferes with the backscatter signal and an electromagnetic velocity meter may have an impact on the environment due to its size.

The ADCP, based on the Doppler technology, allows a faster sampling in sections without in-stream vegetation. Next to the measurement of characteristics of the section and the velocity, an estimation of the discharge is carried out. Although this instrument is an interesting tool, it is rather expensive when compared to the propellers and electromagnetic devices.

An overview of all measurement instruments is given in Table 4.1. The range, accuracy, resolution and measurement technique is mentioned.

From the continuous discharge measurements, it can be seen that all devices are useful for measurements. Due to the presence of vegetation, HIC prefers an estimated discharge which can slightly differ from other values. For lab measurements, all mentioned devices are useful due to the rather 'perfect' conditions. Instruments to perform measurements on the field are determined by the environmental conditions as the presence of vegetation (the propellers), the velocity in the river (range of the instrument), etc.

In the flume of the Hydraulics Laboratory, it is shown that the presence of vegetation disturbs the theoretical logarithmic velocity profile over the water height. A theoretical analysis is described and a wide range of measurements are performed to study stream patterns in and around vegetation and specific attention is paid to the behaviour of floating vegetation.

The flow velocity in the flume is measured with the ADV. For the range of the measurements, this technique delivers accurate values. Eliminating noise was necessary to determine turbulence and Reynolds shear stresses. The x, y and z-velocity was determined in different points. The velocity profile over the depth was measured in three situations: a flume without obstacles, a flume with gravel bottom and a flume with floating plants.

Measurements of the velocity profile in the flume without obstacles show a good agreement with the theoretically derived log-profile. By fitting this profile to the raw data, it is possible to obtain both v* (friction

velocity, m/s) and z_0 (height where the velocity is zero, m). The latter can be converted to k_s, the equivalent grain roughness (m). The calculated characteristics of the flume agree well with the values found in lookup tables. The log profile only applies to the lower part of the flow. At the surface, the velocity will decrease with increasing height caused by secondary currents: velocity vortices within the cross section. The existence of these currents is confirmed by measurements.

Velocity profiles in front of and behind the strip covered with gravel are calculated. The size of the boundary layer can be determined in two ways. The former uses the fitted velocity profile and defines the height of the boundary layer by v = 0.9v_{max}. A peak in stresses occurs within the boundary layer. In the latter, the width of this peak was used. Both definitions gave practically the same results.
It seems that the boundary layer is not fully developed at the end of the grind bottom. Further analysis demands for more extended areas.

Analysis of the velocity profiles between the surface floating plants shows differences from the log-profile derived for the situation above the bottom of the flume. As the measured profile resembles a tangens hyperbolicus profile, it can be compared with a mixing layer.
Measurements in the flume with hanging plants show 4 areas in the flow. Two of them were already present in the flume without obstacles: the boundary layer at the bottom and the undisturbed layer. The mixing layer with the plants and the area within the plants are added. The plants cause disturbance of the flow and eddies start to appear. The flow turbulence increases. This is seen by the swaying movement of the vegetation (called 'Monami') and the erosion of the gravel layer under the plants.

The dataset gathered in the river Aa and Bierbza river is presented. In the field, the measurement conditions are more difficult due to their variability. Furthermore, the presence of vegetation in the river has a big influence on the velocity measurements. According to the location and the circumstances, one measurement technique is more advisable than another. The use of a calibrated weir is possible when the circumstances allow a link between the discharge and the water height over the weir, eg. in lab conditions. In rivers, single point measurements are often used. The technique is rather time-consuming, but cheap compared to other advanced instruments. The use of an electromagnetic device for example, can solve the problems encountered with the hydrometric propellers in vegetated rivers. Furthermore, together with performing velocity measurements, also

the bottom profile is measured, which is useful information for modelling purpose. Although the calibration formula of the weir is difficult to use in the river Aa due to the lack of registration of its position, this way of continuous measuring is preferable. Its results agree with the measured discharges downstream using other techniques. An accurate determination of the water level over the weir is necessary to obtain a sufficient accuracy. A propeller is installed on a fixed position to get continuous information on velocities in the river Aa. It can be seen that using a fixed velocity measurement instrument leads to a good indication for the discharge if discontinuous discharge measurements are used to correct the velocity measurements. Further, the advantage of continuous measurements for flood wave measurement is illustrated.

The amount of biomass in the studied reach of the river Aa is determined by using an invasive technique, a mowing device, determining the amount of macrophytes per surface area. The evolution of macrophyte biomass density in the study area was monitored by quantitative sampling on a monthly base. The heterogeneity of the vegetation in the river causes uncertainty and spreading of the results.

References

[1] V. T. Chow, D. R. Maidment, and L. W. Mays. *Applied Hydrology*. McGrawHill, New-York, 1988.

[2] ISO. *International organization for standardization*, 2006. `http://www.iso.ch`.

[3] R.W. Herschy. *Hydrometry: principles and practices*. Wiley Interscience Publication, 1978. ISBN 0471996491.

[4] M.C. Stone and R.H. Hotchkiss. *Evaluating velocity measurements techniques in shallow streams*. Journal of Hydraulic Research, 45(6):752–762, 2007.

[5] C. Ward and M. Tepper. *The use of Doppler instruments for measuring velocity and discharge in streams less than 1.5 m depth*. Technical report, SonTek/YSE Inc., 2004.

[6] J. Bass, G. Wharton, and J. Cotton. *Flow disturbance by instream macrophytes, a hot wire anemometry and scaffold systemfor measuring finescale velocity patterns and mapping sediment deposits and habitat structures*. Poster, 2005. University of London.

[7] J. Fenton. *The application of numerical methods and mathematics to hydrography*. In Proc. 11th Australasian Hydrographic Conference, pages 1–16, 2002.

[8] F. Thomas. *Open channel flow measurement using international standards: introducing a standards programme and selecting a standard*. Flow Measurement and Instrumentation, (13):303–307, 2002.

[9] M. Voet, P. Cabus, and T. Van Hoestenberghe. *Ultrasone snelheidssensoren bij het meten van debieten in onbevaarbare waterlopen*. Water, Nieuwsbrief, 2004.

[10] J.A. Westphal, D.B. Thompson, G.T. Stevens, and C.N. Strauser. *Stage-discharge relations on the middle Mississippi River*. Journal of Water Resources Planning and Management, (48-53), jan-feb 1999.

[11] L. Van Poucke. *Doorlichting Methodologie voor het uitvoeren van debietmetingen*. Technical report, Ghent University, 2002. Report of the Hydraulics Lab (Department of Civil Engineering); in order of the WLB.

[12] M. Rahimpour and M.F. Maghrebi. *Prediction of stage-discharge curves in open channels using a fixed-point velocity measurement*. Flow Measurement and Instrumentation, 17(5):276–281, 2006.

[13] N. Kouwen. *Using vegetation properties to predict flow resistance and erosion rates*. In Vegetated channels: hydraulic, morphological and ecological aspects, Trento, Italy, February 2003. International workshop on riparian forest.

[14] OTT. *Flow measurement*. `http://www.ott-hydrometry.de`, 2007.

[15] Valeport. *Current and open channel flow meters*. `http:\\www.valeport.co.uk`, 2007.

[16] *ADV Precise Measurements of 3D fluid flow*. Documentation of the Nortek ADV.

[17] L. Van Poucke. *Ijking van de stuw op de Aa te Poederlee*. Report of the Hydraulics Lab, Department of Civil Engineering, in order of the VLM, Ghent University, 1999.

[18] K. Buis, C. Anibas, K. Bal, R. Banasiak, L. De Doncker, N. Desmet, M. Gerard, S. Van Belleghem, O. Batelaan, P. Troch, R. Verhoeven, and P. Meire. *Fundamentele studie van uitwisselingsprocessen in rivierecosystemen - gentegreerde modelontwikkeling*. Water, 2007.

[19] S. Van Belleghem, K. Bal, N. Desmet, K. Buis, E. de Deckere, P. Meire, J.P. Vanderborght, F. Dehairs, N. Brion, and L. De Brabandere. *Macrophytes and nutrient dynamics in the upper reaches of the Schelde basin (Manudyn II): Part 2: global change, ecosystems and biodiversity*. Technical report, University of Antwerp-Universit Libre de Bruxelles-Free University of Bruxelles, 2007.

[20] N. Desmet, S. Van Belleghem, P. Seuntjens, T. Bouma, K. Buis, and P. Meire. *Quantification of the impact of macrophytes on oxygen dynamics and nitrogen retention in a vegetated lowland river*. Physics and Chemistry of the Earth, 2008.

[21] J. Simunek, M.Y. van Genuchten, and M. Sejna. *The Hydrus-1D Software package for simulating the movement of water, heat, and multiple solutes in variably saturated media. Version 3.0. Hydrus Software Series 1.* Technical report, Department of Environmental Sciences. University of California Riverside., Riverside, California, USA, 2005. 270 p.

[22] M. Jonckheere. *Evaluatie van debietmetingen aan de hand van chemische methodes op rivieren: theoretische aspecten*. Master's thesis, Ghent University, 2007. Faculty of Sciences.

[23] E.M. Shawn. *Hydrology in practice*. Taylor and Francis, 1983.

[24] W. Boiten. *Hydrometry*, chapter Dilution Methods, pages 111–118. Francis and Taylor publishers, 2000.

[25] R. Verhoeven. *Hydrografie en hydrometrie*. Ghent University, Faculty of Engineering, 2000.

[26] ISO. *ISO 9555-1: Measurement of liquid flow in open channels - Tracer dilution methods for the measurement of steady flow - Part 1: General*. Technical report, International Organisation for Standardisation, Genve, 1994.

[27] R.W. Herschy. *Streamflow Measurement*, chapter Dilution gauging, pages 352–381. Londen, E & FN Spon, 2 edition, 1995.

[28] R.D. Moore. *Introduction to salt dilution gauging for streamflow measurement. Part 2: Consatnt-rate injection*. In Streamline Watershed Management Bulletin, volume 8, pages 11–15. 2004.

[29] K.E. White. *Hydrometry: principles and practices*, chapter Dilution methods, pages 111–148. Wiley Interscience Publication, 1978. ISBN 0471996491.

[30] R. Hudson and R. Fraser. *Introduction to salt dilution gauging for streamflow measurement. Part 4: the mass balance or dry injection method*. Streamline Watershed Management Bulletin, 2005. 9(1), 6-12.

[31] J. Demuytere. *Evaluatie van debietmetingen aan de hand van chemische methodes op rivieren: praktische aspecten,*. Ghent University, Faculty of Sciences, 2007.

[32] T.R. Marshall and P.F. Lee. *An inexpensive and lightweight sampler for the rapid collection of aquatic macrophytes*. Journal of Aquatic Plant Management, (32):77–79, 1994.

[33] R. Herschy. *The uncertainty in a current meter measurement*. Flow Measurement and Instrumentation, (13):281–284, 2002.

[34] HIC. *Methodology for the discharge measurements (in Dutch) - Methodologie voor het uitvoeren van debietmetingen*. Technical report, Flanders Hydraulics Research - Hydrological Information Centre, 2000.

[35] S. Moeskops. *Stromingspatronen in rivieren door de aanwezigheid van macrofyten*. Master's thesis, Ghent University, 2007. Faculty of Engineering.

[36] J.R. Welty, C.E. Wicks, R.E. Wilson, and G. Rorrer. *Fundamentals of momentum, heat and mass transfer*. John Wiley and Sons, 4th edition, 2000. 759 blz.

[37] V. T. Chow. *Open Channel Hydraulics*. McGrawHill, New-York, 1959.

[38] M. Kummu. *Roughness characteristics and velocity profile in vegetated and non-vegetated channel*. Master's thesis, Helsinki University of Technology, 2002.

[39] W.H. Graf and M.S. Altinakar. *Fluvial Hydraulics: flow and transport processes in channels of simple geometry*, page 681. Wiley, England, 1998. ISBN 0-471-97714-4.

[40] Z. Liu. *Sediment Transport*. Technical report, Aalborg University, 2001.

[41] J.C. Green. *Velocity and turbulence distribution around lotic macrophytes*. Aquatic Ecology, 39(1-2):1–10, 2005.

[42] E. Keirsebelik. *Studie van de numerieke modellering van oppervlaktewater ten behoeve van de gentegreerde modellering van rivierecosystemen*. Master's thesis, Ghent University, 2009.

[43] J. Jarvela. *Flow resistance in environmental channels: focus on vegetation*. Water resources publications, Helsinki University of Technology, 2004.

[44] C.A.M.E. Wilson. *Open channel flow through different forms of submerged flexible vegetation*. Journal of Hydraulic Engineering, 129:847–853, 2003.

[45] H.M. Nepf. *Drag, turbulence, and diffusion in flow through emergent vegetation*. Water resources Research, 35(2):479–489, 1999.

[46] H.M. Nepf and E.R. Vivoni. *Flow structure in depth-limited, vegetated flow*. Journal of Geophysical Research, 105:547–557, 2000.

[47] F. Lopez and M.H. Garcia. *Mean flow and turbulent structure of open-channel flow through non-emergent vegetation*. Journal of Hydraulic Engineering, 127(5):392–402, 2001.

[48] M. Righetti and A. Armanini. *Flow resistance in open channel flows with sparsely distributed bushes*. Journal of Hydrology, 269(1-2):55–64, 2002.

[49] M.J. Baptist, V. Babovic, J. Rodriguez Uthurburu, M. Keijzer, R.E. Uittenbogaard, A. Myn ett, and A. Verwey. *On inducing equations for vegetation resistance*. Journal of Hydraulic Research, 45(4):435–450, 2007.

[50] M. Ghisalberti and H.M. Nepf. *Mixing layers and coherent structures in vegetated aquatic flows*. Journal of Geophysical research, 107(C2):3.1–3.11, 2002.

[51] J.C. Green. *Velocity and turbulence distribution around lotic macrophytes*. Aquatic Ecology, 39(1-2):1–10, 2005.

[52] J. Jarvela. *Flow resistance of flexible and stiff vegetation: a flume study with natural plants*. Journal of Hydrology, 269(1-2):44–54, 2002.

[53] J.C. Green. *Modelling flow resistance in vegetated streams: review and development of new theory*. Hydrological Processes, 19(6):1245–1259, 2005.

[54] J. Welty, C. Wicks, R. Wilson, and G. Rorrer. *Fundamentals of Momentum*. Wiley Interscience, 2001.

[55] I. Nezu. *Open-channel flow turbulence and its research prospect in the 21st century*. Journal of Hydraulic Engineering, 131(4):229–246, 2005.

[56] N.S. Cheng. *Power-law index for velocity profiles in open channel flows*. Advances in Water Resources, pages 1775–1784, 2007.

[57] H. Schlichting. *Boundary-layer theory*. 1979.

[58] V. Ferro and G. Baiamonte. *Flow velocity profiles in gravel-bed rivers*. Journal of Hydraulic Engineering, 120(1):60–80, 1994.

[59] K.V.N. Sarma, P. Lakshminarayana, and Lakshmana R. *Velocity distribution in smooth rectangular open channels*. Journal of Hydraulic Engineering, 109(2):270–289, 1983.

[60] P. Stearns. *A reason why the maximum velocity of water flowing in openc channels is below the surface*. In Transactions of teh American Society of Civil Engineers, pages 331–338, 1983.

[61] A. Cardoso, W. Graf, and G. Gust. *Uniform flow in a smooth open channel*. Journal of Hydraulic Research, pages 27–32, 1989.

[62] W. Nezu and R. Rodi. *Open-channel flow measurements with laser Doppler anemometer*. pages 335–355, 1986.

[63] S.Q. Yang, S.K. Tan, and S.Y. Lim. *Velocity distribution and dip-phenomenon in smooth uniform open channels*. Journal of Hydraulic Engineering, pages 1179–1186, 2004.

[64] D. Coles. *The law of the wake in the turbulent boundary layer*. Journal of Fluid Mechanics, (1):191–226, 1956.

[65] J. Finnigan. *Turbulence in plant canopies*. Annual review of Fluid Mechanics, pages 519–571, 2000.

[66] U. Stephan and D. Gutknecht. *Hydraulic resistance of submergend flexible vegetation*. Journal of Hydrology, 269(1-2):27–43, 2002.

[67] H. Nepf and E. Vivoni. *Turbulence structure in depth limited vegetated flows: transition between emergent and submerged regimes*. In 28th IAHR Conference, 1999. Graz.

[68] F.G. Carollo, V. Ferro, and D. Termini. *Flow velocity measurements in vegetated channels*. Journal of Hydraulic Engineering, 128(7):664–673, 2002.

[69] P. Viaene and H. Vereecken. *Stromingsweerstand tengevolge van waterplanten*. Technical report, Flanders Hydraulics, 2001. Rapport Ministerie van de Vlaamse Gemeenschap, Departement Leefmilieu en Infrastructuur, Administratie Milieu, Land-en Waterbeheer, Afdeling Water, Model 566.

[70] H. Vereecken, J. Baetens, P. Viaene, F. Mostaert, and P. Meire. *Ecological management of aquatic plants: effects in lowland streams*. Hydrobiologia, 570:205–210, 2006.

[71] E. Cornet. *Personal information*.

[72] L. Van Poucke. *Ijking van de stuw op de Aa te Poederlee*. Technical report, Ghent University, Hydraulics Laoratory, 1995.

[73] N. Desmet and S. Vanbelleghem. *Personal communication*.

5
Data Processing

In this chapter, lab and field measurement results are analysed and discussed in more detail. Some physical processes such as the influence of obstacles and vegetation on the characteristics in the laboratory flume are studied. Further, the importance of Manning's coefficient is stressed and the parameters which influence its value are evaluated. Also blockage aspects in rivers are studied.

1 Flume data

1.1 Influence of obstacles on velocity profiles

1.1.1 Measurement set-up

In the flume (glass, length 12 m, width 70 cm) in the Hydraulics Laboratory, obstacles are installed to check the velocity disturbance. The obstacles are wooden planks, tree branches and foil respectively for each measurement [1]. Three of these elements are placed in one cross-section, at 17.5 cm, 35 cm and 52.5 cm from the flume wall, which results in a symmetrical set-up. The obstacles are fixed on a plate, which is placed at 5.98 m from the upstream boundary. The plate has a length of 2.51 m and in front of and behind the plate a transition slope of 0.50 m is applied. The obstacles are positioned at 1.65 m from the front of the plate (Fig. 5.1).

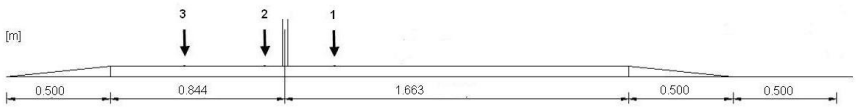

Figure 5.1: Flume set-up, with position of the obstacles and indication of the meaasurement points

Velocities are measured with an electromagnetic device (Valeport, flat sensor), 25 cm in front of, 10 cm behind and 50 cm behind the obstacles. Point measurements are carried out in a grid of 5 cm by 5 cm. Two water heights (20 cm, 50 cm) and corresponding discharges (125 l/s and 155 l/s) are selected. Pictures of the measurement set-up are presented below (Fig. 5.2).
Discharge values are determined by use of the calibration formula of the upstream weir or by measuring the velocities (Chapter 4). Calculation of the discharge out of single point velocity measurements leads to accurate results when a sufficient number of measuring points is sampled [2].

Figure 5.2: Flume experiments with wooden planks (H = 20 cm, H = 50 cm)

Figure 5.3: Flume experiments with branches (H = 20 cm, H = 50 cm)

Figure 5.4: Flume experiments with foil (H = 20 cm, H = 50 cm)

1.1.2 Measurement results

The results of the velocity measurements are summarized in this paragraph. The tables present the velocity values and the absolute deviation for each kind of obstacles.

Measurements 25 cm in front of the obstacles Due to the obstacles, at this position, higher water levels are registered and consequently, the velocities will decrease (the discharge does not change). The more rigid the obstacle, the more the water level rises and the velocity decreases. For a discharge of 125 l/s, an average water level of 205 mm is measured in the empty flume, in front of the wooden planks. Values up to 242 mm are measured while lower values are seen in front of the branches (220 mm) and the foil (210 mm). This is the case if the obstacle rises above the water surface, for water levels twice as high as the obstacle, the back water effect is not noticable (H = 50 cm). The decrease in velocity due to wall friction disappears on a distance of 12.5 cm from the wall. Further, the velocity decrease in front of the obstacles is a global effect and does not indicate the position of the obstacles. Fluctuations of the velocity are smaller than the measurement error of the measuring instrument. The velocity profile over the water height follows a logarithmic profile, with a deviation at the water surface due to friction with the air (Fig. 5.6).

	Q = 125 l/s			Q = 155 l/s		
	uniform velocity [m/s]	abs. deviation	water level [cm]	uniform velocity [m/s]	abs. deviation	water level [cm]
no obstacle	0.853	0.022	20.5	0.454	0.007	50.0
wooden planks	0.734	0.010	24.2	0.475	0.005	50.0
branches	0.803	0.019	22.0	0.455	0.007	50.0
foil	0.822	0.020	21.0	0.461	0.007	50.0

Table 5.1: Uniform velocities 25 cm in front of the obstacles for different types of obstacles and different discharges

Measurements 10 cm behind the obstacles Immediately behind the obstacle, the stream flow is influenced and the water is pushed against the obstacles. The velocity increases at the positions behind the obstacles and decreases at the positions between the obstacles. For the lower water level, the ratio between the two velocities (on a vertical behind and on a vertical in between) is given by values of 71 % (wooden planks), 63 % (branches) and 81 % (foil). For a water level of 500 mm, ratios are 73 %, 82 % and 87 %. The highest difference is noticed for the branches rising up above the water level, which is not expected since the water also flows through the branches. Values of the water level (205 for the empty flume) behind the obstacles are 160 mm behind and 220 mm between the wooden planks (both at 10 cm behind the obstacles), 170 mm behind and 200 mm between the branches and 190 mm behind the foil. For the higher water level, the water level fluctuations are negligible. Also here, the water level decrease is conform the velocity increase. Between the obstacles, the logarithmic velocity profile is found, while behind the obstructions all kinds of curves are measured. The flexible foil is pushed down and the minimum velocity is shifted from the bottom to the bending point. The measurement error increases compared to the section in front of the obstacles due to both; the higher fluctuations on the velocity and the higher inaccuracy of the measurement device for higher velocities.

	Q = 125 l/s			Q = 155 l/s		
	uniform velocity [m/s]	abs. deviation	water level [cm]	uniform velocity [m/s]	abs. deviation	water level [cm]
wooden planks	1.078	0.029	16.0/22.0	0.471	0.005	49.9
branches	0.935	0.025	17.0/20.0	0.455	0.007	49.5
foil	0.912	0.024	19.0	0.459	0.007	49.5

Table 5.2: Uniform velocities 10 cm behind the obstacles for different types of obstacles and different discharges

Measurements 50 cm behind the obstacles Here, the velocities are higher behind the wooden planks and lower in between, which is opposite of the results in the section just behind the obstruction. For the wooden branches and foil, the mesured pattern is the same as before. In general, a decrease in velocity is measured compared to the section 10 cm behind the obstructions. For the lower water level, the ratio between the two velocities (on a vertical in between and on a vertical behind) is given by values of 81 % (wooden planks), 83 % (branches) and 83 % (foil). For a water level of 500 mm, ratios are 98 %, 94 % and 94 %. The difference in velocities behind and in between the obstacles is decreased at this larger distance behind the obstacles (compared with the measurements at 10 cm behind the obstacles). This is due to the larger wetted cross section at the same discharge. Here, measured water levels are (initial 205 mm), 218 mm (wooden planks), 220 mm (branches) and 210 mm (foil). For branches and foil, the water level reaches the same level as in front of the obstacles. Also, the velocity profiles are 'recovering' and are logarithmic. The influence of the air friction is noticed and the position of the obstacles cannot be concluded out of the velocity profiles. The influence of the obstacle is decreasing. For water levels lower than the obstruction height, the measurement error is determined by the deviation of the measuring device. For higher water levels, low velocities can occur behind the obstacles and the standard deviation on the measurements is determining (Chapter 4).

	Q = 125 l/s			Q = 155 l/s		
	uniform velocity [m/s]	abs. deviation	water level [cm]	uniform velocity [m/s]	abs. deviation	water level [cm]
no obstacle	0.848	0.021	20.5	0.453	0.007	50.0
wooden planks	0.835	0.011	21.8	0.476	0.005	50.7
branches	0.830	0.020	22.0	0.453	0.007	50.0
foil	0.808	0.020	21.0	0.457	0.007	50.0

Table 5.3: Uniform velocities 50 cm behind the obstacles for different types of obstacles and different discharges

Fig. 5.5, 5.6 and 5.7 depicts velocity results of the flume measurements with the foil obstacles. Results are shown at the three measurement positions and for a discharge of 125 l/s (H = 20 cm). More graphs of the measured velocities are available in [1].

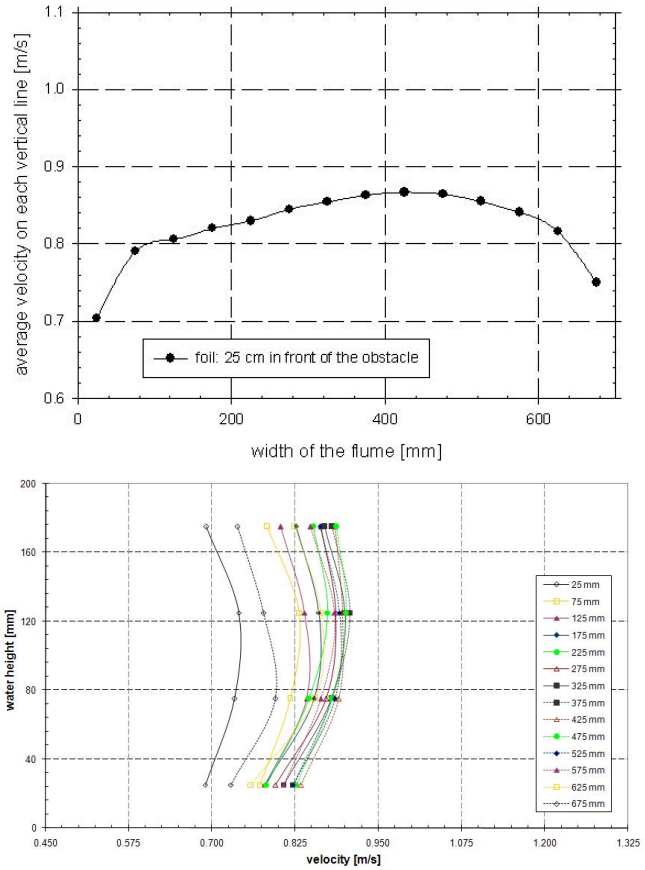

Figure 5.5: Flume experiments with foil (H = 20 cm, Q = 125 l/s), average velocities on each vertical line (1) and velocity profile on each vertical line (2)

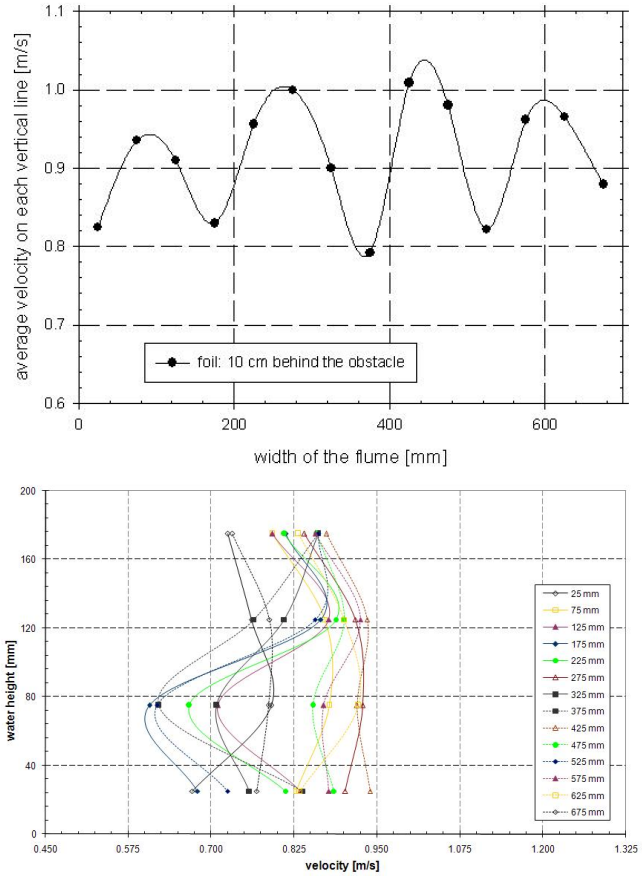

Figure 5.6: Flume experiments with foil (H = 20 cm, Q = 125 l/s), average velocities on each vertical line (1) and velocity profile on each vertical line (2)

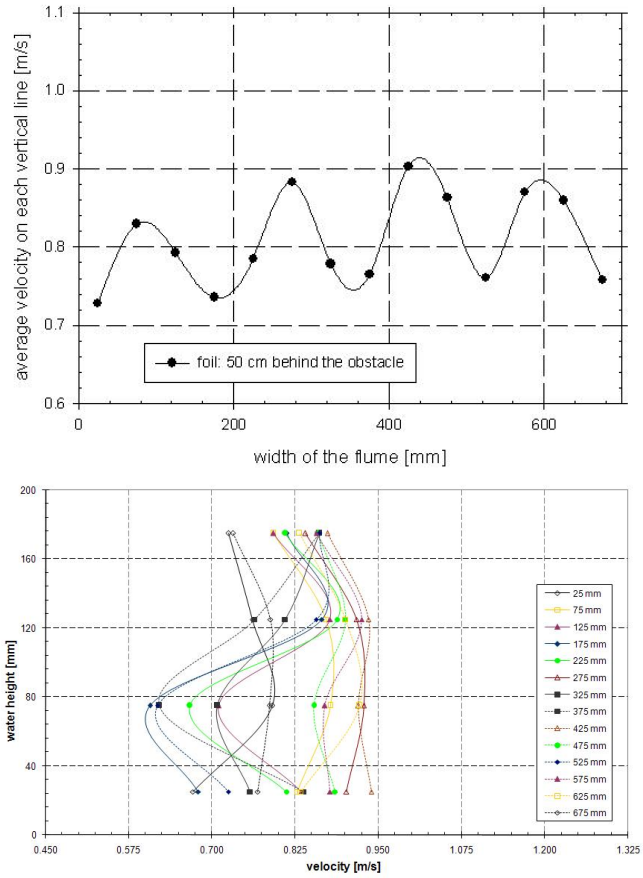

Figure 5.7: Flume experiments with foil (H = 20 cm, Q = 125 l/s), average velocities on each vertical line (1) and velocity profile on each vertical line (2)

1.2 Flow resistance of floating plants

1.2.1 Introduction

Vegetation alters the properties of the waterway and the flow. In a laboratory flume, the flow resistance of floating plants was studied. The objective was to check similarities and differences with the influence of submerged and nonsubmerged plants from which several studies are available. The roughness value is expressed by Manning's coefficient. Special attention is paid to the determination of the water surface slope. Tests were carried out under different circumstances of discharge and water level.
The research showed that the properties of floating plants are comparable

with plants with limited influence on the flow, placed at the bottom of the flume. For floating plants, the impermeable vegetation forms an obstruction to the flow. Manning's coefficient is determined as a function of flow characteristics. This experimental work and extensive analysis allows better understanding of the behaviour of floating plants and contributing to the management of the water courses.

It is often shown that flow in rivers and waterways slows down within and in the proximity of vegetation [3, 4]. Presence of vegetation increases the water level upstream of these plants and screens the flow behind the vegetated area. Consequently, higher resistance against flows occurs. To allow the same discharge in the river when compared to the situation without vegetation, the difference in water levels in front of and behind the vegetation has to increase resulting in backwater influence in the upstream part of the river. Due to the occurence of macrophytes, the drainage capacity of the river decreases, leading to higher flood risks during peak flow. To assess this risk, and determine the effect of the vegetation on flood levels, Manning's roughness coefficient was calculated [5–10].

The goal of this research is to determine the properties of the surface-floating vegetation (roughness coefficient and permeability) to allow better understanding of flow in overgrown waterways. All experiments with vegetation were performed with *Hydrocotyle ranunculoides* ('floating pennywort'), an invasive, widespread; 'alien' freshwater plant. Its rapid growth and high biomass (dry mass of 1,5 kg/m^2) leads to a high influence on the flow.
The measurement test set-up and the test series are described in Chapter 4.

1.2.2 Flow resistance of the flume without obstacles

Determination of Manning's coefficient by tables and compound formulas In this section we try to determine Manning's coefficient of the flume without obstacles making use of data from literature. Values from the look-up tables [11] are as follows: 0.009 m$^{-1/3}$s (glass), 0.010 m$^{-1/3}$s (wood stave) and 0.016 m$^{-1/3}$s (uncoated cast iron).
Next to that, determination of the compound Manning coefficient for the flume, constructed of a metal bottom and glass side walls, is performed using the formulas of [12, 13]. Different expressions are proposed for channels with side walls from varying materials (Table 5.4 and Table 5.5). These formulas are based on Manning's coefficient of all individual parts, which makes determination of the value of Manning's coefficient for the combinated set-up uncertain and difficult. The formulas are based on the total

resistance force which is the sum of the subarea resistance forces (formulas a, c, d in Table 5.4 and Table 5.5) and the total shear velocity which is the weighted sum of the subarea shear velocity (formulas b, e, f in Table 5.4 and Table 5.5) [12–14]. Values are gathered in Table 5.4, for measurements I, II and III performed at the locations as indicated in Fig. 4.17. Equations (Table 5.4 and Table 5.5) which give results lower than the minimum Manning coefficient (for glass) and higher than the maximum Manning coefficient (for iron), mentioned by [11], are not retained as they are physically not possible. So, only formula a and b in Table 5.4 and Table 5.5 are taken into consideration. Considering the values from the look-up tables and the results in Table 5.4 and Table 5.5 (formula a and b), Manning's coefficient of the flume is determined: a Manning value of 0.009 $m^{-1/3}s$ is retained for the test section and 0.012 0.013 $m^{-1/3}s$ for the other parts of the flume.

	a $\sqrt{\frac{1}{P}\sum n_i^2 P_i}$	b $\frac{\sum n_i P_i}{P}$	c $\sqrt{\frac{R^{1/3}}{P}\sum \frac{n_i^2 P_i}{R_i^{1/3}}}$
meas. I	0.009	0.009	0.008
meas. II	0.010	0.010	0.009
meas. III	0.013	0.013	0.012

Table 5.4: Manning's coefficient for measurements at different locations in the flume, calculated according different formulas [12, 13]: Part 1

	d $\sqrt{\frac{\sum n_i^2 P_i R_i^{2/3}}{PR^{2/3}}}$	e $\frac{\sum n_i P_i / R_i^{1/6}}{P/R^{1/6}}$	f $\frac{\sum n_i P_i / R_i^{1/3}}{P/R^{1/3}}$
meas. I	0.012	0.004	0.013
meas. II	0.012	0.004	0.013
meas. III	0.017	0.005	0.018

Table 5.5: Manning's coefficient for measurements at different locations in the flume, calculated according different formulas [12, 13]: Part 2

Determination of Manning's coefficient from measurements and making use of other theoretical considerations or formulas As the determination of Manning's coefficient using the Bresse equation or Manning's formula requires accurate measurement of the water levels (0.1 mm should be obtained), which is difficult in the rather short flume, some other methods have been used to determine Manning's coefficient and to compare it with the results from previous section.

[15] proposed a method based on the Reynolds stresses (Eq.(3.38)). This formula is only useful over the water depth where the stresses show a linear distribution ($z_1 < z < z_2$, with z_1 and z_2 boundary values of the

linear distribution). This linear area is depicted at Fig. 5.8 and is according results in [15]. The slope of the linear line is used in Eq.(3.38), resulting in a water surface slope of 124*10^{-6} and a Manning coefficient of 0.0123 $m^{-1/3}s$.

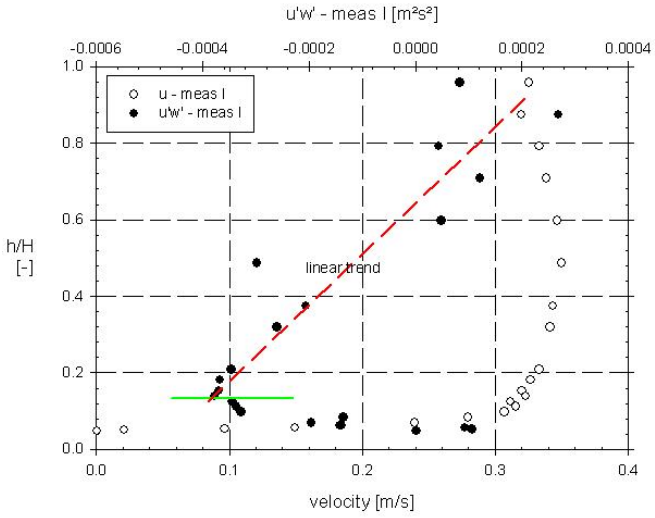

Figure 5.8: Velocity values u and results $\overline{u'w'}$ according standard Reynolds decomposition for measurement I

[16] describes the roughness using the energy losses (Eq.(3.39)):

Results of use of both formulas (Eq.(3.38) and Eq.(3.39)) are gathered in Table 5.6.

Also, other formulations (see Chapter 3) to determine Manning's coefficient are proposed such as the formula of Colebrook-White, Thijsse or Reinius.

Colebrook-White (Eq.(5.1)) calculates iteratively the roughness coefficient f (Eq.(3.33)) as a function of the Reynolds number Re [-], the hydraulic radius R [m] and the equivalent roughness k_s [m]. The equations of Thijsse and Reinius are adapted forms of the equation of Colebrook-White (which is for circular flumes). Berlamont [17] proposes an alternative formulation [18] (C_1 = 2.03, C_2 = 12.2, C_3 = 3.033). Most of these formulations are set up for relations $B/H >> 2$, while in the lab experiments, B/H is about 2. The expression of [19] is used for conditions where B/H equals 2 (C_1 = 2.0, C_2 = 14.8, C_3 = 2.8). Results are presented in Table 5.6.

$$\frac{1}{\sqrt{f}} = -C_1 log(\frac{k_s}{C_2 R} + \frac{C_3}{4Re\sqrt{f}}) \tag{5.1}$$

	measurement I	measurement II	measurement III
Tables (section 1.2.2)	0.009	0.009	0.012 - 0.013
[15]	0.012	0.009	-
[16]	0.001	0.002	-
[18]	0.011	0.010	0.013
[19]	0.010	0.009	0.012

Table 5.6: Manning's coefficient according to different approximations, measurements I, II and III according to Fig. 4.22

Discussion Four formulas were used to calculate n without the needs to determine the surface slope but making use of measured velocities and cross section characteristics. The first was the Colebrook- White equation, adapted according to [18] and [19]. [20] and [16] used the profile of the Reynolds stresses to determine the slope. Only the three first formulas delivered acceptable values. [16] resulted in deviant values. For measurement III, before the raised section, no linear profile was measured and so Eq.(3.38) and Eq.(3.39) cannot be used. From this, it follows that all methods show their proper inconveniences: using tables may lead to a too large range of possible Manning values. Measuring the slope of the water surface has an unsatisfactory accuracy and the formulas of [20] and [16] require a labour intensive gauging of the velocity profile (where accuracy might also be doubtful). However, by comparing the results of different approaches a reliable estimation of the Manning coefficient should be possible. In our case, Manning's coefficient of the flume is determined: a Manning value of 0.009 to 0.010 $m^{-1/3}s$ is retained for the test section and 0.012 0.013 $m^{-1/3}s$ for the other parts of the flume.

1.2.3 Flow resistance of floating plants

Introduction The degree of submergence is determined by the blockage which is determined by (0.07/water level) because the plants are put 7 cm under the water surface of the flume. The measurement set-up is presented in Fig. 4.21.

Water levels were measured at 4 points (Fig. 4.22): 2 points in front of the vegetation patches, 1 in between and 1 behind the plants. Comparison of water levels in front of and over the plants, with inherent Manning coefficient, is possible. The effect of the vegetation on the Manning's coefficient is based on the distinction between n_b (Manning coefficient of the flume without obstacles, measured between point 4 and 3 at Fig. 4.22), n_{pl} (Manning's coefficient over the vegetated flume, so the effects of the empty flume and vegetation are included) and n_{eff} (Manning's coefficient of the plants). n_{eff} is Manning's coefficient due to the plants with exclusion of roughness influences of the flume without obstacles. Its value is based on

$S_{f,eff}$ by $h_{tot} = S_{f,eff} * L_{veg} + S_{f,b} * L_{tot}$ (Fig. 5.9). $S_{f,pl}$ and n_{pl} are characteristics of the 4.50 m test reach of the flume (Fig. 4.22, between tube 1 and 3), where only part has been covered with floating vegetation. These values are only used to determine $S_{f,eff}$. $S_{f,b}$ and n_b are characteristics of the empty flume and $S_{f,eff}$ and n_{eff} are linked to the vegetation in the flume, effects of the the flume without obstacles are not included according to Fig. 5.9. So, in the vegetated area, the effect of the plants is studied separately from the effect of the flume.

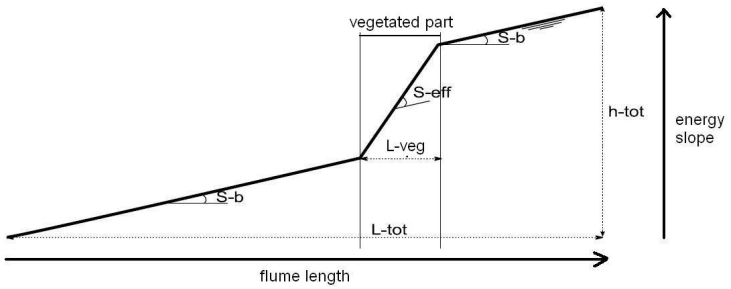

Figure 5.9: Calculation of Manning's coefficient in the flume, with $S_b = S_{f,b}$ and $S_{eff} = S_{f,eff}$

As mentioned before, influence of measurement errors decreases due to presence of a large water surface slope (large velocity, low water level) over the vegetation or by a longer vegetated zone. Here, the vegetated area is 2*0.35 m, while literature shows examples of 3 to 6 m [21, 22].

Two series of measurements are carried out. One with a constant reference water level and varying discharges, the second with a varying water level and discharge.

Determination of Manning's coefficient from measurements and making use of Manning's formula Besides using tables and predefined values, solution of the Manning equation (Eq.(3.34)) yields the roughness of the flume without obstacles. In the empty flume, it is assumed that the velocities are uniformly distributed in every cross section, which allows simplification of the flow pattern and use of the Manning equation. Calculation of Manning's coefficient is based on the determination of the friction slope S_f. This value is composed of the water surface slope (a) and the difference in velocity energy (b) in the flume (Eq.3.36).

The friction slope S_f is written as $S_{f,b}$ for the measurements in the flume without obstacles and as $S_{f,eff}$ for measurements in the flume with the floating plants.

The kinematic wave approximation [17] assumes that the velocity energy term does not change due to limited velocity and water level changes. Then, the water surface slope equals the energy slope.

In case of the blank flume, height differences are so small, that very precise readings are required. Even in the situation with vegetation placed in the flume, in which the slope of the water surface is considerably larger than in case of the flume without obstacles, a large accuracy is necessary. Different instruments to measure the water level were investigated. The gauging errors of divers (0.005 m) and mechanical gauges (0.0015 m) were found to be too big so finally precise measurements for calculating the slope of the water surface were obtained by using a gauge tube with a damper based on the principle of communicating vessels (Fig. 4.22). In order to obtain maximal accuracy, the distance between up- and downstream gauging locations was taken as big as possible. It is clear that the measurement error increases with shorter distance and lower velocities.

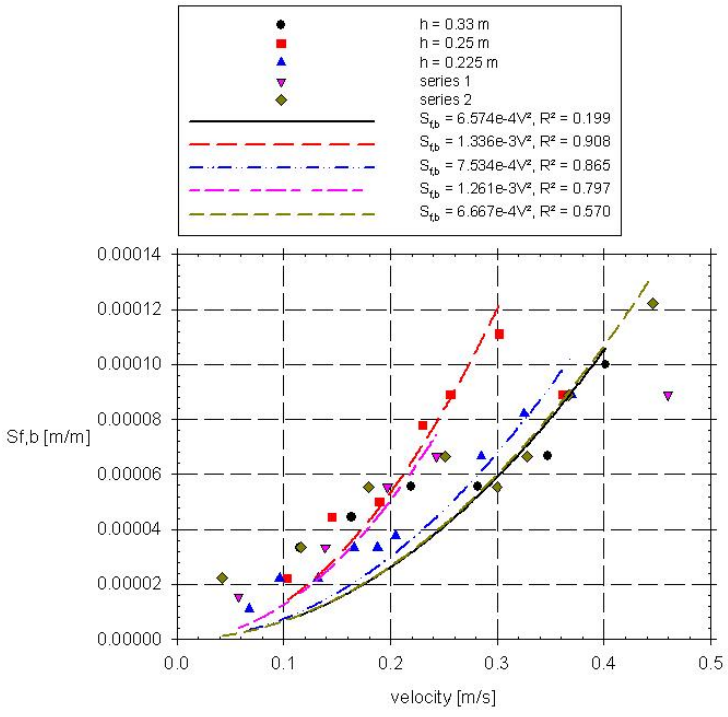

Figure 5.10: Water surface slope of the empty flume for different series of measurements, as a function of velocity

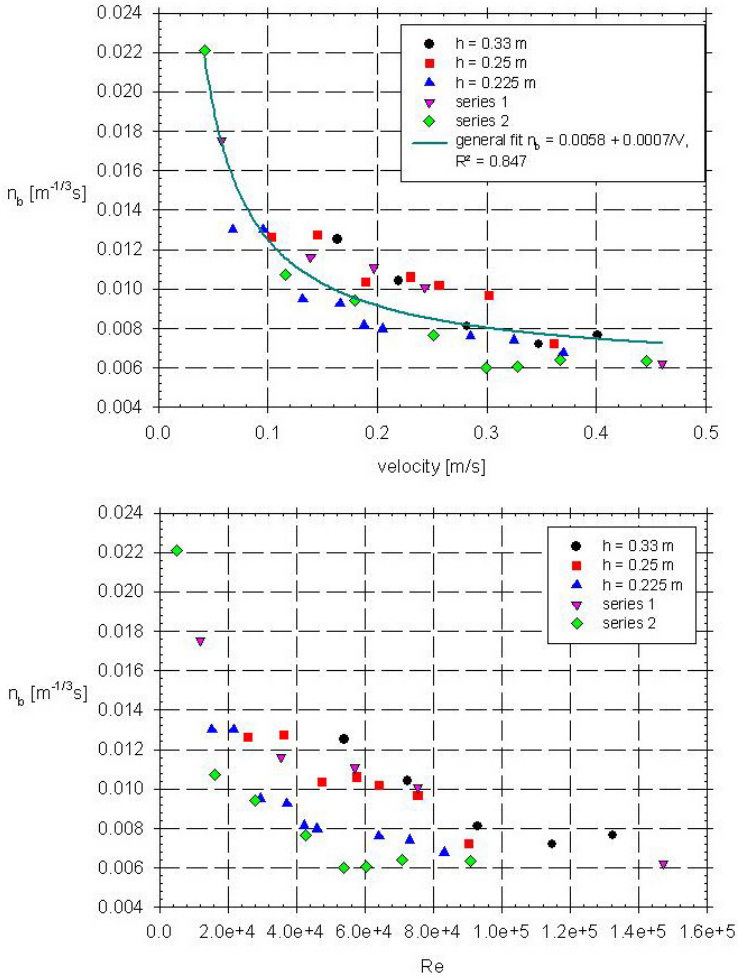

Figure 5.11: Manning's coefficient of the empty flume for different series of measurements, as a function of velocity (top) and Reynolds number (bottom)

The water surface slope $S_{f,b}$ and the average velocity in the flume without obstacles show a quadratic correlation. This relation is added in Fig. 5.10. For two measurement series (h = 0.25 m and series 1), the measurement point for the highest velocity is not taken into account for fitting. These points are not following the quadratic relation. The fit for h = 0.25 m and for series 2 enclose most of all the measurement points. Deviations are largest for the smallest velocity values. The values between 0.009 $m^{-1/3}s$ and 0.016 $m^{-1/3}s$ are proposed by look-up tables [11] and are considered as indicative values. In a second phase, measurements are performed (Fig.

5.11). At Fig. 5.11, it is seen that 2 points are higher than the 0.016 value and a cloud of points is found below the 0.009 value. Values up to 0.006 are calculated. This only confirms the indicative aspect of the look-up tables and the value tabulated for glass and therefore its properties will not agree with the properties of the glass in the flume. The two highest points are not incorporated in the quadratic relation of Fig. 5.11, however one of them follows this trend and both of them follow the trend plotted in Fig. 5.11.
The correlation between $S_{f,b}$ and velocity V is clearly not determined by the water level. The correlation between $S_{f,b}$ and V is in agreement with the expressions for the roughness coefficient i.e. the Manning equation. Fig. 5.11 shows Manning's coefficient of the flume without obstacles for the different measurement series, as a function of the velocity (top,a) and, as a function of the Reynolds number (bottom,b). Manning's coefficient is varying between 0.006 $m^{-1/3}s$ and 0.013 $m^{-1/3}s$. An overall fit is added in Fig. 5.11a, the relation between Manning's coefficient and the velocity is according to the Manning equation ($n \sim 1/V$ with R^2 = 0.847) and is as follows:

$$n_b = 0.00058 + \frac{0.0007}{V} \tag{5.2}$$

Manning's coefficient n is determined according look up tables and is calculated using Manning's formula, based on measurements of slope of the water surface. Due to the small height differences, reading errors had a large effect (Fig. 5.10 and Fig. 5.11) in determining the slope in the situation of the flume without obstacles. Therefore, the roughness coefficient is determined in other way as well.

Constant reference water level In this test, the reference water level is taken just upstream the test section. The downstream weir position is adapted to keep the reference water level constant and to study only one variabele: the discharge. Three series of measurements were carried out, corresponding with water levels of 0.225 m, 0.250 m and 0.330 m. For each of the measurements series, the slope of the water surface is determined over the vegetated part of the flume and $S_{f,pl}$ and $S_{f,eff}$ are calculated. Simultaneously, n_{pl} and n_{eff} are determined (Fig. 5.12).

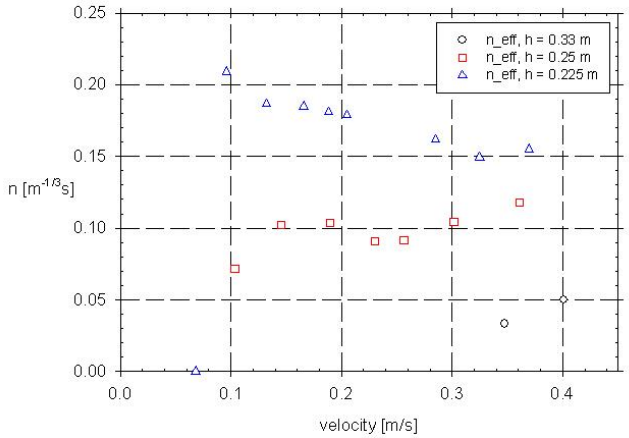

Figure 5.12: Manning's coefficient only due to influence of the floating plants n_{eff}

It is seen that n_{eff} is more or less constant for different velocities (in the same measurement series). For n_{eff}, values of 0.15 to 0.20 $m^{-1/3}s$ (series 1, h = 0.225 m), 0.10 $m^{-1/3}s$ (series 2, h = 0.25 m) and 0.05 $m^{-1/3}s$ (series 3, h = 0.33 m) are found. In the empty flume values were varying from 0.006 $m^{-1/3}s$ to 0.013 $m^{-1/3}s$ (Fig. 5.11 and Fig. 5.12). In the management of water courses, these values can be used as an indication of the resistance caused by floating pennywort, in combination with the bottom roughness values.

It is shown that the vegetational influence decreases with increasing water level due to the smaller relative influence of the obstruction of the flow. A decreasing waterlevel from 0.33 m to 0.25 m or from 0.25 m to 0.225 m, which is a rise of obstruction of 10 %, results in doubling of the Manning coefficient (Fig. 5.12). According to literature values of bottom roughness [13, 23], the n-value is mentioned to be constant for different water levels (Manning's equation). So the increased roughness coefficient is due to the higher obstruction by vegetation.
In combination with the results in the empty flume, values for Manning's coefficient caused by floating plants are found: the n-value varies only little for constant water level. Different measurements under the same conditions result in a rather accurate determination of Manning's coefficient. The value of n strongly depends on the water height in the flume. Change of water level corresponds to a change of blockage and a change of Manning's coefficient. The variation of the Manning coefficient with varying water depth is rather limited, while the Manning coefficient is strongly

varying with the velocity in the flume without obstacles. In presence of floating plants, a clear variation of Manning's value with the water depth is demonstrated. It must be noticed that for high water levels, and a relative lower influence of the vegetation, the vegetational influence almost disappears.

The water surface slope over the plants is proportional to the square of the velocity according the roughness equations (e.g. Manning, Chézy): aV^b. This is confirmed by the measurements: for the different series of measurements, the value of the power b is 2.141 (h = 0.225 m), 1.967 (h = 0.25 m) and 3.229 (h = 0.33 m) (Fig. 5.13). For the first two series, b approximates the value of 2. For the third series, the number of measurements is probably too small to draw conclusions. The same calculations are carried out for $S_{f,eff}$ (according Fig. 5.9) with similar results. Deviations are a little higher due to the cumulative error on the water level measurements of the empty and vegetated flume in $S_{f,eff}$. Further, the mentioned equations for uniform flow are not valid in the area with floating plants, due to the change in water level over the plants. Use of the Bresse equation (Eq.(3.31)) is the appropriate method.

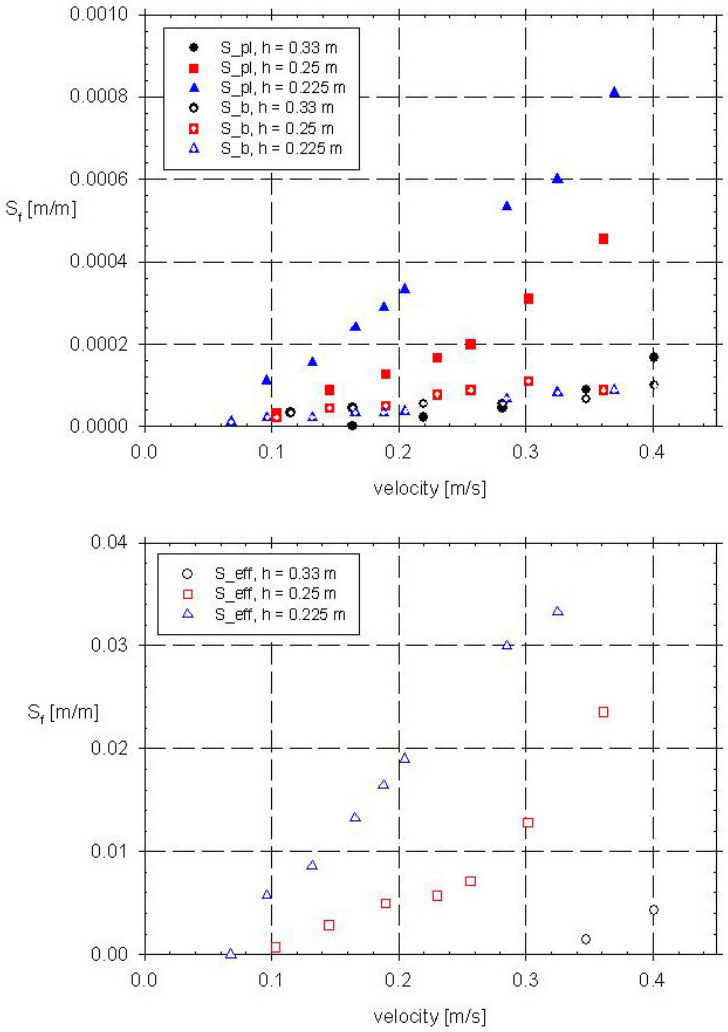

Figure 5.13: Surface water slope of the empty flume $S_{f,b}$, of the vegetated area $S_{f,pl}$ and surface water slope only due to influence of the floating plants $S_{f,eff}$

Different configurations (plants collected in April or May) are compared with the results of [22] where sedges and willows were placed on the bottom of the flume. This flume has following dimensions: 50 m long, 1.1 m wide, 1.3 m deep and the vegetational test area has a length of 6 m. Water levels from 0.25 to 0.80 m and discharges from 40 to 292 l/s are measured. Various discharges were used, while the water level was kept constant. The roughness coefficient f, coefficient of Darcy Weisbach (Eq.(3.33)),

is used. The results of [22] and our lab measurements are plot in Fig. 5.14, respectively left and right.

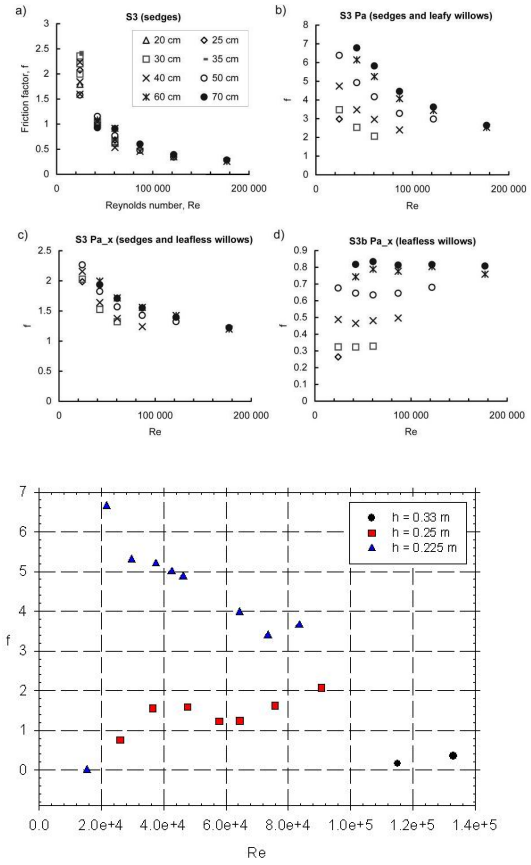

Figure 5.14: Results of 'f' according [22] (top) and according the performed lab measurements (bottom)

Comparison of the f-value of [22] and the lab experiments (Fig. 5.14) shows the similarity of the impact on the roughness coefficient of the floating plants (lab) and plants on the bottom [22]. The properties of the floating vegetation correspond with those of leafy willows (plants taken mid May) and leafless willows (plants taken in April). [22] mentionned that the f-value is more or less independent of Reynolds number for leafless willows, which have a small frontal area. For similar water levels, the roughness coefficient for floating vegetation is somewhat higher than for vegetation on the bottom as shown in the tests of [22]. For vegetation on the bottom, the

roughness increases with higher water level while for the floating vegetation the roughness decreases with increasing water level due to the lower relative blockage of the biomass. The tests performed with floating vegetation gave similar results as the measurements with plants on the bottom as described in different sources [22]. Due to the geometrical differences and the different flume set-up, exact values are difficult to compare.

Varying water level In a next step of the research, both discharge and water level in the flume are varied. The method used for analysis of the measurement results is based on literature review. Two series of measurements are carried out, for two different positions of the downstream weir. Water height and discharge in the flume are related by the calibration formula of the downstream weir:

$$Q = 2.408 * (h - h_0)^{1.5} \tag{5.3}$$

with Q [m^3/s] = discharge, h [m] = water level over the weir, h_0 [m] = height of the weir for each of the positions of the downstream weir. Based on this correlation, the study results in the study of only one parameter.

Study of the resistance of the flow based on the characteristics of the flow is performed by setting up a correlation between Manning's coefficient and the product VR as reported by [24, 25]. It is based on the principle of different regimes of plant flattening with increasing flow. When the grasses are not fully covered by the flow, Manning's coefficient will increase slowly as VR increases, as a result of increasing vibration. Indeed, the plant movement increases with increasing velocity. However, when the vegetation is totally submerged and is forced to bend, resistance will then decline. Minimum resistance values are obtained when the product VR is sufficiently large to force the plants to become fully flattened.
Further quantitative analysis is based on the graphs in the Technical Report of the Department of Natural Resources and Water concerning the soil conservation measures [26]. The analysis is based on the n-VR relationship which refers to the fact that n varies with the product of velocity and hydraulic radius. Under the influence of velocity and depth of flow, vegetation tends to bend and oscillate continuously. Such conditions have an effect on the behaviour of flow and this behaviour varies as the velocity and depth of flow changes. Curves for 5 degrees of vegetal reaction on stream flow are developed by [27] and [28]. These degrees are coupled to the average height of the vegetation. The measured values are compared with the figures (Fig. 5.15).

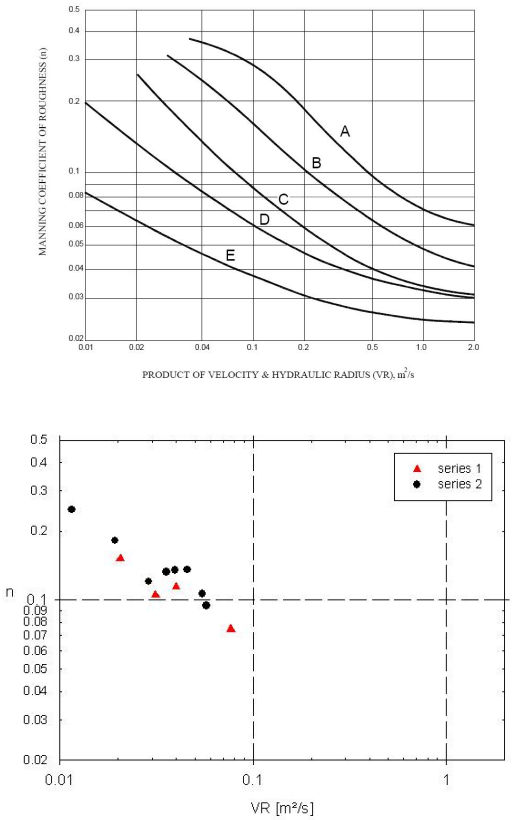

Figure 5.15: Relation between Manning's coefficient and the product of the velocity and the hydraulic radius for plants with low and very low influence on the flow: literature values (top) and measured values (bottom)

The resistance properties of the floating plants agree with the properties of plants on the bottom (between curve B and C) which both have limited influence on the stream flow. Also the downward trend for higher velocities is remarked.

In contrast of Manning's coefficient in the flume with constant water level, here, Manning's coefficient varies little with the water level. The ratio n_{eff}/n_b is independent of the water level for a given position of the downstream weir (and so, a serie of measurements). However, the influence of the water level is seen in Fig. 5.16: the relation n_{eff}/n_b is higher for lower water level (series 1 compared to series 2).

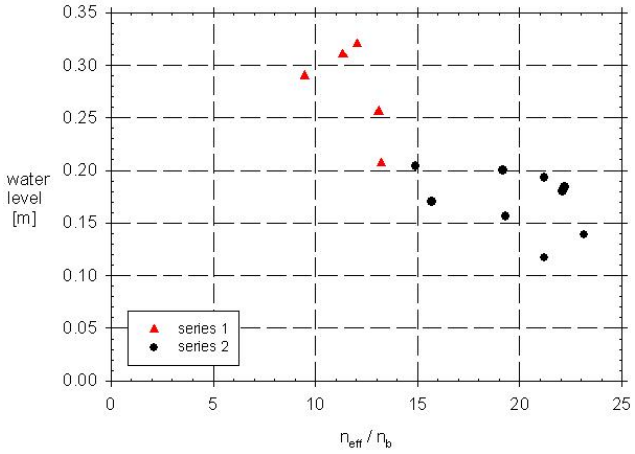

Figure 5.16: Relation n_{eff}/n_b to the water level for measurements with floating plants

Related to this conclusion, the blockage factor is introduced. Calculation of the blockage coefficient is carried out to study the obstruction properties of the macrophytes in the river. The proportion of a single cross-section blocked by plants is used:

$$B_X = A_V/A \tag{5.4}$$

A_V = part of the cross-section taken by plants [m^2]; A = area of the wetted cross section [m^2]; B_X = cross-sectional blockage factor [-].

For lower water levels, the relative obstruction (the blockage) is higher such as the relation n_{eff}/n_b (Fig. 5.16). This correlation is also incorporated in the analytical expression for the effective Manning coefficient according [24]:

$$n_{eff} = \frac{R^{\frac{2}{3}}\sqrt{S_f}}{BV_p + (1-B)\frac{R^{\frac{2}{3}}\sqrt{S_f}}{n_b}} = \frac{n_b}{1-B} \tag{5.5}$$

including values of V_p (velocity within the plants) [m/s], the hydraulic radius R [m] and the blockage B [-], which is the cross-sectional blockage factor B_X. Due to the large biomass density (in the area with floating vegetation), the velocity within the plants is negligible. The blockage is determined by (0.07/water depth) because the plants are put 7 cm under the

water surface of the flume.

A second formula is used to determine the relation between n_{eff} measured and n_{eff} calculated [29]:

$$n_{eff} = \sqrt{R^{\frac{4}{3}}(\frac{C_d B}{2gL} + \frac{n_b^2}{R^{4/3}})} \tag{5.6}$$

with L, the length of the vegetated area and C_d the drag coefficient which was measured.

Results are gathered in Fig. 5.17. n_{eff} as a function of the blockage value is depicted in Fig. 5.17a. A linear trend can be remarked. First, n_{Green} and $n_{Rigetti}$ are plotted against n_{eff} and a linear relation is observed for the theoretical expression of [24]. It is found that the correlation for n_{Green} is good, especially for higher water levels (Fig. 5.17). Using Eq.(5.6), larger deviations are remarked. Here, n_{Green} and the value of n from the lab measurements show an opposite relation. These are due the difficulty to determine C_d. Further, the correlation between n_{eff} measured and n_{eff} calculated is not constant. Next, n_{eff}, calculated according the theoretical formulas, is more or less constant as a function of n_b, but with an off-set difference. On the other hand, the measured n_{eff} changes with n_b. Formulas 5.10 and 5.6 are developed for vegetated reaches with also vegetation on the bottom. So, the study of n_b is already influenced by vegetation. Both formulas are not useful for further study of floating plants.

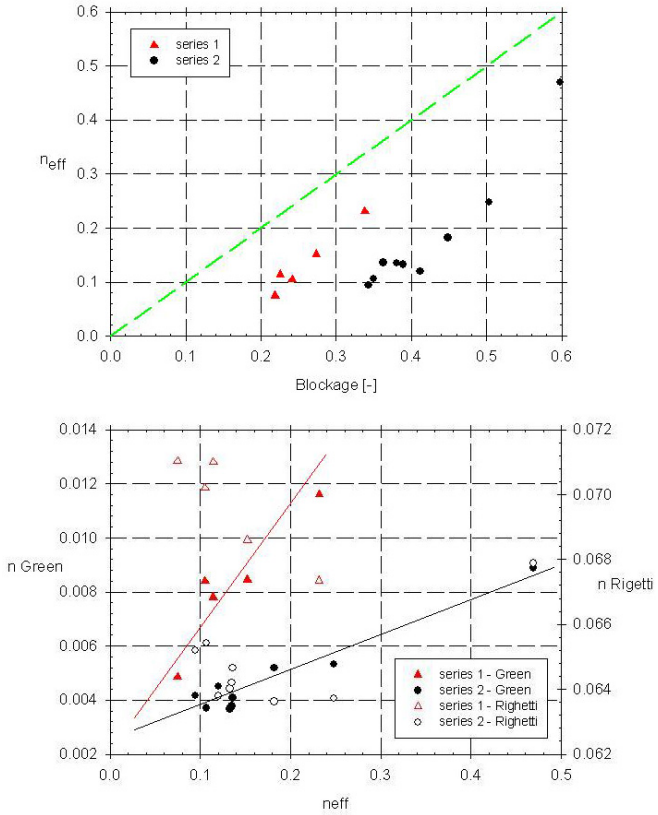

Figure 5.17: Manning's coefficient related to the blockage value (a, top) and Manning's coefficient according Green and Righetti compared to the effective Manning coefficient (b, bottom)

It is not clear if deviant values are due to measurement errors or to a varying relation. Three methods are compared: n_{eff} = f(n_b) (calculated from measurements), f(n_b, B) and f(n_b, Cd, L, Rh) (both calculated from the formula). Formulations of Green and Righetti comprise more parameters than the constant ratio between n_{eff} and n_b (Fig. 5.16). Formulas of Green and Righetti are comparable, but Righetti is more difficult to use due to the larger amount of parameters. The problem with all the expressions is that the ratio n_{eff} measured, to n_{eff} calculated is more or less constant but different from 1. An extra factor, influenced by the water level and so the amount of blockage, has to be added.

The drag coefficient C_d shows the combined effect of the backwater effect in front of the plants and the roughness coefficient [30]. Both effects

include a force on the plants. The value of C_d is determined by the shape of the stems, the leaves, the density, etc. The test set-up is not changed during the measurements and the value of C_d is kept constant. Constant values of C_d are proposed, based on literature: 1.5 [31], 1.0 [22], 1.25 or 1.75 [23]. However, in our lab measurements, values from 50 up to 130 are registered [32], varying with the Reynolds number. The reason for these high values is the little surface perpendicular to the flow (side of the frame). In fact, the large horizontal bottom surface area plants - flow is also responsible for transfer of forces. The dependence of the Reynolds number is also seen in [23, 33] and is due to the varying properties of the flow when passing the obstacle [34]. Shear stress in the contact surface of flow and vegetation causes a force in the direction of the flow.
During the measurements, the frames with plants are moving due to the flow and the cords (that hold the frames) are located under a slope. The total friction force of the flow on the plants is given by $F = 0.5 C_d V^2 A$ with F[N] = drag force = force component in the direction of the flow velocity, A[m^2] = surface area perpendicular to the flow (0.05 m^2), ρ[kg/m^3] = mass density of the water, C_d[-] = drag coefficient and V = the velocity of the fluid [35]. An equilibrium is calculated between the gravity force and the drag force: $\tan \theta = mg/F$ with g = gravity acceleration [m/s^2] and m = mass of the plants which is determined (4.8 kg/frame). Fig. 5.18 shows the forces on the floating plants.

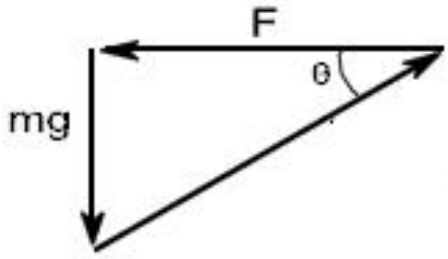

Figure 5.18: Forces on the floating plants for determination of the drag coefficient

During the measurements, the angle θ was measured and the drag coefficient calculated.

Additional to the relation n_{eff}-VR, the correlation $S_{f,eff}$-VR and $S_{f,eff}$-V is checked. The correlation is found to be linear, deviations are distributed randomly around the fitted value. For zero velocity, no effect

of the vegetation is measured and $S_{f,eff}$ has to be zero which is approximately confirmed by Fig. 5.19.

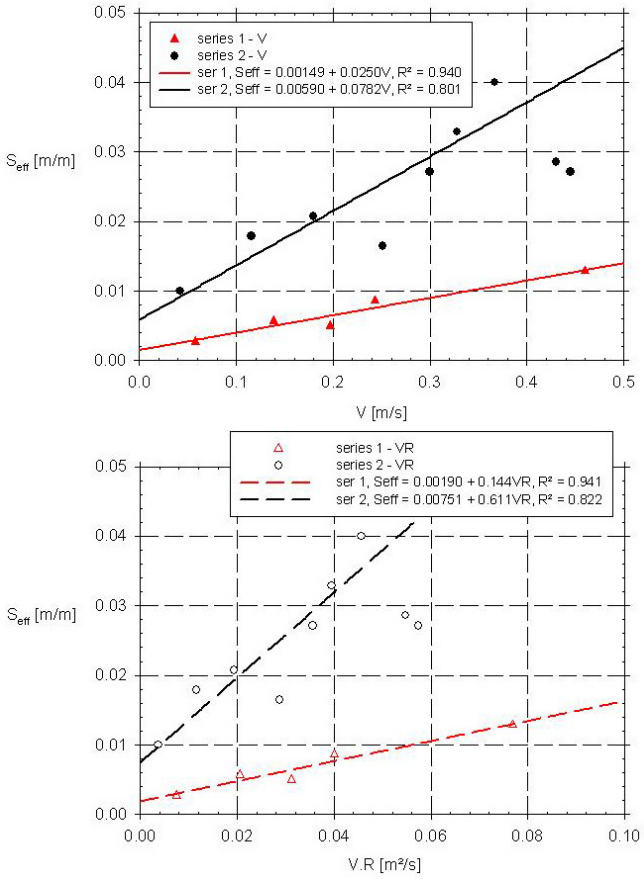

Figure 5.19: Correlation between $S_{f,eff}$ and V and correlation between $S_{f,eff}$ and V.R for measurements with floating plants

As well as the velocity, also the water level is important; even for equal flow velocities, the vegetational influence is largest for lower water levels due to the larger blockage and higher relative obstruction while the roughness remains constant.

As a relation between $S_{f,eff}$ and V was found, as well as a relation between $S_{f,b}$ and V (empty flume), the relation S_f-V may better describe the flow characteristics than the Manning coefficient.

Summarizing, it seems that addition of Manning's coefficient of the the

flume without obstacles and Manning's coefficient of the floating plants is possible. [30] advises against that approximation for plants on the bottom due to the fact that bottom roughness is dependent on the presence of vegetation. This is not the case for the floating plants; the bottom roughness and the vegetational roughness are independent. The resistance behaviour of floating plants and grassy plants (5 to 15 cm) on the bottom is comparable.

Discussion Two different series of tests have been performed:

- A constant reference water level, only changing the discharge by adapting the level of the downstream weir;
- A constant level of the weir, different discharge and water levels.

The first situation was easy to analyse as there was only one changing variable, the average velocity. Manning's n (n_{eff}), only caused by the vegetation, remained constant. Three different measurement series were performed, with each time a different water level. The difference in water level (0.225 - 0.33) remained limited, and by this also the influence of the difference in water height on drag and turbulence. Nevertheless, analysis showed an important influence of the water level on Manning's n. This means that the obstruction of the water by the plants is an important component in the flow resistance [21, 23, 36]. It can be described by means of the blockage factor. The values of the roughness coefficient were compared with experiments done by [22]. The properties of floating vegetation correspond with leafy willows (plants taken mid May) and leafless willows (plants taken in April). The tests performed with floating vegetation gave similar results as the measurements with plants on the bottom as described in different sources [22].

In the second situation, where both the water level and the discharge changed, analysis was more difficult as Manning's n did not stay constant. The values of Manning's coefficient could be compared with curves given by the USCS [3]. The floating vegetation corresponds to vegetation with an average effect on the flow. As with the previous series, analysis showed the influence of the blockage factor: n caused by the plants turned out to be related to n_b/1-B.

1.3 Variation of Manning's coefficient

1.3.1 Variation of Manning's coefficient over the length of the channel

Macrophyte properties are influencing the roughness of the river and so Manning's coefficient. To check general properties of rivers and to get an idea of discharges and water levels, it is sufficient to calculate a 'general' (including the effects over the reach) Manning coefficient over the reach. In reality, Manning's coefficient is varying over the length of the river and over the channel width. Furthermore, particular changes will influence the water surface level. As the vegetation varies along and across a river, by consequence, Manning's roughness coefficient is not a constant.
Using the Strive model, the variation of Manning's coefficient over the length of the river is investigated first, without changes over the width.

Calculations using Strive, with variation of Manning's coefficient over the length of the reach, are resulting in following conclusions [1]. The channel has a length of 1400 m, zero slope and a rectangular cross section with bottom width 5 m. The discharge is constant and equals 20 m^3/s and the downstream water level is 2 m. Calculations are performed in 57 sections (or 'nodes') over the reach. The overall Manning coefficient is 0.01 $m^{-1/3}s$. In one section, a value of 0.1 $m^{-1/3}s$ is chosen. The location of this section is varied from upstream to downstream for different calculations, not only to check the influence of the different Manning coefficients, but also the check the influence of the location of this different value. Using formulas (3.36) and (3.34), an average Manning coefficient of 0.0217 $m^{-1/3}s$ is obtained.
As a result, the upstream water level is 2.87 m, independent of the location of the section with higher Manning value. The more sections are marked with a higher Manning coefficient, the higher the upstream water level. This level only depends on the number of sections with higher Manning coefficient, not on the location of the sections.
A second set of calculations is based on a value of Manning's coefficient of 0.01 $m^{-1/3}s$ for half of the sections and 0.1 $m^{-1/3}s$ for the other half of the channel. The location of the sections with high and low Manning coefficients is varied several times, but the upstream water level does not change.
As a result, for a constant discharge, one can say that mowing of vegetation to lower the upstream water level may happen in any part of the river. For varying discharge, however, the drained discharge is higher and the downstream water level will rise compared to the initial situation [17], while the upstream water level is lower. To avoid inundation, removing the vegetation in the downstream part of the river is advisable.

As a third conclusion: the higher the Manning coefficient and at the more locations this higher value occurs, the higher the upstream water level will be.

1.3.2 Variation of Manning's coefficient over the width of the channel

In-stream vegetation is not only varying over the length but also over the width of the channel. Nowadays, computer programs for 3D simulations, where Manning's coefficient is attributed at each point, exist [37–39] and allow detailed calculations. Similar calculations cannot be carried out by the Strive model. As an alternative, 1D equations can be used for each part of the section individually next to addition of lateral mass transport terms [40, 41]. For these methods, no global Manning coefficient is calculated. On the other hand, the water transport module in Strive is based on the solution of the Saint-Venant equation with only one global Manning coefficient. Therefore, this value has to be calculated out of the roughness values for some separated parts of the channel. The general formula is given by [13]:

$$n[m^{-1/3}s] = \int_P w_i n_i dP = \sum_i w_i n_i \tag{5.7}$$

with coefficient of weight w_i for Manning's coefficient n_i and wetted perimeter P.

Different possibilities for the coefficient of weight are published. [13] gives an overview of values for w based on the geometrical characteristics of the section as the wetted perimeter P, the hydraulic radius R and the wetted cross section A. The coefficient of weight in [42] is based on the discharge through each part of the cross section. [43] proposed an expression based on the velocity distribution.
Not only the coefficient of weight influences the equation for the global Manning coefficient, also the width of the different parts of the cross section is important [40]. The roughness is a characteristic of the cross section borders but the internal boundaries are also important. Calculation of the wetted area is based on the geometry of these internal boundaries. The calculation of the wetted perimeter only takes into account the roughness at the borders, but not the internal shear stresses, which is not correct [40]. For permanent uniform flow, including secondary flow, the slope of the energy line will differ for the parts of the cross section, even if the slope of the water level is equal.

The different methods to calculate the global Manning coefficient are gathered in Table 5.7 [1]. The first method is based on the discharges: the

total discharge in the cross section is the sum of the discharges in the different parts of the cross section [17]. The second method says that the total wetted area of the cross section is the sum of the area of all parts of the cross section. The velocity and the energy slope are constant over the cross section [17]. The last method is based on the wetted perimeter: the total wetted perimeter of the cross section is the sum of the wetted perimeters of all parts of the cross section. Velocity and energy slope are constant over the width of the channel.

	assumption	global n value
method 1	Q = $\sum Q_i$	n = $(\frac{AR^{2/3}}{\sum \frac{A_i R_i^{2/3}}{n_i}})$
method 2	A = $\sum A_i$	n = $(\frac{\sum P_i n_i^{3/2}}{P})^{2/3}$
method 3	P = $\sum P_i$	n = $(\frac{A}{\sum \frac{A_i}{n_i^{3/2}}})^{2/3}$

Table 5.7: Formulas for global Manning coefficient calculation

Some calculations are carried out to check the accuracy of these formulas. A rectangular cross section, width 15 m and water level 5 m is chosen. The section is splitted in B1 (with n1) and B2 (with n2), and B1 + B2 = B. With a second value of the water level of 8 m, the influence of the water height is checked. For n1 = n2 = 0.1 $m^{-1/3}s$, and different split of the section, the results are shown in Table 5.8. The global n value differs for method 1. For method 2 and 3, the global n value equals the expected value of 0.1 $m^{-1/3}s$ and the water level in the reach is of no importance.

global n value	B1 = 0 m	B1 = 0 m	B1 = 7.5 m	B1 = 7.5 m	B1 = 15 m	B1 = 15 m
	h = 5 m	h = 8 m	h = 5 m	h = 8 m	h = 5 m	h = 8 m
method 1	0.0862	0.0820	0.1000	0.1000	0.0862	0.0820
method 2	0.1000	0.1000	0.1000	0.1000	0.1000	0.1000
method 3	0.1000	0.1000	0.1000	0.1000	0.1000	0.1000

Table 5.8: Influence of the formula and the water level on Manning's coefficient ([$m^{-1/3}s$])

Same calculations are carried out for different n values: n1 = 0.01 $m^{-1/3}s$ and n2 = 0.1 $m^{-1/3}s$ (Table 5.9). Only the 3rd method results into logic values. This result is also expected for method 2, but due to the definition (P1 = H + B1 and P2 = H + B2), also for B1 = 0, P1 is taken into account (and different from zero). So, this formula is not useful for a constant Manning coefficient over the cross section. The water level does not influence Manning's value in method 3.

global n value	B1 = 0 m	B1 = 0 m	B1 = 7.5 m	B1 = 7.5 m	B1 = 15 m	B1 = 15 m
	h = 5 m	h = 8 m	h = 5 m	h = 8 m	h = 5 m	h = 8 m
method 1	0.08618	0.08196	0.01818	0.01818	0.00862	0.00820
method 2	0.08663	0.08256	0.06432	0.06432	0.03703	0.04295
method 3	0.10000	0.10000	0.01555	0.01555	0.01000	0.01000

Table 5.9: Influence of the formula and the water level on Manning's coefficient ([$m^{-1/3}s$])

The third method gives the same value if Manning's coefficient is equal for each part of the cross section (Table 5.8). Also the second method gives these results, but pays too much importance on high Manning coefficients, even if they are only occurring in a small part of the cross section (Table 5.9). The third method is contrary to that. Therefore, the global n value, based on this method, is probably an underestimation.

Previous methods are built into the Strive code to perform calculations with a variable Manning coefficient over the length and the width of the channel. The water surface slope in a rectangular channel of 1400 m length and 5 m width is studied, the downstream water level is 2 m and the discharge 20 m^3/s. Simulations are carried out with different Manning coefficient over the width of the channel, the Manning coefficient is 0.01 $m^{-1/3}s$ and starting from the borders, a value of 0.1 is applied over varying distances. This means that the cross section is divided into three parts with higher Manning coefficient applied to the side parts. In Table 5.10, the width with higher n value starting from the borders is mentioned. Also the upstream water level is mentioned. The influence on a river where the biomass grows from the borders to the middle is seen. The result of method 1 is physically not possible, method 3 attributes much influence to the lower Manning coefficients in the section while in method 2, the back water effect is significant.

width with higher n value	upstream water level		
	method 1	method 2	method 3
borders	2.22 m	6.00 m	2.43 m
0.5 m	2.31 m	6.26 m	2.53 m
1 m	2.46 m	6.48 m	2.69 m
1.5 m	2.74 m	6.68 m	2.95 m
2 m	3.38 m	6.87 m	3.53 m
2.4995 m	7.03 m	7.04 m	7.03 m

Table 5.10: Values for the upstream water level for varying value of Manning's coefficient over the width of the channel

In a second verification, a higher n value is attributed to a part of the channel with a width of 3 m. The distance between this zone and the border is varied. For method 2 and 3, the position of the 3m-zone with higher n value is not influencing the result. For method 1, the calculation of the global Manning coefficient is influenced by the position and the relative width of the different zones. The back water effect is more important if the higher rouhghness zone is located more in the middle. Border vegetation is less important than vegetation central in the stream. This is according [44].

2 Field data

The data from the measurement campaigns allow to determine the variation of the roughness coefficient (friction factor or Manning's coefficient n [$m^{-1/3}s$]) as a function of time, type and density of vegetation, hydraulic parameters, etc.

2.1 Manning formula and Bresse equation

As different approaches show great variability of n, they do not guarantee accurate values for the roughness coefficient and a determination of the roughness starting from measurements is recommended. Therefore, some assumptions are made: first, the bottom slope and the cross sections are supposed to be stable, so sediment transport and transformation of the channel bed are not included. Further, the friction factor or roughness coefficient (expressed by Manning's coefficient n) is set as a constant value in the channel and at the banks. The flow is regarded in a 1-dimensional way, with uniform velocity over the cross section. Manning's coefficient n has been calculated in two ways: first, when uniform flow is supposed, the energy slope is equal to the bottom slope and n is obtained from the Manning equation. Second, when the Bresse equation is used, steady state flow is assumed and the roughness coefficient n is calculated from the energy slope.

Using Cowan's formula [45] for the river Aa leads to values from 0.04 $m^{-1/3}s$ for winter situations (low amount of vegetation) to 0.15 $m^{-1/3}s$ for summer situations (high amount of vegetation). Using the tables with Manning values mentioned in [11], leads to the same range of values. The calculated Manning coefficient, based on measurements of water level and velocity, confirms these values for autumn and spring situations, but during summer, Manning coefficients are much higher and can reach values up to 0.4 and even 0.5 $m^{-1/3}s$. Therefore, it is advised to consider Man-

ning's coefficient as the result of the Bresse equation.

In Fig. 5.20, the calculation of Manning's coefficient is carried out for the upstream part of the river Biebrza, from Lipsk to Sztabin. The resulting water levels between Lipsk and Sztabin obtained by using Manning's coefficient from Bresses equation correspond very well with the measurements while these obtained by using Manning's coefficient from the Manning formula return larger values of the water levels in the downstream part (neighbourhood of Sztabin) of the reach. The results using Bresse's equation are much more accurate than those from the Manning equation. Using the Manning formula, Manning's coefficient is 0.16 $m^{-1/3}s$ upstream Lipsk, for Lipsk to Ostrowie, this value is 0.27 $m^{-1/3}s$ and for the downstream part, Manning's coefficient is 0.65 $m^{-1/3}s$. Use of the Bresse equation, has resulted in more accurate values for the downstream part; in the neighbourhood of Sztabin (last two points), Manning's coefficient was 0.4 $m^{-1/3}s$, while this value was 0.5 $m^{-1/3}s$ for the other points between Sztabin and Ostrowie.

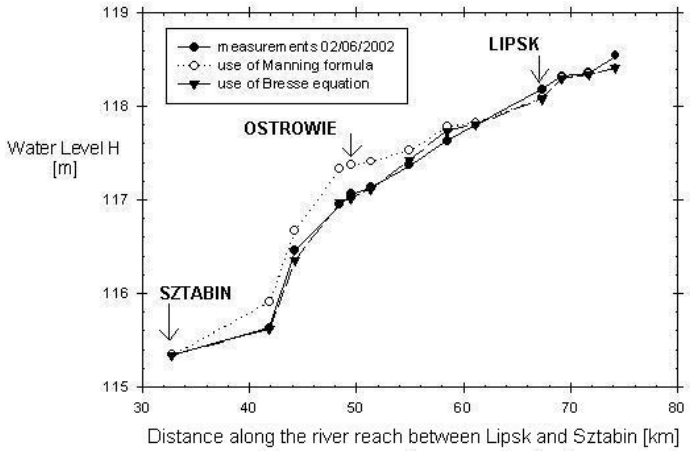

Figure 5.20: Comparison between measured water levels and the values (calculated using Manning's coefficient n) obtained from Manning's and Bresse's equation

Due to the wide range of factors influencing Manning's roughness coefficient, accurate measurement is difficult and very extensive. Therefore, a well established model allows to compute Manning's coefficient for any discharge on any location. However, a large amount of data over a sufficient long period is necessary to set up such a model.

2.2 Manning's coefficient as a function of time

The variation of Manning's coefficient as a function of time has been investigated in the river Aa. Manning's coefficient for the river Aa is calculated according to three different approaches, in the following mentioned as 'Approach 1', 'Approach 2' and 'Approach 3'. 'Approach 1' calculates the roughness coefficient directly using Manning's equation. Second way (Approach 2) of calculating Manning's coefficient is by using the numerical model Hec-Ras solving the complete Saint- Venant equations (in steady state conditions known as the Bresse equation). Fitting allows to determine the roughness value. 'Approach 3' is similar to 'Approach 2' but is using a simplified river geometry. These three calculation methods for Manning's coefficient are applied and calculations are carried out separately for both the discharges measured up- and downstream.
For each of the monthly measurements, Manning's coefficient is plotted in Fig. 5.21, starting from September 04 for two years. The different calculation methods are indicated with a different symbol. Using the same approach, the Manning values based on both the up- and downstream discharge values are very similar.

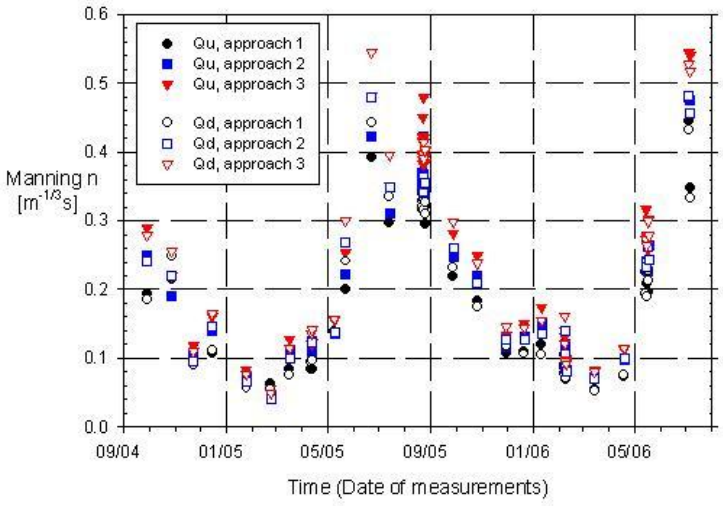

Figure 5.21: Manning's coefficient n for the upstream (Qu) and downstream (Qd) value of Q: comparison of the values calculated using three approaches: Manning's equation given by Eq.(3.34) (1), fitting based on the Saint-Venant (Bresse) equations (HEC-RAS)(2), and fitting using an average section (3)

For the measurements of November 05, January and February 06, differences in Manning's coefficient are negligible. The scatter is larger for the measurements of September, May and June, which is probably due to the larger amount of vegetation. During winter, the presence of vegetation remains rather small and constant, while during spring and summer, Manning's coefficient increases rapidly with the amount of vegetation.
From this, a seasonal trend is observed in the value of Manning's coefficient with low values appearing in January, February (winter), a slight increase in March and April and a fast rise in May and June. Then, the resistance remains high during summer. During winter, most plants have disappeared, yielding lower flow resistance and a decreasing roughness coefficient.
As can be seen, during spring, Manning's coefficients are up to 10 times higher than the values during winter.

Based on the results in Fig. 5.21, a curve is fitted to the trend in the n-values. The best fit is obtained by using a polynomial function (power 6). Six curves are calculated , for each of the 'Approaches'. For each of the curves, the correlation coefficient is calculated and shown in Table 5.11. As can be seen, the correlation is slightly better for the upstream discharges. Besides, the numerical approach (2) (Hec-Ras model, based on the Bresse equation for steady flow) turns into the best fit, so, this method will be used for all further calculations. This corresponds also with the findings of Fig. 5.20, where larger deviations are noticed for the results of the simplified Manning equation.

R^2	Qupstream	Qdownstream
Approach 1	0.8903	0.8725
Approach 2	0.8993	0.8895
Approach 3	0.8980	0.8884

Table 5.11: Values of the correlation coefficient for the fitted curve and the measured values, calculated for each of the 'Approaches' (Manning's equation given by Eq.(3.34) (1), fitting based on the Saint-Venant (Bresse) equations (HEC-RAS)(2), and fitting using an average section (3)) for both the upstream and downstream discharge

From the findings in Table 5.11, it is also concluded that using a simplified geometry doesn't affect very much the accuracy of the calculations. Therefore, the occurring geometry is simplified to rectangular or trapezoidal cross sections.

From Fig. 5.21, some variation over the season '04-'05 and '05-'06 can be seen, but the difference in these two years is not significant.

2.3 Manning's coefficient as a function of distance and water level

As the roughness is strongly dependent on the vegetation density, Manning's coefficient varies with distance due to the various amount of vegetation through the river. This variation was investigated on the river Biebrza (Poland) in the reach between Rogozynek and Rogozyn, more than 5 km long, where Manning's coefficient is calculated in 7 sections (Fig. 5.22). In each of the cross sections, the water level H and the discharge Q have been measured in June 05 during a steady flow situation. The results are shown in Table 5.12 and Fig. 5.23.

	Water Level H [m TAW]	Distance [m]	Cum. dist. [m]	Q [m^3/s]	n (Qmeas.) [$m^{-1/3}s$]	n (Qav.) [$m^{-1/3}s$]
1	119.029		0	0.380		
2	119.105	272	272	0.350	0.172	0.178
3	119.557	1541	1813	0.390	0.317	0.303
4	119.667	667	2480	0.340	0.085	0.090
5	119.780	869	3349	0.370	0.068	0.063
6	120.114	1223	4572	0.350	0.082	0.083
7	120.190	608	5180	0.365	0.140	0.134

Table 5.12: Reach Rogozynek (downstream) - Rogozyn (upstream) of Biebrza River: measured water levels H and discharges Q in June 05 as a function of distance from the upstream boundary, and calculated Manning coefficients n

Manning's coefficient is calculated based on the Manning formula, once with the discharge (Qmeas) measured in each section, once with the average discharge (Qav = 0.367 m^3/s) of all sections. Water levels to calculate the energy slope S_f are measured in each section. The average discharge is used to look at the deviations due to the influence of the accuracy of the discharge measurement. Because of the comparable discharges in each section, the deviations are small. In spite of the constant discharge, Manning's coefficient differs from one location to another. The smaller influence of the different discharges is also clear when the values for Manning's coefficient calculated with the different discharge values are compared. Manning's coefficient value is very similar in both cases. The big rise in Manning's coefficient between section 2 and 3 is due to an obstruction, a piece of wood, in the river. It shows that these natural and temporal situations can have a big influence on the calculation results.

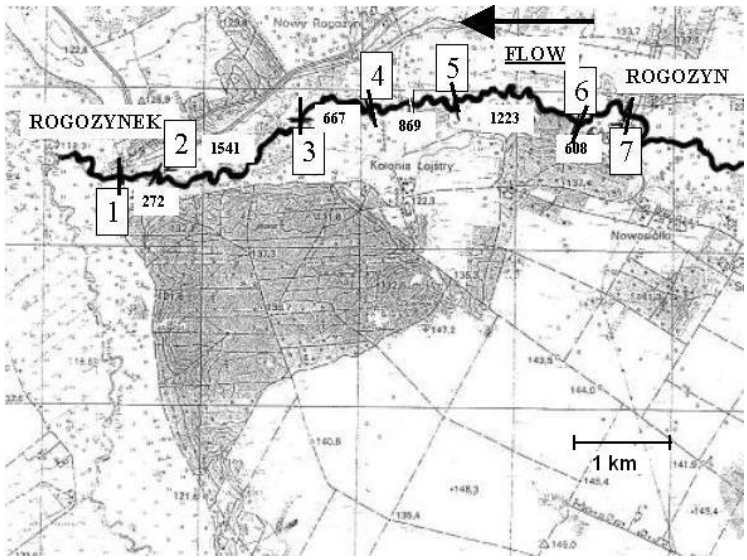

Figure 5.22: Measurement points in the reach between Rogozyn and Rogozynek

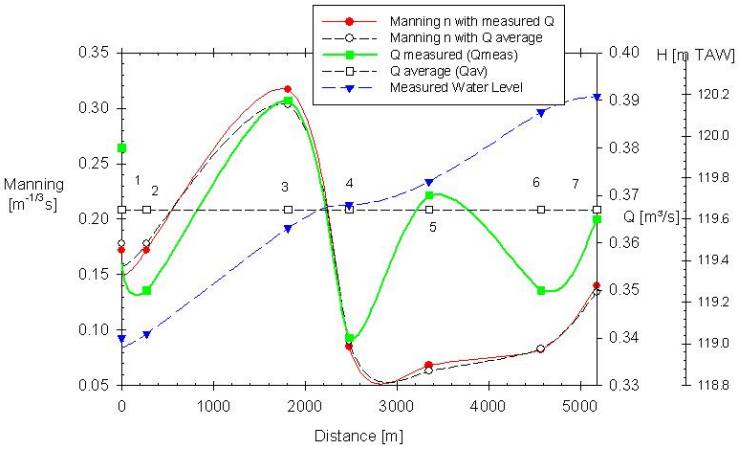

Figure 5.23: Measured discharge Q, measured water level H and calculated Manning's coefficient n in the reach between Rogozyn and Rogozynek

2.4 Manning's coefficient in relation to discharge and biomass

2.4.1 Literature review

Vegetation growth drastically influences water levels and flow patterns in lowland rivers. As soon as plants start to grow in spring, the flow resistance increases to reach a maximum in early summer.

The universities of Ghent and Antwerp are conducting scientific research in the river Aa in Belgium in order to better understand the relation between aquatic weed growth and the hydraulic capacity of the river and to come to a more accurate determination of the different influencing parameters.

Velocity measurements are performed and studied in multiple cross-sections on a regular base. Discharge calculations are based on velocity measurements, which deliver important information about structural characteristics of the river, presence of vegetation, etc. Removing the vegetation allows for determining species and vegetation density as well as for studying the influence of plants on flow distribution and patterns. It is shown that the roughness coefficient, influenced by the amount of biomass, is an important parameter for the hydraulic characteristics of the river. The presence of macrophytes and their blockage characteristics are studied and a relation between discharge, biomass and roughness coefficient is set up.

This leads to more reliable results in the application of hydraulic models for river management and river restoration purposes.

River flow is caused by the runoff of precipitation. On a natural undeveloped river system, the fluctuations in discharge result from variations in the duration, frequency, intensity and areal cover of precipitation and in the catchment characteristics which control the rate and the amount of runoff [2]. So, stream flow is governed by the geometry of the river, the bottom slope, the discharge, the occurring water levels and the flow resistance (described by Manning's coefficient n).

The presence of vegetation on the riverbed has an influence on the hydrodynamic characteristics of the flow; moreover, a seasonal variation of the vegetation causes variation of the depth of flow and variation of the roughness. Vegetation affects the fluvial processes as exchange of sediment, nutrients and contaminants [46, 47]. Here, the vegetation are macrophytes with spatial and temporal variation. The variation of vegetation is expressed as a change in flow resistance characteristics which has consequently a major effect on the flow, i.e. on the hydraulic capacity of the river.

Many unshaded lowland rivers are showing abundant aquatic vegetation growth in spring and summer. The presence of these aquatic plants (macrophytes) will affect river hydraulics as well as biochemical and ecological processes. Inside the vegetation, reduced flow velocities are promoting sedimentation and retention of fine sediments, organic matter and nutrients, whereas erosion prevails in the bare channels that are meandering along the macrophyte patches [48–51]. As such, macrophytes are supporting structural and functional heterogeneity in the river, which is favouring habitat and species diversity [52]. Therefore, macrophytes are considered to play a key role in the ecosystem functioning of rivers [53–55].

The European Union imposes a good quality of surface water by 2015 as laid down in the 'Water Framework Directive' (2000/60 EG). This includes not only a better water quality but also structural interventions in the rivers. A better water quality influences the macrophytes in rivers and so, the drainage of the river. Therefore, the ecological and hydraulic function of the macrophytes has to be understood. The vegetation influences the resistance of the channel bed and banks which, as a major modelling parameter, is important for the prediction of floods since aquatic plants can lead to a substantial rise of the water level [56, 57].

[58] developed a model describing the influence of in-stream vegetation growth on the hydraulic characteristics of streams in different ways. This amount of vegetation determines the flow characteristics (by change in resistance coefficient, average water depth and velocity). This model is known as the conceptual model of Watson [58]. According to this model, the Manning coefficient is not only influenced by the plant growth, but also by the water velocity and the water depth. These hydraulic parameters also influence the amount of macrophytes. So plant cover is an important parameter which changes the flow (Manning's coefficient, water depth and water velocity) for varying discharge. As Manning's coefficient is closely linked to the amount of vegetation (biomass), the variation of hydraulic characteristics can be predicted with the model of Watson. It indicates that if plant cover, discharge and velocity in the river increase, then Manning's coefficient, the mean depth and the water level will decrease. Watson showed that Manning's coefficient is strongly influenced by the seasonal variation of vegetation growth. It was studied that decreasing resistance corresponds with an increasing discharge and the effect is more evident for higher vegetation density. Certainly for small discharges, the density of the plants is a distinctive factor. During peak growth of the vegetation (April - June), the biomass as well as Manning's coefficient are

inversely proportional to the flow velocity in the water course [59], which is also clearly illustrated in the conceptual model of Watson [58].

In general, Manning's coefficient is inversely proportional to the discharge, as well for the percentage of vegetation in a certain cross section as for the biomass density [g/m^2] along the river reach. This is also demonstrated in [60], where the results of field measurements are studied, while the effects shown in [61] are the result of laboratory experiments.

On the other hand, [62] and [63] have indicated that the biomass and Manning's coefficient are proportional to the stream flow. An increasing discharge causes an increasing water depth in the river and so there is more space for vegetation growth. As a result, there is an increase in biomass and Manning coefficient. This is also confirmed by [58]. Of course, this situation is not occurring in case of peak discharges, due to the slower response of the macrophytes, but only when the discharge increases significantly over a longer period.

From both previous paragraphs it can be concluded that Manning's coefficient is not only influenced by vegetation growth, as also the average velocity and the water depth are important. Vice versa, velocity and water depth are also influencing the vegetation.

Stephens [64] added that the dimensions of the water course are important. In larger channels (hydraulic radius $R > 6$ m), the seasonal influence is small and Manning's coefficient is more or less stable. For small rivers (cross section smaller then 18.5 m^2) and for average values of the cross sections between 18.5 m^2 and 185 m^2, Manning's coefficient is strongly influenced by the seasonal variation in plant growth. Further, next to the seasonal variation, there is also a daily variation in Manning's coefficient. A large O_2 production during the day causes less flexible stems of the plant (Powell in [2]).

In terms of hydraulics, the aquatic macrophytes are acting as an obstruction to flow, increasing the hydraulic resistance of the river and reducing average flow velocities [52, 58, 65]. Next to these large-scale effects, more complicated flow patterns are developed at the scale of individual macrophyte stands [48], which can influence transport and retention of solutes and particulate matter. In turn, these processes are determining surface water quality, river morphology and habitat development for invertebrates or fishes [4, 55, 66, 67]. Therefore, a sound understanding and quantification of the interaction between flow and macrophytes is important for sustainable river management in terms of water quantity, water quality, geomorphology and ecology.

First, overall macrophyte charcteristics in general are important while also the individual type of plants is playing an important role. For most of the plant species it is shown that a higher vegetation density results in a lower velocity [24]. Floating-leaved plants cause a reduction of the surface velocity as well as submerged plants. Plants, floating on the water surface, will drift together and cause blockage in the river when the discharge is high. A wealthy plant growth can also cause an obstruction of the drainage because of the reduction of the section, which is a problem for small discharges. For higher discharges, plants are pulled down. The inversely proportional relation between discharge and Manning's coefficient ($1/n \sim Q$) is most evident for submerged plants. The relative reduction of the resistance coefficient with increasing discharge is more important for higher vegetation density and higher biomass [68].

For emerged plants (above the water, e.g. reeds), certainly higher discharges can cause problems. The plants, in normal conditions seen above the water, are pushed into the water, by this causing a reduction of the cross section [61]. For emerged plants, the link between discharge and Manning's coefficient is proportional ($n \sim Q$) because an increasing discharge causes an increasing presence of plants in the cross section of the river. Flattening of the vegetation does not appear so that the flow resistance will increase.

Chow [11] found for floating plants values of Manning's coefficient twice as high, while submerged plants can cause a multiplication up till 20 compared to non-vegetated channels. The channels considered in this latter study are comparable to the river studied in this research (a lot of nutrients, a wealthy plant growth and, as a consequence, obstruction of the drainage). When comparing the lowest and the higher values of Manning's coefficient, calculated out of the measurements, the difference between both reaches a factor 10 to 12. Most of the plants in this reach are indeed submerged plants.

The amount of vegetation in a cross section can be expressed by the blockage coefficient [%]. This value presents the part of the cross section obstructed by plants compared to the entire area of the cross section or the proportion of the channel blocked by vegetation [69]. However, there are several types of blockage factors.

First, there is the cross-sectional blockage factor B_X, defined as the proportion of one cross-sections blocked by macrophyte stands. An alternative to this is the surface area blockage factor B_{SA}, which relates the plan surface area of the vegetation to the plan surface area of the channel

(the proportion of the surface area of a study reach containing vegetation). Then, there is a volumetric version of the blockage factor, which relates the volume occupied by the plants to the volume of the selected reach. This is the volumetric blockage factor B_V, defined as the proportion of the volume of a study reach blocked. A fourth blockage factor is the multi-cross sectional blockage.

[70] found that it was easier to measure the surface area ratio for determination of the vegetation. According [44], Fisher's equation is as follows:

$$n[m^{-1/3}s] \quad = \quad 0.0337 + 0.0239\frac{B_{SA}}{VR} \tag{5.8}$$

with V = velocity [m/s]; R = hydraulic radius [m]; n = Manning's coefficient [$m^{-1/3}s$]

However, the surface area of the plants is not directly related to resistance, because it does not take into account the proportion of the channel depth that the plants occupy. The vegetation surface area ratio can only be used if there is a relationship between the surface area of the plants and their volume. For channels with different depths occupied by vegetation, Fisher's equation can not be used. This equation also does not account for the non-linear nature of the n-VR relationships [44]. Several studies have used an equivalent measure of the cross-sectional blockage factor, finding that it has a linear relationship with Manning's n [71, 72]. [24] supposed non-linearity of this relation and plotted a wide range of measurements. Due to large scattering, the hypothesis of a linear or exponential relation is still open [44]. However, flow-channel studies of cylindrical roughness elements have suggested that resistance is only significantly affected above a threshold vegetation density [73], after which there is a sharp increase in resistance and a linear increase with vegetation density thereafter [44, 74].

2.4.2 Influence of vegetation on discharge measurements

In this paragraph, it is checked whether the presence of vegetation influences the quality and the accuracy of the discharge measurements.
In the month of April (2005), discharge measurements were carried out in three sections (S1: 50 m downstream weir 3, S2: 50 m upstream weir 4, S3: 30 m upstream weir 4). In August, measurements were performed in the same downstream and upstream sections. The measurements were performed with an electromagnetic device (Valeport, cylindrical sensor). Results are shown in Table 5.13. Macrophytes were only removed after the measurement, so their influence is not included in the measurements. In

April, the average dry weight of the biomass was 63 g/m^2, while in August (26th), values of 306 g/m^2 were measured.

	Time	Q $[m^3/s]$	A $[m^2]$	R [m]	P [m]	V [m/s]
April						
Section 1a	10:00 - 11:10	2.72	12.858	0.866	14.844	0.211
Section 2a	11:20 - 12:45	2.77	13.108	0.864	15.163	0.211
Section 3a	13:15 - 14:25	2.89	12.813	0.881	15.549	0.225
August						
Section 1b	10:00 - 12:05	1.47	17.119	0.996	17.179	0.086
Section 2b	09:40 - 11:40	1.46	13.626	0.815	16.725	0.107
Section 3b	12:20 - 14:05	1.44	14.479	0.962	15.053	0.099

Table 5.13: Overview of discharge Q, wetted section A, hydraulic radius R, wetted perimeter P and average velocity V for the different sections

Table 5.13 presents the hydraulic characteristics of the sections. As can be seen, notwithstanding the fact that the wetted section A is larger in August then in April, a smaller discharge is calculated which is due to the amount of vegetation. Macrophytes obstruct the flow resulting in lower velocities and higher water levels. The first series of measurements was carried out on April 14th, at the time indicated in the table.

During the campaign of August, field measurements were carried out with different devices in the same cross sections. Next to the propeller, also two different electromagnetic devices (type Valeport, cylindrical sensor) are used. Results are mentioned in Table 5.14. Values between brackets are propeller measurements in non-cleaned sections, which include the influence of the vegetation.
Lower values are measured with propellers; for the electromagnetic devices no differences were seen over the days, as macrophytes were removed in the downstream section on August, 23rd (evening). So, the quality of the discharge measurements is not influenced by the presence of vegetation on condition that the measurements are carried out with an electromagnetic device.

Q [m^3/s]		22/08/05	23/08/05	24/08/05	25/08/05
upstr. section	propeller	0.72	(0.68)	(0.69)	-
	V'port LvH	-	0.80	0.78	0.84
	V'port UA	-	-	-	0.91
downstr. section	propeller	-	0.79	-	-
	V'port LvH	0.73/0.77	0.77	0.80	0.87
	V'port UA	-	-	0.84	0.82

Table 5.14: Results of the discharge measurement (V'port = Valeport) in the upstream and downstream section in the period of August 05

This conclusion is confirmed by measurements performed in June 06 in the Biebrza river (Poland). During a measurement campaign, three sections were selected and the discharge was determined before and after removing vegetation. As can be seen (Table 5.15), the discharges measured with and without vegetation correspond very well.

Q [m^3/s]	with vegetation	without vegetation
Section 1: Novy Rogozyn	0.179	0.181
Section 2: Rogozynek	0.215	0.214
Section 3: Rogozyn	0.225	0.208

Table 5.15: Results of the discharge measurement in Poland, the same cross sections were sampled with and without vegetation

2.4.3 Relation between Manning's coefficient, discharge and biomass

The relation between biomass and Manning's coefficient has been investigated in the river Aa as in correspondence with the discharge measurements, also the biomass has been determined. For most of the plant species it is obvious that a denser vegetation, results in a lower velocity in the reach occupied by macrophytes. Floating plants cause a reduction of the surface velocity, while submerged plants influence the complete vertical velocity distribution. A wealthy plant growth causes an obstruction of the drainage because of the reduction of the section, which is a problem especially for small discharges (low velocities). For higher discharges (high velocities), the plants are pushed down, by this reducing their influence.
For emerged plants (as reed), certainly higher discharges can cause problems if the plants, that in normal conditions can be seen above the water, are pushed into the water and cause a reduction of the cross section. During peak growth of the vegetation (April - June), the biomass as well as Manning's coefficient are inversely proportional to the flow velocity in the water course [61].

Manning's coefficient is linked to the biomass and by this the biomass is a good parameter for the added roughness of the channel. A positive correlation between the biomass and Manning's coefficient was found by Brooker and mentioned in [61].

For low values of the biomass (less then 100 g/m^2), Manning's coefficient is varying between 0.04 and 0.14 $m^{-1/3}s$. This variation is due to different discharges. The lowest values of Manning's coefficient correspond with a zero level of biomass.

It becomes evident again that Manning's coefficient is strongly increasing in spring, due to explosive vegetation growth (Fig. 5.24). During summer, the roughness reaches a peak value. After dying out of the plants, Manning's coefficient is also decreasing. This cycle is almost the same for each year (Fig. 5.21). A sudden fall in the roughness during the vegetation period can be due to the wash away or flattening of a vegetation patch with large discharges. The roughness decreases when the discharge increases. Hence, the variation of Manning's coefficient is influenced by both discharge and vegetation.
Fig. 5.24 shows that lower discharges correspond with higher Manning coefficients. A larger amount of vegetation, reduces the cross sections open to flow so that less water can pass in a given time period. Discharges are varying between 0.6 and 3.2 m^3/s. Manning values range from 0.05 to 0.5 $m^{-1/3}s$. The trend follows Eq.(3.34) and is the same for upstream and downstream measured discharges.

In the following, the relationship between discharge, biomass and Manning's coefficient is investigated in more detail. Two methods to determine the value of Manning's coefficient for numerical modelling are used and are referred to as 'Method 1' and 'Method 2'.
The first method to calculate Manning's coefficient is based on measurements of discharge and water level over the years in the river Aa. The geometry of the cross sections is incorporated in the calculations. For all measurements carried out over three years, Manning's coefficient is calculated using measured discharge and water level and the one-dimensional HecRas model [75]. The Saint-Venant equations are simplified to the Bresse-equation due to the assumption of steady flow during the measurements of discharge and water level (cf. supra).
The second method (Chapter 6) determines a long-term continuous relationship between Manning's coefficient, discharge and biomass. To set up this relationship, Manning's coefficient is calculated using the Strive model for steady flow based on Eq.(3.31) and the geometrical characteristics built in the Strive model. This geometry is simplified, trapezoidal, and in

very good agreement with the measured geometry of the channel. Under these conditions, use of the Manning equation (Eq.3.34) results in the same values as use of the Bresse equation in the Strive model. Measured discharges and water levels are used.

As Manning's coefficient turns out to be an important calibration parameter, further attention is paid to its value. Manning's coefficient is calculated according to 'Method 1' and shown in Fig. 5.24a as a function of time. The discharge measured at the upstream boundary is indicated as Q-upstream and the discharge at the downstream boundary is Q-downstream. For each of the measured discharge values and the corresponding geometrical characteristics, Manning's coefficient is calculated.
Fig. 5.24a shows the time variation of measured biomass density and calculated Manning coefficient with monthly intervals between September 04 and April 07. The correlation between biomass and Manning's coefficient is clear. Low values for both are seen during winter (November to April), high values during spring and summer (June to September). More biomass results in a higher Manning coefficient [76]. So, the biomass is a good indicator for the roughness of the channel.
In 2006 the explosive biomass growth phase started later than in 2005 and quite high biomass densities were maintained until the end of September. Since light and temperature are major triggers for biological processes, that shift can be assigned to the meteorological conditions. In 2006 night frost continued until the second half of April, whilst in 2005 night temperatures remained positive from the second half of March onwards. Also solar irradiance was approximately 10% less in spring 2006. On the other hand, September 2006 was extremely dry and relatively hot, resulting in an extension of the growth season. Moreover, the low discharges in September '06 maintained considerable biomass densities since wash out contributes substantially to biomass losses in late summer and in the autumn [77]. The values of the measurements of biomass densities during the measurement campaigns are gathered in Table 5.16.

period	biomass density measured [g/m^2]
april 05	63
august 05	306
february 06	13
may 06	157

Table 5.16: Overview of measured biomass density values during the measurement campaigns

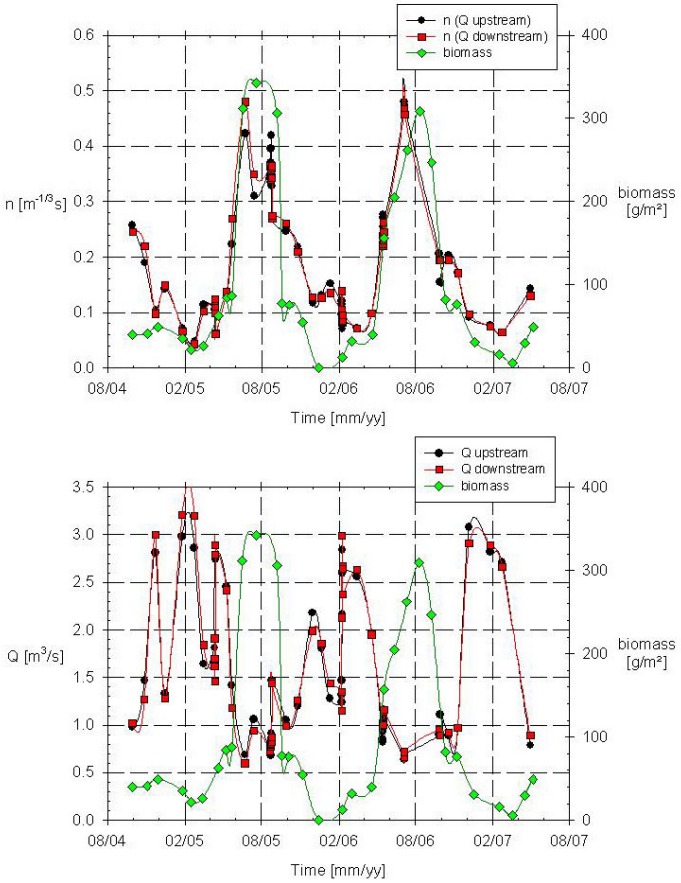

Figure 5.24: Calculated Manning coefficient, measured biomass density (Fig. a, top) and measured discharge upstream and downstream together with the measured biomass density (Fig. b, bottom), in the period from September 04 to April 07 for the river Aa

Fig. 5.24b presents the measured discharges in the upstream and downstream section together with the biomass in the same period.
Manning's coefficient is linked to the discharge by the Bresse equation and a relation with the amount of biomass in the river is remarked. In the following, the relation between these parameters is explored aiming at deriving a general prediction tool for Manning's coefficient as a function of discharge and biomass density, which is applicable for numerical modelling purposes in Strive.

2.4.4 Resistance

A positive correlation between the biomass and Manning's coefficient was found by [59] and mentioned in [61].
Presence of vegetation increases the roughness and decreases the section and by this also the water level for the same discharge value. The vegetational increase of the roughness can also be found, using Cowan's equation where the additional component of the vegetation is expressed by n_4 (Eq.(3.35)). However, these tables are set up for specific situations in particular rivers and give only loose indications.

It becomes evident again that Manning's coefficient is strongly increasing in spring, due to explosive vegetation growth (Fig. 6.24a). During summer, the roughness reaches a peak value. With dying out of the plants, also Manning's coefficient is decreasing.

A sudden fall in the roughness during the vegetation period is probably due to the wash away or flattening of a vegetation patch with large discharges. By this the discharge influences Manning's coefficient. The roughness decreases when the discharge increases. Hence, the variation of Manning's coefficient is influenced by discharge and vegetation. This may explain the variation in the value of Manning's coefficient with similar amount of biomass (Fig. 6.24b). For low values of the biomass (less then 100 g/m^2), Manning's coefficient is varying between 0.04 and 0.14 $m^{-1/3}/s$, due to different discharges. As is indicated in [76], lower discharges correspond with higher Manning coefficients.
As there is no correlation between discharge and biomass and they both influence on Manning's coefficient, a study of the relation between Manning resistance coefficient, amount of biomass and discharge is performed.

The relation between resistance and hydraulic characteristics is already described by a theoretical profile confirmed by data collection. The biomass influence on the velocity distribution in rivers is predominantly described by empirical models which are developed from data collection from natural river channels. These models try to find relationships be-

tween the hydraulic parameters and the presence of vegetation in the channel. They have the advantage that the vegetation parameters (biomass) are easily measured, and they have been proven to work in the conditions for which they were elaborated [24]. The presence of vegetation will obstruct the flow more or less depending on the flattening of the plants, as mentioned before. The architecture and the characteristics of the plant will determine its behaviour under different flow regimes.

In literature [4, 78], the product of the velocity V and hydraulic radius R (replacing discharge) is used to describe the influence of plants on Manning's coefficient. This product is an indication of the value of Manning's n for grasses and grass-like plants, comparable to the river Aa. In Fig. 5.25, the theoretical profile, defined by [79], is plotted together with the measured values for n and VR from Aa measurements from September 2004 to May 2006. V is the average velocity in the river, calculated using the measured velocity field over the cross section. The hydraulic radius R equals the wetted cross section area divided by the wetted length. In addition, [4] also mentions other research where the energy slope and the individual flexibility and stifness of the plants are taken into account.

Fig. 5.25 shows how Manning's coefficient typically changes with an increasing value of the product of the velocity V and the hydraulic radius R, and shows the approximate positions of the six regimes of flattening. When the grasses are not fully covered by the flow, n will increase slowly as VR increases, as a result of increasing movement of the plants. However, when the vegetation is totally submerged and is forced to bend, resistance will then decline. Minimum resistance values are reached when the product VR is sufficiently large to force the plants to become fully flattened ([11, 44]).
Fig. 5.25 shows an area of high resistance (area a:1-2-3), an area with low resistance (area c:5-6) and an area in between (area b:4). In area 'a', the vegetation is largely responsible for the flow resistance, in area 'c' the plants are pushed down by the water so that they have very little influence on the resistance.

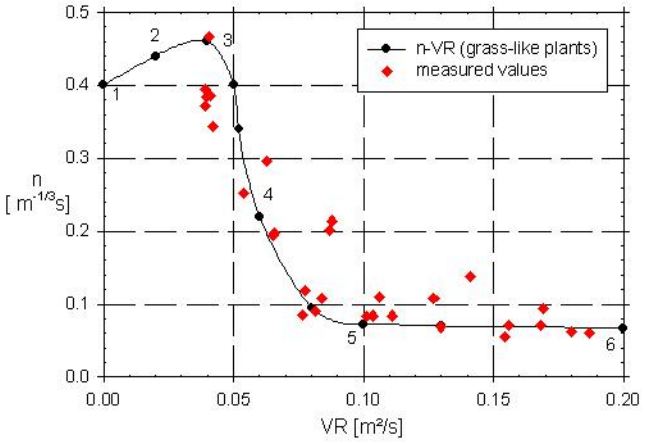

Figure 5.25: The relationship between Manning's n and VR for grass-like plants. The approximate positions of the six regimes of flattening are given. Points are measured values, the fluent line indicates the different regimes as presented in [4]

2.5 Sensitivity analysis of Manning's coefficient comparing the measured values of discharge

It was necessary to check the sensitivity of the results to measurement errors. Therefore, a comparative study of the variation of Manning's coefficient, based on the measurements of Flanders Hydraulics Research, Hydrological Information Centre (HIC) and the measurements of UGent is carried out. Furthermore, the discharge measurements of UGent are compared to the values of HIC and to the values calculated out of the calibration formula of the downstream weir. Therefore, the water height over the flap of the weir is measured. Results for that are in the same range of the measured (Chapter 4, 6.2) and registered values. For the comparison, river characteristics (as the wetted cross section and the river width) are used as measured by UGent.

The Hydrological Information Centre (HIC) of Flanders Hydraulics Research has registered the water levels and the discharge in the studied reach continuously. Manning's coefficient was calculated using the HEC-RAS model, based on the Bresse equation. For each of the monthly measured values, the upstream and downstream discharge is determined. There is only seen a small difference between both values (Fig. 5.26), due to groundwater inflow/outflow, to little tributary inflow between the sections and to inaccuracy of the measurements. Besides, also the discharge

based on the calibration formula of the downstream weir, is calculated. In general, both values are in good agreement. The small deviations that sometimes occur can be explained by vegetation patches disturbing the free flow over the weir.

Three different curves, used for the calculation of Manning's coefficient, are presented in Fig. 5.27. First, Manning's coefficient calculated out of the measured values upstream of UGent (UG measured), second, based on the downstream measured values of UGent, third, Manning's coefficient based on the HIC-values registered at the same moment of the measurements of UGent (HIC measured). All these values are calculated by the numerical model Hec-Ras.
Manning's coefficient is increasing from May until full summer, reaches the highest values in July and is decreasing from October - November on. This trend accompanies the vegetation growth in spring and summer. Maximum values of Manning's coefficient in 2005 are somewhat larger than 0.4 (UGent) and 0.5 (HIC).

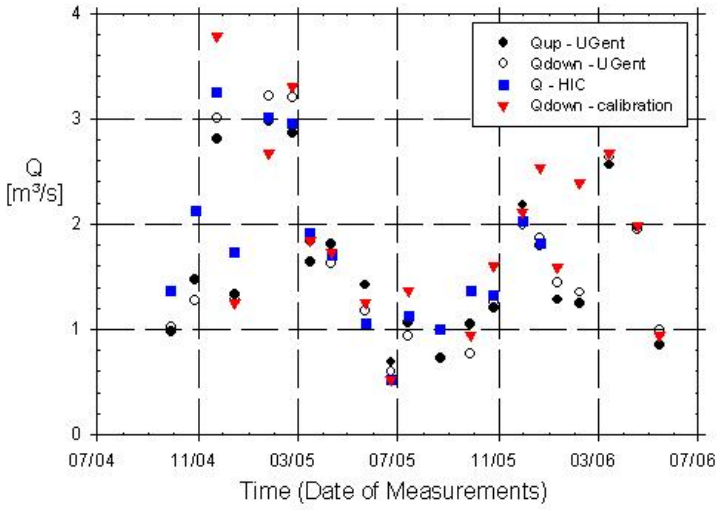

Figure 5.26: Comparison of the discharges; measured by UGent, calculated out of the calibration formula and calculated by HIC, for the period from September 04 to May 06

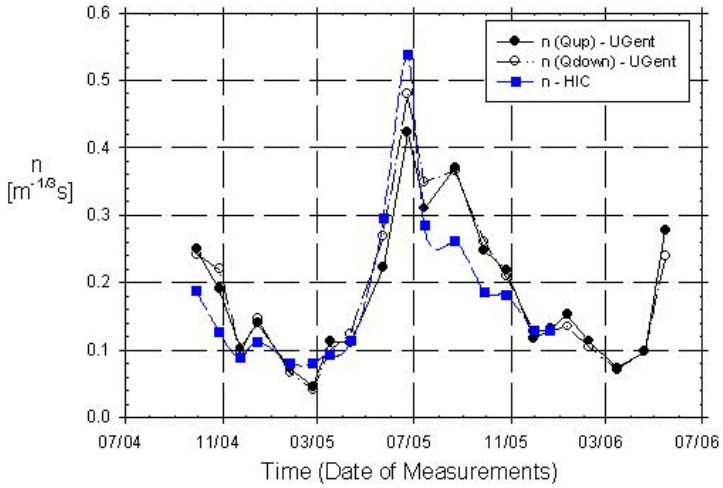

Figure 5.27: Comparison of Manning's coefficients; calculations based on the measurements of UGent and the registrations of HIC

As can be seen, the deviations of Manning's coefficient based on the datasets of UGent are rather small, result of good registration and measurement. Using the discharges estimated by HIC, the differences become bigger. The biggest deviations can be remarked from July 05 to October 05, probably due to the mentioned reason: difference in the discharges based on the estimations of HIC.

This comparison illustrates the importance of accurate information on hydraulic data with regard to the determination of the Manning coefficient as a key-value in numerical modelling.

It is clearly shown that presence of vegetation adds an extra roughness to the channel and influences the water levels. As there is a big variation in the amount of vegetation over the year, the roughness coefficient will change substantially.

2.6 Velocity profiles and biomass

2.6.1 Measurement results

The flow velocity in a channel section usually varies from one point to another. This is due to shear stress at the bottom and at the sides of the channel and due to the presence of the free surface [80]. Theoretically, the water velocity in rivers varies over the section from the bottom of the river to the water surface. This vertical variation is described by the Prandtl

Von Karman profile [11]. In literature, the logaritmic velocity profile is accepted as the basis for defining flow in the case of roughness induced by flexible vegetation [5, 81, 82]. It has been shown that flexible roughness is sufficiently submerged, a logarithmic profile will also develop in the non-vegetated layer.

The velocity profile is given by Prandtl Von Karman's law (5.9):

$$v[m/s] = \frac{v^*}{k} ln \frac{y}{y_0} \tag{5.9}$$

with v = velocity [m/s], V = mean velocity [m/s], result of the integration of Eq.(5.9) = v_{PVK} (velocity on y = 0.37y_n), y = vertical coordinate [m], v^* = shear velocity [m/s], k = 0.4 = Von Karman cte, y_0 = distance from bottom where v = 0 m/s.

This equation describes the logarithmic variation of water velocity within a channel from zero flow at the stream bed to a maximal velocity at the water surface. As can be seen on Fig. 5.28 [83], the profile is influenced by the amount and type of vegetation. The water velocity is lower in vegetated areas. An adaptation to Eq.(5.9) is made by introducing the deflected height of the vegetation [83].

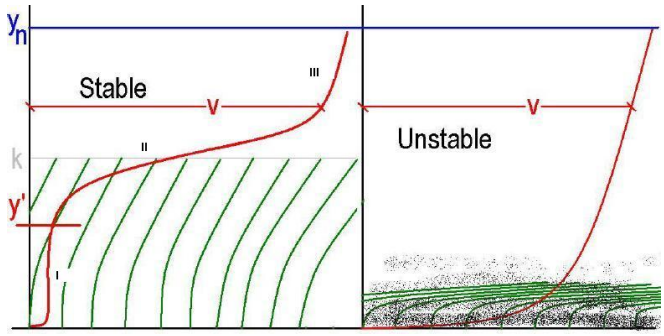

Figure 5.28: Velocity profile over water depth modified by presence of vegetation, for (left graph) stable vegetation and for (right graph) unstable vegetation [83], with y_n = depth of flow [m], k = roughness height in the flow, y' = flexible roughness, as long as y' has some value, there is little shear and the bed and channel is stable

Measured velocity profiles in vegetated zones are S-shaped, as is mentioned by [5] and [84]. For each of these velocity distributions, three zones, separated from each other by relative depth values, are indicated. Zone I is the area where the velocities are very small and show an increasing vertical velocity gradient. In Zone II, the logarithmic velocity profile can

be fitted to the measured velocities and this zone is located above vegetation height. Zone III is characterized by positive vertical velocity gradients which are progressively decreasing until they become zero near the free surface where the measured velocity distribution follows a vertical profile [84].

Furthermore, the velocity is also changing from the left bank to the middle of the river and again to the other bank. This distribution is due to the roughness of the river bed and banks and is similar to the flow distribution in pipes. Theoretically, velocities are largest in the middle of the river and decrease to the river banks [11]. However, temporary measurements in vegetated channels stress the effect of the presence of vegetation. Vegetation patches will disturb this theoretical profile.

In this study, the relation between biomass and erosion (smaller velocities correspond to a larger amount of biomass and less erosion) of the river bed is not clear. This is probably due to the influence of the meandering of the river Aa on the cross-sectional flow patterns. Although, depending on the type of plant, in general, a small velocity corresponds with a big biomass [61].

In small rivers, velocity profiles are rather irregular and the accuracy of the measurements is function of the number of verticals and the number of points at each vertical [85]. For rivers with width comparable to the river Aa, each vertical can be associated with a part of the discharge which is maximum 11 % of the total discharge. At least 11 verticals are gauged. For depths between 94 cm and 150 cm, 5 measurement points are taken (at 1/6, 2/6, etc. to 5/6). This method allows an accuracy better than 5 %, but the method is time intensive. Consequently, in the upstream and downstream section of the river Aa, velocities are measured (black dots in Fig. 5.29 and 5.30) each meter over the width of the section and at regular distances over the vertical (5 to 7 points over 1 to 1.4 m). Gauging sufficient points over the depth allows to generate a velocity profile as shown in Fig. 5.28.

Figures 5.29 and 5.30 show the results of velocity measurements upstream and downstream the selected reach of the river Aa in January (winter) and July (summer). A colour code is applied to the velocity ranges and is indicated as 'velocities in section'.

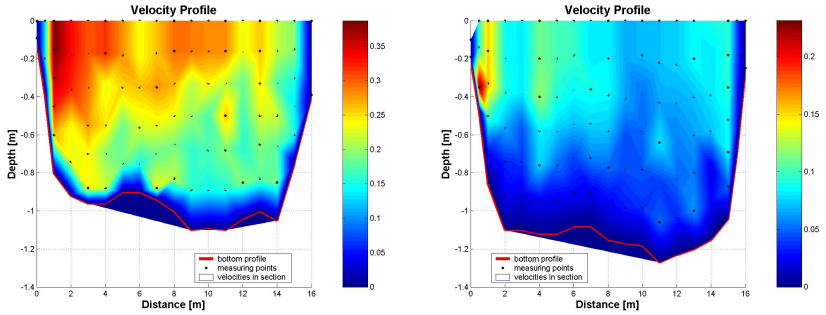

Figure 5.29: Velocity profile in the upstream section of the river Aa on the 25th of January 05 (winter, top) and the 14th of July 05 (summer, bottom)

For Fig. 5.29, following values of these sections in the river Aa are measured. Upstream, the section has a width of 16.0 m, the wetted cross section area varies from 14.00 m^2 in winter conditions to 17.07 m^2 in summer conditions. The measured discharge is 2.99 m^3/s in January and 1.05 m^3/s in July. With these values, an average velocity of 0.213 m/s (max. velocity 0.305 m/s, min. velocity 0.112 m/s) is determined in winter, while a value of 0.062 m/s (max. velocity 0.141 m/s, min. velocity 0.034 m/s) is registered in summer.

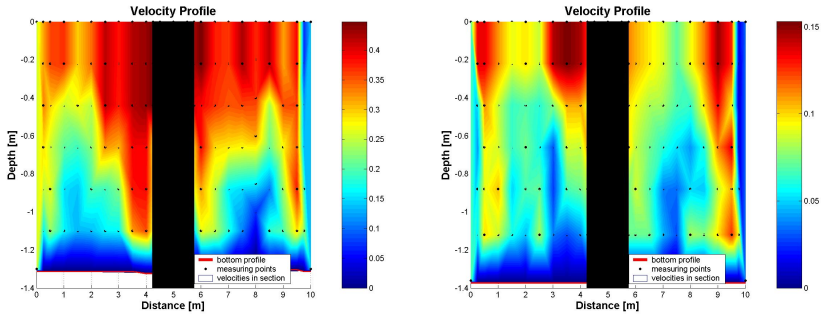

Figure 5.30: Velocity profile in the downstream section of the river Aa on the 25th of January 05 (winter, top) and the 14th of July 05 (summer, bottom)

In Fig. 5.30, the velocity profile is interrupted due to the presence of the wall between the two flaps of the weir at the gauging section. The width is about 10 m and the section is divided into two parts by a central pile. Highest velocities are measured close to the central pile. Discharges varying from 0.94 m^3/s (summer) to 3.21 m^3/s (winter). The average velocity

in the left part is 0.280 m/s, and in the right part 0.266 m/s in the winter period (max. velocity 0.379 m/s, min. velocity 0.137 m/s), somewhat higher then the velocity measured upstream. In July, the velocity near the left bank is 0.077 m/s and near the right bank, the velocity is 0.074 m/s (max. velocity 0.112 m/s, min. velocity 0.033 m/s), also a bit higher then the values measured upstream. This is obviously due to the reduced cross section downstream. The difference between the two parts of the section is negligible. Lowest velocities are measured close to the bottom, higher values are registered near the water surface.

The amount of biomass is very much higher in summer conditions when compared to winter conditions. Average values of dry biomass density and velocity over the studied reach of the river Aa are mentioned. Dry biomass [g/m^2] is measured during winter in the upstream section (44 g/m^2) as well as in the downstream section (27 g/m^2). Values in summer conditions are 351 g/m^2 (upstream) and 450 g/m^2 (downstream).

2.6.2 Velocity distribution

Comparing discharges and velocities, in general, discharges are larger in winter conditions, but the amount of vegetation in the summer leads to lower velocities and by this to a higher wetted cross-section and a lower discharge when compared to winter conditions. Larger velocities are measured during the winter period, as well as larger discharges. Also, water levels are higher in the summer period when a lot of macrophytes are present in the river. They cause higher water levels and lower velocities due to 'obstruction' of the flow.
Velocity variations over the section appear in two directions; vertically close to the bottom, velocities are rather low, near the water surface, higher velocities are registered. Horizontaly, in the left area of the cross section higher values can be found compared to the values in the right part. This is probably due to the curvature of the river. Local deviations in the velocity profile are due to the presence of vegetation patches. These occure in 2005 only in spring and summer conditions but during 2006 over the whole year, due to the mild winter.

The velocity distribution is related to the amount of biomass. In winter, higher average velocities are registered, upstream as well as downstream. This can be linked to the lower amount of biomass. In summer, more biomass is found while the average velocities are lower. Discharges upstream and downstream differ little due to the different time spot at which the measurements are carried out, due to small tributary inflow and due to groundwater exchange. The difference in the amount of biomass upstream

and downstream is due to the heterogeneous growth of macrophytes in the river. Maximum and minimum values of the velocity follow the average values.
The presence of vegetation in the cross section can have big influence on the velocity distribution. The macrophyte patches form an obstacle for a continuous, undisturbed flow. Most of the collected water plants (not for *Potamogeton*) will be found at the bottom of the cross section, so, near to the bottom, the velocity is very low and near to the water surface, higher velocities are registered.

2.7 Biomass blockage

As mentioned in Chapter 4, the amount of biomass is expressed in g/m^2, not taking into account the water depth. For studying effects of blockage, volume dimensions are more useful. Indeed, with increase of discharge and water level, the amount of biomass per m^2 does not change, but the biomass per unit of volume decreases, as well as the effect of blockage. Further, for larger discharges, the plants are pushed down and this reconfiguration will decrease the frontal surface area of the plants in the volume of water. In fact, determination of the volume of the plants compared to the total volume has to be determined. However, this is a topic for future research, because with the techniques used in this research, determination of these volumes is very time consuming and therefore not possible.
At the river Aa, the water depth varies at each section and taking into account this third dimension increases the uncertainty on the results even more. This is not the case in the cross sections where the samples are taken, as there, the water depth is known very accurate.

Calculation of the blockage coefficient is carried out to study the obstruction properties of the macrophytes in the river. The proportion of just a single cross-section blocked by plants is used (Eq.(5.4).

Out of the data in [68], a relation between Manning's coefficient n and the cross-sectional blockage factor B_X is proposed in (Eq.5.10). Situations here are comparable to the ones in the river Aa. In [68] however, more attention is paid to the vegetational component of Manning's coefficient and the blockage.

$$n_{tot} = 0.052exp(0.0258 * B_X) \tag{5.10}$$

n_{tot} = total value of Manning's coefficient; B_X = weighted median of several cross-sectional blockage factors measured at each site.

Using Eq.(5.10) and the correlation of Manning's coefficient and the biomass proposed in Fig. 5.24 (Eq.(6.14)), the blockage for the river Aa is calculated.
Analysis of Eq.(5.10) and Eq.(6.14) shows the same conclusions. There is only blockage of the cross section starting from a certain amount of biomass. A few individual plants are not obstructing the section. A zero blockage of the cross section is related to a Manning coefficient of 0.052 $m^{-1/3}s$, which is low and corresponds to winter situations and a very low amount of biomass. The summer related Manning coefficient is obtained for a cross-sectional blockage around 90 %. Total blockage and the highest biomass values for the river Aa correspond with a Manning coefficient of 0.45 $m^{-1/3}s$, which is according to the measurements. For a zero amount of biomass, Manning's coefficient is 0.063 $m^{-1/3}s$ according Eq.(6.14). This is acceptable for the base value of Manning's coefficient. However, to relate Eq.(5.10) and Eq.(6.14), Eq.(6.14) can be adapted so that for zero biomass, a resistance coefficient of 0.052 $m^{-1/3}s$ is obtained, therefore the value of 0.4628 is changed to 0.4520.
With the value for the wetted cross-section (Eq.(5.4)), calculated from the measurements, and also using Eq.(5.10) and Eq.(6.14), the part of the section obstructed by the vegetation is found (Eq.(5.11)):

$$A_v = \frac{A}{0.0258} ln(\frac{(0.4628 - 0.3998exp(-0.0047 * biomass))}{0.052}) \tag{5.11}$$

Fig. 5.31a presents the blockage factor B_X and Manning's coefficient for the different measurements at the river Aa. Both curves show the same trend; when the amount of vegetation in the channel is higher (spring and summer situation), the channel is more obstructed, the blockage factor is higher and also Manning's coefficient increases. Fig. 5.31b depicts the relation between the blocked cross section of the river Aa and the amount of biomass.

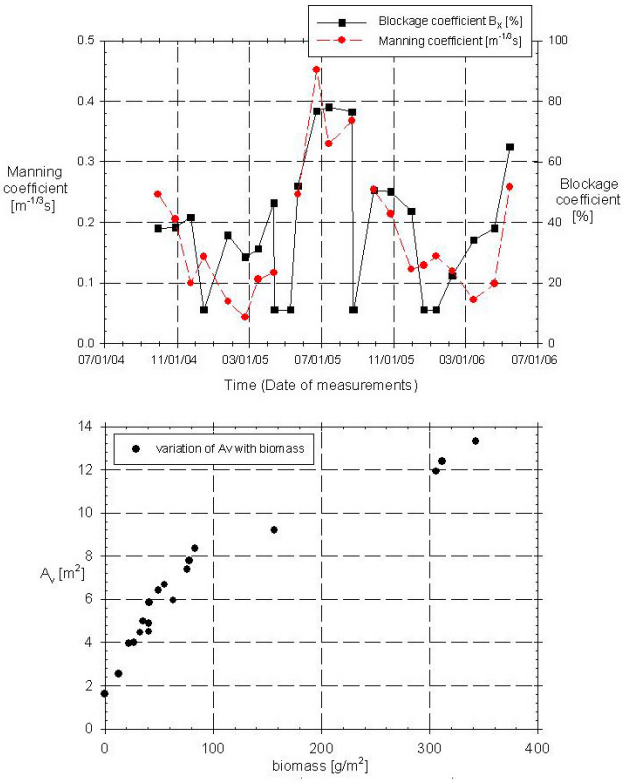

Figure 5.31: Manning's coefficient n and blockage coefficient B for the river Aa as a function of time (top) and obstructed cross section as a function of the measured biomass (bottom)

The amount of biomass of the different types of vegetation are considered all together. However, the different types of growth (emergent, submerged, floating) differ in resistance to flow, blockage and reconfiguration. Considering the river Aa, Potamogeton is present all over the year and determines the plant-hydraulics interaction. Upscaling the results of this research for other rivers (cf. infra) will probably hold different or adapted plant-hydraulic relations.

2.8 Beyond the river Aa

Franklin [86] indicates the limited amount of quantitative information on the relation between flow characteristics and macrophytes, next to the lack of information about the relation between macrophyte behaviour and velocity. This study is a first step in this area. The important role of macrophytes in the structure and functioning of lowland river ecosystems therefore makes understanding the factors controlling the status of macrophytes essential for developing future management strategies for these systems. Velocity and discharge are important in controlling the status of macrophytes in rivers for colonisation, establishment and persistence. In [87], the Manning coefficient of similar lowland rivers as the Aa is checked. The Desselse Nete and the Grote Kaliebeek are studied and the relation between the measured biomass and Manning's coefficient n is investigated. The calculated Manning coefficients and the dry biomass for the river Aa, the study area, are compared with value of the Desselse Nete and the Grote Kaliebeek, bot rivers in the Nete basin (Belgium, province of Antwerp). For the river Aa and the Desselse Nete, an exponential trend is found. For the Grote Kaliebeek, the trend is less clear. The data for this river are collected in the period from May till the end of September. A reach of 170 m is selected to measure the energy slope for the calculation of Manning's coefficient. For higher biomass, extremely high values of the Manning coefficients are registered. The biomass in the Grote Kaliebeek, is only a quarter of the biomass found in the river Aa, and nevertheless the Manning coefficients are higher (up to 1). An explanation could be found in the difference in wetted cross-section where the cross-section of the river Aa is much bigger than the cross-section of the Grote Kaliebeek. For the Desselse Nete, biomasses higher than 1,000 g/m^2 are found. The data are collected by regular measurements in the period from June till the end of September. A reach of 200 m is selected to measure the energy slope for the calculation of Manning's coefficient. For the Desselse Nete, Manning coefficients as well as biomass can be found in the same range as in the river Aa. Also the Biebrza river (Poland) showed analoguous aspects: it is a lowland river dealing with a wealthy vegetation growth influencing the velocity profiles in the river [87].

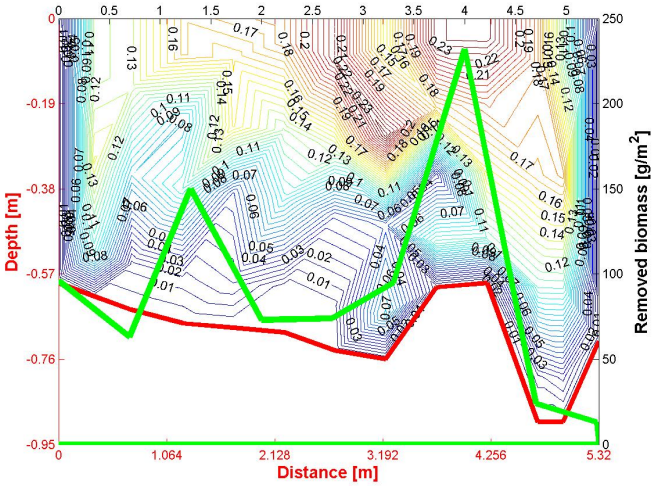

Figure 5.32: Velocity and biomass distribution in a cross section of the Biebrza river near Nowy Rogozyn

Fig. 5.32 shows the velocity distribution in a cross section near Nowy Rogozyn. The section has a width of 5.32 m, the wetted cross section area is 3.72 m^2 and the measured discharge is 0.40 m^3/s. With these values, an average velocity of 0.11 m/s is determined. Lowest velocities are measured close to the bottom, higher values are registered near the water surface. A remarkable higher velocity can be seen on the place where the bottom is less deep. This is supported by the continuity equation: a smaller depth returns into a smaller cross section and corresponds with a larger velocity at the same discharge. After the first discharge measurement, the vegetation in the section is removed. The 'removed biomass', as a function of location in the cross-section, is indicated in Fig. 5.32. The peak value appears together with the peak velocity which can be due to the meandering of the river and to the specific plant species. Most of the collected water plants are found at the bottom of the cross section, so, near the bottom, the velocity is very low and near the water surface, higher velocities are registered. In general, depending on the type of plant, a small velocity corresponds to a big biomass. Furthermore, it seems that removed biomass not really influences the velocity pattern. The velocity pattern was almost equal, before and after removal of the vegetation. Reason for this is to be found in the vegetation upstream of the cleared section. The electromagnetic measurements are clearly not influenced by the vegetation. The relation between biomass and erosion (smaller velocities allow a larger amount of biomass

and cause less erosion) of the river bed is not clear. This is probably due to the influence of the meandering of Biebrza River on the cross-sectional flow patterns.

3 Conclusions

In this chapter processing of the collected data, in the lab flume as well as in the field, is performed. In the flume, measurements are carried out in controlled conditions. Aim is to check the influence of the vegetation on the velocity profiles and Manning's roughness coefficient under different conditions of velocity, discharge and water level. First, the influence of blockage is tested by presence of obstacles. In front of the obstacles, higher water levels are registered and consequently, the velocities will decrease. The more rigid the obstacle, the more the water level rises and the velocity decreases. Immediately behind the obstacle, the stream flow is influenced and the water is pushed against the obstacles. The velocity increases at the positions behind the obstacles and decreases at the positions between the obstacles. This aspect of blockage is very interesting in further research in 2 dimensions concerning the influences of vegetation patches on the flow.

The influence of floating vegetation on the roughness characteristics of flow has been investigated under laboratory circumstances. As this is a new topic in the study of integrated river ecosystems, the information may be useful for setting up guidelines in the management of waterways and flooding protection.
After determination of Manning's coefficient for the flume without obstacles, comparing the results of different methods, the impact of floating vegetation on the value of the Manning coefficient was investigated. It has been shown that determination of Manning's coefficient requires large accuracy due to the small fall of the water level, certainly in the flume without obstacles. Therefore, some theoretical expressions were used to determine the fall and so the Manning coefficient. Two variations of the formula of Colebrook-White were used. Therefore, the value of k_s, the equivalent bottom roughness is necessary and determined out of the velocity profile over the water depth. Also equations of Ghisalberti and Yen are used.

Studying the flume with floating plants, two kinds of analyses are carried out: measurements with constant water level and varying discharge and measurements with both varying discharge and water level. The first series were easy to analyse, only one flow parameter had to be studied. Manning's coefficient caused by the plants was independent of the flow

velocity, but strongly dependent on the water level in the flume. This indicates that the stream flow resistance is especially caused by obstruction. For the series of measurements with constant position of the downstream weir, different formulas are available to determine the resistance based on the properties of the empty flume and the stream flow characteristics. The large influence of the obstruction on the flow is confirmed.

Related to mowing patterns and macrophyte growth in patches in rivers, the Manning coefficient will vary over the width and the length of the channel. The more sections are marked with a higher Manning coefficient, the higher the upstream water level. This level only depends on the number of sections with higher Manning coefficient, not on the location of the sections. As a result, for a constant discharge, one can say that mowing of vegetation to lower the upstream water level may happen in any part of the river. For varying discharge, however, the drained discharge is higher and the downstream water level will rise compared to the initial situation, while the upstream water level is lower. To avoid inundation, removing the vegetation in the downstream part of the river is advisable. The back water effect is more important if the higher rouhghness zone is located more in the middle. Border vegetation is less important than vegetation central in the stream.

In the field, the importance of accurate formulas for determination of Manning's coefficient is checked. Further, the variation of Manning's coefficient as a function of time is indicated, high Manning values occur in full summer, while lowest values are measured in winter situations. These measurement results, varying in time, correspond to a variation of discharge and amount of biomass in the river. So, over a short period, the amount of biomass is constant, but over a year the variation of biomass will largely influence Manning's coefficient. Also local obstructions in the river can largely influence Manning's coefficient. The relation between biomass, discharge and Manning's coefficient is further explored and supported by measurement results over 4 years.
As velocity profiles were investigated in the laboratory flume, results of velocities in the river Aa over the cross section are presented. Due to vegetation growth, the wetted cross section is larger in summer conditions, while velocities are smaller. Presence of biomass in the river results in blockage, this parameter gains importance in 2 dimensions due to the patchy occurrence of macrophytes. Knowing the amount of biomass in the river and the wetted cross section, the part of the cross section blocked by vegetation is calculated.

For the river Aa, as well as for the Biebrza river, an intensive study on the importance of the roughness coefficient is carried out. Hydraulic measurements are performed to set up a data set for implementation in and calibration of numerical models.

An accurate and reliable numerical model must be based on the input of accurately determined characteristics. Some of them, such as topography and discharge, are rather easy to determine, but others, like Manning's coefficient, vary as a function of time.
To build a numerical model, correct calibration data is necessary. Good knowledge of the variation of Manning's coefficient n as a function of time, distance and water stage is needed. Therefore, it is necessary to carry out measurements on a regular basis and to collect hydraulic information all over the year. A numerical model based on a poorly defined Manning coefficient, may introduce large errors in the calculation results, since this roughness coefficient can change up to a factor of ten from winter to summer conditions. A well calibrated model can be very useful for predictions and estimations without measurements.

Manning's coefficient is related to the amount of vegetation, expressed by the biomass and to the discharge. Knowledge of the variation of the biomass as a function of time in combination with the influence of the discharge, should lead to appropriate use of roughness coefficients in modelling surface flow in rivers.

The results of this research clearly show that in vegetated lowland rivers Manning's coefficient varies over the year. In winter time (January and February), when the amount of vegetation is low, the roughness value is also low. In late spring and summer, however (May until August), the number of aquatic plants is much higher, which is resulting in a substantial increase of Manning's coefficient.

Based on frequent discharge, roughness and biomass measurements in the river Aa, an exponential relationship between the Manning coefficient and the amount of vegetation, expressed by the biomass density [g/m^2] is derived. Velocity profile measurements, also revealed that the theoretical velocity profile is disturbed by presence of vegetation patches. Therefore, the biomass influence on the velocity distribution in rivers is described and provides a relationship between the hydraulic parameters and the presence of vegetation in the channel. Similar relationships were found when assessing the vegetation growth either as macrophyte biomass density or as a blockage coefficient, i.e. the blockage of the river cross section by plants.

Calculations for the river Aa are carried out and are compared to results obtained in three other rivers.
Combining the derived relationships and the empirical model with knowledge of the variation of the biomass as a function of time allows for a more appropriate estimate of the resistance coefficient in vegetated rivers. Apart from vegetation growth, also discharge must be taken into account, since river discharge showed to affect the resistance coefficient as well as the hydraulic resistance exerted by plants. Based on the relations that were derived for both, vegetation growth and discharge influences, a better estimation of Manning's coefficient in vegetated rivers can be obtained. This can lead to more reliable results in the application of hydraulic models for river management and river restoration purposes.

References

[1] S. Moeskops. *Stromingspatronen in rivieren door de aanwezigheid van macrofyten*. Master's thesis, Ghent University, 2007. Faculty of Engineering.

[2] R.W. Herschy. *Hydrometry: principles and practices*. Wiley Interscience Publication, 1978. ISBN 0471996491.

[3] H.M. Nepf. *Drag, turbulence, and diffusion in flow through emergent vegetation*. Water resources Research, 35(2):479–489, 1999.

[4] J.C. Green. *Velocity and turbulence distribution around lotic macrophytes*. Aquatic Ecology, 39(1-2):1–10, 2005.

[5] N. Kouwen. *Flow retardance in vegetated open channels*. PhD thesis, University of Waterloo Ontario, 1970. 128 p.

[6] S. Petryk and G. Bosmajian. *Analysis of flow through vegetation*. Journal of the Hydraulics Division, 101(7):871–884, 1975.

[7] T. Helmio. *Unsteady 1D flow model of compound channel with vegetated floodplains*. Journal of Hydrology, 269:89–99, 2002.

[8] A.P. Brooks, G.J. Brierley, and R.G. Millar. *The long-term control of vegetation and woody debris on channel and flood-plain evolution: insights from a paired catchment study in southeastern Australia*. Geomorphology, 51(7-29), 2003.

[9] G.W. Geerling, E. Kater, C. van den Brink, M.J. Baptist, A.M.J. Ragas, and A.J.M. Smits. *Nature rehabilitation by floodplain excavation: the hydraulic effect of 16 years of sedimentation and vegetation succession along the Waal River, Nl*. Geomorphology, 99(1-4):317–328, 2008.

[10] Y.C. Chen, S.P. Kao, J.Y. Lin, and H.C. Yang. *Retardance coefficient of vegetated channels estimated by the Froude number*. Ecological Engineering, 35(7):1027–1035, 2009.

[11] V. T. Chow. *Open Channel Hydraulics*. McGrawHill, New-York, 1959.

[12] B. Yen. *Channel flow resistance: centennial of Manning's formula*, chapter Hydraulic resistance in open channels, pages 1–135. Water Resources Publications, 1991.

[13] B.C. Yen. *Open channel flow resistance*. Journal of Hydraulic Engineering, 128(1):20–38, 2002.

[14] N. Pavlovskii. *Design formula for uniform channels with heterogenuous walls*. Izvestiia Vsesoiuznogo Nauchno-Issledovatel'skogo Instituta Gidrotekhniki, pages 157–164, 1931.

[15] M. Ghisalberti and H. Nepf. *The limited growth of vegetated shear layers*. Water Resources Research, 40(W07502), 2004.

[16] B. Yen. *Open channel flow equations revisited*. Journal of the Engineering Mechanics Division, 99(5):979–1009, 1973.

[17] J. Berlamont. *Theorie van de verhanglijnen*. L. Wouters, 6 edition, 2004.

[18] J. Thijsse. *Formulae for the friction head loss along conduit walls under turbulent flow*. In 3rd IAHR Congress, pages 1–11, 1949. Grenoble.

[19] E. Reinius. *Steady uniform flow in open channels*. 1961. Stockholm, Sweden.

[20] M. Ghisalberti and H.M. Nepf. *Mixing layers and coherent structures in vegetated aquatic flows*. Journal of Geophysical research, 107(C2):3.1–3.11, 2002.

[21] U. Stephan and D. Gutknecht. *Hydraulic resistance of submergend flexible vegetation*. Journal of Hydrology, 269(1-2):27–43, 2002.

[22] J. Jarvela. *Flow resistance of flexible and stiff vegetation: a flume study with natural plants*. Journal of Hydrology, 269(1-2):44–54, 2002.

[23] C. James, A. Birkhead, A. Jordanova, and J. O'Sullivan. *Flow resistance of emergent vegetation*. Journal of Hydraulic Research, 42(4):390–398, 2004.

[24] J.C. Green. *Modelling flow resistance in vegetated streams: review and development of new theory*. Hydrological Processes, 19(6):1245–1259, 2005.

[25] L. De Doncker, P. Troch, R. Verhoeven, N. Desmet, and P. Meire. *Relation between resistance characteristics due to aquatic weed growth and the hydraulic capacity of the river Aa*. River Research and Application, 2008. DOI: 10.1002/rra.1240.

[26] *Soil Conservation Measures - Design manual*, 2008. Queensland Government.

[27] J.E. Garton and J.E. Green. *Improved design procedures for vegetation-lined channels*. Research Report P-814, Oklahoma State University, 1981. Agricultural Experiment Station, Division of Agriculture.

[28] G.H. Findlay and G.A. Ellul. *The application of computers to prepare design tables for grasses waterways and flumes*. Agricultural Engineering, 5:20–24, 1976.

[29] M. Righetti and A. Armanini. *Flow resistance in open channel flows with sparsely distributed bushes*. Journal of Hydrology, 269(1-2):55–64, 2002.

[30] J. Jarvela. *Flow resistance in environmental channels: focus on vegetation*. Water resources publications, Helsinki University of Technology, 2004.

[31] DVWK. *Hydraulische Berechnung von Fliessgewassern*. Technical report, Bonn, 1991.

[32] M. Deneckere. *Stromingspatronen rond en tussen planten*. Master's thesis, Ghent University, Faculty of Engineering, 2008.

[33] A. Armanini, M. Righetti, and P. Grisenti. *Direct measurement of vegetation resistance in prototype scale*. Journal of Hydraulic Research, 43(5):481–487, 2005.

[34] J.R. Welty, C.E. Wicks, R.E. Wilson, and G. Rorrer. *Fundamentals of momentum, heat and mass transfer*. John Wiley and Sons, 4th edition, 2000. 759 blz.

[35] J. Welty, C. Wicks, R. Wilson, and G. Rorrer. *Fundamentals of Momentum*. Wiley Interscience, 2001.

[36] A.F. Lightbody and H.M. Nepf. *Prediction of velocity profiles and longitudinal dispersion in emergent salt marsh vegetation*. Limnology and Oceanography, 51(1):218–228, 2006.

[37] K.S. Erduran and V. Kutija. *Quasi-three-dimensional numerical model for flow through flexible, rigid, submerged and non-submerged vegetation,*. Journal of Hydroinformatics, 5(3):189–202, 2003.

[38] R. Uittenbogaard. *Modelling turbulence in vegetated aquatic flows.*, 2003. International workshop on riparian forest vegetated channels, Trento (Italy).

[39] C.A.M.E. Wilson. *3D numerical modelling of a willow vegetated river/floodplain system*. Journal of Hydrology, 327:13–21, 2006.

[40] B.C. Yen, R. Camacho, R. Kohane, and B. Westrich. *Significance of floodplains in backwater computation*. In 21st IAHR congress, pages 439–445, 1985.

[41] D. Bousmar and Y. Zech. *Momentum transfer for practical flow computations in compound channels*. Journal of Hydraulic Engineering, 125(7):696–706, 1999.

[42] T. Helmio. *Unsteady 1D flow model of compound channel with vegetated floodplains*. Journal of Hydrology, 269:89–99, 2002.

[43] Z. Cao. *Flow resistance and momentum flux in compound open channels*. Journal of Hydraulic Engineering, 132(12):1272–1282, 2006.

[44] J.C. Green. *Effect of macrophyte spatial variability on channel resistance*. Advances in Water Resources, (65):232–243, 2005.

[45] W.L. Cowan. *Estimating hydraulic roughness coefficients*. Agricultural Engineering, 37(7):473–475, 1956.

[46] F.G. Carollo, V. Ferro, and D. Termini. *Experimental investigation of flow characteristics in vegetated channels.* In River Flow 2006, Portugal, 2006.

[47] S. Schneider, F. Nestmann, and B. Lehmann. *Interaction of vegetation, current and sedimantation*. In River Flow 2006, Portugal, 2006.

[48] K. Sand-Jensen and J.R. Mebus. *Fine-scale patterns of water velocity within macrophyte patches in streams*. Oikos, 76:169–180, 1996.

[49] S.J. Clarke and G. Wharton. *Sediment nutrient charcteristics and aquatic macrophytes in lowland English rivers*. Science of The Total Envitonment, 266:103–112, 2001.

[50] M. Schulz, H.P. Kozerski, T. Pluntke, and K. Rinke. *The influence of macrophytres on sedimentation and nutrient retention in the lower River Spree (Germany)*. Water Research, 37:569–578, 2003.

[51] T.G. Horvath. *Retention of particulate matter by macrophytes in a first-order stream*. Aquatic Botany, 78:27–36, 2004.

[52] W.W. Gregg and F.L. Rose. *The effects of aquatic macrophytes on the stream micro-environment*. Aquatic Botany, 14:309–324, 1982.

[53] J.D. Allan. *Stream Ecology: structure and functioning of running waters*. Chapmann and Hall, London, 1995.

[54] D.S. White and S.P. Hendricks. *Chapter 15: Lotic Macrophytes and surface-subsurface exchange processes*, volume In: Streams and ground waters of *Academic Press, San Diego, California*. J.J. Jones and P.J. Mulholland, 2000.

[55] S.J. Clark. *Vegetation growth in rivers: influences upon sediment and nutrient dynamics*. Progress in Physical Geography, 26:159–2002, 2002.

[56] Aminal. *De Kleine Nete, computer modelling as a method, high water control as a target (in Dutch) - computermodellering als methode, hoogwaterbeheer als doel*, 2004. Grontmij Belgroma nv, in order of Aminal.

[57] NVVE. *Waterplanten als graadmeters voor de ecologische toestand van het water: doel, referentie en beoordeling*. 2003. Nederlands-Vlaamse Vereniging voor Ecologie - Werkgroep Water-en Oeverplanten.

[58] D. Watson. *Hydraulic effects of aquatic weeds in U.K. rivers*. Regulated Rivers: Research and Management, (1):211 – 227, 1987.

[59] M.D. Brooker, D.L. Morris, and C.J. Wilson. *Plant flow relationships in the River Wye catchment*. In European Weed Research Society 5th International Symposium on Aquatic Weeds, pages 63 – 70, September 1978.

[60] L. De Doncker, P. Troch, R. Verhoeven, K. Bal, and P. Meire. *Determination of the Manning roughness coefficient influenced by vegetation in the river Aa and Biebrza river*. In review, 2008.

[61] P. Viaene and H. Vereecken. *Stromingsweerstand tengevolge van waterplanten*. Technical report, Flanders Hydraulics, 2001. Rapport Ministerie van de Vlaamse Gemeenschap, Departement Leefmilieu en Infrastructuur, Administratie Milieu, Land-en Waterbeheer, Afdeling Water, Model 566.

[62] S. Ham. *The growth and recession of chalk stream macrophytes*. In Seminar on the Ecology and Management of Chalk Streams, March 1977.

[63] F.H. Dawson. *Seasonal effects of aquatic plant growth on the flow of water in a small stream*. In European Weed Research Society 5th International Symposium on Aquatic Weeds, September 1978.

[64] J.C. Stephens, R.D. Blackburn, D.E. Seaman, and L.W. Weldon. *Flow retardance by channel weeds and their control*. In Journal of the Irrigation and Drainage Division, pages 31–53. Proceedings of the American Society of Civil Engineers, 1963.

[65] H. Vereecken, J. Baetens, P. Viaene, F. Mostaert, and P. Meire. *Ecological management of aquatic plants: effects in lowland streams*. Hydrobiologia, 570:205–210, 2006.

[66] S. Vogel. *Life in moving fluids*. Princeton University Press, Princeton, New Jersy, 1994.

[67] J.D. Madsen, P.A. Chambers, W.F. James, E.W. Koch, and D.F. Westlake. *The interaction between water movement, sediment dynamics and submersed macrophytes*. Hydrobiologia, 444:71–84, 2001.

[68] J.C. Green. *Comparison of blockage factors in modelling the resistance of channels containing submerged macrophytes*. River Research and Applications, (21):671–686, 2005.

[69] R.H. Pitlo. *Oversizing and reuced maintenance in relation to aquatic plant growth and flow resistance*. In Proceedings EWRS, 8th Symp. on Aquatic Weeds, Upsala, pages 167–172, 1990.

[70] K. Fisher. *The hydraulic roughness of vegetated channels*. Technical report, Hydraulics Research Ltd., Wallingford, 1992. Report SR 305.

[71] M.F. Bakry, T.K. Gates, and A.F. Khattab. *Field-measured hydraulic resistance characteristics in vegetation-infested channels*. Journal of Irrigation and Drainage Engineering, 118(2):256–274, 1992.

[72] P.D. Champion and C.C. Tanner. *Seasonality of macrophytes and interaction with flow in a New Zealand lowland stream*. Hydrobiologia, 441:1–12, 2000.

[73] S.J. Bennett, T. Pirim, and B.D. Barkdoll. *Using simulated emergent vegetation to alter stream flow direction within a straight experimental channel*. Geomorphology, 44:115–126, 2002.

[74] F. Lopez and M.H. Garcia. *Mean flow and turbulent structure of open-channel flow through non-emergent vegetation*. Journal of Hydraulic Engineering, 127(5):392–402, 2001.

[75] Hydrologic Engineering Center, US Army Corps of Engineers. *HEC-RAS River Analysis System, Version 2.1.4*, 2004. `http:\\www.hec.usace.army.mil`.

[76] L. De Doncker, P. Troch, R. Verhoeven, K. Bal, and P. Meire. *Influence of aquatic plants on the flow resistance and the hydraulic capacity of vegetated rivers*. In River Flow '06, number ISBN 0-415-40815-6, pages 593–602, Portugal, Lisboa, September 2006.

[77] N. Desmet, S. Van Belleghem, P. Seuntjens, T. Bouma, K. Buis, and P. Meire. *Quantification of the impact of macrophytes on oxygen dynamics and nitrogen retention in a vegetated lowland river*. Physics and Chemistry of the Earth, 2008.

[78] E. Querner. *Aquatic weed control within an integrated water management framework*. PhD thesis, Agriculture University Wageningen, 1993. ISBN 90-5485-122-8.

[79] V.J. Palmer. *A method for designing vegetated waterways*. Agricultural Engineering, 26(12):516–520, 1945.

[80] M.H. Chaudhry. *Open-Channel Flow*. Prentice Hall, 1993.

[81] H.M. Nepf and E.R. Vivoni. *Flow structure in depth-limited, vegetated flow*. Journal of Geophysical Research, 105:547–557, 2000.

[82] J. Jarvela. *Effect of submerged flexible vegetation on flow structure and resistance*. Journal of Hydrology, 307(1-4):233–241, 2005.

[83] N. Kouwen. *Using vegetation properties to predict flow resistance and erosion rates*. In Vegetated channels: hydraulic, morphological and ecological aspects, Trento, Italy, February 2003. International workshop on riparian forest.

[84] F.G. Carollo, V. Ferro, and D. Termini. *Flow velocity measurements in vegetated channels*. Journal of Hydraulic Engineering, 128(7):664–673, 2002.

[85] R. Verhoeven. *Hydrografie en hydrometrie*. Ghent University, Faculty of Engineering, 2000.

[86] P. Franklin, M. Dunbar, and P. Whitehead. *Flow controls on lowland river macrophytes: a review*. Science of the total environment, 400:369–378, 2008.

[87] L. De Doncker, P. Troch, R. Verhoeven, K. Bal, P. Meire, J. Chormanski, D. Miroslaw-Swiatek, and T. Okruszko. *Impact of vegetation development on the hydraulic characteristics and flow patterns in lowland rivers*. In W3M, Wetlands: Monitoring, Modelling, Management, Wierzba, Poland, 2005.

6

Basic validation of the Strive numerical model

The subject of environmental engineering is currently of great interest. Next to the field experiments, numerical models are a fundamental issue. An introduction to coupled hydrodynamic and ecosystem modelling is described. The developed Strive (STream RIVer Ecosystem) model is set up in the Femme-environment and has already proven its worth in a large number of calculations [1, 2]. This chapter presents practical examples and applications of the coupled eco-hydraulic modelling. Special attention is paid to the interaction of vegetation and stream flow. First, the context of the research is presented. Further, the importance of accurate hydraulic modelling is illustrated. The study area and the Strive modelling environment are further developed. Validation of the Strive model is performed and a sensitivity analysis is made to allow better understanding of the different parameters.

1 Implementation of the solution algorithm for the flow equations

The hydrodynamic model for the transmission of the wave in the river has to be implemented in 'Femme'. Differential equations were converted into algebraic equations using the finite difference scheme. Forward discretisation of the equations in time and central discretisation in space is carried out. Implementation of the hydrodynamic model in 'Femme' can be done by using the characteristics of this environment [3]. In this multidisciplinary approach, different research areas have to be integrated to study properly the interaction between surface water and vegetation [4] and 'Femme' will be used for the integrated hydrodynamic - ecological modeling. Therefore, it is not advisable to model complex ecological processes with simplified conceptual hydrodynamic models and a more advanced hydraulic model is necessary.

In Chapter 3, the implementation of the Saint-Venant equations in the Femme framework, leading to the Strive model, is discussed. The flowchart of the Strive model, with most attention paid to the hydraulic module is presented in Appendix B.

A typical sequency of interaction in a model and how this is achieved in 'Femme' is given in Fig. 6.1 and Fig. 6.2. In short the main program gives control to the driving routines of 'Femme' (via the Fortran statement Call XSimulate). The driver then opens and reads the declaration files, and the observed data files. Subroutine XSTART is called, after which the forcing function data are read and the second part of the initialisation is performed (subroutine XSTART2). The userspecific subroutine XSUBMODS is called at each time step. It is also called during steady state calculation. After running the model for the specified time, the subroutine XSTOP is called. 'Femme' takes care of solving the model and writing the output.
A set of models developed in 'Femme' has a hierarchical structure. The model driver is the core of 'Femme' and controls all different models. This is the genetic part, which is common to all models. It consists of a large number of Fortran subroutines and functions performing general modelling tasks. The model driver interacts with a problem-specific part that consits of the declarations of the parameter and constants, the variables and forcing functions and a Fourtran source code that specifies how the differential equations and the output variables are calculated. Several different applications can be run using the same model source, by toggling on or off specific features of the model environment or by linking different data files to the model [3]. Once the Strive model is operational, basic validation and sensitivity analysis is performed. Further, calibration for

coupled modelling is carried out.

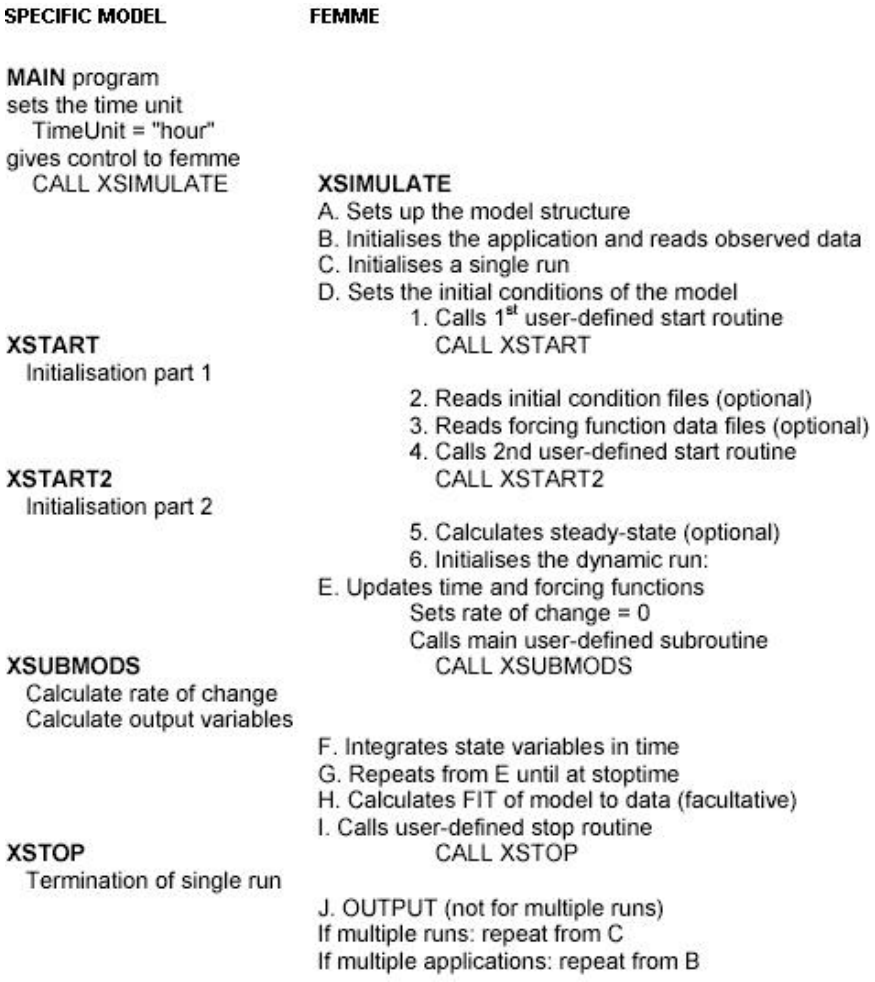

Figure 6.1: Basic structure of a model developed in Femme

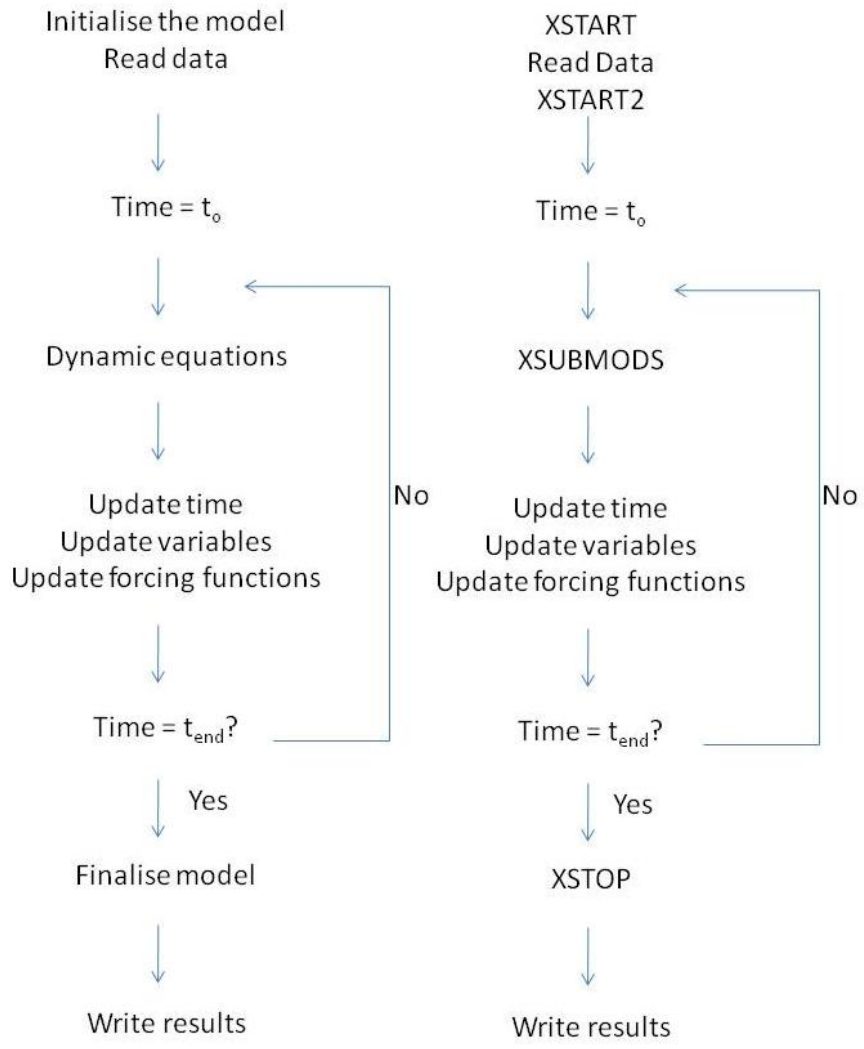

Figure 6.2: Basic structure of a model developed in Femme

2 Flowchart of Strive

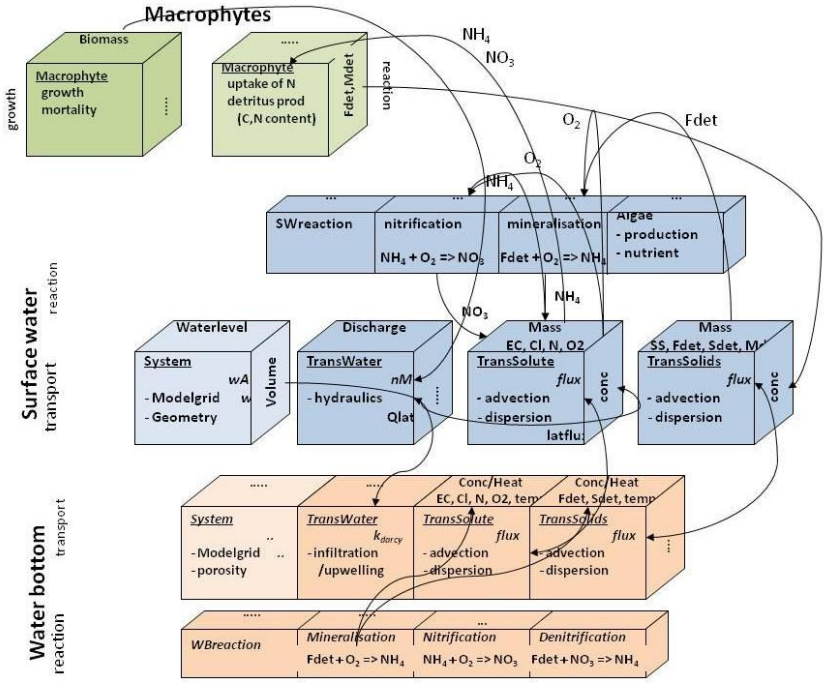

Figure 6.3: Flow chart of Strive (after K. Buis)

The flowchart of Strive shows the most important relations between the model components and so the different processes which take place in the ecosystem. The interaction between the surface water part, the groundwater and the macrophytes is clearly presented. For the water component, aspects of transport and reaction are included. Concerning the macrophytes, their growth as well as their reactive characteristics are described. In the water bottom, the groundwater flow occurs. The groundwater interacts with the surface water. In that part, the geometry of the system and the stream flow, with discharges and water level, are important. Next to that, also solutes and solids are found in the water body and these components are responsible for reactive aspects. Last, there is the vegetation growth in the river, plants grow and die and so, they participate in the reaction processes. Again, here is particularly focussed on the interaction between the stream flow and the presence of vegetation in the river.

3 Boundary conditions in Strive

Here, general information concerning boundary conditions is gathered and a number of indicative calculations are performed.

3.1 General information

In the studied reach of the river Aa, a wave is generated from upstream to downstream and the water levels are measured in several points.
In this subsection, upstream and downstream boundary conditions as the discharge and the water level are based on the data presented by HIC. The discharge or water level is set as an upstream boundary condition, the downstream boundary condition is the downstream water level for the first part of the calculations and the weir formula for the second part of the calculations.
An initialisation period is incorporated and the output is only selected after few seconds to eliminate instabilities in the beginning of the run. The output interval is 360 s. Calculations are carried out with a time step of 36 s.

3.2 Data sets

Two datasets are used to check the influence and importance of the boundary conditions in the Strive model. The datasets used in the calculations are delivered by HIC. The water levels are measured downstream of weir 3 (which is the upstream boundary condition) and upstream weir 4 (downstream boundary condition) (Fig. 1.1). The discharge registered is determined downstream weir 4 and is seen as constant over the reach. Two waves are selected, one in summer (August) and one in winter (January). As the first period is characteristed by one peak discharge, in winter, two small peaks and a varying base flow occur. These examples cover situations which can easily occur. The section is rectangular and the bottom is as measured in the river Aa. The deepest bottom value of each section is used as the constant bottom depth of each section.

August The selected wave dates from the 12th of August 2005 to the 19th of August 2005. The base flow of the discharge during that week is about 1 m^3/s, while on the 15th of August a peak flow of almost 3 m^3/s is registered. The water level during the period of base flow varies from 10.6 m TAW upstream the reach to 10.2 m TAW downstream the reach. During the peak flow, the water level rises with more than 20 cm (Fig. 6.4).

January The selected wave dates from the 1th of January 2005 to the 31th of January 2005. The base flow of the discharge is 2 m^3/s, further, 2 peaks are registered during the month of January with discharge values above 8 m^3/s. The water level over the reach varies between 10.5 (upstream) and 10 m TAW (downstream), with rises of 0.5 m during the period of the peak discharges (Fig. 6.5).

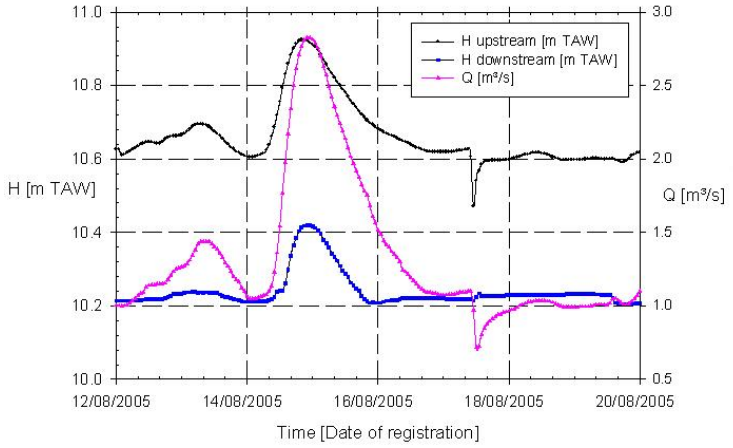

Figure 6.4: Boundary conditions of the river Aa used for the calculation in Strive (August 2005)

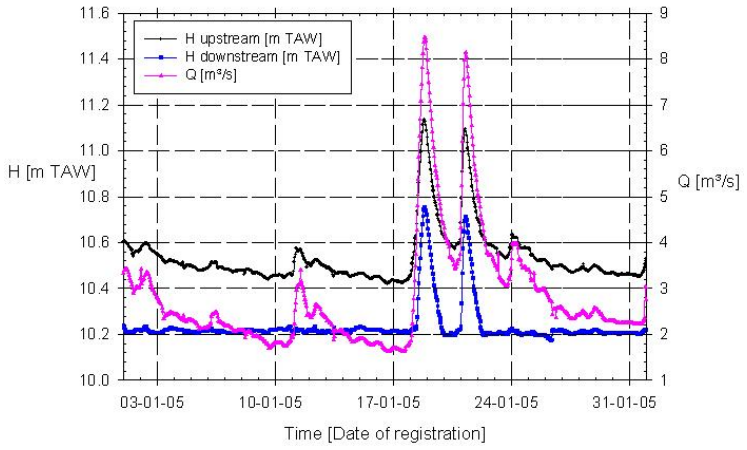

Figure 6.5: Boundary conditions of the river Aa used for the calculation in Strive (January 2005)

3.3 Boundary conditions

Boundary conditions can be implemented in different ways. Upstream and downstream of the research area, measurements of discharge and water level are carried out and these data sets can be used as upstream and downstream values. Next to upstream and downstream water level or discharge, also the link between discharge and water level at the downstream weir can be used. Different combinations can be implemented in the model. All of them are tested and the best results are retained.

One possibility is to see the boundaries as fixed boundaries. The natural situation however is different. At the downstream section of the studied reach, a weir is constructed. At this weir, the discharge is determined by the water height over the weir by Eq.(D.2).

After analysis of the measured values during the last 2 years, following formula is found as a good average:

$$Q = 9.851(Z_{sv} - 9.913)^{1.706} \tag{6.1}$$

with Z_{sv} = water level [m TAW]

In Fig. 6.6 the measured values downstream of the reach are compared to the calculated results to check the weir formula for the period of August. The discharge is indicated, next to the measured water levels upstream and

downstream. The downstream water level is compared to the numerical results using the calibration formula. As can be seen (lowest curves in Fig. 6.6), the results are very similar.

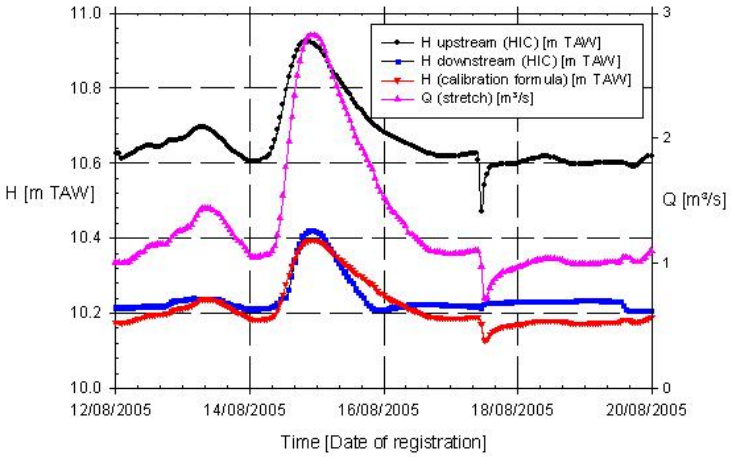

Figure 6.6: Check of the weir formula for the period of August in the river Aa: measured values downstream are compared to the calculated results using the weir formula

3.4 Boundary condition analysis

Different calculations were carried out based on the boundary conditions as measured in the month of January. The water levels measured upstream and downstream the river Aa, next to the discharge in this reach were registered. Starting from 2 of the 3 possible boundary conditions, the calculations were carried out and the results were compared with the registered values.
Therefore, an average value and a peak value of each simulated series of data was calculated and compared to the average and peak values of the registered series. So, the best combination of boundary conditions is selected. Some combinations give rather good results, others do not, but the method of the least squares allows to select the best combination.
Two calculations are carried out and presented in the Table 6.1. In the first column, the combination of implemented boundary conditions is mentioned, so is 'QQ' an indication for discharge as upstream and downstream boundary condition. 'Qf(Z)' means that the discharge is chosen as upstream boundary condition while the calibration formula of the weir is the downstream boundary condition. All used combinations are mentioned in a similar way. For each of the combination of boundary conditions, two

calculations are performed.
For the measured data series of discharge and water level, upstream as well as downstream, the average and peak value of the series is determined. For each of the combinations of boundary condition, a simulation is performed and as for the measured series, the average and peak value of discharge and water level is determined, upstream as well as downstream.
First (column 2 and 3), the least square method is used for the average (QZav, second column) and peak values (QZpeak, third column) of each series. For the discharge, the simulated value is subtracted from the measured value upstream. The square of this result divided by Q_e = 1 m^3/s is added to the square of the same calculation for the downstream discharge. The square root of this value is retained. For the water levels, the same calculation is performed (with Z_e = 1 m). Result of water level calculation and discharge calculation are added (Eq.(6.2)).

$$\begin{aligned} P1 \\ &= (\sqrt{(\frac{Q_{sim} - Q_{meas}}{Q_e} up)^2 + (\frac{Q_{sim} - Q_{meas}}{Q_e} down)^2}) \\ &+ (\sqrt{(\frac{Z_{sim} - Z_{meas}}{Z_e} up)^2 + (\frac{Z_{sim} - Z_{meas}}{Z_e} down)^2}) \end{aligned} \tag{6.2}$$

with Q_{sim} = simulated value of the discharge [m^3/s], Q_{meas} = measured value of the discharge [m^3/s], Z_{sim} = simulated value of the water level [m] and Z_{meas} = measured value of the water level [m]

Second (column 4 and 5), the deviation from the calculated values to the registered value is determined: P2 (Eq.(6.3)). P2 [-] is calculated for average as well as peak values.

$$\begin{aligned} P2 \\ &= \frac{Q_{sim} - Q_{meas}}{Q_{meas}} up + \frac{Q_{sim} - Q_{meas}}{Q_{meas}} down \\ &+ \frac{Z_{sim} - Z_{meas}}{Z_{meas}} up + \frac{Z_{sim} - Z_{meas}}{Z_{meas}} up \end{aligned} \tag{6.3}$$

Results are mentioned in Table 6.1. Here, the calculated value is subtracted from the measured value and this result is divided by the measured value. The results for upstream and downstream discharge and water level, based on average values, are added (QZav, fourth column). The same calculation is carried out for peak values (QZpeak, fifth column).
It can be concluded out of Table 6.1 that the best correspondence of mea-

sured and calculated values will be obtained by using the discharge as upstream boundary condition and the weir formula as downstream boundary condition. Downstream boundary conditions as a fixed discharge or water level will induce a reflection of the wave, which does not correspond with the natural situation.

combination	QZav P1av [-]	QZpeak P1peak [-]	QZav P2av [-]	QZpeak P2peak [-]
QQ	0.349	0.374	0.042	-0.045
QZ	0.202	0.138	-0.018	-0.007
Qf(Z)	0.171	0.105	0.008	0.000
ZQ	0.239	0.169	0.023	0.016
ZZ	3.954	3.362	1.964	0.561
Zf(Z)	1.038	1.209	0.432	0.193

Table 6.1: Boundary condition control with combination of upstream and downstream boundary conditions in the first column and the deviations between measured and simulated values in the other columns

3.5 Boundary condition: influence of Manning's coefficient by changing amount of biomass

Biomass growth is important in the study of river hydraulics. The ecological processes in the system are important with regard to water quality and exchange processes. Nutrients can be found in sediments and suspended solids, the presence of macrophytes in the river assures retaining of the nutrients in the system. When there are no macrophytes which keep the bottom material together, there is a deterioration of the river by washing out of sediments and solids and the adherent nutrients. The growth of biomass is determined by the season of the year, the nutrients, the stream velocity, the amount of light, the macrophyte type, etc. Furthermore, the hydraulics of the river and the biomass growth are processes on a different scale; the amount of plants in the river does not change in the period of changing discharges.

The wave measured in August 2005 is used for calculation. As in the previous section good results were obtained. Two simulations with different boundary conditions are carried out to present the influence of Manning's coefficient on values for discharge and water level. Two types of boundary conditions are used (however the downstream weir formula was selected as the best choice) to exclude influences on Manning's coefficient.

Firstly, the discharge value is the upstream boundary condition in the reach, while the downstream boundary condition is the downstream water level. Secondly, the weir formula is chosen as the downstream boundary condition. Results can be seen in Fig. 6.7. For the selected wave, the upstream and downstream water levels are shown in Fig. 6.7, with in between the different downstream calculated water levels, based on the varying values of Manning's coefficient. For this period in August, Manning's coefficient was calculated, based on the Manning equation (Eq.(3.34)) and some measured values, and resulted in a value of 0.375 $m^{-1/3}s$.
Using the fixed boundary conditions, Manning's coefficient corresponding with the numerical calculation is little higher (0.4 $m^{-1/3}s$ for base flow) (Fig. 6.7). In [1], it was already shown that the calculated Manning coefficients are little higher then the values obtained by the Manning equation. As can be seen on Fig. 6.7, for this wave, variations are only small for the different boundary conditions. However results for base flow are satisfying under different boundary conditions, the simulation of the water level peak is not good. This is due to the dependence of Manning's coefficient on the discharge.

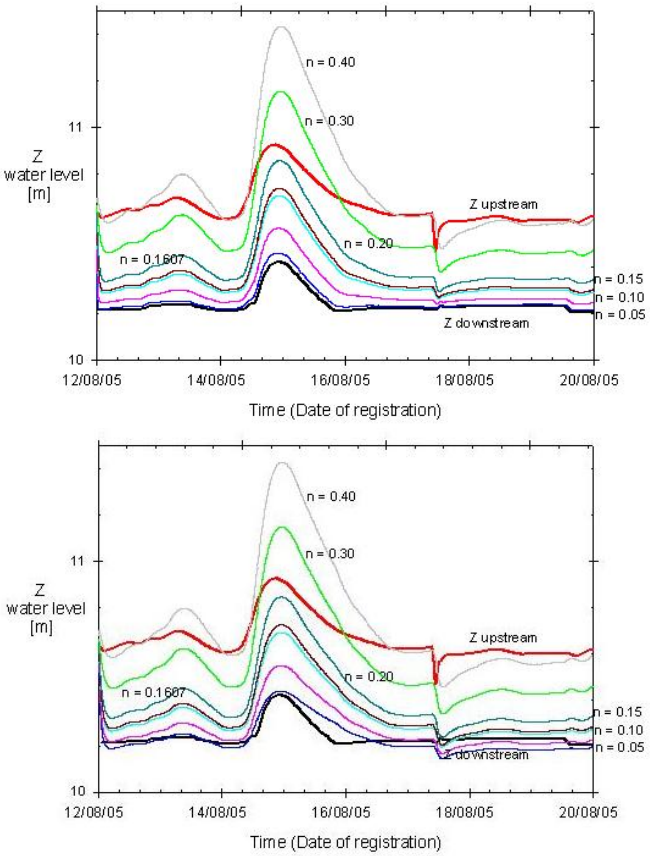

Figure 6.7: Variation of the downstream water level when the calculation is carried out with different values of Manning's coefficient. Boundary conditions are Qup-Zdown (a, top) and Qup-f(Z)down (weir) (b, bottom).

3.6 Sensitivity analysis

For the data registered in January 05 (Fig. 6.5), a sensitivity analysis was carried out. Different values of different parameters (numerical parameters as Δt, Δx and θ and physical parameters as Manning's coefficient and the bank slope) were tested and the results for discharge and water level compared. The results were checked by calculating the average values and the peak value of discharge and water level. As boundary conditions, the discharge was chosen upstream and the formula of the calibrated weir (Eq.(6.1)) was used downstream, as this was selected as the best combination for the studied reach.

The geometry of the river Aa is adapted for the sensitivity analysis and is characterised, firstly, by a flat bottom (8.89 m TAW) and a rectangular cross-section (bottom width of 9.08 m) and, secondly, for a linear bottom slope (from 9.1 m TAW to 8.68 m TAW) and a trapezoidal cross section (slope of 60 °).

Some numerical parameters as the time step Δt of the numerical calculation, the cell size Δx in the grid and θ, a parameter in the numerical scheme are subjected to sensitivity tests. For each of these parameters, no differences were seen as long as the values are within reasonable proportion with the data. It means for example that θ has to be between 0.55 and 1, where 0.7 is proposed as a good value in literature [4, 5]. On the one hand, the time step can not be too large not to miss any peak values, on the other hand, a very small time step leads to calculation difficulties and memory problems. Similar remarks can be given for the choice of the cell size. In this study, an indicative value for the time step is 10 to 20 s. For simulations of hydraulic parameters as discharge and water level, a time step of 20 s is sufficient, but for modelling water quality variables, a smaller timestep of 10 s is required. A cell width between 5 and 15 m is a good value for simulations.

Further, a sensitivity analysis is performed for two physical parameters: Manning's coefficient and the slope of the river banks. The data series of January 05 is selected (HIC data), as well as a bottom with linear slope and a trapezoidal cross section. Upstream boundary condition is the discharge, while the calibration formula of the weir is the downstream boundary condition. First of all, the slope of the river banks was varied between 0 and 75 (0, 30, 45, 60, 75). Results are plotted in Fig. 6.8a and 6.8b. The first figure (a) depicts the peak values of the water level upstream as well as downstream, the second figure (b) shows the average values, for each of the different bank slopes. For the water level, a variation of the upstream water level is seen: the larger the bank angle, the larger the river cross section and the lower the water level. The measured water levels are for one particular situation. Measured and simulated water levels differ little. This is probably due to the choice of the discharge as boundary condition. The discharge values, provided by HIC, are uncertain in the studied reach of the river Aa, due to lack of registration and the disturbance by macrophyte growth.

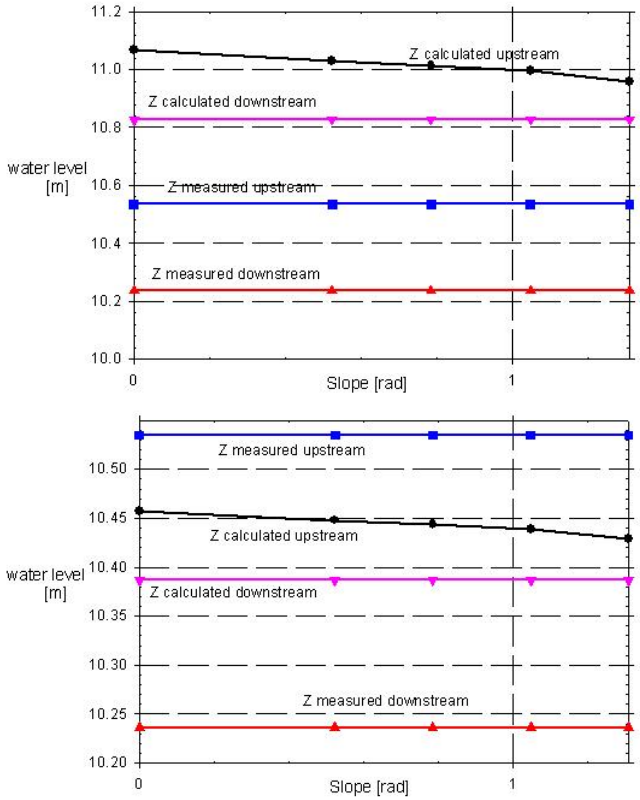

Figure 6.8: Variation of the slope of the banks: peak value (Fig. a, top) and average value (Fig. b, bottom) of the water level for varying slope of the banks

Second series of figures (Fig. 6.9a and Fig. 6.9b) depicts the same calculation for different values of Manning's coefficient (0.024, 0.044, 0.064, 0.084 and 0.104 $m^{-1/3}s$). The calculated Manning coefficient for the month of January is 0.064 $m^{-1/3}s$.
The variations of the upstream water level are linked to the resistance to flow expressed by Manning's coefficient. A higher Manning coefficient causes a higher resistance and therefore higher upstream water levels. For the Manning coefficient calculated from measurements using Eq.(3.34), calculated and measured upstream water level values correspond well (n = 0.064 $m^{-1/3}s$).

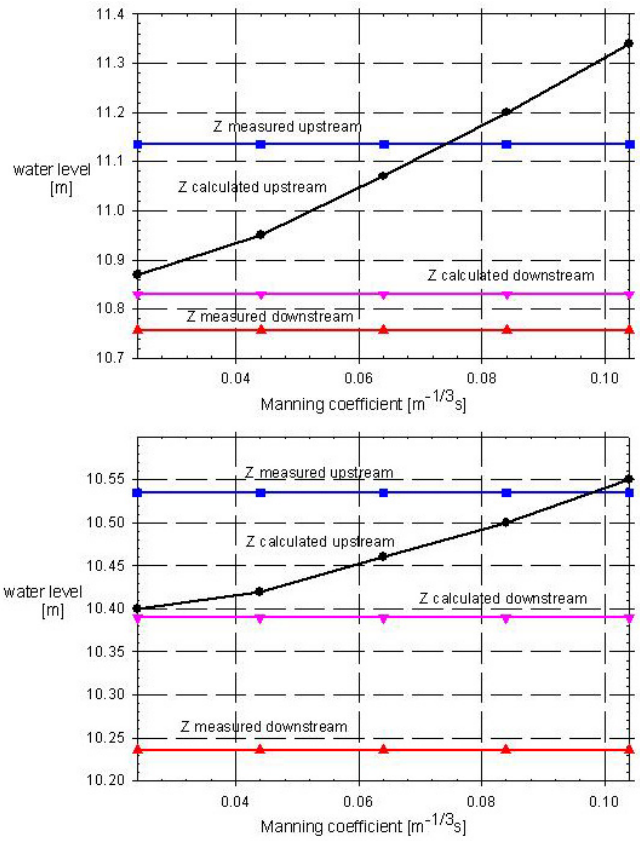

Figure 6.9: Variation of Manning's coefficient: peak value (Fig. a, top) and average value (Fig. b, bottom)

4 Basic validation

4.1 Initial and boundary conditions

Solving the Saint-Venant equations for discharge and water level requires boundary conditions and initial conditions. For transient flow modelling, initial conditions represent the state of the fluid flow at the time when the computation starts, based on the measured data series. Boundary conditions are required on all the boundaries of the solution domain in order to define a specific fluid flow of interest. The imposed conditions must reflect the real situation of the river flow that is being modelled [6]. Upstream boundary conditions describe the time variability of discharge or water level. Similarly, downstream boundary conditions are time series for discharge or water level, or a relation between discharge and water level. For example, the latter can be related to a calibrated weir where the discharge is calculated from the measured water levels and the weir formula.

Next to datasets of measured discharge and water level used as upstream and downstream values, also the link between discharge and water level at the downstream weir can be used. Different combinations of boundary conditions can be implemented in the model. All of them are tested and the best results are retained, based on the comparison of measured and modelled base and peak values.

For example, at the downstream section of the reach, the calibration formula of the weir is given by:

$$Q = a(Z_{sv} - Z_{cr})^b \tag{6.4}$$

with Q = discharge [m^3/s], Z_{sv} = water level [m TAW], Z_{cr} = level of the crest of the weir [m TAW], a and b are coefficients depending of the position of the weir. The formula is only valid for free flow.

After analysis of the values measured over more than 2 years (2005 - 2006) and comparing them with the calibration results of the weir [7], reliable values for a, b and Z_{cr} are found.

4.2 Mass conservation

To check the mass conservation principle, an artificial river channel with a flat bottom and a length of 1400 m is used. The cross section is rectangular and has a bottom width of 5 m. The channel is splitted into two parts of equal length: the first part has an initial water level of 2.20 m, while in the second part, the initial water level is 1.80 m. The upstream and downstream boundaries are closed, so there is no flow into the reach. Manning's

coefficient is first set at 0.01 $m^{-1/3}s$ and at 0.1 $m^{-1/3}s$ in the second set of calculations. For the higher Manning coefficient, corresponding to summer conditions, it takes about 4 hours to come to a stable situation while for the winter conditions, it takes about 8 hours. In the center node, there are big variations of the discharge, but small variations for the water level. Finally, the criterion of mass conservation is fulfilled as, at the end, the water level equals 2.0 m over the entire channel reach.

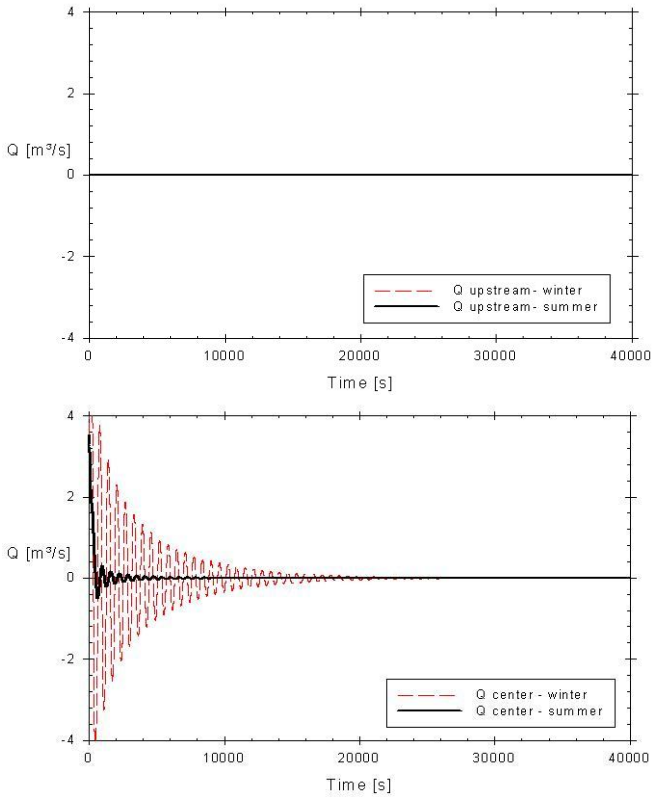

Figure 6.10: Upstream discharge (top) and discharge in the middle of the reach (bottom) for summer and winter conditions

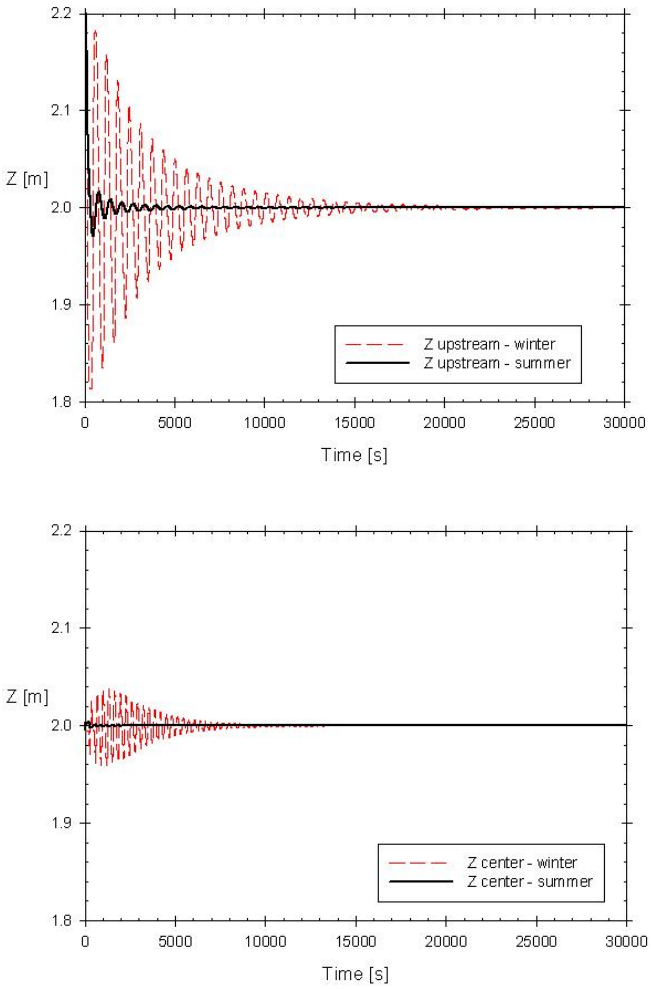

Figure 6.11: Upstream water level (top) and water level in the middle of the reach (bottom) for summer and winter conditions

4.3 System parameters

The numerical solution of the Saint-Venant equations depends on the physical situation, but also on the system parameters. Here, the effect of spatial

and temporal resolution is analysed and the value of the weighting factor θ of the Preissmann scheme is presented.

Number of nodes The number of nodes depends on different aspects. The number has to be sufficiently high to avoid too large calculation cells which are not able to simulate all physical aspects. Also the initial condition is important. The better the initial values agree with a realistic start condition, the fewer boxes are necessary. A small example confirms this statement. A surface water profile is calculated for summer (n = 0.1 $m^{-1/3}s$) and winter (n = 0.01 $m^{-1/3}s$) conditions, with a downstream water level of 2 m and a discharge of 20 m^3/s. The artificial river channel as described before (length 1400 m, width 5 m) is used. Using the Bresse equation results into an upstream water level of 2.43 m for winter situations and 7.05 m in summer conditions (theoretically supposing that the river banks are sufficiently high). The same calculation is carried out using Strive with a variation in the number of nodes (5, 10, 15,..., 50). For the winter situation, the value of 2.43 m is obtained in any case, due to the small difference between the initial and the final situation. For the summer situation, it seems that at least 25 nodes are necessary to come to an accurate result. It has to be added that this example assumes permanent flow.

Timestep Certainly in non-permanent situations, the timestep will be of great importance. In numerical modelling, a good choice of timestep Δt and cell size Δx is necessary. These values have to be sufficiently small to not miss any effects (e.g. peak discharges) and to be sufficiently large to minimize the calculation time. The Courant-Friedrichs-Lewy condition (CFL, [5]) determines a relation between the time step and the grid size to solve the partial differential equations in a convergent way. For an explicit scheme, it means that the solution will be numerical stable if the CFL condition is fulfilled.
This condition can be avoided by using an implicit scheme (as the Preissmann scheme) for solving the Saint-Venant equations. Time steps can be taken larger, which is useful for long simulation periods, keeping the solution stable.

The calculation carried out in the 'mass-conservation' paragraph is repeated for different time steps (1 s, 10 s, 20 s and 50 s). The water level variations need a larger period to stabilize for smaller time steps, so for this aim, smaller time steps are not necessary, while too large time steps cause instabilities. On the other hand, to simulate specific effects, time steps have to be adapted. For example, when taking into account ecologi-

cal processes as conductivity, the time step has to approximate the natural physical process of transportation and dispersion in the river.

Weighting factor The weighting factor θ is used in the Preissmann scheme. A higher θ value underlines the importance of the later point of time. The 'mass conservation' example is carried out with θ values of 0.55, 0.70 and 0.85. The higher the value, the longer the time necessary to come to a stable situation. For non-permanent situations, the optimal value has to be determined for each specific case. For values of θ lower then 0.55, in general, no solutions are found.

4.4 Validation for steady state conditions

First, the problem of steady turbulent open channel flow is studied. The results of the Strive model are compared with analytical calculation results based on Bresse's equation and with numerical results of the program Hec-Ras.

Hec-Ras (Hydrologic Engineering Center, River Analysis System) is a free tool developed by the US Army Corps of Engineers [8]. The program is continuously evaluated and used world wide by hydrological engineers. The program is also based on the Saint-Venant equations, but is not working as an open source. It allows to perform one-dimensional steady and unsteady flow calculations for a full network of natural and man-made channels.

The water surface profile can also be calculated analytically by the Bresse equation which is the simplification of the Saint-Venant equations for steady flow. This is the case when the calculation of the water surface profile is concerned (Q is a constant value). In the most simple form, in steady state conditions and for uniform flow, the Bresse equation is known as the Manning equation.

Several calculations in permanent conditions have been carried out to evaluate the impact of model parameters. The river has a constant rectangular or trapezoidal cross section. Earlier calculations showed that an average geometry is sufficient for calculation of Manning's coefficient and the water surface profile [9]. Further the slope of the river has been changed and 2 cases have been considered; a horizontal slope of 0 m/m and a slope of 0.0002 m/m. The width of the river is 15 m and the length is 1350 m. The calculations are carried out with a constant water level upstream (1.094 m) and downstream (0.56 m) as boundary conditions. Keeping the value of Manning's coefficient constant at a value of 0.1 $m^{-1/3}s$, the three codes (Hec-Ras model, Bresse equation, Strive model) were used to calculate the discharge for both a rectangular and a trapezoidal cross section (Table 6.2).

For a rectangular cross section, discharge values of 2.14 m^3/s (bottom slope 0.000) and 2.82 m^3/s (bottom slope 0.0002) are obtained for each of the 3 ways of calculation. Similar results for both discharges and evolution of the water surface profile are obtained for the trapezoidal section (Fig. 6.12). By this, it is shown that the Saint-Venant equations, as implemented in the Strive model for flow in permanent conditions, delivers accurate results for different values of the bottom slope and bank slope of the cross section.

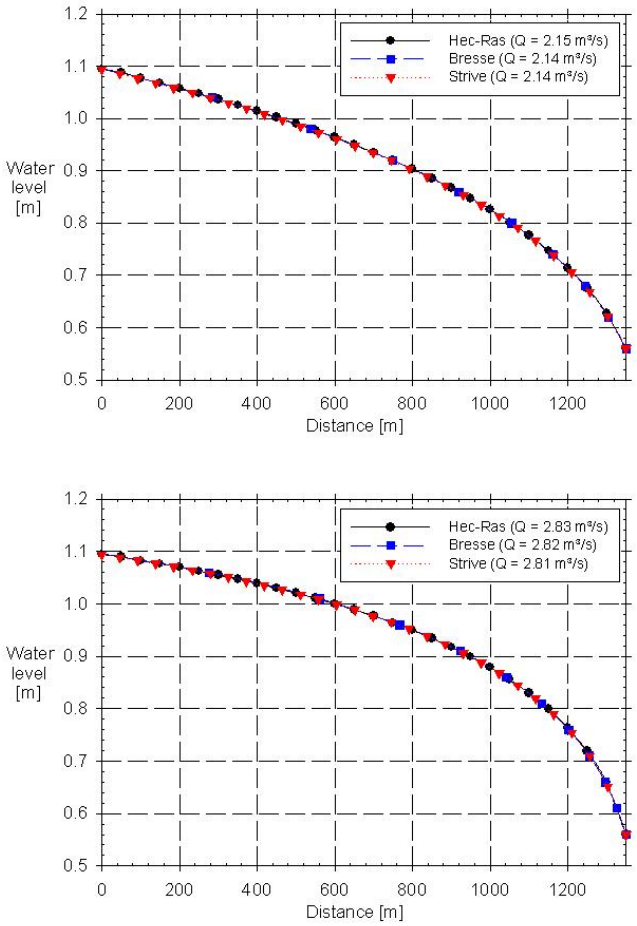

Figure 6.12: Calculation of surface water profiles: for a channel with a rectangular cross section and bottom slope 0 (case 1), bottom slope 0.0002 (case 2)

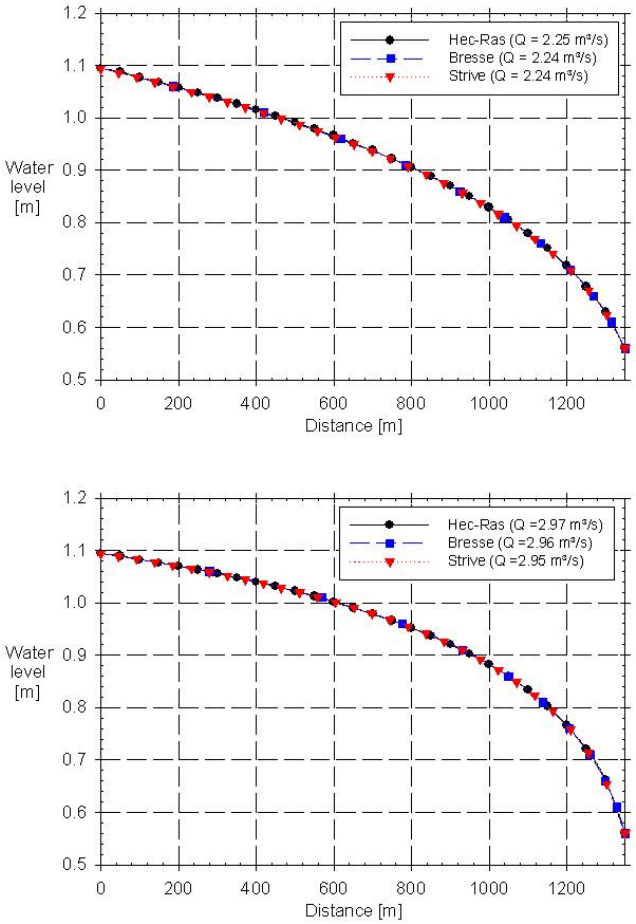

Figure 6.13: Calculation of surface water profiles: for a channel with a trapezoidal cross section (angle of 30 °) and bottom slope 0 (case 3); bottom slope 0.0002 (case 4)

case	S_0 [m/m]	Width [m]	Length [m]	Angle [°]	Z_{up} [m]	Z_{down} [m]
1	0	15	1350	0	1.094	0.56
2	0	15	1350	30	1.094	0.56
3	0.0002	15	1350	0	1.094	0.56
4	0.0002	15	1350	30	1.094	0.56
case	n [$m^{-1/3}s$]	Q_1 [m^3/s]	Q_2 [m^3/s]	Q_3 [m^3/s]		
1	0.1	2.15	2.14	2.14		
2	0.1	2.25	2.24	2.24		
3	0.1	2.83	2.82	2.81		
4	0.1	2.97	2.96	2.95		

Table 6.2: Calculation of surface water profiles (steady state) - with Q_1 = Q(Hec-Ras), Q_2 = Q(Bresse) and Q_3 = Q(Strive)

Due to vegetation and the consequential influence of backwater, the friction slope S_f of a river reach can vary extremely. Figure 6.14a shows the situation in the reach of the river Aa. Two cases are considered, a value of Manning's coefficient of 0.046 $m^{-1/3}s$, which was calculated with the Manning formula (Eq. 3.34) and the measurements of February 05 and a Manning coefficient of 0.423 $m^{-1/3}s$ (June 05). Manning's coefficient is 9 times higher in June when there is a wealthy vegetation. Starting from the same downstream water level and using a discharge of 1 m^3/s, the upstream water level is calculated for both values of n. In June, a value of 10.83 m for the upstream water level is calculated, while 10.20 m is obtained in February; this is a difference of more than 0.60 m due to the presence of vegetation.

Figure 6.14b shows the influence of the discharge on the energy slope S_f. For three different values of the discharge, the water surface profile is calculated. Manning's coefficient does not change. It seems that tripling the discharge results in an increase of the water level of only 0.35 m. So, the impact of the vegetation on S_f is much bigger and explains why a dangerous situation may occur with regard to inundation during summer floods.

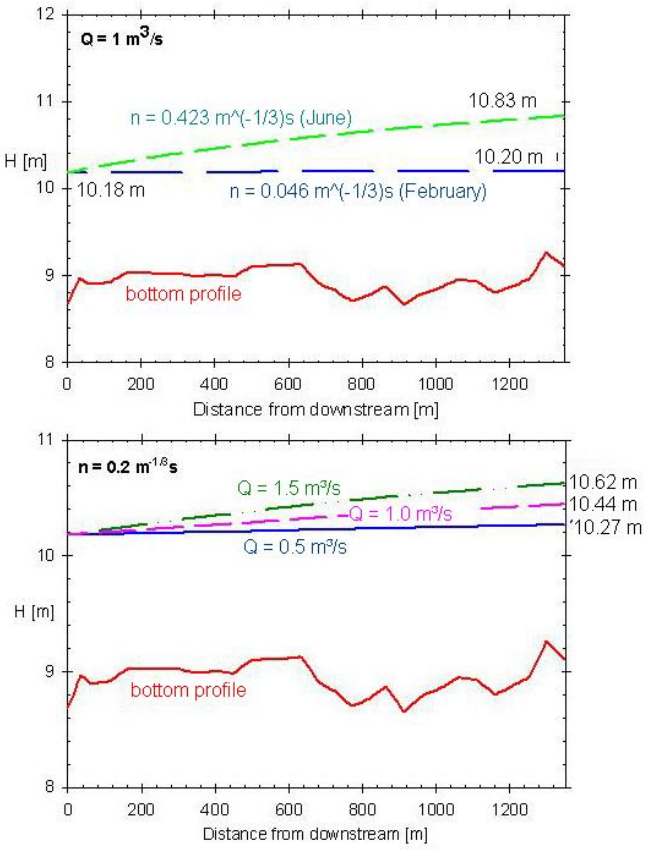

Figure 6.14: Influence of backwater of Manning's coefficient on the water level for a given discharge (a, top) and backwater influence of Manning's coefficient on the discharge for a given amount of vegetation (b, bottom)

4.5 Validation for unsteady state conditions

4.5.1 Propagation of waves

The propagation of a triangular hydrograph in a 10,000 m long channel with rectangular cross section as shown in Fig. 6.15a (bottom width of 10 m) and a zero bottom slope is modelled in Strive using the Saint-Venant equations. The Saint-Venant equations use both boundary conditions (zero upstream and downstream discharge) and need well balanced initial conditions. The initial water level is 1 m, initial discharge is 0 m^3/s. Calculation of the surface water level for permanent steady state flow over the total length of the channel can be a good start and can yield initial condi-

tions. Figure 6.15a shows the results at different sections when Manning's coefficient is kept constant (n = 0.05 $m^{-1/3}s$). At Figure 6.15b, the influence of this friction coefficient in a certain section (x = 2990 m) can be seen. The results indicate the possibility to carry out unsteady state simulations with the Strive model. Time shift and peak flattening are seen on bot Fig. 6.15a and Fig. 6.15b.

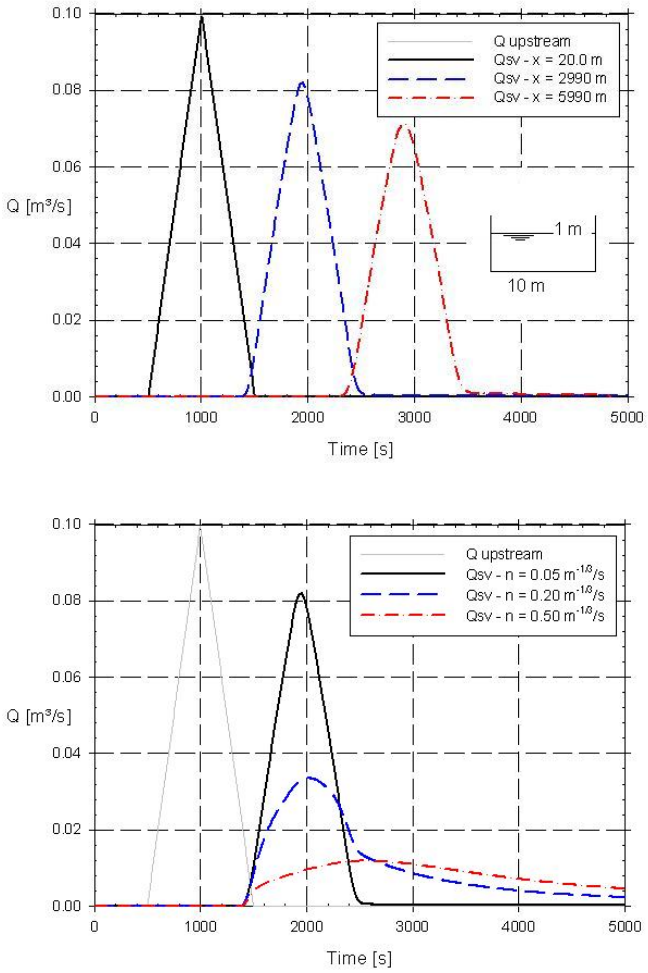

Figure 6.15: Numerical results of wave propagation by use of the Saint-Venant equations: result at different distances (top) and result at the same distance (x = 2990 m) for different values of Manning's coefficient n (bottom)

4.5.2 Comparison with analytical solution

A tidal wave in an open channel is modelled. An analytical solution for this problem is described by Ying [10] and Bermudez [11] and is depicted in Fig. 6.16 in comparison with the results of the numerical solution. The figures show the water level and the velocity over the entire length of the reach. The values are results after 7000 s of calculation.

The bed elevation, Zb(x), with a negative slope, is defined by:

$$Zb(x) = 10 + \frac{40x}{L} + 10sin(\pi(\frac{4x}{L} - \frac{1}{2})) \tag{6.5}$$

with x = the coordinate along the river channel and L = 14000 m, the channel length. The water level is Z(x,t), so initial condition is noted as Z(x, t = 0) = 60.5 m, and the velocity is V(x,t), with V(x, t = 0) = 0 m/s as initial condition.

Boundary conditions are:

$$Z(0,t) = 64.5 - 4.0sin(\pi(\frac{4t}{86400} + \frac{1}{2})) \tag{6.6}$$

$$Q(L,t) = 0.0 \tag{6.7}$$

The analytical solution is given by Bermudez [11]:

$$Z(x,t) = 64.5 - 4.0sin(\pi(\frac{4t}{86400} + \frac{1}{2})) \tag{6.8}$$

$$V(x,t) = \frac{(x-L)\pi}{5400h(x,t)}cos(\pi(\frac{4t}{86400} + \frac{1}{2})) \tag{6.9}$$

with h [m]= waterdepth.

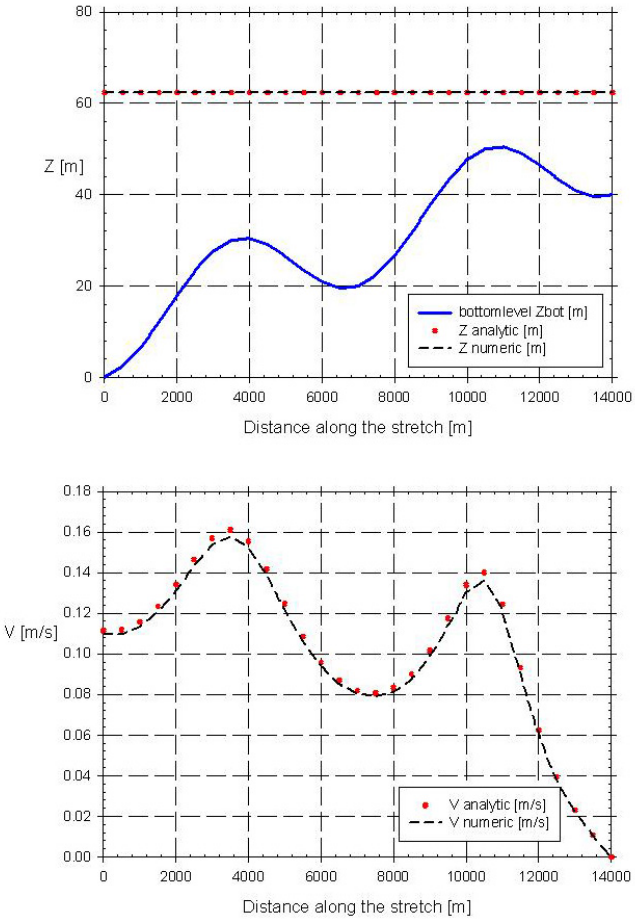

Figure 6.16: Analytical and numerical solution to the tidal wave problem: water level (top) and velocity (bottom) over the entire reach of 14000 m at time t = 7000 s

In both figures, the numeric solution is in good agreement with the analytical solution, which confirms the good functioning of the numerical model. It is capable of accurately predicting water surface level and flow velocity. Comparable results are mentioned by Ying [10].

4.5.3 Comparison of the Hec-Ras results and the Strive results

The problem of steady turbulent open channel flow is studied. The results of the Strive model are compared with numerical results of the program Hec-Ras. By this, it is shown that the Saint-Venant equations, as implemented in the Strive model for flow in permanent conditions, deliver accurate results for different values of the bottom slope and bank slope of the cross section.

5 Sensitivity analysis

5.1 Influence of discharge and biomass on celerity and dispersion of waves

In the following 3 paragraphs, all calculations use an upstream hydrograph Q(t) according to Anderson [12]. The resulting hydrograph at the downstream boundary is calculated as well as the water levels along the reach. The total length of the channel is 5000 m. The channel is rectangular, has a bottom width of 12 m and a bottom level of 8.89 m. The cross section characteristics and the range of the values of discharge and water level are derived from the Aa data. The length of the reach is extended to show clearly the effects and influences in the sensitivity analysis.

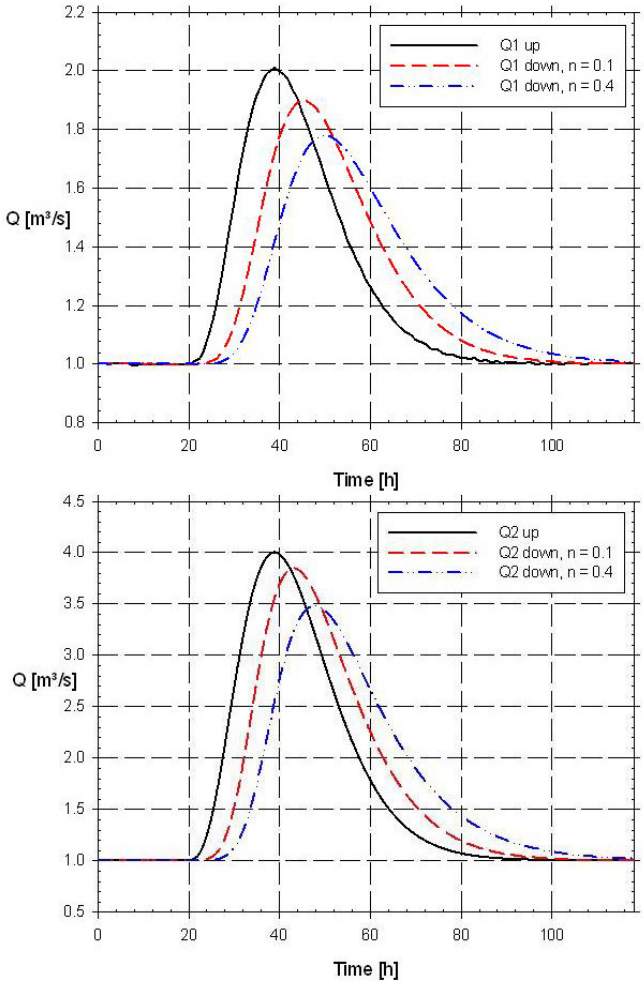

Figure 6.17: Influence of discharge and biomass on celerity and dispersion of waves

Figure 6.17 shows results for different hydrographs, indicated as $Q_1(t)$ and $Q_2(t)$, with a ratio Q_2/Q_1 as mentioned in Fig. 6.19. $Q_1(t)$ has a peak discharge of 2 m^3/s while $Q_2(t)$ reaches peak values of 4 m^3/s. For both, the base flow equals 1 m^3/s. The amount of biomass is expressed by Manning's coefficient. Indeed, analysis in the river Aa showed the relation between the amount of biomass and Manning's coefficient [13]; in the river Aa, 40 g/m^2 corresponds with a Manning coefficient of 0.1 $m^{-1/3}s$, while 0.4 $m^{-1/3}s$ is linked to an amount of macrophytes of 400 g/m^2. The upstream hydrograph is a fixed boundary condition and the downstream

discharge values are mentioned for comparison. For both hydrographs, it seems that the wave celerity (velocity by which a disturbance travels along the flow path) is smaller and the dispersion (tendency of the disturbance to disperse longitudinally if it travels downstream) [14] is larger for higher amount of biomass (higher Manning coefficients, higher roughness). Furthermore, the wave celerity is larger when the discharge increases. This is according to the continuity equation, agrees with larger celerities in streams with larger water levels [15] and corresponds with the larger backwater effect for larger roughness coefficients. Not only the larger dispersion is an effect of the larger vegetation growth but also the slower decrease of the peak value of the wave is due to the higher resistance.
Table 6.3 presents the comparison of downstream discharges for different amounts of vegetation. The value of the peak discharge is mentioned as well as the time after which the peak value occurs.

	Q_{up} m^3/s	Q_{down} (n = 0.1) m^3/s	Q_{down} (n = 0.4) m^3/s
peak			
Q_1	2	1.898 m	1.779 m
Q_2	4	3.844 m	3.481 m
time			
Q_1	0	6 h	11 h
Q_2	0	4 h	9 h

Table 6.3: Comparison of downstream discharges for different amounts of vegetation

5.2 Influence of discharge and biomass on water levels

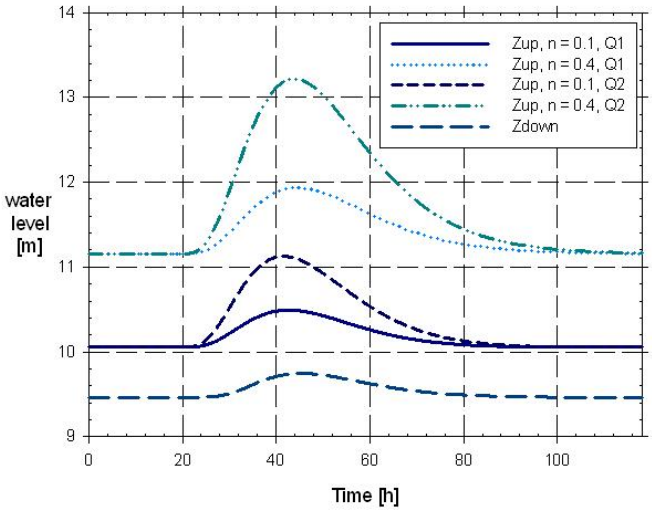

Figure 6.18: Influence of discharge and Manning's coefficient on water levels

Fig. 6.18 depicts the upstream water level for different discharges (hydrograms $Q_1(t)$ and $Q_2(t)$ as above) and for different values of Manning's coefficients. The back water effect is higher for more wealthy vegetation growth and for higher discharges. It can be seen that peak flows (higher discharge) in summer situations (more vegetation and therefore higher resistance described by a higher Manning coefficient) can cause dangerous situations. In case of low heights of the dikes, inundations will occur.

5.3 Influence of discharge on water level

In Fig. 6.19 the impact of the discharge on the water level is checked for increasing discharge. Two different hydrographs are chosen, $Q_1(t)$ and $Q_2(t)$ as in the previous paragraphs, results for $Z_1(t)$ and $Z_2(t)$ are also as above (Fig. 6.18). The relation between the basic hydrograph $Q_1(t)$ and the increased discharge is plotted and shows a peak value of 2. The impact on the water level, however, is much smaller and varies with varying Manning coefficient. For n = 0.1 $m^{-1/3}s$, the relation is 1.06, while for n = 0.4 $m^{-1/3}s$, the relation is 1.10. The impact on the water level is higher for a higher amount of in-stream vegetation. In general, discharges are much more sensitive to changes then water levels and therefore, upstream hydrograph values are preferred above water levels as a boundary condition.

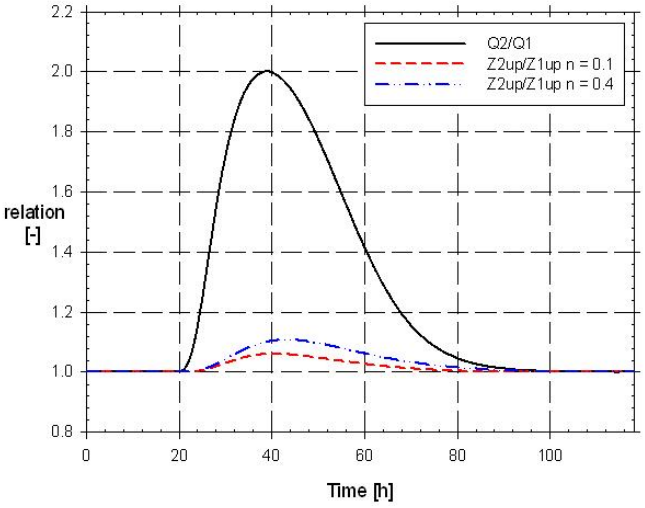

Figure 6.19: Influence of discharge on water level

5.4 Combined influence of discharge and biomass: steady state

The influence of the in-stream vegetation (biomass) is represented by the value of Manning's coefficient (Fig. 5.24). Figure 6.20 shows the situation in a theoretical reach of 5000 m. The cross-section is rectangular and has a bottom width of 12.0 m. There is no slope along the reach and the bottom level is 8.89 m.

Two cases are considered (Fig. 6.20a), a lower Manning coefficient of 0.1 $m^{-1/3}s$, which corresponds with the values in the winter for the river Aa and a higher Manning coefficient of 0.4 $m^{-1/3}s$ (spring and summer values). The Manning coefficient is up to 9 times (0.05 to 0.45 $m^{-1/3}s$) higher in spring when there is a wealthy vegetation [1]. Starting from the same downstream water level (10.20 m) and using a discharge of 1 m^3/s, the upstream water level is calculated for both values of n. In spring, a value of 11.21 m for the upstream water level is calculated, while 10.35 m is obtained in winter; this is a difference of 0.90 m due to the presence of vegetation.

Fig. 6.20b shows the influence of the discharge on the energy slope S_f. For three different values of the discharge (0.5; 1 and 1.5 m^3/s), the water surface profile is calculated. Manning's coefficient is kept constant at 0.1 $m^{-1/3}s$. It is shown that tripling the discharge results in an increase of the water level of only 0.26 m (10.24 m for the lowest discharge, 10.35 m for Q =

m^3/s and 10.50 for the highest value of Q). So, the impact of the vegetation on S_f is much bigger and explains why dangerous situations may occur with regard to inundation during summer floods.

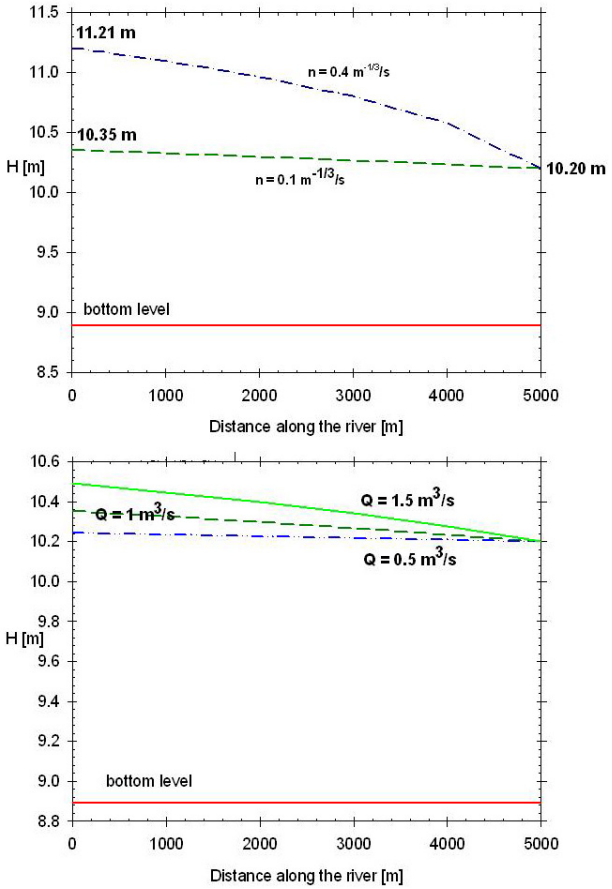

Figure 6.20: Backwater influence of Manning's coefficient on the water level for a given discharge (top) and backwater influence of the discharge on the water level for a given amount of vegetation (bottom)

5.5 Combined influence of discharge and biomass: unsteady state

The impact of a variable amount of vegetation on the stream flow is illustrated. A flood wave, registered in the studied reach of the river Aa, in the period from August, 12th to August, 19th (2005), is used as upstream boundary condition for the calculation (Qupstream). Downstream boundary condition is the registered water level at the downstream weir (Zdownstream). The simulated reach has a length of 5000 m, a rectangular cross section and a bottom width of 12.0 m. The bottom level is 8.89 m. Fig. 6.21 depicts the boundary conditions and the calculated results for Qdownstream and Zupstream for two values of the biomass: in winter conditions (n = 0.1 $m^{-1/3}s$) and in summer conditions (n = 0.4 $m^{-1/3}s$). The variation, with Manning's coefficient, of the downstream discharge is limited, but it is clear that the upstream water level (Zupstream) is strongly influenced by the dense vegetation growth during summer. With increasing values of Manning's coefficient, the downstream discharge peak shows a small time lag and a substantial attenuation.

In Fig. 6.21b and Fig. 6.22, the river banks are indicated. For low vegetation growth, the peak discharge and corresponding water level cause no problems. For higher values of Manning's coefficient, the river banks (11.6 m) will be too low for the peak discharge and neighbouring areas will inundate. Therefore, a good knowledge of the impact of biomass on the roughness of the river is important to build river flood simulation models able to produce reliable results for all seasons of the year. Consequently knowing the maximum allowable flood water level, it becomes possible to determine the value of Manning's coefficient and by this the amount of biomass that can be kept in the river to safely convey a given flood wave. As can be seen from Fig. 6.22, reducing the n-value to 0.205 $m^{-1/3}s$ (which corresponds with an elimination of 75% of the biomass) keeps the flood wave under concern within the banks of the river. In this way, it becomes possible to define a 'safe' biomass management strategy.

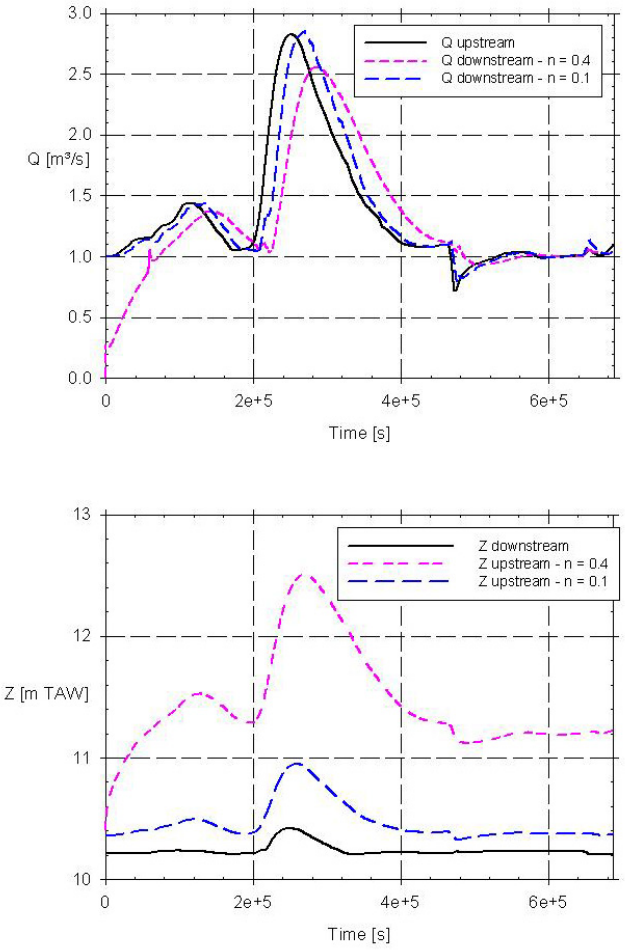

Figure 6.21: Boundary conditions Qupstream and calculated Qdownstream for n = 0.4 $m^{-1/3}s$ and n = 0.1 $m^{-1/3}s$ (top, Fig. 6.21a) and boundary conditions Zdownstream and calculated Zupstream for n = 0.4 $m^{-1/3}s$ and n = $m^{-1/3}s$ (bottom, Fig. 6.21b)

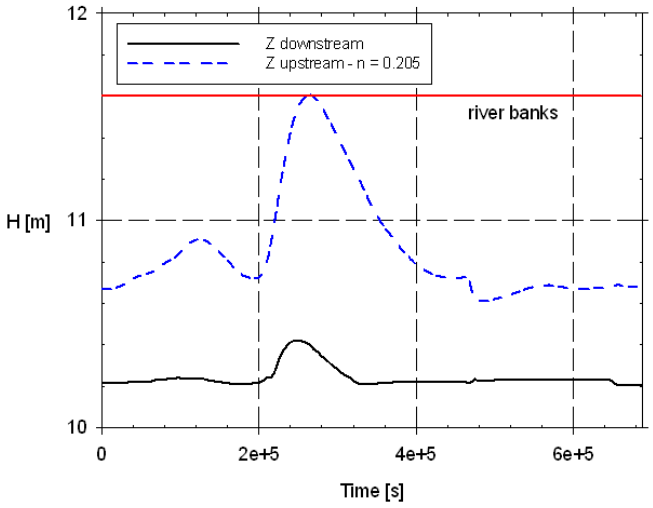

Figure 6.22: Upstream and downstream water level of the flood wave for n = 0.205 $m^{-1/3}s$, with indication of the river bank

6 Calibration process of the coupled Strive model using field data

Discharges and water levels are modelled together with modelling of electrical conductivity. The electrical conductivity can be used as a boundary condition if values of discharge, for example, are difficult to determine. The conductivity is often more easy to measure compared to calculation of discharges where integration of velocities is necessary. Extensive measurement campaigns are carried out to collect a large number of observations and calibration of the model is based on this data set. Further, calibration methods and the discussion of this process is displayed. As a result, it is seen that the developed Strive model can model both, hydrodynamic and ecological processes, in an accurate way. The section highlights the importance of detailed determination of Manning's coefficient, dependent on discharge and amount of biomass, as an important calibration parameter for accurate modelling.

6.1 Introduction

In the field of environmental engineering, numerical modelling of river systems is becoming more and more required. Flow prediction and water management ask for a long-term view, based on numerical models as well

as on measurements in the field. Modelling the free surface flow in creeks and rivers requires the implementation of the Saint-Venant equations describing the flow mathematically, and calibration of the obtained solution, e.g. by evaluating Manning's roughness coefficient as one of the most important model parameters. To come to an accurate hydraulic model, its setup needs a lot of effort in implementing the Saint-Venant equations and calibration of the parameters, including Manning's coefficient.

Manning's coefficient expresses the resistance of the channel to the flow in it. This value is influenced by the bottom material, the meandering of the river, the presence of macrophytes etc. [16]. Manning's coefficient in the Saint-Venant equations is calculated from the friction slope, the discharge and the geometrical characteristics of the channel [14]. It is well-known that Manning's roughness coefficient is the most sensitive parameter and needs to be calibrated carefully [17]. Most of the equations and methods to estimate the flow resistance are based on Manning's coefficient and also describe the flow problem in a simplified but accurate way. This Manning's coefficient is not constant due to the variable discharge [18] and the varying vegetational influence over the year [1, 19]. All model packages focus on the calibration of the roughness parameter which, together with the geometry, is considered to have the most important impact on predicting flow characteristics [20]. Therefore, the focus of this study is an evaluation of the calibration value of the roughness coefficients. This analysis is also driven by the fact that many modellers see the main problem in practical applications as a problem of choosing the 'correct' roughness [20].
In this study, the numerical model Strive model has been used [21–23]. A 1D hydrodynamic model for unsteady free surface flow based on the Saint-Venant equations is coupled to ecosystem exchange processes such as macrophyte growth, transport of solutes and solids, etc. [24]. The Strive model has already established good results [1, 2, 21, 25] and the role of the accuracy of the numerical solution and its impact on model predictions is already investigated.

Interactions between surface water, groundwater and ecological processes are already studied in different fields [26]. Modelling of the interaction processes is studied in [27–31].
An integrated model study of hydraulic, groundwater, biogeochemical and ecological processes is required for the prediction of dynamic ecosystem behaviour, such as retention of matter in a river ecosystem and the associated resilience. However, most of the available models do not allow the integration of surface water flow, groundwater flow and ecosystem processes. Whigham [32] developed a simple water movement model allow-

ing the prediction of the environmental impact of flow scenarios in lowland rivers and their floodplains. The model is a good initial framework, but has its constraints due to its simplification. In a multidisciplinary approach, different research areas have to be integrated to study properly the interaction between surface water and vegetation.

Measurements over the years of discharge, water level and electrical conductivity in the river Aa form a useful dataset for calibration and validation of the Strive model. Influence of discharge and biomass on Manning's coefficient is discussed. Out of all calibration parameters, Manning's coefficient is the most important one. Extensive calibration is carried out to determine the parameters for the best fit between observed and modelled data Two short-term relationships as well as a long-term relationship for Manning's coefficient and discharge is set up and used for modelling. An extensive numerical study is not performed, but attention is paid to the physical processes in the river ecosystem. Numerical results of modelling discharge, water level and electrical conductivity are presented.

6.2 Discussion of parameter uncertainties

The uncertainty on a lot of parameters complicates accurate numerical modelling. Calibration of the model parameters listed hereafter is based on the data sets of the measurement campaigns in 2005 and 2006 in the reach of the river Aa. Some of the parameters have been measured, others are only known in an indicative way:

- The *position of the downstream weir (Angle1,...,4)* is not known due to the lack of registrations. Furthermore, this position can change at any time, following the changes in the water level.
- *The bottom level, upstream and downstream* ($Z_{bottomup}$, $Z_{bottomdown}$). Cross sections in the river Aa have been measured in 1997. The bottom profile may have changed slightly over the years, which introduces uncertainty on the bottom level over the reach.
- *Bottom Width, Bank Angle (the cross sectional geometry)*. These parameters are approximately known according to the same remarks as mentioned above. A trapezoidal geometry is built in the model. Accurate cross section determination is necessary for volume calculation. However, the cross section is more or less variable due to sedimentation and erosion, vegetation growth, obstacles, etc. Furthermore, these processes will also affect each other.

- *The lateral inflow of the Slootbeek ($Q_{Slootbeek}$, $EC_{Slootbeek}$).* Just, downstream of the upstream weir, a lateral inflow of the Slootbeek is present. This (rather small) discharge is not measured and is therefore an unknown parameter. This inflow is already incorporated in the upstream discharge measurement, which is measured downstream the inflow location, but the EC-value is measured upstream the Slootbeek.

- *The value of Manning's coefficient (n).* This parameter determines the roughness in the Saint-Venant equations and is influenced by biomass and discharge (cf. infra), which has consequences for the modelling of base and peak discharges. Due to the short calibration and validation period used (3 to 7 days during the measurement campaign), it has been assumed that the biomass is more or less a constant value during that period. The discharge however will change as flood waves are present.

6.3 Cost function

Arhonditsis [33] conducted an analysis of 153 studies published from 1990 to 2002 to see if modellers follow conventional procedures for the calibration. These procedures include sensitivity analysis, calibration and validation [34].

Sensitivity analysis is the process by which the modeler attempts to evaluate the model sensitivity to the parameters selected, forcing functions or variable submodels [34]. This step is essential for selecting the optimal model structure and complexity because it indicates the accuracy required for the forcing function data and identifies the parts of the model that need to be estimated with great precision. Arhonditsis [33] analysed that only 27.4 % of the studies did a profound quantification of the model sensitivity. Sensitivity of models is obtained by separately perturbing each model parameter and observing the effect on the output of the model. This technique demands for plenty of simulation time, while not giving a lot of additional information. To get information of the variability of the output with change of some parameters, a technique for sensitivity analysis as Monte Carlo is interesting. A Monte Carlo analysis tests the effect of a change in parameter on the numerical result. However, for a model with a large computation time and/or for a wide range of each parameter, a Monte Carlo analysis is not feasible, the number of runs becomes too large, estimated around 10^N, where N is the number of parameters of the model. Then, more efficient sampling methods are available such as the shuffled complex evolution (SCE) method [35, 36].

Calibration is the procedure by which the modeler attempts to find the best fit between computed and observed data by adjusting model parameters. In the analysis by [33], 91.5 % of the models were reported as calibrated by tuning and in almost every study the parameters were based on literature review and not on measurements [33, 37]. This is a method of trial and error and does not ensure that the selected parameter set is the best set and consequently, it is not known if lack of fit is due to errors in the model's structure of due to a bad choice of the parameters [37]. This problem can be solved by application of optimization techniques designed to search the parameter space for combinations of parameters which provide the best fit through minimization of cost functions. Arhonditsis [33] stated that only 8.5 % of the studies used this optimization technique. However, a wide range of skills is developed in the field, Matear [38] and Hurtt [39] used the technique of simulated annealing and Vallino [40] improved marine ecosystem modelling using data assimilation where model and model results were improved based on measurements.
Two categories of methods are available for calibration: the random methods and the directional methods [41, 42]. Some algorithms delivering good results for some application, may fail for others. The first category includes the quasi-random methods as simulated annealing [38, 43, 44], genetic algorithm [40, 45], a pseudo-random search algorithm [46, 47], etc. The second category are the directional methods where the minimum is approached iteratively, using the gradient of the discrepancy of the model to data. The directional methods will provide an minimum depending on the parameter set of the initial guess: a solution will be obtained, but it is doubtful if it is the best solution. Parameters change up to a better solution. Examples are the quasi-Newton and the Levenberg-Marquardt algorithm [41]. In case of correlated parameters, this method often fails. Soetaert [41] advises to start with a random-based method [37] for calibration to get an idea of the parameter space and to come to the final result by a directional method. The first category of methods allows to identify a global minimum which is useful since, due to the non-linearity and the complexity of the ecosystem model, the cost function (cf. infra) will have multiple minima (Fig. 6.23).

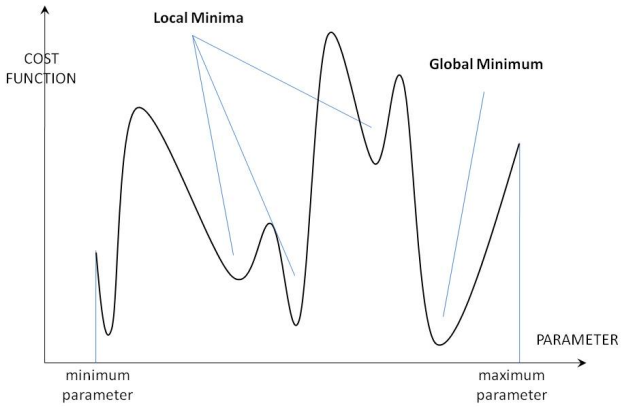

Figure 6.23: Local and global minima of the cost function

Further, calibration routines often fail when parameters are strongly related. Franks [48] used the term 'calibration bias' for the situation where the fit for other parameters is reduced when trying to maximize the fit for a specific parameter. More than 95 % of the models studied [33] did not report results for all parameters and suggested selective interest or selective presentation of the parameters with better results. Another possibility is that the results are not corresponding to the data [48].

Validation is defined as 'whether a model within its domain of applicability possesses a satisfactory range of accuracy consistent with the intended application of the model' [33]. It is an essential step in model reliability.

Models ususally have been used to produce system dynamics based on a given set of equations and parameters. Often, one is more interested in extracting, based on the data, the parameter values or fluxes rather than to predict data from parameter values. This reverse application of models is called inverse modelling. Here, this technique is used for calibration of the model parameters.

As is mentioned in the introductory part, up till now, mathematical techniques of optimization are not often used in ecosystem modeling. However, different techniques are available, all based on minimizing a cost function [33]. The cost function describes the difference between model results and observed data. The parameter set which results in the best fit is searched, as the lower the cost function, the better the model de-

scribes the data. Definitions of the cost function can be found in [37, 49]. Los [50] mentions different ways to determine the 'goodness of fit' by various expressions of the cost function. First, a single parameter cost function (Eq.(6.10)) is calculated for each parameter over the modelled period, and subsequently the single cost functions are combined into the model cost function (Eq.(6.11)).

$$CostFunction = \sum \frac{(ModVal - ObsVal)^2}{\sigma^2} \tag{6.10}$$

$$ModelCostFunction = \sum CostFunction(parameters) \tag{6.11}$$

where ModVal = model value of the parameter; ObsVal = observed value of the parameter and σ^2 = variance.

An 'error' value is used to give more weight to the parameters that are more precisely known and returns the cost function in a dimensionless form. Here, each model parameter is weighed using the variance in the data. The result of the cost function is averaged over the output interval, which is 1 hour for water quantity calculations.

Study of the cost function will result in an optimal solution. However, attention has to be paid: apart from comparison of the mathematical value, interpretation is necessary. For example, wrong (extreme eg.) measurement values will influence the cost function significantly. Furthermore, one large deviation compared to several small differences between observed and calculated values will result in the same value of the cost function.
Variation of one parameter is more determining than another. Good approximation of the bottom level of the river is important. Indeed, introducing wrong bottom values has influence on volume calculations and consequently on electrical conductivities. Next to that, the value of the model cost for the calculations is compared with deviations on average and peak value of discharge, water level and electrical conductivity (cf. infra).

6.4 Manning's coefficient as a function of discharge and biomass

In Chapter 5, it is shown that Manning's coefficient is related to discharge and amount of biomass. In the following, a numerical relation is set up between these three parameters aiming use of it in the Strive model.

In the following, the relationship between discharge, biomass and Manning coefficient is investigated in more detail. Two methods to determine the value of Manning's coefficient for numerical modelling are used and are mentioned as 'Method 1' and 'Method 2'.
The first method to calculate Manning's coefficient is based on measurements of discharge and water level over the years in the river Aa. The geometry of the cross sections is incorporated in the calculations. For all measurements carried out over three years, Manning's coefficient is calculated using measured discharge and water level and the one-dimensional Hec-Ras model [8]. The Saint-Venant equations are simplified to the Bresse-equation due to the assumption of steady flow during the measurements of discharge and water level (cf. supra).
The second method determines a long-term continuous relationship between Manning's coefficient, discharge and biomass. To set up this relationship, Manning's coefficient is calculated using the Strive model for steady flow based on Eq.(3.31) and the geometrical characteristics built in the Strive model. This geometry is simplified, trapezoidal, and in very good agreement with the measured geometry of the channel. Use of this trapezoidal geometry results in slightly (30 %) lower Manning values compared to the ones in Fig. 5.24. Under these conditions, use of Manning's equation (Eq.3.34) results in the same values as use of the Bresse equation in the Strive model.

6.4.1 Long-term (continuous) relationship between Manning's coefficient, discharge and biomass for use in the Strive model

Equations The discrete measurements are used to set up a continuous relationship between Manning's coefficient, the discharge and the biomass. This relationship is used in the Strive model to determine Manning's coefficient based on calculated values for discharge and biomass. Calculations for obtaining Manning's coefficient are performed using 'Method 2'. Use of this trapezoidal geometry results in slightly (30 %) lower Manning values compared to the ones in Fig. 5.24. First, the relations between Manning's coefficient and discharge and between Manning's coefficient and biomass are found. Secondly, all parameters are studied jointly.

Using the data set of Manning's coefficients and related discharges between September 04 and April 07, yields an exponential decay of Manning's coefficient n with increasing discharge Q (see Fig. 6.24a):

$$n = f(Q) \tag{6.12}$$

$$n = 0.0602 + 1.0435exp(-2.2035Q) \tag{6.13}$$

The exponential relation between Manning's coefficient and discharge (Eq.(6.13) and Fig. 6.24a) has an R^2 value of 0.81 and covers all values in an accurate way. The measured discharge ranges between Q = 0.5 m^3/s and Q = 3.2 m^3/s, and related values for the calculated Manning coefficient are n = 0.35 $m^{-1/3}s$ and n = 0.04 $m^{-1/3}s$, resp. The fitted exponential decay function shows good agreement with the data for the whole range of Q values, with somewhat larger scatter between Q = 1.0 m^3/s and Q = 1.4 m^3/s.

A sigmodal curve (R^2 = 0.78) (Eq.(6.14)) is fitted to the values of biomass and Manning's coefficient in Figure 6.24b. For biomass values equal to 0, Manning's coefficient is set to 0.0850 $m^{-1/3}s$. The sigmoide represents well the physical processes which occur between the flow and the vegetation in the flow. For low amount of biomass, Manning's coefficient is low because the macrophytes do not obstruct the flow. The higher the amount of biomass, the higher the resistance to flow and consequently Manning's coefficient. Further, the resistance to flow reaches a certain maximum, independent of the amount of biomass.

$$\begin{aligned} &n = f(biomass) \\ &f = 0.0850 + (0.3025 - 0.0850) * (|(biomass/106.29)|^{|(-3.8033)|})/ \\ &\quad (1 + (|(biomass/106.29)|^{|(-3.8033)|})) \end{aligned} \tag{6.14}$$

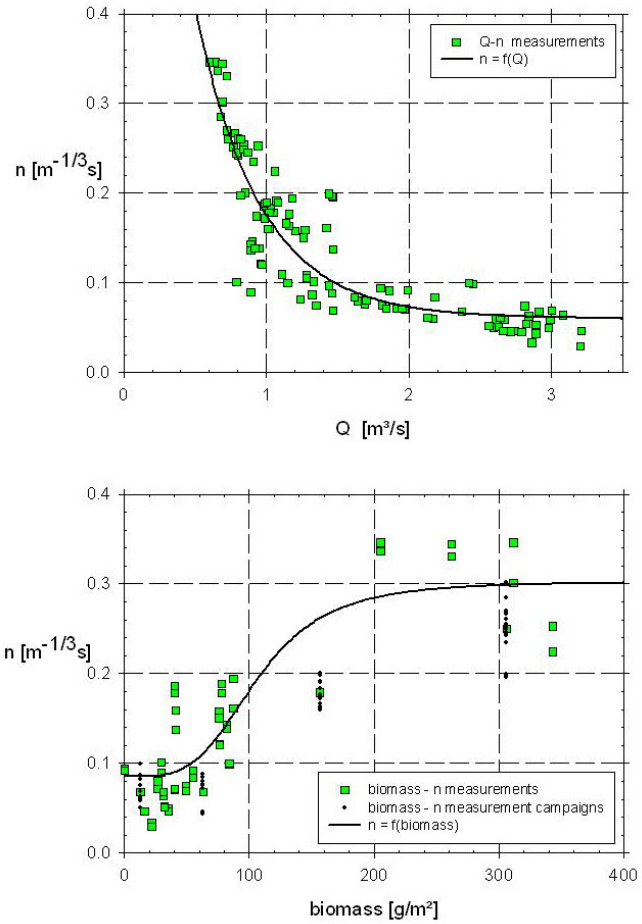

Figure 6.24: Measured data set and empirical fitting of relationship between Manning's coefficient and discharge (Fig. a, top, Eq.6.13) and between Manning's coefficient and biomass density (Fig. b, bottom, Eq.6.14), for the period of September 04 to April 07 in the river Aa

In order to combine the effect of discharge and biomass density on Manning's coefficient, a relation between these three parameters is set up, resulting in Eq.(6.15). In Eq.(6.15), the influence of the biomass is taken into account for 40 %, while the discharges comprise the other part. These values give the best agreement between the measured values and the fitted curves.

$$n = 0.40f(biomass) + 0.56f(Q) \tag{6.15}$$

The physical interaction between the parameters is explained as follows. Low discharges correspond to higher Manning coefficients, certainly in combination with higher biomass values. For a low biomass density, the variation of the discharge is of less importance for the determination of Manning's coefficient, which will not significantly change. The relation is evident; if the river is totally obstructed by vegetation (high n values), the discharge will be low. For small discharges, the influence of the biomass is only small, for larger discharges, Manning's coefficient is increasing with increasing biomass. High discharges and a lot of macrophytes have the largest influence on Manning's coefficient.

Figure 6.25 presents Manning's coefficient n_{meas} calculated out of the measurements (Method 2, Bresse equation with simplified geometrical characteristics and measured discharges and water levels) and the predicted Manning coefficient n_{pred} calculated according to the empirically fitted relationship Eq.(6.15). A reasonable agreement between predicted and measured values is observed. The predicted values yield a small overestimation compared to the measured values for small n-values and a small underestimation for the largest values around n_{pred} = 0.3 $m^{-1/3}s$. The values are varying, with a little spreading, around the central line, which is acceptable for these natural systems. So, Eq.(6.15) gives a good prediction for the calculation of Manning's coefficient in the river Aa using the measured discharges and biomass. The relation between the mentioned values of Manning's coefficient is given by Eq.(6.16):

$$n_{meas} = 1.0887n_{pred} - 0.0164 \tag{6.16}$$

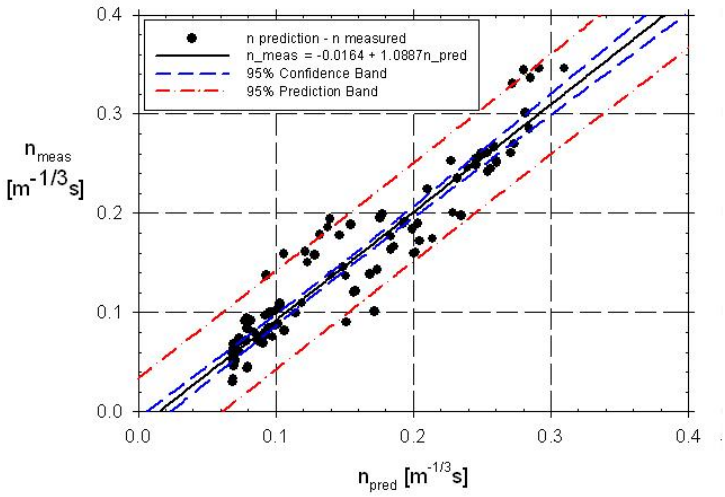

Figure 6.25: Agreement between measurements (Manning's coefficient n_{meas} calculated out of the measurements) and predictions (Manning's coefficient n_{pred} calculated according to Eq.(6.15))

In [25], the relation between Manning's coefficient, biomass and discharge is already introduced. Here, a more detailed analysis is carried out, based on a more elaborated dataset.

Spreading The study of the relationship between biomass, discharge and Manning's coefficient resulted in Eq.(6.15) which delivers globally good results. However, Fig. 6.24 needs some additions: the same biomass density is measured for a large range of discharges. For example, at the end of 2004, constant biomass values around 40 g/m^2 are measured while discharges varying between 1 to 3 m^3/s are seen. This is plotted in Fig. 5.24b. In Fig. 5.24a, for the same period and so for biomass density values around 40 g/m^2 (and corresponding discharges varying between 1 and 3 m^3/s cf. Fig. 5.24b), the same Manning coefficient is calculated (0.1 m$^{-1/3}$s). So, considerable spreading is observed in the dataset.

Fig. 6.26a shows the relationship between discharge and Manning's coefficient together with the deviation on Manning's coefficient when the discharge varies within a range of about 5 %. A measurement error on the discharge of 3 to 5 % is realistic [13]. Consequently, the calculated Manning coefficient, based on the discharge measurements, will also vary. Calculations showed that Manning's coefficient will vary in the same way: an

error on the discharge of 5 %, will lead to an error on Manning's coefficient of 5 %. For large discharges and corresponding small n-values, the consequence on the results is rather small, while for small discharges and larger n-values larger deviations occur. Using these deviant values for modelling will result in errors on the calculation results of discharge and water level.

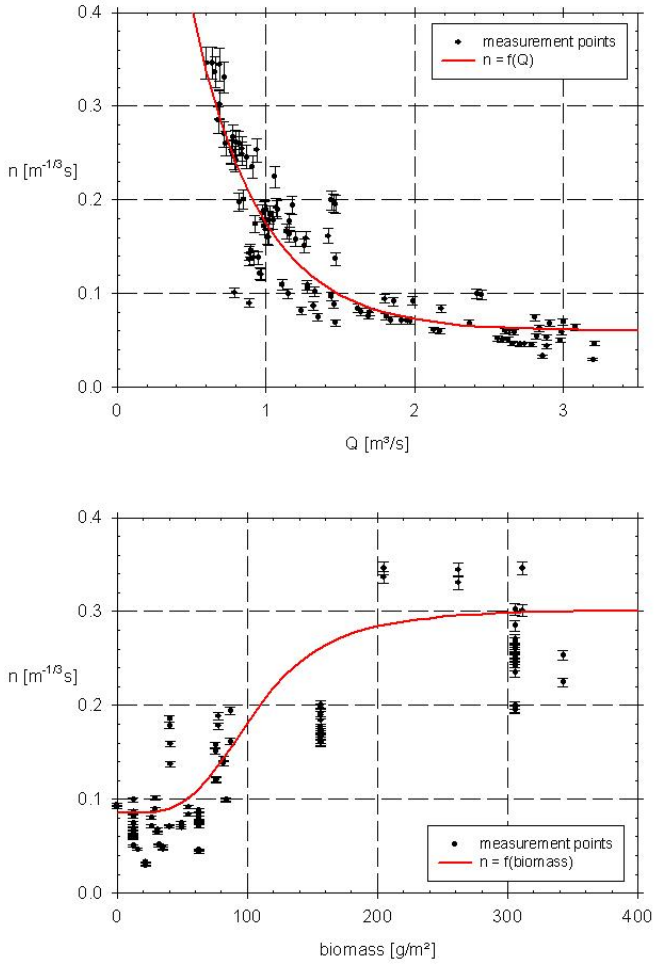

Figure 6.26: Measured data set and relationship Eq.(6.13) between discharge and Manning's coefficient and error band indication for discharge variations with ± 5% (Fig. 6.26a, top) and measured data set and relationship Eq.(6.14) between biomass and Manning's coefficient and error band indication for biomass variations ± 5% (Fig. 6.26b, bottom)

The accuracy of the biomass measurements is strongly related to the amount of biomass. In moderately vegetated channels, the accuracy is up to 5 %, while in channels with dense vegetation growth, this value will strongly increase. Furthermore, at a small scale, the accuracy is most of the time less than 10 %. Calculations showed that a deviation (eg. measurement error) of the biomass of more or less 5 %, results in a deviation of Manning's coefficient of more or less 2 % (Fig. 6.26b) .

Simultaneously, the macrophyte biomass growth cycle can be predicted based on the vegetation growth which depends on temperature and light and the vegetation mortality which is increasing with biomass density. The growth cycle is given in Eq.(6.17) [51] and measured and predicted values of the biomass density are plotted as a function of time in Fig. 6.27. Manning's coefficients are retained as presented in Fig. 5.24.

$$\begin{aligned} biomass(t_1) = {} & biomass(t_0) \\ & + biomass(t_0)([k_{growth} exp(\beta(T - T_0)) \\ & \frac{NH_4}{K + NH_4} \frac{I}{K_I} \frac{daylength}{24} exp(1 - \frac{I}{K_I})] \\ & - [k_{decay} exp(\frac{biomass(t_0)}{K_{biomass}})] \Delta t \end{aligned} \tag{6.17}$$

with biomass(t_1) = amount of biomass density at timestep 1 [g/m^2]; biomass(t_0) = amount of biomass at timestep 0 [g/m^2]; k$_{growth}$ = intrinsic growth rate [1/day]; T = temperature [°C]; T$_0$ = reference temperature [°C] β = temperature correction [1/°C]; NH$_4$ = NH$_4$ concentration [g/l]; I = intensity of light [W/m^2]; K$_I$ = light limitation [W/m^2]; k$_{decay}$ = intrinsic mortality rate [1/day]; K$_{biomass}$ = biomass limitation [g/m^2]

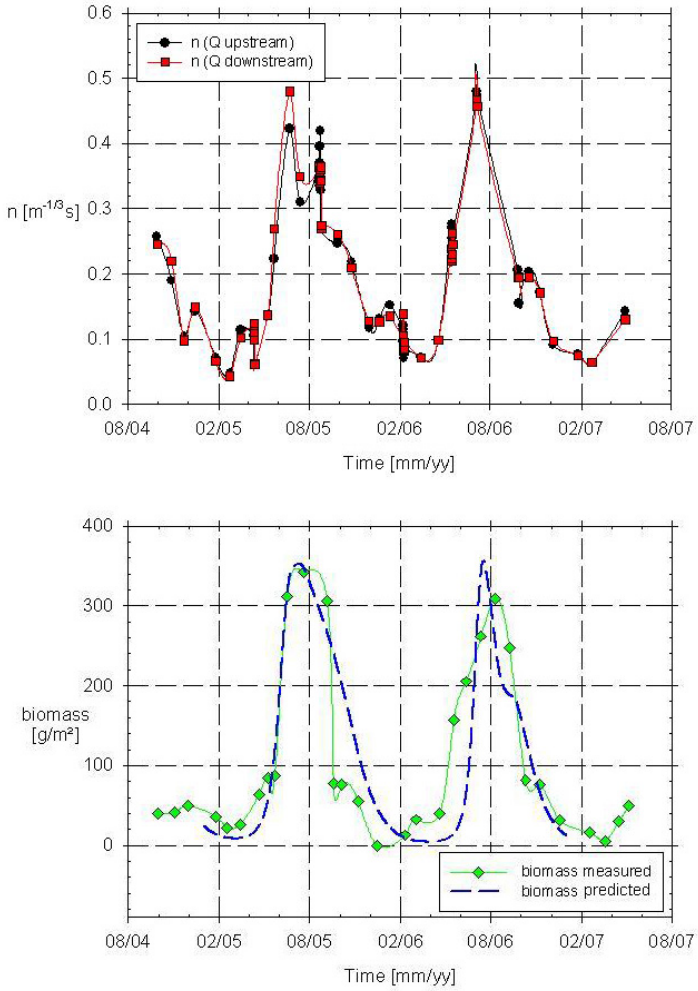

Figure 6.27: Measured and predicted values for Manning's coefficient (top) and for the biomass density (bottom), for the period of September '04 to April '07 in the river Aa

In general, Eq.(6.17) corresponds well to the biomass measurements. However, for specific periods, the deviations are large, eg. biomass measurements of May 06 differ from the model predictions using Eq.(6.17). Based on Eq.(6.15), inaccurate biomass predictions will introduce wrong roughness values into the numerical model and will result in poor modelling results.

6.4.2 Short-term relationships between Manning's coefficient, discharge and biomass during the measurement campaigns for use in the Strive model

After several years of data monitoring and analysis on the river Aa, a long-term general relationship between Manning's coefficient, discharge and biomass has been set up (with n according Method 2, see previous section). In general, this prediction provided by Eq.(6.15) delivers good results.
A second analysis is carried out here by gathering the biomass values, discharges and Manning's coefficient (with n according Method 2) values of the 4 different measurement campaigns and setting up a best-fit relationship, based on the measured values over this period only, to evaluate the accurateness of the predictions. We will refer to this methodology as the short-term analysis. The biomass varies slowly as a function of time, while discharge shows rapid changes over the time. Therefore, a seperate Manning coefficient-discharge relationship under the assumption of constant biomass density for the 4 periods of the measurement campaigns is proposed. These short term relationships are built using Manning's coefficient values calculated in 'Method 2'.

In a third analysis, both the long-term and the short-term based relationships between Manning's coefficient and discharge (using the data set) have not been used, but instead, for each measurement campaign, an iterative procedure has been applied to obtain a best match between measured and modelled values for discharge, water levels and electrical conductivity, by adjusting empirically the relationship between Manning's coefficient and discharge, comparing the values of the cost function.

Both methods and relationships from the above analysis, respectively, are used in the following: a simple best-fit to the measurements of a single measurement campaign *(n-best-fit-to-measurements)* and an empirical relationship which results in the best agreement in the numerical model results *(n-best-fit-for-modelling)*. For each measurement campaign, the value of the biomass is kept constant and Manning's coefficient is expressed as a function of discharge (cf. Table 6.4).

The ranges of the discharges measured during the measurement campaigns are also indicated in Table 6.4. For the period of August, three measurements of the peak value are not taken into account (cfr. infra).

period	$n_{best-fit-to-measurements}$	$n_{best-fit-for-modelling}$	Q range
February 2006	$0.0922Q^{-0.46}$	$0.094Q^{-0.41}$	$1 < Q < 3$
May 2006	$0.1794Q^{-0.381}$	0.2104-0.0288Q	$0.7 < Q < 1.2$
April 2005	$0.1397Q^{-1.089}$	0.0899-0.0195(Q-1.6)	$1.2 < Q < 2$
August 2005	$0.2201Q^{-0.663}$	$0.215Q^{-0.64}$	$0.5 < Q < 1.5$

Table 6.4: Short-term Manning-discharge relationships for the 4 measurement campaigns, using a best fit to the measurements and a best agreement for the numerical model results, and the range of the discharge [m^3/s]

6.4.3 Comparison of different methods for Manning calculation

As discussed in the two previous sections, the prediction of Manning's coefficient as a function of the discharge can be achieved using three relationships (i.e. one long-term and 2 short-term approaches) yielding different relationships. A comparison of these methods is carried out for the periods of the 4 measurement campaigns and the results are plotted in Fig. 6.28. Next to the measured data set during each measurement campaign (points with associated error band, cf. Fig. 6.26), three relationships are depicted. First, a simple best fit curve to the measurements is plotted (solid curve). Secondly, the relationship yielding the best agreement between modelled and measured values for the discharge, water level and electrical conductivity is shown (dashed curve). Thirdly, the long-term general relationship between Manning's coefficient, discharge and biomass (Eq.(6.15)) is depicted (dash-dotted curve). All calculations are carried out for the period of the measurement campaigns and so for the range of discharges measured over these periods.
It is questioned if one method for setting up a n-Q relationship is more appropriate than another and if Eq.(6.15) is suitable for overall modelling with the Strive model.

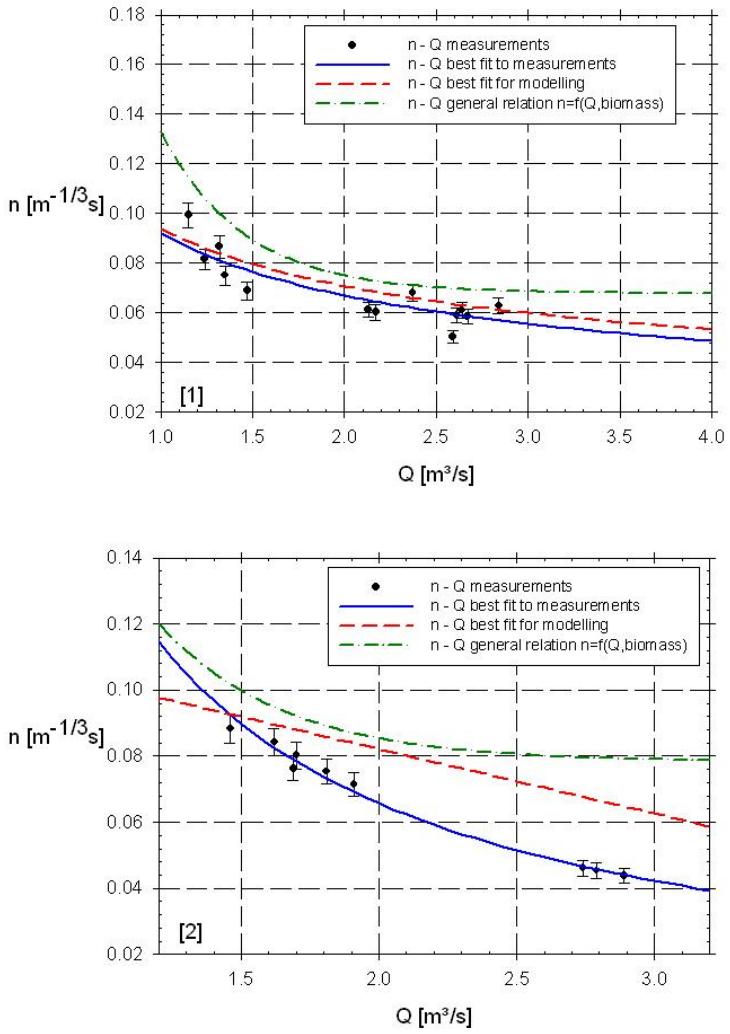

Figure 6.28: Relationships n-Q for the measurement campaigns of February 2006 (1, top) and April 2005 (2, bottom). The measurement values (points with associated error band) are plotted together with the best fit to these measurements (solid curve), the curve with the best results for the numerical model (dashed curve) and the result using the general relation between Manning's coefficient, biomass and discharge (dash-dotted curve).

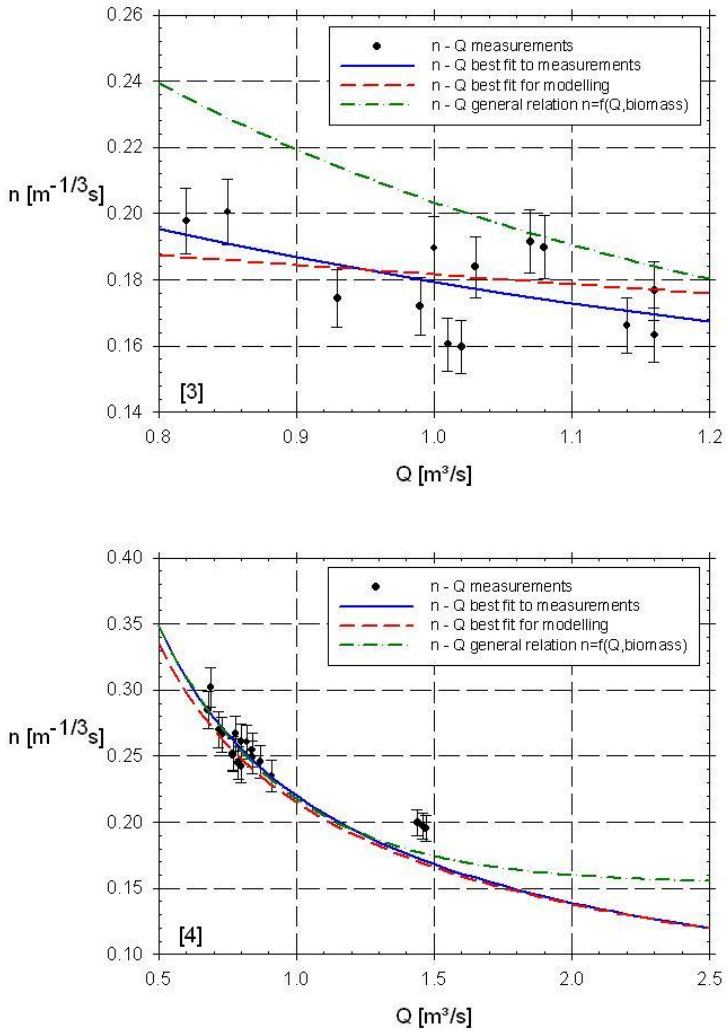

Figure 6.29: Relationships n-Q for the measurement campaigns of May 2006 (3, top) and August 2005 (4, bottom). The measurement values (points with associated error band) are plotted together with the best fit to these measurements (solid curve), the curve with the best results for the numerical model (dashed curve) and the result using the general relation between Manning's coefficient, biomass and discharge (dash-dotted curve).

Manning's coefficients for August (4, summer) are higher than for April and May (2, 3, spring) and February (1, winter). In general, the correspondance between the different ways of calculating the Manning coefficient as a function of discharge is large. Further conclusions over the quality of the mentioned n-Q relationships are related to the simulation results for discharge, water level and electrical conductivity of the numerical Strive model and can be found in the next paragraph. Certainly for the periods of February and August, the Manning coefficients predicted according to the different methods are almost equal. A larger spreading is observed for the results of April and May. The value of the discharge determines the range of Manning's coefficient for the different n-Q relationships.

6.4.4 Long-term simulations

The aim of numerical modelling is the study of different scenarios as the organisation of mowing actions in rivers, prediction of inundation risks, etc. Therefore, the integrated modelling package Strive is developed. For this objective, long-term simulations are useful. The Strive code is able to model longer time series and here, a simulation over a period of 1 year is performed to stress the value of the code.
In the reach of the river Aa, HIC provides discharges and upsream and downstream water levels. As is mentioned before (chapter 4, 6.1.2 and chapter 6, 2.6), discharges are not retained as boundary conditions. Weirs are important for the water level regulation in the study area. Therefore, the upstream water level is the upstream boundary condition and and the calibration formula of the weir is chosen as the downstream boundary condition (Eq.(D.2)). As the position of the weir is not registered, an average value of 30 °is chosen.
the channel has a length of 1450 m and a linear bottom slope (0.0002 m/m). The bottom width is 9.0 m and the channel banks have a slope of 45 °.
A simulation is performed for the data series of 2005 (365 days). The time step is 60 s and results are plotted each hour. Manning's coefficient is determined by discharge and amount of biomass in the reach by Eq.(6.15). The discharge is calculated in each time step and the biomass is given by Fig. 6.30, resulting from measurements and found in [52].

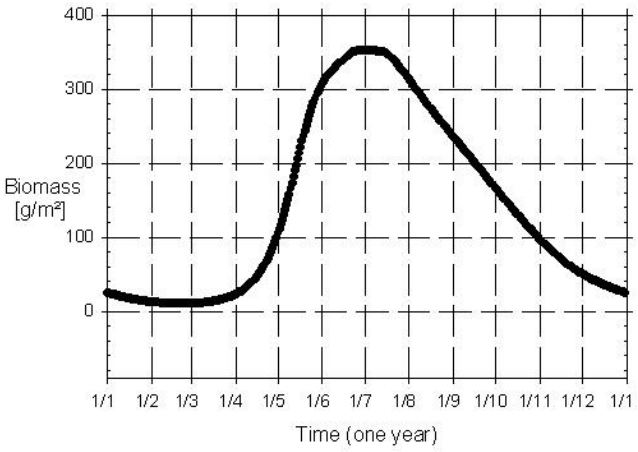

Figure 6.30: Variation of the amount of biomass over the year

Indicative results are plotted below. Comparison with measured data is not useful due to the lack of weir information. Fig. 6.31 presents discharge values, in the upstream as well as in the downstream section of the reach. The variation of the discharge over the reach is only small. Fig. 6.31 depicts values of the water level, in the upstream as well as in the downstream section of the reach. The series in the upstream section is the upstream boundary condition. The variation of the Manning coefficient over the year is shown. The biomass cycle and the variation of the discharge are clearly included in the result. These results confirm the good working of the Strive code, also for long-term objectives.

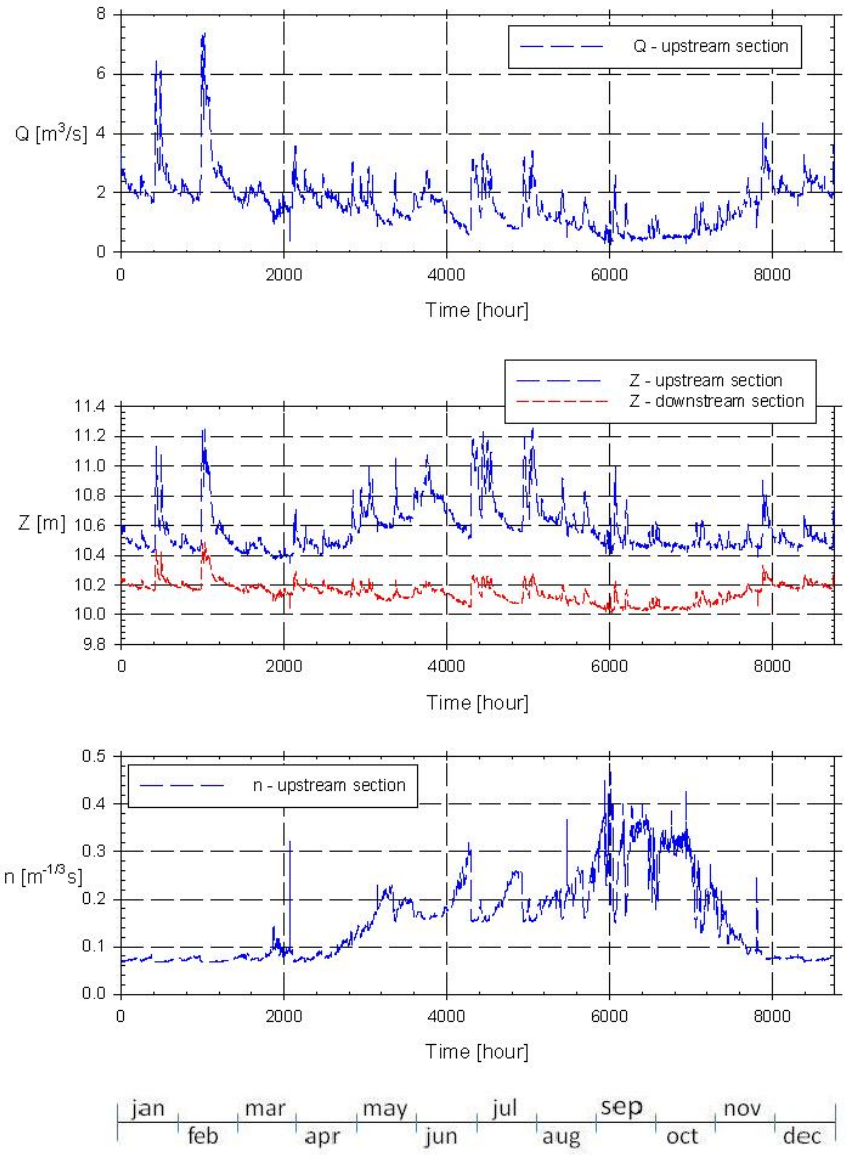

Figure 6.31: Simulation values of the discharge, the upstream and downstream water level and the variation of Manning's coefficient over the year

7 Conclusions

Part of chapter 6 reports basic aspects of integrated modelling. Data analysis showed the large influence of in-stream vegetation (biomass) on the roughness parameter in the Saint-Venant equations. The Strive model was developed to incorporate the surface water model into an environmental environment. Data collection was carried out in the river Aa over three years. This extended data set, based on hydraulic as well as biological and chemical parameters, allows calibration of the Strive model, which results in a well tested code with accurate and reliable results.

The model is tested in steady state as well as in unsteady state conditions and is compared to analytical solutions as well as to other numerical (Hec-Ras) solutions. A sensitivity analysis is carried out to get familiar with the interaction of biomass and the hydraulic parameters. Study of the possible boundary conditions confirms that the discharge as upstream boundary and the calibration formula of the weir as downstream boundary condition results into the most accurate values. The interaction between discharge, water level and electrical conductivity is shown. Based on the hydrodynamic aspect of the study, first aim is to model discharges and water levels in an accurate way. Therefore, not only the best fit between measured and modelled results is considered, but also specific attention is paid to model peak as well as base flow. Modelling of the electrical conductivity is important for calculation of retention and residence time. The Strive model returns accurate results of the different variables, including the large impact of the presence of biomass.

Over the year, the amount of vegetation is linked to the seasonal cycle. The combination of a wealthy vegetation growth and summer storms can cause flood problems. A well-considered integrated river management needs to balance the requirements from the ecosystem with regard to water quality and the need for a safe flood protection policy. For a reach of the river Aa, the correlation between discharge, biomass in the river and the resistance coefficient is demonstrated based on field measurements and hydraulic modelling. Calculation results show the influence of the resistance on both flow and water levels. Taking into account the environmental conditions (living area, agricultural land, etc.), peak values of the discharge have to be reduced e.g. for safety reasons. Therefore, a sound vegetation control policy can contribute to control flood water levels, at the same time guaranteeing the quality of the ecosystem.

Measurements as well as modelling showed that the Manning coefficient depends on discharge and biomass and is the most important parameter for the model. The Manning coefficient is calculated according 2 methods. Firstly, the measured cross-sections are used with the measured discharges and the Bresse equation in the Hec-Ras model. Secondly, the Strive model calculated the Manning coefficient using a simplified geometry. The last Manning coefficient is the parameter used for further analysis. 3 relationships between Manning and discharge are set up, 2 short-term and 1 long-term relationship. The long-term relationship, including biomass, for Manning coefficient and discharge causes deviations on modelling discharge, water level and electrical conductivity. Therefore, for each measurement campaign, short-term relationships between discharge and Manning coefficient are set up, based on the idea that the biomass is kept constant over that small period. A long-term relationship allows continuous modelling but includes sometimes large spreading on the results inherent to natural processes. Short-term relationships are very accurate but labour intensive. The first short-term relationship is expressed in the best fit between numerical and measured values, where the second short-term relationship is based on a simple best fit through the measured values. Afterwards, comparison of all 3 formulations of the Manning coefficient is made. It seemed that deviations on water level and electrical conductivity are small, while differences on peak discharges will reach up to 20 %. The accuracy, using the different relationships, depends on the spreading, which is inherent in natural processes, of the measured value compared to the relationship. A calibration and validation analysis based on a cost function delivers an objective criterion for studying model results. Literature review and analysis [33] showed that more than 90 % of the calibration in ecosystem modelling is based on trying to find the best fit between computed and observed data by adjusting model parameters, without analysis of measurements or use of optimisation techniques. The Strive model and the above analysis allow a well-founded study of hydraulic and ecological processes.

References

[1] L. De Doncker, P. Troch, R. Verhoeven, K. Bal, and P. Meire. *Influence of aquatic plants on the flow resistance and the hydraulic capacity of vegetated rivers*. In River Flow '06, number ISBN 0-415-40815-6, pages 593–602, Portugal, Lisboa, September 2006.

[2] L. De Doncker, P. Troch, R. Verhoeven, N. Desmet, and P. Meire. *Influence of vegetation on the propagation of flood waves*. In M. Rahman and C. Brebbia, editors, Applied Fluid Mechanics, number 512 in WIT Transactions on Engineering Sciences , 59, pages 331–340, 2008.

[3] K. Soetaert, V. de Clippele, and P. Herman. *Femme: a flexible environment for mathematically modelling the environment*. NIOO: Netherlands Institute of Ecology, 2006.

[4] K. Mahmood and V. Yevjevich, editors. *Unsteady flow in open channels*, volume 1. Water Resources Publications, 1975.

[5] J.A. Cunge, F.M. Holly, and A. Verwey. *Practical aspects of computational river hydraulics*. Pitman Advanced Publishing Program, 1980.

[6] P. Bates. *Applications in environmental hydraulics*. Wiley, 2005.

[7] L. Van Poucke. *Ijking van de stuw op de Aa te Poederlee*. Technical report, Ghent University, Hydraulics Laoratory, 1995.

[8] Hydrologic Engineering Center, US Army Corps of Engineers. *HEC-RAS River Analysis System, Version 2.1.4*, 2004. `http:\\www.hec.usace.army.mil`.

[9] L. De Doncker, P. Troch, and R. Verhoeven. *Influence of aquatic weed growth on the flow resistance of the river Aa*. In 6th FirW PhD Symposium, Belgium, 2005. Ghent University.

[10] X. Ying and S. Wang. *Improved implementation of teh HLL approximate Riemann solver for one-dimensional open channel flows*. Journal of Hydraulic Research, 46(1):21–34, 2008.

[11] A. Bermudez and M.E. Vazquez. *Upwind methods for hyperbolic conservation laws with source terms*. Computers and Fluids, 23(8):1049–1071, 1994.

[12] B. Anderson, I. Rutherford, and A. Western. *An analysis of the influence of riparian vegetation on the propagation of flood waves*. Environmental Modelling and Software, (21):1290–1296, 2006.

[13] L. De Doncker, P. Troch, R. Verhoeven, K. Bal, and P. Meire. *Determination of the Manning roughness coefficient influenced by vegetation in the river Aa and Biebrza river*. In review, 2008.

[14] V. T. Chow. *Open Channel Hydraulics*. McGrawHill, New-York, 1959.

[15] R. Verhoeven. *Waterbeheer en waterbeheersing. Course for civil engineers. Part C: 'Afvoer en berging van water'.* 2006.

[16] W.L. Cowan. *Estimating hydraulic roughness coefficients*. Agricultural Engineering, 37(7):473–475, 1956.

[17] D. Jinkang, X. Shunping, X. Youpeng, X. Chong-yu, and P. Singh Vijay. *Development and testing of a simple physically-based distributed rainfall-runoff model for storm runoff simulation in humid forested basins*. Journal of Hydrology, 336(3-4):334–346, 2007.

[18] V. T. Chow, D. R. Maidment, and L. W. Mays. *Applied Hydrology*. McGrawHill, New-York, 1988.

[19] J.C. Green. *Effect of macrophyte spatial variability on channel resistance*. Advances in Water Resources, (65):232–243, 2005.

[20] F. Pappenberger, K. Beven, H. Morrit, and S. Blazkova. *Uncertainty in the calibration of effective roughness parameters in Hec-Ras using inundation and downstream level observations*. Journal of Hydrology, 302(1-4):46–69, 2005.

[21] L. De Doncker, P. Troch, R. Verhoeven, K. Buis, and P. Meire. *Coupled ecosystem-hydrodynamic modelling using Femme*. 2008. In review.

[22] K. Buis. *Strive: Modelling riverecosystems - Manual*. Technical report, University of Antwerp, 2009.

[23] K. Buis. *Strive: Modelling riverecosystems*. 2009. In preparation.

[24] K. Buis, C. Anibas, K. Bal, R. Banasiak, L. De Doncker, N. Desmet, M. Gerard, S. Van Belleghem, O. Batelaan, P. Troch, R. Verhoeven, and P. Meire. *Fundamentele studie van uitwisselingsprocessen in rivierecosystemen - gentegreerde modelontwikkeling*. Water, 2007.

[25] L. De Doncker, P. Troch, R. Verhoeven, N. Desmet, and P. Meire. *Relation between resistance characteristics due to aquatic weed growth and the hydraulic capacity of the river Aa*. River Research and Application, 2008. DOI: 10.1002/rra.1240.

[26] E.S.J. Dollar. *Fluvial geomorphology*. Progress in Physical Geography, 28(3):405–450, 2004.

[27] G. Steinebach, S. Rademacher, P. Rentrop, and M. Schulz. *Mechanisms of coupling in river flow simulation systems*. Journal of Computational and Applied Mathematics, 168:459–470, 2004.

[28] Y. Lian, I. Chi Chan, J. Singh, M. Demissie, V. Knapp, and H. Xie. *Coupling of hydrologic and hydraulic models for the Illinois River Basin*. Journal of Hydrology, 344:210–222, 2007.

[29] D. Yuan, B. Lin, and R. Falconer. *A modelling study of residence time in a macro-tidal estuary*. Estuarine, Coastal and Shelf Science, 71(3):401–411, 2007.

[30] K. Ebrahimi, R. Falconer, and B. Lin. *Flow and solute fluxes in integrated wetland and coastal systems*. Environmental Modelling and Software, 22(9):1337–1348, 2007.

[31] B. Bockelmann, E. Fenrich, B. Lin, and R. Falconer. *Development of an ecohydraulics model for stream and river restoration*. Ecological Engineering, 22(4-5):227–235, 2004.

[32] P.A. Whigham and W.J. Young. *Modelling river and floodplain interactions for ecological response*. Mathematical and Computer Modelling, 33:635–647, 2001.

[33] G. Arhonditsis. *Evaluation of the current state of mechanistic aquatic biogeochemical modeling*. Marine Ecology Progress Series, 271:13–26, 2004.

[34] S.E. Jorgensen. *Integration of ecosystem theories: a pattern*. Kluwer, Dordrecht, 1997.

[35] Q. Duan, V.K. Gupta, and S. Sorooshian. *Effective and efficient global optimization for conceptual rainfall-runoff models*. Water Resources Research, 28:1015–1031, 1992.

[36] J.A. Vrugt, H.V. Gupta, W. Bouten, and S. Sorooshian. *A shuffled complex evolution metropolis algorithm for optimization and uncertainty assessment of hydrologic model parameters*. Water Resources Research, 39(8):1201, 2003.

[37] M. Kawamiya. *Numerical model approaches to address recent problems on pelagic ecosystems*. Journal of Oceanography, 58:365–378, 2002.

[38] R.J. Matear. *Parameter optimization and analysis of ecosystem models using simulated annealing: a case study at station P*. Journal of Marine Research, 53:571–607, 1995.

[39] G.J. Hurtt and R.A. Armstrong. *A pelagic ecosystem model calibrated with BATS and OWSI data*. Deep-Sea Research I, 46:27–61, 1999.

[40] J.J. Vallino. *Improving marine ecosystem models: use of data assimilation and mesocosm experiments*. Journal of Marine Research, 58(117-164), 2000.

[41] K. Soetaert, V. de Clippele, and P. Herman. *Femme, a flexible environment for mathematically modelling the environment*. Ecological Modelling, (151):177–193, 2002.

[42] K.J. Beven. *Rainfall-runoff modelling. The primer*. 2001.

[43] J. Kruger. *Simulated annealing: a tool for data assimilation into an almost steady model state*. Journal of Physical Oceanography, 23:679–693, 1993.

[44] G.C. Hurtt and R.A. Armstrong. *A pelagic ecosystem model calibrated with BATS data*. Deep-sea Research II, 43(2-3):653–683, 1996.

[45] D.E. Goldberg. *Genetic algorithms in search, optimization and machine learning*. Addison-Wesley Publishing Company, 1989.

[46] W.L. Price. *A controlled random search procedure for global optimisation*. The Computer Journal, 20:367–370, 1979.

[47] W.L. Price. *Global optimization by controlled random search*. Journal of Optimization Theory and Applications, 40(3):333–347, 1983.

[48] P.J.S. Franks. *Coupled physical-biological models in oceanography*. Reviews of Geophysics, 33(S1):1177–1188, 1995.

[49] M.J.R. Fasham, G.T. evans, D.A. Kiefer, M. Creasey, and H. Leach. *The use of optimization techniques to model marine ecosystem dynamics at the JGOFS station*. Philosophical Transactions: Biological Sciences, 348(1324):203–209, 1995.

[50] F.J. Los, M.T. Villars, and M.W.M. van der Tol. *A 3-dimensional primary production model (BLOOM/GEM) and its applications to the southern North Sea (coupled physical -chemical-ecological model)*. Journal of Marine Systems, 74(1-2):259–294, 2008.

[51] N. Desmet, S. Van Belleghem, P. Seuntjens, T. Bouma, K. Buis, and P. Meire. *Quantification of the impact of macrophytes on oxygen dynamics and nitrogen retention in a vegetated lowland river*. Physics and Chemistry of the Earth, 2008.

[52] N. Desmet, S. Van Belleghem, P. Seuntjens, and P. Meire. *Water quality modelling in vegetated rivers*. In Man and River Systems - Interactions among rivers, their watersheds, and the sociosystem, Paris, 2006. The 2nd international symposium on Man and River Systems.

7

Integrated modelling using Strive

In the previous chapters, the Strive model has been developed in the Femme environment. An extended dataset for calibration of the model has been collected and validation of the model has been performed. The first calculations have shown the accuracy of the Strive model. In this chapter, aspects of integrated modelling using Strive are studied in more detail. Results of the Strive model are compared to experimental data, attention is paid to the choice and use of the boundary conditions in the numerical model and tributaries and inundation areas are modelled. The propagation of waves and the combined influence of discharge and biomass is already illustrated in Chapter 6. Further, aspects of water quantity (discharge and water level) and aspects of water quality (electrical conductivity, chloride) are investigated. Finally, an introduction to reactive processes (nitrate, oxygen, etc.) is incorporated in the model.

1 Tributaries: lateral in- or outflow

it is necessary to add the possibility of lateral in- or outflow in the model. For example, in the studied reach of the river Aa, there are a few small tributaries. Some of them are only dry canals, not carrying water most of the time. One of them however, is a small creek and adds, just downstream of the upstream weir, a certain amount of water to the main river.
Two possibilities are incorporated: first, the case of lateral outflow at a certain location and second, distributed in- or outflow over a certain distance along the river (e.q. groundwater in- or ouflow). Further, this lateral connection introduces the aspect of water exchange between river and inundation areas.

A measured flood wave (period from the 12th to the 20th of August 2005) is chosen as boundary condition. The measured upstream discharge is the upstream boundary condition and the calibration formula of the weir is the downstream boundary condition. Similar results are seen with other types of boundary conditions (e.g. use of water level upstream etc., cf. infra). Further, the simplified geometry of the Aa is used for the modelling. A measured depth, which includes a varying bottom profile, and an averaged width (i.e. the same width for all the sections) is used. Fig. 7.1a and Fig. 7.1b show the discharge and water level at different sections along the river Aa. These figures have to be compared to both Fig. 7.2a and Fig. 7.2b. Fig. 7.1a shows the discharges over the reach at 7 sections (distributed over 1350 m). The reach is divided into 30 sections, numbered from upstream (1) to downstream (30). Time shift and peak flattening of the discharge is only small, while the water level decreases from upstream (section 1) to downstream (section 30) (Fig. 7.1b). In Fig. 7.2a, a lateral outflow at location x = 800 m (section 18) is implemented, consequently, also the water level is lower over the entire reach (Fig. 7.2b). Looking to the graphs of the discharges, it can be seen that extracting a discharge of 0.01 $m^3/s/m$ along one cell leads to a decrease in discharge of almost 0.5 m^3/s, which is as expected because cross sections are taken each 50 m (corresponds with the distance of a 'cell' or 'box' in the model). Comparing the water levels, it seems that due to the lateral extraction of water, a general decrease in water level can be remarked over the entire reach. When the volume of water decreases, the water level will also decrease.

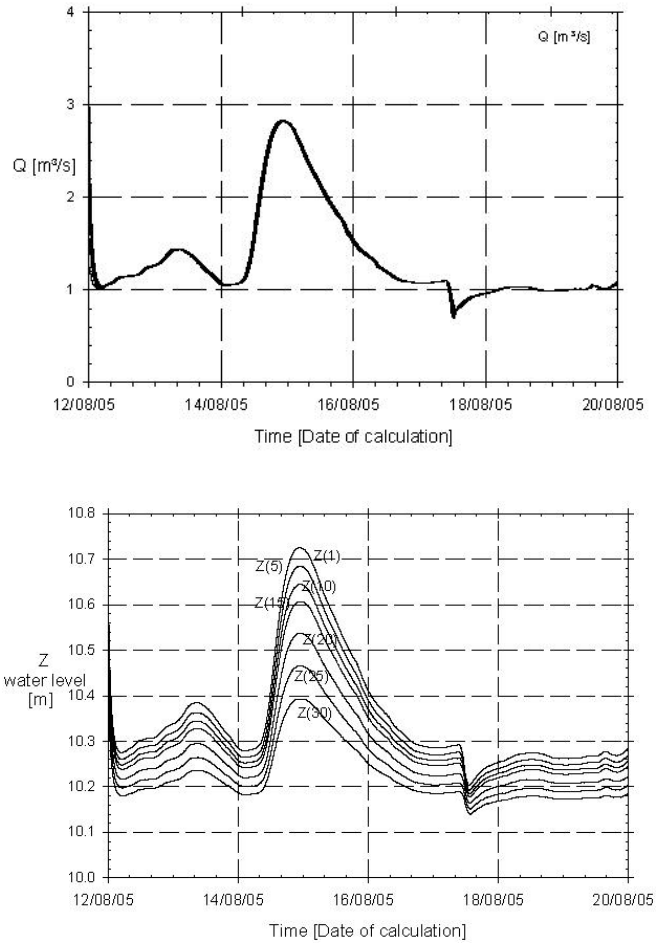

Figure 7.1: Calculation of discharge (a, top) and water level (b, bottom) at different sections of the river Aa. The discharge in 7 sections is hardly changing, while the water level decreases from upstream (1) to downstream (30).

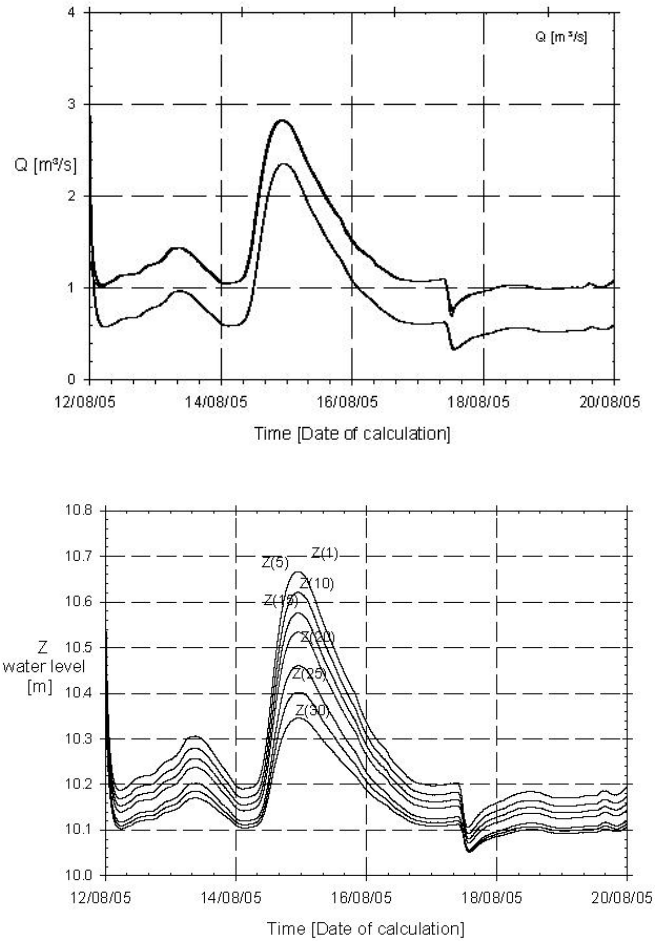

Figure 7.2: Calculation of discharge (a, top) and water level (b, bottom) at different sections of the river Aa, extracting a lateral inflow at a distance of 800 m (section 18). The discharge decreases in all sections downstream section 18, while the water level decreases over the entire reach.

2 Flood plains

As inundation areas are an important part in the study of the river hydraulics, a specific module for flooding is developed and calibrated in The Hydraulics Laboratory.

2.1 Inundations: theoretical view

2.1.1 Introduction

The river water is stored in the main channel as long as the water level does not exceed the river bank crest. During a flood, the water flows laterally over the banks into the floodplains. When the river is saturated the water is stored in the external floodplain. The storage in the floodplain causes flattening of the peak discharges in the wave. During periods of lower discharge, this volume of water slowly returns to the main channel, the water stored externally flows laterally from the floodplains to the main channel. The total volume of the water flow is consequently spreaded in time.
The described physical process is implemented in the numerical model. The water flow between a river and its floodplain ('storage cells') is modelled in different ways.

2.1.2 Water levels in the river channel and the storage basin

Depending on the water levels in the river basin (z_j) and the storage basin (z_b) and the height of the weir ((z_d), treshold value), water flows in the inundation area or in the river channel. Measuring or calculating the volume in the flooding area, allows to calculate the water height. Depending on the water levels, different situations are considered (Fig. 7.3).

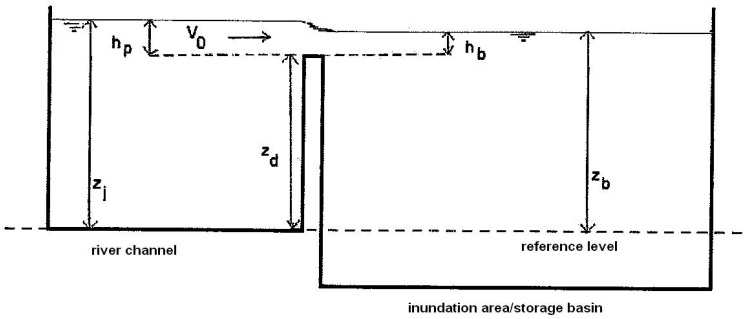

Figure 7.3: Definition sketch of the different water levels and water heights relative to the reference level, which is the bottom of the river channel at the downstream boundary

1. $z_j < z_d$ and $z_b < z_d$: the water level in the river channel is lower than the threshold value as well as the water level in the storage basin. No lateral flow occurs.

2. $z_b < z_d < z_j$: the water level in the river channel is higher than the threshold value, the water level in the storage basin is smaller. Water flows from the river to the basin and free overflow occurs, the water level in the flooding zone does not influence the discharge.

3. $z_d < z_b < z_j$: both water levels, in the river channel and in the storage basin, are higher than the threshold value. The water level of the river channel is higher than the water level in the flooding zone and submerged flow occurs from the river to the flooding zone.

4. $z_d < z_j < z_b$: both water levels, in the river channel and in the storage basin, are higher than the threshold value. The water level of the river channel is lower than the water level in the flooding zone and submerged flow occurs, from the flooding area back to the river channel.

5. $z_j < z_d < z_b$: the water level in the river channel is lower then the threshold value and both levels are lower than the water level in the storage basin. Free flow occurs from the storage basin to the river channel.

2.2 Solution methods for the numerical model

2.2.1 Internal storage: use of weirs (Method 1)

The water flow between main channel and storage cells is modelled by weirs [1, 2]. A calibration of all the banks along a river (all the 'weirs' from

the river to its storage cells and between those cells) is an intensive task and therefore a disadvantage of the method. Besides, these banks change all the time due to the processes of erosion and sedimentation and plant growth. However, this method gives very satisfying results compared to experimental data. By using this technique, one can simulate floods within all kinds of configurations, including these with multiple storage cells connected to each other. The one dimensional model is extended to a quasi two-dimensional model, by studying the interaction between the main channel and the floodplain. Storage cells reflect the retention and storage capacity of the floodplains. The storage cells, as an internal boundary condition, are implemented in the Saint-Venant equations [3].

The influence of the cells is directly implemented in the coefficients of the set of linear difference equations. The model uses a 1D representation of the river's main channel but storage cells are connected to the main channel. In general, a floodplain is modelled as a bypass channel if the water flow is dominant to the water storage. Then, the flow in the floodplain contributes substantially to the flow in the main channel. A floodplain is modelled as a storage cell if the water storage is dominant to the water flow. Storage cells are connected with each other so water can flow from one cell to another, depending from the relative water level in the cell and the relative elevation of the cells. One assumes that there is no water flow inside a cell [2, 4, 5]. An important point to obtain a realistic flood routing with the Strive model, and therefore a good prediction of the residence time of the water in the river system, an appropriate method has to be implemented to slow down the flow between the storage cells eg. by adapted roughness coefficients of the storage zones (section 4.4.2.2).

This method supposes a weir between river channel and floodplain. The discharge is determined by the calibration relation of the weir and the upstream water level. For each of the 5 situations corresponding the different water levels, the coefficients in the Double Sweep algorithm to solve the Saint-Venant equations are changed according the equations mentioned into detail in Appendix E.

2.2.2 Internal storage: relation discharge and flooding area (Method 2)

The second method [2, 3, 6] focuses on the relation between the change of the surface of the flooding area and the water height in the flooding area (and the water height over the weir) which both determine the discharge flowing out of the river (in the flooding area). Flow out or in the storage basin is based on the differences in water levels between river and storage

area. This method has the big disadvantage that the water level in the storage basin needs to be equal to the water level in the river channel for calculation. This is the case when the simulation starts with a 'filled' storage basin. So, one cannot simulate a situation with free overflow from the river into an empty storage cell.

The Saint-Venant equations describe non permanent flow in open channels and are not able to describe local discontinuities, as storage areas are internal boundary conditions, in rivers. Therefore, the coefficients used in the Double Sweep algorithm (Chapter 3) are adapted to obtain compatibility. The method is explained in detail in Appendix E.

2.2.3 External storage

Using techniques based on 'external storage', the discharge is determined by using weir equations [7, 8]. The inundation area is a place of storage and connected to the river by a weir. The discharged flow mass over this weir is calculated using the weir equation, based on the upstream water level and the geometric parameters of the weir. The downstream water level is also important in case of submerged overflow. This method calculates the discharge over the weir separately. In the numerical model, the module containing this overflow discharge is connected to other modules and calculations. Advantage of this method is the clarity of discharge values and therefore, the dimensions of flooding surfaces. Further, the module for tributary and groundwater in- or outflow is fully developed and is suitable for this type of lateral in- or outflow. Contrary, the advantages of the Saint-Venant equations and its storage possibilities are not incorporated.
This module is developed theoretically, but is not implemented yet in the Strive model for the river Aa. This implementation should only be illustrative, flooding is not yet a topic at the river Aa.

2.3 Experimental setup

Numerical calculations are carried out and validated based on measurements in an experimental setup. Fig. 7.4 shows a definition sketch and an overview photo of the flume in the lab. The model flume includes a rectangular channel, width 40 cm, height 43 cm and length 12.41 m. An upstream weir and downstream gate are added to the channel. Discharges up to 32 l/s are studied. The upstream weir allows an accurate determination of the discharge, the downstream gate allows regulation of the water level in the flume. Aside the channel, one big inundation area is added. This flooding area can be divided into three parts and also three lateral weirs, width 30

cm, are included in the flume construction. Interconnection of the 3 flood plains is also possible.

Fig. 7.5 shows the simulation scheme. Dimensions are indicated in cm at the figure on the left.

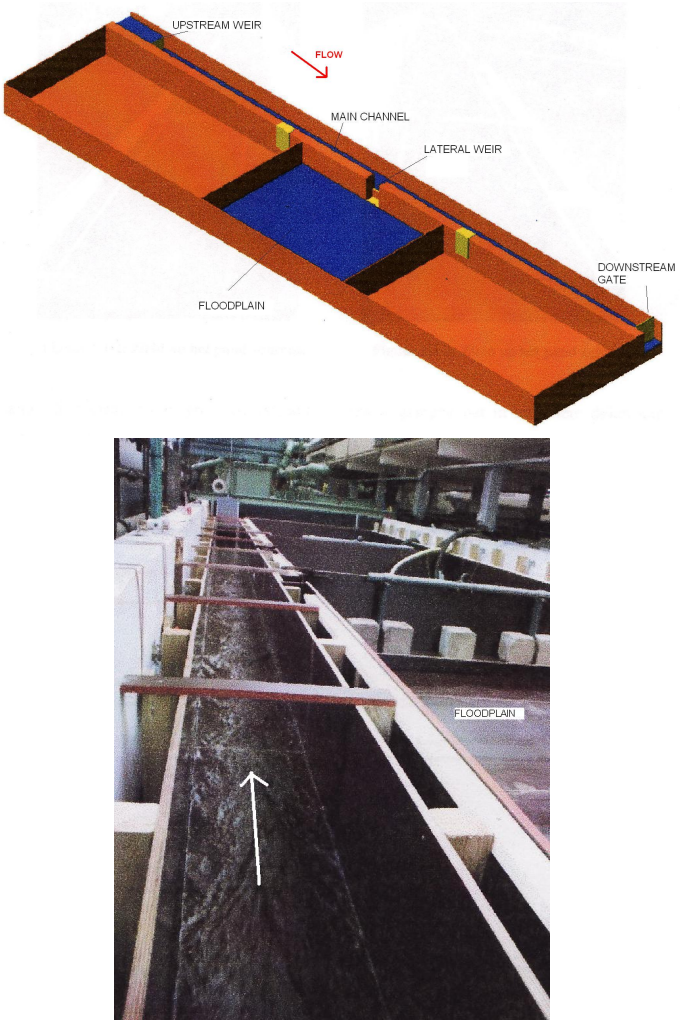

Figure 7.4: Laboratory test flume: definition sketch (top) and overview photo (bottom)

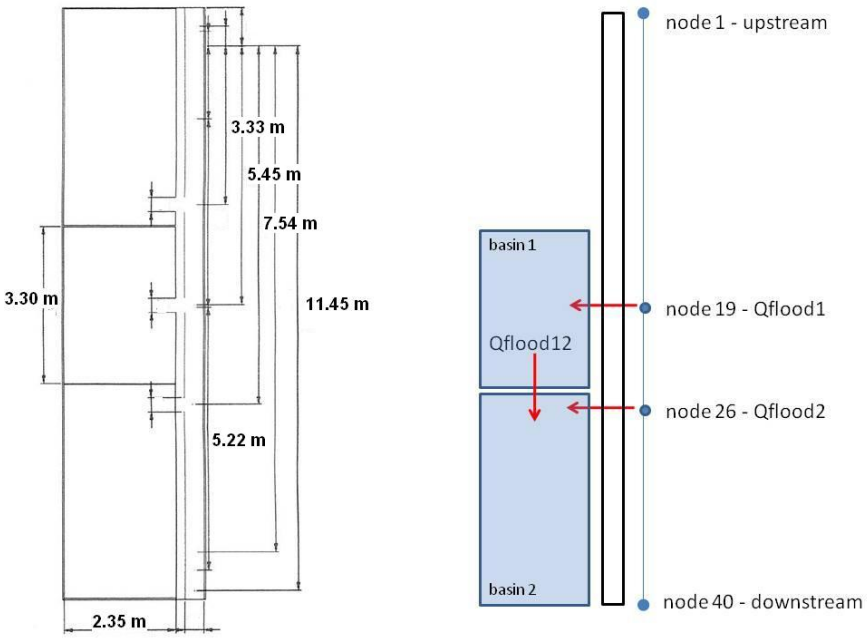

Figure 7.5: Laboratory test flume: dimensions and simulation scheme

2.4 Numerical results

2.4.1 Implementation of one storage basin

Two methods of internal storage are implemented in the Strive code. For the second method, only situations with higher water level than the treshold value are taken into account. The first method allows all possibilities of flow (from river channel to storage basin and vice versa) and is not limited to one flooding zone. Fig. 7.6 presents the flowchart for the implementation of a storage basin in the Strive code including the values coupled to the experimental setup. V_{0a} is the volume of the filled storage basin, V_{0b} is theoretically the same value. However, in the experiments is seen that the transition from one situation into another not always happens at a fixed parameter value. The volume V_{0b} is little higher than the volume V_{0a}. Theoretically, submerged flow starts from V_{0a}, practically, situation 2 occurs until V_{0b} is reached. The same situation is seen between situation 3 and 4, here, the transition parameters are numerically determined based on the measured values. Additional, it is checked that the water height corresponding with the final volume of the storage basin never exceeds the treshold value and that inundation occurs if the treshold value is reached.

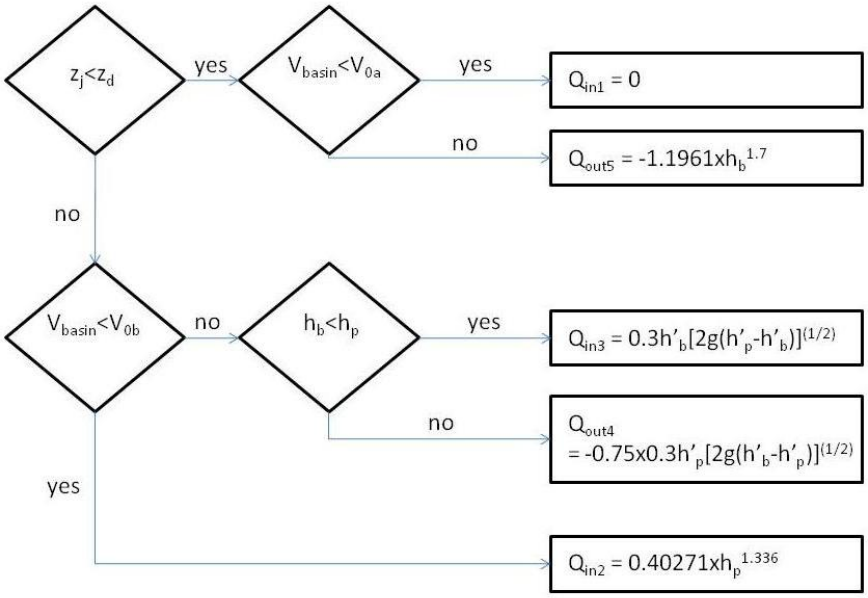

Figure 7.6: Flowchart for the implementation of a storage basin in the Strive code according the method with the weirs

In the previous chapters, considerations about the roughness of rivers are discussed. When studying floods, also the roughness of the inundation areas is important. During a flood, the characteristics of the cross section are completely different than during periods of normal discharge. During the greatest part of the year, the water flows only in the main channel. Plants can grow on the floodplains without any problems. This causes a roughness which is much higher in the floodplain then in the main channel. This different roughness can be incorporated in the model by using an average roughness or by using different roughness values. The first technique is based on the average discharge in the total section which is the same as the total discharge in the section with the different roughness. This method assumes a uniform velocity distribution. However, use of different roughness is a more realistic approach. Due to the larger amount of vegetation in the floodplains, there the average speed of the flow is smaller. The greatest part of the discharge flows through the main channel and just a small part of it flows through the floodplains [4, 5]. This approach is of large importance if stream flow in the flood plains is incorporated in the model.

In the experimental set-up in this research, several discharges are chosen and Manning's coefficient is determined under these steady state conditions and for different heights of the downstream gate. A Manning coefficient of 0.012 $m^{-1/3}s$ is calculated and retained for the modelling.

A wave is measured in the main channel of the experimental set-up. The calibration formulas of the weirs (upstream, downstream and sideward, [3]) determine the discharges in the flume and from the channel to the floodplains. First (Fig. 7.7a), there is no connection between channel and floodplain and the water flows in the channel. The upstream boundary condition is based on the measured discharge series (Qup - measured), while downstream an equation is set up linking the discharge to the opening height of the gate. The measured values are compared with the simulation results and it seems that the Strive model presents analoguous simulation results as the values obtained in the experimental set-up. Fig. 7.7 depicts the results. The simulated discharge downstream (Qdown - modelled) corresponds to the measured discharge (Qdown - measured). Due to friction, time shift and flattening of the discharge peak is remarked. Second, a connection between the channel and the floodplain is realised. The floodplain, that allows storage of the water, also causes peak flattening of the wave. Fig. 7.7b shows the result, the floodplain is empty at the beginning of the measurement and calculation. Measured and modelled values are in good agreement and the flooding discharge is determined as a function of time (Qflood). Deviations are due to measuring errors.

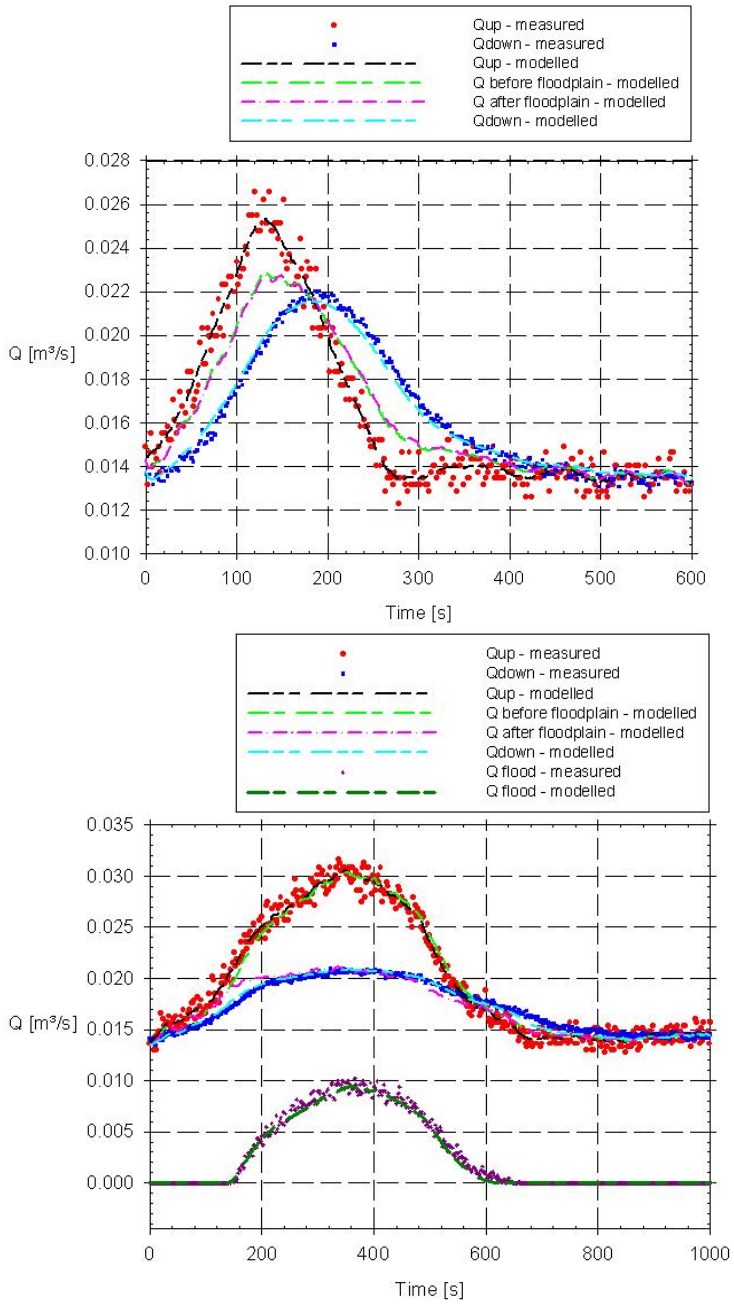

Figure 7.7: Wave in a river channel without (a, top) and with (b, bottom) floodplain

Fig. 7.8, 7.9, 7.10 and 7.11 present measured discharge and water level for a flood wave in the experimental set-up. Respectively method 1 and method 2 are used for calculation of the flooding discharge. The discharge is rather high and the opening height of the downstream gate is 2 cm. This height causes the largest deviations, due to the largest deviations on the calibration formula [3]. This deviation and the deviation on the inundation volume are responsible for small differences between measured and simulated values. The storage basin is filled at the beginning of the simulation. The timestep for calculation is 2 s, which allows registration of all discharge variations. The upstream boundary condition is the measured discharge series in the lab.
Using the first method, it is seen that the downstream simulated discharge corresponds well with the measured wave. The largest deviations are remarked at the descending part of the wave. The flooding starts when a part of the wave in the channel flows into the storage basin (positive in the flood graph). The discontinuity in the flood wave is due to the start of the submerged overflow, with a flooding discharge that equals Q_{in3} (Fig. 7.8). Transition from one situation into another, without mass loss and taking into account the physical conditions in the lab, will introduce discontinuities. The flow is not immediately submerged, the first part of the flow of the flood wave is described by Q_{in2}. Numerically, the scheme of Fig. 7.6 is incorporated and no difficulties occur in the transition from free overflow to submerged flow.
The transition from Q_{out4} to Q_{out5} in the descending part also shows a small discontinuity. This is caused by free flow which is obtained faster than the value of the weir height z_d will allow. The difference between measured and modelled values in the descending part of the wave is even more clear when considering the water levels (Fig. 7.9). The exact point of transition is subject of calibration.

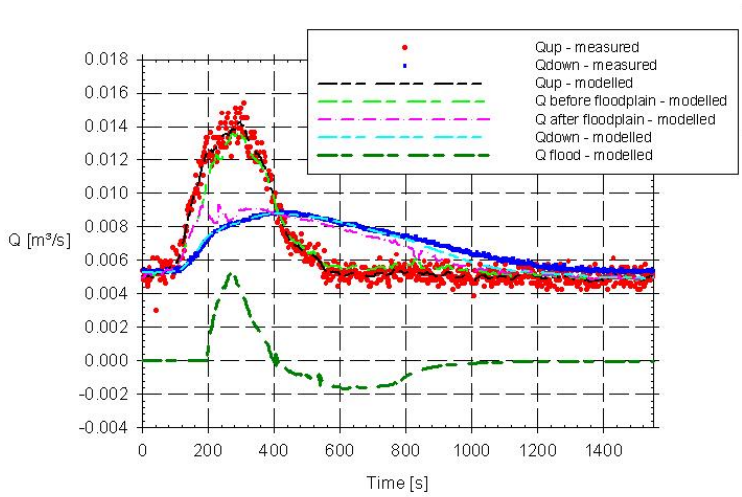

Figure 7.8: Comparison of a measured flood wave with a modelled flood wave (method 1), upstream and downstream values

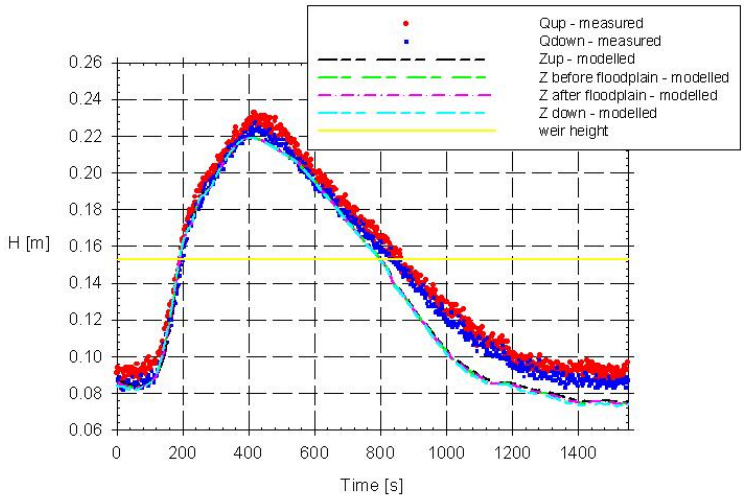

Figure 7.9: Comparison of measured and simulated water levels for the flood wave of Fig. 7.8 (method 1), upstream and downstream values

Fig. 7.10 and 7.11 show the results using the second method. The cel width (0.30 m), the timestep (2s) and the value of Manning's coefficient (0.012 $m^{-1/3}s$) for the numerical calculation do not change compared to previous simulations. The θ value in the Preissmann scheme equals 0.9 and the surface area of the storage basin is 7.77 m^2. At the beginning of the measurement and simulation, the storage area is filled. Consequently, the water level in the storage basin rises equally to the water level in the river channel. Considering the discharge behind the storage basin, oscillation is seen. At the end of the reach, the same oscillation (but weaker) is noticed. Probably, reason for that is the same as for the discontinuities occurring with method 1. The theoretical points of transition between the particular situations need adaptation to the effective moments of transition which results into accurate numerical and physical values. The discontinuity at the downstream end of the channel is due to analoguous reasons.
This second method cannot describe free flow from the storage basin to the river channel, this discharge is thus underestimated and the water volume retained in the storage basin is too large.

As a conclusion, this technique results into good results in case of submerged flow. During moments of transition and for free flow, deviations and oscillations occur. It seems that submerged flow does not immediately occur if the water level in the storage basin equals the water level in the channel. Situation 2 continues for a little moment and the water level is little heigher than the weir height when situation 3 starts. For each transition, the lab measurements and the numerical modelling results into little different values than the theoretical values, taking into account that the water height corresponding with the total volume of the storage basin never exceeds the weir level and that the inundation starts if the weir level is reached.

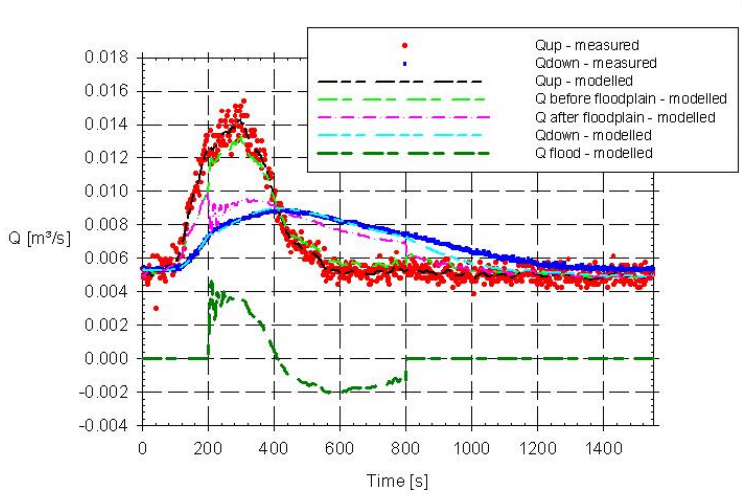

Figure 7.10: Comparison of a measured flood wave with a modelled flood wave (method 2), upstream and downstream values

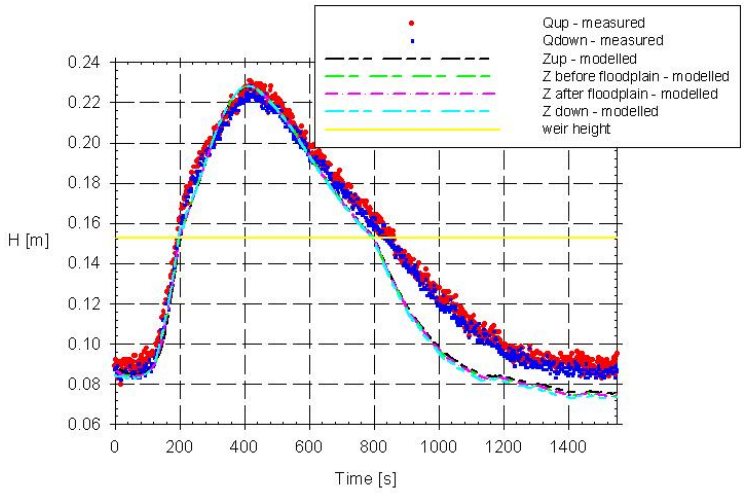

Figure 7.11: Comparison of measured and simulated water levels for the flood wave of Fig. 7.10 (method 2), upstream and downstream values

2.4.2 Implementation of two storage cells

In the previous, one storage cell connected with the river is implemented. In inundation areas, a river has often two banks which can flood. The height of the left and right river bank will differ and determines when the flood event occurs. The flooding can start at one bank, while the other bank does not flood yet. So, more than one storage cell has to be implemented and connected with one cell or node of the river. The modelling of two storage cells, one for each river bank, connected with one node is theoretically considered in [1, 3]. Both storage cells have an influence on the water stage in the river and therefore they influence each other. Eighteen different situations are considered in [1, 3]. The effect on the coefficients of the continuity equation is according the principles in the previous paragraph, results are gathered in [1–3], the momentum equation does not change.

The flooding area of the experimental setup is divided into three parts (Fig. 7.4). The study of two storage basins, separately and interconnected, is discussed in [3]. Two storage basins are connected in two different cells or nodes of the river. The calibration formula of the middle side weir, connecting the river channel and the storage basin, is set-up. The other side weirs, connecting the river channel with the first and third part of the storage basin are assumed to correspond with this calibration formula. For numerical simulation, the river channel is split up in 40 cells or nodes. A first storage basin is connected to node 19, node 26 is connected with a second part of the basin. The geometrical characteristics of the storage basin and its different parts are well known. Calculations for different cases are performed with the storage basins filled or empty and with one basin filled and the other basin empty at the beginning of the simulation. Results are mentioned below.

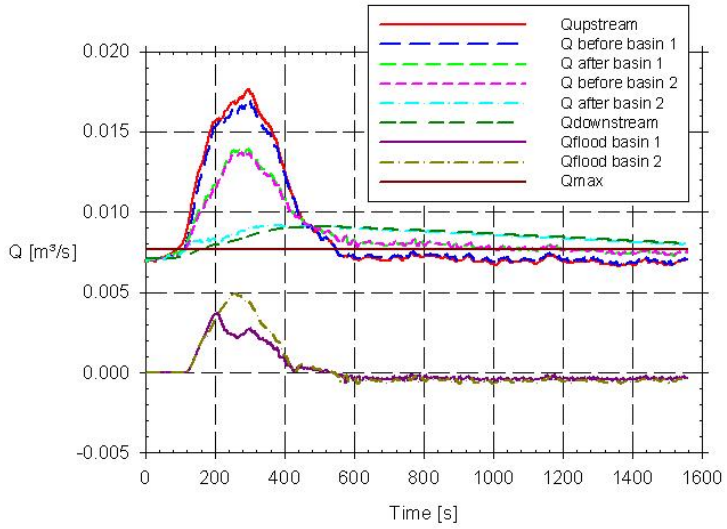

Figure 7.12: Simulation of a flood wave through a channel connected with two storage basins. The storage basins are filled at the beginning of the simulation, they are not mutually connected.

In Fig. 7.12, both storage basins are filled, the time step equals 2 s, θ is 0.7, the Manning coeficient is 0.012 $m^{-1/3}s$. Discontinuities in the flood curves are due to the transitions between two situations (cf. supra). A rather equal flow from the storage basins to the river channel is remarked, due to the high discharges. The discharge flowing in the river channel is close to the maximum allowed discharge in the channel. Therefore, the water level over the channel is high, even higher than the weir height. The volume of water in the storage basins only flows slow back to the channel, submerged flow occurs. The downstream discharge also stays higher than the upstream discharge after passing of the peak discharge.

To complete this study, the channel is linked with two storage basins, mutually connected by a weir and a flood wave is measured and simulated. Calibration formulas for the weir connecting the two basins are supposed to be equal to the formulas for flow from the basin to the river channel. Depending on the water levels in the two basins, 5 situations (section 5.1.2) are considered, similar to flow from river channel to storage basin and vice versa. Due to the presence of non-calibrated weirs, the results plotted below (Fig. 7.13) are only indicative, but representative for the inundation part in the Strive model.

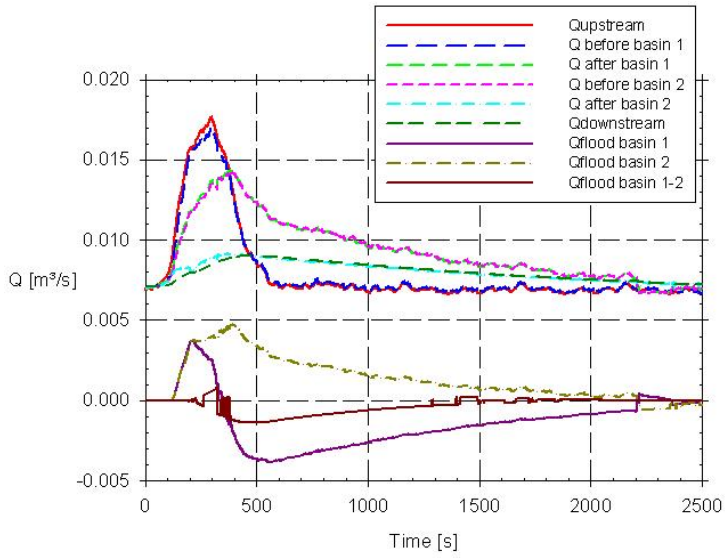

Figure 7.13: Simulation of a flood wave through a channel connected with two storage basins. The storage basins are filled at the beginning of the simulation, they are mutually connected.

For Fig. 7.13, the parameters are equal to the parameters in the previous situation (time step equals 2 s, θ is 0.7, the Manning coeficient is 0.012 $m^{-1/3}s$). The wave is spreaded over a longer time period. The downstream discharge is only slowly reaching the original value. This is due to the large temporal storage in the two basins. It is also seen that water which is flowing in the downstream basin is returning to the upstream basin. This way of emptying, when the peak of the wave is passed, is faster than water which is flowing back to the river channel. Consequently, the downstream basin will not empty in the channel but in the upstream basin. Further, the water levels downstream the upstream basin remain too high. The water level in the upstream basin is decreasing, which allows the emptying of the downstream basin. So, the water leaves the downstream storage area through the upstream basin. This is seen in the discharge curve between the two basins which turns out to be negative. At the end of the simulation, the rest of the stored water in the downstream basin is leaving the basin into the channel. The described situation is due to the relation between the storage basins and the calibration formulas. In reality, the upstream basin will have a higher bottom level and the flow will not return.

3 Coupled modelling results

3.1 Introduction

River variables as discharge, water level and electrical conductivity (EC) are related. In the river Aa, upstream and downstream water levels are measured continuously. Discharges as well as the EC-value are measured during measurement campaigns. EC is a measure for the amount of total dissolved solids (TDS) which is an indication for the water quality, TDS is an aggregate indicator of presence of a broad array of chemical contaminants. Comparing peak values of the electrical conductivity upstream and downstream allows to estimate the travelling time of the tracer. Together with values of the water volume in the reach, the discharge can be calculated. As sometimes discharge determination in rivers is difficult, measurement of EC and water level Z allows use of these variables as boundary conditions.
Different datasets are selected for model calibration. Boundary conditions are the upstream water level and the downstream discharge-water level relation. Discharges, which are more sensitive to variations, cannot be used for calibration due to the limited amount of data available.

The simulation is rather complicated due to the uncertainty on a lot of parameters: the position of the downstream weir is not registered en therefore not known, the bottom depth, bottom width and wetted cross section in the reach are not known exactly, calculated Manning coefficients are approximative, etc. All parameters have to be determined to achieve an accurate solution. An important parameter is Manning's coefficient, based on biomass and discharges, which has consequences for the modelling of base and peak discharges. Manning's coefficient is calibrated based on the data set of measurements [9].

3.2 Water quality linked to electrical conductivity

3.2.1 Results of measurement campaigns

February 2006 Modelling of discharge, water level and electrical conductivity for the period from February, 6th to February, 13th is carried out using the Strive model. Manning's coefficient is the most important calibration parameter and is predicted in Strive according to the three different methods (cf. supra). The additional inflow from the Slootbeek turned out to be negligible and this inflow discharge is set to 0. The flap-position of the downstream weir changes in time and the angle varies. This change in position is seen on Fig. 7.14b, 7.15b and 7.16b where a sudden fall or rise of

the water level is plotted. The flap position of the downstream weir varies from 31.8°to 28.9°over 27.2°and 30.9°.
Fig. 7.14, 7.15 and 7.16 show the time evolution of the measured and modelled discharge, water level and EC-values in the river Aa. In Fig. 7.14, the numerical result from the run yielding the best agreement with the measured discharges is plotted. The exponential relation (Table 6.4, column 3) results in good agreement for modelling the peak value of the floodwave. Measured discharges upstream as well as downstream are close to the modelled values (Fig. 7.14a). In Fig. 7.14b, the upstream water level (boundary condition), and the downstream water level are plotted. The peak value as well as the base flow are simulated very well. The changes in the first and the last part of the values are due to changes in the position of the downstream weir. It can be seen that results are very sensitive to this weir position. Fig. 7.14c shows modelled and measured conductivity values which are in accordance. Comparing peak values upstream and downstream allows to estimate the travelling time of the tracer. Using water volume values in the reach, the discharge can be calculated. Thus, the EC value is also useful in situations where no discharge measurement is possible.

Fig. 7.15 shows the results for discharge, water level and electrical conductivity using the relation based on the best fit to the measurement values (Table 6.4, column 2). For the discharge, values of the base flow are equal to the values in Fig. 7.14, while the peak is simulated less accurate: the peak values are slightly higher. The modelled water level shows good agreement with the measured values as is also the case for the electrical concuctivity where results are equal to those in Fig. 7.14. Differences between modelled and measured values occur for the last part of the time period.

Results using Eq.(6.15) are depicted in Fig. 7.16. The differences between the measured and modelled discharge values are large, as is also the case for the water level. For the electrical conductivity, the (important) peak values are modelled well, but differences are seen during base flow. Modelled discharges as well as water levels are too low compared to the measured values. This is due to an overestimation of Manning's coefficient based on Eq.(6.15) when compared to the measured values (cf. infra).

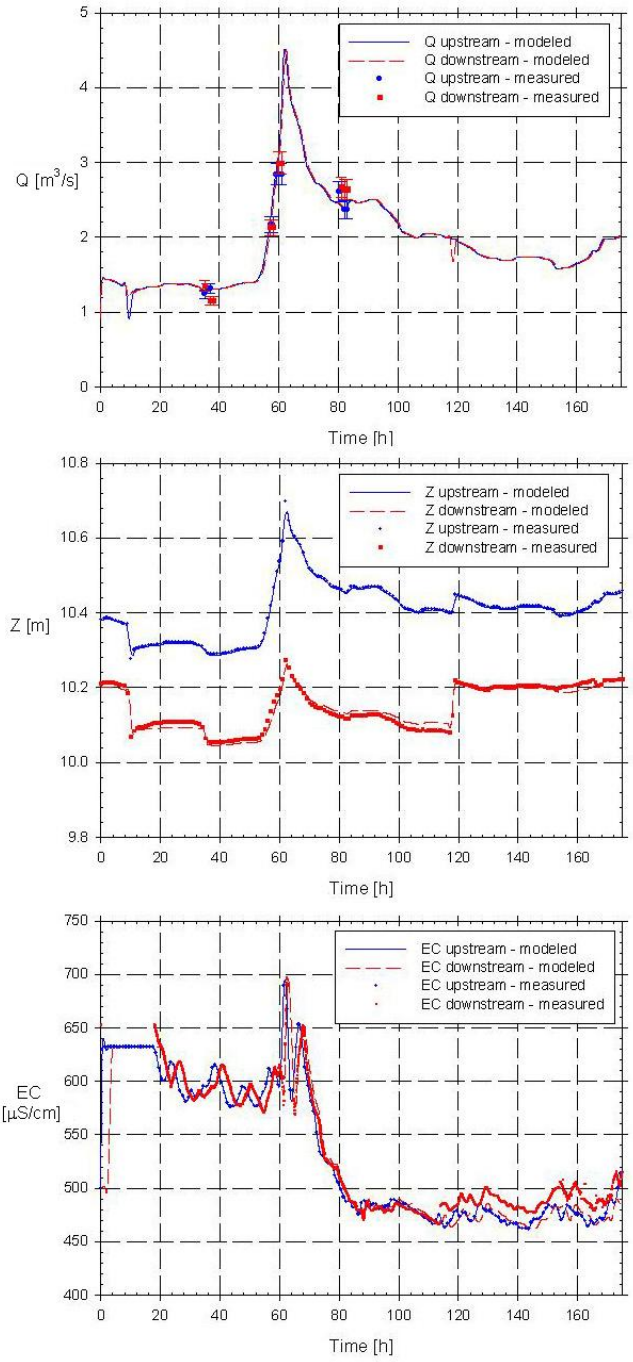

Figure 7.14: Modelled and measured values of discharge, water level and electrical conductivity from February 6th, to February 13th, upstream and downstream of the studied reach in the river Aa according to the best fit for the numerical model

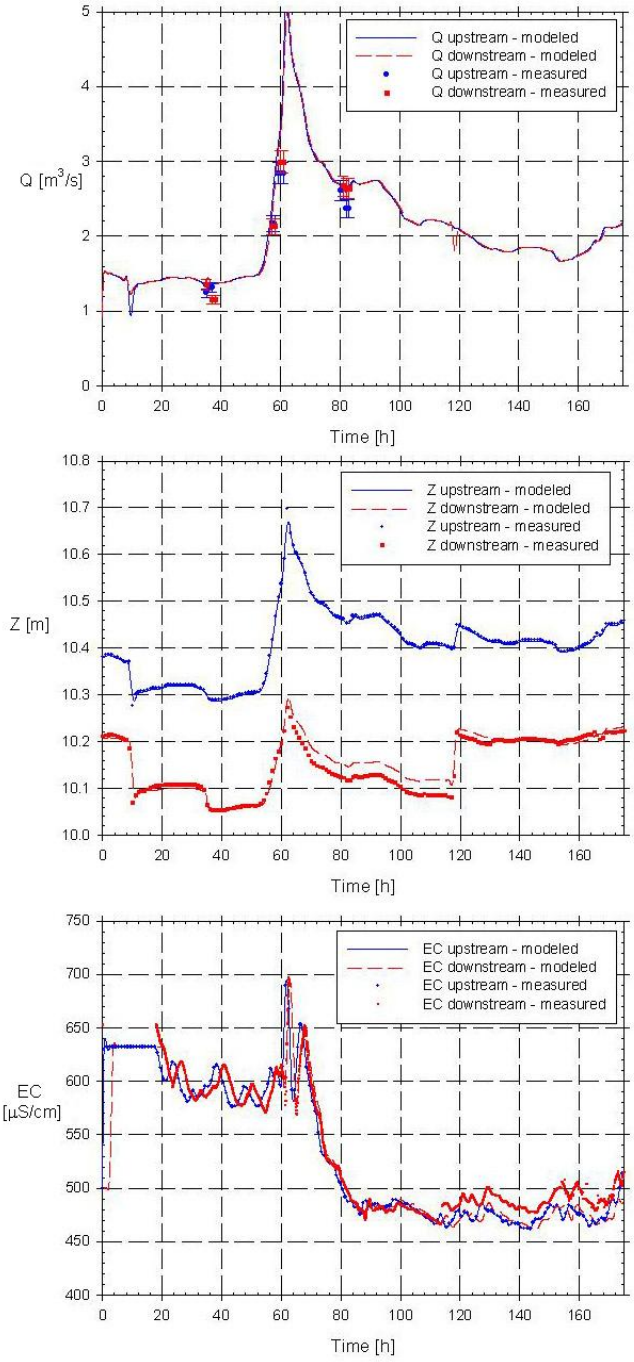

Figure 7.15: Modelled and measured values of discharge, water level and electrical conductivity from February 6th, to February 13th, upstream and downstream of the studied reach in the river Aa according to the best fit to the measurements

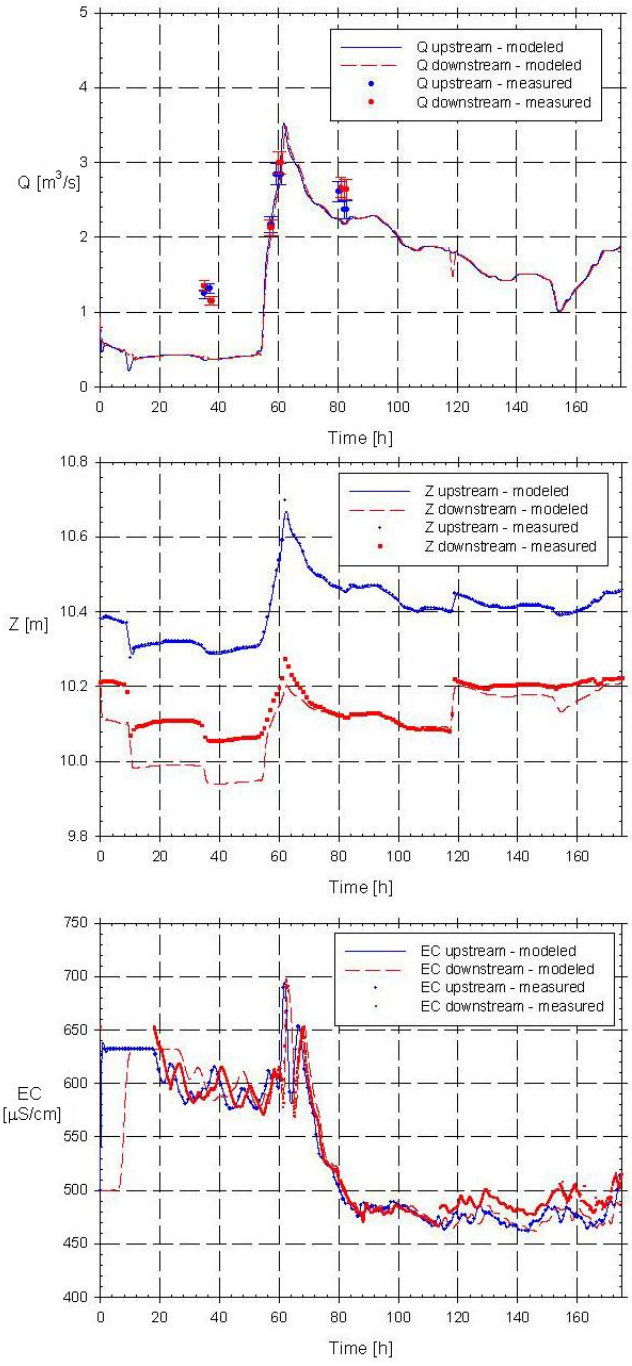

Figure 7.16: Modelled and measured values of discharge, water level and electrical conductivity from February 6th, to February 13th, upstream and downstream of the studied reach in the river Aa according to the general Manning-discharge-biomass relationship

May 2006 Similar simulations are carried out for the measurement campaign in May 2006. The fixed values for the channel geometry (the bottom depth, bottom slope, bank angle and bottom width) are used, in addition with the adapted values for the position of the downstream weir (Angle = 33.3 °) and the inflow from the Slootbeek (a discharge of 0.05 m^3/s with EC of 635 μS/cm). These values are obtained from the electrical conductivity, measured upstream and downstream. As the Slootbeek causes a dilution effect to the water in the river Aa, from upstream to downstream, discharge and electrical conductivity from the Slootbeek are incorporated to complete the balances correctly. Due to little variation in the water level, the position of the downstream weir is kept constant during the measurements.
Simulation of discharge and water level using the relationship yielding the best agreement between modelled and measured values for discharge, water level and electrical conductivity (Fig. 7.17) are according to the measurement values. Most modelled discharge results are within the 3 to 5 % accuracy range [10]. Also for the electrical conductivity, the simulated trend follows the measurements, although a time delay of about three hours is observed. Upstream and downstream measured values are very similar. The simulated water volume needs more time to pass through the channel from upstream to downstream. A solution can be obtained by increasing the cross section or decreasing the roughness coefficient, but with consequently bad results for discharge and water level. Time periods, linked to the electrical conductivity, are simulated well, so for calculation of residence time and retention time, the model works good. Difficulties with simulating the EC-values are probably due to errors in the registration. Regarding the discharges (an average value of 1.02 m^3/s) and the average wetted cross section during the measurement campaigns (13.35 m^2), a translation of EC-values of 5 hours is expected. This estimation is according the modelled values (Fig. 7.17c).

Fig. 7.18 shows the result based on the best fit to the measurements. Results are very similar to Fig. 7.17. Only peak discharges are simulated slightly larger.

For the results based on the general relation between Manning's coefficient and discharge (Fig. 7.19), larger deviations are found. Here also, modelled results for discharge and water level are below the measured value due to the overestimation of Manning's coefficient calculated by Eq.(6.15) for the studied period. Values of the simulated electrical conductivity are similar to the results based on the other methods.

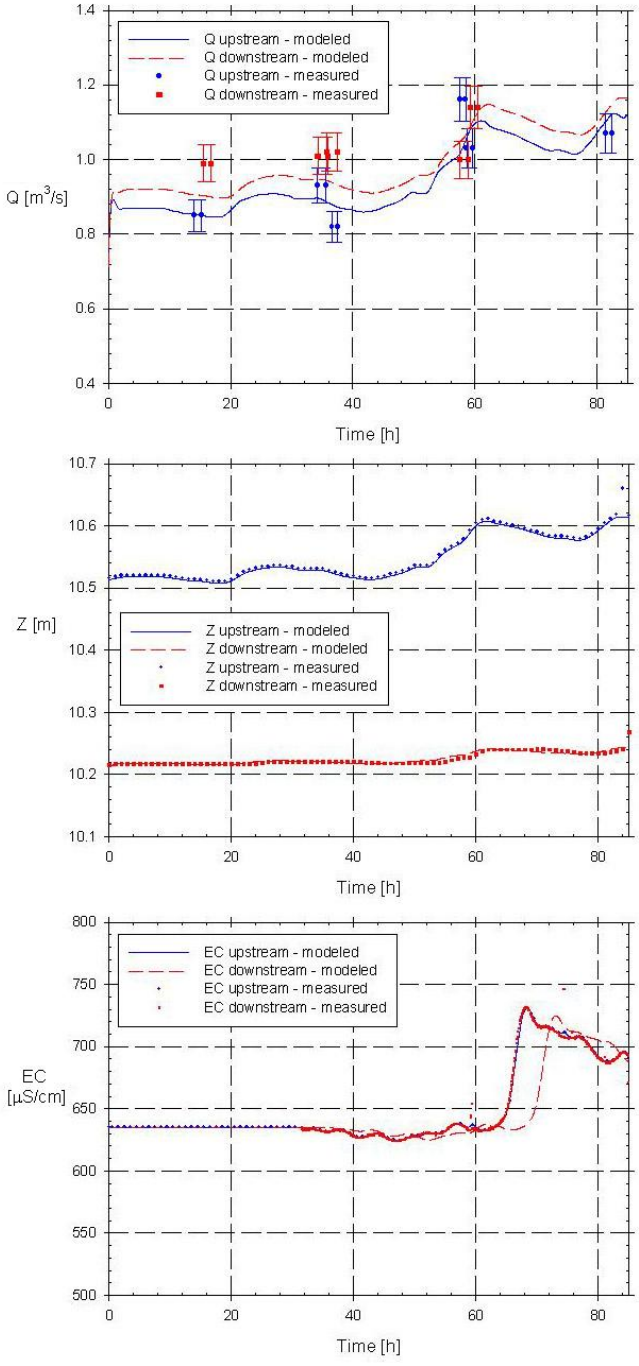

Figure 7.17: Modelled and measured values of discharge, water level and electrical conductivity from May 15th, to May 18th, upstream and downstream of the studied reach in the river Aa according to the best fit for the numerical model

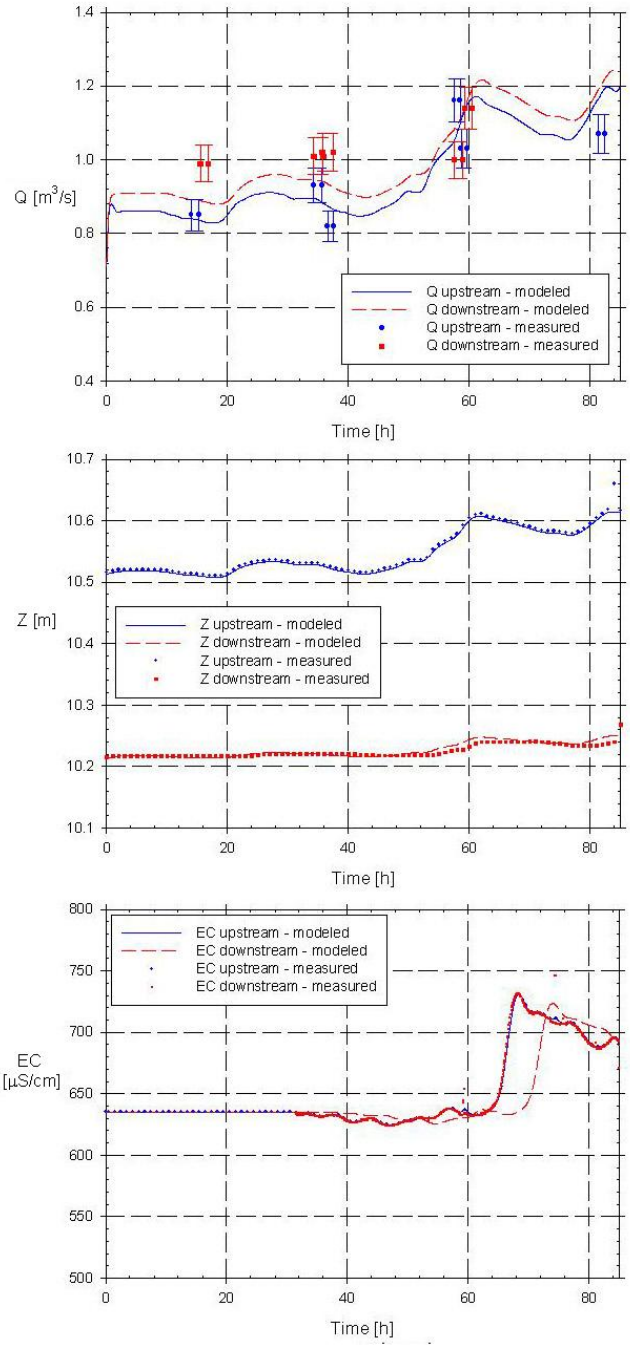

Figure 7.18: Modelled and measured values of discharge, water level and electrical conductivity from May 15th, to May 18th, upstream and downstream of the studied reach in the river Aa according to the best fit through the measurements

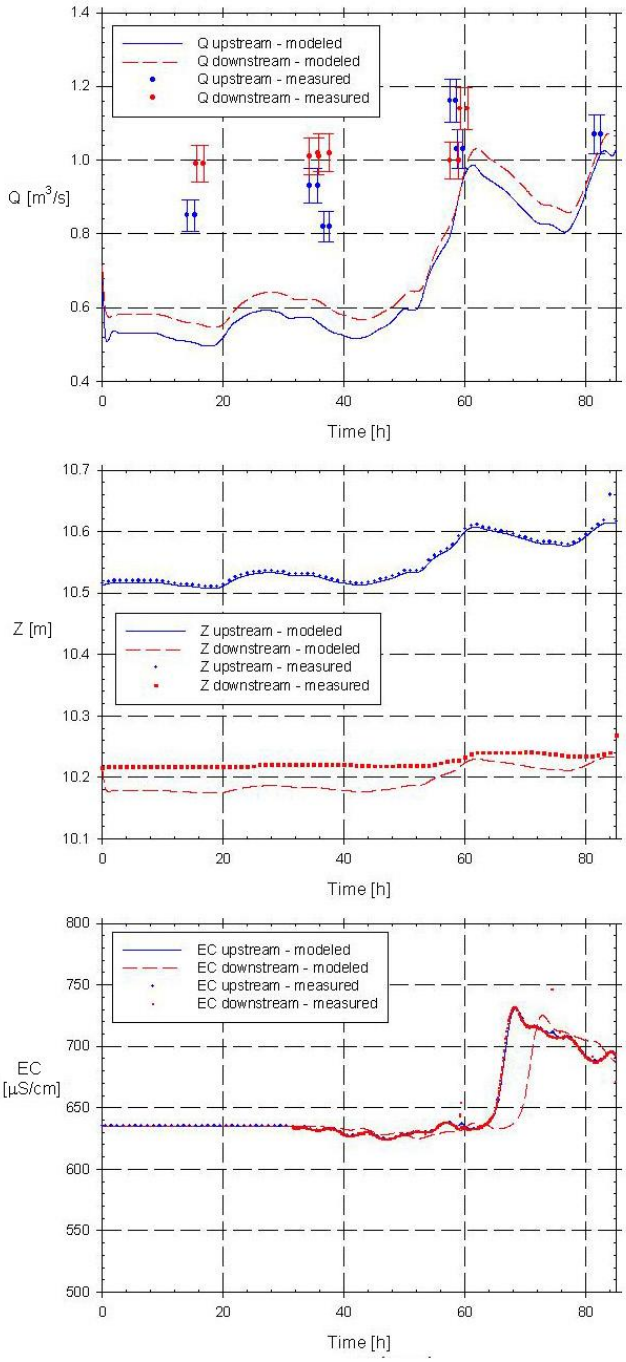

Figure 7.19: Modelled and measured values of discharge, water level and electrical conductivity from May 15th, to May 18th, upstream and downstream of the studied reach in the river Aa according to the general Manning-discharge-biomass relationship

April 2005 For the measurement campaign of April 2005, basic calibrated parameters are used and completed with an inflow of the Slootbeek of 0.05 m^3/s (EC = 520 μSS/cm) and a flap angle of the downstream weir of 29.5°. Discharge, water level and electrical conductivity are simulated very accurate by the model, using the best fit for this numerical model (Fig. 7.20).
Using the best fit to the measurements (Fig. 7.21) results in an approximate modelling of base values, but in large deviations for the peak discharges and water levels. Studying the electrical conductivity, a time delay is remarked for the same peak values. Modelled peak discharges and peak water levels are overestimated and linked to an underestimation of Manning's coefficient.
Using the general relation between Manning's coefficient (Fig. 7.22) and discharge results in approximate, but slightly underestimated, modelling results.

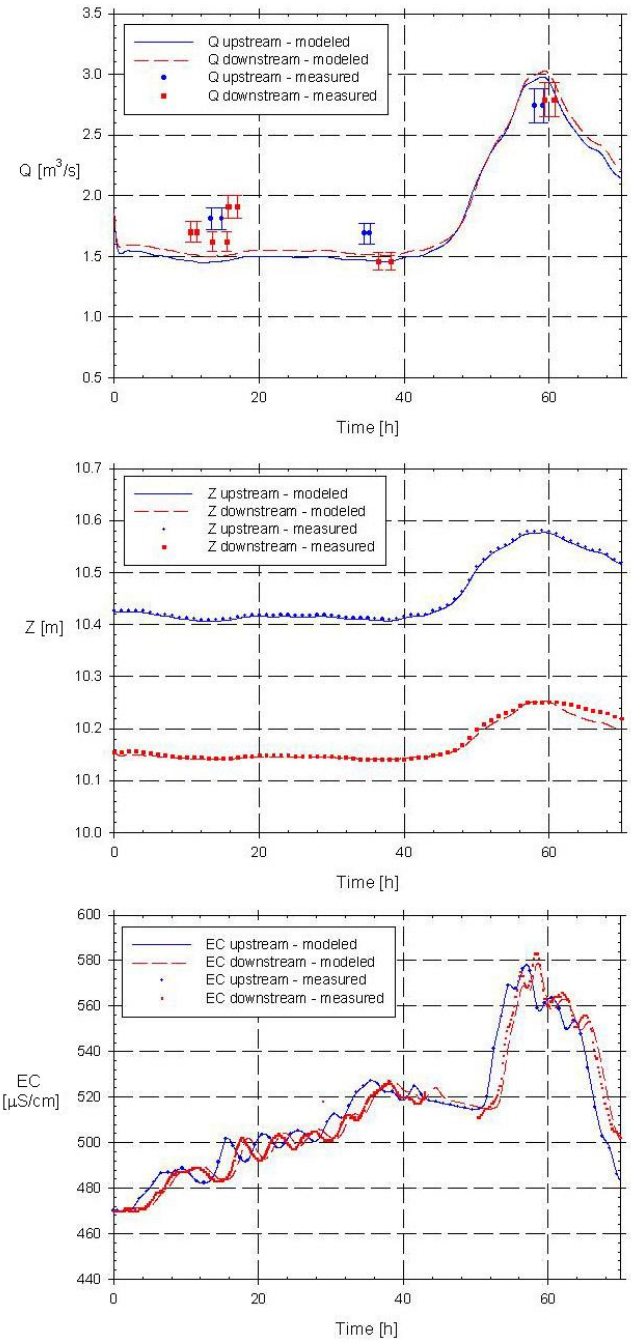

Figure 7.20: Modelled and measured values of discharge, water level and electrical conductivity from April 12th, to April 14th, upstream and downstream of the studied reach in the river Aa according the best fit for the numerical model

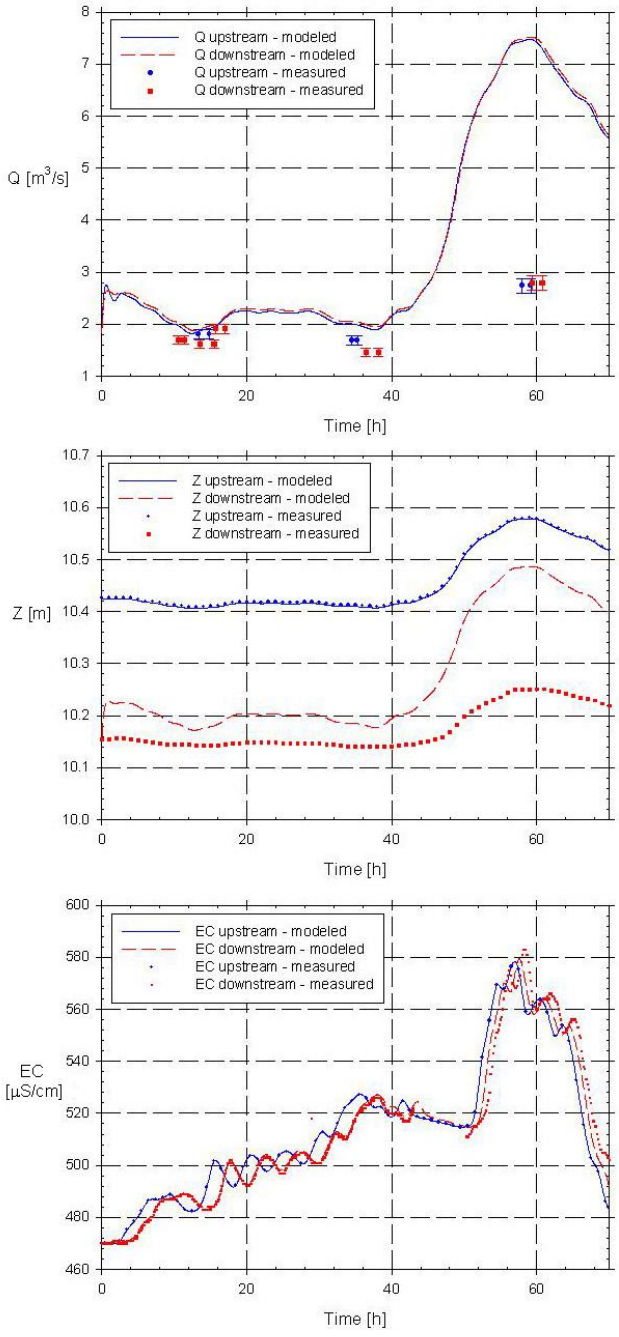

Figure 7.21: Modelled and measured values of discharge, water level and electrical conductivity from April 12th, to April 14th, upstream and downstream of the studied reach in the river Aa according the best fit through the measurements

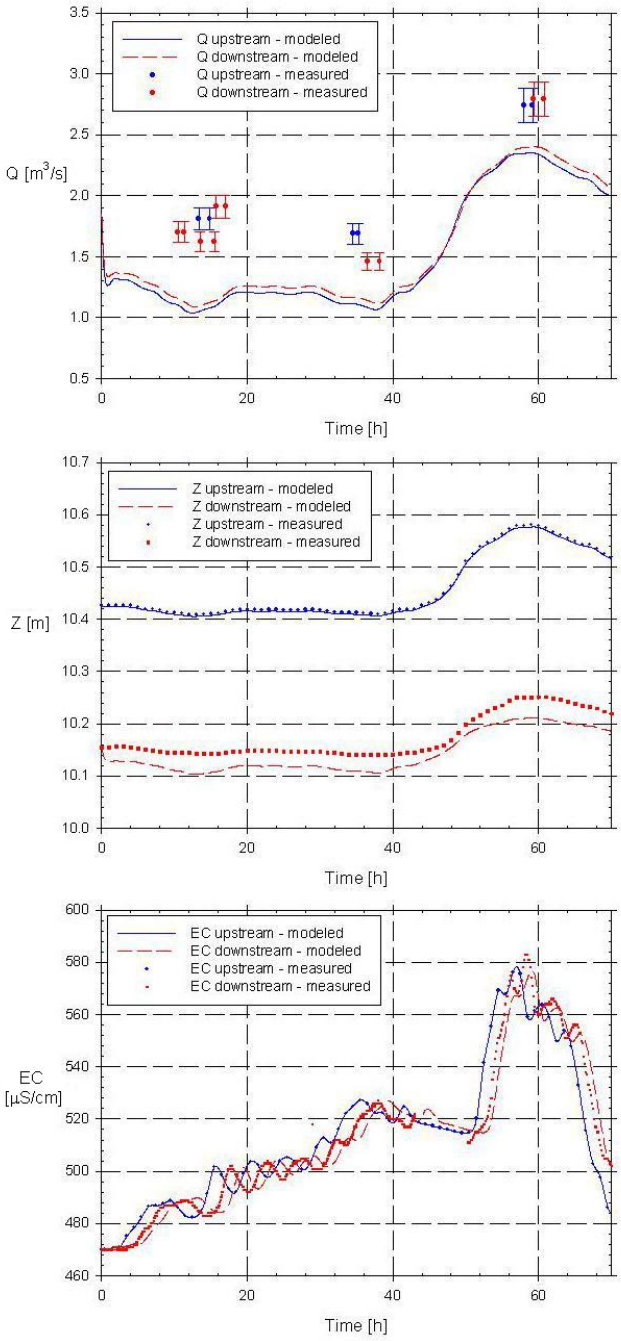

Figure 7.22: Modelled and measured values of discharge, water level and electrical conductivity from April 12th, to April 14th, upstream and downstream of the studied reach in the river Aa according the general Manning-discharge-biomass relationship

August 2005 In August 2005, an inflow of the Slootbeek of 0.02 m^3/s is incorporated in the calculations (EC = 565 μSS/cm), the flap angle is 33.5°. Using Manning's coefficient causing the best fit for the numerical model (Fig. 7.23), water level is simulated very accurate, while good results are obtained for base flow discharges, but not for the peak value. This deviation can be due to wrong measurements, although 3 different measurements are carried out in that period. As an indication, comparison with the HIC values is performed. The HIC (Hydrologic Information Centre from Flanders Hydraulic Research [11]) presents data from a wide range of rivers in Flanders and measures larger values in the more downstream part of the studied reach. All measurements are carried out with the same instrument and probably errors occur in the calibration formula of the Valeport sensor. Another explanation is that these are no error in measurements, but the modelling result is wrong, eg. due to errors in the Manning formula. However, deviant formulas do not result in good approximation of the water levels and do not result in better agreement for the discharges. Furthermore, EC-values are modelled well , which is an indication that the modelled discharge values are rather accurate. Therefore, due to their uncertainty, the measured peak values for the discharge are not taken into account for the determination of Manning's coefficient

The results of Fig. 7.24, where the best fit through the measurements for the value of Manning's coefficient is used, are equal to the results in Fig. 7.23.

Use of the general relation between Manning's coefficient and discharge (Fig. 7.25) results in good agreement between modelled and measured values for the base values, but in lower modelled values for the peak discharge (and so a time delay on the electrical conductivity). Also the modelled values of the downstream water levels are slightly smaller.

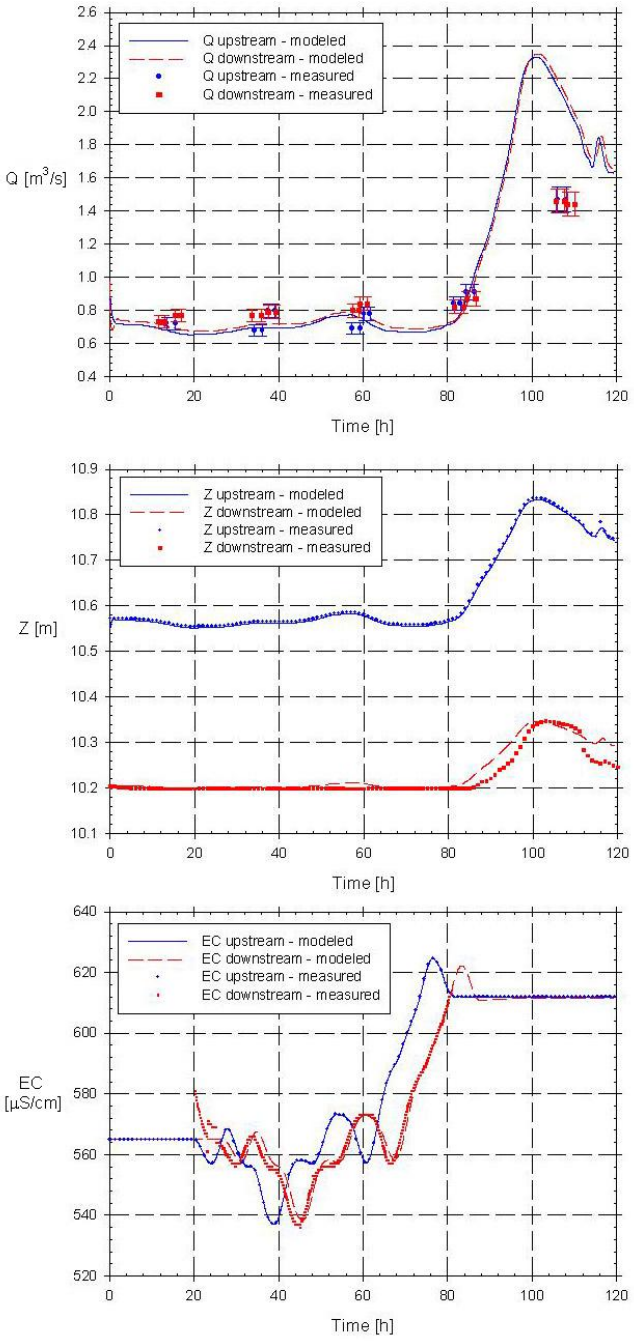

Figure 7.23: Modelled and measured values of discharge, water level and electrical conductivity from August 22nd, to August 26nd, upstream and downstream of the studied reach in the river Aa according to the best fit for the numerical model

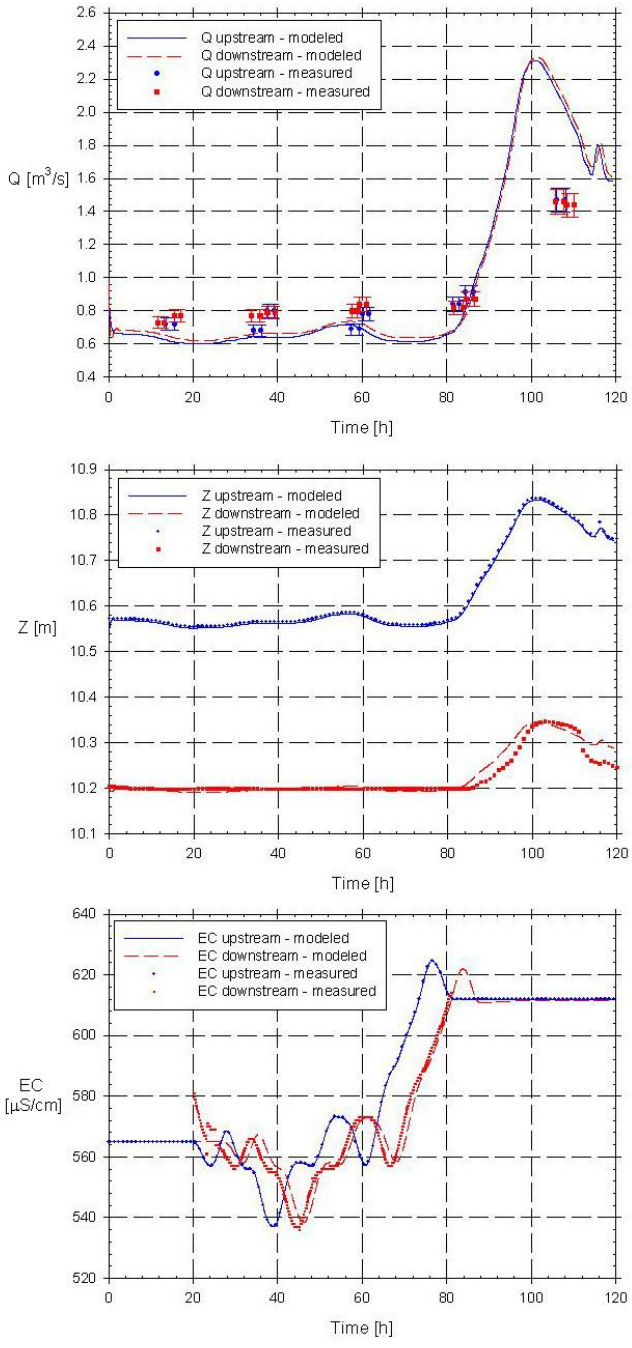

Figure 7.24: Modelled and measured values of discharge, water level and electrical conductivity from August 22nd, to August 26nd, upstream and downstream of the studied reach in the river Aa according to the best fit through the measurements

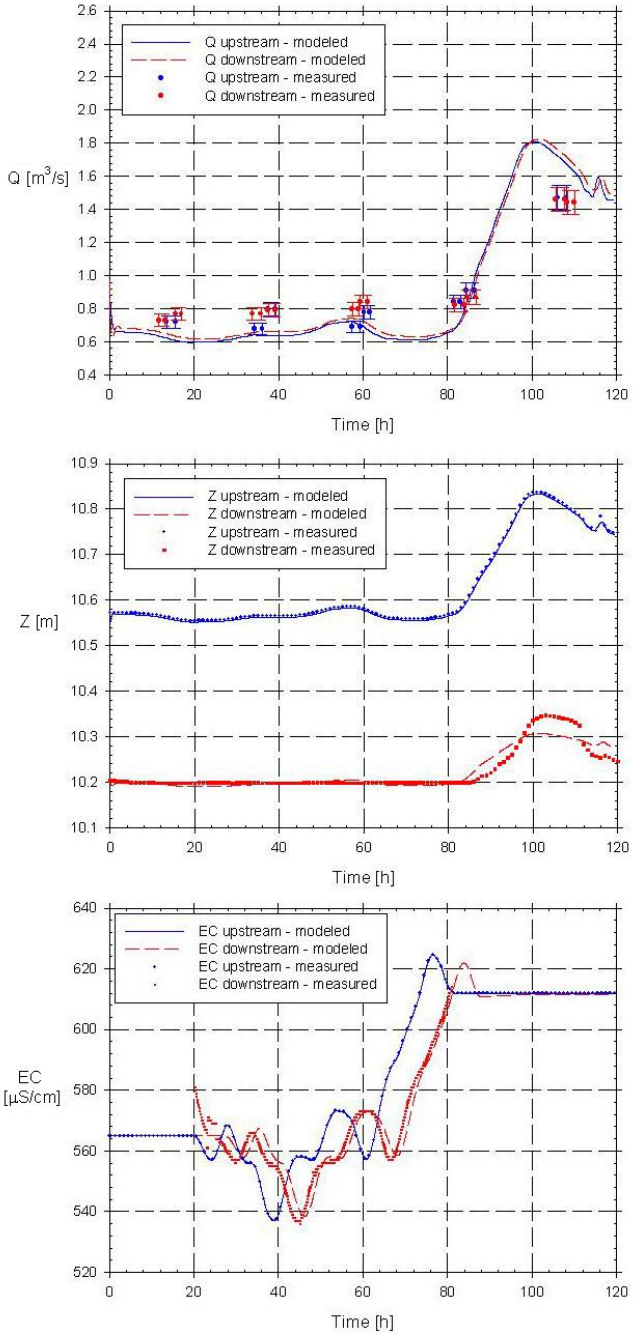

Figure 7.25: Modelled and measured values of discharge, water level and electrical conductivity from August 22nd, to August 26nd, upstream and downstream of the studied reach in the river Aa according to the general Manning-discharge-biomass relationship

3.2.2 Discussion

Manning coefficient during the measurement periods The measurement campaigns have been used to check the relationship between the Manning coefficient and the discharge. Obviously, good results are obtained by using the short-term relationship (Table 6.4, column 3), based on the relationship yielding the best agreement between modelled and measured values for discharge, water level and electrical conductivity. A best fit through the measurements (Table 6.4, first column) returns in good (February, May, August) or reasonable agreement (April). For one measurement campaign compared to another, the results will differ due to deviation of the measurements compared to the curve of Eq.(6.15). Comparison is plotted in Fig. 7.26. Fig. 7.26a shows measurements in the n-Q graph compared to Eq.(8), while Fig. 7.26b compares the calculated values based on measurements of discharge and water level and the simplified geometry in the Strive model with the predicted values (Eq.(6.15)) of Manning's coefficient. For the measurements of August, measured and predicted values for Manning's coefficient are in good agreement, while more spreading is seen on the points of May. These points are situated under the central line (Fig. 7.26b). This aspect is also found for the points of February and April. For both, the predicted values (n_{pred}) of Manning's coefficient are higher then the calculated values (n_{meas}) which causes lower values for discharge and water level. The correspondance for August is large. Taking into account the natural environment and the properties of field measurements, the obtained accuracy and spreading is good.

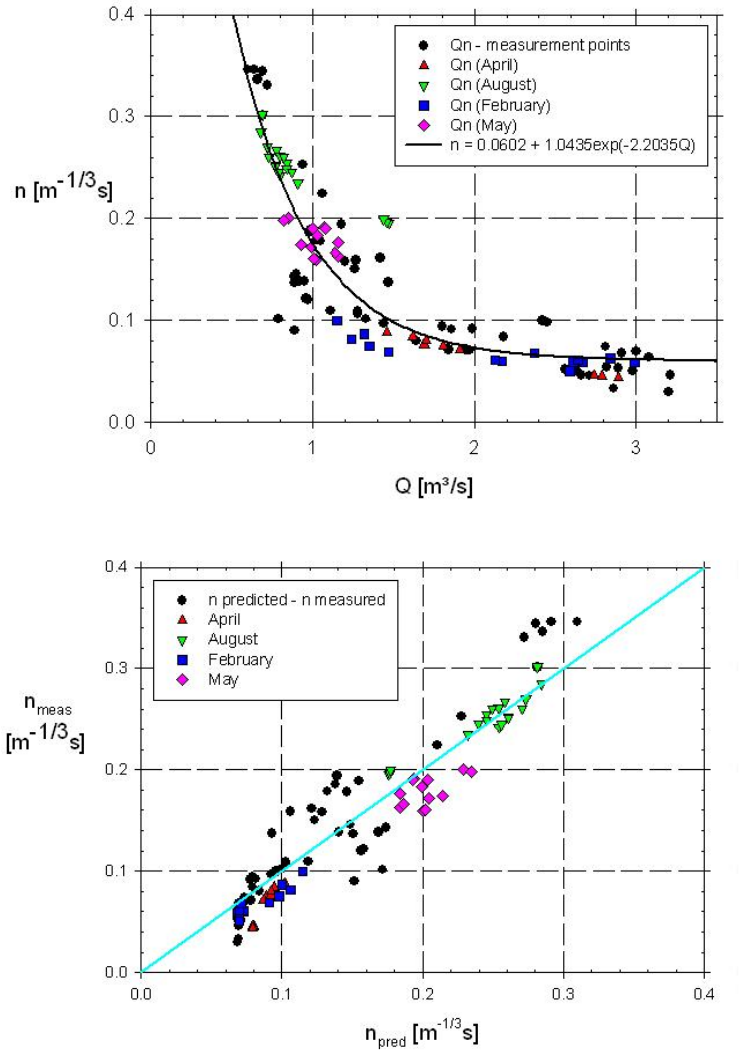

Figure 7.26: Relation between Manning's coefficient and discharge together with the measured values and indications of the measurement campaign (Fig. 21a, top) and values of the measurement campaigns compared to the Manning values calculated with Eq.(13) (Fig. 21b, bottom)

Accuracy of the modelling results For all 4 measurement periods and different Manning relations, the accuracy of the modelling results, for discharge, water level and electrical conductivity, is checked and compared in

Table 7.1. Therefore, peak and average values of all variables over the measurement period are calculated. Peak and average values for the water level and the electrical conductivity at the upstream boundary are not taken into account. These variables are boundary conditions for the numerical model and therefore, differences which occur due to numerical deviations between model and measurements are lower than 1 %. Discharges are measured in a discontinuous way and therefore, maximum and average values are not determined. Therefore, the deviations concerning discharge in Table 7.1 are calculated in a different way.
For water level and electrical conductivity, results of the numerical model (with three different Q-n relationships) are compared to the measured values and deviations [%] are calculated. All deviations are small, only for the water level in the period of April, differences are substantially, due to the large error when calculating peak values with Manning's coefficient based on the best Q-n fit through the measurements. For the discharge, no comparison for the best Q-n fit through the measurements and for Manning's coefficient based on Eq.(6.15) with the measurements was possible. In an indicative way, comparison is made to the method using Manning's coefficient for the best Q-n fit for the numerical model. Using the relationship between discharge, biomass and Manning's coefficient (Eq.(6.15)) introduces deviations from 7 % to 28 %. Deviations on the peak discharge reach 20 %. Using Manning's coefficient based on the best fit through the measurements results in little predictable deviations.
As a conclusion, use of Eq.(6.15) is the most interesting for overall modelling with the Strive model. Deviations for water level and electrical conductivity are within an acceptable range. Deviations for discharge are difficult to determine due to the lack of a continuous data set of measurements. However, discharge values are the most sensitive to variations in Manning's coefficient.
Comparing of the cost function shows good or reasonable agreement between modelled and measured values. In the cost function value, the agreement of discharge, water level and electrical conductivity is incorporated. Lowest values are observed if the Manning coefficient-discharge relationship is based on the best fit of the numerical model with the measurements. The global relationship yields good results for the period of August where measured values correspond well with the long-term relationship.

	Q peak up [m^3/s]	Q peak down [m^3/s]	Q aver. up [m^3/s]	Q aver. down [m^3/s]	Z peak down [m]	Z aver. down [m]	EC peak down [μS/cm]	EC aver. down [μS/cm]	Total cost [-]
February 2006									
measured values									
fit numerical model					-0.94	-0.57	-1.60	0.81	24.07
fit measurements	13.28	13.75	7.70	7.70	1.88	0.47	-1.27	0.81	28.1
global correlation	-20.82	-22.80	-24.50	-24.52	-5.20	-4.84	-2.01	0.43	79.2
April 2005									
measured values									
fit numerical model					0.17	-0.47	-0.72	1.19	16.1
fit measurements	151.08	148.33	96.65	94.05	20.50	9.59	-0.62	1.19	458.8
global correlation	-20.90	-20.68	-16.74	-16.34	-3.48	-2.79	-1.41	1.12	32.9
May 2006									
measured values									
fit numerical model					-2.40	0.00	-3.05	-1.76	30.9
fit measurements	6.14	6.78	1.05	2.02	-1.54	0.00	-2.90	-1.74	34.8
global correlation	-7.89	-6.78	-24.82	-26.26	-2.40	-0.29	-3.22	-1.83	189.6
August 2005									
measured values									
fit numerical model					0.00	0.80	1.34	2.63	70.4
fit measurements	-0.90	-0.89	-4.79	-4.72	-0.16	0.36	1.27	2.59	72.4
global correlation	-22.49	-22.35	-11.52	-11.37	-3.21	-0.18	1.27	2.58	44.9

Table 7.1: Comparison of the results for discharge, water level and electrical conductivity at the upstream and downstream boundary using the different relationships between Manning's coefficient and discharge [%] ('aver.' = average values). The result of the cost function is added.

Conclusions Field measurements in the downstream part of the river Aa lead to a large dataset useful for further analysis and use. This dataset is used for calibration of the modelling parameters of the Strive model, a 1D hydrodynamic model based on the Saint-Venant equations. Based on the hydrodynamic aspect of the study, first aim is to model discharges and water levels in an accurate way. Therefore, not only the best fit between measured and modelled results is considered, but also specific attention is paid to the modelling of peak as well as base flow. Modelling of the electrical conductivity is important for calculation of retention and residence time.

Measurements as well as modelling showed that Manning's coefficient depends on discharge and biomass and is the most important parameter for the model. Manning's coefficient is calculated according 2 methods. Firstly, the measured cross-sections are used with the measured discharges and the Bresse equation in the Hec-Ras model. Secondly, the Strive model calculated Manning's coefficient using a simplified geometry. The last Manning coefficient is the parameter used for further analysis. 3 relationships between Manning and discharge are set up, 2 short-term and 1 long-term relationship. The long-term relationship, including biomass, for Manning's coefficient and discharge (Eq.(6.15)) causes deviations on modelling discharge, water level and electrical conductivity. Therefore, for each measurement campaign, short-term relationships between discharge and Manning coefficient are set up, based on the idea that the biomass is kept constant over that small period. The first short-term relationship is expressed in the best fit between numerical and measured values, where the second short-term relationship is based on a simple best fit through the measured values. Afterwards, comparison of all 3 formulations of Manning's coefficient is made. It seemed that deviations on water level and electrical conductivity are small, while differences on peak discharges will reach up to 20 %. The accuracy, using the different relationships, depends on the spreading, which is inherent in natural processes, of the measured value compared to the relationship. A calibration and validation analysis based on a cost function delivers an objective criterion for studying model results. As ecosystem modelling is often based on trial and error, the Strive model and the above analysis allow a well-founded study of hydraulic and ecological processes.

3.3 Modelling of water quality variables

3.3.1 Introduction

As is indicated in the previous sections, the Strive model provides in accurate modelling results for discharge, water level and electrical conductivity. Next to these hydraulic quantitative variables and the conductivity, also amounts of chloride (Cl^-), a conservative tracer and some reactive components, as ammonium (NH_4^+), nitrate (NO_3^-), and oxygen (O_2), are measured in the river Aa. Therefore, some first modelling attempts of these components are described in this paragraph, taking into account the presence of macrophytes in the study area. It has to be added that this work is written from a hydraulic point of view, i.e. stream flow based on the Saint-Venant equations, and so, the in-depth study of ecological processes and their relation to the presence of in-stream vegetation, is beyond the scope of this work. The role of macrophytes in nutrient dynamics in macrophyte rich lowland rivers is described in [12, 13].

The water quality observed in rivers is determined by input and transformation processes. Neglecting the organic pollutants, heavy metals or other toxic compounds influencing the water quality, the functioning is basically determined by the cycle of life. The process of photosynthesis performed by algae or waterplants merges CO_2, water and sunlight into organic matter and oxygen. Modelling water quality means that the components of this reaction (oxygen, pH, organic matter or BOD and algae or chlorophyll) and the performers of this reaction (algae and bacteria) should be involved [14–16]. However, to perform the cycle of life, there is more: nutrients for instant nitrogen. The form of nitrogen used by algae can be ammonium or nitrate. These are very important compounds because the algae growth is determined by the most scarce building block (light availability, CO_2 or nitrogen). The classic water problem is eutrophication: a stimulation of primary production (algae growth) because more nutrients are added to the water system than normally and massive growth of algae take place. Regarding nitrogen, also other processes are of importance, namely nitrification and denitrification. So, for water quality purposes, nitrate and ammonium should be measured.

Chloride determines, next to other ions, the salt concentration in the river, which has consequences for the fauna and flora in the river. In zones with high concentrations, chloride might determine or select biological organisms. Oxygen is an atmospheric gas which dissolves partly in water and helps with the purification of the water. Photosynthesis is a process that converts carbon dioxide into organic compounds, especially sugars,

using the energy from sunlight. Also oxygen is added to the water in this process. The saturation degree of oxygen of the water is determined by the temperature of the water. Therefore, the saturation percentage of oxygen is used. This is the measured amount of oxygen in percentage of the saturation percentage at that temperature. Values of the saturation percentage of oxygen vary most of the time between 80 % and 120 % but also lower and higher values were found [14]. Low values indicate biological decomposition, high values are due to large primary production by the algae or macrophytes. Further, also ammonium and nitrate are important for the river ecosystem (Fig. 7.27) [17]. Fig. 7.28 depicts the flow of nitrogen particularly in rivers. Bioavailable inorganic nitrogen consists mainly of nitrate and ammonia, which is immobilized by autotrophs and microbial heterotrophs in biofilms or in suspension, and by higher plants. Assimilatory uptake refers to nutrients that are incorporated into cellular constituents and are potentially available to higher trophic levels. Excretion, decomposition, and production of exudates are the principal pathways by which elements are recycled to an inorganic state. Various dissimilatory transformations of inorganic forms of nitrogen by bacteria add to the complexity of the nitrogen cycle. Cyanobacteria and other microorganisms capable of nitrogen fixation transforms N2 gas into ammonia. Nitrification, which takes place under aerobic conditions, and denitrification, which takes place under anaerobic conditions, further influence the quantities and availability of dissolved inorganic nitrogen (DIN) [15].

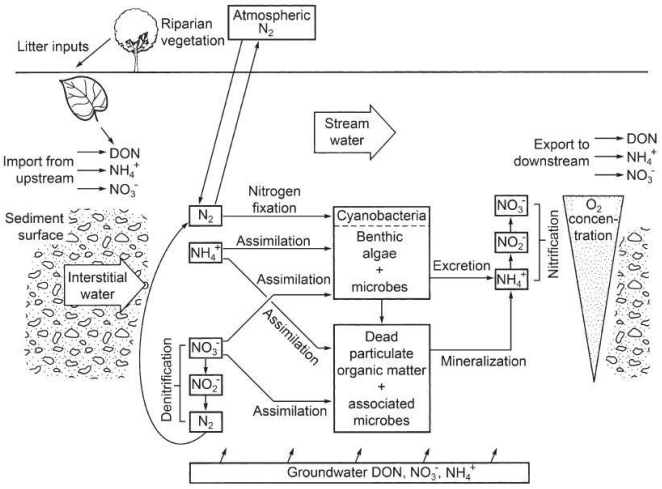

Figure 7.27: Schematic representation of the flow of nitrogen through the environment. The importance of bacteria in the cycle is immediately recognized as being a key element in the cycle, providing different forms of nitrogen compounds assimilable by higher organisms [15]

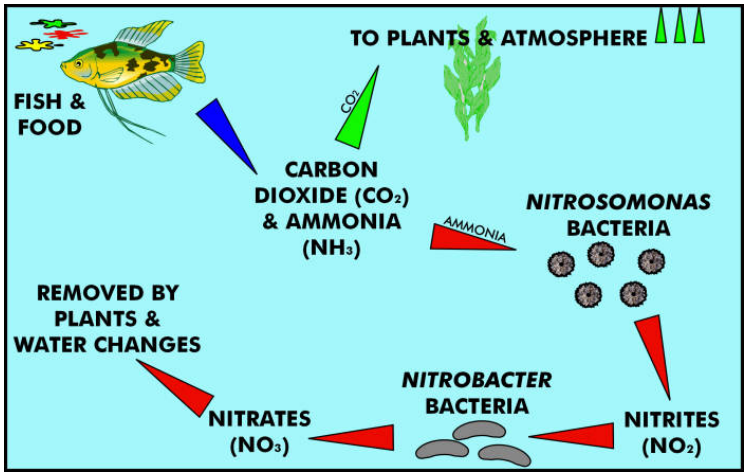

Figure 7.28: Schematic representation of the flow of Nitrogen in rivers (figure from http://www.iowas.co.uk/)

When a plant or an animal dies, or when an animal expels waste, the initial form of nitrogen is organic. Bacteria convert the organic nitrogen

back into ammonium, a process called ammonification or mineralization. High ammonium concentrations indicate pollution in the river.

Oxidation of ammonium to nitrate (nitrification) uses a lot of oxygen from the river. The conversion of ammonia to nitrates is performed by nitrifying bacteria. The primary stage of nitrification, the oxidation of ammonia (NH_3) is performed by bacteria which converts ammonia to nitrites (NO_2^-). Other bacterial species are responsible for the oxidation of the nitrites into nitrates (NO_3^-) [2]. A lot of nitrate, next to phosphate, results in eutrophication of the river. So, it is important for the nitrites to be converted to nitrates because accumulated nitrites are toxic to plant life. Denitrification is the reduction of nitrates back into the largely inert nitrogen gas (N_2), completing the nitrogen cycle. This process is performed by bacterial species in anaerobic conditions.
Calculations in the following are based on the best fit for the numerical model with the observed data. Differences with other approaches (Chapter 6) are only small. Measurements of all conservative and reactive tracers are performed with the described probes (Chapter 4).

3.3.2 The Strive package

An extra module, describing the flow of solutes, is incorporated in the Strive model. This module describes the transport of tracer or nutrients in the longitudinal direction. The flux of tracer or reactive variables is based on the discharge and the concentration. This leads to updated concentrations based on mass changes in a compartment.

The advection-dispersion-reaction equation (Eq.(7.1)) is the base for water quality modelling i.e. transport and reaction of chemicals in surface water [15, 16, 18]. This states that the change in concentration is the result of change in input and output (transport) and transformation of the compound (reaction). The use of tracers is important to get the transport right. So chloride and conductivity should be measured.

$$\frac{\partial C}{\partial t} = -\nu\frac{\partial C}{\partial x} + D_L\frac{\partial^2 C}{\partial x^2} - \frac{\partial r}{\partial t} \tag{7.1}$$

where C = concentration in water [mol/kg water], t = time [s], ν = water flow velocity [m/s], x = distance [m], D_L = hydrodynamic dispersion coefficient [m^2/s] and r = concentration in the solid phase [expressed as mol/kg water]. Considering the right part of the expression: the first term represents advective transport (transport related to the velocity of the wa-

ter), the second represents dispersive transport (fading concentration gradients by diffusion and differences in velocity of the water), and the third one is the change in concentration due to reactions (r in the same units as C).

Modelling discharge and water level is performed using the Saint-Venant equations. As the aim of this research is to end up with suggestions for integrated modelling, including water quality modelling [19], the advection-dispersion-reaction equation (Eq.(7.1)) is incorporated.
As the discharge was not available as upstream boundary condition for modelling discharge and water level, modelling of the electrical conductivity was performed as an extra check of the results. There (subsection 7.2), the Saint-Venant equations were already coupled with the advection-dispersion equation.
The Saint-Venant equations describe the hydraulics, discharge and water level, of rivers. So, they form the core module of an integrated river ecosystem. As next to flow, also transport is important in a coupled model, the advection-dispersion reaction is incorporated. The first term, representing the advective part, is exactly the coupling of the transport aspect with the flow (aspect) Saint-Venant equations. The second part, the dispersive transport, is also incorporated in the model, but is negligible for the study of the river Aa. This is concluded from measurements up- and downstream, the cloud of measured points does not show dispersive effects. The third part, the reactive part, has to be added to the model when modelling reactive tracers as ammonium, nitrate and oxygen. This extensive study is beyond the scope of this research.

The implementation of the water quality aspects in Strive is performed according the advection part of (Eq.(7.1)).

3.3.3 Calculation information

The time step of the calculations is 10 s, which is more critical than for the hydraulic parameters. As the number of calculation points in time and space (grid points) has to be sufficient to model all effects, this smaller timestep leads to better convergence which is important for mass balances. The output is plotted each hour.
The figures in the following focus on the interval of time of the measurements where the time is mentioned in hours. For interpretation of some of the results, the date and explicit time are interesting (eg. day-night) and mentioned in Table 7.2. The time at which the first measurement is performed is indicated, as well as the hour at which the quality measure-

ments started compared to the hydraulic measurements. The measurements started at the time indicated in column 3. The first measurement point is mentioned in column 2, where 0 h equals the time in column 3. Only the period of time of the measurements is plotted at the following figures.

Month	First measurement point	Time
February 06	38h	Feb, 7th 14h
April 05	0h	April, 12th 0h
May 06	31h	May, 16th 7h
August 05	25h	August, 23rd 1h

Table 7.2: Interval of time of the measurements during the different measurement campaigns. The explicit time is mentionned together with the indication of time in the following figures.

For better interpretation of the results, information about the temperature during the measurement campaigns is added (Table 7.3). The temperature is measured by the RMI (Royal Meteorological Institute of Belgium) in the neighbouring weather station of Geel. Mentioned values are averaged day values. Also temperature values of the water are continuously (with probes) or in water samples measured. The water temperature is an average value of upstream and downstream measured values, but differences are very small (0.1 °). Values are added in Table 7.3.

Month	Min. temp. [°C]	Min. water temp. [°C]	Aver. temp. [°C]	Aver. water temp. [°C]	Max. temp. [°C]	Max. water temp. [°C]
February 06 (6-13th)	1.2	-	3.4	-	5.8	-
April 05 (12-14th)	10.8	10.7	11.4	11.7	12.1	13.6
May 06 (15-18th)	15.9	16.6	16.2	17.5	16.4	21.1
August 05 (22-26th)	15.0	16.7	17.0	17.9	18.9	19.5
February 06	3.1	-	2.7		7.6	
April 05	6.0		11.0		15.9	
May 06	7.4		14.8		19.6	
August 05	12.7		17.8		22.9	

Table 7.3: Minimum, maximum and average temperature values during the period of the measurement campaigns and during the month of the measurement campaigns. Minimum, maximum and average water temperature during the period of the measurements.

3.3.4 Modelling results

3.3.4.1 Conservative tracers: EC and Cl^- The first modelling attempt is based on stream flow without dilution or reaction effects. In fact, reactive processes do not appear for conservative components. Indeed, due to the conservative behaviour of EC and Cl^-, all of this component is available upstream as well as downstream the reach. As a result, peak and base values of EC and Cl^- over the reach have to be equal.

Upstream and downstream Cl^- values do not agree totally due to some dilution effects over the reach [12]. The same effect was seen for the electrical conductivity (section 7.2.1). Two effects are possible: groundwater exchange and lateral in- or outflow. It was shown that groundwater contributions are of minor importance in the studied river reach since [23] concluded that only at the first part of the upstream weir, some seepage could be detected. Therefore, the observed diluted chloride signal in the downstream stations must be linked to the Slootbeek inflowing water holding lower Cl^- concentrations [14]. The dilution factor was modelled via the measured chloride values of the Aa and is rather small, comparing the small discharge of the Slootbeek to the one in the river Aa. From this, the discharge of the Slootbeek could be estimated which gave almost equal result as the measured values. Results are mentionned in Table 7.4. Like this, after the calibration step for the electrical conductivity, the modelling of chloride is a validation step of the Strive model for non-reactive tracers, which is successfull.

Month	Q [m^3/s]	EC [$\mu S/cm$]	Cl^- [mg/l]
February 06	0	-	-
April 05	0.05	520	58.5
May 06	0.05	635	77
August 05	0.02	565	60

Table 7.4: Discharge, electrical conductivity and chloride values for the Slootbeek during the different measurement campaigns

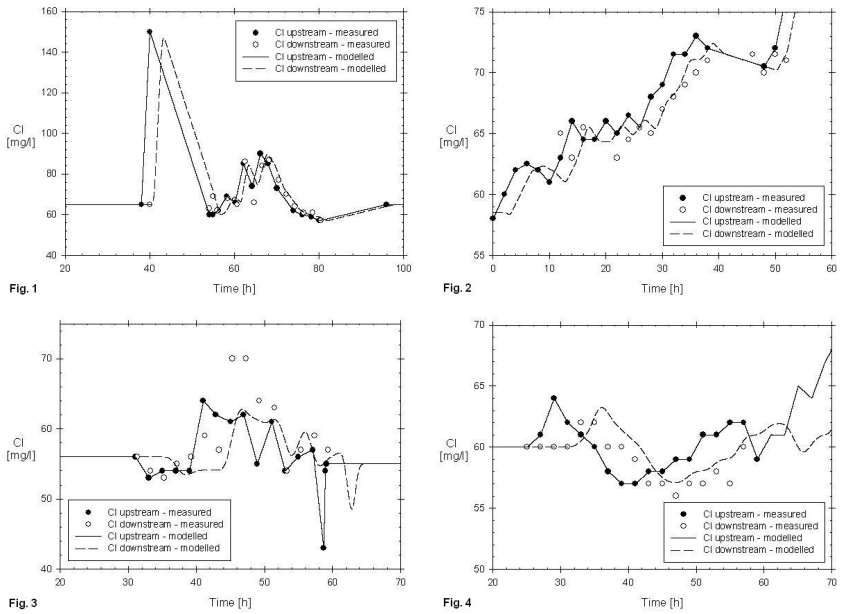

Figure 7.29: Tracer chloride values [mg/l] at the upstream weir and at the downstream weir for the different measurement campaigns (February (1), April (2), May (3) and August (4)) campaigns plotted as a function of time [h]

Fig. 7.14, 7.17, 7.20 and 7.23 already presented the values for the electrical conductivity, taking into account the values of Table 7.4.

The behaviour of the tracer element chloride during the measurement campaigns is shown in Fig. 7.29. Dilution is already incorporated when modelling discharge, water level and electrical conductivity and therefore, the chloride value of the Slootbeek is put at the same value as the chloride value of the river Aa. In reality, the amount of tracer in the Slootbeek will be lower compared to the river Aa. The studied reach receives treated sewage due to the presence of a wastewater treatment plant upstream [14]. As only a small number of measurements or indicative values are available and taking into account the small discharge of the Slootbeek compared to the discharge of the Aa, the chloride value of the Slootbeek is not determining for further calculation. Furthermore, analysis in the following shows that the amount or concentration of (conservative or reactive) tracer in the Slootbeek has only low influence on the modelling values. The dilution effect is small as is explained in the above paragraph. As the discharge of the Slootbeek is already determined for the electrical conductivity and

good calibration values are obtained here, the error on the tracer values in the Slootbeek will be negligible. chloride pulses were quite variable over the measured time period in all seasons and values were always highest at the upstream weir, but whereas the difference with the downstream weir is negligible. Deviations between measurements and model are due to the limited resolution of the measurements.

Table 7.5 presents the values of the tracers and nutrients in the Slootbeek. Only in April 05, measured values are available and comparable to the results of the numerical simulation. The chloride value is 61.13 ($\pm$ 23.45) mg/l, for ammonium 0.86 ($\pm$ 0.81) mg/l is registered and 2.17 ($\pm$ 0.22) mg/l is the result for nitrate. Taking into account the standard deviation, the followed modelling procedure returns accurate values.

Month	Q [m^3/s]	EC [$\mu S/cm$]	Cl^- [mg/l]	O_2 [mg/l]	NO_3^- [mg/l]	NH_4^+ [mg/l]
February 06	0	-	-	-	-	-
April 05	0.05	520	58.5	10.51	2.27	0.24
May 06	0.05	635	56	8.25	2.3	0.28
August 05	0.02	565	60	8.3	1.6	-

Table 7.5: Values of tracer and nutrients in the Slootbeek used for modelling of the periods of the measurement campaigns

3.3.4.2 Reactive components: NH_4^+, NO_3^- and O_2 In [12], indicative values for a couple of tracers are mentionned. Mean values [mg/l] for NH_4^+, NO_3^- and Cl^- in the river Aa are determined during 2003 to 2004, a period of 2 years, and result in 0.65 ($\pm$ 0.69) for NH_4^+, 2.92 ($\pm$ 1.52) for NO_3^- and 61 ($\pm$ 17) for Cl^-. More specific, in August 2003, values between 0.1 and 1.0 are measured for NH_4^+ and from 4.5 to 7.0 for NO_3^-. In May 2004, values between 0.15 and 0.45 are measured for NH_4^+ and from 2.0 to 2.25 for NO_3^-.

Table 7.6 presents the range of the measured values during the measurement campaigns for Cl^-, NH_4^+, NO_3^- and O_2. These values are all lower than the standards of water quality presented in Vlarem (Flemish legislation concerning the environment).

Month	Cl^- [mg/l]	NH_4^+ [mg/l]	NO_3^- [mg/l]	O_2 [mg/l]
February 06	65-140	1.5-5.0	1.0-2.0	60-95 [%]
April 05	55-75	0.25-2.0	2.0-2.75	7.0-10.0
May 06	53-70	0.25-0.55	2.5-5.0	7.0-11.0
August 05	56-64	-	1.6-3.0	3.0-12.0

Table 7.6: Range of measured values of Cl^-, NH_4^+, NO_3^- and O_2, during the measurement campaigns

Measured and modelled values of some reactive components are depicted in Figures 7.30 (ammonium), 7.31 (nitrate) and 7.32 (oxygen) which show the behaviour of the major nutrients during the measurement campaigns. Transport effects are already incorporated by use of the advection-dispersion equation as is explained for non-reactive tracers, but it is seen that reaction effects (third part of Eq.(7.1)) are much more important. Indeed, differences between modelled and measured reactive values are still large.
As for chloride, the nutrient profiles showed large variations over the measured periods. Ammonium and nitrate variations were irregular within the measurement periods with large peaks and troughs. This highlights the irregular sources of ammonium and nitrate for the river, probably linked to the management of the wastewater discharge located upstream from the studied section [12]. These dynamics make it easier to model and validate transport features. Oxygen, a reactive component, has a day-night cycle which is a point of particular interest when modelling.

Fig. 7.30 depicts measurements of downstream values which are more or less the same than the upstream values in the month of February, a time lag can be reamrked. A peak is observed in the late evening. In april, values are quite constant, upstream as well as downstream, with a large peak at the end of the measurements. In May, downstream measured values are larger than the upstream measurements. Downstream values of ammonium for the period of August are below the detection limit of the measurement instrument and are not incorporated in the modelling procedure. For all periods, the difference between upstream and downstream measurements is quite variable.

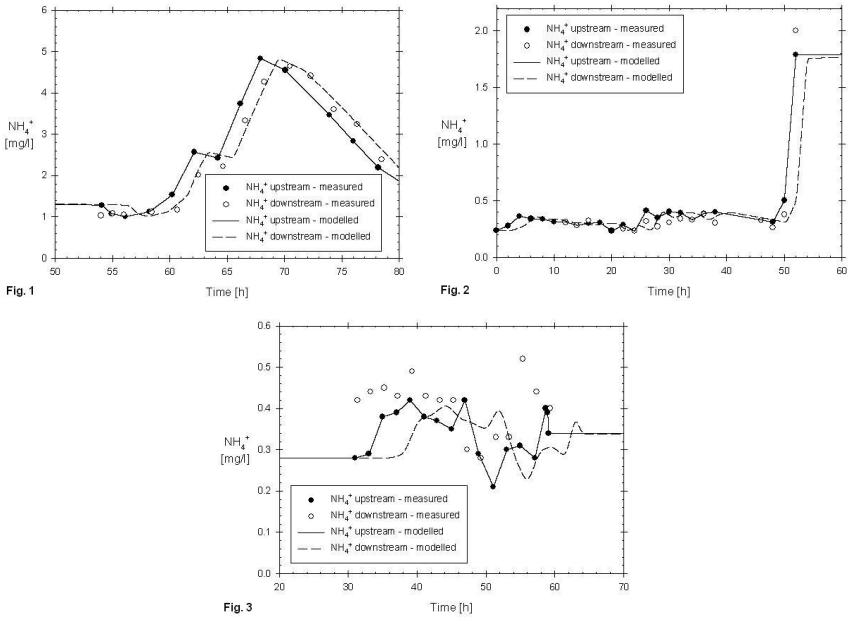

Figure 7.30: N-NH_4^+ values [mg/l] at the upstream weir and at the downstream weir for the different measurement campaigns (February (1), April (2), and May (3)) plotted as a function of time [h]. Downstream values of ammonium for the period of August are below the detection limit of the measurement instrument and are not incorporated in the modelling procedure.

For all periods, the measured values are quite variable, upstream as well as downstream (Fig. 7.31). Highest values are measured in April and May. In August, a clear peak is observed with larger upstream values when compared to the downstream values. For the other periods, there is no (net) reaction.

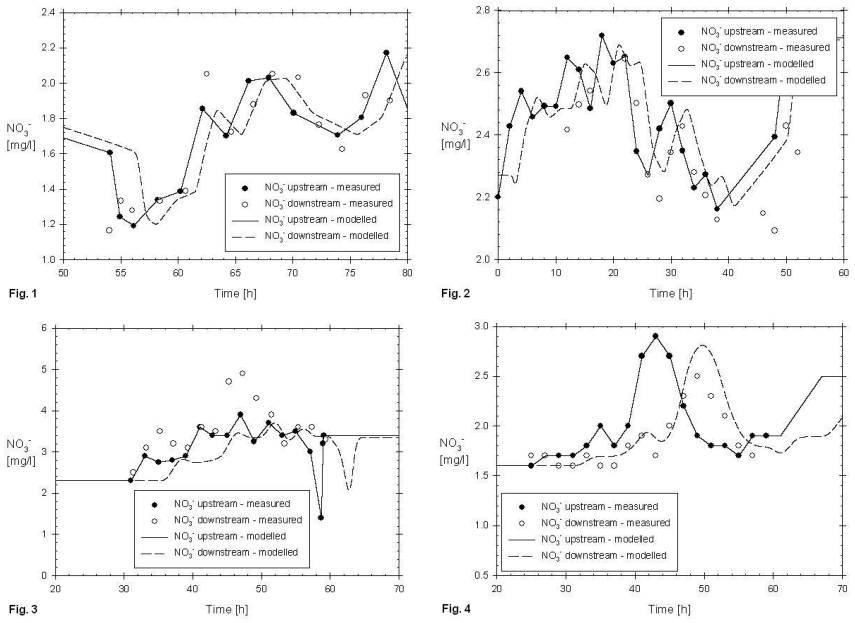

Figure 7.31: N-NO_3^- values [mg/l] at the upstream weir and at the downstream weir for the different measurement campaigns (February (1), April (2), May (3) and August (4)) plotted as a function of time [h]

The variation of oxygen during the measurements is presented in Fig. 7.32. Large variations over the day are registered with lower measured values downstream compared to upstream for the periods of April and smaller upstream measured values for the periods of May and August. A mass balance, implemented in the model, would give a clear picture on influx, outflux and retention/storage in the reach segment.

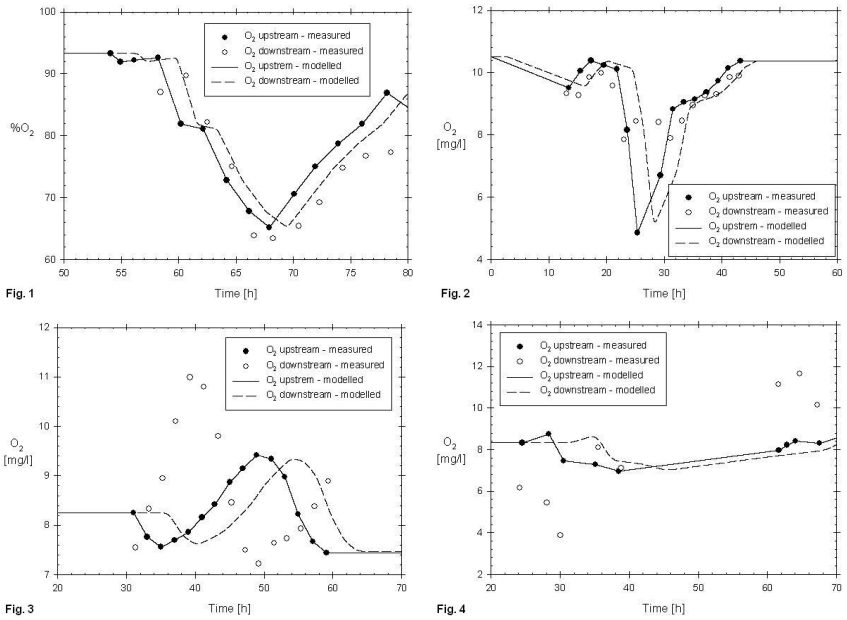

Figure 7.32: Oxygen values [mg/l] at the upstream weir and at the downstream weir for the different measurement campaigns (February (1), April (2), May (3) and August (4)) plotted as a function of time [h]

3.3.4.3 Comments

February In February, the Slootbeek does not add any water to the river Aa. This is confirmed by checking the chloride values in the reach (Fig. 7.29a). Downstream modelled values correspond well with the upstream values. Also the groundwater exchange is negligible. A chloride peak of 140 mg/l is measured, while lower values vary between 60 and 90 mg/l. The percentage of oxygen is between 60 and 95 %. The amount of oxygen in the water is low. Nitrate values vary from 1.0 to 2.0 mg/l. These values are lower than the average values for the river Aa as mentioned in [12], due to the lower plant activity in the river during the winter

season. For ammonium, values from 1.5 to 5 mg/l occur, which are higher than the average values. Results for February are very accurate due to the low pace of biochemical processes in winter periods.

April In the month of April, the Slootbeek adds a discharge of 0.05 m^3/s. The electrical conductivity of the Slootbeek is 520 μS/cm (cf. supra) and the value of chloride is fixed at 58.5 mg/l. Modelling of the downstream profiles of nitrate, ammonium and oxygen will include reactive processes. However, these preliminary results, only including the transport and dilution of the tracers, already show a reasonable agreement between modelled and measured values. Reducing or increasing the concentration values of the tracers in the Slootbeek is not influencing the modelling results greatly, due to its small discharge. Thus, no (net) reaction activity is taken place.

May In May, the same procedure as for the other periods is followed. The Slootbeek adds a discharge of 0.05 m^3/s, the electrical conductivity is set to 635 μS/cm (see section 7.2) and the chloride value is equal to the initial value for the measurement campaign in the river Aa, 56 mg/l. Also for oxygen, nitrate and ammonium the initial conditions for the model (which are the values measured at the beginning of the measurement campaign) are used (Table 7.5) for the Slootbeek. Changing these values does not result in better modelling results. The model results for ammonium and nitrate, only taking the transport processes into account, give lower values compared to the measured data. This suggests that a balance between ammonification (producing ammonium), nitrification (producing nitrate, consuming ammonium) and denitrification (producing nitrogen, consuming nitrate) has to be found. Additionally, a reasonable agreement between model and measurements, not including reaction processes can indicate a low biochemical activity (eg. less macrophytes in the river), but can also indicate an equivalence between production and consumption of nutrients. A last remark concerns the modelling of oxygen, which clearly shows the lack of modelling the day-night cycle typical for oxygen. During the day, the amount of oxygen increases due to photosynthesis, durinh night, photosynthesis stops and the plants start respiring which decreases the amount of oxygen in the water. Further, the spreading between lowest and highest values is bigger in the downstream section.

August In August, a small discharge (0.2 m^3/s) of the Slootbeek is added to adjust the values of discharge, water level and electrical conductivity. This amout is also used for modelling the values of chloride, which

vary between 56 and 65 mg/l. The amount of chloride in the Slootbeek is chosen equal to the initial chloride value in the measurement period in the river Aa. A variation of the amount of chloride in the Slootbeek does not result in better agreement. Downstream values of nitrate are below the detection limit of the measurement instrument and are not incorporated in the modelling procedure. The downstream modelled values of oxygen and nitrate show that the dilution of these variables from upstream to downstream is not sufficient. For oxygen, the bigger variation downstream compared to upstream is remarked as well as the day-night cycle. Besides this influence, reaction processes will take place in the reach. For this modelling, the nitrate and oxygen values in the Slootbeek are chosen equal to the initial values in the river Aa. Adapting the amount of nitrate in the Slootbeek does not strongly affect the modelling result: reducing the ammount of nitrate from 1.6 mg/l to 0 mg/l reduces the peak value from 2.88 mg/l to 2.77 mg/l. Therefore, the values measured in the river Aa are also used for modelling the Slootbeek inflow. Also for oxygen, variation of the amount of oxygen in the Slootbeek does not greatly affect the modelling results. On the other hand, the values of the Slootbeek are not measured and are in this modelling phase (without reaction effects) only indicative.

3.3.5 Conclusions

The dilution factor, due to lateral input of the Slootbeek, included in further modelling calculation of the nutrient patterns, did not explain all of the variations over the length of the study section in most cases. This is especially true for N-NH_4^+ in the growing season. Modelling purposes which incorporate a reaction or production term between the upstream and downstream weir of the study section will show better results for all available nitrogen components.
Downstream modelled nutrient profiles compared to the measured ones highlight the occurrence of non-conservative processes especially during the summer months (August) where we observe lower N-NH_4^+ concentrations (in August, values were lower than the detection limit of the measuring instrument) and higher N-NO_3^- concentrations than expected from mixing-dilution.
For each of the situations, a reaction rate term which is representing the non-conservative processes can be computed by taking the difference between modelled mixing-dilution curve and observed profiles. As is seen, a 'disappearance' of ammonium and nitrate occurs during summer while a production of the respective nutrients between the upstream and downstream weir is expected during winter. These processes are not that clear.

Incorporating a reaction or production factor between the upstream and downstream weir supposes good results for ammonium and nitrate.
In the oxygen rich study section, we may assume that a part of the present N-NH_4^+ is converted to N-NO_2^- and NO_3^- [24]. It is also expected that still a considerable amount of N-NH_4^+ has disappeared during the flow time, especially in the growing season and it is clear that the river macrophytes do play a role in the uptake of N-NH_4^+ in the growing season while in late autumn and winter, their role is negligible. The amount of biomass can be compared with the average N-NH_4^+ concentrations in the surface water for each campaign so that the contribution of the standing biomass could be obtained. More measurements are, and particularly a more detailed analysis with reaction processes is, necessary to draw any conclusions.
Fosfate measurements and modelling is not performed. Reactions involving P-PO_4^{3-} are more complex: sediment sorption (as an abiotic process) has been shown as a substantial factor in phosphorus (P) retention [25, 26]. Furthermore, the organic matter content of sediment also influences the ability of sediments to adsorb P [27] as well as present concentrations of iron and calcium [26]. Sediments are also responsible for the nitrogen removal, they interfere with the dynamics of oxygen and nitrogen [12].
For all nutrients, the reaction rates will be highest at the peak of the growing season, namely in August. Most important ammonium and nitrate sink is represented by macrophyte uptake which had a preference for ammonium. Preference for ammonium by macrophytes was previously shown by several studies [24, 28–30].

4 Conclusions

Remarks concerning the choice of boundary conditions are formulated in the previous chapter. A combination of discharges upstream and the relation between the water level and the discharge downstream (calibration formula of the weir) results in the most accurate modelling values in the river Aa. However, these data series are not always available. Therefore, use of tracer values (as the electrical conductivity) is also tested and seemed a useful alternative.

Aspects of integrated modelling are studied more in detail. Lateral in- or outflow is incorporated in the Strive model. Lateral in- or outflow at a certain point as well as distributed in- or outflow is modelled.

As an extension to lateral in- and outflow, inundation areas are added to the model. Different solution methods are considered and different cases,

depending on the water level in the channel and in the flooding cell, are discussed. An experimental setup is tested and several situations, including 1 or 2 storage areas connected with the river, are simulated. The Strive model allows to include the aspect of flooding for short rivers. For longer distances, an appropriate method has to be implemented to slow down the flow between the storage cells. A time delay of the water flowing in the inundation area compared to the flow in the river channel has to be incorporated to obtain a more realistic flood routing with the coupled Strive model, and therefore a good prediction of the residence time of the water in the river system.

Based on the hydrodynamic aspect of the study, first aim is to model discharges and water levels in an accurate way. Therefore, not only the best fit between measured and modelled results is considered, but also specific attention is paid to model peak as well as base flow. Modelling of the electrical conductivity is important for calculation of retention and residence time.
Integrated ecosystem modelling using the Strive package allows simulating aspects of both water quantity (discharge, water level) and water quality (here chloride, ammonium, nitrate, oxygen). Simulations for 4 measurement campaigns over the year are performed and result in very accurate values. An extra module for the reaction processes involving these nutrients has to be added.
The stream flow is modelled well using the Saint-Venant equations, transport is coupled to this flow by the advection-dispersion equation. Using this equation for the different measurement campaigns results into good agreement between modelled and measured values for conservative tracers as the electrical conductivity and the amount of chloride in the river. Also for reactive tracers, good results are obtained when the reaction rate in the river is low (eg. during the winter months). The University of Antwerp has dedicated its research to determining the reaction processes in the river Aa. Measurements are performed and waiting for analysis and incorporation in the Strive model.

References

[1] M. Van Lysebettens. *Numerical modelling of the interaction between a river and its floodplains*. Master's thesis, Ghent University, 2006.

[2] P. Troch. *Mathematische simulatie van niet-permanente stroming op een waterwegennet*. Master's thesis, Ghent university, 1991.

[3] F. Declercq. *Overstromingsgebieden: experimentele opzet en numerieke modellering in 'Femme'*. Master's thesis, Ghent University, 2007. Faculty of Engineering.

[4] S.R. Durzans. *Stormwater conveyance modeling and design, first edition*. Haestad Press, 2003. ISBN 0 967580 8 7.

[5] R. Moussa. *Criteria for the choice of flood routing methods in natural channels with overbank flow*. Wethydro: Center of excellence in wetland hydrology: model application for wetland hydrology and hydraulics. 2004. ISBN 83 7244 620 2.

[6] K. Mahmood and V. Yevjevich, editors. *Unsteady flow in open channels*, volume 1. Water Resources Publications, 1975.

[7] J. Berlamont. *Theorie van de verhanglijnen*. L. Wouters, 6 edition, 2004.

[8] V. T. Chow. *Open Channel Hydraulics*. McGrawHill, New-York, 1959.

[9] L. De Doncker, P. Troch, R. Verhoeven, K. Buis, N. Desmet, and P. Meire. *Importance of Manning's coefficient for the calibration of the coupled Strive model*. 2009. In review.

[10] L. De Doncker, P. Troch, R. Verhoeven, K. Bal, and P. Meire. *Determination of the Manning roughness coefficient influenced by vegetation in the river Aa and Biebrza river*. Environmental Fluid Mechanics, 9(5):549–567, 2009.

[11] *Flanders Hydraulic Research*. online, 2009. `http://www.watlab.be/`.

[12] S. Van Belleghem, K. Bal, N. Desmet, K. Buis, E. de Deckere, P. Meire, J.P. Vanderborght, F. Dehairs, N. Brion, and L. De Brabandere. *Macrophytes and nutrient dynamics in the upper reaches of the Schelde basin (Manudyn II): Part 2: global change, ecosystems and biodiversity*. Technical report, University of Antwerp-Universit Libre de Bruxelles-Free University of Bruxelles, 2007.

[13] T.C.M. Brock. *Waterplanten en waterkwaliteit*. Number 45. Stichting Uitgeverij Koninklijke Nederlandse Natuurhistorische Vereniging, 1988. ISBN 90-5011-014-2.

[14] K. Buis, N. Desmet, and S. Vanbelleghem. *Personal communication*, 2009.

[15] J.D. Allan and M.M. Castillo. *Stream Ecology: Structure and function of running waters*. Number ISBN 978-1-4020-5583-6. Springer Netherlands, 2007.

[16] R.V. Thomann and J.A. Mueller. *Principles of surface water quality modeling and control*. Number ISBN 978-0060466770. Prentice Hall, 1997.

[17] R.C. Nijboer and P.F.M. Verdonschot. *Variabele selection for modelling effects of eutrophication on stream and river ecosystems*. Ecological Modelling, 177(1-2):17–39, 2004.

[18] A.D. Rubio, A. Zalts, and C.D. El Hasi. *Numerical solution of the advection-reaction-diffusion equation at different scales*. Environmental Modelling and Software, 23(1):90–95, 2008.

[19] E.C. Ani, S. Wallis, A. Kraslawski, and S. Agachi. *Development, calibration and evaluation of two mathematical models for pollutant transport in a small river*. Environmental Modelling and Software, 24(10):1139–1152, 2009.

[20] K. Soetaert and P.M.J. Herman. *Carbon flows in the Westerschelde (The Netherlands) evaluated by means of the ecosystem modle (MOSES)*. Hydrobiologia, (311):247–266, 1995.

[21] K. Soetaert and P.M.J. Herman. *Estimating estuarine residence times in the Westerschelde (The Netherlands) using a box model with fixed dispersion coefficients*. Hydrobiologia, (311):215–224, 1995.

[22] K. Soetaert and P.M.J. Herman. *Nitrogen dynamics in the Westerschelde (The Netherlands) estimated by means of the ecosystem model MOSES*. Hydrobiologia, (311):225–246, 1995.

[23] P. Meire, R. Verhoeven, P. Troch, F. De Smedt, and O. Batelaan. *Fundamentele studie van uitwisselingsprocessen in ecosystemen*. Technical report, Research Foundation - Flanders, 2007.

[24] M. Scholz and M. Trepel. *Water quality characteristics of vegetated groundwater-fed ditches in a riparian peatland*. Science of the Total Environment, 332:109–122, 2004.

[25] I. Fox, M.A. Malati, and R. Perry. *The adsorption and release of phosphate from sediments of a river receiving sewage effluent*. Water Research, 23(6):725–732, 1989.

[26] W.A. House and M.S. Warwick. *Interactions of phosphorus with sediments in the River Swale, Yorkshire, UK*. Hydrological Processes, 13(7):1103–1115, 1999.

[27] D.R. Smith, B.E. Haggard, E.A. Warnemuende, and C. Huang. *Sediment phosphorus dynamics for three tile fed drainage ditches in Northeast Indiana*. Agricultural Water Management, 71(1):19–32, 2005.

[28] D.S. Nichols and D.R. Keeney. *Nitrogen nutrition of Myriophyllum spicatum: uptake and translocation of 15N by shoots and roots*. Freshwater Biology, 6:145–154, 1976.

[29] K.R. Reddy, J.C. Tucker, and W.F. Debusk. *The role of Egeria in removing nitrogen and phosphorus from nutrient enriched waters*. Journal of Aquatic Plant Management, 25:14–19, 1987.

[30] N. Cedergreen and T.V. Madsen. *Nitrate reductase activity in roots and shoots of aquatic macrophytes*. Aquatic Botany, 76:203–212, 2003.

8 Conclusions

1 Specific research results

A river is part of an integrated ecosystem where interactions between surface water, groundwater and ecological processes take place. In literature, a lot of research was performed considering aspects of water, sediments, solutes, etc. in zones of interaction. This work adds research on the synthesis of physical and ecological descriptions in one model structure to analyse land-water interaction. Attention is particularly paid to the presence of in-stream vegetation and its effect on discharge, water level and also on water quality variables. Measurements are performed in a laboratory flume and in the field where two study areas are considered: the river Aa (Belgium) and the Biebrza river (Poland). The mentioned interactions are incorporated in an integrated model with an important hydraulic component as the driving force of the ecological processes.

The search for a model structure which allows analysis and simulation of interactions in the integrated ecosystem includes a literature study. A large amount of available model packages is considered. Although some model codes are good for describing several aspects of integrated modelling, none of them meet the requirements for integrated ecosystem modelling (widely available code, extended flow equations, no black box, attention for water quality aspects). Therefore, a totally new code, the Strive package, is developed in an existing environment ('Femme').

In this Strive package, the hydraulic component is based on the Saint-Venant equations. An important parameter in the Saint-Venant equations is Manning's coefficient calculated from the energy slope. In steady state conditions and assuming uniform flow, Manning's coefficient is determined by Manning's equation.

The quality and accuracy of a numerical model strongly depends on the data available to build and to calibrate the model. Therefore, regular measurement campaigns are an important tool.
Hydraulic measurements are performed in the laboratory flume and in the field. Instrumentation and methods are explained in detail. Traditional techniques are sometimes difficult to use, for one, to measure flow velocities through vegetation. Hydrometric propellers can be fouled in vegetation. For acoustic devices, the vegetation interferes with the backscatter signal and an electromagnetic velocity meter may have an impact on the environment due to its size. The ADCP, based on the Doppler technology, allows a faster sampling in sections without in-stream vegetation.

In the flume of the Hydraulics Laboratory, it is shown that the presence of vegetation disturbs the theoretical logarithmic velocity profile over the water depth. A theoretical analysis is described and a wide range of measurements is performed to study stream patterns in and around vegetation and specific attention is paid to the behaviour of floating vegetation.
Measurements of the velocity profile in the flume without obstacles show a good agreement with the theoretically derived log-profile. The log profile only applies to the lower part of the flow. At the surface, the velocity will decrease with increasing depth caused by secondary currents: velocity vortices within the cross section. The existence of these currents is confirmed by measurements.
Velocity profiles in front of and behind the strip covered with gravel are calculated. The size of the boundary layer can be determined in two ways. The former uses the fitted velocity profile and defines the height of the boundary layer by v = 0.9v_{max}. A peak in stresses occurs within the boundary layer. In the latter, the width of this peak was used. Both definitions gave practically the same results. It seems that the boundary layer is not fully developed at the end of the grind bottom. Further analysis demands for more extended areas.
Analysis of the velocity profiles between the surface floating plants shows differences from the log-profile derived for the situation above the bottom of the flume. As the measured profile resembles a tangens hyperbolicus

profile, it can be compared with a mixing layer. Measurements in the flume with hanging plants show 4 areas in the flow. Two of them were already present in the flume without obstacles: the boundary layer at the bottom and the undisturbed layer. The mixing layer with the plants and the area within the plants are added. The plants cause disturbance of the flow and eddies start to appear. The flow turbulence increases. This is seen by the swaying movement of the vegetation (called 'Monami') and the erosion of the gravel layer under the plants.

The dataset gathered in the river Aa and Bierbza river is presented. In the field, the measurement conditions are more difficult due to their variability. Furthermore, the presence of vegetation in the river has a big influence on the velocity measurements. According to the location and the circumstances, the use of a calibrated weir is possible. In rivers, single point measurements are often used. The use of an electromagnetic device for example, can solve the problems encountered with the hydrometric propellers in vegetated rivers. Although the calibration formula of the weir is difficult to use in the river Aa due to the lack of registration of its position, this way of continuous measuring is preferable. Its results agree with the measured discharges downstream using other techniques. An accurate determination of the water level over the weir is necessary to obtain a sufficient accuracy.
The amount of biomass in the studied reach of the river Aa is determined by using an invasive technique, a mowing device, determining the amount of macrophytes per surface area. The evolution of macrophyte biomass density in the study area was monitored by quantitative sampling on a monthly base. The heterogeneity of the vegetation in the river causes uncertainty and spreading of the biomass results.

In the flume, the influence of the vegetation on the velocity profiles and Manning's roughness coefficient under different conditions of velocity, discharge and water level, is checked. First, the influence of blockage is tested by presence of obstacles. In front of the obstacles, higher water levels are registered and consequently, the velocities will decrease. The more rigid the obstacle, the more the water level rises and the velocity decreases. Immediately behind the obstacle, the stream flow is influenced and the water is pushed against the obstacles. The velocity increases at the positions behind the obstacles and decreases at the positions between the obstacles. This aspect of blockage is very interesting in further research in 2 dimensions concerning the influences of vegetation patches on the flow.

The influence of floating vegetation on the roughness characteristics of flow has been investigated under laboratory circumstances. As this is a new topic in the study of integrated river ecosystems, the information is useful for setting up guidelines in the management of waterways and flooding protection. It has been shown that determination of Manning's coefficient requires large accuracy due to the small fall of the water level, certainly in the flume without obstacles. Manning's coefficient caused by the plants was independent of the flow velocity, but strongly dependent on the water level in the flume. This indicates that the stream flow resistance is especially caused by obstruction.

Related to mowing patterns and macrophyte growth in patches in rivers, Manning's coefficient will vary over the width and the length of the channel. The more sections are marked with a higher Manning's coefficient, the higher the upstream water level. This level only depends on the number of sections with higher Manning's coefficient, not on the location of the sections. As a result, for a constant discharge, mowing of vegetation to lower the upstream water level may happen in any part of the river. For varying discharge, however, the drained discharge is higher and the downstream water level will rise compared to the initial situation, while the upstream water level is lower. To avoid inundation, removing the vegetation in the downstream part of the river is advisable. The back water effect is more important if the higher roughness zone is located more in the middle. Border vegetation is less important than vegetation central in the stream.

In the field, the variation of Manning's coefficient as a function of time is indicated, high Manning values occur in full summer, while lowest values are measured in winter situations. These measurement results, varying in time, correspond to a variation of discharge and amount of biomass in the river. The relation between biomass, discharge and Manning's coefficient is further explored and supported by measurement results over 4 years.
As velocity profiles were investigated in the laboratory flume, results of velocities in the river Aa over the cross section are presented. Due to vegetation growth, the wetted cross section is larger in summer conditions, while velocities are smaller. Presence of biomass in the river results in blockage, this parameter gains importance in 2 dimensions due to the patchy occurrence of macrophytes. Knowing the amount of biomass in the river and the wetted cross section, the part of the cross section blocked by vegetation is calculated. Quantitative information on the relation between flow

characteristics and macrophytes is limited, next to the lack of information about the relation between macrophyte behaviour and velocity. Therefore, calculations for the river Aa are carried out and are compared to results obtained in three other rivers.

The Strive model was developed to incorporate the surface water model into an environmental package. Data collection was carried out in the river Aa over three years. This extended data set, based on hydraulic as well as biological and chemical parameters, allows calibration of the Strive model, which results in a well tested code with accurate and reliable results.

The model is tested in steady state as well as in unsteady state conditions and is compared to analytical solutions as well as to other numerical, hydraulic, (Hec-Ras) solutions. A sensitivity analysis is carried out to get familiar with the interaction of biomass and the hydraulic parameters. Study of the possible boundary conditions confirms that the discharge as upstream boundary and the calibration formula of the weir as downstream boundary condition results into the most accurate values. Therefore, use of tracer values (as the electrical conductivity) is also tested and seemed a useful alternative. The interaction between discharge, water level and electrical conductivity is shown. Based on the hydrodynamic aspect of the study, first aim is to model discharges and water levels in an accurate way. Therefore, not only the best fit between measured and modelled results is considered, but also specific attention is paid to model peak as well as base flow. Modelling of the electrical conductivity is important for calculation of retention and residence time. Calculation results show the influence of the resistance on both flow and water levels.

The performed measurements resulted in a dataset useful to study physical processes in rivers and flumes. In a second phase, this dataset was also used for calibration and validation of the Strive model. Discharge, water level, but also values of the electrical conductivity are used to determine the values of the parameters in the Strive model. The most important parameter in the flow equations is Manning's coefficient [1, 2].

Measurements as well as modelling showed that Manning's coefficient depends on discharge and biomass and is the most important parameter for the model. Three relationships between Manning and discharge are set up, 2 short-term and 1 long-term relationship. The long-term relationship, including biomass, for Manning's coefficient and discharge causes deviations on modelling discharge, water level and electrical conductivity.

Therefore, for each measurement campaign, short-term relationships between discharge and Manning's coefficient are set up, based on the idea that the biomass is kept constant over that small period. A long-term relationship allows continuous modelling but includes sometimes large spreading on the results inherent to natural processes. Short-term relationships are very accurate but labour intensive. Afterwards, comparison of all 3 formulations of Manning's coefficient is made. It seemed that deviations on water level and electrical conductivity are small, while differences on peak discharges will reach up to 20 %. The accuracy, using the different relationships, depends on the spreading of the measured value compared to the relationship. A calibration and validation analysis based on a cost function delivers an objective criterion for studying model results. As ecosystem modelling is often based on trial and error, the Strive model and the above analysis allows a well-founded study of hydraulic and ecological processes.

Aspects of integrated modelling are studied more in detail. Lateral in- or outflow at a certain point as well as distributed in- or outflow is incorporated in the Strive model. As an extension to lateral in- and outflow, inundation areas are added to the model. Different solution methods are considered and different cases, depending on the water level in the channel and in the flooding cell, are discussed. An experimental setup is tested and several situations, including 1 or 2 storage areas connected with the river, are simulated. The Strive model allows to include the aspect of flooding for short rivers. Use of these methods in longer rivers indicates problems concerning the physical interpretation of wave propagation. The velocity of the wave in the river channel and the velocity of the wave in the flooding area need further study.

Integrated ecosystem modelling using the Strive package allows simulating aspects of water quantity (discharge, water level) and water quality (here chlorine, ammonium, nitrate, oxygen). The stream flow is modelled well using the Saint-Venant equations, transport is coupled to this flow by the advection-dispersion-reaction equation. Using this equation for the different measurement campaigns results into good agreement between modelled and measured values for conservative tracers as the electrical conductivity and the amount of chlorine in the river. Also for reactive tracers, good results are obtained when the reaction rate in the river is low (e.g. during the winter months). The University of Antwerp has dedicated its research to determining the reaction processes in the river Aa. Measurements are performed and waiting for analysis and incorporation

in the Strive model. Summarizing, integrated ecosystem modelling using the Strive package allows simulating aspects of water quantity (discharge, water level) and water quality (here chlorine, ammonium, nitrate, oxygen).

2 Other results of the FWO project

The study area considered in the FWO project, a part of the river Aa, has a length of almost 1.5 km, is located between two weirs and is characterized by a wealthy macrophyte growth. The biomass of the vegetation is measured over the years and results in maximum values of 500 g/m^2 [3–5]. Mass balances are performed for different periods throughout the year during measurement campaigns and allow a first analysis of transport and retention in the river. Discharge measurements at the upstream and downstream weir give water balances as a result. The different methods used result in comparable values [6]. Lateral water exchange between the river and the groundwater is researched by temperature measurements in the water bottom [7]. A strong spatial variation is found and is integrated to come to an estimation of the water exchange [8–10]. The groundwater flux for the whole study area is about 0.1 m^3/s while the surface water discharge varies between 1 to 3 m^3/s.

Based on water balances and the measured concentrations, balances for nutrients are formulated [11, 12]. [11] concluded that during the growth season of the macrophytes, 5 to 13 % of the incoming nitrogen is captured in the river reach. Further experiments to determine ammonium and nitrate uptake, for different conditions of nutrient concentration and stream velocity, are performed in a flume and described in [13, 14]. The ammonium uptake by plants was the largest. Taking into account the measured nitrogen uptake velocity of the plants and the measured biomass density, in the river Aa, the plants only take 3 to 13 % of the total nitrogen retention [11, 12, 15, 16]. Also lower stream velocities and higher denitrification by presence of macrophytes will lead to an indirect nitrogen retention.

Based on measurements, process relations for implementation in a river-ecosystem model are built. The water flow (discharge and water level) is strongly influenced by the resistance to flow, e.g. by the amount of in-flow vegetation. The effect of macrophytes on the stream flow is expressed by the Manning coefficient [17–19] which is up to 10 times higher in summer as in winter conditions. The macrophyte growth cycle is modelled, based on measured data, light and temperature [3]. The biomass has a high grow and die velocity which has consequences for the amount of nutrients in the

system. Model results show that the presence of macrophytes in the river enlarge the residence time of the water in the river [20]. Further, experiments in the flume are performed to obtain a relation between the morphology of the plants (emergent, submerged, floating) and the resistance to flow [21–23]. These low scale results are difficult to implement in river ecosystem models.

The difficulty with the development of integrated numerical ecosystem models, which have to describe feedback relations in and between the different parts of the system, is that all parts are situated in their own model environment. In this project, the integrated modelling is performed in the 'Femme' environment [24, 25]. This structure allows the integration of different processes. This model development resulted in the Strive code for describing ecosystem processes [26, 27].

3 Recommendations for further research

At the end of this work, aspects for further research are gathered.

A 1D approach of river flow is a good start. A lot of processes are already incorporated in the model code. A 1D study also allows use of the Saint-Venant equations which are solvable in a short computer calculation time. The world of ecosystems is complex and a 1D study allows comprehension in the best possible way. However, the flow structure in rivers with substantial macrophyte growth, common in most lowland streams, is 3-dimensional. This has important implications for hydraulic modelling as velocities occur in 3 directions and obstructions in the river as biomass patches are no 1D objects. 2D or even 3D research allows more detailed knowledge of flow and transport in rivers.
As a continuation of the current research, the forthcoming project (*'Linking optical imaging techniques and 2D modelling for studying spatial heterogeneity in vegetated streams and rivers'*, Fonds voor Wetenschappelijk Onderzoek) is waiting to start. The measurement techniques, code and the interaction processes used and studied in this research will be studied in 2 dimensions. Then, the implementation of inundation areas, as a quasi 2D or full 2D technique, gains importance. Filling and emptying of storage basins is an important topic in the study of river hydraulics. The study of the size and the location of the flooding area results in guidelines for management.

Attention has to be paid to the simplification of the measurements. The determination of the discharge with propellers or electromagnetic instru-

ments in rivers, as is done in this research, is an intensive task. It demands for good equipment, trained people and a lot of time. Concerning the river Aa, registration of the position of the downstream weir in the studied reach and use of the calibration formula and the registration of the water level already allows continuous determination of the discharge.

Understanding the extent of energy losses through turbulence production may be a useful avenue for moving towards a less empirically based approach to flow resistance [28]. Here, additional turbulence production through the interaction of the flow with the vegetation is controlled in a rudimentary way.

Here, an extended study concerning the river Aa is performed, including plenty of results. A next step in ecosystem research is the use of the results in other river systems. Are the obtained formulas useful in other rivers and river systems? How we have to deal with larger or smaller river systems, with other types of macrophytes, with other amounts of biomass, with other bottom types?
Attention to this aspect is paid by implementing Biebrza river in the Strive model. Up till know, results are very limited due to the lack of data and measurement results available. Thesis work (*'Numerical modelling of the Biebrza river (Poland) using the Strive model'*, *'Ecohydraulic modelling of the Crocodile river and the Hartbeespoortdam using Strive (South Africa)'* and *'Modelling of the waterflow and pollutant transport in the Oranjerivier (South Africa)'*) continues the extension to other study areas.
As the Strive package is used in several projects, a manual is useful and in preparation.

Furthermore, in-stream vegetation does not occur in a single position. Macrophyte growth in rivers is typically patchy and, therefore, experimental work should be directed towards understanding the effect of vegetation patches or individual large plants and their arrangement on the flow dynamics. In order to understand flow resistance and help in the management of aquatic vegetation in rivers where flood defence is an important consideration, the contribution of the different components of the flora at different seasons, flow depths and velocities must be recognized and quantified.

Finally, interchange with biochemical researchers is important to include the modelling of reactive tracers in rivers. Transport is already included by the advection-dispersion equation, but calibration concerning the different ecological processes in river ecosystems is necessary.

References

[1] L. De Doncker, P. Troch, R. Verhoeven, K. Buis, N. Desmet, and P. Meire. *Numerical simulation of the interaction between ecological processes and surface water flow making use of the coupled Strive model*. Journal of Hydroinformatics, 2009. In review.

[2] L. De Doncker, P. Troch, R. Verhoeven, K. Buis, N. Desmet, and P. Meire. *Importance of Manning's coefficient for the calibration of the coupled Strive model*. River Research and Applications, 2009. In review.

[3] N. Desmet, S. Van Belleghem, P. Seuntjens, and P. Meire. *Water quality modelling in vegetated rivers*. In Man and River Systems - Interactions among rivers, their watersheds, and the sociosystem, Paris, 2006. The 2nd international symposium on Man and River Systems.

[4] S. Van Belleghem. *Macrophytes in the Nete catchment*. 2009. In preparation.

[5] S. Van Belleghem, E. De Deckere, K. Bal, and P. Meire. *Estimating macrophyte biomass in a lowland river: a critical analysis of different methods*. 2009. In preparation.

[6] L. De Doncker, P. Troch, and R. Verhoeven. *Accuracy of discharge measurements in a vegetated river*. Flow Measurement and Instrumentation, 19:29–40, 2008.

[7] C. Anibas, O. Batelaan, K. buis, A. Getachew, P. Meire, and R. Verhoeven. *Determination of groundwater fluxes in the Belgian Aa river via sensing and simulation of streambed temperatures*. Surface Water - Groundwater Interactions: process understanding, conceptualization and modelling (IAHS Publication), 32, 2009. in review.

[8] C. Anibas, O. Batelaan, K. Buis, P. Meire, and R. Verhoeven. *Kwantificering van grondwater-oppervlakte water interactie: analyse van temperatuur gradinten in de rivierbedding van de Aa*. Water, 2007.

[9] C. Anibas, O. Batelaan, K. Buis, L. De Doncker, N. Desmet, S. Van Belleghem, and P. Troch. *Interactions between groundwater flow, stream flow and plant growth in lowland rivers*. In preparation.

[10] C. Anibas, O. Batelaan, K. Buis, L. De Doncker, and P. Troch. *Quantification of the groundwater-surface water interaction by measuring temperature gradients in the streambed*.

[11] N. Desmet, S. Van Belleghem, P. Seuntjens, T. Bouma, K. Buis, and P. Meire. *Quantification of the impact of macrophytes on oxygen dynamics and nitrogen retention in a vegetated lowland river*. Physics and Chemistry of the Earth, 2008.

[12] S. Van Belleghem, K. Buis, N. Brion, N. Desmet, E. De Deckere, F. Dehairs, and P. Meire. *The role of macrophytes in nutrient dynamics in a macrophyte rich lowland river in Belgium*. 2009. In preparation.

[13] N. Desmet, S. Van Belleghem, T. Bouma, L. Van Duren, E. De Deckere, K. Buis, P. Seuntjens, and P. Meire. *Nitrogen uptake by macrophytes on the effect of N-form, current velocity and location*. In preparation.

[14] S. Van Belleghem, N. Desmet, K. Buis, E. De Deckere, L. Van Duren, T. Bouma, and P. Meire. *The assimilation of 15N by three different macrophytes under enforced stream conditions in a flume*. 2009. In preparation.

[15] N. Desmet, S. Van Belleghem, P. Seuntjens, and P. Meire. *Quantifying the contribution of plant uptake to nutrient retention: example of a vegetated river*. In Tartu University, editor, Wetland Pollutant Dynamics and Control, Proceedings of the International Symposium WETPOL 2007, 2007.

[16] S. Van Belleghem, K. Bal, N. Desmet, E. De Deckere, and P. Meire. *The role of macrophyte biomass in nutrient assimilation in a Belgian lowland river (the Aa)*. 2009. In preparation.

[17] L. De Doncker, P. Troch, R. Verhoeven, K. Bal, and P. Meire. *Determination of the Manning roughness coefficient influenced by vegetation in the river Aa and Biebrza river*. In review, 2008.

[18] L. De Doncker, P. Troch, R. Verhoeven, N. Desmet, K. Buis, and P. Meire. *Stromingsweerstand in rivieren door de aanwezigheid van macrofyten*. Water, 2007.

[19] L. De Doncker, P. Troch, R. Verhoeven, N. Desmet, and P. Meire. *Relation between resistance characteristics due to aquatic weed growth and the hydraulic capacity of the river Aa*. River Research and Application, 2008. DOI: 10.1002/rra.1240.

[20] K. Buis, C. Anibas, K. Bal, R. Banasiak, L. De Doncker, N. Desmet, M. Gerard, S. Van Belleghem, O. Batelaan, P. Troch, R. Verhoeven, and P. Meire. *Fundamentele studie van uitwisselingsprocessen in rivierecosystemen - gentegreerde modelontwikkeling*. Water, 2007.

[21] K. Bal, T. Bouma, K. Buis, E. Struyf, and P. Meire. *Trade-offs related to aquatic plant-growth strategies: how to maximize light interception while minimizing drag?* In preparation.

[22] N. Desmet, L. De Doncker, S. van Belleghem, P. Seuntjens, T. Bouma, K. Buis, R. Verhoeven, and P. Meire. *About the effect of submerged, floating and emergent freshwater macrophytes on flow and transport (I) - Velocity profiles, turbulence and flow resistance*. In preparation.

[23] N. Desmet, L. De Doncker, S. van Belleghem, P. Seuntjens, T. Bouma, K. Buis, R. Verhoeven, and P. Meire. *About the effect of submerged, floating and emergent freshwater macrophytes on flow and transport (I) - Scale dependent dispersion in relation to flow velocity, biomass density and plant morphology*. In preparation.

[24] K. Soetaert, V. de Clippele, and P. Herman. *Femme, a flexible environment for mathematically modelling the environment*. Ecological Modelling, (151):177–193, 2002.

[25] K. Soetaert, V. de Clippele, and P. Herman. *Femme: a flexible environment for mathematically modelling the environment*. NIOO: Netherlands Institute of Ecology, 2006.

[26] K. Buis. *Strive: Modelling riverecosystems - Manual*. Technical report, University of Antwerp, 2009.

[27] K. Buis. *Strive: Modelling riverecosystems*. 2009. In preparation.

[28] P. Naden, P. Rameshwaran, O. Mountford, and C. Robertson. *The influence of macrophyte growth, typical of eutrophic conditions, on river flow velocities and turbulence production*. Hydrological Processes, (20):3915–3938, 2006.

9
Appendix

A

Coefficients of the Saint-Venant equations

Continuity equation:

$$H_j \Delta z_{j+1} + I_j \Delta Q_{j+1} = \quad C_j \Delta z_j + D_j \Delta Q_j + G_j \tag{A.1}$$

$$\begin{aligned}
H_j &= 1 - 4\theta \frac{\Delta t}{\Delta x} \frac{Q_{j+1} - Q_j}{(B_{j+1} + B_j)^2} (tan(Tal_{j+1}) + (tan(Tar_{j+1})) \\
&\quad - q_{lat} 4\theta \Delta t (tan(Tal_{j+1}) + (tan(Tar_{j+1})) \frac{1}{(B_{j+1} + B_j)^2} && \text{(A.2)} \\
I_j &= 4\theta \frac{\Delta t}{\Delta x} \frac{1}{B_{j+1} + B_j} && \text{(A.3)} \\
C_j &= -1 + 4\theta \frac{\Delta t}{\Delta x} \frac{Q_{j+1} - Q_j}{(B_{j+1} + B_j)^2} (tan(Tal_j) + (tan(Tar_j)) \\
&\quad + q_{lat} 4\theta \Delta t (tan(Tal_j) \\
&\quad + (tan(Tar_j)) \frac{1}{(B_{j+1} + B_j)^2} && \text{(A.4)} \\
D_j &= I_j && \text{(A.5)} \\
G_j &= - 4 \frac{\Delta t}{\Delta x} \frac{Q_{j+1} - Q_j}{B_{j+1} + B_j} - q_{lat} 4\Delta t \frac{1}{(B_{j+1} + B_j)} && \text{(A.6)}
\end{aligned}$$

Momentum equation:

$$H_j^{'}\Delta z_{j+1} + I_j^{'}\Delta Q_{j+1} = \quad C_j^{'}\Delta z_j + D_j^{'}\Delta Q_j + G_j^{'} \tag{A.7}$$

$$\begin{aligned} H_{1j}^{'} &= \theta\frac{\Delta t}{\Delta x}g(A_{j+1} + A_j + B_{j+1}(z_{j+1} - z_j)) \\ &\quad +g\theta\Delta t\frac{Q_{j+1}|Q_{j+1}|}{k_{j+1}^2}(B_{j+1} - \frac{2A_{j+1}dk_{j+1}}{k_{j+1}}) \end{aligned} \tag{A.8}$$

$$I_{1j}^{'} = 2g\theta\Delta t\frac{A_{j+1}|Q_{j+1}|}{k_{j+1}^2} \tag{A.9}$$

$$\begin{aligned} C_{1j}^{'} &= -\theta\frac{\Delta t}{\Delta x}gB_j(z_{j+1} - z_j) + \theta\frac{\Delta t}{\Delta x}g((A_{j+1} + A_j) \\ &\quad -g\theta\Delta t\frac{Q_j|Q_j|}{k_j^2}(B_j - \frac{2A_j dk_j}{k_j}) \end{aligned} \tag{A.10}$$

$$D_{1j}^{'} = -2g\theta\Delta t\frac{A_j|Q_j|}{k_j^2} \tag{A.11}$$

$$\begin{aligned} G_{1j}^{'} &= -g\frac{\Delta t}{\Delta x}(z_{j+1} - z_j)(A_{j+1} + A_j) \\ &\quad -g\Delta t(\frac{A_{j+1}Q_{j+1}|Q_{j+1}|}{k_{j+1}^2} + \frac{A_j Q_j(|Q_j|)}{k_j^2}) \end{aligned} \tag{A.12}$$

$$
\begin{aligned}
H'_{2j} &= -\frac{1}{2}\left(\frac{Q_{j+1}B_{j+1}}{A_{j+1}} + \frac{Q_jB_j}{A_j}\right) - \theta\alpha\frac{\Delta t}{\Delta x}\left((Q_{j+1}-Q_j)\left(\frac{Q_{j+1}B_{j+1}}{A^2_{j+1}}\right)\right. \\
&\quad -\theta\frac{\Delta t}{\Delta x}B_{j+1}\left(\frac{Q^2_{j+1}}{A^2_{j+1}} + \frac{Q^2_j}{A^2_j} - \frac{Q^2_{j+1}}{A^3_{j+1}}(A_{j+1}-A_j)\right) \\
&\quad +\theta\frac{\Delta t}{\Delta x}g(A_{j+1}+A_j+B_{j+1}(z_{j+1}-z_j)) \\
&\quad +g\theta\Delta t\frac{Q_{j+1}|Q_{j+1}|}{k^2_{j+1}}\left(B_{j+1} - \frac{2A_{j+1}dk_{j+1}}{k_{j+1}}\right) \\
&\quad +\theta g\Delta t q_{lat}\frac{Q_{j+1}B_{j+1}}{A^2_{j+1}} \qquad \text{(A.13)} \\
I'_{2j} &= 1 + 2\alpha\frac{\Delta t}{\Delta x}\left(\frac{Q_{j+1}}{A_{j+1}} + \frac{Q_j}{A_j} - \frac{Q_j}{A_{j+1}} - \left(\frac{2Q_{j+1}}{A^2_{j+1}}\right)(A_{j+1}-A_j)\right) \\
&\quad +2g\theta\Delta t\frac{A_{j+1}|Q_{j+1}|}{k^2_{j+1}} - q_{lat}\Delta t\frac{\theta}{A_{j+1}} \qquad \text{(A.14)} \\
C'_{2j} &= \frac{1}{2}\left(\frac{Q_{j+1}B_{j+1}}{A_{j+1}} + \frac{Q_jB_j}{A_j}\right) + \theta\frac{\Delta t}{\Delta x}\left((Q_{j+1}-Q_j)\frac{Q_jB_j\alpha_j}{A^2_j}\right) \\
&\quad -\theta\frac{\Delta t}{\Delta x}\alpha B_j\left(\frac{Q^2_{j+1}}{A^2_{j+1}} + \frac{Q^2_j}{A^2_j} + \frac{Q^2_j}{A^3_j}(A_{j+1}-Aj)\right) \\
&\quad -\theta\frac{\Delta t}{\Delta x}gB_j(z_{j+1}-z_j) + \theta\frac{\Delta t}{\Delta x}g((A_{j+1}+A_j) \\
&\quad -g\theta\Delta t\frac{Q_j|Q_j|}{k^2_j}\left(B_j - \frac{2A_jdk_j}{k_j}\right) \\
&\quad -\theta\Delta t q_{lat}\frac{Q_jB_j}{A^2_j} \qquad \text{(A.15)} \\
D'_{2j} &= -1 + \theta\frac{\Delta t}{\Delta x}\left(Q_{j+1}\left(\frac{1}{A_j} - \frac{1}{A_{j+1}}\right) + \left(\frac{-2Q_j}{A_j}\right) - (A_{j+1}-A_j)\frac{2Q_j}{A^2_j}\right) \\
&\quad -2g\theta\Delta t\frac{A_j|Q_j|}{k^2_j} + q_{lat}\Delta t\frac{\theta}{A_j} \qquad \text{(A.16)} \\
G'_{2j} &= -\frac{\Delta t}{\Delta x}\left(\left(\frac{Q_{j+1}}{A_{j+1}} + \frac{Q_j}{A_j}\right)(Q_{j+1}-Q_j) + \left(\frac{Q^2_{j+1}}{A^2_{j+1}} + \frac{Q^2_j}{A^2_j}\right)(A_{j+1}-A_j)\right. \\
&\quad -g(z_{j+1}-z_j)(A_{j+1}+A_j) \\
&\quad -g\Delta t\left(\frac{A_{j+1}Q_{j+1}|Q_{j+1}|}{k^2_{j+1}} + \frac{A_jQ_j(|Q_j|)}{k^2_j}\right) \\
&\quad \left.+q_{lat}\Delta t\left(\frac{Q_{j+1}}{A_{j+1}} + \frac{Q_j}{A_j}\right)\right) \qquad \text{(A.17)}
\end{aligned}
$$

$$
\begin{aligned}
H_{3j}^{'} &= -\frac{1}{2}(\frac{Q_{j+1}B_{j+1}}{A_{j+1}} + \frac{Q_jB_j}{A_j}) + \theta\frac{\Delta t}{\Delta x}(-(Q_{j+1}-Q_j)(\frac{Q_{j+1}B_{j+1}\alpha_{j+1}}{A_{j+1}^2}) \\
&\quad -\theta\frac{\Delta t}{\Delta x}B_{j+1}(\frac{Q_{j+1}^2\alpha_{j+1}}{A_{j+1}^2} + \frac{Q_j^2\alpha_j}{A_j^2} - \frac{Q_{j+1}^2}{A_{j+1}^3B_{j+1}}((A_{j+1}-A_j)(2\alpha_{j+1}B_{j+1}))) \\
&\quad +\theta\frac{\Delta t}{\Delta x}g(A_{j+1}+A_j+B_{j+1}(z_{j+1}-z_j)) \\
&\quad +g\theta\Delta t\frac{Q_{j+1}A|Q_{j+1}|}{k_{j+1}^2}(B_{j+1} - \frac{2A_{j+1}dk_{j+1}}{k_{j+1}}) \\
&\quad +\theta\Delta t q_{lat}\frac{Q_{j+1}B_{j+1}}{A_{j+1}^2} \qquad \text{(A.18)} \\
I_{3j}^{'} &= 1+\theta\frac{\Delta t}{\Delta x}(\frac{Q_{j+1}}{A_{j+1}} + \frac{Q_j}{A_j} + \frac{Q_{j+1}-Q_j}{A_{j+1}} - (A_{j+1}-A_j)(\frac{2Q_{j+1}}{A_{j+1}^2}) \\
&\quad -2g\theta\Delta t\frac{A_{j+1}|Q_{j+1}|}{k_{j+1}^2} - q_{lat}\Delta t\frac{\theta}{A_{j+1}} \qquad \text{(A.19)} \\
C_{3j}^{'} &= \frac{1}{2}(\frac{Q_{j+1}B_{j+1}}{A_{j+1}} + \frac{Q_jB_j}{A_j}) + \theta\frac{\Delta t}{\Delta x}((Q_{j+1}-Q_j)\frac{Q_jB_j\alpha_j}{A_j^2}) \\
&\quad -\theta\frac{\Delta t}{\Delta x}B_j(\frac{Q_{j+1}^2\alpha_{j+1}}{A_{j+1}^2} + \frac{Q_j^2\alpha_j}{A_j^2} + \frac{Q_j^2}{A_j^2}((A_{j+1}-Aj)(-\frac{2\alpha_jB_j}{A_j}))) \\
&\quad -\theta\frac{\Delta t}{\Delta x}gB_j(z_{j+1}-z_j) + \theta\frac{\Delta t}{\Delta x}g((A_{j+1}+A_j) \\
&\quad -g\theta\Delta t\frac{Q_j|Q_j|}{k_j^2}(B_j - \frac{2A_jdk_j}{k_j}) \\
&\quad -\theta\Delta t q_{lat}\frac{Q_jb_j}{A_j^2} \qquad \text{(A.20)} \\
D_{3j}^{'} &= -1+\theta\alpha\frac{\Delta t}{\Delta x}(Q_{j+1}(-\frac{1}{A_j} + \frac{1}{A_{j+1}}) + (A_{j+1})(\frac{2Q_j}{A_j^2}) \\
&\quad -2g\theta\Delta t\frac{A_j|Q_j|}{k_j^2} + q_{lat}\Delta t\frac{\theta}{A_j} \qquad \text{(A.21)} \\
G_{3j}^{'} &= -\frac{\Delta t}{\Delta x}(\alpha(\frac{Q_{j+1}}{A_{j+1}} + \frac{Q_j}{A_j})(Q_{j+1}-Q_j) - (\frac{Q_{j+1}^2}{A_{j+1}^2} + \frac{Q_j^2}{A_j^2})\alpha(A_{j+1}-A_j) \\
&\quad +g(z_{j+1}-z_j)(A_{j+1}+A_j)) \\
&\quad -g\Delta t(\frac{A_{j+1}Q_{j+1}|Q_{j+1}|}{k_{j+1}^2} + \frac{A_jQ_j|Q_j|}{k_j^2}) \\
&\quad +q_{lat}\Delta t(\frac{Q_{j+1}}{A_{j+1}} + \frac{Q_j}{A_j}) \qquad \text{(A.22)}
\end{aligned}
$$

B
Strive: flowchart

ModelComponents

- initialisation of variables needed in other routines (volumes, concentration)
  System
  TimestepIni
- processes in the surface water
  Reaction
- specific compartments in the river or stream
  MacrophyteGrowth
  MacrophyteReaction
- specific lateral connections
  Slootbeek
- transport in the stream or river
  TransWater
  TransSolute
  TransSolids
- mass balances and specific output formulations
  SysPropwater
  SysPropSolute

PROGRAM Strive
use ModuleTime (to know time units in Femme)
TimeUnit = 'sec' (specify time units)
call XSimulate() (gives control to Femme)

XSTART() (model initialisation BEFORE reading initial conditions and forcing files)
InitialiseSystem
InitialiseTimestepIni
InitialiseReaction
InitialiseMacrophyteGrowth
InitialiseMacrophyteReaction
InitialiseSlootbeek
InitialiseTransWater
InitialiseTransSolute
InitialiseTransSolids
InitialiseSysPropwater
InitialiseSysPropSolute

* initialisatie variabelen (=0)
* initialisatie 'default initial situation'
* effective values by parameters.dec (<> 0)

- <WriteToScreen@StartOnly>
- <ToggleOffReadingForcingFunctions>

InitialiseSystem

- use ModuleComBlock (to have access to declarations in XmoduleDeclaration.f90, makes available the values of the parameters and variables that were declared in the declaration files)
- use ModuleInterface (to get acces to internal functions, eg. XGetCurrentTime)

- BoxLength=StreamLength/(NoI-1)
- Distance(I)=...
- InitDistance(I)=
- Initialisation of

- Zbot(I) = f(Zbottombegin, ZbottomEnd)
- Zwaterlevel(I) = f(ZwaterlevelBegin, ZwaterlevelEnd)
- Discharge(I) = f(DischargeBegin, DischargeEnd)
- Dwarsdoorsnede (Trap: WidthBottom(I)=constant, Tal(I) = Tal-Constant, Tar(I)=tarConstant)

InitialiseTimestepIni
use ModuleComBlock

InitialiseReaction
use ModuleComBlock

InitialiseMacrophyteGrowth
use ModuleComBlock
- initialise state variable: MacrophyteBiomass(I)
- create constant forcing: Growth, Mortality = 0; Temp, Ilight = constant

InitialiseMacrophyteReaction
use ModuleComBlock
-Q10fac?
-calculation of Macrophyte$_{Nuptakerate}$

InitialiseSlootbeek
use ModuleComBlock
-BoxIntegerCalc: distances become boxes

InitialiseTransWater
use ModuleComBlock (to have access to declarations in XmoduleDeclaration.f90)
use ModuleInterface

- Initialisation of:

- ([Q/Z/H]sv(I)=[Q/Z/H]T0)
- Qsv(I)=Discharge(I)
- Zsv(I) = Zwaterlevel(I)
- Qlat(I) = f(qlatBegin, qlatEnd)

- Initialisation of variables:

- $[E/F/L/M/N]_{ds}$=0

- Delta[Q/Z]=0
- set zj,zj1,Qj,Qj1,qlatj = 0
- set aj,aj1,bj,bj1,kj,kj1 = 0
- set dPj,dPj1,dRj,dRj1,Dkj,Dkj1 = 0

- up-and downstream boundary conditions:

Q/Z [Up/Down]stream$_{oldtimelevel}$ = [Q/Z]T0

set theta,alfa

InitialiseTransSolute
use ModuleComBlock
initial concentration of solutes: ECt0, Clt0, O2t0, NO3t0, NH4t0

InitialiseTransSolids
use ModuleComBlock
initial concentration of solids (direct or calcpFdet(?)): Fdet(M)t0, Sdet(M)t0, SSt0

InitialiseSysPropWater
use ModuleComBlock

InitialiseSysPropSolute
use ModuleComBlock

- read *.frc files (by using helping variables, bv. Qupstream = fQupstream)
- read *.ini files (directly reading of variables, bv. Zbot - Distance - Value)

XSTART2() (model initialisation AFTER reading initial conditions and forcing files)
InitialiseSystem2
InitialiseTimestepIni2
InitialiseReaction2
InitialiseMacrophyteGrowth2
InitialiseMacrophyteReaction2
InitialiseSlootbeek2
InitialiseTransWater2

InitialiseTransSolute2
InitialiseTransSolids2
InitialiseSysPropwater2
InitialiseSysPropSolute2

*calculation of derived variables based on the initial situation or the reading in of *.ini en *.frc-files

InitialiseSystem2

- use ModuleComBlock
- useModuleInterface
- berekening van [wA,wP,wWidth](I) (case trapezium!)
- berekening van VolumewA(I), VolumeQ(I), VolumewAtot, VolumeQtot

InitialiseTimestepIni2
use ModuleComBlock

InitialiseReaction2
use ModuleComBlock

InitialiseMacrophyteGrowth2
use ModuleComBlock

InitialiseMacrophyteReaction2
use ModuleComBlock
calculation pFdet (?)

InitialiseSlootbeek2
use ModuleComBlock

InitialiseTransWater2
use ModuleComBlock
useModuleInterface

- determination of Manning coefficient and angle of the weir
- hydraulic model with cte Q value

InitialiseTransSolute2
use ModuleComBlock

- calculate state variables from concentrations: ECmass(I), Clmass(I), O2mass(I), NO3mass(I), NH4mass(I)
- longitudinal dispersion: bulkdispersion(I)

InitialiseTransSolids2
use ModuleComBlock

InitialiseSysPropWater2
use ModuleComBlock

- calculation of reference situation
  - Qlattot=0
  - [VolumeRef(I)=Volume(I)]
  - [WaterStorage, WaterStoragerate, WaterLatFlux, WaterReaction](I) = 0
  - Lateral exchange
  - VolumeTotRef = VolumeTot
  - WaterStorageTot, WaterLatFlucTot, WaterreactionTot, WaterMBTotRun, VolumeRunUpstream, VolumeRunDownstream, DischargeVoltotRun, Qlattotrun = 0

InitialiseSysPropSolute2
Total mass of components in the surface water is calculated.
Comparison with a reference situation is made.
For each solute a subroutine is called that generates the mass balances.
In here the initial conditions are set.

XSUBMODS() [for each timestep]
DynamicsSystem
DynamicsTimestepIni
DynamicsReaction
DynamicsMacrophyteGrowth
DynamicsMacrophyteReaction
DynamicsSlootbeek
DynamicsTransWater

DynamicsTransSolute
DynamicsTransSolids
DynamicsSysPropwater
DynamicsSysPropSolute

- boundary conditions as a function of time

- <> (state) variables in <> different types of models are changed into one state variable

DynamicsSystem
berekening van [wA,wP,wWidth](I) (case trapezium!)
berekening van VolumewA(I), VolumeQ(I), VolumewAtot, VolumeQtot

DynamicsTimestepIni2
use ModuleComBlock
calculation of concentration based on mass and volume: EC(I) = ECmass(I)/Volume(I)

DynamicsReaction2
use ModuleComBlock
- temp. dependency: Q10 factor for mineralisation rate and other processes
- mineralisation and decomposition, decay constants at the temperature (rFdet, rSdet, rFdetM, rSdetM, Fdet(M)min, Sdet(M)min, FdetMdecomp
- nitrification in the surface water: rnitri, nitrification(I)
- formulation of the rate of change of state variables: dFdet(M)Mass(I), dSdet(M)Mass(I), dO2Mass, dNH4mass, dNO3Mass

DynamicsMacrophyteGrowth2
Use ModuleComBlock
Use ModuleInterface
Calculate MacrophyteBiomassAVG/MacrophyteBiomassInterface
Macrophytegrowth:
- constant
- model with (boundary/forcing from sinusfunction of T and I) or (data from forcing file)

DynamicsMacrophyteReaction2
Use ModuleComBlock
- uptake of nutrients from the surface water: MaphyNuptakeM2(growth)

- integration to the whole river: dNH4mass, dO2mass
- production of macrophyte detritus: Mdetprod (FdetMprod+SdetMprod), dFdetMass, dSdetMass

DynamicsSlootbeek2
Use ModuleComBlock
Calculation of Qlatbox and dECmass, taking into account lateral flow

DynamicsTransWater
use ModuleComBlock
useModuleInterface

Determination up-and downstream boundary conditions as a function of the chosen type (constant (DischargeBegin), function of forcing (fQupstream))
Qupstream
Zupstream
Qdownstream
Zdownstream

- Determination of the Manning coefficient (constant/function)
- Determination of Qlat

Type of model according Wave Model: kin, par, sv, Q=cte

Case Saint Venant
DeltaT=XGetTimeStep()
DeltaX=BoxLength
Loopcounter=0+1=1!!

IF LoopCounter>=1 THEN
tt=XGetCurrentTime()
$T_{oldlevel}$=$T_{newlevel}$
$T_{newlevel}$= $T_{newlevel}$+DeltaT
DSCounter=0+1=1

Forward Sweep
$[E/F]_{ds}$(1) (from upstream BCs)
n,Talj,Talj1,Tarj,Tarj1
Hj(I),Ij(I),Cj(I),Dj(I),Gj(I)
$[L/M/N]_{ds}$(I)

H1j(I),I1j(I),C1j(I),D1j(I),G1j(I)
$[E/F]_{ds}$(I+1)

Backward Sweep
Delta[Z/Q](N) (from downstream BCs)
[Q/Z]sv(N)
Delta[Z/Q](I)
[Q/Z]sv(I)
[Q/Z][Up/Down]stream$_{oldtimelevel}$=f[Q/Z][Up/Down]stream

calculation of hydraulic characteristics
[wR,nM,K](I) (case trapezium!)
Update of Zwaterlevel and Qdischarge
ENDIF

DynamicsTransSolute2
use ModuleComBlock
useModuleInterface
- calculation of longitudinal dispersion
- upstream and downstream boundary conditions of the tracer
- subroutines: transport of tracers in the longitudinal direction (EC, Cl, O2, NO3, NH4)
- subroutine [Flux and dMass]
o Calculate the rate of mass change for the first compartment
o Calculate the rate of mass change for the last compartment
o Calculate the rate of mass change for the compartments inbetween

DynamicsTransSolids2
use ModuleComBlock
useModuleInterface
- Calculate the concentrations based on the total mass and volume (Fdet(M), Sdet(M))
- calculation of longitudinal dispersion
- upstream and downstream boundary conditions of the tracer
- subroutines: transport of tracers in the longitudinal direction (Fdet, Sdet, FdetM, SdetM, SS)
- subroutine [Flux and dMass]
o Calculate the rate of mass change for the first compartment
o Calculate the rate of mass change for the last compartment
o Calculate the rate of mass change for the compartments inbetween

DynamicsSysPropWater2
use ModuleComBlock
useModuleInterface
- Qlattot berekenen
- XGetTimeStep
- Calculation of WaterStorage and WaterLatFlux
- Calculation of Residence Time
- Calculation of Retention Time

DynamicsSysPropSolute2
use ModuleComBlock
useModuleInterface
- Subroutine SoluteMBdyn
- Subroutine SoluteRetention

XSTOP() FinaliseSystem
FinaliseTimestepIni
FinaliseReaction
FinaliseMacrophyteGrowth
FinaliseMacrophyteReaction
FinaliseSlootbeek
FinaliseTransWater
FinaliseTransSolute
FinaliseTransSolids
FinaliseSysPropwater
FinaliseSysPropSolute

<WriteResults>

END PROGRAM Strive

C

Parameters and variables in Strive

initial conditions		
[System-Parameters]		
Dischargebegin, DischargeEnd	m^3/s	initial discharge
ZwaterlevelBegin, ZwaterlevelEnd	m	initial water stage
boundary condition		
[TransWater-Parameters]		
UpstreamBoundaryType (Qup, Zup)		boundary condition
DownstreamBoundaryType (Qdown, Zdown, QZdown)		boundary condition
QUpstreamBoundaryType	m^3/s	boundary condition (Constant, Forcing, Sine)
ZUpstreamBoundaryType	m	boundary condition (Constant, Forcing, Sine)
QDownstreamBoundaryType	m^3/s	boundary condition (Constant, Forcing, Sine)
ZDownstreamBoundaryType	m	boundary condition (Constant, Forcing, Sine)
[TransWater-Forcings]		
fZUpstream	m	upstream boundary condition Z
fQUpstream	m^3/s	upstream boundary condition Q
fZDownstream	m	downstream boundary condition Z
fQDownstream	m^3/s	downstream boundary condition Q

Table C.1: Conventions (Part I)

physical characteristics		
[System-Parameters]		
StreamLength	m	total length of the modelled river
WidthBottomConstant	m	section width at bottom for rectangular/trapezodal cross-section
Zbottombegin, ZbottomEnd	m	initial conditions for bottom level
TalConstant, TarConstant		angle of river banks
Talj, Talj1, Tar, Tarj1		angle of river banks
[TransWater-Parameters]		
S_0	m/m	bottom slope S0 = sin(bottom angle) (NL: bodemverhang)
S_f	m/m	friction slope (NL: energieverhang)
qlatBegin, qlatEnd		initial parameters for linear lateral inflow
alfa		velocity distribution factor
run parameters		
[TransWater-Parameters]		
TotTime	s	total time
Toldlevel	s	tn, old time level
Tnewlevel	s	tn+1, new time level
LoopCounter	-	counter for general loop
DSCounter	-	counter for loop of double sweep algorithm
[TransWater-Constants]		
g	m/s^2	gravity
theta	-	factor for numerical stability
state variable declaration		
[TransWater-Variables]		
Discharge(NoI)	m^3/s	discharge for numerical model
Qkin(NoI)	m^3/s	discharge for kinematic equation
Hkin(NoI)	m	water height for kinematic equation
Qpar(NoI)	m^3/s	discharge for parabolic equation
Hpar(NoI)	m	water height for parabolic equation
[System-Variables]		
Zwaterlevel(NoI)	m	waterlevel for numerical model

Table C.2: Conventions (Part II)

ordinary variable declaration		
[TransWater-Variables]		
Qsv(NoI)	m^3/s	discharge for SV model
Zsv(NoI)	m	water level for SV model
qlat(NoI)	m^3/sm	lateral inflow
$QUpstream_{oldtimelevel}$	m^3/s	upstream boundary condition in previous loop (SV)
$ZUpstream_{oldtimelevel}$	m	upstream boundary condition in previous loop (SV)
$QDownstream_{oldtimelevel}$	m^3/s	downstream boundary condition in previous loop (SV)
$ZDownstream_{oldtimelevel}$	m	downstream boundary condition in previous loop (SV)
QUpstream	m^3/s	upstream boundary condition in new loop (SV)
ZUpstream	m	upstream boundary condition in new loop (SV)
QDownstream	m^3/s	downstream boundary condition in new loop (SV)
ZDownstream	m	downstream boundary condition in new loop (SV)
constanteQ	m^3/s	constant discharge as upstream boundary
double sweep variables		
[TransWater-Variables]		
E_{ds}(NoI)		
F_{ds}(NoI)		
L_{ds}(NoI)		
M_{ds}(NoI)		
N_{ds}(NoI)		
DeltaZ(NoI)		
DeltaQ(NoI)		

Table C.3: Conventions (Part III)

helping values		
[TransWater-Variables]		
celerity(NoI)		wave celerity
Kdispx(NoI)		dispersion coefficient
tt		
nom		
hulp		
hulp1		
hulp2		
hulp3		
hulp4		
aax		
[numerical discretisation]		
Δ T		time step
Δ X		cell distance
'section' parameters		
[TransWater-Variables]		
K(NoI)		conveyance
R, dRj, dRj1, wR(NoI)	m	hydraulic radius
n, nM(NoI)	$m^{-1/3}s$	Manning friction coefficient
aj	m^2	simplified wetted area at time n
aj1	m^2	simplified wetted area at time n+1
bj	m	section width at surface at time tn
bj1	m	section width at surface at time tn
kj		conveyance at time tn (Manning)
kj1		conveyance at time tn+1 (Manning)
dkj, dkj1		
dPj, dPj1		
zj	m	water level at time tn
zj1	m	water level at time tn+1
Qj	m^3/s	Qsv at time tn
Qj1	m^3/s	Qsv at time tn+1
qlatj	$m^3/s/m$	lateral inflow
continuity equation variables		
[TransWater-Variables]		
Hj(NoI)		
Ij(NoI)		
Cj(NoI)		
Dj(NoI)		
Gj(NoI)		

Table C.4: Conventions (Part IV)

momentum equation variables		according method 1, 2, 3
[TransWater-Variables] H1j(NoI) H2j(NoI) H3j(NoI) I1j(NoI) I2j(NoI) I3j(NoI) C1j(NoI) C2j(NoI) C3j(NoI) D1j(NoI) D2j(NoI) D3j(NoI) G1j(NoI) G2j(NoI) G3j(NoI)		
reach variables		
[System-Variables]		
Distance(NoB)	m	Distance to upstream boundary of centre of boxes
IntDistance(NoI)	m	Distance to upstream boundary of begin of boxes
BoxLength	m	Length of stream boxes
wA(NoI)	m^2	wetted cross-sectional area
wP(NoI)	m	wetted perimeter
wWidth(NoI)	m	section width at surface (NL: kombergingsbreedte, i.e. breedte aan wateroppervlak)
WidthBottom(NoI)	m	section width at bottom
Zwaterlevel	m	water level for numerical model
Zbot(NoI)	m	bottom level for SV model
Tal(NoI)	rad	angle of left bank
Tar(NoI)	rad	angle of right bank
[System-Constants] NoB NoI		
macrophyte characteristics		
[Macrophyte-Variables]		
biomassinterface(NoI)	g/m^2	amount of biomass at the interfaces of cells
biomass(NoB)	g/m^2	amount of biomass in the cells
macrophytes(NoB)	g/m^2	variable amount of vegetation in the reach
[Macrophyte-Parameters] BiomassType		
[Macrophyte-Forcings]		
MacrophyteValue	g/m^2	amount of biomass in the time

Table C.5: Conventions (Part V)

mass balance characteristics		
[Mass Balance-Parameters]		
VolumeCalcFactor		
[Mass Balance-Variables]		
Volume(NoB)	m^3	volume in each cell
VolumeMBCheck	m^3	volume based on waterlevels
VolumeQCheck	m^3	volume based on discharge
VolumeINtot	m^3	total incoming volume
VolumeOUTtot	m^3	total outgoing volume
VolumeStart	m^3	initial volume
DifMBandQ	m^3	difference between TotVolumeMB and TotVolumeQ
TotVolumeMB	m^3	total volume based on waterlevels
TotVolumeQ	m^3	total volume based on discharge

Table C.6: Conventions (Part VI)

D

Calibration of weir 4 at the river Aa

The calibration formula, for different positions of the downstream weir in the measurement reach, mentioned above, was determined in 1995 by the Hydraulics Laboratory (UGent) [1], using a scale model (scale: $1/5$) of the weir in the lab. Water levels were measured with electronic balances (accuracy 0.2 mm +/- 0.1 mm), discharge was registered with an electromagnetic discharge meter (accuracy 0.2 % of the exact value). The angle of the flap of the weir varied over 0, 10, 20, 30, 40 and 50 °, for submerged and free overflow. For an angle of 60 °, only measurements for free overflow were performed.

Expressions for the discharge over the weir are given in Eq. (D.1) and (D.2). Coefficients of these equations are gathered in Table D.1. The scale model is presented in Figure D.1 together with the parameters of the equations (h_{opw} = upstream water level [m TAW], h_{afw} = downstream water level [m TAW], h_{kr} = crest level [m TAW], a , b, m and n = parameter values in Eq. (D.1) and (D.2)).

Submerged flow

$$Q = a(h_{opw} - h_{kr})^b(1 - (\frac{h_{afw} - h_{kr}}{h_{opw} - h_{kr}})^m)^{(\frac{1}{n})} \quad \text{(D.1)}$$

Free flow

$$Q = a(h_{opw} - h_{kr})^b \quad \text{(D.2)}$$

Angle of weir [°]	h_{kr} [m TAW]	a	b	n	m
0	8.830	9.247	1.662	1.457	59.02
10	9.200	10.250	1.705	1.501	9.443
20	9.564	9.980	1.712	1.441	6.540
30	9.913	9.851	1.706	1.612	7.317
40	10.237	9.663	1.719	1.950	6.187
50	10.532	9.498	1.761	2.120	4.443
60	10.800	9.559	1.776	-	-

Table D.1: Calibration parameters

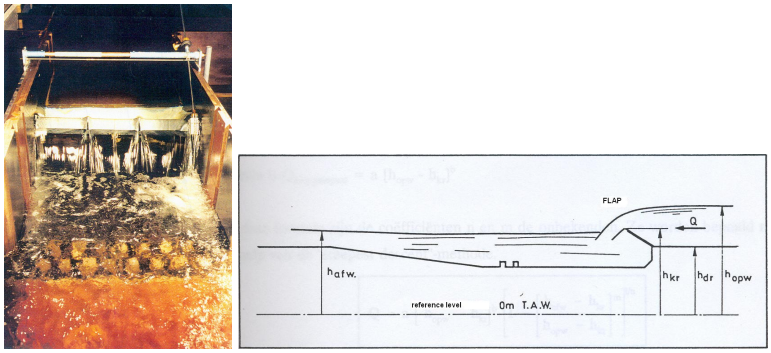

Figure D.1: The river Aa: scale model of the downstream weir and parameters used for the calibration of the weir

For coefficients a and b, following expressions are obtained, in which θ is the angle of the flap (°):

$$a = 9.565 + 0.02675\theta - 0.0005005\theta^2 \quad \text{(D.3)}$$

$$b = 1.675 + 0.001111\theta + 0.0000088869\theta^2 \quad \text{(D.4)}$$

Using these coefficients and for different positions of the weir following graph (Fig. D.2) is obtained by giving the relationship between discharge and upstream water level.

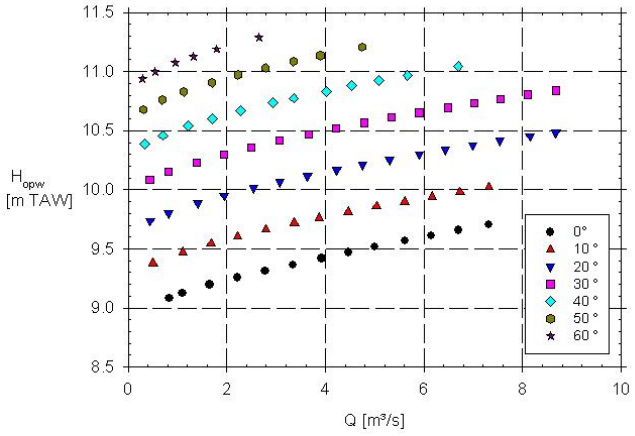

Figure D.2: Discharge for different positions of the weir and upstream water level, results of the calibration process

References

[1] L. Van Poucke. *Ijking van de stuw op de Aa te Poederlee*. Report of the hydraulics lab, department of civil engineering, in oder of the vlm, Ghent University, 1999.

E

Flood plains: solution methods for the numerical model

1 Internal storage: use of weirs (Method 1)

z_j<z_d and z_b<z_d: No flow exchange between the main channel and the storage cell. The continuity equation and the momentum equation do not change between node j and j+1.

z_b<z_d<z_j: The general equation for free flow over a weir is given by Poleni [1]:

$$Q_{in2} = \frac{2}{3} C_d l \sqrt{2g} h_p^{3/2} \tag{E.1}$$

with C_d is the loss coefficient, l is the width of the weir (which is smaller or equal to the distance between node 1 and j+1) and h_p is as indicated at Fig. 7.3. Eq.(E.1) determines the discharge flowing into the storage basin at node j. This internal boundary condition changes the continuity equation and momentum equation because a certain volume of water is taken out of the wave. During the forward sweep of the double sweep algorithm one calculates the coefficients E_j and F_j from the coefficients of node j-1. To continue the calculation, the coefficients in node j+1 are necessary. Consequently, the coefficients L_j, M_j and N_j are necessary to calculate Δz_j during the backward sweep when Δz_{j+1} and ΔQ_{j+1} are already known. All

these coefficients depend on the transition from node j to j+1 [2]. So if one wants to implement the effect of the cell on the wave, one has to interfere directly on the coefficients of the Saint-Venant continuity and momentum equation.

The continuity equation is:

$$Q_{j+1}^{n+1} = Q_j^{n+1} - Q_{in2} \tag{E.2}$$

and the momentum equation:

$$z_{j+1}^{n+1} = z_j^{n+1} \tag{E.3}$$

One can easily see that both sets of equations are complementary. The SaintVenant equations take care of the shifting and the flattening of the wave peak due to storage and the dissipation of energy by friction. Eq.(E.2) introduces the storage of a volume in the cell at time step n+1. The meaning of Eq.(E.3) is that no extra energy is dissipated or no extra volume is stored by bottom friction due to the presence of the storage cell.

In Eq.(E.2), Q_{in2} is written as follows:

$$Q_{in2} = \frac{2}{3} C_d l \sqrt{2g} (z_j^{n+1} - z_d)^{3/2} \tag{E.4}$$

and using Eq.(3.28):

$$Q_{in2} = \frac{2}{3} C_d l \sqrt{2g} (z_j^{n} + \Delta z_j - z_d)^{3/2} \tag{E.5}$$

This expression is not linear in Δz_j and it is impossible to make it linear in Δz_j in analytical way. To solve this problem, a linear approximation of Eq.(E.5) is made by using a 1st order Taylor development in the vicinity of zero. This approximation is accurate under the condition that the value of Δz_j stays sufficiently small [3].

The general form of the first order Taylor development in the vicinity of x_0 is:

$$f(x) \approx f(x_0) + (x - x_0) f'(x_0) \tag{E.6}$$

Eq.(E.5) and Eq.(E.6) lead to:

$$Q_{in2} \approx \frac{2}{3} C_d l \sqrt{2g} \left[(x_0 + z_j^n - z_d)^{\frac{3}{2}} + (\Delta z_j - x_0) \frac{3}{2} \sqrt{x_0 + z_j^n - z_d} \right] \tag{E.7}$$

This equation is linear in Δz_j and with x_0 = 0, Eq.(E.2) results into:

$$Q_{j+1}^{n+1} = Q_j^{n+1} - \frac{2}{3} C_d l \sqrt{2g} \left[z_j^n - z_d)^{\frac{3}{2}} + (\Delta z_j) \frac{3}{2} \sqrt{z_j^n - z_d} \right] \tag{E.8}$$

Using Eq. (3.29) gives:

$$\begin{aligned} Q_{j+1}^n + \Delta Q_{j+1} & \\ &= Q_j^n + \Delta Q_j - \frac{2}{3} C_d \sqrt{2g} l (z_j^n - z_d)^{\frac{3}{2}} \\ &- C_d l (\Delta z_j) \frac{3}{2} \sqrt{2g(z_j^n - z_d)} \end{aligned} \tag{E.9}$$

Substitution in Eq.(3.19) leads to adapted coefficients to indicate the influence of the storage area.

$$H = 0 \tag{E.10}$$
$$I = 1 \tag{E.11}$$
$$C = -C_d l \sqrt{2g(z_j - z_d)} \tag{E.12}$$
$$D = 1 \tag{E.13}$$
$$G = Q_j - Q_{j+1} - \frac{2}{3} C_d \sqrt{2g} l (z_j - z_d)^{\frac{3}{2}} \tag{E.14}$$

For the momentum equation, Eq.(E.3) is written as

$$z_{j+1}^n + \Delta z_{j+1} = z_j^n + \Delta z_j \tag{E.15}$$

and the coefficients in the Saint Venant equations are as follows:

$$H' = 1 \tag{E.16}$$
$$I' = 0 \tag{E.17}$$
$$C' = 1 \tag{E.18}$$
$$D' = 0 \tag{E.19}$$
$$G' = z_j - z_{j+1} \tag{E.20}$$

$\mathbf{z}_d$<$\mathbf{z}_b$<$\mathbf{z}_j$: Here, the water level in the channel and the water level in the inundation area are higher than the treshold and the water level in the channel is higher than the water level in the flooding cell, so, water will flow from channel to storage zone. The used formulas model the treshold between channel and inundation area as a submerged weir. The discharge over the weir will depend on the water level in the channel and on the water level in the inundation area. The discharge is given by [1]:

$$Q_{in3} = C_d l h_b \sqrt{2g(h_p + \tfrac{V_0^2}{2g}) - h_b} \tag{E.21}$$

V_0 is neglected by assuming that the water flow between the main channel and the inundation cell is only dependent on the water level of channel and cell.
The continuity equation is:

$$Q_{j+1}^{n+1} = Q_j^{n+1} - Q_{in3} \tag{E.22}$$

and the momentum equation equals Eq.(E.3).
These equations are valid on time step n+1. Q_{in3} is written as follows:

$$\begin{aligned} Q_{j+1}^n + \Delta Q_{j+1} & \\ &= Q_j^n + \Delta Q_j - C_d l h_b \sqrt{2g(z_j^n} \\ &+ \Delta z_j - z_d - h_b) \end{aligned} \tag{E.23}$$

This equation is not linear in Δz_j and a first order Taylor development in the vicinity of zero has to be applied [2–4] resulting in following coefficients of the continuity equation:

$$H = 0 \tag{E.24}$$
$$I = 1 \tag{E.25}$$
$$C = \frac{-C_d l h_b \sqrt{2g}}{2\sqrt{z_j - z_d - h_b}} \tag{E.26}$$
$$D = 1 \tag{E.27}$$
$$G = Q_j - Q_{j+1} - C_d l h_b \sqrt{2g(z_j - z_d - h_b)} \tag{E.28}$$

The coefficients in the momentum equation equal Eq.(E.17) to (E.20).

z_d<z_j<z_b: The water flows from the storage cell to the river channel, both levels are higher than the treshold level. The used formulas model the treshold between channel and inundation area as a submerged weir. The discharge from the inundation area to the river is given by:

$$Q_{out4} = C_d l h_b \sqrt{2g(h_p + \frac{V_0^2}{2g}) - h_b} \tag{E.29}$$

As one assumes that there is no water flow in a storage cell, V_0 = 0 and the continuity equation is:

$$Q_{j+1}^{n+1} = Q_j^{n+1} + Q_{out4} \tag{E.30}$$

The momentum equation equals Eq.(E.3). Eq.(E.30) results into:

$$Q_{j+1}^n + \Delta Q_{j+1} = Q_j^n + \Delta Q_j + C_d l (z_j^n + \Delta z_j - z_d) \sqrt{2g(h_b - z_j^n - \Delta z_j + z_d)} \tag{E.31}$$

Taylor development in the vicinity of zero leads to following coefficients of the continuity equation:

$$H = 0 \tag{E.32}$$
$$I = 1 \tag{E.33}$$
$$C = C_d l [\sqrt{2g(h_b - z_j + z_d)} - (z_j - z_d) \frac{g}{\sqrt{2g(h_b - z_j + z_d)}}] \tag{E.34}$$
$$D = 1 \tag{E.35}$$
$$G = Q_j - Q_{j+1} + C_d l (z_j - z_d) \sqrt{2g(h_b - z_j + z_d)} \tag{E.36}$$

The coefficients in the momentum equation equal Eq.(E.17) to (E.20).

z_j<z_d<z_b: Here, the water level in the storage area is higher than the treshold and water flows from the flooding cell back to the river channel. The general equation for free flow over a weir is given by Poleni [1]:

$$Q_{out5} = \frac{2}{3} C_d l \sqrt{2g} h_b^{3/2} \tag{E.37}$$

h_b is as indicated at Fig. 7.3. Eq.(E.37) determines the discharge flowing into the storage basin at node j.

The continuity equation is:

$$Q_{j+1}^{n+1} = Q_j^{n+1} + Q_{out5} \tag{E.38}$$

Eq.(E.37) and Eq.(E.38) lead to:

$$Q_{j+1}^n + \Delta Q_{j+1} = Q_j^n + \Delta Q_j + \frac{2}{3} C_d \sqrt{2g} l h_b^{\frac{3}{2}} \tag{E.39}$$

The previous leads to adapted coefficients to indicate the influence of the storage area.

$$\begin{aligned} H &= 0 && \text{(E.40)} \\ I &= 1 && \text{(E.41)} \\ C &= -C_d l \sqrt{2g(z_j - z_d)} && \text{(E.42)} \\ D &= 1 && \text{(E.43)} \\ G &= Q_j - Q_{j+1} + \frac{2}{3} C_d \sqrt{2g} l (h_b)^{\frac{3}{2}} && \text{(E.44)} \end{aligned}$$

For the momentum equation, Eq.(E.3), the coefficients are identical to the ones in the other situations (Eq.(E.17 to E.20)).

2 Internal storage: relation discharge and flooding area (Method 2)

Consider a storage basin linked to the river. When the coefficients E and F are computed, they are found automatically for point j as they were for point j-1. To continue the computations, the coefficients E_{j+1} and F_{j+1} are needed. The coefficients E_{j+2} and F_{j+2}, etc. may then be computed by recurrence. The coefficients L_j, M_j and N_j are also necessary to compute Δz_j in the backward sweep if Δz_{j+1} and ΔQ_{j+1} are known. These coefficients depend upon the characteristics of the transition between the nodes j and j+1. If the velocity in the cross sections j and j+1 are equal and the water level in the storage basin (z_b) equals the water level in the river channel (z_j), then continuity equation and momentum equation are written according Eq.(E.45) and Eq.(E.46), with Q the discharge from the river into the basin.

$$Q_{j+1}^{n+1} = Q_j^{n+1} - Q^{n+1} \tag{E.45}$$

$$z_j^{n+1} = z_{j+1}^{n+1} = z_b^{n+1} \tag{E.46}$$

Comparing with Eq.(3.19) and Eq.(3.20) allows to easily read the coefficients. The continuity of the volume stored in the basin leads to the equation:

$$V_b = A_b * z_b \tag{E.47}$$

$$\frac{\partial V_b}{\partial t} = A_b \frac{\partial z_b}{\partial t} = Q \tag{E.48}$$

where A_b is the horizontal water surface area of the basin [m^2], with A_b = $A_b(z_b)$.
Eq.(E.45) and Eq.(3.29) substituted in Eq.(E.48) results into:

$$Q_{j+1}^{n+1} = Q_j^{n+1} - \frac{A_b^{n+1}(z_b)}{\Delta t}\Delta z_b \tag{E.49}$$

$$Q_{j+1}^{n} + \Delta Q_{j+1} = Q_j^n + \Delta Q_j - \frac{A_b^{n+1}(z_b)}{\Delta t}\Delta z_b \tag{E.50}$$

$$= Q_j^n + \Delta Q_j - (\frac{A_b^n}{\Delta t} + (\frac{\partial \Delta b}{\partial z_j \Delta t})\Delta z_j)\Delta z_j \tag{E.51}$$

$$= Q_j^n + \Delta Q_j - \frac{A_b^n}{\Delta t}\Delta z_j \tag{E.52}$$

Comparing with Eq.(3.19) results in following coefficients of the continuity equation:

$$H = 0 \tag{E.53}$$
$$I = 1 \tag{E.54}$$
$$C = -\frac{A_b}{\Delta t} \tag{E.55}$$
$$D = 1 \tag{E.56}$$
$$G = Q_j - Q_{j+1} \tag{E.57}$$

Discretisation of Eq.(E.46) leads to:

$$z_{j+1}^{n+1} = z_j^{n+1} \tag{E.58}$$

and with Eq.(3.28):

$$z_{j+1}^{n} + \Delta z_{j+1} = z_j^{n} + \Delta z_j \tag{E.59}$$

Comparing Eq.(3.20) with Eq.(E.59) results in following coefficients of the momentum equation.

$$H^{'} = 1 \tag{E.60}$$
$$I^{'} = 0 \tag{E.61}$$
$$C^{'} = 1 \tag{E.62}$$
$$D^{'} = 0 \tag{E.63}$$
$$G^{'} = z_j - z_{j+1} \tag{E.64}$$

These coefficients replace the original coefficients in the Saint Venant equations if the water level in the river channel exceeds the height of the banks (the treshold value or height of the weir). Under this condition, the Double Sweep algorithm uses these new coefficients to solve the Saint Venant equations for this particular node.

References

[1] J. Berlamont. *Theorie van de verhanglijnen*, page 239. L. Wouters, 6 edition, 2004.

[2] P. Troch. *Mathematische simulatie van niet-permanente stroming op een waterwegennet*. Master's thesis, Ghent university, 1991.

[3] M. Van Lysebettens. *Numerical modelling of the interaction between a river and its floodplains*. Master's thesis, Ghent University, 2006.

[4] F. Declercq. *Overstromingsgebieden: experimentele opzet en numerieke modellering in 'Femme'*. Master's thesis, Ghent University, 2007. Faculty of Engineering.